UNIVERSITÉ DE LORRAINE | BIBLIOTHÈQUES UNIVERSITAIRES

AVERTISSEMENT
DROIT D'AUTEUR

Ce document est le fruit d'un long travail approuvé par le jury de soutenance et mis à disposition de l'ensemble de la communauté universitaire élargie.

Il est soumis à la propriété intellectuelle de l'auteur. Ceci implique une obligation de citation et de référencement lors de l'utilisation de ce document. Toute contrefaçon, plagiat ou reproduction illicite encourt une poursuite pénale.

Contact bibliothèque : ddoc-theses-contact@univ-lorraine.fr
(Cette adresse ne permet pas de contacter les auteurs)

Code de la Propriété Intellectuelle. articles L 122. 4
Code de la Propriété Intellectuelle. articles L 335.2- L 335.10

UNIVERSITÉ DE LORRAINE
34 COURS LÉOPOLD — CS 25233
54052 NANCY CEDEX
TÉL : 03 54 50 54 00
CONTACT@UNIV-LORRAINE.FR
WWW.UNIV-LORRAINE.FR

THÈSE

pour obtenir le grade de

Docteur de l'Université de Lorraine

Spécialité « Énergie et Mécanique »

présentée et soutenue publiquement par

Guillaume ETIENNE

le 08 juillet 2026

Performance and Degradation of Ionomer Membranes for Fuel Cells between 70°C and 100°C *Ex Situ* and *In Situ* Approaches

Performances et dégradations des membranes ionomères pour pile à combustible entre 70°C et 100°C Approches ex situ et in situ

---

École Doctorale

SIMPPÉ – Sciences et Ingénierie des Molécules, des Produits, des Procédés, et de l'Énergie

Unité de Recherche

LEMTA, UMR 7563, CNRS, Université de Lorraine

Composition du jury

Rapporteure	Hakima MENDIL JAKANI	Directrice de recherche – CEA, SyMMES, Grenoble
Rapporteur	Bruno AMÉDURI	Directeur de recherche – CNRS, ICGM, Montpellier
Examinatrice & Présidente du jury	Corine BAS	Professeure – Université Savoie Mont-Blanc, LEPMI, Chambéry
Examinateur	Laurent REY	Ingénieur R&D – Symbio, Lyon
Examinateur	Sylvain BRIMAUD	Scientist and Team Leader – ZSW, Baden-Württemberg
Examinateur	Marian CHATENET	Professeur – Université Grenoble Alpes, LEPMI, Grenoble
Directeur de thèse	Olivier LOTTIN	Professeur – Université de Lorraine, LEMTA, Nancy
Co-directrice	Assma EL KADDOURI	Maître de Conférences – Université de Lorraine, LEMTA, Nancy
Invité	Arnaud MORIN	Directeur de recherche – CEA, LITEN, Grenoble
Invité	Julia MAINKA	Maître de Conférences – Université de Lorraine, LEMTA, Nancy
Invité	Jérôme DILLET	Ingénieur de recherche – CNRS, LEMTA, Nancy

Douter de tout ou tout croire, ce sont deux solutions également commodes, qui l'une et l'autre nous dispensent de réfléchir.
Henri Poincaré

Remerciements

Voici la conclusion de ces quatre années de thèse réalisées au LEMTA. A mes débuts, je me disais que trois ans représentaient une durée considérable pour un sujet de recherche, mais je me rends compte aujourd'hui que ces années sont passées à une vitesse folle. Voici maintenant venu le temps de remercier toutes les personnes qui m'ont accompagné au cours de cette aventure. Elles sont très nombreuses, mais je vais essayer de faire de mon mieux pour n'oublier personne.

Mes remerciements s'adressent tout d'abord à mon jury de thèse. Je vous suis très reconnaissant pour le temps que vous avez consacré à l'évaluation de mon travail ainsi que pour vos commentaires. Les questions et discussions engagées se sont révélées très instructives et inspirantes, et je ne manquerai pas de m'en inspirer pour de futures expérimentations. J'espère avoir un jour l'occasion de (re)travailler avec vous.

Je tiens également à remercier chaleureusement mes encadrants de thèse, Olivier et Assma. Tout d'abord, pour m'avoir donné l'opportunité de participer à ce projet mais également pour avoir cru en moi. Je ne saurais énumérer toutes les choses que vous m'avez apprises, tant elles sont nombreuses. Néanmoins, je tiens à vous remercier chaleureusement pour votre pédagogie et pour le cadre que vous avez instauré. La liberté de tester des expériences, votre disponibilité pour répondre à mes questions, toujours avec bienveillance, ainsi que les nombreuses discussions scientifiques que nous avons eues ne m'ont jamais donné l'impression d'un emploi, mais d'un véritable travail d'équipe. C'est grâce à cet environnement que j'ai toujours pu me sentir libre d'aller plus loin. Encore merci !
Je remercie également Julia pour sa bienveillance, ses bons conseils et sa disponibilité. Merci pour toutes ces discussions qui m'ont beaucoup apporté et m'ont permis de grandir en tant que chercheur. Je remercie également Aouatef, avec qui j'ai pu travailler sur ce projet. Au-delà de ton aide précieuse lors des expérimentations, ta bonne humeur et tes rires permanents ont beaucoup apporté.

Je ne saurais également exprimer suffisamment ma reconnaissance à Jérôme et Kévin pour la conception des bancs d'expérimentation. Votre travail constitue la base de tout ce qui a pu être réalisé au cours de cette thèse. Merci pour votre travail et votre implication, ainsi que pour votre disponibilité dès qu'un problème apparaissait.
Un grand merci à toutes les personnes qui ont pu m'aider pendant ces années. Gaël, Sophie, Feina, Jean-Christophe, merci d'avoir toujours pris le temps de répondre à mes questions.

Je tiens particulièrement à remercier Meriem. Meriem, tu m'as tout appris sur les piles : leur montage, leur fonctionnement. Merci d'avoir pris le temps de tout m'expliquer avec autant de bonne humeur et de joie de vivre. Je ne crois pas t'avoir déjà vue négative. Une positivité constante et une grande gentillesse sont les meilleurs mots que je pourrais utiliser pour te décrire. Merci !

Merci à tous mes amis de la fac qui m'ont soutenu ainsi qu'à tous les doctorants. Merci à Kolo, Valentin, Joïc, William, Christine pour ces bons moments passés dans le bureau. Merci également à tous les doctorants avec qui j'ai pu partager de nombreux moments. Emeric, Thomas, Maxime, Emilie et Kaoutar, merci pour tous ces moments partagés du début à la fin de cette thèse, dans les bons

comme dans les mauvais moments ! Kaoutar, je ne saurais assez te remercier pour le soutien que tu m'as apporté. Merci pour les conversations, les pauses café et les rires. "Chère amie", merci d'avoir été là, avec ta bienveillance et ta bonne humeur. Je garderai précieusement tous ces moments partagés.
Bien évidemment, j'adresse mes remerciements à Giuseppe, grand frère de tous les doctorants et père spirituel. Ta bonne humeur, ta compassion et tes bons conseils ont constitué un précieux soutien. Ta gentillesse et ta bienveillance font de toi une personne à part, toujours présente avec les bons mots et les bons conseils. Merci pour tous ces bons moments au labo, à Montpellier, à Lucerne...

Je tiens à remercier chaleureusement toutes les personnes du laboratoire avec qui j'ai eu la chance de partager de nombreux bons moments, aussi bien autour d'un café qu'en dehors du laboratoire. Un grand merci aux anciens doctorants comme aux membres du personnel du laboratoire pour leur gentillesse, leur bonne humeur et leur convivialité, qui ont contribué à rendre ces années de thèse particulièrement agréables.

Enfin, je tiens à remercier ma famille pour sa présence, son soutien et son aide tout au long de ce parcours. Merci pour votre patience, votre confiance et vos encouragements, qui m'ont permis d'avancer avec sérénité et de persévérer dans les moments plus difficiles. Votre soutien m'a été précieux et je vous en suis sincèrement reconnaissant.

Sommaire

Remerciements

Introduction

1. State of the art

1 State of the art 10

1.1 The different components of a PEMFC and their role 10

1.1.1 The proton exchange membrane fuel cell 10

1.2 The bipolar plate (BP) 12

1.2.1 Role, composition, and morphology 12

1.2.2 Degradation mechanisms 13

1.3 Gas Diffusion Layer (GDL) 14

1.3.1 Role, composition, and morphology 14

1.3.2 Degradation mechanisms 17

1.4 Electrodes 18

1.4.1 Role, composition, and morphology 18

1.4.2 Degradation mechanisms 20

1.5 The ionomer membrane 23

1.5.1 Role, composition and families 23

1.5.2 Degradation mechanisms 25

2 Impact of operating temperature on fuel cell and components performance/durability 29

2.1 Fuel cell performance and durability from standard to high temperatures 29

2.1.1 Fuel cell performance 29

2.1.2 PEMFC durability 32

2.2 Component performance and durability from standard to high temperatures 34

2.2.1 Bipolar plates 34

2.2.2 Gas Diffusion Layers 35

2.2.3 Catalyst layers 36

2.2.4 Ionomer membrane 40
3 Conclusions 43
References 44

2. PEMFC performance at higher operating temperature

1 Introduction 64
2 Materials & methods 67
2.1 MEA and break-in protocol 67
2.2 Polarization curves and Electrochemical Impedance Spectroscopy 68
2.2.1 Polarization curves with imposed current density (galvanostatic mode) 68
2.2.2 Polarization curves and EIS in potentiostatic mode 68
2.3 Accelerated Stress Test (AST) 69
3 Performance mapping 70
3.1 Impact of operating conditions on PEMFC performance 70
3.2 Impact of relative humidity at 95°C – possible issues with membrane hydration and oxygen diffusion 74
3.3 Origin of voltage drop at 95°C 76
3.4 R_{hf} measurements during the AST 78
3.5 R_{hf} measurements at intermediate temperature 79
4 Discussion : on the main factors limiting the FC performance in the 90°C-100°C temperature range 80
5 Local behavior assessment at 95°C 83
5.1 Local i and R_{hf} measurements with the state-of-the-art membrane 84
5.2 Effect of membrane thickness on MEA hydration 85
6 Conclusion 86
References 88

3. sPEEK Membranes : A Review of Structural and Physicochemical Properties

1 Introduction 98
2 PEEK sulfonation 99
3 Microstructure & Morphology 101
4 Physicochemical properties 104
4.1 Sorption, water uptake 105
4.2 Conductivity 107
4.3 Other transport properties 110

4.4 Mechanical properties . . . 112
5 Ionomer durability . . . 115
5.1 sPEEK during *ex situ* degradation tests . . . 115
5.2 sPEEK durability during fuel cell operation . . . 117
6 Impact of manufacturing process . . . 118
6.1 Casting solvent . . . 119
6.2 Pretreatment . . . 121
6.2.1 Soaking treatments . . . 121
6.2.2 Crosslinking . . . 123
7 Conclusions/perspectives . . . 124
References . . . 126

4. sPEEK-based MEA performances

1 Introduction . . . 140
2 Materials & methods . . . 143
2.1 sPEEK pretreatment . . . 143
2.1.1 Drying step . . . 144
2.2 Catalyst Coated Backing (CCB) based MEA . . . 145
2.3 Catalyst Coated Membrane (CCM) based MEA . . . 146
2.4 Test-bench, single cell, and performance mapping . . . 147
2.5 Polarization curves and Electrochemical Impedance Spectroscopy (EIS) . . . 148
3 Results . . . 149
3.1 sPEEK-based MEA *vs.* Nafion . . . 149
3.2 Impact of sPEEK pretreatment : *sPEEK nanostructured vs. sPEEK standard* . . . 150
3.3 Impact of operating conditions . . . 152
3.4 Comparison of electrodes deposition method effect . . . 154
3.5 Effect of *Nafion overcoat* thickness on CCB MEA performance . . . 157
4 Discussion . . . 158
5 Conclusion . . . 160
References . . . 161

5. PFSA-based durability at higher operating temperature and comparison with alternative membrane

1 Introduction . . . 168
2 Materials, methods & protocol . . . 169

2.1 Materials & methods . . . 169
2.2 Protocol . . . 170
3 Durability evaluation of state-of-the-art materials . . . 172
3.1 Impact of operating parameters on MEA performance evolution . . . 172
3.2 Post-mortem analysis . . . 182
3.3 Summary and discussion . . . 188
4 Comparison with alternative membrane ionomers . . . 191
4.1 sPEEK durability : effect of pretreatment and comparison with PFSA membranes durability . . . 191
4.2 Effect of *Nafion overcoat* and electrodes deposit method (CCM) on sPEEK durability . . . 194
4.3 Summary and discussion . . . 197
5 Conclusions . . . 198
References . . . 201

6. *Ex situ* durability measurements in vapor phase

1 Introduction . . . 206
2 Materials & methods . . . 208
2.1 Materials . . . 208
2.2 Methods . . . 209
3 Preliminary tests : sPEEK vs NR211 and parameters adjustment . . . 210
4 Impact of chemical and coupled chemical-mechanical stresses on sPEEK membrane . . . 214
4.1 sPEEK chemical structure . . . 214
4.2 Crystallinity evolution through FTIR measurements . . . 218
4.3 Impact on fuel cell performance . . . 220
4.4 Discussion . . . 222
5 Conclusions . . . 225
References . . . 227
6 Appendix . . . 231

Conclusions & perspectives

Résumé

Introduction

General context

Energy has become a critical driver in modern society. The development of industry and technologies, combined with rising living standards, has led to a sharp increase in energy demand. For example, global energy demand doubled between 1980 and 2021, reaching 171 650 TWh [1]. This demand is largely met by the extensive use of fossil resources–mainly oil, gas, and coal, which account for 30%, 23%, and 28% of total energy supply [2], respectively. Due to their ease of extraction and widespread availability, fossil fuels remained the preferred energy source, particularly in countries with large industrial sectors and in developing nations [3]. Although fossil fuels offer certain advantages, the International Energy Agency (IEA) predicts that global demand will peak before 2030 and decline afterward. Several factors contribute to this trend, including dependence on imports, fuel price volatility in a complex geopolitical context, which create severe interdependencies between countries. Additionally, since fossil fuels are a major contributor to global warming, policies are increasingly aimed at limiting the rise in global temperature, which is linked to more frequent natural disasters and worsening air pollution [4]. In this context, numerous countries have developed strategies centered on hydrogen as an energy vector. This versatile fuel is already used in various sectors, such as refining and chemical processes (figure 1), with 100 Mt consumed worldwide–of which only 1 Mt is low-emission H_2–and 0.9 Mt consumed in France in 2024 [5, 6].

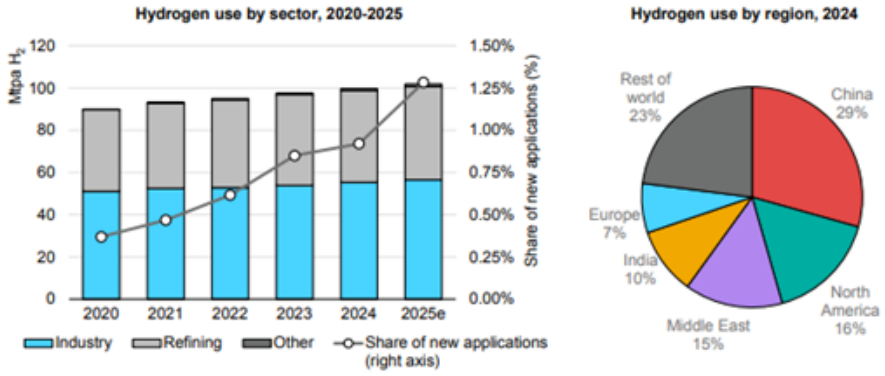

FIGURE 1 – Hydrogen demand by sector and by region between 2020 and 2025 [5].

Hydrogen offers numerous advantages, which explains the significant investments in this emerging industry :

- **Production independence :** hydrogen can be produced independently of fossil fuels, and thus other countries, using electrolyzers and water. However, different electrolyzer technologies exist, and some rely on noble metals, making their production dependent on countries that possess these critical materials. On the other hand, prospecting missions are currently conducted to es-

timate the potential of native hydrogen. Although estimating global H_2 reserves and natural H_2 production of earth is challenging, preliminary measurements suggest substantial potential. In France, research has identified a large hydrogen deposit estimated at 46 Mt [7]. Other deposits have also been discovered worldwide, some already being exploited, such as in Mali [8]. Despite uncertainties, native hydrogen is believed to exist in many countries (figure 2).

- **Versatility of use :** hydrogen can be employed in multiple ways. Through direct combustion or electrochemical reactions, heat or electricity can be produced for stationary and transportation applications. Additionally, electricity produced via electrochemical reactions emits no pollutant, enabling cleaner processes across various sectors.
- **Energy storage potential :** unlike electricity, which is difficult to store and requires large numbers of batteries that may contain critical metals, hydrogen offers a practical storage solution. This capability is particularly valuable for managing renewable electricity, whose intermittency can cause grid instabilities. Solar energy can be converted into hydrogen, especially in regions with abundant sunlight, such as Africa [9]. Offshore wind energy is another promising option, as wind is more consistent at sea than on land. Various architectures are under consideration, including offshore electricity generation combined with onshore hydrogen production, or both offshore electricity and hydrogen production with subsea or platform storage [10].

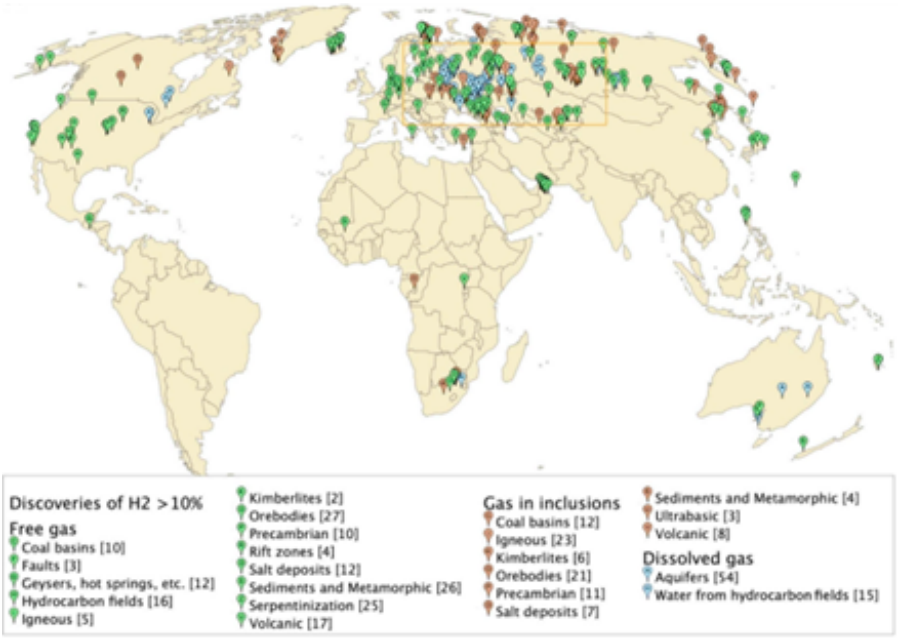

FIGURE 2 – World map illustrating locations where hydrogen concentrations greater than 10% have been detected [11].

Hydrogen production is currently based on fossil fuels, accounting for 95% of global hydrogen output through steam reforming and gasification processes [12]. This results in 920 Mt of CO_2 emissions for hydrogen production worldwide in 2023 [13]. In France, hydrogen consumption amounts to 1 Mt, while production reaches 0.9 Mt, generating 11.5 Mt CO_2–approximately 3% of national carbon dioxide emissions [14]. To develop a robust hydrogen sector, the French government launched a hydrogen deployment plan for the energy transition in 2018 [14]. The plan sets several objectives, including the development of an innovative French hydrogen industry, the decarbonization of existing industry processes involving hydrogen consumption, and the development of hydrogen technologies and knowledge through research supported by the French National Research Agency (ANR). To achieve these goals, a research program called PEPR-H2, comprising 20 R&D projects, is being set up from 2022 to

accelerate the development of hydrogen production, consumption, and storage technologies, as well as conversion systems, experimental platforms and cross-cutting activities such as life cycle analysis and socio-economic studies [15].

Part of the PEPR-H2 project focuses on fuel cell technologies. The general principle is to consume hydrogen and oxygen, often contained in air, to produce electricity. There are different types of fuel cells, whose specific features reflect the applications in which they are best suited. Depending on the characteristics of the fuel cell, such as operating temperature, power density and start-up time, stationary or portable applications are possible. Low-temperature fuel cells, such as PEMFC (*Proton Exchange Membrane Fuel Cell*) and AFC (*Alkaline Fuel Cell*), are suitable for stationary and portable applications because of their high-power density, high efficiency and fast start-up time. SOFC (*Solid Oxide Fuel Cell*) and MCFC (*Molten Carbonate Fuel Cell*) operate at high temperatures and require a long start-up time. However, the robustness and high efficiency of these systems when operating with heat recovery make them suitable for stationary applications such as large-scale stationary power generation, combined heat and power systems, industrial applications, etc. As described, both portable and stationary applications are suitable for fuel cell use. Different sectors are targeted :

- Stationary applications with power densities ranging from kW to MW. Fuel cells can be used in power stations to supply and balance the electricity grid. For example, they can be incorporated into an uninterruptible power supply (UPS) system in important applications such as hospital [16], or into an integrated power system (IPS) [17].
- Portable systems with applications in aerospace, unmanned aerial vehicles, space, transport, etc. Even if PEMFC are not yet competitive in the transport sector, trucks, trains, buses and marine applications require greater autonomy and power density, which cannot be provided by batteries but could be by fuel cells.

Therefore, using different fuel cells according to the application could decarbonize a large part of the society. Power generation by gas and coal-fired power stations could be replaced by fuel cell facilities with SOFC and MCFC. Heavy duty transportation could be decarbonized using high-power density as PEMFC or AFC. One of the main sources of pollution in France is the transport sector, which accounted for 34% of national greenhouse gas emissions in 2023, equivalent to 126.8 Mt $CO_{2,\,eq}$. The majority of these emissions come from personal vehicles (23.7% of national $CO_{2,\,eq}$ emissions), while the remainder is divided among heavy goods vehicles (8.2%), rail (0.1%), maritime transport (0.7%) and air transport (1.2%) (figure 3) [18].

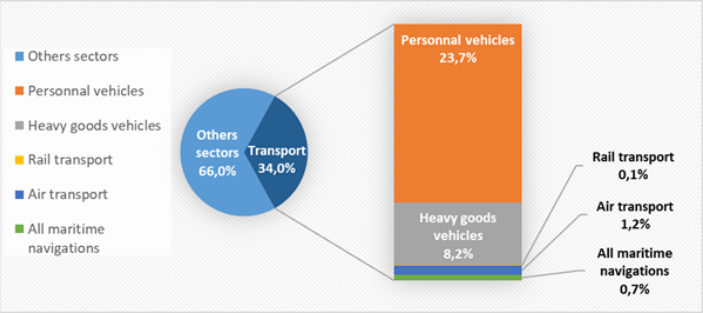

Means of transport	Emissions (Mt CO_2 eq)
Personnal vehicles	88.4
Heavy goods vehicles	30.7
Rail transport	0.4
Air transport	2.7
All maritime navigations	4.5

FIGURE 3 – Summary of emissions transport sector emissions in 2023 [18].

According to available data, the transport sector has a significant part to play in decarbonization. For smaller vehicles, batteries are preferred because the overall energy chain–from hydrogen production to consumption–is less efficient with hydrogen than with direct electricity. Consequently, battery-powered vehicles are less polluting over the entire life cycle compared to fuel cell vehicles,

due to the additional emissions generated during hydrogen production. The Carbone 4 society estimated an emission rate of 95 $gCO_{2,\,eq}$/km for a fuel cell car powered by hydrogen produced using the current French energy mix, compared to 85 $gCO_{2,\,eq}$/km for a battery-electric car using the same energetic mix [19]. Despite these differences, both options still represent a substantial reduction in greenhouse gas emissions compared to conventional internal combustion vehicles (*e.g.*, diesel cars ⇔ 242 $gCO_{2,\,eq}$/km). However, applying fuel cell technology to personal vehicles remains challenging due to logistical issues, including hydrogen transport and storage at gas stations.

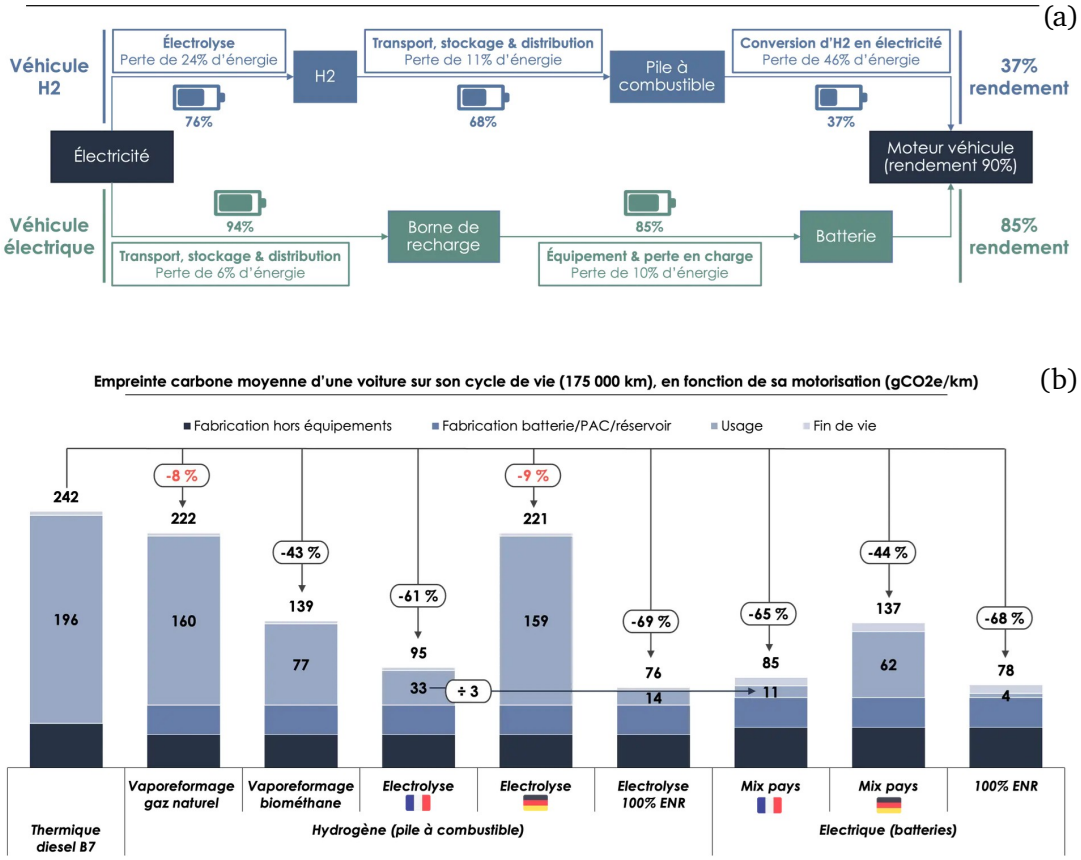

FIGURE 4 – H_2 and electric vehicle powertrain (a) and vehicle emissions according to its fuel type, calculated over its entire life cycle, based on the country's electricity mix (b)[19].

While fuel cells are not well suited for personal vehicles, batteries are difficult to integrate into heavy transport due to the excessive weight of the system. For example, providing the power and range required for heavy transport, such as lorries, would require approximately 3 tonnes of lithium batteries, compared with only 500 kg for a 150 kW PEMFC. It is therefore evident that an alternative power source must be considered for heavy transport. As noted above, PEMFC or AFC systems are suitable candidates due to their high-power density and rapid response to sudden power demands.

Thesis context

Although PEMFC systems present significant potential for heavy-transport applications, material limitations still exist, and further improvements are required to accelerate their development. Current systems operate at temperatures around 70-80°C using well-established materials. However, an increasing number of studies are focusing on higher operating temperatures, *i.e.*, 80-120°C for Intermediate-

Temperature PEMFC (IT-PEMFC) and above 140°C for High-Temperature PEMFC (HT-PEMFC). Raising the operating temperature enables two main advantages :

- **Enhanced catalyst tolerance to impurities :** most hydrogen currently used is produced from fossil fuels, a process that generates impurities such as CO, CO_2 and CH_4 [20]. These species can interact with catalyst particles, reducing the available electrochemical surface area [21] and thus decreasing fuel cell performance. Higher operating temperatures improve catalyst tolerance to impurities due to increased kinetics of hydrogen oxidation and oxygen reduction, potentially lowering costs by enabling the use of less pure hydrogen.
- **Improved system compactness :** for transport applications, system size is a critical parameter. Increasing the operating temperature reduces the required size of heat exchangers and, consequently, the overall system volume.

In this context, the PEMFC95 project was launched in 2019 with the aim of developing a PEMFC capable of operating with high performance and durability at 95°C. Several tasks were defined to address this challenge :

- **Assess the impact of a higher operating temperature on PEMFC performance and durability :** to this end, single cells ranging from 25 cm^2 to 100 cm^2, as well as mini-stacks, are employed to evaluate overall performance and characterize the state of materials in various operating conditions.
- **Synthesis of new materials (Gas Diffusion Layer, Electrodes and membrane) :** these materials are designed to withstand harsher operating conditions and demonstrate improved durability.
- **Life Cycling Analysis (LCA) :** this task aims to estimate the environmental impact associated with the synthesis of the new materials, as well as the operation and recycling costs.

Among these tasks, our laboratory (LEMTA) focuses on evaluating the performance and durability of MEA at elevated temperatures during fuel cell operation. In this context, this thesis aims at investigating on membrane performance and durability between 70°C and 95°C.

It is widely recognized that PerFluoroSulfonic acid Long-Side Chain (PFSA-LSC) ionomer membranes are the benchmark at conventional temperatures, but they are not fully operational at higher temperatures, primarily due to excessive dehydration. However, only a few studies have explored the use of PFSA-LSC membrane while limiting the increase in operating temperature. The development of more efficient commercial materials raises questions about the traditionally accepted operational limits.

With this context, this work aims to evaluate the performance and durability of a state-of-the-art PFSA-LSC membrane. Simultaneously, part of this work investigates the feasibility of using sulfonated poly(ether ether ketone) (sPEEK) membrane. Known for its superior thermal and mechanical properties compared with PFSA-LSC, sPEEK also offers the advantages of being cheaper and less polluting, making it an attractive alternative. The results of this work are structured into six chapters, which are summarized below :

- **Chapter 1 :** a state-of-the-art overview detailing PEMFC operating principles and describing each component, including its composition and degradation mechanisms under standard and elevated operating temperatures.
- **Chapter 2 :** a study on the impact of temperature on the performance of a commercial MEA based on a 12 μm state-of-the-art membrane. Both global and local measurements were conducted to precisely assess the effect of operating conditions, such as temperature and gas inlet relative humidity.
- **Chapter 3 :** a dedicated literature review on sPEEK, placed just before the chapter presenting the experimental results on sPEEK. This review has been deliberately presented as a separate

chapter in order to ease the reading of the general state of the art (chapter 1).

- **Chapter 4 :** characterizations to assess the feasibility of using sPEEK ionomer at intermediate temperatures, including performance mapping. A comparison is then conducted between Catalyst-Coated Backing and Catalyst-Coated Membrane configurations to evaluate the influence of the electrode deposition method on hydrocarbon-based membrane.
- **Chapter 5 :** an evaluation of the durability of a commercial MEA with the aim to assess the effect of operating parameters, particularly temperature, on component degradation. Additional measurements were performed to evaluate the durability of sPEEK membranes and compared them with Nafion 211 and the commercial MEA.
- **Chapter 6 :** a study of sPEEK durability in a vapor phase, performed using a specially designed experimental bench capable of generating a controlled atmosphere with precise temperature, relative humidity, and mechanical constraints, in order to investigate membrane aging under well-defined environmental conditions.

Références

[1] C. général au développement DURABLE, *International*, https ://www.statistiques.developpement-durable.gouv.fr/edition-numerique/chiffres-cles-energie-2024/11-international.php.

[2] *World*, https ://www.iea.org/world/energy-mix, s.d.

[3] E. INSTITUTE, *Statistical review of world energy*, https ://www.energyinst.org/statistical-review/home.

[4] « World Energy Outlook 2023, » rapp. tech.

[5] U. REMME, « Global Hydrogen Review 2025, » rapp. tech., 2025.

[6] « L'hydrogène Aujourd'hui et Demain - Rapport, » Académie des Sciences, rapp. tech., 2024.

[7] *Un gisement géant d'hydrogène en Lorraine ?* https ://lejournal.cnrs.fr/articles/un-gisement-geant-dhydrogene-en-lorraine.

[8] L. RUFFINE et al., « Hydrogène naturel : Etat des connaissances scientifiques, juridiques et d'acceptabilité sociale, inventaire mondial, zones d'intérêts sur le territoire français, » rapp. tech., 2025.

[9] A. FOPAH-LELE et al., « Solar electricity storage through green hydrogen production : A case study, » *International Journal of Energy Research*, t. 45, n° 9, p. 13 007-13 021, 2021, ISSN : 1099-114X. DOI : 10.1002/er.6630

[10] Z. WANG et al., « Subsea energy storage as an enabler for floating offshore wind hydrogen production : Review and perspective, » *International Journal of Hydrogen Energy*, t. 71, p. 1266-1282, 2024, ISSN : 03603199. DOI : 10.1016/j.ijhydene.2024.05.329

[11] V. ZGONNIK, « The occurrence and geoscience of natural hydrogen : A comprehensive review, » *Earth-Science Reviews*, t. 203, p. 103 140, 2020, ISSN : 00128252. DOI : 10.1016/j.earscirev.2020.103140

[12] *IFPEN | Tout savoir sur l'hydrogène*, https ://www.ifpenergiesnouvelles.fr/enjeux-et-prospective/decryptages/energies-renouvelables/tout-savoir-lhydrogene.

[13] « GHG emissions of hydrogen and its derivatives – Global Hydrogen Review 2024 – Analysis, » rapp. tech

[14] « Plan de Déploiement de l'hydrogène Pour La Transition Énergétique, » rapp. tech., p. 26.

[15] *PEPR Hydrogène ✓-*, https ://www.pepr-hydrogene.fr/.

[16] Y. ZHAN et al., « Intelligent uninterruptible power supply system with back-up fuel cell/battery hybrid power source, » *Journal of Power Sources*, t. 179, n° 2, p. 745-753, 2008, ISSN : 03787753. DOI : 10.1016/j.jpowsour.2007.12.113

[17] P. GUPTA et al., « A Critical Review on Hydrogen Based Fuel Cell Technology and Applications, » *The Chemical Record*, t. 24, n° 1, e202300295, 2024, ISSN : 1528-0691. DOI : 10.1002/tcr.202300295

[18] « Emissions de Gaz à Effet de Serre et de Polluants Atmosphèriques En France | 1990-2023, » Secten, Rapport Secten Éd.2024, p. 561.

[19] *L'hydrogène pourra-t-il contribuer à décarboner les voitures ? | Carbone 4*, https ://carbone4.com/fr/analyse-hydrogene-decarbonation-voitures.

[20] Y. Kim et al., « Hydrogen Purity : Influence of Production Methods, Purification Techniques, and Analytical Approaches, » *Energies*, t. 18, n° 3, p. 741, 2025, ISSN : 1996-1073. DOI : 10.3390/en18030741

[21] Y. Qin et al., « Effect of hydrogen impurities on hydrogen oxidation activity of Pt/C catalyst in proton exchange membrane fuel cells, » *Clean Energy*, t. 7, n° 1, p. 139-147, 2023, ISSN : 2515-4230, 2515-396X. DOI : 10.1093/ce/zkac085

Chapter 1

State of the art

1 State of the art 10
1.1 The different components of a PEMFC and their role 10
1.1.1 The proton exchange membrane fuel cell 10
1.2 The bipolar plate (BP) 12
1.2.1 Role, composition, and morphology 12
1.2.2 Degradation mechanisms 13
1.3 Gas Diffusion Layer (GDL) 14
1.3.1 Role, composition, and morphology 14
1.3.2 Degradation mechanisms 17
1.4 Electrodes 18
1.4.1 Role, composition, and morphology 18
1.4.2 Degradation mechanisms 20
1.5 The ionomer membrane 23
1.5.1 Role, composition and families 23
1.5.2 Degradation mechanisms 25
2 Impact of operating temperature on fuel cell and components performance/durability . 29
2.1 Fuel cell performance and durability from standard to high temperatures 29
2.1.1 Fuel cell performance 29
2.1.2 PEMFC durability 32
2.2 Component performance and durability from standard to high temperatures 34
2.2.1 Bipolar plates 34
2.2.2 Gas Diffusion Layers 35
2.2.3 Catalyst layers 36
2.2.4 Ionomer membrane 40
3 Conclusions 43
References 44

1 State of the art

1.1 The different components of a PEMFC and their role

1.1.1 The proton exchange membrane fuel cell

A Proton Exchange Membrane Fuel Cell (PEMFC) is an electrochemical device that converts chemical energy into electrical energy. It is generally made of a series of elementary cells assembled to form a *stack*.

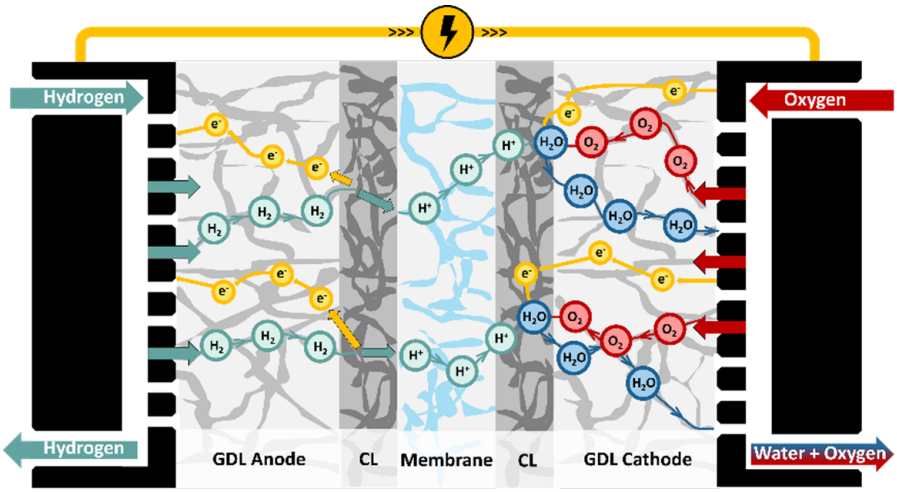

FIGURE 1.1 – Schematic diagram of a PEMFC operating under oxygen.

Each cell is composed of bipolar plates and Gas Diffusion Layers (GDL), which distribute the reactant gases to the electrodes, also called catalyst layers (CL), separated by an ionomer membrane. The cell is supplied with hydrogen on one side through the bipolar plates. The hydrogen then diffuses through the GDL to reach the electrode known as the anode. On the opposite side, the gas is either air or pure oxygen, which is convoyed to the cathode CL. Oxidation and reduction reactions occur at the electrodes, enabled by the potential difference between them and their separation by the electronically insulating membrane. The reactions are as follows :

- Hydrogen Oxidation Reaction (HOR) at the anode :

$$H_2 \longrightarrow 2H^+ + 2e^- \tag{1.1}$$

  The protons cross the membrane to reach the cathode, while the electrons are conducted through an external circuit to perform electrical work.

- Oxygen Reduction Reaction (ORR) at the cathode :

$$\frac{1}{2}O_2 + 2H^+ + 2e^- \longrightarrow H_2O \tag{1.2}$$

The overall reaction is therefore :

$$\frac{1}{2}O_2 + H_2 \longrightarrow H_2O + Q + W_{elec} \tag{1.3}$$

Assuming ideal gas behavior, the potential difference between the electrodes driving the reaction can

be expressed using the Nernst equation :

$$E = E^0 + \frac{RT}{2F} ln\left(\frac{a_{O_2}^{1/2} a_{H_2O}}{a_{H_2O}}\right) = E^0 + \frac{RT}{2F} ln\left(P_{O_2}^{1/2} P_{H_2O}\right) \tag{1.4}$$

- E^0, the reversible cell voltage
- R=8.314 J.K^{-1}.mol^{-1}, the ideal gas constant
- F=96485 C.mol^{-1}, the Faraday constant
- T=25°C

The potential difference is therefore directly related to the concentrations of the reactants, expressed in terms of their partial pressures. Under standard conditions, the reversible Open-Circuit Voltage (OCV), *i.e.*, in the absence of any current flow, is 1.23 V. However, this value is also influenced by operating conditions such as temperature [1, 2] and by various phenomena that reduce the potential to approximately 1 V. These include hydrogen permeation through the membrane, which leads to a decrease in the cathode potential [1, 2]. The oxidation of certain materials, such as platinum [3] and carbon, as well as catalyst contamination by specific gases, also contributes to lowering the Open-Circuit voltage (OCV).
During operation, the cell produces an electric current, which results in voltage losses mainly due to three mechanisms :

- At low current densities, activation losses significantly reduce cell voltage. These losses are influenced by several parameters, such as the composition of the electrodes, including the type of carbon, the amount of ionomer and particularly the active platinum surface [4].
- At medium current densities, ohmic losses cause a linear decrease in cell voltage. Each material is characterized by a specific resistance, determined by its composition. For example, the ionomer content in the electrodes affects protons and-indirectly through the I/C ratio-electrons transfer [4], while the thickness and porosity of the GDL influence the electrical (or electronic) resistance of the cell [5, 6].
- At high current densities, mass transport losses become predominant [7]. Water production and the large flow of air or oxygen required to feed the cell can lead to phenomena such as oxygen dilution and transport resistance, both of which are affected by parameters such as the porosity and thickness of the GDL.

The wide range of possible applications leads to different operating conditions and, consequently, to varying levels of performance losses. This diversity highlights the need for research into materials specifically adapted to each intended application. To achieve consistent power densities in mobile applications, the cells are connected in series to form a stack, which increases the overall system voltage and, therefore, the generated power. Today, different stack sizes are designed according to the targeted application : from 100 to 400 kW for medium and heavy trucks, 1.5 to 3 MW for trains, and 4 to 60 MW for boats [8].

During operation, the cell is subjected to multiple stress factors, which may originate from chemical, mechanical and/or thermal sources :

- The acidic environment at medium temperature of the cell can lead to the corrosion of bipolar plates [9]. In addition, the direct combination of hydrogen and oxygen results in the formation of hydrogen peroxide, which can decompose into free radicals that chemically attack both the membrane and the ionomer in the electrodes.
- The production of water and heat can generate significant internal mechanical stresses, particularly in the membrane and the electrodes, potentially leading to irreversible deformation.

- As the cell produces current, the temperature of the membrane-electrode assembly (MEA) increases. Like mechanical stresses, temperature cycling during operation can induce structural changes within the materials.

The choice of materials is therefore crucial for designing a high-performance fuel cell that remains durable in such an aggressive environment. The following sections present each component, its composition, functional properties and the degradation mechanisms described in the literature.

1.2 The bipolar plate (BP)

1.2.1 Role, composition, and morphology

The bipolar plates consist of ribs and channels that enable the gases to circulate in contact with the gas diffusion layers (GDL). Their main functions are as follows [10, 11] :

- To ensure a homogeneous distribution of gases in contact with the diffusion layers.
- To remove the gases, heat and excess water produced by the reaction, while also serving as a medium for the cooling circuit.
- To ensure electron conduction.

The design of these plates must also provide sufficient mechanical strength for the stack while minimizing gas pressure losses [12]. As research has advanced, several standard rib and channel configurations have been developed (figure 1.2).

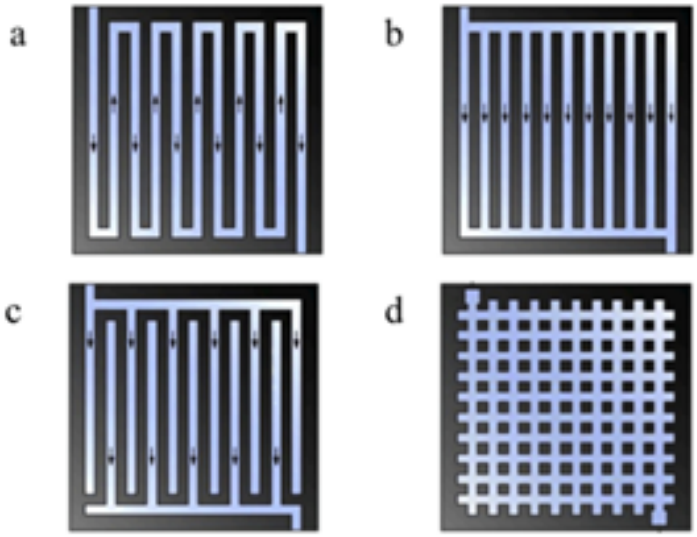

FIGURE 1.2 – Examples of bipolar plates configuration : serpentine (a), parallel (b), interdigitated (c) and pin-type or columns [12].

Numerous numerical studies have compared these different designs. Serpentine channels have shown varying results depending on their dimensions and number, with the optimum configuration differing according to the applied experimental conditions [13, 14]. For example, the number of channels affects the gas velocity, among other parameters. A smaller number of channels can result in a greater amount of water being removed [15], which is beneficial under humid conditions but detrimental under dry conditions. Overall, bipolar plates with serpentine channels cause higher gas pressure losses than other designs but provide better homogeneity in gas distribution at the interface with the GDL [16]. Rostami et al. [17] compared several bipolar plate geometries based on different criteria and

observed that, although straight parallel channels exhibited lower gas pressure losses than serpentine ones, the pressure distribution was significantly less homogeneous in straight channels. Furthermore, evaluation of the membrane temperature showed that the plate design affects heat removal : a greater temperature difference between the membrane and the bipolar plates was observed for parallel channels than for serpentine channels over a current density range of 0.1 to 1 $A.cm^{-2}$.

Despite this, the conclusions of studies comparing the distribution of current and temperature between parallel and serpentine channels vary. Most often, serpentine channels are reported to be more efficient [18, 19], although some studies present opposite results [20]. These discrepancies are mainly attributed to the number and dimensions of the channels [21-24]. For example, Ding et al. [25] observed significant differences in performance at high current densities depending on the depth of straight parallel channels, which were linked to reduced oxygen transport resistance and improved water removal. Today, the trend is to develop specific designs that optimize parameters such as water drainage, gas distribution, and so on. Several numerical studies have shown performance improvements with modified conventional designs, such as channel blocking at specific points, wavy channel shapes, and other innovative geometries [20, 26, 27].

Nowadays, bipolar plates are manufactured from metals such as titanium and stainless steel, metal alloys based on aluminium and nickel, graphite and composite materials [22, 28, 29]. The use of metal alloy-based materials offers several advantages, including low machining costs and high mechanical strength. However, their low corrosion resistance is a drawback, which can be mitigated by depositing thin protective films. Bipolar plates made of graphite benefit from the intrinsic properties of this material, including low density, good corrosion resistance (section 1.2.2) and excellent thermal and electrical conductivity. On the other hand, their high porosity, brittleness and low mechanical strength require thicker bipolar plates, which increases the overall system cost. Composite materials combine the advantages of the two previous materials but their high contact resistance and relatively high cost still limit their large-scale industrial development. Finally, several studies have investigated the use of graphene-based coatings to enhance the corrosion resistance of metal bipolar plates [29, 30].

1.2.2 Degradation mechanisms

Although the durability of bipolar plates is generally not considered a limiting factor for fuel cell performance and durability, the aggressive environment within a PEMFC can lead to their corrosion. Numerous studies have therefore focused on the durability of metallic bipolar plates. In addition to the loss of mechanical, thermal and electrical properties, the release of metal cations can catalyze the decomposition of H_2O_2 *via* Fenton-type reactions, leading to the formation of radicals (section 1.5.2), thereby accelerating the degradation of other components such as the ionomer in the electrodes and the membrane. From the plate's perspective, different degradations have been described in the literature [9, 31] :

- Pinhole formation, caused by gradual erosion of the plate surface over time. This phenomenon may occur even when the cell is not in operation, except in cases where strict measures are applied to remove residual water. Nevertheless, this mechanism is very slow, although it depends on the material used.
- Active metal dissolution forming metallic cation and surface passivation by oxidation, which leads to the formation of a protective but resistive oxide layer.

Active metal dissolution	**Passive metal dissolution**	**Transpassive metal dissolution**
• Cations are formed at the metal-electrolyte interface • Soluble ions are formed and dissolved into the electrolyte • Higher dissolution rate than passive dissolution	• Surface of the metal is covered with a thin oxide layer • Cations are formed at the metal-film interface • Cations migrate across the film to the film-electrolyte • Lower dissolution rate than active dissolution	• Dissolution of the passive film • Surface state is not well-defined, and the surface may or may not be covered by an oxide
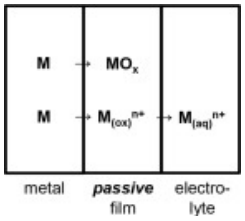	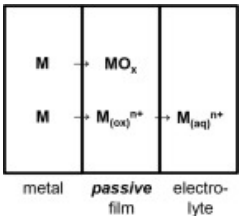	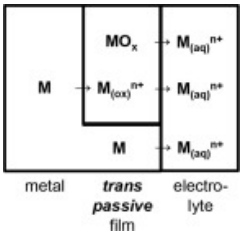

TABLE 1.1 – Taken from *Transient stainless-steel dissolution and its consequences on ex situ bipolar plate testing procedures* [32].

In addition, metallic ions can migrate and poison catalyst sites. They may also interact in the electrodes with oxygen to form oxides on the cathode side, whereas they may be reduced to the metallic side by hydrogen on the anode side. These species can then remain in the electrodes and block pores, impacting fuel cell performance, or be removed by convective flows [9].
Various studies have investigated the accelerated aging of bipolar plates using an *ex situ* approach to simulate fuel cell environment, *i.e.*, in an acidic medium at typical operating temperatures. Ren et al. [33] applied potential cycles to stainless steel bipolar plate SS316L. In an acidic solution (0.5 mmol/L H_2SO_4) with a pH of 3 and containing 2 ppm of HF ions, potential variations representative of operating and start/stop cycles were imposed. Corrosion current measurements and SEM imaging revealed that more severe corrosion occurred under potential cycling than under potentiostatic conditions. Furthermore, the degradation increased as the amplitude of the applied potential cycles widened. High potentials promote the dissolution of chromium species, which typically occurs during start/stop phases of fuel cell operation. Conversely, the potentials encountered under normal operating conditions favor the dissolution of iron species.

1.3 Gas Diffusion Layer (GDL)

1.3.1 Role, composition, and morphology

The gas diffusion layers (GDL) are porous layers positioned between the bipolar plates and the electrodes. They are characterized by a macroporous structure with pore sizes ranging from 10 to 30 µm. The GDL fulfills several key functions [34] :

- Conducting the transport of gases from the bipolar plates to the electrodes.
- Conducting electrons from the electrode to the bipolar plate on the anode side, and from the bipolar plate to the electrode on the cathode side.

- Removing the water and the heat produced during the electrochemical reaction.

The porosity and thickness of the GDL are considered key parameters for the proper operation of the PEMFC. Xia et al. [5] investigated the impact of these two parameters on the performance of a PEMFC operating at high temperature. A reduction in porosity leads to lower gas diffusion to the catalyst sites [35, 36], but increases electronic conductivity [37], thereby reducing the ohmic resistance of the material. Regarding GDL thickness, increasing it improves the uniformity of gas distribution between the ribs and the channels in contact with the catalyst layers, but also increases the resistance to gas diffusion. Furthermore, since the GDL plays a crucial role in removing the water produced by the cell, its properties must be optimized according to the flow-field design, particularly the channel dimensions.

Liu et al. [38] studied the optimum GDL thickness as a function of channel thickness. Since wet operating conditions cause higher voltage losses with thinner GDL, due to larger water concentration gradients between the ribs and channels, the use of deeper channels improves water removal. Based on this observation, the authors established an optimum GDL thickness as a function of channel depth and current density, corresponding to the cell's water production rate.

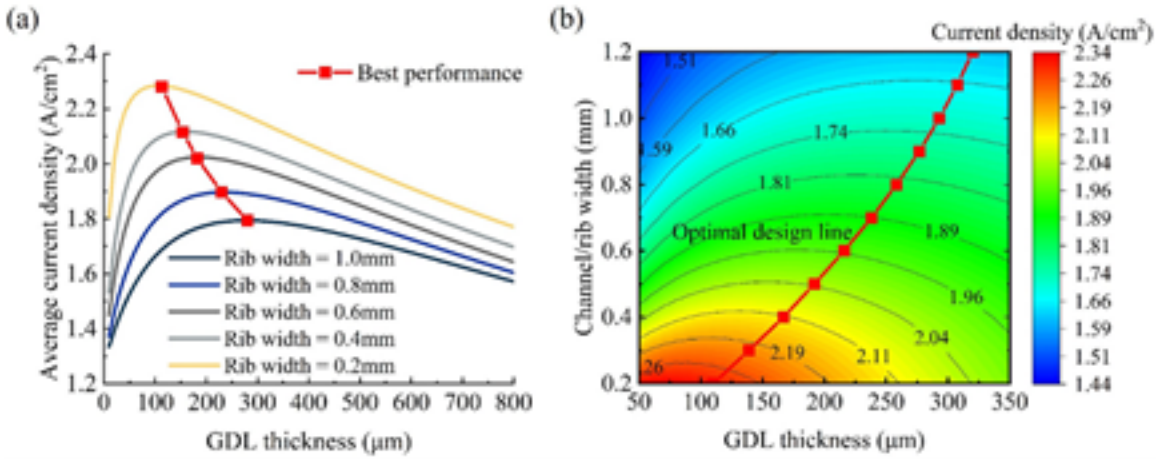

FIGURE 1.3 – Average current density as a function of GDL thickness for different rib widths (a), current density mapping for channel/rib width as a function of GDL thickness (b) [38].

It can therefore be understood that an optimum set of GDL parameters exists, particularly at high current densities [39], where water production strongly affects oxygen transport. Moreover, this optimum is highly dependent on the other cell components.

GDL are generally made of carbon fibers due to the advantageous properties of this material, *i.e.*, high gas permeability, mechanical properties that allow the MEA to be supported under compression, excellent corrosion resistance, and high electrical conductivity [40-42]. Several manufacturing methods exist, leading to different morphologies. The most common GDL types are carbon cloth, carbon paper and carbon felt [40] (figure 1.4). Carbon cloth exhibits a regular structure owing to the weaving of carbon fiber bundles, unlike carbon paper, in which straight and rigid fibers are randomly interlaced. Carbon felt also presents a random structure, composed of so-called *spaghetti-shaped* fibers [34]. These structural differences result in distinct properties, particularly in terms of electrical resistance [43], porosity and gas transport.

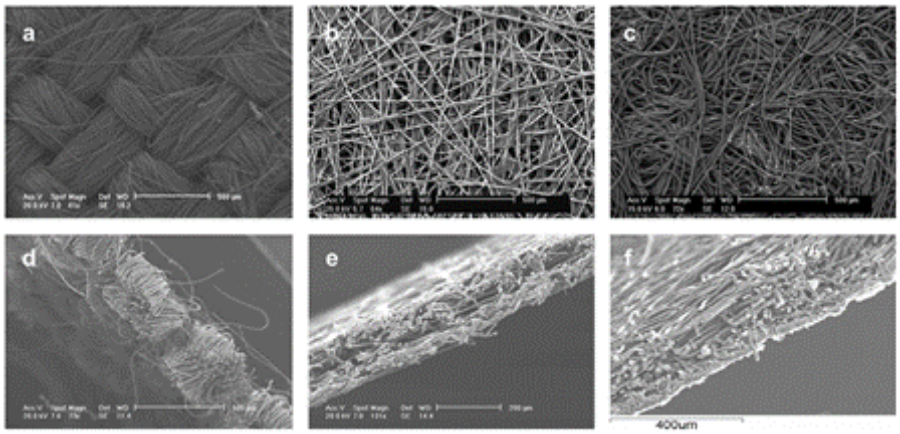

FIGURE 1.4 – SEM images of GDL fibers surface (top row) and cross-sections (bottom row) of carbon cloth (a-d), carbon paper (b-e) and carbon felt (c-f) [44].

In parallel with these developments, several research projects have focused on the development of alternative materials and manufacturing processes aimed at improving the intrinsic characteristics of GDL, enhancing their durability, and reducing production costs. Particular attention has been paid to the following materials :

- **Graphite/graphene**, for its excellent mechanical properties and high electrical conductivity [45, 46]. Lee et al. [47] demonstrated that incorporating graphite into carbon black improved permeability by increasing surface roughness and average pore size, reduced the ohmic resistance of the material, provided that a good interface was maintained with the electrodes, and increased the elastic limit.
- **Carbon nanotubes (CNT)**, for their thermal and electrical properties [48, 49]. Although CNTs are more commonly used in the microporous layer and electrodes, some studies have evaluated their performance as a GDL material [50, 51]. Zhang et al.[52] reported a decrease in pore size distribution and electrical resistance with increasing CNT loading. Under dry conditions (80°C, 26% RH), this resulted in improved voltage at low and medium current densities, attributed to better water retention, while performance under high humidity remained similar. However, mass transport limitations can occur at high current densities, depending on CNT loading, due to water accumulation.
- **Carbon fibers** derived from biomass (*e.g.*, cellulose, coconut fiber, bamboo, etc [42]), which help reduce costs and promote more environmentally sustainable manufacturing processes [53].

Alternative materials have also been investigated, such as metals (aluminium, titanium, nickel, etc [34, 54]), which allow control over permeability, pore shape, and porosity, as well as aerogels [55], although the latter are considered more difficult to develop on an industrial scale [34]. From a processing standpoint, the electrospinning technique has attracted particular interest because it enables, among other advantages, control over fiber alignment and diameter, thereby optimizing porosity and improving water and heat management [56]. Another approach involves perforating the GDL on the cathode side to create wider pathways for the removal of water produced during operation [57].

A hydrophobic coating is applied to the pores to improve water removal, generally based on PTFE (polytetrafluoroethylene). In several studies, other hydrophobic additives have been tested, such as PFPE (perfluoropolyethers) [58, 59], due to their chemical and thermal stability and high hydrophobicity [60]. However, this coating can negatively affect the GDL structure by reducing electrical conductivity [61, 62] and porosity [63], altering the pore size distribution, and modifying heat transfer within the material. Indeed, several studies have reported an increase in heat transfer with higher

PTFE content in GDL [64, 65]. The content of hydrophobic additives must therefore be optimized to achieve a compromise between improved water management and reduced electrical conductivity, diffusion, and gas permeability.

To improve the material's performance, a microporous layer (MPL) is applied onto the diffusion layer on the electrode side. Its porosity is lower than that of the macroporous layer, which enhances electrical contact between the catalytic layer and the GDL [66] while improving water management [67]. The MPL consists of a carbon-based structure (carbon black, carbon nanotubes, graphene etc.) and includes a hydrophobic coating made of materials similar to those used for the macroporous layer, generally PTFE [68]. For the same reasons, the architecture and carbon black content influence properties such as gas permeability, which is directly related to porosity.

1.3.2 Degradation mechanisms

The gas diffusion layers constitute the medium through which the various reactants and reaction products are transported. The performance of the cell is therefore directly linked to the transport capacity of this material, both for delivering reactants to the catalytic sites and for removing water toward the bipolar plates. Although no electrochemical reactions occur within the GDL, the operating conditions and oxidizing environment of the cell are detrimental to its properties. GDL degradation mechanisms can be classified into three main categories [69] :

- Mechanical damage during operation is primarily caused by compression of the MEA, which can lead to deformation of the carbon fibers, particularly at the rib/channel junctions where localized stresses are highest. Additionally, carbon loss can occur due to erosion by fluids and material dissolution. Carbon corrosion is also possible through electrochemical reactions at low potential ; however, the reaction kinetics are very slow, so their impact is considered negligible.

$$C + 2H_2O = CO_2 + 4H^+ + 4e^- \qquad E_0 = 0.207 \text{ V vs. RHE} \qquad (1.5)$$

$$C + H_2O = CO + 2H^+ + 2e^- \qquad E_0 = 0.518 \text{ V vs. RHE} \qquad (1.6)$$

  In addition, several studies found that acidic conditions and the presence of oxygen in water could lead to material losses of carbon and PTFE, as well as oxidation of the pore surface.
- Damage caused by the start/stop procedure can occur, due to a phenomenon called hydrogen starvation : inhomogeneities in hydrogen concentration on the anode side induce high local potentials that can exceed 1.4 V on the cathode side, accelerating the kinetics of carbon corrosion. Accelerated stress tests (ASTs) consisting of start and stop cycles have been developed to study carbon corrosion [70, 71], but they focus mostly on the cathode catalyst layer. Under extreme conditions, freeze/thaw cycles following start/stop procedures can lead to PTFE loss and mechanically stress the carbon fibers, potentially causing fracture.
- Periods of gas operation without electrical production–*i.e.*, at open circuit voltage (OCV)–are conducive to the formation of hydrogen peroxide (H_2O_2) and associated radicals (section 1.5.2). The result is an oxidizing environment that promotes the formation of surface oxides due to carbon corrosion and PTFE loss. To a lesser extent, carbon corrosion can also cause a loss of mass and, consequently, a reduction in GDL thickness, porosity and pore size.

All these modifications lead to changes in the properties and structure of the GDL. Several studies have reported a significant reduction in GDL thickness, particularly in regions with high water content [72-74]. This reduction is accompanied by a decrease in mechanical properties and an increase in pore size, indicating degradation of the internal structure. In addition, these studies observed a loss of hydrophobicity, evidenced by a higher contact angle with water. Such structural changes result in

poorer *in situ* performance, especially at high current densities where water production is elevated, leading to flooding and mass transport limitations.

1.4 Electrodes

1.4.1 Role, composition, and morphology

The electrodes–the anode on the hydrogen side and the cathode on the air/oxygen side–are the sites where the electrochemical reactions occur. They are located between the gas diffusion layer (through which the gas is conveyed) and the ionomer membrane, which acts as a separator between the two catalyst layers. To ensure proper reaction performance, the electrodes must allow :

- Diffusion of reactants to the catalytic sites.
- Removal of the water and heat produced during the cathodic reaction.
- Proton conduction toward the membrane and electronic conduction toward the diffusion layers.

To meet these needs, electrodes are composed of catalysts that promote oxidation-reduction (redox) half-reactions. In PEMFC, platinum is the reference catalyst due to its high catalytic activity. Numerous studies have sought to improve the properties of the catalyst layer–such as electron transfer, carbon monoxide tolerance, catalytic activity, durability etc.–by synthesizing platinum-based alloys with various metals [75-77]. For example, Pt/Ni alloys exhibit twice the ORR activities of a graphitized carbon black-supported Pt catalyst in RDE in liquid electrolyte, while being at least as stable [78]. Platinum-iron alloys have demonstrated excellent catalytic activity with a high degree of structural ordering but relatively large particle size, whereas platinum-cobalt alloys exhibit both high catalytic activity and resistance to dissolution [79].

Since the oxidation-reduction reactions occur on the surface of the catalyst, it is essential to maximize the accessible surface area to minimize the amount of catalyst required. For this reason, catalyst particles are dispersed on a porous carbon support that conducts electrons to the gas diffusion layers. Carbon black has traditionally been used due to its low cost, high availability, large surface area, and good electrical performance [80]. However, the presence of micropores that can trap catalyst particles, and its poor corrosion resistance have led researchers to explore alternative carbon-based supports. The desired properties include a high surface area and porosity, good thermal and electrical conductivity, and high durability. With this in mind, several morphologies have been developed, such as carbon nanotubes (CNT), nanofibers (CNF), nanospheres (CNS), graphene, mesoporous carbon, carbon gels and so on. These carbons have different structures from carbon black, giving them interesting properties, particularly in terms of surface area, porosity, and durability [80, 81]. Performance can also be enhanced through graphitization or surface doping. In the first case, heat treatment is used to modify the structure [82], thereby influencing the material's properties [83, 84]. Depending on the temperature and duration of the treatment, a more or less pronounced improvement can be observed including, among other things, changes in pore distribution, increased active surface area, and greater corrosion resistance–all of which contribute to improved performance and durability during fuel cell operation. In the second case, doping the carbon support with a heteroatom such as nitrogen, sulfur, boron, etc [85-87], enhances functional properties such as catalytic activity, water management, mass and proton transport, platinum particle size and dispersion, electrical conductivity, and durability–for example, by influencing hydrogen peroxide decomposition [88]. Other non-carbon supports have also been investigated, such as silicon carbide (SiC), iridium oxide (IrO_2), titanium dioxide (TiO_2), etc., which generally offer improved durability but sometimes lower performance compared with commercial Pt/C catalysts [89, 90].

At the same time, an ionomer phase in contact with the catalyst particles enables proton conduction

from the anode to the membrane and from the membrane to the cathode. In addition, the choice of ionomer binder ensures strong cohesion between the electrodes and the membrane, as this is essential for achieving a good interfacial contact and, consequently, improved cell performance. Pu et al. [91] demonstrated this by reporting a higher open circuit voltage (OCV). In addition, the ionomer should exhibit the following properties :

- **High proton conductivity**, to enable rapid proton transfer within the electrode.
- **Electronic insulation**, to ensure that electrons generated during the reaction are removed via the external electrical circuit.
- **Good water absorption capacity**, contributing to proton transfer.
- **High durability** under chemical, mechanical, and thermal stresses.

Several types of ionomers have been investigated in recent years, including :

- **Perfluorosulfonic acid (PFSA)-based ionomers**–These consist of a hydrophobic backbone with attached pendant side chain, the length of which determines the ionomer type : short-side chain (SSC-PFSA) or long-side chain (LSC-PFSA). Characterized by excellent properties such as high proton conductivity and strong chemical durability, these ionomers are regarded as the benchmark materials.
- **Sulfonated hydrocarbon-based ionomers**–Because the presence of fluorine in PFSAs entails a costly and environmentally harmful manufacturing process, much research has focused on the synthesis of hydrocarbon-based ionomers [92], which are cheaper and less polluting to produce. Despite these advantages, limited proton conductivity under low relative humidity and lower chemical stability remain major obstacles to their development. Nonetheless, various hydrocarbon ionomers have been explored, such as Pemion [93], sulfonated poly(arylene ether ketone) (sPAEK) [94], among others.

The amount of ionomer used, determined by the ionomer-to-carbon ratio I/C is crucial for proper electrode operation. Structurally, incorporating the ionomer into the carbon matrix tends to reduce the number of macropores and shift the size distribution toward smaller diameter pores. This structural change directly affects performance, as increasing the I/C ratio leads to higher proton conductivity but also greater ohmic resistance, either favorable or unfavorable, respectively, for overall cell performance. In addition, oxygen transport on the cathode side is significantly affected. First, the Knudsen resistance, which is associated with oxygen transport through interactions with pore surfaces, increases as pore size decreases and, consequently, as the I/C ratio increases. Second, the local oxygen transport resistance of the ionomer increases at excessive I/C ratios, due to an increase in average ionomer thickness, whereas intermediate values enable coverage of more catalyst sites, enhancing the ECSA [95]. Changes in the I/C ratio therefore have a non-linear impact on this parameter. Finally, during operation, a high ionomer content leads to a higher water content and thus higher proton conductivity, which is beneficial under dry operating conditions but detrimental under wet conditions, causing electrode flooding, pore blockage, and reduced access of reactants to the catalytic sites. Consequently, the optimal I/C ratio depends not only on the operating conditions but also on the materials used, explaining the wide range of optimal values reported in the literature [96, 97].

The region combining the carbon support, ionomer binder, and catalyst particles is commonly referred to as the *triple phase boundary*. As mentioned earlier, the selection of these three electrode components–as well as their proportions–is crucial for both the performance and durability of the PEMFC. Determining the optimal "recipe" is particularly challenging, as it strongly depends on the intended operating conditions (*e.g.*, operating temperature, humidity, etc).

1.4.2 Degradation mechanisms

The durability of the three electrode components depends on the operating conditions of the cell, such as the gas relative humidity (RH), cell temperature, applied current density, local potential, etc [98, 99]. Each component undergoes its own degradation mechanisms, contributing to a reduction in the catalyst's active surface area and, consequently, a decrease in the overall performance of the system.

Catalyst degradation

The aging of platinum catalysts leads to a reduction in the active surface area available for electrochemical reactions. The degradation mechanisms can be classified into two groups [100-102] :

- **Migration/coalescence mechanism :** in this process, Pt particles aggregate to form larger particles. Two phenomena can contribute to this :
  - Like the mechanisms occurring in the GDL, carbon corrosion causes increased electrical insulation and/or Pt agglomeration, with the detachment of Pt particles from the carbon support and/or the ionomer, thereby reducing the catalyst's active surface area.
  - Migration and coalescence involve the movement of Pt particles on the carbon support surface. To minimize surface energy, the Pt particles agglomerate, forming larger particles with a lower surface-to-volume ratio.
- **Platinum dissolution mechanism :** Pt particles dissolve, diffuse, and subsequently redeposit. Several electrochemical reactions are responsible for the detachment of Pt particles [103], the first being the direct electrochemical dissolution of platinum :

$$Pt \longrightarrow Pt^{2+} + 2e^- \qquad E^0 = 1.19 + 0.029 log[Pt^{2+}] \tag{1.7}$$

(1.8)

The second reaction involves the formation of platinum oxide followed, by its dissolution :
Oxidation/reduction reactions

$$Pt + H_2O \longrightarrow PtO + 2H^+ + 2e^- \qquad E^0 = 0.98 - 0.059\,pH \tag{1.9}$$

$$PtO + H_2O \longrightarrow PtO_2 + 2H^+ + 2e^- \qquad E^0 = 1.045 - 0.059\,pH \tag{1.10}$$

Dissolution/redeposition reactions

$$Pt + H_2O \longrightarrow PtO + 2H^+ + 2e^- \qquad E^0 = 0.98 - 0.059pH \tag{1.11}$$

$$PtO_2 + 4H^+ + 2e^- \longrightarrow Pt^{2+} + 2H_2O \qquad E^0 = 0.84 - 0.12pH - 0.03log(Pt^{2+}) \tag{1.12}$$

This reaction can be divided into two distinct mechanisms based on the cation deposition site :

- The first mechanism, known as *Ostwald electrochemical ripening*, corresponds to the dissolution of platinum followed by the redeposition of Pt species on the carbon support, near other particles, to minimize surface energy. The consequences are similar to those of migration and coalescence, namely an increase in particle size and a reduction in the catalyst's active surface area. However, the two mechanisms can be distinguished by the crystalline structure and particle size distribution. In the case of Ostwald ripening, the particle size distribution shifts toward larger particles, with the peak corresponding to small particles

progressively diminishing, reflecting their gradual consumption. In contrast, during migration and coalescence, the distribution peak broadens toward larger particle sizes.

- The second mechanism involves the dissolution of platinum followed by its precipitation within the membrane. After dissolution, Pt particles diffuse–driven by the concentration gradient or electroosmotic flow–toward the membrane, or even as far as the anode, where they are chemically reduced by hydrogen, which is present due to the crossover phenomenon. The position of the resulting platinum band has been observed experimentally and depends primarily on the extent of hydrogen crossover through the membrane.

Carbon support degradation

Acidic environments (pH<1) with high water content, abundant oxygen, and high electrode potentials-such as those occurring during start/stop cycles or under flooding conditions where reactants cannot reach the catalytic sites-are potentially degrading for the carbon support. The degradation mechanisms are close to those described for GDL degradation, with the additional contribution of platinum-catalyzed carbon corrosion at potentials above 0.5 V. Likewise, the loss of electrode structure can adversely affect transport properties due to changes in porosity and morphology, impacting both the removal of reaction products and the transport of reactants to the catalytic sites. The entrapment of ionomer and platinum particles further contributes to the reduction in the number of triple phase boundary sites where electrochemical reactions occur.

Ionomer binder degradation

While the mechanisms of ionomer degradation in the membrane are well established, those of the ionomer binder within the electrode are not well understood, despite its assumed predominant role in electrode performance. Several studies have reported compositional changes, notably a reduction in fluorine content [104-106]. Similarly, it has been shown that the thickness of the ionomer film can decrease on both the anode and cathode sides during accelerated stress tests (AST) [106, 107]. However, the underlying degradation mechanisms are difficult to identify, largely because the electrode composition is often similar to that of the membrane, *i.e.*, PFSA-based. As a result, quantifying degradation–particularly through the analysis of the degradation products–is challenging to distinguish from membrane degradation. To address this issue, several studies have employed alternative characterization techniques such as small-angle neutron scattering (SANS), microscopy, nuclear magnetic resonance (NMR), etc. Chabot et al. [108] applied two AST protocols : one at open-circuit voltage with humidity cycling targeting the membrane (AST-M), and a second cycling between 0.5 and 1-1.5 V targeting the electrodes (AST-C), particularly the carbon support. In both cases, carbon support degradation was observed. Further X-ray photoelectron spectroscopy (XPS) analysis revealed that the fluorine-to-carbon support ($F/C_{carbon\ support}$) ratio decreased after AST-C, while the $F/C_{ionomer}$ ratio of the ionomer remained relatively stable. This result was interpreted as a loss of ionomer from the surface of the carbon support, without degradation of the ionomer backbone. In contrast, during AST-M, XPS measurements showed a decrease in the sulfur-to-fluorine (S/F) ratio of the ionomer, suggesting degradation of the ionomer binder's pendant side chains, although the precise origin of this degradation was not confirmed. Overall, several mechanisms may contribute to the loss of electrode properties related to the ionomer binder : (i) carbon corrosion leading to ionomer detachment from the carbon surface, and (ii) chemical degradation of the ionomer side chain, which remains to be fully elucidated.

El Kaddouri et al. [109] studied the degradation of a PFSA-based ionomer binder with a MEA aged for 10,400 h under constant-current operation. XRD measurements revealed an increase in crystallinity on both the anode and cathode sides, attributed either to radical attack on the side chains or to an unzipping mechanism, and thus more generally to chemical degradation of the ionomer. They corroborated this hypothesis by detecting a degradation product of the Nafion side chain, namely 1,1,2,2-tetrafluoro-2-(1,2,2-tetrafluoroethoxy) ethanesulfonic acid. Several studies support the hypothesis of radical attack on the side chain, with observations indicating the loss of sulfonic groups [106, 107]. In parallel, ionomer migration has been observed, leading to a redistribution of the ionomer into larger aggregates. However, quantifying this degradation remains challenging, as it does not account for degradation products removed by the cell water or for those originating from the membrane that may become trapped within the electrodes.

Humidity cycling can also induce structural changes in the ionomer [110]. Du et al. [111] associated water loss with drying of the ionomer film, leading to local mechanical stresses that could cause local delamination between the ionomer and the carbon support. They further identified ionomer detachment and redistribution as an additional mechanism of performance losses. Yin et al. [112] observed similar trends, including an increase in cracks in the electrode due to plastic deformation and enhanced ionomer migration as relative humidity increased. These structural changes contribute to performance losses, manifested as higher ohmic resistance and a reduction in the carbon/ionomer/catalyst triple-phase boundary area. In addition, ionomer migration into the pores can increase oxygen transport resistance at the catalyst surface. Moreover, similar to carbon corrosion, this phenomenon promotes the detachment of catalyst particles, contributing significantly to the loss of electrochemically active surface area (ECSA) [113].

(a) (b)

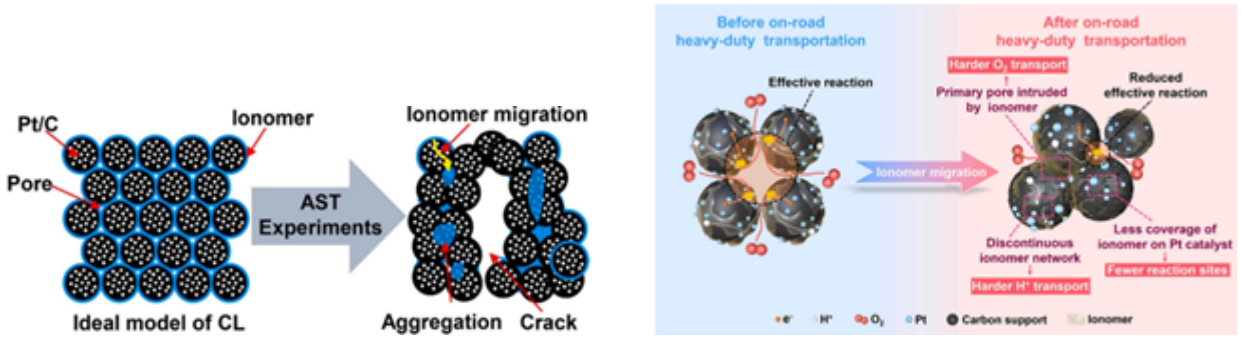

FIGURE 1.5 – Ionomer migration in catalyst layers due to humidity cycling [114] (a) and consequences of ionomer migration after 1000h of on-road-heavy-duty transportation [113] (b).

Overall, the number of studies addressing ionomer binder degradation mechanisms remains limited, with some focusing only on durability and performance loss. Nevertheless, it has been observed that ionomer loss, resulting in decreased proton conductivity, constitutes a key degradation pathway for ionomer binders, whether caused by carbon corrosion or ionomer detachment. In parallel, chemical degradation mechanisms may occur through radical attacks on the ionomer's pendant side chains, leading to a reduction in ion exchange capacity (IEC) and, consequently, proton conductivity. However, the observation of these degradation processes is highly dependent on the accelerated aging conditions, and a more comprehensive understanding of these mechanisms would require more targeted and extensive studies.

1.5 The ionomer membrane

1.5.1 Role, composition and families

The proton exchange membrane acts as a solid electrolyte. It must exhibit several key properties to ensure reliable operation and long-term durability [115, 116] :

- High proton (H^+) conductivity.
- High water transport properties.
- Impermeability to gases.
- Electronic insulation.
- Good and durable physicochemical properties to maintain consistent performance against chemical, mechanical and thermal stresses, which can affect its microstructure and, consequently, degrade its functional properties.

The membrane structure corresponds to that of an ionomer, *i.e.*, a polymer with ionic groups enabling proton conduction. In this configuration, the backbone consists of a hydrophobic polymer responsible for providing the mechanical properties. Attached to this backbone are pendant side chains containing sulfonic acid groups, which enable proton conduction. From this structure arise all the functional properties that determine the suitability of the membrane for fuel cell operation. Several families of ionomers have been considered based on their composition (figure 1.6) [116] :

- **Perfluorinated ionomers** consist of a highly hydrophobic fluorinated backbone to which fluorinated pendant side chains terminated by sulfonic groups are attached. Owing to the high electronegativity of fluorine, which forms strong bonds with carbon atoms, this type of ionomer exhibits excellent properties such as high chemical stability and enhanced acidity of the sulfonic groups, leading to easier proton dissociation and, consequently, high proton conductivity. These ionomers can be divided into several types depending on the length of their side chain, which directly affects their physicochemical properties. Long-Side-Chain (LSC) ionomers, such as Nafion, have long been considered the reference materials because of their high proton conductivity and chemical durability. In contrast, Short-Side-Chain (SSC) ionomers are now being considered for operation at higher temperatures and under dry conditions, owing to their higher crystallinity and greater water uptake in low-humidity environment. It is also worth noting that ionomers with intermediate side-chain lengths have been developed by 3M.
- **Non-fluorinated ionomers** consist of an aliphatic or hydrocarbon backbone containing ring structures. One of their main advantages is that a wide range of polymers (such as PESF, PEK, PEEK, polyimides, etc.) can be functionalized through nucleophilic substitution, with flexibility in the choice of substitution sites. In addition, the absence of fluorine makes these polymers less expensive and easier to recycle while their fabrication is less polluting. From a physicochemical properties standpoint, their backbone confers high thermal and mechanical stability, as well as a high glass transition temperature.
- **Acid-base complexes** result from the combination of an acid and an ionomer. A typical example is phosphoric acid-doped polybenzimidazole ($PBI/H_3PO_{4)}$, which exhibits promising properties for high-temperature fuel cells (HT-PEMFC), owing to its proton conductivity and reduced dependence on humidity at elevated temperature.

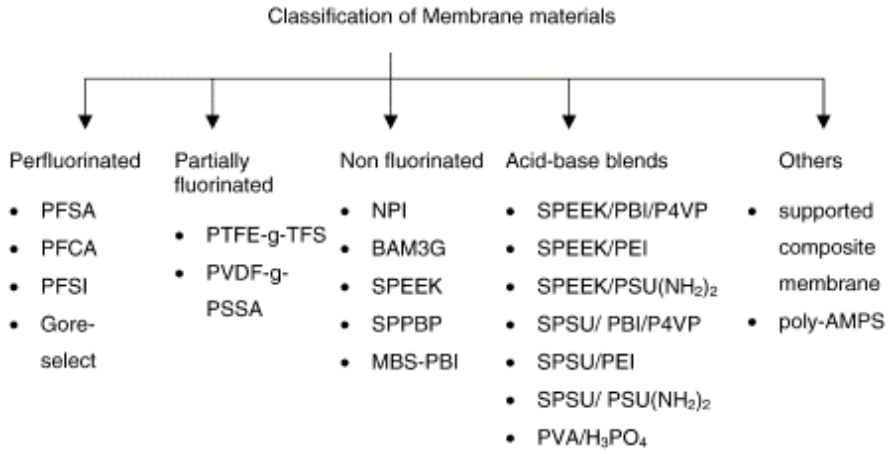

FIGURE 1.6 – Ionomer classification [116]. Note that the BAM3G ionomer is partially fluorinated.

The backbone and side-chain structures are determining factors for the physicochemical properties of ionomers. They are responsible for the major differences observed between the different ionomer families. In addition, two ionomers with the same structure can be distinguished by their number of sulfonic groups, represented by the ion-exchange capacity parameter (IEC), which corresponds to the number of millimoles of sulfonic acid groups per gram of dry polymer. This parameter strongly influences both the microstructure and the physicochemical properties of the material [117-121] :

- **Microstructure :** increasing the IEC leads to a decrease in ionomer crystallinity. Conversely, a reduction in the number of sulfonic acid groups restricts segmental motion, resulting in a higher glass transition temperature. In addition, at high equivalent weights (corresponding to a low ion-exchange capacity), the ionomer tends to exhibit a more crystalline structure, which inhibits H_2 transport and therefore reduces gas permeability compared with an amorphous structure.
- **Water uptake and proton conductivity :** a higher IEC increases ionomer hydrophilicity, leading to greater water uptake. The increased water content promotes the formation of larger hydrophilic clusters and their percolation, which enhances proton conduction pathways and results in higher proton conductivity. However, it has also been noticed that excessive water content can dilute proton concentration and thus decrease proton conductivity.
- **Mechanical properties :** variations in IEC strongly affect the mechanical behavior of the ionomer. An increase in sulfonic group concentration can compromise mechanical integrity due to excessive water absorption or reduced crystallinity [122]. For sPEEK, Parnian et al. [123] observed that an increase in IEC, and consequently in the degree of sulfonation (DS), led to a substantial decrease in the elastic modulus and tensile strength, accompanied by a significant increase in elongation at break. This was attributed to the more amorphous structure resulting from the higher degree of sulfonation.

LT-PEMFC currently operate with PFSA ionomers due to their superior proton conductivity and chemical stability. However, the limited proton conductivity at elevated temperature (*i.e.*, above 90-100°C) has prompted further research into alternative membrane materials. Although several studies have focused on hydrocarbon-based ionomers such as sPEEK, their shortcomings in terms of chemical stability and proton conductivity under low-humidity conditions have hindered their widespread use. To overcome these limitations, various ionomer modifications have been developed to improve physicochemical properties, including mechanical ones, proton conductivity, chemical durability etc.

- **Mechanical properties** can be enhanced through several processes. Structural modifications can be induced by crosslinking reactions or thermal treatments. Mechanical reinforcement can also

be achieved by incorporating polymers such as PTFE, electrospun matrix, inorganic fillers etc [124] :

- **Cross-linking reactions** involve creating chemical bonds either between different ionomers or within a single ionomer to enhance mechanical properties. Several pathways are possible, such as the conversion of sulfonic acid side chains or the use of polymers with crosslinkable functional groups. Zhou et al. [125] prepared crosslinked Nafion 212 with poly(vinylidene fluoride) (PVDF) and observed lower water uptake, swelling ratio, and proton conductivity as the PVDF content increased. However, the composite membrane exhibited significantly improved mechanical properties, with higher tensile strength. Crosslinking can also be induced through thermal treatment. Hou et al. [126] reported a gradual transition from ductile to brittle behavior in sPEEK ionomer, accompanied by a significant increase in Young's modulus and tensile strength.
- **Polymer-fiber reinforcement**, such as the introduction of polytetrafluoroethylene (PTFE), has been widely employed to enhance mechanical stability. Siracusano et al. [127] observed reduced dimensional changes and higher mechanical properties (Young's modulus and stress at break) in PTFE-reinforced SSC-PFSA. The electrospinning method enables the formation of uniform polymer nanofibers. Although this approach may reduce proton conductivity (mostly due to a lower PFSA content and depending on the type of reinforcing polymer) significant improvements in mechanical properties have been reported [128].

- **Water uptake and proton conductivity** can be improved by doping the membrane with another materials. Rao et al. [129] incorporated metal-organic frameworks (MOF) into Nafion and observed higher water uptake and proton conductivity compared to the recast Nafion membrane. Thmaini et al. [130] compared Nafion membranes reinforced with SiO_2, TiO_2 and ZnO nanoparticles combined with sepiolite fibers. They reported enhanced water retention capacity with the addition of nanofillers, as well as higher proton conductivity.
- **Chemical stability** can be enhanced by adding radical scavengers [131]. Liu et al. [132] incorporated ferrocyanide and ferricyanide into PFSA and hydrocarbon matrices and compared their physicochemical properties, fuel cell performance, and durability, with those of pristine and Ce^{+}-doped sPEEK and Nafion membranes. Although both Ce^{3+}-modified membranes exhibited improved durability during open-circuit voltage tests, they also showed lower proton conductivity and, consequently, reduced fuel cell performance compared to pristine membranes. In contrast, membranes reinforced with Fc(II) and Fc(III) exhibited higher proton conductivity, fuel cell performance and chemical durability than both pristine and Ce^{3+}-reinforced membranes. Therefore, improving chemical durability can simultaneously enhance ionomer stability and physicochemical properties.

1.5.2 Degradation mechanisms

The fuel cell environment involves multiple stress factors that can lead to the deterioration of membrane properties. Thermal, mechanical and chemical stresses can affect the membrane microstructure and, consequently, its physicochemical properties. These degradation pathways are coupled and can mutually accelerate one another, thereby increasing the overall degradation rate. For example, mechanical damage can alter the microstructure through the formation of cracks and pinholes, resulting in increased gas crossover that, in turn, accelerates chemical degradation (subsection 1.5.2). Conversely, chemical attacks on specific bonds within the ionomer can modify its mechanical properties, facilitating the formation of pinholes and cracks during wet/dry operational cycles. Similarly, localized heating caused by electrochemical reaction can alter the ionomer's properties in specific regions, further intensifying chemical and mechanical degradation. De Bruijn et al. [133] and Robert et al. [134] detailed

the various coupled degradation mechanisms affecting PFSA ionomers (figure 1.7).

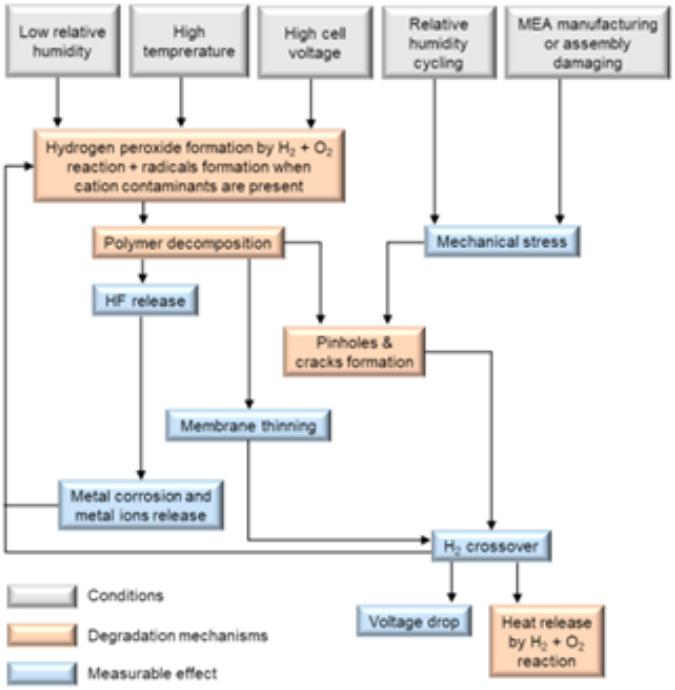

FIGURE 1.7 – Coupled degradation ways encountered during fuel cell operation [134].

The coupling of degradation pathways applies to all ionomer systems. Although hydrocarbon-based ionomers release aromatic fragments instead of fluoride, the resulting microstructural damages are analogous to those observed in PFSA-based membranes.
In the following subsections, the different degradation pathways–chemical, mechanical, and thermal– are discussed separately to provide a detailed overview of the different stress factors.

Chemical degradation

Chemical degradation originates from the reaction between hydrogen and oxygen, leading to the formation of hydrogen peroxide (H_2O_2), which subsequently decomposes into radicals that attack specific bonds within the ionomer. The formation of H_2O_2 can occur on both the anode and cathode sides. The most frequently cited mechanisms are as follows [135-137] :

- **Cathode side :** incomplete reduction of oxygen at the catalyst surface at potentials below 0.67 V vs. SHE :

$$O_2 + 2H^+ + 2e^- \longrightarrow H_2O_2 \qquad E^0 = 0.67V\,vs.SHE \tag{1.13}$$

- **Anode side :** oxygen from crossover, although the ionomer membrane is relatively impermeable, may combine with adsorbed hydrogen on catalyst sites

$$H_2 \longrightarrow 2H^{\cdot} \tag{1.14}$$
$$H^{\bullet} + O_2 \longrightarrow HOO^{\cdot} \tag{1.15}$$
$$HOO^{\bullet} + H^{\bullet} \longrightarrow H_2O_2 \tag{1.16}$$

- **On both sides**, thanks to gas crossover, the direct reaction between O_2 and H_2 can also directly

form H_2O_2.

$$O_2 + H_2 \longrightarrow H_2O_2 \tag{1.17}$$

The presence of H_2O_2 is not inherently detrimental to the ionomer membrane. However, elevated temperature [138] or the presence of metallic cations originating from gas impurities or corrosion of bipolar plates can induce its decomposition into free radicals [139, 140], which are harmful to the membrane.
Another mechanism of radical formation proposed involves the direct reaction of hydrogen and oxygen at the catalyst surface, thanks to gas crossover [141] :

$$H_2 + O_2 \longrightarrow 2HO^{\bullet} \qquad \textit{(thanks to Pt catalyst)} \tag{1.18}$$

$$HO^{\bullet} + H_2 \longrightarrow H_2O + H^{\bullet} \tag{1.19}$$

$$H^{\bullet} + O_2 \longrightarrow HOO^{\bullet} \tag{1.20}$$

PFSA degradation pathways have been widely studied and can be summarized into four mechanisms (figure 1.8) [136]. These pathways produce different degradation products, including the release of HF species. It should be noted that the length of the side chain significantly affects ionomer chemical stability. Higher chemical stability has been observed in PFSA SSC ionomers, attributed to the absence of ether groups and tertiary carbon atoms [142, 143]. However, during fuel cell operation, the durability also depends on membrane thickness, which influences gas crossover and, consequently, radical production [144].

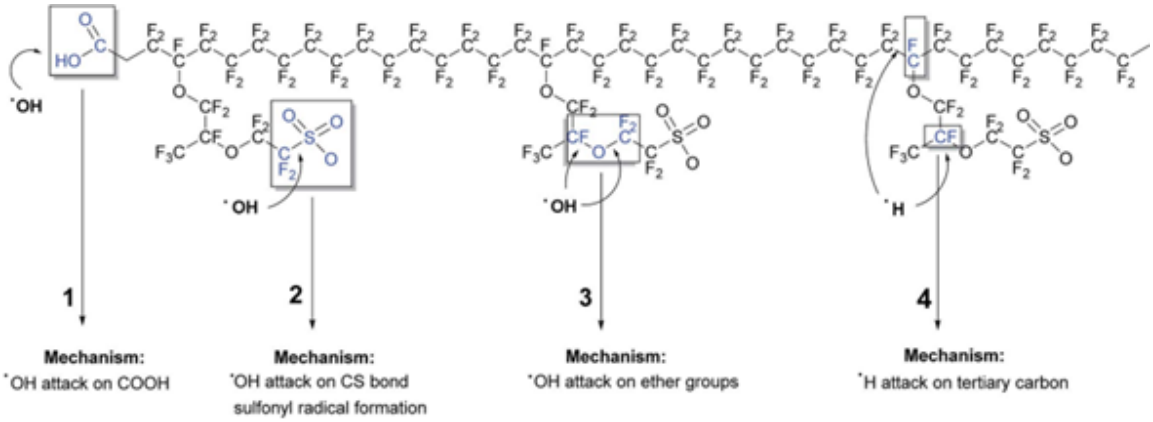

FIGURE 1.8 – Main mechanisms describing radical attacks on PFSA ionomer [136].

Although hydrocarbon ionomer membranes have been less extensively studied, a few works have identified the main degradation pathways of these ionomers. For hydrocarbon-based ionomers, most studies report the radical attacks on aromatic rings as the primary degradation mechanism [145, 146]. Lawrence et al. [147] identified two types of radical attacks for sulfonated poly(arylene ether sulfone) (sPAES) : desulfonation, which affects performance, and chain scission, which impacts fuel cell lifetime. Using FTIR spectroscopy, they observed that chain scission was the predominant mechanism, highlighting durability issues of the ionomer. Hübner et al. [145] reached similar conclusions in their study of hydrocarbon degradation. They reported that the main reaction involves the addition of $HO^{\bullet}$ radicals to the aromatic ring for various sulfonated hydrocarbon-based ionomers (figure 1.9). It should be noted that some radical attacks, such as those on ether bonds, are pH-dependent and are not observed at pH lower than 5.

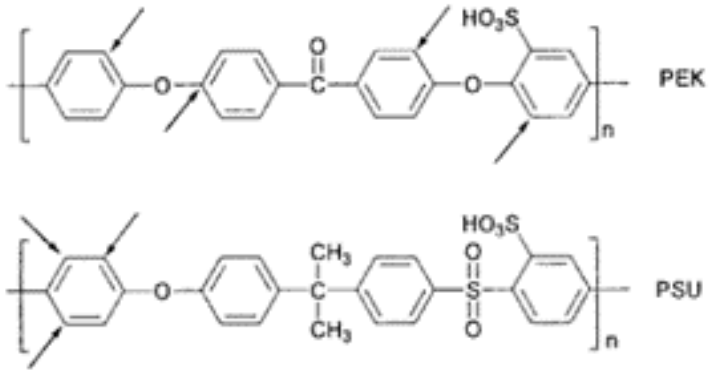

FIGURE 1.9 – Potential HO radicals attack sites in several sulfonated hydrocarbon-based ionomers [145].

In addition, Panchenko et al. [148] observed using thermodynamic calculations that, for sPEEK and PSU ionomers, several pathways leading to sulfonic groups loss are initiated by $HO^{\bullet}$ radical attacks on aromatic rings, highlighting significant durability issues.

Chemical degradation directly affect ionomer thickness, through chain scission, leading to membrane thinning and pinhole formation. Another consequence is a decrease in water uptake and proton conductivity. These changes are detrimental as they negatively impact fuel cell performance and durability [105, 149, 150].

1.5.2.1 Morphological changes and mechanical degradation

During fuel cell operation, the ionomer membrane is mechanically solicited, and its dimensions depend on its water content. The membrane exhibits a high-water content at elevated gas RH and high current load, leading to swelling and significant local stresses. At low gas RH and/or low current load, drying of the membrane induces shrinkage, and consequently, reduced local stresses. Under severely dry conditions (high temperature combined with low RH), the MEA hydration state can change abruptly, resulting in sudden MEA dehydration at high current density. This phenomenon has been discussed previously [151], and will be examined further in the next chapter. Several studies have conducted hygrothermal tests as aging tests to assess the impact of these morphological changes and observed corresponding variations in physicochemical and mechanical properties [152] :

- Shi et al. [153] observed an increase in storage modulus, which they attributed to the formation of anhydride species, previously observed during hydrothermal tests [154, 155].
- A decrease in water uptake and proton conductivity [153, 154].
- A decrease in water permeability, water diffusivity and gas diffusivity (H_2, O_2 and CO_2), attributed to structural changes associated with anhydride species formation [156]. Moreover, the increase in gas permeability with water content is less pronounced after aging, as the water content is also lower.

Although these changes are reversible with appropriate treatment, such as boiling acid [152], this approach is not feasible at the stack scale. Consequently, the alteration of membrane properties impacts performance and durability during prolonged operation.

The MEA also undergoes stress cycling due to repeated humidification and drying steps. Several studies have conducted accelerated mechanical aging tests using RH cycling, either through variations in gas RH [157] or through load cycling [158, 159] to mimic fuel cell operation. Although such tests allow for harsh membrane aging, the resulting changes in ionomer properties strongly depend on the

specific conditions. Tang et al. [160] observed significant differences in H_2 crossover, with an exponential increase when cycling between soaking and 25% RH, but only a slight increase when cycling between 100 and 25% RH. Nevertheless, they found that cycling with stress levels well below the tensile strength was sufficient to induce significant elongation, demonstrating that low-stress cycling can cause permanent deformations. Regardless of the specific parameters, RH cycling induces mechanical aging that affects the membrane's structure [161], leading to :

- A significant increase in H_2 permeation current and a decrease in OCV, attributed to crack propagation and pinhole formation [162-164].
- Changes in mechanical properties, with a transition from ductile to brittle behavior. Han et al. [162] reported lower storage modulus, loss modulus, and ultimate strain for PFSA membrane after hydrothermal cycles. A similar behavior was observed for hydrocarbon-based ionomers (sPEEK), with a transition to brittle behavior ; however, an increase in Young modulus was measured [165].
- A decrease in performance. Choi et al. [166] observed a reduction in produced electrical power with PFSA-based membranes, from 0.938 to 0.608 $W.cm^{-2}$ after 5000 cycles between 0 and 150% RH (2min/2min). Although almost no changes in chemical structure were detected, cracks and delamination of the PEM/cathode interface were observed, illustrating the detrimental effects of RH cycling. Huang et al. [157, 167] reported a similar trend, with a higher voltage degradation rate when cycling between 0 and 62% RH than between 62 and 100% RH, due to increased H_2 permeation current.

These consequences can be aggravated by manufacturing defects that occur during the electrode-membrane assembly process or during MEA integration into the stack, where non-uniform stresses may develop between the ribs and the channels.

2 Impact of operating temperature on fuel cell and components performance/durability

2.1 Fuel cell performance and durability from standard to high temperatures

As mentioned previously, increasing the operating temperature of PEMFC is mainly driven by their use in transport applications, particularly heavy-duty transport. The objective of raising the temperature is to reduce the heat that must be removed, thereby decreasing the size of the system through smaller heat exchangers, while simultaneously enhancing electrode kinetics, which may allow operation with impure hydrogen and thus reduce production costs [168]. However, performance and durability are inevitably affected by this temperature increase. Indeed, issues such as membrane and electrode drying, as well as overall durability, can compromise the well-established operation of PEMFC at usual temperatures. In the following sections, we first review the impact of temperature on MEA performance and durability to provide a global overview and then examine each component individually to better understand the influence of operating temperature on fuel cell behavior.

2.1.1 Fuel cell performance

It is generally accepted that increasing the PEMFC operating temperature from low to intermediate temperature, *e.g.*, from approximately 40 to 70-80°C, leads to enhanced performances. Ozen et al. [169] observed an increase in power density, particularly at high current densities between 50 and 80°C under humid conditions, which they attributed to a decrease in proton transfer resistance. This

effect is minimal in the kinetic region (low current densities) but becomes significant at high current densities. Nevertheless, Ge et al. [170] reported an increase in ohmic resistance at high current densities for a MEA operating at 68°C due to membrane dehydration caused by localized temperature rises within the CCM. Alongside the increase in proton conductivity, Kadjo et al. [171] reported improvements in oxygen reduction kinetics and a reduction in mass transport resistance, consistent with other studies [168, 172] that attributed the performance gain to increased gas diffusivity. Furthermore, they suggested that higher temperatures reduce water condensation, thereby preventing fuel cell flooding, which is known to impede gas transport and create unstable operating points. As a result, performance improvements are particularly notable at high current densities, where excessive water production can hinder reactant transport.

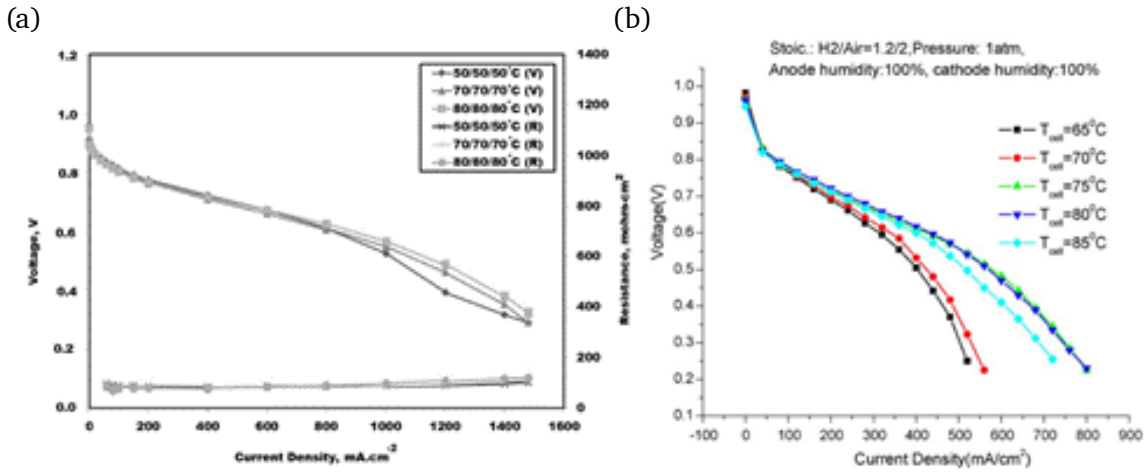

FIGURE 1.10 – Effect of operating temperature at 100% gas inlet RH under H_2/air [169] (a) and [172] (b).

Although increasing temperature generally enhances performance, particularly at high current densities [173], temperatures above 80-90°C have been shown to cause a decline in open-circuit voltage (OCV) due to cathode mixed potential and increased H_2 crossover [1]. In parallel, we also observed reduced performance between 70°C and 95°C [151], mainly due to changes in MEA hydration and oxygen dilution (chapter 2), consistent with the study by Yin et al. [174]. Using a PEM fuel cell model, Wang et al. [175] reported an increase in performance when the temperature rose from 60 to 80°C, attributed to enhanced electrodes kinetics and faster O_2 transfer. However, at 90°C, they observed a larger temperature gradient between the cathode catalyst layer and the coolant, which induced a water outflow from the cathode, leading to membrane dehydration and consequently reduced fuel cell performance. Murthy et al. [176] observed a decrease in performance between 70 and 90°C at high current densities (from 2 $A.cm^{-2}$ in their study) under humid conditions with a gas pressure of 101 kPa. They hypothesized that the drop in oxygen partial pressure, resulting from the increase in water vapor partial pressure rather than MEA dehydration, was responsible for the performance decline at higher temperatures, as also reported in another study [177]. Conversely, when the gas pressure was increased to 202 kPa, the trend reversed : at high current densities, higher performance was observed at 90°C, attributed to the increase in membrane conductivity with temperature. In addition, several studies have reported improved performance with increasing gas pressure at elevated temperatures, due to higher O_2 concentration and enhanced membrane hydration [151, 175].

Humid conditions at higher temperatures can therefore be detrimental to fuel cell performance, as the oxygen partial pressure decreases. Zhang et al. [178] studied oxygen transport between 80 and 120°C. The resistance to oxygen transport arises from three different contributions : transport through the gas diffusion layer, through the microporous layer and through the catalyst layer. They observed

a decrease in total resistance with decreasing gas pressure at any temperature and with increasing temperature at constant pressure. The authors argued that higher temperatures promote faster water evaporation, leading to less residual liquid water and, consequently, easier oxygen transfer. Overall, it should be noted that interdiffusion between two gas components is proportional to temperature and inversely proportional to operating pressure, explaining the increased oxygen diffusion with increasing cell temperature (equation 1.21 [179]).

$$\frac{PD_{AB}}{(P_{cA}P_{cB})^{1/3}(T_{cA}T_{cB})^{5/12}(1/M_A+1/M_B)^{1/2}} = a\left(\frac{T}{\sqrt{T_{cA}T_{cB}}}\right)^b \tag{1.21}$$

Increasing the operating temperature at fixed gas relative humidity produces therefore competitive effects : it improves gas diffusivity and reaction kinetics (beneficial), but also increases oxygen dilution and reduces the oxygen partial pressure (detrimental). The latter effect can be mitigated by increasing the operating pressure, thanks to higher O_2 concentration and improved membrane hydration [175].

Butori et al. [180] further examined the effect of oxygen partial pressure and humidification between 80 and 120°C at 200 kPa pressure. At 70% RH, a decrease in voltage was observed across the entire polarization curve with increasing operating temperature from 80 to 100 and 120°C, with an increase in high-frequency resistance (R_{hf}) at 0.105 A.cm^{-2}, mainly representative of the membrane hydration state. This indicates a lower hydration state at higher temperatures. However, the iR-corrected polarization curves still showed voltage differences, consistent with Xu et al. [181] observations, showing that membrane resistance is not solely responsible for the voltage variation. To isolate the effect of oxygen dilution, they conducted a second experiment in which both oxygen partial pressure and gas RH were kept constant. Under these conditions, IR-corrected polarization curves at different temperatures agreed well in the kinetic region, demonstrating that the reduction in oxygen partial pressure at higher temperatures contributes to the voltage drop. They also reported a voltage decrease at medium and high current densities when reducing the gas RH from 100 to 70 and 40% at 100°C and 200 kPa gas pressure, highlighting the importance of maintaining adequate MEA hydration. Xu et al. [181] stated that cell performance was more impacted by oxygen partial pressure and MEA hydration than the temperature between 80 and 120°C, under 50 and 100% gas inlet RH. Thus, increasing the temperature at constant RH induces a decrease in MEA hydration, resulting in higher membrane resistance. Although this observation was obtained under intermediate temperatures and humid conditions that differ from automotive operation, it illustrates the dependence of performance on hydration at higher temperature [182]. Some studies have nevertheless examined the effect of cell temperature under drier conditions. For example, Zhang et al. [183] performed fuel cell tests with Nafion 112 under dry conditions (0% RH) and observed an increase in performance up to 60°C, attributed to improved reaction kinetics, followed by a decrease in performance from 80°C to 120°C due to increased MEA dehydration outweighing the kinetic gains. In another study, Zhang et al. [184] investigated the effect of RH at 120°C under ambient pressure and reported a significant drop in performance with decreasing RH. They measured an increase in membrane resistance, charge-transfer resistance, and mass transport resistance. According to the authors, substantial dehydration of the catalyst layers leads to a reduction in the oxygen reduction reaction rate. Moreover, the lower water content in the catalyst layer increases the resistance to proton transport and reduces reactant transport across the ionomer film [185]. On the membrane side, dehydration increases the resistance to proton transfer. Saleh et al. [186] summarized the main limiting factors at 70 and 90°C under various RH conditions : at 70°C, performance at low and medium current densities is governed by reaction kinetics and ohmic resistance, while performance at high current densities is limited by mass transport. At 90°C, MEA drying becomes the dominant factor causing the performance loss, highlighting the strong dependence of cell performance on gas RH. Moreover, Chen et al. [187] stated that the decline in performance was due more to reduced humidity than to the temperature increase

itself.

In summary, increasing the operating temperature has mixed effects on PEMFC operation [174, 188] :

- **Benefits** mainly arise from enhanced gas diffusivity and improved electrode kinetics.
- **Drawbacks** are mainly related to MEA hydration, which is highly dependent on the operating conditions. Increasing the operating pressure improves MEA hydration and reactant partial pressures (as discussed in the next chapter) but simultaneously reduces gas diffusivity. Likewise, the gas relative humidity (RH) strongly influences the MEA hydration state :
  - **At high RH**, a significant decrease in oxygen partial pressure and increased oxygen dilution may occur.
  - **At low RH**, substantial membrane and electrode dehydration may develop, leading to an increase in R_{hf} and resulting in a pronounced voltage drop. Chen et al. [187] stated that the decline in performance was due more to reduced humidity than to the temperature increase itself.

The impact of temperature on MEA behavior is therefore highly dependent on the operating conditions. Increasing the temperature at a given inlet gas relative humidity creates a trade-off between, on the one hand, improved reaction kinetics and gas diffusivity and, on the other hand, reduced MEA hydration, decreased reactant partial pressures, and increased dilution by water vapor. Enhancing one parameter, such as MEA hydration through higher operating pressure or increased inlet gas relative humidity, may have detrimental effects, for example by reducing gas diffusivity. This illustrates the competing effects on fuel cell performance between MEA dehydration and mass-transport. In the following sections, we briefly discuss the influence of operating temperature on fuel cell durability and on each MEA component, in order to provide a clearer understanding of the challenges associated with these operating conditions.

2.1.2 PEMFC durability

Automotive conditions involve applying variable load setpoints, depending on the required power density, under relatively dry conditions. Several studies have examined MEA durability under such conditions and at usual temperatures using accelerated stress tests consisting of load cycling, sometimes including OCV periods to accelerate MEA degradation. However, they reported that the findings varied due to differences in materials and test conditions. Nandjou et al. [189] observed a higher voltage degradation at 80°C during the cyclic test, compared to stationary one. Microcracks and pinholes were detected in the membrane, leading to premature MEA failure without significant chemical degradation. In contrast, stationary conditions did not cause sudden failure but resulted in delamination at high water content and corrosion of the bipolar plates. The authors concluded that elevated or varying water content and relative humidity induce several degradation modes, particularly membrane pinholes and microcracks responsible for sudden loss of cell functionality, while only one degradation mode was linked to local temperature, with negligible consequence on cell lifetime under the tested conditions. Tian et al. [190] reported that the decrease in electrochemically active surface area at 65°C caused by carbon corrosion and Pt particle growth (section 1.4.2) was the main degradation factor for the MEA after an accelerated stress test involving load cycle and OCV periods under various gas relative humidities, as no evolution in membrane gas permeation was observed.

Given these differences, it is difficult to establish a general trend regarding MEA durability under automotive conditions. Nevertheless, significant degradation has been observed both at the catalyst level, reducing MEA performance, and in the membrane, sometimes leading to sudden cell shutdown.

In parallel with automotive conditions, a few studies have examined the impact of operating temperature on MEA durability. Eriksson et al. [191] investigated the effect of temperature in the 80-120°C range under constant load and 70% gas RH. They observed a higher performance degradation rate with increasing temperature, resulting in lower cell potential and OCV, mainly attributed to increased hydrogen crossover and decreased ionic conductivity. They concluded that ionomer degradation–both in the membrane and the catalyst layer–was the primary cause of fuel cell failure, associated with increased gas permeation and pinholes formation. Moreover, they found that the degradation rate of the ionomer in the cathode catalyst layer increased with increasing temperature from 80 to 100°C. Similarly, Kakinuma et al. [182] reported lower membrane durability at 120°C under OCV condition, leading to a significant decrease in membrane thickness. The application of an AST involving load cycling between 80 and 120°C at 80% gas RH also resulted in a higher degradation rate at higher temperature, consistent with Han et al. [162], who reported a higher performance decrease at 95°C than at 85°C during RH cycling.
However, under drier conditions (20% RH) at 120°C, the decrease in ECSA was lower than that observed at 80°C and 80% gas RH, which the authors attributed to the dependence of Pt oxidation on water activity. Lu et al. [192] conducted an accelerated stress test on a 10 kW-stack at 95°C under load cycling conditions. They reported a higher degradation rate at 95°C compared with 70°C (1.44% vs. 0.567% @1 $A.cm^{-2}$), particularly near the coolant outlet where the temperature was higher. Degradation was observed in each component, including the corrosion of the bipolar plates and carbon support, loss of PTFE in the GDL and ionomer in the catalytic layer, as well as aggregation and growth of Pt particles. Additionally, microstructural defects were observed in the membrane, associated with increased permeation. The authors suggested that these defects in the PEM were induced by repeated swelling/contraction cycles during load cycling, along with increased free radical generation at higher temperatures. Furthermore, material losses (PTFE in the GDL, ionomer in the CL and the PEM), led to thickness reduction, thereby decreasing the mechanical integrity of the components. They concluded that the combined structural degradation and material losses were responsible for the higher overall degradation rate observed at higher temperature.

Moreover, although component degradation is often considered separately for clarity, the degradation processes of fuel cell components are strongly coupled. Shi et al. [193] investigated the mechanical degradation of a NR211-based CCM under humidity cycling (0-120% RH) at 70, 80, and 90°C using 4D X-ray computed tomography. They reported significantly reduced durability with increasing temperature, evidenced by an earlier increase in H_2 crossover. This was attributed to more severe CL buckling and crack formation resulting from temperature-induced changes in mechanical properties and plastic deformation within the CCM. They proposed a CCM failure mechanism in which cracks in the GDL induce CL buckling during RH cycling, leading to plastic strain deformation. This promotes crack formation in the CL, generating stress concentrations that ultimately drive crack propagation in the membrane. Increased temperature was found to exacerbate CL buckling, leading to premature CCM failure.

To summarize, increasing the operating temperature under low gas RH likely affects MEA durability, particularly under load-cycling conditions resulting in degradation or even premature MEA failure, due to components aging :

- MEA failure can occur due to excessive membrane degradation, characterized by thinning and pinholes formation [194]. This is mainly attributed to the increase in membrane permeability with temperature, although hydrogen crossover is also dependent on membrane hydration, and thus, gas RH [174, 181, 195].
- Catalyst layer state affects MEA performance degradation. Higher degradation rate has been observed at constant gas RH with increasing cell operating temperature. However, this trend can

be mitigated under lower gas RH, since higher water activity accelerates Pt degradation.

Therefore, increasing the operating temperature may only slightly affect the MEA performance degradation rate if an adequate gas RH is maintained, but it can still lead to rapid degradation or even sudden cell failure.

In the following subsections, we review the impact of temperature on the performance and durability of each MEA component. Although this review is not exhaustive, it provides a better understanding of the potential results that could be obtained during our experimental work.

2.2 Component performance and durability from standard to high temperatures

2.2.1 Bipolar plates

There are relatively few studies on the effect of operating temperature on bipolar plate (BP) performance and durability during PEMFC operation. Nevertheless, *ex situ* investigations have reported a significant impact of temperature on both performance and durability.

Akhtar et al. [196] developed bipolar plates made of multi-walled carbon nanotubes, natural graphite, and epoxy. They reported decreased mechanical properties, such as Young's modulus and shore hardness, with increasing temperature, which is detrimental to durability. They also observed increased electrical conductivity, consistent with the study of Husaini et al. [197], which is beneficial for fuel cell efficiency. In contrast, Ghosh et al. [198] reported stable shore hardness and electrical conductivity up to 175°C for graphene reinforced carbon-polymer composite BP, highlighting the strong dependence of BP properties on material composition.
Fan et al. [199] investigated the properties of stainless steel with gold/titanium nitride (Au/TiN/SS) composite coating at various temperatures. They reported that increasing the temperature accelerated H^+ diffusion, promoting dissolution of TiN, reducing Au adhesion. This resulted in lower surface coverage of Au and higher interfacial contact resistance (ICR), which tends to reduce fuel cell performance. Moreover, several studies reported a decrease in thermal conductivity with increasing temperature [200, 201], which may adversely affect overall system efficiency, by increasing cooling demand under high load, and reduced other component durability due to local hot spots.

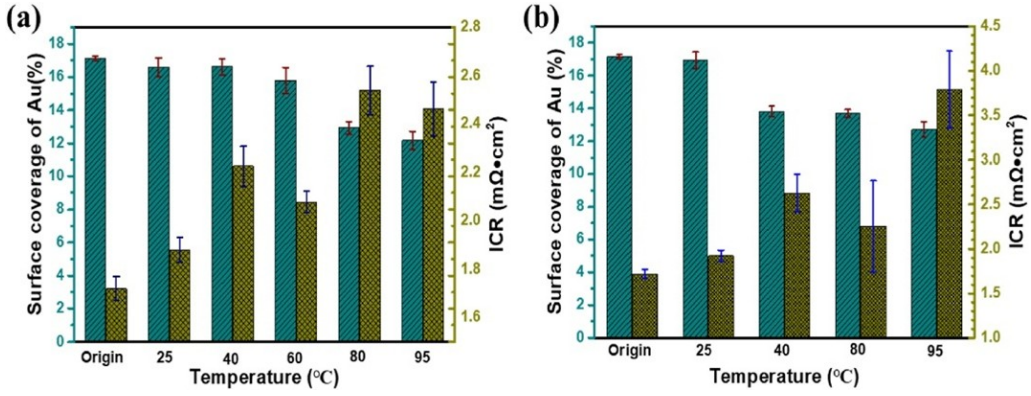

FIGURE 1.11 – Evolution of the surface coverage of Au and the interfacial contact resistance at various temperature after polarization at 0.67 V polarization for 24h (a) and 1.43 V polarization for 1h (b) [199].

In addition, it is widely accepted that higher temperature accelerates corrosion process [199, 202, 203], although most studies have been conducted in an *ex situ* way. Nevertheless, Lu et al. [192] performed an accelerated stress test at 95°C on a 10-kW stack using load cycling. They observed cracks, corrosion holes in SEM images, and significant surface elemental changes on the anode Ru-

coated metallic (Ti) BP, indicating coating degradation. These changes led to a substantial increase in corrosion current, from 0.41 to 7.87 and 10.68 $\mu A.cm^{-2}$ after the AST, depending on the location. In contrast, the graphite cathode BP exhibited stable elemental composition but an increased number of defects, attributed to the brittle nature of graphite.

Overall, BP performance and durability are significantly affected by temperature, although the consequences strongly depend on BP composition. In terms of properties, decreases in mechanical properties, along with increases in interfacial contact resistance and electrical conductivity, have been reported with adverse effects on fuel cell performance. Regarding durability, most available studies found have been conducted in *ex situ* way, but they consistently indicate that corrosion rates increase at higher temperature. In addition, temperature-induced changes in mechanical properties of certain BP materials may promote defect formation. These effects can lead to reduced fuel cell performance due to both changes in BP properties and degradation of other components. In particular, dissolution of metallic elements from metallic BP can enhance free radical formation, which negatively affects ionomer durability. Therefore, appropriate BP composition and manufacturing process designed for higher operating temperatures are essential to ensure a reliable fuel cell operation.

2.2.2 Gas Diffusion Layers

As previously stated, one of the main challenges in operating PEMFC at intermediate temperatures is maintaining appropriate MEA humidification. Although few studies have focused on the design of the GDL/MPL assembly, this component remains essential since it governs, among other functions, heat and water management.

Some authors have investigated performance evolution as a function of GDL composition. Eom et al. [204] evaluated the performance of a PEMFC operating between 65 and 80°C with gas RH varying between 25, 50 and 100%, using GDL with different PTFE loadings ranging from 10 to 30 wt%. At 80°C, GDL with higher PTFE loading (20-30 wt%) exhibited better performance, whereas a low loading was more effective at lower temperatures. Increasing the PTFE content reduces GDL porosity, thereby enhancing water retention, which is beneficial under dry, high temperature conditions [205] but detrimental under wet conditions due to an increased risk of flooding. Nishimura et al. [206] investigated the impact of GDL thickness at 80 and 90°C under 40 and 80% RH, using a Nafion 115 membrane. They found that employing a thinner GDL improved fuel cell performance due to enhanced water management and gas diffusivity, as well as a more uniform temperature distribution. In fact, a thinner GDL promotes a higher water vapor concentration gradient, resulting in an increased diffusive flux, which is further amplified at higher temperature [207]. In a subsequent study, Nishimura et al. [208] examined the performance of MEA operating in the temperature range of 90-100°C with and without MPL, under relatively humid conditions (80/80%, 40/80%, and 80/40% at anode/cathode). They observed that incorporating an MPL was detrimental for fuel cell performance and concluded that the MPL has a negative effect when used with a thin PEM and GDL at high temperature. Moreover, they reported a more homogeneous temperature distribution in the absence of the MPL.

Yildirim et al. [209] synthesized a 30 µm-thick, self-supported MPL on the anode side, containing polyvinylidene fluoride (PVDF) in the range of 20-40%. When they compared the fuel cell performance with a commercial GDL (Freudenberg H14Cx483) at 95-120°C and low gas RH, they observed higher cell voltages across the polarization curve with the synthesized MPL. This improvement was attributed to lower high-frequency resistance resulting from enhanced water management. However, it is difficult to isolate the direct impact of reduced thickness on fuel cell performance, since the tested GDL differed in composition. Using a different hydrophobic agent and varying its content can substantially alter the GDL's characteristics–reducing hydrophobicity and permeability while increasing electrical resistivity

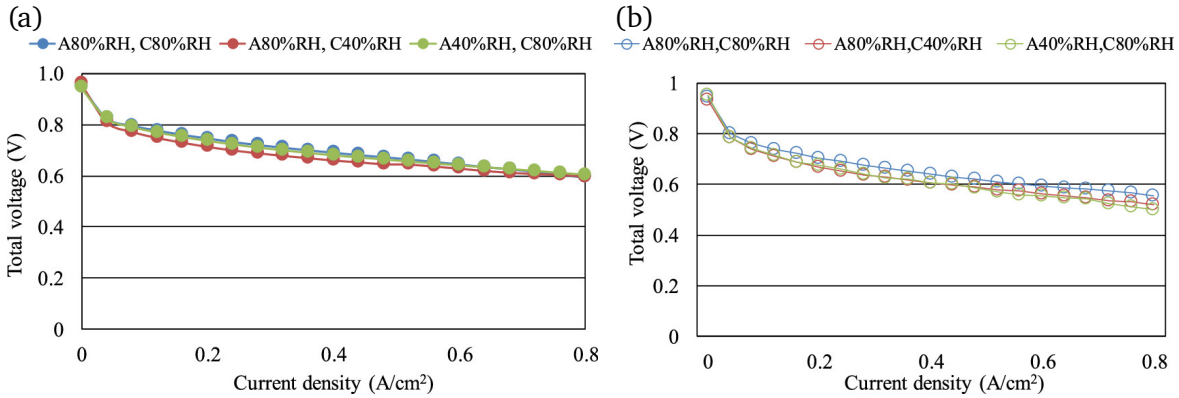

FIGURE 1.12 – Polarization curves at 90°C and different RH conditions without MPL (a) and with MPL (b) [208].

and porosity in the synthesized MPL. Nevertheless, these studies indicate that significant performance differences can be achieved through the optimization of GDL parameters such as composition, thickness, etc. Although relatively few studies have focused on GDL behavior in fuel cells operating at intermediate temperatures, the cited works highlight marked differences in heat and water management compared with operation at standard temperatures. The GDL therefore plays a significant role in ensuring reliable and efficient fuel cell performance.

In addition, increasing the cell operating temperature can affect the properties of the GDL and, consequently, the overall fuel cell durability. Chen et al. [210] reported reduced GDL stiffness at 90°C compared to 25°C and 60°C, attributed to the softening of adhesive polymers or resins used in the carbon fiber composites and PTFE at higher temperature. Scanning electron microscopy (SEM) images revealed that GDL compressed at 90°C sustained greater mechanical damages due to epoxy resin softening. Wu et al. [211] evaluated GDL durability at 120°C under elevated flowrate over 200h. Following an accelerated stress test, they observed reduced electrical resistivity and hydrophobicity, associated with PTFE losses. This is consistent with Lu et al. [192] work, who reported a structural breakdown (higher on the cathode side) of the GDL after a 100h-driving cycle AST at 95°C, characterized by carbon corrosion and PTFE losses, inducing degraded mechanical properties and changes in pore size. These changes led to lower fuel cell performance and increased mass transport losses. Chen et al. [212] also conducted a coupled chemical/mechanical stress test using a MEA incorporating GDL with holes of different sizes. They observed significant crack propagation in both the catalyst layer and membrane, as well as membrane thinning near the GDL holes, depending on hole size. These findings highlight the critical importance of employing mechanically and chemically durable GDL to ensure long-term MEA operation.

2.2.3 Catalyst layers

As mentioned earlier, compositional adjustments are necessary at higher operating temperatures to maintain good performances :

- **SSC and LSC ionomer :** perfluorosulfonic acid (PFSA) ionomers with long side chain (LSC) are currently the most widely used due to their good proton conductivity and high chemical durability. Nevertheless, several studies have focused on PFSA Short Side Chain (PFSA-SSC) ionomers because of their higher water retention capacity and proton conductivity [142, 213]. This results in greater water uptake and, consequently, higher proton conductivity under equivalent temperature and relative humidity conditions. Li et al. [214] reported a proton conductivity exceeding 0.1 $S.cm^{-1}$ for PFSA-SSC with an equivalent weight (EW) of 720 over a temperature

range of approximately 30-70°C (at RH=60%), whereas PFSA-LSC with an EW of 1100 exhibited conductivities not exceeding 0.03 S.cm^{-1}. This implies lower membrane resistance and improved performance, particularly under low gas RH, as observed at medium-to-high current densities.

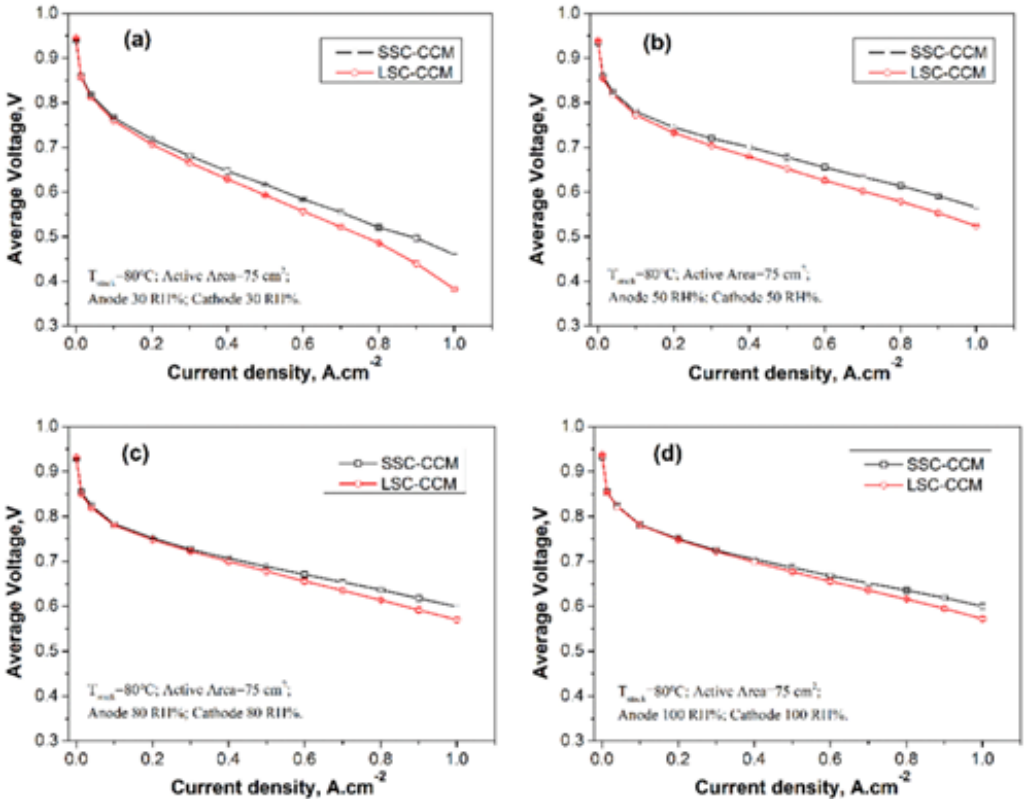

FIGURE 1.13 – polarization curves of SSC and LSC MEA operating at 80°C, 30% EH (a), 50% RH (b), 80% RH (c) and 100% RH (d) [214].

Jeon et al. [215] observed similar performances between PFSA-LSC and SSC MEA under fully humidified conditions (RH=100%) at 75 and 90°C. However, the performance of PFSA-LSC MEA decreased significantly at 120-140°C and 40% RH compared with the PFSA-SSC MEA. Impedance spectroscopy measurements performed at 0.6 V revealed increased membrane and charge-transfer resistance in the PFSA-LSC MEA, indicating greater dehydration of the MEA and a consequent decrease in cell performance. In contrast, the higher water uptake capacity of PFSA-SSC enables better performance under dry conditions. Although the number of studies remains limited, the properties of PFSA-SSC suggest that this ionomer is a promising candidate for use in the catalyst layers operating under automotive conditions. Furthermore, the use of hydrocarbon-based ionomer is envisaged to eliminate the use of fluorinated compounds, which are both environmentally concerning and costly. However, fabricating electrodes based on hydrocarbon ionomers requires precise control of the ionomer content to avoid excessive swelling and reduced gas permeability in the catalyst layer [216].

- **Ionomer content :** as discussed in the section 1.4.1, the ionomer content is a key parameter, as it determines, among other factors, the hydrophilicity and gas permeability of the electrode. In theory, dry operating conditions may require a higher ionomer content to maintain sufficient hydration within the electrode and efficient proton transport, especially since permeability tends to decrease under dry conditions. The optimal ionomer content also depends on the operating

point : at low and medium current densities, a higher ionomer content is beneficial to sustain adequate hydration. Conversely, at high current densities, excessive ionomer content can block catalyst sites [217] and cause flooding or mass transport limitations due to increased water production and oxygen dilution.
Gatto et al. [218] investigated the effect of ionomer content in catalyst layers using PFSA-LSC. The layers were hot-pressed onto the same ionomer membrane and tested in a single cell under H_2/O_2 at various temperature (80-130°C) and RH. The authors found that the relationship between performance and ionomer content strongly depended on the operating conditions of the fuel cell. At 1 A.cm^{-2}, an increase in cell voltage was observed for ionomer contents of 50-60 wt% as the temperature increased from 80°C to 110°C, followed by a decrease at 130°C. For ionomer contents of 30 and 40 wt%, the cell voltage decreases progressively from 100°C to 130°C and from 80 to 130°C, respectively. An ionomer content of 40 wt% yielded the best performance at 80-100°C/100% RH, whereas 30 and 50 wt% showed better performances at 130°C/100% RH. However, at 130°C/100% RH, the 50 wt% sample exhibited mass transport limitations at high current densities compared to the 30wt%. When performance was evaluated at 110°C under various RH values for the 50 wt% ionomer content, only a minor influence of gas humidity was observed. This was attributed to a sufficient ionomer content to maintain adequate MEA humidification. Nguyen et al. [216] investigated the effect of an ionomer gradient within the catalyst layer compared with a homogeneous Ionomer-to-Carbon (I/C) ratio. A hydrocarbon-based ionomer was used as the binder in the cathode CL (with PFSA-LSC ionomer at the anode) and sprayed onto a hydrocarbon-based membrane. The cathode CL was divided into two sublayers : one near the GDL with a low I/C ratio and another neat the membrane with a high I/C ratio. The low I/C sublayer, located adjacent to the GDL accounted for 75% of the total Pt loading (0.3 mg.cm^{-2}), while the high I/C sublayer near the membrane represented 25% of the total Pt loading (0.1 mg.cm^{-2}). Under automotive conditions (95°C / 50% RH), the cathode CL with I/C ratios of 0.2 (near the GDL) and 0.4 (near the membrane) delivered the best performance, even slightly outperforming the homogeneous PFSA-LSC cathode (I/C=0.4). The authors attributed this improvement to the lower ionomer content near the GDL, which enhances oxygen permeability, while a higher I/C ratio near the membrane is beneficial at low current densities.

- **Carbon support :** the type of carbon support plays a significant role in both performance and durability, as notable changes have already been observed at typical operating temperature [219]. Ott et al. [220] compared different carbon support, including N-doped and commercial materials, under conditions of 90°C/30% RH and 65°C/90% RH, referred to as dry and wet conditions, respectively. They reported significant differences in fuel cell performance : the best performing material under wet conditions performed among the worst under dry conditions. The authors stated that a well-defined pore structure is essential to enable ionomer penetration and improve Pt accessibility, as the lack of water cannot compensate for discontinuities in the ionomer film discontinuities. Although we could not find other studies examining the carbon support under dry conditions/at intermediate temperature, these results highlight the drastic changes in catalytic layer operation.

Although compositional adjustments are made at higher operating temperatures to maintain good performance, durability may still be affected. Lu et al. [192] reported significant structural damage in the CL after a driving cycle AST at 95°C compared to conventional operating conditions. Similar to operation at usual temperatures, catalyst layer degradation can occur through three main pathways : degradation of the catalyst particles, the carbon support and the ionomer binder :

- Strandberg et al. [221] tested four MEA with different membranes and catalyst layers, subjecting them to 15k-voltage cycles (0.6-3/0.95V-3s) at 80, 100 and 120°C under 100% gas RH. While only a small performance decrease was observed when increasing the temperature from 80 to 100°C, the degradation was significantly higher at 120°C. This was primarily attributed to greater ECSA losses. Pt particle growth was found to be more pronounced at higher temperatures, with the rate depending on the initial particle size, smaller particles being less stable. However, the drop in performance at 120°C could not be fully explained by ECSA losses and hydrogen crossover alone and was therefore also attributed to increased mass transport limitations resulting from microstructural changes in the catalyst layer. Kakinuma et al. [182] reached similar conclusions when comparing MEA aging at 80°C/80% RH and 120°C/80% RH, observing a more significant decrease in ECSA after load cycling at higher temperature. Furthermore, when the same test was performed at 120°C under dry conditions (20% RH), lower ECSA losses were recorded. The authors concluded that Pt degradation is accelerated by both temperature and water activity, while Pt diffusion may be mitigated under low gas RH.
- Carbon corrosion kinetics are accelerated at higher temperatures [222]. Consequently, increasing the cell operating temperature can exacerbate carbon support degradation during both start-up/shut-down processes [223], load cycling [194] and normal operation. Yang et al. [224] observed greater performance and ECSA losses during a load-cycling AST at 95°C compared to 75°C, both at 50% RH. In addition to larger Pt particle growth, they reported more defects in the cathode carbon support at the higher temperature, including a less ordered structure and lower graphitization, which was related to enhanced carbon support electrochemical oxidation at higher temperature. Zhao et al. [225] investigated carbon corrosion during 100 hours at 1.6 $A.cm^{-2}$, 65 and 90°C. The greater performance loss observed at 90°C was attributed to increased ECSA degradation. Scanning electron microscopy (SEM) images revealed more severe carbon corrosion at 90°C than at 65°C in regions where flooding was absent. At the same time, operating at higher temperature helps to prevent liquid water accumulation in specific areas of the MEA, thereby reducing carbon corrosion. These results highlight the importance of water management, which can be facilitated by operating at higher temperatures.
- There are currently few studies on ionomer binder degradation [226], especially at intermediate temperature. Eriksson et al. [191] observed an increased resistance of the ionomer, as well as a notable increase in the I/C ratio and in ionomer loading, with increasing temperature through ASTs conducted at 80, 100, and 120°C at 70% gas RH under constant load. Lu et al. [192] reported a decreased content of F and Pt elements after a 100h-driving cycle AST at 95°C, indicating potential ionomer binder degradation. Young et al. [105] conducted an accelerated stress test at 1V, 90°C and 100% RH for 440h, evaluating two different ionomer contents in the cathode catalyst layer. They observed significant degradation, manifested as reduced ECSA and increased ionic resistance ; however, no data were provided on morphological changes in the ionomer. Lower durability was noted for the sample with higher ionomer content, although this sample contained a higher Pt loading. Shahgaldi et al. [227] reported an opposite trend under different testing conditions. Nevertheless, Yoo et al. [228] found that, in a MEA subjected to load cycling at 80°C under humid conditions, ionomer binder degradation was less pronounced than degradation of the carbon support or catalyst.

As a summary, the performance and durability of the catalyst layer are highly sensitive to opera-

ting conditions. From the aforementioned studies, it is evident that fuel cell performance at higher temperatures depends strongly on the type of ionomer and its content. Optimizing these parameters can enhance water retention, which is particularly important under dry conditions, such as those encountered in automotive applications. Carbon support examinations under wet and dry conditions demonstrated the essential role of ionomer coverage in the catalyst layer in compensating for the lack of water and, consequently, improving Pt accessibility.

In terms of durability, higher operating temperatures accelerate catalyst degradation, although this effect can be mitigated by lower gas RH, as water activity is a key factor in catalyst degradation. No studies specifically addressing ionomer binder degradation in the catalyst layer were identified. Nevertheless, given that membrane ionomer degradation increases at higher temperatures and low RH (see the next section), it is likely that similar degradation occurs within the catalyst layer.

2.2.4 Ionomer membrane

Membrane properties are strongly influenced by operating conditions, particularly temperature. The microstructure undergoes reorganization due to segmental motions of the polymer backbone and side chains, which are temperature-dependent [153]. As detailed in the next chapter (chapter 3), each ionomer is characterized by several transition temperatures (α, β, γ) corresponding to structural rearrangement. Without going into details that will be discussed later, changes in microstructure lead to variations in ionomer properties, as outlined below :

- Significant changes in mechanical properties have been observed with increasing temperature, notably a decrease in the storage modulus [153, 229, 230]. Tang et al. [231] confirmed these results and additionally reported a decrease in tensile strength and an increase in elongation at break with increasing temperature. These properties are highly dependent on the membrane

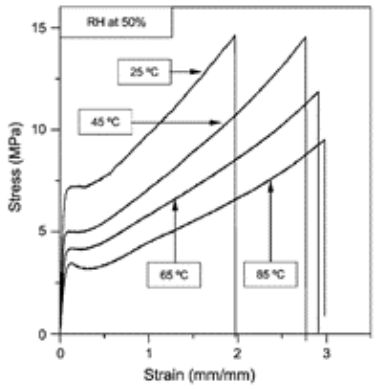

FIGURE 1.14 – Stress-strain curves at different temperatures and 50% RH [231].

hydration state. Zhao et al. [232] observed, for Nafion 1035, a decrease in the elastic modulus with increasing water activity below the thermal transition temperature (around 70°C). However, at temperatures above the thermal transition (approximately 80°C), the elastic modulus of dry Nafion 1035 was systematically lower than that of samples with water activity.
- Although no significant differences in water sorption were observed at different temperatures [232], several studies have reported higher swelling and water uptake with increasing temperature [231, 233]. Regarding proton conductivity, Xiao et al. [233] observed that it was strongly dependent on water activity but only weakly influenced by temperature. Barique et al. [234] reached similar conclusions in their study of Nafion 212 in the 80-100°C temperature range. They also observed an increase in proton conductivity up to 80°C, particularly at high RH, above which

no significant changes were measured. They suggested that ion-water channels could not expand further at higher temperatures due to the attainment of morphological and thermodynamic equilibrium around 80°C. The slight increase in proton conductivity at constant RH between 80 and 100°C could therefore result from higher proton mobility [233]. It is worth noting that Maldonado et al. [235] reported a significantly stronger effect of temperature on proton conductivity for Nafion 212 and 115.

- Higher temperature is associated with higher water diffusion [236] and gas permeability coefficients [237]. Butori et al. [195] reported an increase in H_2 crossover with temperature and pressure. Interestingly, they observed an increase in hydrogen crossover with RH at 80°C, whereas this trend was no longer observed at 100°C. They explained that, at constant total pressure and RH, increasing temperature leads to a decrease in H_2 partial pressure and, consequently, a lower crossover rate, even though membrane permeability increases. Operating at higher temperatures than usual and under low RH could therefore promote H_2 crossover and, in turn, accelerate chemical degradation. The phenomenon also depends on operating pressure, as H_2 crossover and permeability increase up to around 90-100°C, beyond which a decrease is observed. Harilal et al. [238] suggested that H_2 permeability is enhanced by the presence of liquid water within the membrane until it evaporates at higher temperatures.

These changes in physico-chemical properties significantly affect the durability of the ionomer. As a key component of the fuel cell, the ionomer membrane has been extensively studied through both *ex situ* and *in situ* approaches. Although substantial improvements in fuel cell materials may alter the conclusions of earlier studies, several general trends have been established through accelerated stress tests conducted at various temperatures and RH conditions on different ionomer membranes. To better understand the influence of temperature, the results of AST can be analyzed according to the dominant degradation mechanisms involved :

- **Chemical degradation :** Eriksson et al. [191] conducted AST at 80, 100, and 120°C at 70% gas RH under constant load and observed increased pinhole formation at higher temperatures, attributed to increased membrane permeability, affecting MEA lifetime. Sethuraman et al. [239] carried out AST on Nafion 112 and biphenyl sulfone hydrocarbon (BPSH-35) membranes, maintaining OCV until MEA failure. Under H_2/O_2 atmosphere at 25% RH, they observed reduced chemical stability with increasing cell temperature– specifically, MEA lifetimes of 498h and 25h at 80°C and 120°C, respectively. The OCV decay occurred in two distinct stages : an initial period of gradual, nearly linear decay corresponding to membrane thinning, followed by a rapid OCV drop associated with pinhole formations. The authors attributed this accelerated membrane degradation to a higher H_2O_2 production rate at elevated temperatures and low RH, as also reported by several studies [240-242].
  Chen et al. [243] investigated the influence of RH at intermediate temperature (90°C) by performing OCV tests on Nafion 112 (50 µm) for 120 h at 36, 55, and 82% RH. Although ATR-FTIR analysis revealed no major structural changes between the different conditions, low RH caused a decrease in the intensity and area of all characteristic peaks. Combined with higher emission rates of degradation products and a lower IEC, this indicated that low RH promotes accelerated degradation, particularly of the side chains. This led to the formation of defects and pinholes at low RH, whereas no such damage was observed at higher RH.
  This low-humidity degradation resulted in more pronounced decreases in the ionomer's physical and chemical properties : proton conductivity declined due to the loss of sulfonic acid groups during chain scission, and mechanical properties deteriorated, with notably reduced tensile and breaking strength. These findings are consistent with those from Zhao et al. [244], who observed greater OCV degradation with increasing operating temperature (from 64 to 95°C) and decreasing RH (from 60 to 30% at 95°C). They also reported that the effect of temperature was

minor during the first 50 hours but became significant thereafter, resulting in a much shorter MEA lifetime at 95°C/60% RH (168 hours) compared to 64°C/60% RH (over 700 hours).

- **Mechanical degradation :** mechanical aging can induce severe performance losses and membrane properties changes. Lu et al. [192] conducted a 100h-drive cycle AST at 95°C and reported reduced mechanical properties of the membrane, indicating the transition from a ductile to a brittle behavior. Marrony et al. [245] performed load-cycling tests using hydrocarbon-based (sPEEK) and PFSA-based (Nafion) membranes. For the Nafion membrane, they observed a decrease in both mechanical and electrochemical properties at 90°C, leading to failure after 41 load cycles. The OCV monitoring results were consistent with those reported by Sethuraman et al. [240], showing a stable OCV up to 39 cycles, followed by a sharp drop indicating membrane failure. For the sPEEK membrane, durability was found to be very low, with failure occurring after only 88 and 3 load cycles at 80 and 90°C, respectively. When testing thicker membranes with the same ionomers, improved durability was observed, attributed to enhanced mechanical properties and reduced gas crossover. This is consistent with the work of Shi et al. [193], who attributed the premature crack formation observed in CCM under RH cycling at 90°C to the degradation of the membrane's mechanical properties.
  Similarly, Trogisch et al. [194] conducted AST involving load-cycling steps of 10 s each, between 0.6 and 0.88 V, at 68 and 105°C. While the test at 68°C endured up to 82k cycles, the test at 105°C failed after only 25k cycles. A noteworthy detail was the absence of characteristic signals on the polarization curves after 10k cycles, foreshadowing the eventual MEA failure at 105°C. Based on *ex situ* analyses, the authors observed significantly greater structural defects at 105°C, evidenced by a higher number of larger holes, though not correlated with the current distribution. They attributed these findings to the operating temperature approaching the polymer's glass transition temperature, which may have intensified membrane creep and led to irreversible deformations. Han et al. [162] investigated the durability of CCM through RH cycling below and above its glass transition temperature. Although the RH range was not identical (0-120% at 85°C and 0-80% at 95°C), they reported fewer but larger cracks and greater delamination between the membrane and the catalyst layer, as well as more brittle behavior after aging at 95°C, leading to earlier failure.
  Overall, these results highlight the (much) greater mechanical fatigue experienced at higher temperatures, exacerbating deformations within the ionomer and leading to the formation of pinholes.
- **Chemical and mechanical degradation pathways** are coupled. For example, RH cycling generates mechanical stresses that promote the formation of pinholes and cracks, increasing H_2 crossover and enhancing H_2O_2 generation, which in turn accelerates chemical degradation. Although few studies have focused on coupled degradation at intermediate temperature, the underlying mechanisms are similar to those occurring for each individual pathway ; however, the overall degradation rate is expected to be higher, as lower durability has been reported in the previous section. Lai et al. [246] conducted accelerated stress tests at 80 and 90°C using load cycling between 0.05 and 1.2 A.cm^{-2} at constant reactant flowrate, under 30% gas RH and 3 bar, on a MEA incorporating a PFSA-based membrane. They reported an earlier failure at higher temperature, characterized by an earlier onset of H_2 crossover and higher voltage degradation. Using localized diagnostics, they showed that the most severe membrane thinning coincided with regions subjected to strong hydration/dehydration cycling, experiencing high mechanical stress and water flux, rather than the drier regions. The authors concluded that membrane degradation results from a synergistic interaction between mechanical stress and chemical attack rather than from dry conditions alone.

Overall, the membrane undergoes significant changes at higher temperature, particularly near its

glass transition, where major microstructural modifications occur, leading to altered physicochemical properties. Changes in water uptake and mechanical properties strongly impact fuel cell performance and durability, especially under driving-cycling operating conditions. For example, Lu et al. [192] reported significant structural changes in the membrane after a 100h-drive cycle AST at 95°C, in contrast to a 600h-drive-cycle AST at 75°C, where the membrane exhibited no cracks or cavities [247]. Similarly, changes in gas permeability significantly affect chemical durability, and increased degradation under drier conditions promotes gas crossover, accelerating degradation and potentially leading to fuel cell shutdown. Overall, membrane performance and durability are critical determinants of fuel cell reliability, as membrane failure directly results in fuel cell shutdown.

3 Conclusions

Although research on PEMFC operating at intermediate temperatures between 90°C and 100°C remains limited, it appears that increasing the operating temperature can be detrimental to both the performance and durability of the fuel cell, as well as to each of its components. Therefore, adapting the operating conditions is essential to enable higher operating temperatures while still using materials like those employed in LT-PEMFC.

Increasing the operating temperature enhances gas diffusivity ; however, it decreases the oxygen partial pressure (and increases oxygen dilution) at equivalent gas RH. Reducing the gas RH can mitigate these issues but may lead to MEA dehydration, thereby reducing fuel cell performance. Ensuring a proper fuel cell operation therefore requires increasing the operating pressure to improve MEA hydration and oxygen partial pressure, while limiting the gas RH. Low air stoichiometry is also required to prevent MEA drying. Overall, this highlights the importance of water-balance within the cell to ensure high performance at higher operating temperatures [194].

From a durability perspective, studies agree that MEA lifetime and performance durability are significantly reduced at higher temperature, with higher degradation rates for all components. MEA performance durability is negatively impacted by the reduced durability of the catalytic layer, through accelerated degradation of the catalyst particles, the carbon support, and the ionomer, while sudden MEA failure can occur due to reduced membrane durability. Indeed, membrane mechanical durability tends to decrease as the operating temperature approaches the glass transition temperature of the ionomer. Similarly, chemical durability is also reduced, likely due to a possible increased H_2O_2 production–especially under dry conditions. Nevertheless, a lack of data appears to establish operating conditions that mitigate degradation. Reducing gas RH may mitigate catalyst particle degradation but could simultaneously accelerate membrane degradation. However, Eriksson et al. [191] observed that reducing the load by half at 100°C and 70% gas RH during aging (1.3 to 0.65 $A.cm^{-2}$) resulted in a lower performance degradation rate-similar to that observed at 80°C-although Pt degradation was higher.

Although a few studies established operating conditions that maintain both adequate performance and durability at intermediate temperatures, it is clear that operation under such conditions, particularly at low humidities, requires careful optimization. Specific parameters, such as gas pressure and relative humidity, can affect component properties, including ionomer ionic conductivity and hydrogen permeability [195]. It is therefore essential to characterize the effect of temperature under a range of operating conditions while evaluating their impact on MEA durability. In addition, although significant durability limitations have been reported for conventional ionomers, new membranes have been mechanically reinforced and impregnated with radical scavengers to extend their lifetime. It is therefore of great interest to evaluate both the performance and durability of state-of-the-art materials.

References

[1] J. Zhang et al., « PEM Fuel Cell Open Circuit Voltage (OCV) in the Temperature Range of 23°C to 120°C, » *Journal of Power Sources*, Special Issue Including Selected Papers Presented at the Second International Conference on Polymer Batteries and Fuel Cells Together with Regular Papers, t. 163, n° 1, p. 532-537, 2006, ISSN : 0378-7753. DOI : 10.1016/j.jpowsour.2006.09.026

[2] R. K. Abdul Rasheed et al., « Experimental Investigation of Open Circuit Voltage during Start-up Process of HT-PEMFC, » *Electrochimica Acta*, t. 186, p. 353-358, 2015, ISSN : 0013-4686. DOI : 10.1016/j.electacta.2015.10.157

[3] V. B. Silva et al., « Hydrogen-Fed PEMFC : Overvoltage Analysis during an Activation Procedure, » *Journal of Electroanalytical Chemistry*, t. 671, p. 58-66, 2012, ISSN : 1572-6657. DOI : 10.1016/j.jelechem.2012.02.013

[4] J. Thepkaew et al., « Key parameters of active layers affecting proton exchange membrane (PEM) fuel cell performance, » *Energy*, t. 33, n° 12, p. 1794-1800, 2008, ISSN : 03605442. DOI : 10.1016/j.energy.2008.08.008

[5] L. Xia et al., « Optimization of gas diffusion layer in high temperature PEMFC with the focuses on thickness and porosity, » *Applied Energy*, t. 300, p. 117 357, 2021, ISSN : 03062619. DOI : 10.1016/j.apenergy.2021.117357

[6] J. H. Chun et al., « Numerical modeling and experimental study of the influence of GDL properties on performance in a PEMFC, » *International Journal of Hydrogen Energy*, t. 36, n° 2, p. 1837-1845, 2011, ISSN : 03603199. DOI : 10.1016/j.ijhydene.2010.01.036

[7] F. Cai et al., « Proton Exchange Membrane Fuel Cell (PEMFC) Operation in High Current Density (HCD) : Problem, Progress and Perspective, » *Energy Conversion and Management*, t. 307, p. 118 348, 2024, ISSN : 0196-8904. DOI : 10.1016/j.enconman.2024.118348

[8] D. A. Cullen et al., « New roads and challenges for fuel cells in heavy-duty transportation, » *Nature Energy*, t. 6, n° 5, p. 462-474, 2021, ISSN : 2058-7546. DOI : 10.1038/s41560-021-00775-z

[9] H. Tawfik et al., « Metal bipolar plates for PEM fuel cell—A review, » *Journal of Power Sources*, t. 163, n° 2, p. 755-767, 2007, ISSN : 03787753. DOI : 10.1016/j.jpowsour.2006.09.088

[10] Y. Wang et al., « Fundamentals, materials, and machine learning of polymer electrolyte membrane fuel cell technology, » *Energy and AI*, t. 1, p. 100 014, 2020, ISSN : 26665468. DOI : 10.1016/j.egyai.2020.100014

[11] Z. Xu et al., « Towards mass applications : A review on the challenges and developments in metallic bipolar plates for PEMFC, » *Progress in Natural Science : Materials International*, t. 30, n° 6, p. 815-824, 2020, ISSN : 10020071. DOI : 10.1016/j.pnsc.2020.10.015

[12] K. Xiong et al., « Modeling, design, materials and fabrication of bipolar plates for proton exchange membrane fuel cell : A review, » *Applied Energy*, t. 301, p. 117 443, 2021, ISSN : 03062619. DOI : 10.1016/j.apenergy.2021.117443

[13] V. Velisala et al., « Numerical Simulation and Experimental Comparison of Single, Double and Triple Serpentine Flow Channel Configuration on Performance of a PEM Fuel Cell, » *Arabian Journal for Science and Engineering*, t. 43, n° 3, p. 1225-1234, 2018, ISSN : 2191-4281. DOI : 10.1007/s13369-017-2813-7

[14] R. Boddu et al., « Development of bipolar plates with different flow channel configurations for fuel cells, » *Journal of Power Sources*, t. 189, n° 2, p. 1083-1092, 2009, ISSN : 03787753. DOI : 10.1016/j.jpowsour.2008.12.156

[15] Y. Wu et al., « Effect of Serpentine Flow-Field Design on the Water Management of Polymer Electrolyte Fuel Cells : An in-Operando Neutron Radiography Study, » *Journal of Power Sources*, t. 399, p. 254-263, 2018, ISSN : 0378-7753. DOI : 10.1016/j.jpowsour.2018.07.085

[16] N. Abbaspour, « Numerical and Experimental Approach for Bipolar Plates in PEM Fuel Cells : Novel Designs of Fluid Domain, » PhD Thesis, Université d'Avignon, 2020.

[17] L. Rostami et al., « A 3D CFD Model of Novel Flow Channel Designs Based on the Serpentine and the Parallel Design for Performance Enhancement of PEMFC, » *Energy*, t. 258, p. 124 726, 2022, ISSN : 0360-5442. DOI : 10.1016/j.energy.2022.124726

[18] J. Shen et al., « Evaluation Criterion of Different Flow Field Patterns in a Proton Exchange Membrane Fuel Cell, » *Energy Conversion and Management*, t. 213, p. 112 841, 2020, ISSN : 0196-8904. DOI : 10.1016/j.enconman.2020.112841

[19] H.-C. Chiu et al., « A Three-Dimensional Modeling of Transport Phenomena of Proton Exchange Membrane Fuel Cells with Various Flow Fields, » *Applied Energy*, Smart Grids, t. 96, p. 359-370, 2012, ISSN : 0306-2619. DOI : 10.1016/j.apenergy.2012.02.060

[20] T. Wilberforce et al., « Design Optimization of Proton Exchange Membrane Fuel Cell Bipolar Plate, » *Energy Conversion and Management*, t. 277, p. 116 586, 2023, ISSN : 0196-8904. DOI : 10.1016/j.enconman.2022.116586

[21] D. H. Jeon et al., « The Effect of Serpentine Flow-Field Designs on PEM Fuel Cell Performance, » *International Journal of Hydrogen Energy*, t. 33, n° 3, p. 1052-1066, 2008, ISSN : 0360-3199. DOI : 10.1016/j.ijhydene.2007.11.015

[22] Q. Liu et al., « A review of proton exchange membrane fuel cell's bipolar plate design and fabrication process, » *Journal of Power Sources*, t. 538, p. 231 543, 2022, ISSN : 03787753. DOI : 10.1016/j.jpowsour.2022.231543

[23] T. Henriques et al., « Increasing the Efficiency of a Portable PEM Fuel Cell by Altering the Cathode Channel Geometry : A Numerical and Experimental Study, » *Applied Energy*, t. 87, n° 4, p. 1400-1409, 2010, ISSN : 0306-2619. DOI : 10.1016/j.apenergy.2009.09.001

[24] X.-D. Wang et al., « Numerical Study on Channel Size Effect for Proton Exchange Membrane Fuel Cell with Serpentine Flow Field, » *Energy Conversion and Management*, t. 51, n° 5, p. 959-968, 2010, ISSN : 0196-8904. DOI : 10.1016/j.enconman.2009.11.037

[25] Q. Ding et al., « Performance of Parallel, Interdigitated, and Serpentine Flow Field PEM Fuel Cells with Straight or Wavelike Channels, » *Journal of Energy Engineering*, t. 146, n° 5, p. 04 020 054, 2020, ISSN : 1943-7897. DOI : 10.1061/(ASCE)EY.1943-7897.0000701

[26] Y. Zhou et al., « Optimal Design of a Cathode Flow Field for Performance Enhancement of PEM Fuel Cell, » *Applied Energy*, t. 343, p. 121 226, 2023, ISSN : 0306-2619. DOI : 10.1016/j.apenergy.2023.121226

[27] Z. Zhang et al., « Optimal Design of Locally Improved Structure for Enhancing Mass Transfer in PEMFC Cathode Flow Field, » *International Journal of Hydrogen Energy*, t. 57, p. 798-811, 2024, ISSN : 0360-3199. DOI : 10.1016/j.ijhydene.2024.01.092

[28] X. Gao et al., « Research progress and prospect of the materials of bipolar plates for proton exchange membrane fuel cells (PEMFCs), » *International Journal of Hydrogen Energy*, t. 50, p. 711-743, 2024, ISSN : 03603199. DOI : 10.1016/j.ijhydene.2023.09.005

[29] P. C. Okonkwo et al., « A review of bipolar plates materials and graphene coating degradation mechanism in proton exchange membrane fuel cell, » *International Journal of Energy Research*, t. 46, n° 4, p. 3766-3781, 2022, ISSN : 1099-114X. DOI : 10.1002/er.7428

[30] A. K. Arya et al., « Graphene-Coated Ni–Cu Alloys for Durable Degradation Resistance of Bi-Polar Plates for Proton Exchange Membrane Fuel Cells : Remarkable Role of Alloy Composition, » *Small*, t. 20, n° 39, p. 2 305 320, 2024, ISSN : 1613-6829. DOI : 10.1002/smll.202305320

[31] E. Pahon et al., « A Review of Accelerated Stress Tests Dedicated to Proton Exchange Membrane Fuel Cells – Part I : Fuel Cell Component Level, » *Journal of Power Sources*, t. 546, p. 231 895, 2022, ISSN : 0378-7753. DOI : 10.1016/j.jpowsour.2022.231895

[32] X. Li et al., « Transient Stainless-Steel Dissolution and Its Consequences on *Ex*-Situ Bipolar Plate Testing Procedures, » *International Journal of Hydrogen Energy*, t. 45, n° 1, p. 984-995, 2020, ISSN : 0360-3199. DOI : 10.1016/j.ijhydene.2019.10.191

[33] P. Ren et al., « Corrosion of Metallic Bipolar Plates Accelerated by Operating Conditions in a Simulated PEM Fuel Cell Cathode Environment, » *Renewable Energy*, t. 194, p. 1277-1287, 2022, ISSN : 0960-1481. DOI : 10.1016/j.renene.2022.05.153

[34] F. Lee et al., « Alternative architectures and materials for PEMFC gas diffusion layers : A review and outlook, » *Renewable and Sustainable Energy Reviews*, t. 166, p. 112 640, 2022, ISSN : 13640321. DOI : 10.1016/j.rser.2022.112640

[35] P. Irmscher et al., « Impact of Gas Diffusion Layer Mechanics on PEM Fuel Cell Performance, » *International Journal of Hydrogen Energy*, t. 44, n° 41, p. 23 406-23 415, 2019, ISSN : 0360-3199. DOI : 10.1016/j.ijhydene.2019.07.047

[36] Z. Zhang et al., « Study of the Mechanical Behavior of Paper-Type GDL in PEMFC Based on Microstructure Morphology, » *International Journal of Hydrogen Energy*, t. 45, n° 53, p. 29 379-29 394, 2020, ISSN : 0360-3199. DOI : 10.1016/j.ijhydene.2020.07.240

[37] S.-Y. Jing et al., « Effects of Porosity and Porosity Distribution in Gas Diffusion Layer on the Performances of Proton Exchange Membrane Fuel Cell, » *Journal of Power Sources*, t. 613, p. 234 957, 2024, ISSN : 0378-7753. DOI : 10.1016/j.jpowsour.2024.234957

[38] H. Liu et al., « Investigation on the Optimal GDL Thickness Design for PEMFCs Considering Channel/Rib Geometry Matching and Operating Conditions, » *Energy*, t. 282, p. 128 780, 2023, ISSN : 0360-5442. DOI : 10.1016/j.energy.2023.128780

[39] P. Yang et al., « Effects of Gas Diffusion Layer Porosity Distribution on Proton Exchange Membrane Fuel Cell, » *Energy Technology*, t. 9, n° 7, p. 2 001 012, 2021, ISSN : 2194-4288, 2194-4296. DOI : 10.1002/ente.202001012

[40] S. Park et al., « A Review of Gas Diffusion Layer in PEM Fuel Cells : Materials and Designs, » *International Journal of Hydrogen Energy*, XII International Symposium on Polymer Electrolytes : New Materials for Application in Proton Exchange Membrane Fuel Cells, t. 37, n° 7, p. 5850-5865, 2012, ISSN : 0360-3199. DOI : 10.1016/j.ijhydene.2011.12.148

[41] H. Yang et al., « Carbon Cloth Based on PAN Carbon Fiber Practicability for PEMFC Applications, » *International Journal of Hydrogen Energy*, 2008 International Hydrogen Forum (HyForum2008), t. 35, n° 7, p. 2791-2795, 2010, ISSN : 0360-3199. DOI : 10.1016/j.ijhydene.2009.05.019

[42] A. Vinod et al., « Recent Advancements in Lignocellulose Biomass-Based Carbon Fiber : Synthesis, Properties, and Applications, » *Heliyon*, t. 9, n° 3, e13614, 2023, ISSN : 2405-8440. DOI : 10.1016/j.heliyon.2023.e13614

[43] D. Qiu et al., « Electrical Resistance and Microstructure of Typical Gas Diffusion Layers for Proton Exchange Membrane Fuel Cell under Compression, » *Applied Energy*, t. 231, p. 127-137, 2018, ISSN : 0306-2619. DOI : 10.1016/j.apenergy.2018.09.117

[44] A. El-kharouf et al., « *Ex-Situ* Characterisation of Gas Diffusion Layers for Proton Exchange Membrane Fuel Cells, » *Journal of Power Sources*, t. 218, p. 393-404, 2012, ISSN : 0378-7753. DOI : 10.1016/j.jpowsour.2012.06.099

[45] Y. Zhang et al., « Breaking the Trade-Off Between Electrical Conductivity and Mechanical Strength in Bulk Graphite Using Metal–Organic Framework-Derived Precursors, » *Advanced Science*, t. 12, n° 9, p. 2 416 210, 2025, ISSN : 2198-3844. DOI : 10.1002/advs.202416210

[46] P. Trogadas et al., « Carbon as Catalyst and Support for Electrochemical Energy Conversion, » *Carbon*, t. 75, p. 5-42, 2014, ISSN : 0008-6223. DOI : 10.1016/j.carbon.2014.04.005

[47] H.-F. Lee et al., « Improvement in physical properties of single-layer gas diffusion layers using graphene for proton exchange membrane fuel cells, » *RSC Advances*, t. 8, n° 40, p. 22 506-22 514, 2018. DOI : 10.1039/C8RA02062K

[48] D.-K. Lee et al., « Electrical and Thermal Properties of Carbon Nanotube Polymer Composites with Various Aspect Ratios, » *Materials*, t. 15, n° 4, p. 1356, 2022, ISSN : 1996-1944. DOI : 10.3390/ma15041356

[49] C. Jose et al., « Carbon Nanotubes for Energy Applications, » in *Carbon Nanotubes for Energy and Environmental Applications*, Apple Academic Press, 2022, ISBN : 978-1-003-18961-9.

[50] J. Tang et al., « Carbon Nanotube Free-Standing Membrane as Gas Diffusion Layer in Hydrogen Fuel Cells, » *Micro & Nano Letters*, t. 1, n° 1, p. 62-65, 2006. DOI : 10.1049/mnl:20065030

[51] P. H. Maheshwari et al., « CNT Membrane as a Free Standing Electrode for PEM Fuel Cell, » *Journal of The Electrochemical Society*, t. 161, n° 12, F1146, 2014, ISSN : 1945-7111. DOI : 10.1149/2.0201412jes

[52] X.-F. Zhang et al., « Single-Walled Carbon Nanotube Interlayer Modified Gas Diffusion Layers to Boost the Cell Performance of Self-Humidifying Proton Exchange Membrane Fuel Cells, » *International Journal of Hydrogen Energy*, t. 48, n° 79, p. 30 899-30 908, 2023, ISSN : 0360-3199. DOI : 10.1016/j.ijhydene.2023.04.250

[53] L. Q. Hoa et al., « Carbon-Based Nanomaterials in Biomass-Based Fuel-Fed Fuel Cells, » *Sensors*, t. 17, n° 11, p. 2587, 2017, ISSN : 1424-8220. DOI : 10.3390/s17112587

[54] Y. Zhang et al., « A Metallic Gas Diffusion Layer and Porous Media Flow Field for Proton Exchange Membrane Fuel Cells, » *Journal of Power Sources*, t. 543, p. 231 847, 2022, ISSN : 0378-7753. DOI : 10.1016/j.jpowsour.2022.231847

[55] M. Glora et al., « Integration of Carbon Aerogels in PEM Fuel Cells, » *Journal of Non-Crystalline Solids*, t. 285, n° 1, p. 283-287, 2001, ISSN : 0022-3093. DOI : 10.1016/S0022-3093(01)00468-9

[56] M. Balakrishnan et al., « Designing Tailored Gas Diffusion Layers with Pore Size Gradients via Electrospinning for Polymer Electrolyte Membrane Fuel Cells, » *ACS Applied Energy Materials*, t. 3, n° 3, p. 2695-2707, 2020. DOI : 10.1021/acsaem.9b02371

[57] S. Lan et al., « Comprehensive Analysis on the Influence of Perforated Structure on Mass Transfer and Performance of Gas Diffusion Layer, » *Renewable Energy*, t. 246, p. 122 897, 2025, ISSN : 0960-1481. DOI : 10.1016/j.renene.2025.122897

[58] P. Gallo Stampino et al., « Investigation of Hydrophobic Treatments with Perfluoropolyether Derivatives of Gas Diffusion Layers by Electrochemical Impedance Spectroscopy in PEM-FC, » *Solid State Ionics*, "Fuel Cells-Energy Conversion" Proceedings of Symposium X EMRS Spring Meeting 2011, t. 216, p. 100-104, 2012, ISSN : 0167-2738. DOI : 10.1016/j.ssi.2012.03.032

[59] P. G. Stampino et al., « Surface Treatments with Perfluoropolyether Derivatives for the Hydrophobization of Gas Diffusion Layers for PEM Fuel Cells, » *Journal of Power Sources*, t. 196, n° 18, p. 7645-7648, 2011, ISSN : 0378-7753. DOI : 10.1016/j.jpowsour.2011.04.039

[60] A. Figoli et al., « Innovative Hydrophobic Coating of Perfluoropolyether (PFPE) on Commercial Hydrophilic Membranes for DCMD Application, » *Journal of Membrane Science*, t. 522, p. 192-201, 2017, ISSN : 0376-7388. DOI : 10.1016/j.memsci.2016.08.066

[61] R. Kuwertz et al., « Influence of PTFE Content in Gas Diffusion Layers Used for Gas-Phase Hydrogen Chloride Electrolysis with Oxygen Depolarized Cathode, » *Journal of The Electrochemical Society*, t. 163, n° 9, F988-F997, 2016, ISSN : 0013-4651, 1945-7111. DOI : 10.1149/2.0261609jes

[62] H. Su et al., « The Effect of Gas Diffusion Layer PTFE Content on The Performance of High Temperature Proton Exchange Membrane Fuel Cell, » *International Journal of Electrochemical Science*, t. 11, n° 4, p. 2919-2926, 2016, ISSN : 1452-3981. DOI : 10.1016/S1452-3981(23)16151-7

[63] R. R. Rashapov et al., « Characterization of PEMFC Gas Diffusion Layer Porosity, » *Journal of The Electrochemical Society*, t. 162, n° 6, F603, 2015, ISSN : 1945-7111. DOI : 10.1149/2.0921506jes

[64] T. Chen et al., « Study on the Characteristics of GDL with Different PTFE Content and Its Effect on the Performance of PEMFC, » *International Journal of Heat and Mass Transfer*, t. 128, p. 1168-1174, 2019, ISSN : 0017-9310. DOI : 10.1016/j.ijheatmasstransfer.2018.09.097

[65] N. Alhazmi et al., « The In-Plane Thermal Conductivity and the Contact Resistance of the Components of the Membrane Electrode Assembly in Proton Exchange Membrane Fuel Cells, » *Journal of Power Sources*, t. 241, p. 136-145, 2013, ISSN : 0378-7753. DOI : 10.1016/j.jpowsour.2013.04.100

[66] C.-J. Tseng et al., « Effects of Microstructure Characteristics of Gas Diffusion Layer and Microporous Layer on the Performance of PEMFC, » *Energy Conversion and Management*, t. 51, n° 4, p. 677-684, 2010, ISSN : 0196-8904. DOI : 10.1016/j.enconman.2009.11.011

[67] J. T. Gostick et al., « On the Role of the Microporous Layer in PEMFC Operation, » *Electrochemistry Communications*, t. 11, n° 3, p. 576-579, 2009, ISSN : 1388-2481. DOI : 10.1016/j.elecom.2008.12.053

[68] Y. Yang et al., « Recent Progress of the Gas Diffusion Layer in Proton Exchange Membrane Fuel Cells : Material and Structure Designs of Microporous Layer, » *International Journal of Hydrogen Energy*, t. 46, n° 5, p. 4259-4282, 2021, ISSN : 0360-3199. DOI : 10.1016/j.ijhydene.2020.10.185

[69] Y. Pan et al., « Gas Diffusion Layer Degradation in Proton Exchange Membrane Fuel Cells : Mechanisms, Characterization Techniques and Modelling Approaches, » *Journal of Power Sources*, t. 513, p. 230 560, 2021, ISSN : 0378-7753. DOI : 10.1016/j.jpowsour.2021.230560

[70] A. Lamibrac et al., « Local Degradations Resulting from Repeated Start-ups and Shut-downs in Proton Exchange Membrane Fuel Cell (PEMFC), » *Energy Procedia*, t. 29, p. 318-324, 2012. DOI : 10.1016/j.egypro.2012.09.038

[71] O. Lottin et al., « Experimental Results with Fuel Cell Start-up and Shut-down. Impact of Type of Carbon for Cathode Catalyst Support, » *ECS Transactions*, t. 69, n° 17, p. 1065, 2015, ISSN : 1938-5862. DOI : 10.1149/06917.1065ecst

[72] T. Ha et al., « Experimental Study on Carbon Corrosion of the Gas Diffusion Layer in Polymer Electrolyte Membrane Fuel Cells, » *International Journal of Hydrogen Energy*, t. 36, n° 19, p. 12 436-12 443, 2011, ISSN : 0360-3199. DOI : 10.1016/j.ijhydene.2011.06.098

[73] K. Xu et al., « Degradation Mechanism Analysis of Substrate and Microporous Layer of Gas Diffusion Layer in Proton Exchange Membrane Fuel Cell, » *Fuel*, t. 358, p. 130 198, 2024, ISSN : 0016-2361. DOI : 10.1016/j.fuel.2023.130198

[74] J. Sim et al., « Effects of Carbon Corrosion on Proton Exchange Membrane Fuel Cell Performance Using Two Durability Evaluation Methods, » *Renewable Energy*, t. 190, p. 959-970, 2022, ISSN : 0960-1481. DOI : 10.1016/j.renene.2022.04.015

[75] Z. A. Che Ramli et al., « Evaluating Electrocatalytic Activities of Pt, Pd, Au and Ag-based Catalyst on PEMFC Performance : A Review, » *International Journal of Hydrogen Energy*, t. 104, p. 463-486, 2025, ISSN : 0360-3199. DOI : 10.1016/j.ijhydene.2024.04.177

[76] R. Sgarbi et al., « Impact of Transition Metals and Electrocatalyst Layer Thickness on the Pt-Based Cathodes of Proton Exchange Membrane Fuel Cells – Do Multimetallic Electrocatalysts Necessarily Yield an Improved Performance ? » *Advanced Energy Materials*, t. n/a, n° n/a, p. 2 403 212, ISSN : 1614-6840. DOI : 10.1002/aenm.202403212

[77] L. Dubau et al., « Durability of Pt3Co / C Cathodes in a 16 Cell PEMFC Stack : Macro/Microstructural Changes and Degradation Mechanisms, » *Journal of The Electrochemical Society*, t. 157, n° 12, B1887, 2010, ISSN : 1945-7111. DOI : 10.1149/1.3485104

[78] Q. Labarde et al., « Evaluation of Carbon-Capped PtNi Nanoparticles Supported on Graphitized Carbon Black – from Rotating Disk Electrode to Unit Proton Exchange Membrane Fuel Cell Operated at 95 °C, » *Electrochimica Acta*, t. 537, p. 146 910, 2025, ISSN : 0013-4686. DOI : 10.1016/j.electacta.2025.146910

[79] Z. Zhou et al., « Progress of Pt and Iron-Group Transition Metal Alloy Catalysts with High ORR Activity for PEMFCs, » *Journal of Electroanalytical Chemistry*, t. 959, p. 118 165, 2024, ISSN : 1572-6657. DOI : 10.1016/j.jelechem.2024.118165

[80] S. Sharma et al., « Support Materials for PEMFC and DMFC Electrocatalysts—A Review, » *Journal of Power Sources*, t. 208, p. 96-119, 2012, ISSN : 0378-7753. DOI : 10.1016/j.jpowsour.2012.02.011

[81] S. Shahgaldi et al., « Improved Carbon Nanostructures as a Novel Catalyst Support in the Cathode Side of PEMFC : A Critical Review, » *Carbon*, t. 94, p. 705-728, 2015, ISSN : 0008-6223. DOI : 10.1016/j.carbon.2015.07.055

[82] M. Endo et al., « Microstructural Changes Induced in “Stacked Cup” Carbon Nanofibers by Heat Treatment, » *Carbon*, t. 41, n° 10, p. 1941-1947, 2003, ISSN : 0008-6223. DOI : 10.1016/S0008-6223(03)00171-4

[83] W. S. Jung, « Study on Durability of Pt Supported on Graphitized Carbon under Simulated Start-up/Shut-down Conditions for Polymer Electrolyte Membrane Fuel Cells, » *Journal of Energy Chemistry*, t. 27, n° 1, p. 326-334, 2018, ISSN : 2095-4956. DOI : 10.1016/j.jechem.2017.05.012

[84] Y. Devrim et al., « Investigation of the Effect of Graphitized Carbon Nanotube Catalyst Support for High Temperature PEM Fuel Cells, » *International Journal of Hydrogen Energy*, Hydrogen Energy Technologies for Mitigating Global Warming, t. 45, n° 5, p. 3609-3617, 2020, ISSN : 0360-3199. DOI : 10.1016/j.ijhydene.2019.01.111

[85] H. N. Yang et al., « Effect of Boron-Doping Levels in Pt-B-graphene on the Electrochemical Properties and Cell Performance of High Temperature Proton Exchange Membrane Fuel Cells, » *Electrochimica Acta*, t. 209, p. 430-439, 2016, ISSN : 0013-4686. DOI : 10.1016/j.electacta.2016.05.114

[86] S. Ott et al., « Understanding the Performance Increase of Catalysts Supported on N-Functionalized Carbon in PEMFC Catalyst Layers, » *Journal of The Electrochemical Society*, t. 169, n° 5, p. 054 520, 2022, ISSN : 1945-7111. DOI : 10.1149/1945-7111/ac6e4d

[87] A. Kozhushner et al., « Heteroatom-Doped Carbon Supports with Enhanced Corrosion Resistance in Polymer Electrolyte Membrane Fuel Cells, » *Energies*, t. 16, n° 9, p. 3659, 2023, ISSN : 1996-1073. DOI : 10.3390/en16093659

[88] V. Goellner et al., « Degradation by Hydrogen Peroxide of Metal-Nitrogen-Carbon Catalysts for Oxygen Reduction, » *Journal of The Electrochemical Society*, t. 162, n° 6, H403, 2015, ISSN : 1945-7111. DOI : 10.1149/2.1091506jes

[89] J. Lobato et al., « Enhancement of High Temperature PEMFC Stability Using Catalysts Based on Pt Supported on SiC Based Materials, » *Applied Catalysis B : Environmental*, t. 198, p. 516-524, 2016, ISSN : 0926-3373. DOI : 10.1016/j.apcatb.2016.06.011

[90] A. Pătru et al., « Pt/IrO2–TiO2 Cathode Catalyst for Low Temperature Polymer Electrolyte Fuel Cell – Application in MEAs, Performance and Stability Issues, » *Catalysis Today*, Electrocatalysis, t. 262, p. 161-169, 2016, ISSN : 0920-5861. DOI : 10.1016/j.cattod.2015.09.009

[91] X. Pu et al., « Understanding of Hydrocarbon Ionomers in Catalyst Layers for Enhancing the Performance and Durability of Proton Exchange Membrane Fuel Cells, » *Journal of Power Sources*, t. 493, p. 229 671, 2021, ISSN : 0378-7753. DOI : 10.1016/j.jpowsour.2021.229671

[92] E. Balogun et al., « Catalyst layers for fluorine-free hydrocarbon PEMFCs, » *Electrochimica Acta*, t. 401, p. 139 479, 2022, ISSN : 00134686. DOI : 10.1016/j.electacta.2021.139479

[93] H. Nguyen et al., « Hydrocarbon-based Pemion™ proton exchange membrane fuel cells with state-of-the-art performance, » *Sustainable Energy & Fuels*, t. 5, n° 14, p. 3687-3699, 2021, ISSN : 2398-4902. DOI : 10.1039/D1SE00556A

[94] J. E. Chae et al., « Hydrocarbon-Based Electrode Ionomer for Proton Exchange Membrane Fuel Cells, » *International Journal of Hydrogen Energy*, ICAE 2019 – Symposium 6 : Advanced Materials and Devices for Fuel Cell and Electrolysis Technologies, t. 45, n° 57, p. 32 856-32 864, 2020, ISSN : 0360-3199. DOI : 10.1016/j.ijhydene.2020.03.003

[95] P. A. García-Salaberri et al., « Local oxygen transport resistance in polymer electrolyte fuel cells : origin, dependencies and mitigation, » *Frontiers in Energy Research*, t. 12, 2024, ISSN : 2296-598X. DOI : 10.3389/fenrg.2024.1357325

[96] Z. Wen et al., « Optimization of the Ionomer-to-Carbon Ratio in the Cathode Catalyst Layer of PtCoMn/C Alloy Catalysts, » *International Journal of Electrochemical Science*, t. 18, n° 6, p. 100 152, 2023, ISSN : 1452-3981. DOI : 10.1016/j.ijoes.2023.100152

[97] Y. V. Yakovlev et al., « Ionomer Content Effect on Charge and Gas Transport in the Cathode Catalyst Layer of Proton-Exchange Membrane Fuel Cells, » *Journal of Power Sources*, t. 490, p. 229 531, 2021, ISSN : 0378-7753. DOI : 10.1016/j.jpowsour.2021.229531

[98] Z. Yang et al., « Systematic Study on the Impact of Pt Particle Size and Operating Conditions on PEMFC Cathode Catalyst Durability, » *Journal of The Electrochemical Society*, t. 158, n° 11, B1439, 2011, ISSN : 00134651. DOI : 10.1149/2.081111jes

[99] R. K. Ahluwalia et al., « Achieving 5,000-h and 8,000-h Low-PGM Electrode Durability on Automotive Drive Cycles, » *Journal of The Electrochemical Society*, t. 168, n° 4, p. 044 518, 2021, ISSN : 1945-7111. DOI : 10.1149/1945-7111/abf507

[100] P. C. Okonkwo et al., « Platinum Degradation Mechanisms in Proton Exchange Membrane Fuel Cell (PEMFC) System : A Review, » *International Journal of Hydrogen Energy*, t. 46, n° 29, p. 15 850-15 865, 2021, ISSN : 0360-3199. DOI : 10.1016/j.ijhydene.2021.02.078

[101] L. Dubau et al., « A review of PEM fuel cell durability : materials degradation, local heterogeneities of aging and possible mitigation strategies, » *WIREs Energy and Environment*, t. 3, n° 6, p. 540-560, 2014, ISSN : 2041-840X. DOI : 10.1002/wene.113

[102] B. V.-D. Vion-Dury, « Mécanismes de vieillissement des électrocatalyseurs de pile à combustible de type PEMFC, » PhD Thesis, Université de Grenoble, 2011.

[103] S. Hegde et al., « Automotive PEM Fuel Cell Catalyst Layer Degradation Mechanisms and Characterisation Techniques, Part II : Platinum Degradation, » *International Journal of Hydrogen Energy*, t. 143, p. 179-212, 2025, ISSN : 0360-3199. DOI : 10.1016/j.ijhydene.2025.05.034

[104] F.-Y. Zhang et al., « Quantitative Characterization of Catalyst Layer Degradation in PEM Fuel Cells by X-ray Photoelectron Spectroscopy, » *Electrochimica Acta*, t. 54, n° 16, p. 4025-4030, 2009, ISSN : 0013-4686. DOI : 10.1016/j.electacta.2009.02.028

[105] A. P. Young et al., « Ionomer Degradation in Polymer Electrolyte Membrane Fuel Cells, » *Journal of The Electrochemical Society*, t. 157, n° 3, B425, 2010, ISSN : 1945-7111. DOI : 10.1149/1.3281899

[106] Y. Xiao et al., « Degradation Behavior of Ionomer in the Cathode Catalyst Layer of Polymer Electrolyte Fuel Cells, » *Applied Energy*, t. 389, p. 125 759, 2025, ISSN : 0306-2619. DOI : 10.1016/j.apenergy.2025.125759

[107] T. Morawietz et al., « High-Resolution Analysis of Ionomer Loss in Catalytic Layers after Operation, » *Journal of The Electrochemical Society*, t. 165, n° 6, F3139, 2018, ISSN : 1945-7111. DOI : 10.1149/2.0151806jes

[108] F. Chabot, « Analyse de la structure et des propriétés du conducteur protonique des électrodes de PEMFC par diffusion de neutrons aux petits angles et par électrochimie : impact des cycles accélérés de dégradations, » PhD Thesis, Université Grenoble Alpes, 2022.

[109] A. El Kaddouri, « Mise En Évidcence de La Dégradation Du Liant Ionomère Dans Les Électrodes de Pile à Combustible, » PhD Thesis, Université de Grenoble, 2014.

[110] E. Colombo et al., « An Innovative Accelerated Stress Test Representative of Automotive PEMFC Degradation Mechanisms Validated on 1000 Hours Real-World Operation, » *Journal of Power Sources*, t. 580, p. 233 376, 2023, ISSN : 0378-7753. DOI : 10.1016/j.jpowsour.2023.233376

[111] F. Du et al., « Effects of PEMFC Operational History under Dry/Wet Conditions on Additional Voltage Losses due to Ionomer Migration, » *Journal of The Electrochemical Society*, t. 167, n° 14, p. 144 513, 2020, ISSN : 1945-7111. DOI : 10.1149/1945-7111/abc83f

[112] Y. Yin et al., « Ionomer Migration within PEMFC Catalyst Layers Induced by Humidity Changes, » *Electrochemistry Communications*, t. 109, p. 106 590, 2019, ISSN : 1388-2481. DOI : 10.1016/j.elecom.2019.106590

[113] C. Yue et al., « Decomposition on the Degradation Mechanism of the Cathode Catalyst Layer under 1000 h of On-Road Heavy-Duty Transportation, » *Journal of Energy Storage*, t. 104, p. 114 426, 2024, ISSN : 2352-152X. DOI : 10.1016/j.est.2024.114426

[114] M. Haque et al., « Navigating Challenges and Possibilities for Improving Polymer Electrolyte Membrane Fuel Cells via Pt Electrocatalyst, Support and Ionomer Advancements, » *International Journal of Hydrogen Energy*, t. 85, p. 30-47, 2024, ISSN : 0360-3199. DOI : 10.1016/j.ijhydene.2024.08.323

[115] B. Smitha et al., « Solid Polymer Electrolyte Membranes for Fuel Cell Applications—a Review, » *Journal of Membrane Science*, t. 259, n° 1, p. 10-26, 2005, ISSN : 0376-7388. DOI : 10.1016/j.memsci.2005.01.035

[116] S. J. Peighambardoust et al., « Review of the Proton Exchange Membranes for Fuel Cell Applications, » *International Journal of Hydrogen Energy*, t. 35, n° 17, p. 9349-9384, 2010, ISSN : 0360-3199. DOI : 10.1016/j.ijhydene.2010.05.017

[117] X. Luo et al., « Water, proton, and oxygen transport in high IEC, short side chain PFSA ionomer membranes : consequences of a frustrated network, » *Physical Chemistry Chemical Physics*, t. 13, n° 40, p. 18 055-18 062, 2011, ISSN : 1463-9084. DOI : 10.1039/C1CP22559F

[118] E. Moukheiber et al., « Investigation of Ionomer Structure through Its Dependence on Ion Exchange Capacity (IEC), » *Journal of Membrane Science*, t. 389, p. 294-304, 2012, ISSN : 0376-7388. DOI : 10.1016/j.memsci.2011.10.041

[119] S. Banerjee et al., « Impact of degree of sulfonation on microstructure, thermal, thermomechanical and physicochemical properties of sulfonated poly ether ether ketone, » *Polymer*, t. 109, p. 176-186, 2017, ISSN : 00323861. DOI : 10.1016/j.polymer.2016.12.030

[120] H. Eskandari et al., « Humidity-Dependent Hydration and Proton Conductivity of PFSA Ionomer Thin Films at Fuel-Cell-Relevant Temperatures : Effect of Ionomer Equivalent Weight and Side-Chain Characteristics, » *ACS Applied Materials & Interfaces*, t. 14, n° 45, p. 50 762-50 772, 2022, ISSN : 1944-8244. DOI : 10.1021/acsami.2c12667

[121] K. Takeuchi et al., « Hydrogen Permeation in Hydrated Perfluorosulfonic Acid Polymer Membranes : Effect of Polymer Crystallinity and Equivalent Weight, » *The Journal of Physical Chemistry C*, t. 123, n° 33, p. 20 628-20 638, 2019, ISSN : 1932-7447. DOI : 10.1021/acs.jpcc.9b05502

[122] S. J. Hamrock et al., « Proton Exchange Membranes for Fuel Cell Applications, » *Journal of Macromolecular Science, Part C*, t. 46, n° 3, p. 219-244, 2006, ISSN : 1532-1797. DOI : 10.1080/15583720600796474

[123] M. J. Parnian et al., « Comprehensive investigation of physicochemical and electrochemical properties of sulfonated poly (ether ether ketone) membranes with different degrees of sulfonation for proton exchange membrane fuel cell applications, » *Energy*, t. 125, p. 614-628, 2017, ISSN : 03605442. DOI : 10.1016/j.energy.2017.02.143

[124] S. Subianto et al., « Physical and chemical modification routes leading to improved mechanical properties of perfluorosulfonic acid membranes for PEM fuel cells, » *Journal of Power Sources*, t. 233, p. 216-230, 2013, ISSN : 03787753. DOI : 10.1016/j.jpowsour.2012.12.121

[125] B. Zhou et al., « Proton Exchange Membranes Based on Semi-Interpenetrating Polymer Networks of Nafion® and Poly(Vinylidene Fluoride) via Radiation Crosslinking, » *International Journal of Hydrogen Energy*, t. 36, n° 11, p. 6809-6816, 2011, ISSN : 0360-3199. DOI : 10.1016/j.ijhydene.2011.02.115

[126] H. Hou et al., « Crosslinked SPEEK membranes : Mechanical, thermal, and hydrothermal properties, » *Journal of Materials Research*, t. 27, n° 15, p. 1950-1957, 2012, ISSN : 0884-2914, 2044-5326. DOI : 10.1557/jmr.2012.151

[127] S. Siracusano et al., « Reinforced Short-Side-Chain Aquivion® Membrane for Proton Exchange Membrane Water Electrolysis, » *International Journal of Hydrogen Energy*, t. 47, n° 35, p. 15 557-15 570, 2022, ISSN : 0360-3199. DOI : 10.1016/j.ijhydene.2022.03.061

[128] M. S. Mu'min et al., « Electrospun Phosphonated Poly(Pentafluorostyrene) Nanofibers as a Reinforcement of Nafion Membranes for Fuel Cell Application, » *Journal of Membrane Science*, t. 685, p. 121 915, 2023, ISSN : 0376-7388. DOI : 10.1016/j.memsci.2023.121915

[129] Z. Rao et al., « Proton Conductivity of Proton Exchange Membrane Synergistically Promoted by Different Functionalized Metal–Organic Frameworks, » *ACS Applied Materials & Interfaces*, t. 9, n° 27, p. 22 597-22 603, 2017, ISSN : 1944-8244. DOI : 10.1021/acsami.7b05969

[130] N. Thmaini et al., « Nanoarchitectonics of Fibrous Clays as Fillers of Improved Proton-Conducting Membranes for Fuel-Cell Applications, » *Applied Clay Science*, t. 242, p. 107 019, 2023, ISSN : 0169-1317. DOI : 10.1016/j.clay.2023.107019

[131] Z. Rui et al., « Understanding of Free Radical Scavengers Used in Highly Durable Proton Exchange Membranes, » *Progress in Natural Science : Materials International*, t. 30, n° 6, p. 732-742, 2020, ISSN : 1002-0071. DOI : 10.1016/j.pnsc.2020.08.013

[132] X. Liu et al., « Durability enhancement of proton exchange membrane fuel cells by ferrocyanide or ferricyanide additives, » *Journal of Membrane Science*, t. 629, p. 119 282, 2021, ISSN : 03767388. DOI : 10.1016/j.memsci.2021.119282

[133] F. D. Bruijn et al., « Review : durability and degradation issues of pem fuel cell components, » *Fuel Cells*, t. 8, n° 1, p. 3-22, DOI : 10.1002/fuce.200700053

[134] M. Robert, « Impact of Degradation and Aging on Properties of PFSA Membranes for Fuel Cells, » PhD thesis, Université de Lorraine, 2021.

[135] M. Daoudi, « Performances et Durabilité Des Membranes Alternatives Aux Membranes PFSA, » PhD Thesis, Université de Lorraine, 2023.

[136] M. Zatoń et al., « Current understanding of chemical degradation mechanisms of perfluorosulfonic acid membranes and their mitigation strategies : a review, » *Sustainable Energy & Fuels*, t. 1, n° 3, p. 409-438, 2017. DOI : 10.1039/C7SE00038C

[137] A. B. LaConti et al., « Mechanisms of membrane degradation, » in *Handbook of Fuel Cells*, John Wiley & Sons, Ltd, 2010, ISBN : 978-0-470-97400-1.

[138] C. Perrot, « Mécanismes de dégradation des membranes polyaromatiques sulfonées en pile à combustible, » PhD Thesis, Université Joseph-Fourier - Grenoble I, 2006.

[139] M. P. Rodgers et al., « Fuel Cell Perfluorinated Sulfonic Acid Membrane Degradation Correlating Accelerated Stress Testing and Lifetime, » *Chemical Reviews*, t. 112, n° 11, p. 6075-6103, 2012, ISSN : 0009-2665. DOI : 10.1021/cr200424d

[140] A. Pozio et al., « Nafion Degradation in PEFCs from End Plate Iron Contamination, » *Electrochimica Acta*, t. 48, n° 11, p. 1543-1549, 2003, ISSN : 0013-4686. DOI : 10.1016/S0013-4686(03)00026-4

[141] L. Ghassemzadeh et al., « Chemical Degradation of Nafion Membranes under Mimic Fuel Cell Conditions as Investigated by Solid-State NMR Spectroscopy, » *The Journal of Physical Chemistry C*, t. 114, n° 34, p. 14 635-14 645, 2010, ISSN : 1932-7447. DOI : 10.1021/jp102533v

[142] J. Li et al., « Understanding the Short-Side-Chain Perfluorinated Sulfonic Acid and Its Application for High Temperature Polymer Electrolyte Membrane Fuel Cells, » *RSC Advances*, t. 4, p. 3944-3965, 2014. DOI : 10.1039/c3ra43735c

[143] S. Shahgaldi et al., « The impact of short side chain ionomer on polymer electrolyte membrane fuel cell performance and durability, » *Applied Energy*, t. 217, p. 295-302, 2018, ISSN : 03062619. DOI : 10.1016/j.apenergy.2018.02.154

[144] K. Talukdar et al., « Comparative investigation into the performance and durability of long and short side chain ionomers in Polymer Electrolyte Membrane Fuel Cells, » *Journal of Power Sources*, t. 439, p. 227 078, 2019, ISSN : 03787753. DOI : 10.1016/j.jpowsour.2019.227078

[145] G. Hübner et al., « EPR investigation of HO / radical initiated degradation reactions of sulfonated aromatics as model compounds for fuel cell proton conducting membranes, » *Journal of Materials Chemistry*, t. 9, n° 2, p. 409-418, 1999. DOI : 10.1039/A807129B

[146] L. Gubler et al., « Perspective—Prospects for Durable Hydrocarbon-Based Fuel Cell Membranes, » *Journal of The Electrochemical Society*, t. 165, n° 6, F3100, 2018, ISSN : 1945-7111. DOI : 10.1149/2.0131806jes

[147] J. Lawrence et al., « The Degradation Mechanism of Sulfonated Poly(Arylene Ether Sulfone)s in an Oxidative Environment, » *Journal of Membrane Science*, t. 325, n° 2, p. 633-640, 2008, ISSN : 0376-7388. DOI : 10.1016/j.memsci.2008.08.027

[148] A. Panchenko, « DFT investigation of the polymer electrolyte membrane degradation caused by OH radicals in fuel cells, » *Journal of Membrane Science*, t. 278, n° 1-2, p. 269-278, 2006, ISSN : 0376-7388. DOI : 10.1016/j.memsci.2005.11.010

[149] G. A. Futter et al., « Physical Modeling of Chemical Membrane Degradation in Polymer Electrolyte Membrane Fuel Cells : Influence of Pressure, Relative Humidity and Cell Voltage, » *Journal of Power Sources*, t. 410–411, p. 78-90, 2019, ISSN : 0378-7753. DOI : 10.1016/j.jpowsour.2018.10.085

[150] K. Hongsirikarn et al., « Effect of H2O2 on Nafion® Properties and Conductivity at Fuel Cell Conditions, » *Journal of Power Sources*, t. 196, n° 6, p. 3060-3072, 2011, ISSN : 0378-7753. DOI : 10.1016/j.jpowsour.2010.11.133

[151] G. Etienne et al., « On the Main Factors Limiting the Performance of State-of-the-Art Polymer Electrolyte Membrane Fuel Cells in the 90–100 °C Temperature Range, » *Electrochimica Acta*, t. 541, p. 147 320, 2025, ISSN : 0013-4686. DOI : 10.1016/j.electacta.2025.147320

[152] A. Kusoglu et al., « New Insights into Perfluorinated Sulfonic-Acid Ionomers, » *Chemical Reviews*, t. 117, n° 3, p. 987-1104, 2017, ISSN : 0009-2665. DOI : 10.1021/acs.chemrev.6b00159

[153] S. Shi et al., « Impact of hygrothermal aging on structure/function relationship of perfluorosulfonic-acid membrane, » *Journal of Polymer Science Part B : Polymer Physics*, t. 54, n° 5, p. 570-581, 2016, ISSN : 1099-0488. DOI : 10.1002/polb.23946

[154] F. M. Collette et al., « Hygrothermal aging of Nafion®, » *Journal of Membrane Science*, t. 330, n° 1-2, p. 21-29, 2009, ISSN : 03767388. DOI : 10.1016/j.memsci.2008.11.048

[155] S. M. Clapham et al., « Degradation of Perfluorosulfonic Acid Membrane Water Permeance via Formation of Sulfonic Acid Anhydrides, » *ECS Transactions*, t. 50, n° 2, p. 1011, 2013, ISSN : 1938-5862. DOI : 10.1149/05002.1011ecst

[156] S. Naudy et al., « Influence of Hygrothermal Aging on the Gas and Water Transport Properties of Nafion® Membranes, » *Journal of Membrane Science*, t. 451, p. 293-304, 2014, ISSN : 0376-7388. DOI : 10.1016/j.memsci.2013.10.013

[157] B. T. Huang et al., « Experimental Investigation of Air Relative Humidity (RH) Cycling Tests on MEA/Cell Aging in PEMFC Part I : Study of High RH Cycling Test With air RH at 62%/100%, » *Fuel Cells*, t. 12, n° 3, p. 335-346, 2012, ISSN : 1615-6846, 1615-6854. DOI : 10.1002/fuce.201100060

[158] S. Touhami et al., « Anode aging in polymer electrolyte membrane fuel Cells I : Anode monitoring by ElectroChemical impedance spectroscopy, » *Journal of Power Sources*, t. 481, p. 228 908, 2021, ISSN : 03787753. DOI : 10.1016/j.jpowsour.2020.228908

[159] W. Aït-Idir, « Performance et durabilité des piles à combustible basse température à faible chargement en platine, » PhD Thesis, Université de Lorraine, 2024.

[160] H. Tang et al., « A Degradation Study of Nafion Proton Exchange Membrane of PEM Fuel Cells, » *Journal of Power Sources*, t. 170, n° 1, p. 85-92, 2007, ISSN : 0378-7753. DOI : 10.1016/j.jpowsour.2007.03.061

[161] D. Qiu et al., « Mechanical failure and mitigation strategies for the membrane in a proton exchange membrane fuel cell, » *Renewable and Sustainable Energy Reviews*, t. 113, p. 109 289, 2019, ISSN : 13640321. DOI : 10.1016/j.rser.2019.109289

[162] S. Han et al., « Investigation of Mechanical Degradation in Catalyst-Coated Reinforced Membranes under in-Situ Hydrothermal Cycles, » *International Journal of Hydrogen Energy*, t. 58, p. 279-288, 2024, ISSN : 0360-3199. DOI : 10.1016/j.ijhydene.2024.01.131

[163] Y.-H. Lai et al., « Viscoelastic Stress Model and Mechanical Characterization of Perfluorosulfonic Acid (PFSA) Polymer Electrolyte Membranes, » in *ASME 2005 3rd International Conference on Fuel Cell Science, Engineering and Technology*, American Society of Mechanical Engineers Digital Collection, 2008, p. 161-167. DOI : 10.1115/FUELCELL2005-74120

[164] B. Wu et al., « The degradation study of Nafion/PTFE composite membrane in PEM fuel cell under accelerated stress tests, » *International Journal of Hydrogen Energy*, t. 39, n° 26, p. 14 381-14 390, 2014, ISSN : 03603199. DOI : 10.1016/j.ijhydene.2014.02.142

[165] S. H. Mirfarsi et al., « Study of mechanical degradation of sulfonated poly (ether ether ketone) membrane using ex-situ hygrothermal cycles for polymer electrolyte fuel cell application, » *Journal of Power Sources*, t. 401, p. 73-84, 2018, ISSN : 03787753. DOI : 10.1016/j.jpowsour.2018.08.067

[166] S. R. Choi et al., « Assessing the Degradation Pattern and Mechanism of Membranes in Polymer Electrolyte Membrane Fuel Cells Using Open-Circuit Voltage Hold and Humidity Cycle Test Protocols, » *Materials Science for Energy Technologies*, t. 5, p. 66-73, 2022, ISSN : 2589-2991. DOI : 10.1016/j.mset.2021.12.001

[167] B. T. Huang et al., « Experimental Investigation of Air Relative Humidity (RH) Cycling Tests on MEA/Cell Aging in PEMFC Part II : Study of Low RH Cycling Test with Air RH at 62%/0%, » *Fuel Cells*, t. 12, n° 3, p. 347-355, 2012, ISSN : 1615-6846, 1615-6854. DOI : 10.1002/fuce.201100061

[168] S. Wasterlain et al., « Study of Temperature, Air Dew Point Temperature and Reactant Flow Effects on Proton Exchange Membrane Fuel Cell Performances Using Electrochemical Spectroscopy and Voltammetry Techniques, » *Journal of Power Sources*, t. 195, n° 4, p. 984-993, 2010, ISSN : 0378-7753. DOI : 10.1016/j.jpowsour.2009.08.084

[169] D. N. Ozen et al., « Effects of Operation Temperature and Reactant Gas Humidity Levels on Performance of PEM Fuel Cells, » *Renewable and Sustainable Energy Reviews*, t. 59, p. 1298-1306, 2016, ISSN : 1364-0321. DOI : 10.1016/j.rser.2016.01.040

[170] N. Ge et al., « Membrane Dehydration with Increasing Current Density at High Inlet Gas Relative Humidity in Polymer Electrolyte Membrane Fuel Cells, » *Journal of Power Sources*, t. 422, p. 163-174, 2019, ISSN : 0378-7753. DOI : 10.1016/j.jpowsour.2019.03.001

[171] A. J. .-. Kadjo et al., « Improvement of Proton Exchange Membrane Fuel Cell Electrical Performance by Optimization of Operating Parameters and Electrodes Preparation, » *Journal of Power Sources*, t. 172, n° 2, p. 613-622, 2007, ISSN : 0378-7753. DOI : 10.1016/j.jpowsour.2007.05.019

[172] Q. Yan et al., « Steady State and Dynamic Performance of Proton Exchange Membrane Fuel Cells (PEMFCs) under Various Operating Conditions and Load Changes, » *Journal of Power Sources*, t. 161, n° 1, p. 492-502, 2006, ISSN : 0378-7753. DOI : 10.1016/j.jpowsour.2006.03.077

[173] H. Askaripour, « Effect of Operating Conditions on the Performance of a PEM Fuel Cell, » *International Journal of Heat and Mass Transfer*, t. 144, p. 118 705, 2019, ISSN : 0017-9310. DOI : 10.1016/j.ijheatmasstransfer.2019.118705

[174] T. Yin et al., « Experimental Investigation and Comprehensive Analysis of Performance and Membrane Electrode Assembly Parameters for Proton Exchange Membrane Fuel Cell at High Operating Temperature, » *Energy Conversion and Management*, t. 315, p. 118 740, 2024, ISSN : 0196-8904. DOI : 10.1016/j.enconman.2024.118740

[175] Q. Wang et al., « Dynamic Thermal and Mass Transport in PEM Fuel Cells at Elevated Temperatures and Pressures : A 3D Model Study, » *Fuel*, t. 381, p. 133 623, 2025, ISSN : 0016-2361. DOI : 10.1016/j.fuel.2024.133623

[176] M. Murthy et al., « The Effect of Temperature and Pressure on the Performance of a PEMFC Exposed to Transient CO Concentrations, » *Journal of The Electrochemical Society*, t. 150, n° 1, A29, 2002, ISSN : 1945-7111. DOI : 10.1149/1.1522383

[177] H. Chen et al., « Influencing Sensitivities of Critical Operating Parameters on PEMFC Output Performance and Gas Distribution Quality under Different Electrical Load Conditions, » *Applied Energy*, t. 255, p. 113 849, 2019, ISSN : 0306-2619. DOI : 10.1016/j.apenergy.2019.113849

[178] J. Zhang et al., « Experimental and Numerical Simulation Study of Oxygen Transport in Proton Exchange Membrane Fuel Cells at Intermediate Temperatures (80 °C–120 °C), » *Membranes*, t. 14, n° 4, p. 72, 2024, ISSN : 2077-0375. DOI : 10.3390/membranes14040072

[179] Bird Robert Byron, *Transport Phenomena*, Revised 2nd edition. New York [etc : John Wiley & Sons, Inc., 2007, ISBN : 978-0-470-11539-8.

[180] M. Butori et al., « The Effect of Oxygen Partial Pressure and Humidification in Proton Exchange Membrane Fuel Cells at Intermediate Temperature (80–120 °C), » *Journal of Power Sources*, t. 563, p. 232 803, 2023, ISSN : 0378-7753. DOI : 10.1016/j.jpowsour.2023.232803

[181] H. Xu et al., « Effect of Elevated Temperature and Reduced Relative Humidity on ORR Kinetics for PEM Fuel Cells, » *Journal of The Electrochemical Society*, t. 152, n° 9, A1828, 2005, ISSN : 1945-7111. DOI : 10.1149/1.1984351

[182] K. Kakinuma et al., « The Possibility of Intermediate–Temperature (120 °C)–Operated Polymer Electrolyte Fuel Cells using Perfluorosulfonic Acid Polymer Membranes, » *Journal of The Electrochemical Society*, t. 169, n° 4, p. 044 522, 2022, ISSN : 0013-4651, 1945-7111. DOI : 10.1149/1945-7111/ac624b

[183] J. Zhang et al., « PEM fuel cells operated at 0% relative humidity in the temperature range of 23–120°C, » *Electrochimica Acta*, t. 52, n° 15, p. 5095-5101, 2007, ISSN : 00134686. DOI : 10.1016/j.electacta.2007.02.002

[184] J. Zhang et al., « PEM fuel cell relative humidity (RH) and its effect on performance at high temperatures, » *Electrochimica Acta*, t. 53, n° 16, p. 5315-5321, 2008, ISSN : 00134686. DOI : 10.1016/j.electacta.2008.02.074

[185] S. Nakamura et al., « The Diffusion Overpotential Increase and Appearance of Overlapping Arcs on the Nyquist Plots in the Low Humidity Temperature Test Conditions of Polymer Electrolyte Fuel Cell, » *Journal of Power Sources*, t. 186, n° 2, p. 278-285, 2009, ISSN : 0378-7753. DOI : 10.1016/j.jpowsour.2008.10.022

[186] M. M. Saleh et al., « Exploring the Effects of Symmetrical and Asymmetrical Relative Humidity on the Performance of H2/Air PEM Fuel Cell at Different Temperatures, » *Journal of Power Sources*, t. 164, n° 2, p. 503-509, 2007, ISSN : 0378-7753. DOI : 10.1016/j.jpowsour.2006.11.065

[187] D. Chen et al., « High-Temperature Performance and Degradation Mechanisms of Proton Exchange Membrane Fuel Cells : Experimental Investigation at 95–105, » *Applied Thermal Engineering*, t. 280, p. 128 341, 2025, ISSN : 1359-4311. DOI : 10.1016/j.applthermaleng.2025.128341

[188] Y. Lu et al., « Unveiling Stack-Level Performance Heterogeneity in Proton Exchange Membrane Fuel Cells under Elevated Temperature and Pressure Conditions, » *Electrochimica Acta*, t. 537, p. 146 854, 2025, ISSN : 0013-4686. DOI : 10.1016/j.electacta.2025.146854

[189] F. Nandjou et al., « Impact of Heat and Water Management on Proton Exchange Membrane Fuel Cells Degradation in Automotive Application, » *Journal of Power Sources*, t. 326, p. 182-192, 2016, ISSN : 0378-7753. DOI : 10.1016/j.jpowsour.2016.07.004

[190] T. Tian et al., « Accelerated life-time test of MEA durability under vehicle operating conditions in PEM fuel cell, » *Frontiers in Energy*, t. 11, n° 3, p. 326-333, 2017, ISSN : 2095-1701, 2095-1698. DOI : 10.1007/s11708-017-0489-z

[191] B. Eriksson et al., « The effect of temperature and load as a stressor for proton exchange membrane fuel cells durability at intermediate temperatures, » *Journal of Power Sources*, t. 658, p. 238 258, 2025, ISSN : 03787753. DOI : 10.1016/j.jpowsour.2025.238258

[192] Y. Lu et al., « Degradation Mechanism Analysis of a Fuel Cell Stack Based on Perfluoro Sulfonic Acid Membrane in Near-Water Boiling Temperature Environment, » *Renewable Energy*, t. 234, p. 121 166, 2024, ISSN : 0960-1481. DOI : 10.1016/j.renene.2024.121166

[193] S. Shi et al., « The Role of Temperature in Mechanical Degradation of Catalyst Coated Membrane in Fuel Cell : A 4D in-Situ Investigation Based on X-ray Computed Tomography, » *Applied Energy*, t. 393, p. 126 098, 2025, ISSN : 0306-2619. DOI : 10.1016/j.apenergy.2025.126098

[194] N. Trogisch et al., « Degradation of Automotive PEM Fuel Cells under Accelerated Stress Tests – The Effect of High Operating Temperature, » *Journal of Power Sources*, t. 649, p. 237 408, 2025, ISSN : 0378-7753. DOI : 10.1016/j.jpowsour.2025.237408

[195] M. Butori et al., « Ionic Conductivity and Hydrogen Crossover for IT-PEMFCs : Influence of Pressure, Temperature, Relative Humidity and Reinforcement, » *International Journal of Hydrogen Energy*, t. 95, p. 1158-1170, 2024, ISSN : 0360-3199. DOI : 10.1016/j.ijhydene.2024.06.286

[196] M. N. Akhtar et al., « Multi-Component MWCNT/NG/EP-based Bipolar Plates with Enhanced Mechanical and Electrical Characteristics Fabricated by Compression Moulding, » *Ceramics International*, t. 44, n° 12, p. 14 457-14 464, 2018, ISSN : 0272-8842. DOI : 10.1016/j.ceramint.2018.05.059

[197] T. Husaini et al., « Effect of Temperature on the Mechanical Performance of Highly Conductive Composites for HT-PEMFC Application, » *Jurnal Kejuruteraan*, t. SI1, p. 25-30, 2018. doi : 10.17576/jkukm-2018-si1(1)-04

[198] A. Ghosh et al., « Carbon-Polymer Composite Bipolar Plate for HT-PEMFC, » *Fuel Cells*, t. 14, n° 2, p. 259-265, 2014, issn : 1615-6854. doi : 10.1002/fuce.201300186

[199] H.-Q. Fan et al., « Solution Acidity and Temperature Induced Anodic Dissolution and Degradation of Through-Plane Electrical Conductivity of Au/TiN Coated Metal Bipolar Plates Used in PEMFC, » *Energy*, t. 254, p. 124 453, 2022, issn : 0360-5442. doi : 10.1016/j.energy.2022.124453

[200] S. Banerjee et al., « Impact of Graphite on Thermomechanical, Mechanical, Thermal, Electrical Properties, and Thermal Conductivity of HDPE/Copper Composites, » *Fuel Cells*, t. 20, n° 2, p. 116-130, 2020, issn : 1615-6854. doi : 10.1002/fuce.201900004

[201] H. Sadeghifar et al., « Thermal Conductivity of a Graphite Bipolar Plate (BPP) and Its Thermal Contact Resistance with Fuel Cell Gas Diffusion Layers : Effect of Compression, PTFE, Micro Porous Layer (MPL), BPP out-of-Flatness and Cyclic Load, » *Journal of Power Sources*, t. 273, p. 96-104, 2015, issn : 0378-7753. doi : 10.1016/j.jpowsour.2014.09.062

[202] Y. Yang et al., « Factors Affecting Corrosion Behavior of SS316L as Bipolar Plate Material in PEMFC Cathode Environments, » *International Journal of Hydrogen Energy*, ICCE-2011, t. 37, n° 18, p. 13 822-13 828, 2012, issn : 0360-3199. doi : 10.1016/j.ijhydene.2012.04.026

[203] C. Jin et al., « Temperature-Relevant Degradation in Amorphous Carbon Coated SS316L Bipolar Plates for PEMFC, » *Surface and Coatings Technology*, t. 484, p. 130 767, 2024, issn : 0257-8972. doi : 10.1016/j.surfcoat.2024.130767

[204] K. Eom et al., « Optimization of GDLs for High-Performance PEMFC Employing Stainless Steel Bipolar Plates, » *International Journal of Hydrogen Energy*, t. 38, n° 14, p. 6249-6260, 2013, issn : 0360-3199. doi : 10.1016/j.ijhydene.2012.12.061

[205] A. Chandan, « Investigating Electrodes for Intermediate Temperature Polymer Electrolyte Fuel Cell (IT-PEFC) : GDL Material Properties and their Influence, » in *5th European PEFC & H2 Forum*, 2015.

[206] A. Nishimura et al., « Heat and Mass Transfer Analysis in Single Cell of PEFC Using Different PEM and GDL at Higher Temperature, » *International Journal of Hydrogen Energy*, The 2nd International Symposium on Hydrogen Energy and Energy Technologies (HEET-2018), t. 44, n° 56, p. 29 631-29 640, 2019, issn : 0360-3199. doi : 10.1016/j.ijhydene.2019.05.192

[207] S. Lal et al., « Determination of Water Evaporation Rates in Gas Diffusion Layers of Fuel Cells, » *Journal of The Electrochemical Society*, t. 165, n° 9, F652, 2018, issn : 1945-7111. doi : 10.1149/2.0831809jes

[208] A. Nishimura et al., « Impact of Microporous Layer on Heat and Mass Transfer in a Single Cell of Polymer Electrolyte Fuel Cell Using a Thin Polymer Electrolyte Membrane and a Thin Gas Diffusion Layer Operated at a High-Temperature Range, » *ACS Omega*, t. 6, n° 22, p. 14 575-14 584, 2021. doi : 10.1021/acsomega.1c01693

[209] K. Yildirim et al., « 30 μm Thin Anode Gas Diffusion Layers for Optimized PEM Fuel Cell Operation at 120 °C and Low Relative Humidity, » *Advanced Energy and Sustainability Research*, t. 5, n° 2, p. 2 300 179, 2024, issn : 2699-9412. doi : 10.1002/aesr.202300179

[210] Y. Chen et al., « An Investigation of the Compressive Behavior of Polymer Electrode Membrane Fuel Cell's Gas Diffusion Layers under Different Temperatures, » *Polymers*, t. 10, n° 9, p. 971, 2018, issn : 2073-4360. doi : 10.3390/polym10090971

[211] J. Wu et al., « In situ accelerated degradation of gas diffusion layer in proton exchange membrane fuel cellPart I : Effect of elevated temperature and flow rate, » *Journal of Power Sources*, t. 195, n° 7, p. 1888-1894, 2010, ISSN : 03787753. DOI : 10.1016/j.jpowsour.2009.10.022

[212] Y. Chen et al., « Impact of through-plane gas diffusion layer holes on fuel cell membrane durability deciphered by four-dimensional in-situ X-ray computed tomography visualization, » *Journal of Power Sources*, t. 652, p. 237 627, 2025, ISSN : 03787753. DOI : 10.1016/j.jpowsour.2025.237627

[213] Y. Garsany et al., « Improving PEMFC Performance Using Short-Side-Chain Low-Equivalent-Weight PFSA Ionomer in the Cathode Catalyst Layer, » *Journal of The Electrochemical Society*, t. 165, n° 5, F381, 2018, ISSN : 1945-7111. DOI : 10.1149/2.1361805jes

[214] T. Li et al., « Performance Comparison of Proton Exchange Membrane Fuel Cells with Nafion and Aquivion Perfluorosulfonic Acids with Different Equivalent Weights as the Electrode Binders, » *ACS Omega*, t. 5, n° 28, p. 17 628-17 636, 2020. DOI : 10.1021/acsomega.0c02110

[215] Y. Jeon et al., « Temperature-dependent performance of the polymer electrolyte membrane fuel cell using short-side-chain perfluorosulfonic acid ionomer, » *International Journal of Hydrogen Energy*, t. 39, n° 22, p. 11 690-11 699, 2014, ISSN : 03603199. DOI : 10.1016/j.ijhydene.2014.05.105

[216] H. Nguyen et al., « Improving the efficiency of fully hydrocarbon-based proton-exchange membrane fuel cells by ionomer content gradients in cathode catalyst layers, » *Materials Advances*, t. 3, n° 23, p. 8460-8468, 2022. DOI : 10.1039/D2MA00761D

[217] Y. Song et al., « Dependence of high-temperature PEM fuel cell performance on Nafion® content, » *Journal of Power Sources*, t. 154, n° 1, p. 138-144, 2006, ISSN : 03787753. DOI : 10.1016/j.jpowsour.2005.04.001

[218] I. Gatto et al., « Optimization of Perfluorosulphonic Ionomer Amount in Gas Diffusion Electrodes for PEMFC Operation under Automotive Conditions, » *Electrochimica Acta*, t. 165, p. 450-455, 2015, ISSN : 0013-4686. DOI : 10.1016/j.electacta.2015.03.068

[219] G. Lee et al., « In Situ Durability of Various Carbon Supports against Carbon Corrosion during Fuel Starvation in a PEM Fuel Cell Cathode, » *Nanotechnology*, t. 30, n° 8, p. 085 402, 2019, ISSN : 0957-4484, 1361-6528. DOI : 10.1088/1361-6528/aaf48c

[220] S. Ott et al., « Impact of Carbon Support Meso-Porosity on Mass Transport and Performance of PEMFC Cathode Catalyst Layers, » *ChemCatChem*, t. 13, n° 22, p. 4759-4769, 2021, ISSN : 1867-3899. DOI : 10.1002/cctc.202101162

[221] L. Strandberg et al., « PEMFC Catalyst Layer Degradation at Intermediate Temperatures (80°C, 100°C, and 120°C), » *Fuel Cells*, t. 25, n° 3, e70009, 2025, ISSN : 1615-6854. DOI : 10.1002/fuce.70009

[222] C. Cremers et al., « DEMS and Online Mass Spectrometry Studies of the Carbon Support Corrosion under Various Polymer Electrolyte Membrane Fuel Cell Operating Conditions, » *Journal of The Electrochemical Society*, t. 165, n° 6, F3307, 2018, ISSN : 1945-7111. DOI : 10.1149/2.0331806jes

[223] N. Linse et al., « Quantitative Analysis of Carbon Corrosion during Fuel Cell Start-up and Shut-down by Anode Purging, » *Journal of Power Sources*, t. 219, p. 240-248, 2012, ISSN : 0378-7753. DOI : 10.1016/j.jpowsour.2012.07.037

[224] D. Yang et al., « Post-Mortem Analysis of Degradation Behavior in Catalyst Layers of Proton Exchange Membrane Fuel Cell under near-Water Boiling Temperature, » *Fuel*, t. 406, p. 136 914, 2026, ISSN : 0016-2361. DOI : 10.1016/j.fuel.2025.136914

[225] J. Zhao et al., « Effects of Operating Temperature on the Carbon Corrosion in a Proton Exchange Membrane Fuel Cell under High Current Density, » *Energy Conversion and Management : X*, t. 10, p. 100 087, 2021, ISSN : 2590-1745. DOI : 10.1016/j.ecmx.2021.100087

[226] S. Hegde et al., « Automotive PEM Fuel Cell Catalyst Layer Degradation Mechanisms and Characterisation Techniques, Part I : Carbon Corrosion and Binder Degradation, » *International Journal of Hydrogen Energy*, t. 118, p. 268-299, 2025, ISSN : 0360-3199. DOI : 10.1016/j.ijhydene.2025.02.402

[227] S. Shahgaldi et al., « Influence of Ionomer Structures and Ratios on Performance and Degradation of PEM Fuel Cells, » *ECS Transactions*, t. 83, n° 1, p. 71, 2018, ISSN : 1938-5862. DOI : 10.1149/08301.0071ecst

[228] D. Yoo et al., « In Situ Analysis of Binder Degradation during Catalyst-Accelerated Stress Test of Polymer Electrolyte Membrane Fuel Cells, » *Materials*, t. 17, n° 17, p. 4425, 2024, ISSN : 1996-1944. DOI : 10.3390/ma17174425

[229] X. Luo et al., « Thickness Dependence of Proton-Exchange-Membrane Properties, » *Journal of The Electrochemical Society*, t. 168, n° 10, p. 104 517, 2021, ISSN : 1945-7111. DOI : 10.1149/1945-7111/ac2973

[230] E. Sgreccia et al., « Mechanical properties of proton-conducting sulfonated aromatic polymer membranes : Stress–strain tests and dynamical analysis, » *Journal of Power Sources*, t. 195, n° 23, p. 7770-7775, 2010, ISSN : 03787753. DOI : 10.1016/j.jpowsour.2009.09.061

[231] Y. Tang et al., « An experimental investigation of humidity and temperature effects on the mechanical properties of perfluorosulfonic acid membrane, » *Materials Science and Engineering : A*, t. 425, n° 1-2, p. 297-304, 2006, ISSN : 09215093. DOI : 10.1016/j.msea.2006.03.055

[232] Q. Zhao et al., « Mechanical properties of perfluoro sulfonated acids : The role of temperature and solute activity, » *Journal of Polymer Science Part B : Polymer Physics*, t. 51, n° 11, p. 915-925, 2013, ISSN : 0887-6266, 1099-0488. DOI : 10.1002/polb.23284

[233] P. Xiao et al., « Understanding of temperature-dependent performance of short-side-chain perfluorosulfonic acid electrolyte and reinforced composite membrane, » *International Journal of Hydrogen Energy*, t. 39, n° 28, p. 15 948-15 955, 2014, ISSN : 03603199. DOI : 10.1016/j.ijhydene.2014.01.204

[234] M. A. Barique et al., « Effect of Elevated Temperatures on the States of Water and Their Correlation with the Proton Conductivity of Nafion, » *ACS Omega*, t. 3, n° 1, p. 349-360, 2018. DOI : 10.1021/acsomega.7b01765

[235] L. Maldonado et al., « Characterization of polymer electrolyte Nafion membranes : Influence of temperature, heat treatment and drying protocol on sorption and transport properties, » *Journal of Membrane Science*, t. 389, p. 43-56, 2012, ISSN : 03767388. DOI : 10.1016/j.memsci.2011.10.014

[236] N. V. Trinh et al., « Characteristics of Water Transport of Membrane Electrolyte over Selected Temperature for Proton Exchange Membrane Fuel Cell, » *Polymers*, t. 14, n° 15, p. 2972, 2022, ISSN : 2073-4360. DOI : 10.3390/polym14152972

[237] M. Schalenbach et al., « Gas Permeation through Nafion. Part 1 : Measurements, » *The Journal of Physical Chemistry C*, t. 119, n° 45, p. 25 145-25 155, 2015, ISSN : 1932-7447. DOI : 10.1021/acs.jpcc.5b04155

[238] Harilal et al., « Physicochemical Properties of Short-Side-Chain Perfluorosulfonic Acid Membranes at Elevated Temperatures, » *Solid State Ionics*, t. 419, p. 116 747, 2025, ISSN : 0167-2738. DOI : 10.1016/j.ssi.2024.116747

[239] V. A. Sethuraman et al., « Durability of Perfluorosulfonic Acid and Hydrocarbon Membranes : Effect of Humidity and Temperature, » *Journal of The Electrochemical Society*, t. 155, n° 2, B119, 2007, issn : 1945-7111. doi : 10.1149/1.2806798

[240] V. A. Sethuraman et al., « Hydrogen Peroxide Formation Rates in a PEMFC Anode and Cathode : Effect of Humidity and Temperature, » *Journal of The Electrochemical Society*, t. 155, n° 1, B50, 2007, issn : 1945-7111. doi : 10.1149/1.2801980

[241] C. Chen et al., « H2O2 Formation under Fuel-Cell Conditions, » *ECS Transactions*, t. 11, n° 1, p. 1127-1137, 2007, issn : 1938-5862, 1938-6737. doi : 10.1149/1.2781025

[242] C. Chen et al., « Modeling of H2O2 Formation in PEMFCs, » *Electrochimica Acta*, t. 54, n° 16, p. 3984-3995, 2009, issn : 0013-4686. doi : 10.1016/j.electacta.2009.02.021

[243] C. Chen et al., « The Effect of Humidity on the Degradation of Nafion® Membrane, » *Polymer Degradation and Stability*, t. 94, n° 9, p. 1436-1447, 2009, issn : 0141-3910. doi : 10.1016/j.polymdegradstab.2009.05.016

[244] N. Zhao et al., « Effects of Fuel Cell Operating Conditions on Proton Exchange Membrane Durability at Open-Circuit Voltage, » *Fuel Cells*, t. 20, n° 2, p. 176-184, 2020, issn : 1615-6854. doi : 10.1002/fuce.201900173

[245] M. Marrony et al., « Durability study and lifetime prediction of baseline proton exchange membrane fuel cell under severe operating conditions, » *Journal of Power Sources*, t. 182, n° 2, p. 469-475, 2008, issn : 03787753. doi : 10.1016/j.jpowsour.2008.02.096

[246] Y.-H. Lai et al., « Accelerated Stress Testing of Fuel Cell Membranes Subjected to Combined Mechanical/Chemical Stressors and Cerium Migration, » *Journal of The Electrochemical Society*, t. 165, n° 6, F3217, 2018, issn : 1945-7111. doi : 10.1149/2.0241806jes

[247] T. Chu et al., « Performance Degradation and Process Engineering of the 10 kW Proton Exchange Membrane Fuel Cell Stack, » *Energy*, t. 219, p. 119 623, 2021, issn : 0360-5442. doi : 10.1016/j.energy.2020.119623

Chapter 2

PEMFC performance at higher operating temperature

1 Introduction **64**
2 Materials & methods **67**
2.1 MEA and break-in protocol 67
2.2 Polarization curves and Electrochemical Impedance Spectroscopy 68
2.2.1 Polarization curves with imposed current density (galvanostatic mode) 68
2.2.2 Polarization curves and EIS in potentiostatic mode 68
2.3 Accelerated Stress Test (AST) 69
3 Performance mapping **70**
3.1 Impact of operating conditions on PEMFC performance 70
3.2 Impact of relative humidity at 95°C – possible issues with membrane hydration and oxygen diffusion 74
3.3 Origin of voltage drop at 95°C 76
3.4 R_{hf} measurements during the AST 78
3.5 R_{hf} measurements at intermediate temperature 79
4 Discussion : on the main factors limiting the FC performance in the 90°C-100°C temperature range **80**
5 Local behavior assessment at 95°C **83**
5.1 Local i and R_{hf} measurements with the state-of-the-art membrane 84
5.2 Effect of membrane thickness on MEA hydration 85
6 Conclusion **86**
References **88**

Contexte

This work corresponds to a published article entitled '*On the main factors limiting the performance of state-of-the-art polymer electrolyte membrane fuel cells in the 90–100 °C temperature range*' (DOI. 10.1016/j.electacta.2025.147320). It presents a comprehensive study of the effect of elevated temperatures on the performance of a commercial MEA based on a state-of-the-art membrane. Assessments of the effects of operating parameters on performance, as well as the phenomena responsible for the limitations observed at high current densities, are also provided.

1 Introduction

Thanks to their high-power density, rapid start-up and shutdown, and good efficiency, PEMFC are suitable for many applications, particularly in heavy transport [1]. PEMFC are divided into several categories : low temperature (LT-PEMFC) below 90°C, intermediate temperature (IT-PEMFC) above 80°C/90°C but still using PFSA (PerFluoroSulfonic Acid) or more generally ionomer membranes, and high temperature (HT-PEMFC) above 120°C using PBI membranes. During operation, hydrogen undergoes oxidation on the anode side while oxygen undergoes reduction at the cathode. This results in the production of electrical work, water, and heat which must be removed by an external cooling system. Increasing the temperature of the Fuel Cell (FC) can therefore reduce the size of the cooling system, which is advantageous when space is limited, as is often the case in many transport applications. In addition, increasing cell temperature is believed to improve half-reactions kinetics and thus electrodes tolerance to platinum poisoning by gases such as carbon monoxide or sulfur compounds [2, 3]. Most studies deal with LT-PEMFC but some works considered HT-PEMFC because of their better tolerance to hydrogen impurities [4, 5], easier water management with suitable materials [6] to prevent flooding and better thermal management [7, 8]. However, performance and durability remain major obstacles due to high corrosion of bipolar plates and severe degradation of electrodes and membranes [6, 9, 10]. IT-PEMFC have some of the advantages of the HT-PEMFC, such as tolerance to catalyst poisoning and better thermal management while offering good performance and using well-known PFSA membrane like those of LT-PEMFC, *i.e.*, with interesting durability.

IT-PEMFC operating conditions generally correspond to temperatures between 90 and 120°C and low relative humidity. Consequently, a key parameter of the system is MEA hydration. Long-side-chain PFSA polymer is known to perform well at low temperatures but suffers from dehydration at high temperatures and low RH, leading to an increase in membrane resistance and therefore to a decrease in proton conductivity [11-14] and performance. Short-side-chain PFSA have been developed as electrolyte membranes and as ionomers in electrodes due to their superior water retention capacity at high temperatures [15, 16]. Particularly at intermediate temperature, membranes and catalyst layers made with SSC-PFSA perform better than when using LSC-PFSA [17, 18]. Stassi et al. [19] for instance reported better performances of SSC-PFSA at 130°C, 100% RH, 3 bars compared with LSC-PFSA, while Zhao et al. [20] observed significantly better performances of SSC-based MEA at 95°C, particularly with gas inlet RH equal to 30%. Several authors carried out electrochemical impedance spectroscopy measurements at different temperature and RH, observing a lower high frequency resistance (R_{hf}) with the SSC-PFSA membrane than with the LSC-PFSA membrane, which is explained by greater water uptake at high temperature and low RH [19, 20]. Using molecular simulations, other studies report a better connectivity and a more homogeneous distribution of water cluster at intermediate hydration state for SSC than LSC, which implies a higher proton conductivity of the membrane and therefore better performances [21-23]. In parallel, several groups have developed membranes based on hydrocarbon ionomer, which are mechanically more stable, cheaper and fluorine-free [24-26], and give interesting

performances, although highly dependent on gas inlet RH [27].

One way to improve FC operation at intermediate temperatures, especially under dry conditions, consists in adapting the FC materials, such as the type of ionomer for the membrane and electrodes or the ionomer/carbon ratio in the electrodes. Another way consists of applying intermediate conditions such as low relative humidity and a temperature below 100°C, while adapting the operating conditions when needed to allow the use of well-established materials as in the LT-PEMFC. Hickner et al. [28] studied the water content inside an operating PEMFC as a function of current density and cell temperature under fully humidified conditions : for cell temperatures between 40 and 80°C and a constant air stoichiometry equal to 2, they noted a decrease in the water content of the cell with temperature, which was more pronounced at higher current density. Indeed, higher fuel cell temperature improves the water removal capacity through the gas flow. The problems of dehydration of the MEA induced by the operating temperature of the fuel cell could therefore be compensated by appropriately choosing the operating point in terms of air stoichiometry and gas inlet RH.

Several groups studied how air stoichiometry [29, 30] and/or current density [31] governed the MEA hydration. Kim et al. [32] observed that stable performance at 70°C was linked to precise air stoichiometry as a function of the current density. Cho et al. [33] considered the impact of the air flow rate on the cathode side at 120°C and several RH (10 to 35%) for different current densities : they observed that a low air flow rate implies a lack of reactant while a high flow rate induces dehydration of the MEA by excessive water removal, leading to voltage drops. For catalyst layers, Cho et al. [33] observed that a high ionomer binder content implies slightly better performance at low and medium current densities, but lower performance at high current density where mass transport problems may occur, including flooding. Also at 10% RH, they observed that the FC high-frequency resistance firstly decreases with increasing current density and thus water production, before a sharp increase at 0.2 $A.cm^{-2}$ due to the dehydration of the MEA, which they justify by the electro-osmosis flux becoming more important than water back-diffusion from the cathode to the anode, as has been observed in several studies [34, 35]. Such a membrane drying phenomenon is expected to happen at significantly higher current densities with state-of-the-art components.

Several works investigated the behavior of fuel cells at different current densities using impedance spectroscopy, mainly to separate the voltage drop associated with charge transfer, mass transfer and membrane ionic resistance, *i.e.*, high frequency resistance. These phenomena were then related to the characteristics of the membrane and electrodes to provide a better understanding of fuel cell operation, depending on the operating point. Many focused on a small range of current densities : for example, Reshetenko et al. [36] observed significant variations in the parameters of the catalytic layer between 50 and 400 $mA.cm^{-2}$ at 80°C. A large increase in proton conductivity in the catalytic layer was also observed when the current density increases while the double layer capacity decreases, which can be explained respectively by a higher water content and better proton transport. Tang et al. [13] studied the evolution of the voltage drop due to charge transfer, membrane resistance and mass transport between 0.1 and 1.9 $A.cm^{-2}$ at 100% RH, 80 and 120°C. For both temperatures, they observed that the charge transfer resistance, mainly responsible for the voltage drop at low current densities, decreases as current density increases in accordance with the impedance theory. In parallel, the high frequency resistance, assumed to be governed mainly by the membrane, decreases very slightly, or even remains constant, with increasing current density. They also reported better mass transfer parameters with increasing temperature, especially at high current densities, which they did not explain.

Although these studies provide detailed data on FC operation under various conditions, they primarily focus on high relative humidity and/or typical operating temperatures (table 2.1), which differ significantly from the conditions that are targeted in heavy mobility. In addition, in most cases the MEA materials used in the above-mentioned studies are neither recent nor representative of the present state

of the art ; nowadays thinner membranes and more optimized ink deposition processes are the norm. The observations and conclusions are therefore difficult to compare with those of previous studies, which reinforced our motivation to consider the impact of conditions close to those for heavy transport systems-*i.e.*, 95°C, our reference temperature, and low relative humidity-on the performance of state-of-the-art MEA.

Cell T (°C)	i range ($A.cm^{-2}$)	Air/cathode		Hydrogen/anode		Membrane		Authors	Ref.
		Stoichiometry/ flowrate	RH (%)	Stoichiometry/ flowrate	RH (%)	Type	Thickness (μm)		
40-60-80	0-1.5	2	100	90 L/h	100	Nafion 112	50	Hickner et al.	[28]
60	0.5-1.5	2, 4, 6							
120	0.05-0.38	4.2-14.7 (L/h)	10-35	2.58 (L/h)	10.0-35.0	Aquivion	30	Cho et al.	[33]
70	0.1-0.5	0-4	0-100	2	100	Nafion 115	100	Mérida et al.	[37]
49-57	0.15-0.4	1.6	25-122	1.3	25-122	Not disclosed		Moçotéguy et al.	[38]
60	0.3-0.8	3	100	1.4	100	Nafion 112	50	Malevich et al.	[39]
80	0.05-0.4	9.5	50	2	100	Gore	16-18	Reshetenko et al.	[36]
80-120	0.1-1.9	60 (L/h)	100	18 (L/h)	100	Nafion 112	50	Tang et al.	[13]
68	0-3	60 (L/h)	50-100	60 (L/h)	50-100	Not disclosed		Ge et al.	[40]
52	0.05-0.4	4	Dry to humidification (lower than 100%)	Not disclosed	Dry to humidification (lower than 100%)	Nafion	30	Ciureanu et al.	[41]
60	0.2-1.2	2.5-3.5	40-100	1.5	40-100	Not disclosed	15	Miao et al.	[42]
80	0.1-1.5	4.0-8.0	50-100	2.0-3.0	30-100	Nafion XL	27.5	Najafi et al.	[43]
80	0.05-0.9	>10 (O_2)	30-70	>10	30-70	Not disclosed		Schiefer et al.	[44]
70	0-2	30 (L/h)	40-80	90 (L/h)	40-80	Not disclosed	15	Xia et al.	[45]
120	0.1-1.5	45 (L/h)	25-100	60 (L/h)	25-100	Nafion 112	50	Zhang et al.	[46]

TABLE 2.1 – Non-exhaustive list of current density, operating conditions and materials in various literature studies

Although SSC-PFSA is generally considered a better candidate according to the existing literature, this study explores the feasibility of using LSC-PFSA at intermediate temperatures. To this end, we operated a commercial MEA at temperatures up to 105°C, taking 95°C and 70°C as the reference cases. The gas inlet relative humidity (RH) was maintained at low to moderate levels (*i.e.*, 20 to 50% RH) to simulate conditions similar to those encountered in automotive applications. Electrochemical impedance spectroscopy was performed to study the evolution of the high frequency resistance R_{hf}, as a marker of MEA hydration, as well as the parameters representative of oxygen transport & cathode kinetics. This work was done using state-of-the art 12 µm thick LSC-PFSA membrane and electrode materials. Particularly, we were interested in performance limitations and focused on high current densities, where mass transfer resistance and the lack of reactants are usually considered as the main phenomena responsible for voltage drop at usual operating temperatures. However, it was observed that depending on the operating conditions, MEA dehydration could become a significant factor limiting performance, since low gas relative humidity combined with high cell temperature may affect the membrane hydration state [47]. In addition, high current densities can lead to local membrane heating, further contributing to its drying out [40]. As a result, the phenomena limiting cell performance under these conditions may differ from those typically observed at standard operating temperatures.

2 Materials & methods

2.1 MEA and break-in protocol

MEA performances were mostly measured using a single cell with 50 straight parallel channels 0.15 mm deep at the anode and 0.25 mm deep at the cathode (figure 2.1(a)). Another cell was also used, in occasions, corresponding to earlier designs (*e.g.*, serpentine channels, figure 2.1(b)). In both cases, the plates were made of gold-coated 316L stainless steel.

(a)

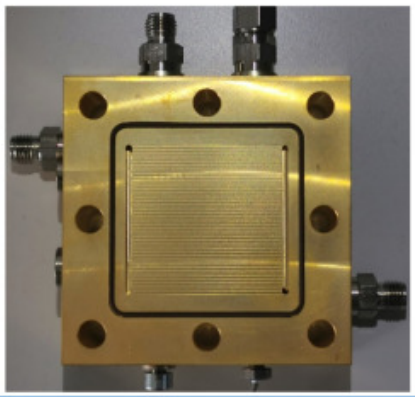

Number of channels	Depth	
	Anode	Cathode
50	0.15 mm	0.25 mm

(b)

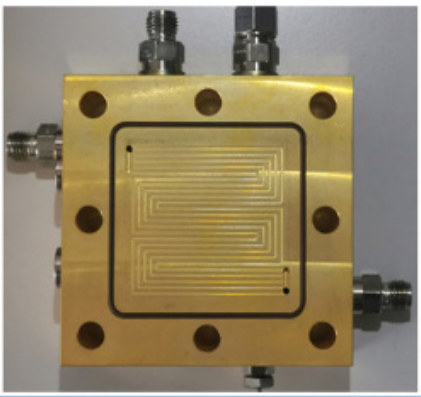

Number of channels	Depth	
	Anode	Cathode
5	0.3 mm	0.6 mm

FIGURE 2.1 – Straight parallel channels (a) and serpentine channels (b) bipolar plates.

The cell was operated in counter-flow, its temperature being imposed thanks to an oil circulation loop. For every experiment, 25 cm^2 commercial MEA were used, consisting of :

- Anode : Pt/HSAC 50 wt% (Tanaka TKK TEC10E50E) - 0.1 $mg.cm^{-2}$
- Cathode : Pt/HSAC 50 wt% (Tanaka TKK TEC10E50E) - 0.3 $mg.cm^{-2}$
- Ionomer binder : Nafion® D2020CS for both anode and cathode side with an ionomer/carbon ratio equal to 0.8
- Ionomer membrane : Gore 788.12
- Gas diffusion layer (GDL) : Freudenberg H14CX653

A 25% compression rate was applied to each GDL using two 100 μm PTFE gaskets and one 25 μm polyethylene naphthalate (PEN) film.

Before any performance characterization, each MEA was subjected to a conditioning (break-in) protocol, consisting of potentiostatic steps at OCV (30 s), 0.6 V (45 s) and 0.3 V (60 s) for about 2h. The cell temperature was set to 70°C, gas pressure and relative humidity (RH) were imposed at 1 bar and 50% RH ; the stoichiometry was set to 1.5 for hydrogen and 3 for air, calculated on the measured current density at each imposed voltage. External parameters such as cell temperature, gas RH, pressure and stoichiometries were controlled.
For performance mapping, all the external parameters were varied, except for the hydrogen stoichiometry, which was deliberately set to a low value (1.25) to approach real-life operating conditions. After the performance mapping, the gas pressure and air stoichiometry were fixed to the values giving the best performances (*i.e.*, reference conditions : 3 bar and an air stoichiometry equal to 3), so that only the gas RH and cell temperature were varied.

2.2 Polarization curves and Electrochemical Impedance Spectroscopy

2.2.1 Polarization curves with imposed current density (galvanostatic mode)

Firstly, performance mapping was done by measuring the polarization curves in galvanostatic mode, *i.e.*, by imposing the current density. Each polarization curve was recorded after a 30-minute constant current stage (1 A.cm^{-2}) to begin from an identical starting point. The current density was then varied in 100 s steps, starting from OCV (Open Circuit Voltage), until the FC voltage dropped below 0.3 V. Then, the current density was decreased following the same protocol, *i.e.*, by 100 s steps, up to OCV. The average voltage value corresponding to each current density value was then calculated by considering the last 50 s of the increasing and decreasing steps. The cell temperature, air stoichiometry, pressure and gas RH are specified in each case.

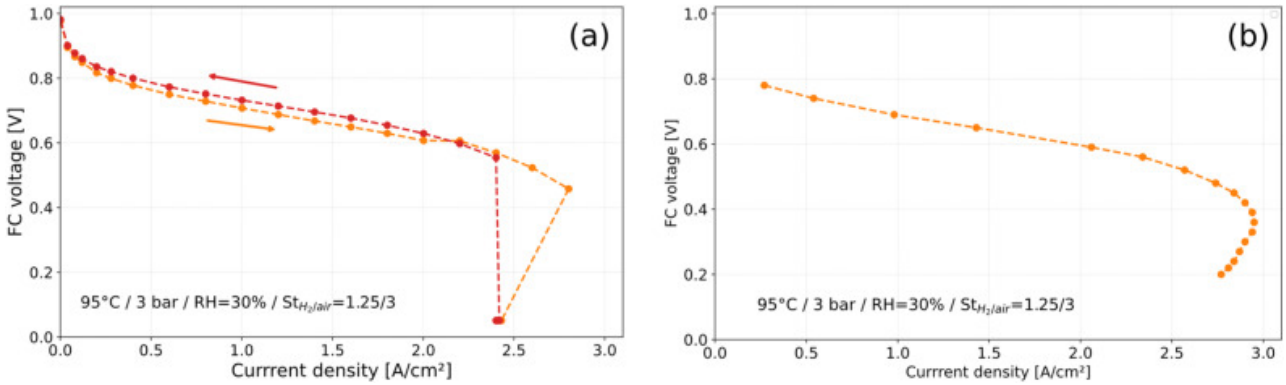

FIGURE 2.2 – Polarization curve in galvanostatic mode (a) and in potentiostatic mode (b) ; potentiostatic polarization curves prove more stable at high current density and this makes it possible to perform EIS simultaneously.

However, although similar to what we had done in previous works [26, 48, 49] this way of measuring the polarization curves resulted in serious voltage instabilities at high current density, especially at high temperature (*i.e.*, 95°C) and low gas inlet RH, as illustrated in figure 2.2(a). Similarly, it was not possible to perform Electrochemical Impedance Spectroscopy (EIS) in galvanostatic mode in the high current density region of the polarization curves, because of sudden voltage drops ; consequently, it was not possible to study the cause of that voltage drop.

2.2.2 Polarization curves and EIS in potentiostatic mode

Since measuring the polarization curves and performing EIS in galvanostatic mode proved difficult at high current density, *i.e.*, near unstable operating points, the MEA behavior was instead studied in potentiostatic mode. In this approach, EIS was performed simultaneously with the recording of the polarization curves, rather than separately in galvanostatic mode. EIS was used to evaluate the high-frequency resistance R_{hf} as well as other impedance parameters and thus assess the hydration state of the MEA and/or the oxygen transport impedance.

- Before measuring each point on the polarization curve, a 30 min, 1.5 A.cm^{-2}, constant current step was performed to avoid any discrepancies linked to the FC hydration history. The polarization curves were measured by decreasing the FC voltage from approximately 0.8 V (maximum value corresponding to about 0.25 A.cm^{-2}) down to 0.2 V. Each step lasted 30 minutes to ensure that the current density value reading corresponded to a stable operating point. Hydrogen and air flow rates had to be adjusted several times to achieve a stoichiometry of 1.25 and 3 based on

the measured current density (*i.e.*, reference conditions, as mentioned at the end of the previous section).

- EIS measurements were carried out at the end of each constant voltage steps. A small sinusoidal disturbance was imposed on the voltage setpoint, and the current density response was recorded simultaneously. For full-spectrum measurements, the frequency range was from 25 kHz to 0.02 Hz. When R_{hf} values only were needed, the minimum frequency was increased to 500 Hz to save time. In both cases, the amplitude of the disturbance was set between +/- 10 to 4% of the voltage measurement. At low voltage, the disturbance was reduced to the minimum value to avoid altering the state of the MEA. However, our tests showed that at high current density and low voltage, there was no significant effect of the amplitude of the disturbance, especially at high frequency, at least in the tested range (+/- 2 to %).

2.3 Accelerated Stress Test (AST)

The accelerated stress test used in this study was introduced in previous works [48, 50-53]. It does not target one specific component of the MEA but is designed to induce a global aging, including a decrease in the electrode surface area, chemical and mechanical stress to the membrane and ionomer. Such an AST was chosen because of its ability to combine stress factors that induce coupled mechanical and chemical degradation of the membrane and the electrodes. Its effectiveness has been demonstrated in previous works on MEA durability, showing a significant decrease in performance due to ECSA degradation and, in some cases, membrane breaking [48-53]. It consists of the repetition of a 60 s sequence (figure 2.3) that is divided into two parts while the gas flow rates are kept constant, based on a stoichiometry of 1.25/3 (*i.e.*, our reference conditions) when the current density is the highest :

- A 43 s load cycling stage between a current density value corresponding to 0.55 V for the pristine MEA-for 3 s-and Open Circuit Voltage (OCV)-for 2 s. This load, *i.e.*, potential, cycling stage is well-known to induce aging of the Catalyst Layer (CL) [54, 55] ; in addition, one can also observe a FC voltage undershoot in figure 2.3 when the current density increases, which may be the marker of membrane and/or CL drying. Note that in our case, the current density was equal to about 2.2 $A.cm^{-2}$ at 0.55 V, with 30% inlet RH and 3 bar operation pressure.
- A 17 s OCV stage to induce chemical aging of the membrane and ionomer in the electrodes [56],[57], as well as MEA drying, due to relatively low gas inlet RH (30%) and thus a mechanical aging due to swelling and contraction cycling [52]. As mentioned above, humidity cycling may also occur during load cycling.

The cell temperature was set to 95°C and the relative humidity of the gas at 30%. AST periods of 2 days were applied to the MEA, between which performance and state of the MEA were characterized using polarization curves and impedance spectroscopy at imposed voltage, as described above.

A total of four two-day periods of AST and characterization were conducted to determine whether electroosmotic drag or heat generation primarily governs membrane drying at high current densities. The investigation was motivated by the fact that aging affects the current density at a given fuel cell voltage, thereby influencing both electroosmotic water flux through the membrane and heat production.

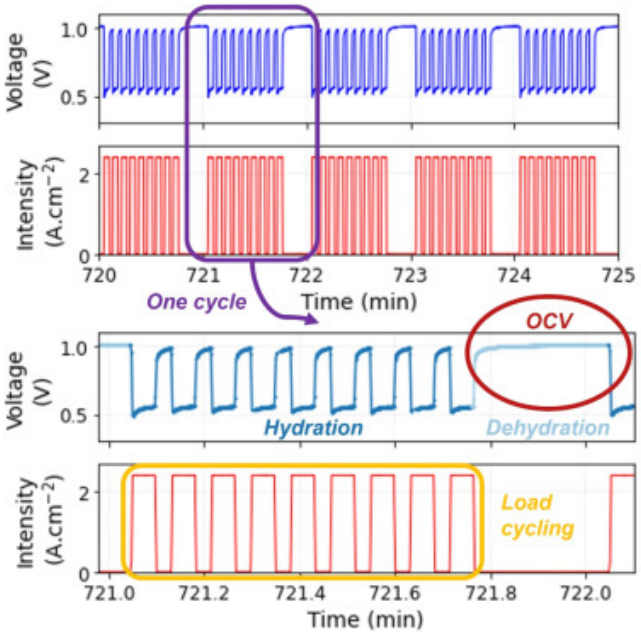

FIGURE 2.3 – Representation of the accelerated stress test used with the presentation of the repeated 60 s cycle divided in three parts : load cycle (yellow) for electrodes aging, OCV (red) for chemical aging, and hydration/dehydration cycle (dark and light blue) for mechanical aging.

3 Performance mapping

3.1 Impact of operating conditions on PEMFC performance

The research data repository contains all the data presented in this article [58].
PEMFC temperature, as well as gas relative humidity, pressure and air stoichiometry were varied to optimize operating conditions and to investigate the impact of a higher temperature. A total of 44 different cases have been tested (table 2.2) while, as mentioned above, the hydrogen stoichiometry was always maintained at 1.25.

T (°C)	RH (%)	P (bar)	St (air)
70	50	1	2–2.5–3–4–5
		2–3	2–2.5–3
	80	1	2–2.5–3–4–5
		2–3	2–2.5–3
95	30	1–2–3	2–2.5–3–4–5
		2–3	2–2.5–3
	50	1	2–2.5–3–4–5
		2–3	2–2.5–3

TABLE 2.2 – Range of operating condition tested for performance mapping.

Note that these experiments were also performed using the five-channel serpentine cell (figure 2.1(b)). Since the performance was lower and the observations and conclusions were similar, we chose, for the sake of simplicity, to present only the results obtained with the straight parallel channel cell. The

polarization curves in galvanostatic mode (figure 2.4) include error bars representing the difference between measurements taken during increasing and decreasing current density (section 2.2.1). Large vertical error bars, such as those observed at high current densities-particularly at 95°C-indicate significant hysteresis between the forward and backward current scans, and instabilities. The horizontal error bars (*i.e.*, those on the current density values) reflect unstable operating conditions that prevent precise control of the setpoint.

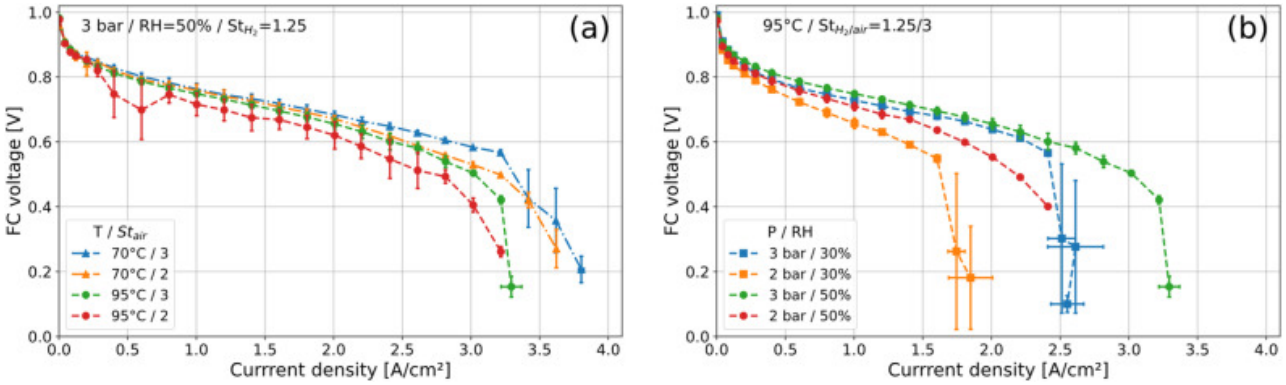

FIGURE 2.4 – Polarization curves in galvanostatic mode : impact of temperature and air stoichiometry at 3 bar/50% RH and St(H_2) =1.25 (a) and impact of gas pressure and relative humidity at 95°C and St(H_2/air) =1.25/3 (b).

Not all of the data are presented here, as the volume of data was too large to be displayed in full without impacting clarity. Nevertheless, the complete dataset allowed us to highlight the following trends :

- As expected, increasing the FC operating pressure enhances performance, particularly at high current densities. Lu et al. [59] reported that the primary benefit of increased back pressure in PEMFC arises from improved membrane hydration, which leads to higher membrane conductivity. In contrast, the associated increase in reactant partial pressure contributes only marginally to the cell voltage. Furthermore, the influence of operating pressure on FC performance is most pronounced under conditions of low gas inlet RH [60]. These findings agree with our R_{hf} measurements (table 2.4), for both temperature and at all current densities that were tested. There was a more pronounced decrease in R_{hf} with increasing gas pressure at 20% RH. A similar trend was observed at 95°C, however, the impact of RH on this trend could not be verified for all current densities, as certain operating conditions did not allow operation at certain specific current densities.
  The operating pressure is beneficial for the hydration of the membrane and the catalyst layers [61], but it also leads to a decrease in the diffusivity of oxygen and water vapor [59]. The cathode compartment environment is a multi-species system containing liquid water, water vapor, oxygen, and nitrogen, which makes it challenging to calculate a global diffusion coefficient for a single component. However, the interdiffusion D_{AB} between two gases components can be calculated, using the molar mass, critical pressure and critical temperature of the two components, as well as the operating pressure and temperature [62] :

$$\frac{PD_{AB}}{(P_{cA}P_{cB})^{1/3}(T_{cA}T_{cB})^{5/12}(1/M_A+1/M_B)^{1/2}} = a\left(\frac{T}{\sqrt{T_{cA}T_{cB}}}\right)^b \tag{2.1}$$

  Where a and b are dimensionless constants, P and T are the temperature and pressure of the system. PcA, TcA and MA (respectively PcB, TcB and MB) are the critical pressure, critical

temperature and molar mass of species A (respectively species B).

The values in table 2.3 show that increasing the operating pressure significantly reduces interdiffusion for any gas pair. For example, increasing the pressure from 1 to 3 bar results in a threefold decrease in all the interdiffusion coefficients. In that regard, one might be tempted to attribute the instabilities observed at high temperature and high current density in figure 2.4 to limitations in oxygen diffusion. However, oxygen diffusion alone does not account for the instabilities, resulting in large error bars, at high current densities in the polarization curves, indicating that a more detailed analysis of the experimental results is necessary.

D ($cm^2.s^{-1}$)						
Species	O_2/N_2		O_2/H_2O		H_2O/N_2	
P (bar)	1	3	1	3	1	3
T (°C)						
25	0.208	0.069	0.254	0.085	0.266	0.089
40	0.228	0.076	0.285	0.095	0.298	0.099
50	0.241	0.080	0.307	0.102	0.321	0.107
60	0.255	0.085	0.329	0.110	0.344	0.115
70	0.269	0.090	0.353	0.118	0.369	0.123
80	0.284	0.095	0.377	0.126	0.394	0.131
90	0.299	0.100	0.403	0.134	0.421	0.140
95	0.306	0.102	0.416	0.139	0.435	0.145
100	0.314	0.105	0.429	0.143	0.449	0.150

TABLE 2.3 – Diffusion coefficient for several pair of gases.

- Increasing the gas inlet RH up to 50% (at 95°C) or 80% (at 70°C) also improves the FC performances. Zhang et al. [47] observed an approximately five-fold decrease in membrane resistance (from approximately 700 to 140 $m\Omega.cm^2$) when the relative humidity at the gas inlet increased from 25 to 100% at 120°C. They associated this result with an increase in membrane water content and thus, in ionic conductivity. This is confirmed by our R_{hf} measurements, which show a substantial decrease between 20 and 50% RH across all current densities and pressures at 95°C. For example, at 3 bar and 1.5 $A.cm^{-2}$, R_{hf} drops from 87 to 41 $m\Omega{\cdot}cm^2$. A similar trend is observed at 70°C, although it is significantly less pronounced-for instance, R_{hf} decreases only slightly, from 35 to 32 $m\Omega{\cdot}cm^2$ at 1.5 $A.cm^{-2}$. However, these results are only valid through the range of parameters tested : Xu et al. [63] came to a different conclusion when increasing the gas inlet RH from 50 to 90% RH at 90°C and 1.5 atm : despite the decrease in membrane resistance, the performance was lower at 90% RH due to a higher resistance to oxygen transport. This was explained by the greater amount of water brought in by the gases and produced by the electrochemical reaction, hindering oxygen diffusion. Indeed, the oxygen inlet molar fraction decreases from 14.8 to 10.5% when the gas inlet RH increases from 50 to 90% at 1.5 atm, while the water molar fraction increases from 29.6 to 49.9%.
- Increasing the air stoichiometry increases the performance, especially at high current densities. At 3 bars, the increase in performances is mainly noticeable at high current densities, contrary to 1 and 2 bar where the gain in voltage can be observed over a larger current density range. Wang et al. observed that the optimal air stoichiometry value was depending on the operating point [64] : high current densities require a higher air stoichiometry to avoid gas starvation [7]

and to evacuate the excess water produced ; however, a higher air stoichiometry can also entail MEA dehydration, especially for dry conditions, leading to a decrease in the membrane's water content and therefore proton conductivity, resulting in a-sometimes severe-drop in performance. This finding is in line with our measurements, which demonstrate that at 95°C, 30% RH (rather dry conditions), there is no observed increase in performance with increasing air stoichiometry. Further characterization revealed that a sharper decrease in performance is observed in drier conditions, for example at temperatures of 95°C and relative humidity levels of 20%.

- Increasing the FC temperature while keeping all other parameters constant negatively impacts performance. Notably, this decline is observed across the entire polarization curve (figure 2.4) and attempts to optimize operating conditions-such as adjusting air stoichiometry, gas inlet relative humidity, and back pressure-failed to compensate for the performance loss.
  Although catalyst activity and proton conductivity are generally enhanced by elevated temperatures [65-68], several studies also suggest that higher temperatures, especially under low humidity conditions, increase the rate of water evaporation [69-71]. This results in reduced membrane hydration, which significantly lowers proton conductivity and FC efficiency [17, 72, 73]. For instance, Wu et al. [74] observed an increase in proton conductivity from 0.079 S.cm^{-1} at 20°C to 0.210 S.cm^{-1} at 60°C, followed by a decline at higher temperatures ; similarly, Jeon et al. [18] reported that raising the operating temperature at constant relative humidity (RH) increases both R_{hf}, which reflects membrane hydration, and the charge transfer resistance. In addition, the positive effect of temperature increase on the reaction kinetics can be balanced by detrimental mass transfer effects (*e.g.*, decrease of the oxygen solubility) [75]. For all the current densities and RH tested (table 2.4), we observed similar trends, *i.e.*, much higher R_{hf} values at 95°C than at 70°C, particularly at 1 and 2 bar. At 3 bar and 50% RH, the variation in R_{hf} between 70 and 95°C is much smaller, indicating that the effect of temperature on hydration is more significant at low RH and low pressure.

R_{hf} (Ohm.cm^2)		Gas inlet RH : 20%			Gas inlet RH : 30%			Gas inlet RH : 50%		
i (A.cm^{-2})	T (°C)	1 bar	2 bar	3 bar	1 bar	2 bar	3 bar	1 bar	2 bar	3 bar
1	70	0.097	0.045	0.036	0.072	0.039	0.034	0.050	0.035	0.033
	95	–	0.177	0.094	0.168	0.096	0.066	0.070	0.054	0.043
1.5	70	0.103	0.042	0.035	0.070	0.037	0.033	0.049	0.033	0.032
	95	–	–	0.087	–	0.099	0.059	0.081	0.053	0.041
2	70	–	0.040	0.032	0.085	0.037	0.031	0.054	0.033	0.031
	95	–	–	–	–	–	0.057	0.104	0.056	0.041

TABLE 2.4 – R_{hf} measurements with imposed current density at different current densities and for various temperature, pressure and gas inlet RH.

Note that the R_{hf} values reported in table 2.4 were measured in galvanostatic mode (section 2.2.1), which could only be applied at relatively low current densities due to the current/voltage instabilities observed in figure 2.4. The slight general decrease in R_{hf} from 1 to 2 A.cm^{-2} aligns with trends reported in the literature [13, 33, 38, 40, 42, 73, 76] and suggests progressive membrane hydration in the low-current-density region of the polarization curve [77].
However, the significantly higher R_{hf} values at 95°C compared to 70°C-particularly at 1 and 2 bar-may indicate membrane hydration challenges at elevated temperatures. Additionally, the increased hysteresis between the forward and backward current scans in the polarization curves at high current densities under high-temperature, low-RH conditions (figure 2.4) further supports the possibility of membrane

and ionomer hydration issues. While some of the hysteresis may be due to the formation/reduction of platinum oxides, the process being dependent on temperature and humidification [77, 78], it is likely that the increase in error bars at high current densities is mainly related to hydration of the MEA. Based on these initial observations, we further investigated the impact of gas inlet relative humidity (RH) at high temperature (*i.e.*, 95°C) to better understand the primary cause of the voltage drop observed at high current densities. For simplicity, the results presented below were performed under reference conditions : a gas back pressure of 3 bar, with hydrogen and air stoichiometries set to 1.25 and 3, respectively. These conditions corresponded to the best performance observed.

3.2 Impact of relative humidity at 95°C – possible issues with membrane hydration and oxygen diffusion

To gain a deeper understanding of the MEA behavior at 95°C, performance tests were carried out with various gas inlet relative humidities, in the reference conditions defined above. Note that, unless otherwise stated, we always considered identical RH values on the hydrogen side and on the oxygen (air) side. According to the literature, an increase in RH induces a decrease in the cell resistance, usually associated with a better hydration of the membrane and possibly the ionomer in the CL, resulting in higher proton conductivity [38, 79-81] and better performances [38, 82]. Indeed, we observed an increase in performances at 95°C with relative humidity from 20 to 40%, which is in line with the quoted literature (figure 2.5). However, there was no significant increase in performance at 70°C between 20% RH and 40% RH and above 40% RH at 95°C, although the studies cited above report an increase in the ionomer proton conductivity with relative humidity, up to 100% RH. Therefore, there must be at least one additional phenomenon in competition with the increase in proton conductivity : possibly, as mentioned in the previous section, some difficulties in oxygen diffusion [63].

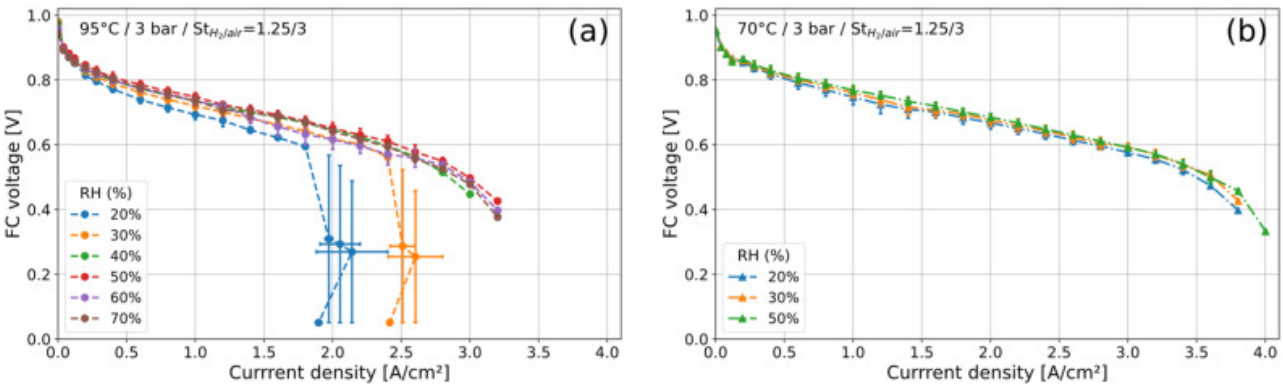

FIGURE 2.5 – Polarization curves in reference conditions (St(H_2/air) = 1.25/3, P = 3 bar, symmetrical RH) at various RH at 95°C (a) and 70°C (b).

In addition, low gas inlet RH leads to severe current and voltage instabilities, as evidenced by the large error bars in figure 2.5. These large error bars arise from both a significant voltage drop at high current densities and strong hysteresis between the forward and backward current scans : the lower the gas inlet RH, the more pronounced these instabilities. Impedance spectroscopy was performed at 95°C and at several RH and current density values to better capture the MEA behavior (figure 2.6).

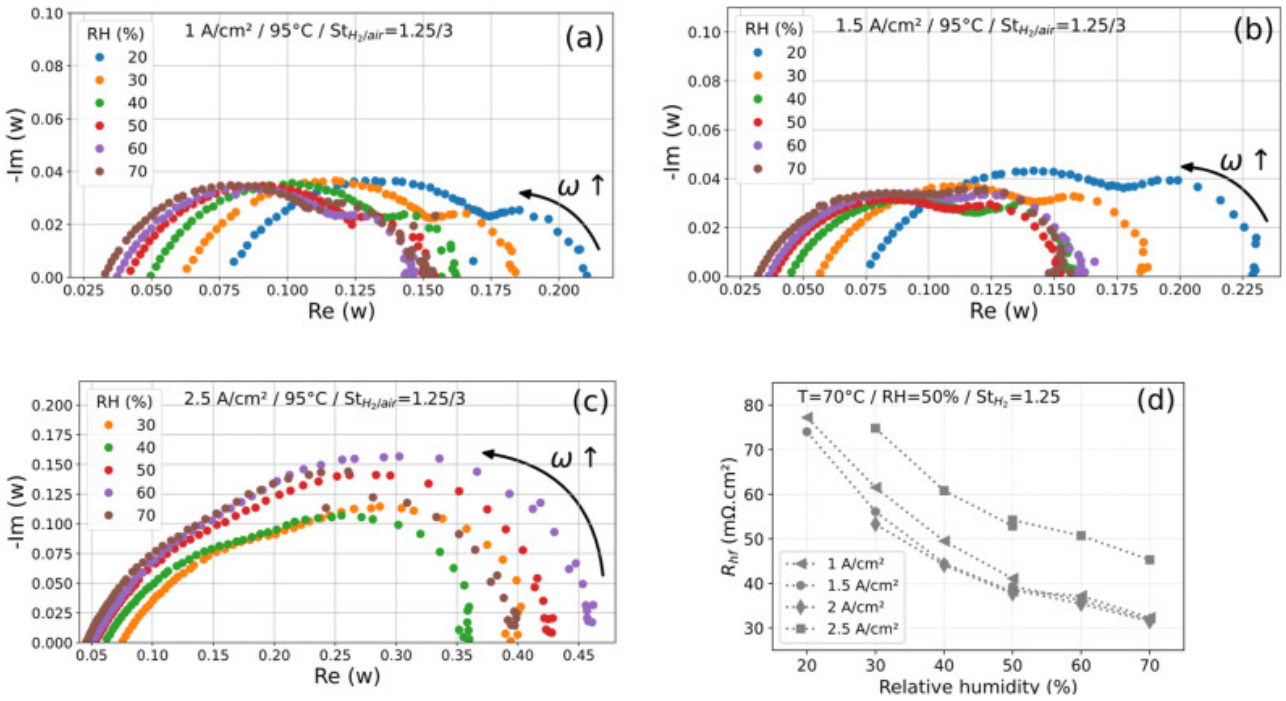

FIGURE 2.6 – Impedance spectra recorded in galvanostatic mode at 1 (a), 1.5 (b), and 2.5 A.cm^{-2} (c) and 95°C under different relative humidities. R_{hf} measurements at different current densities and relative humidities at 95°C (d).

Impact of gas inlet RH

As expected, we observed a decrease in R_{hf} with increasing relative humidity across all the current density tested (1, 1.5 and 2.5 A.cm^{-2}, figure 2.6(a-b-c)) reflecting improved hydration of both the membrane and the ionomer. However, at the highest current densities-2.5 A.cm^{-2}, figure 2.6(c)-an increase in the mass transfer (low-frequency) loop is also observed, possibly indicating higher resistance to oxygen diffusion. This behavior may be attributed to oxygen dilution and/or reactant starvation, potentially caused by the combined effects of increased RH and the higher water production by the fuel cell. Overall, it appears there is a trade-off between the performance gains from enhanced MEA hydration and the losses due to increased mass transport resistance. This trade-off could explain the absence of significant performance improvement above 40% RH at 95°C.

Impact of current density

Paradoxically, increasing the current density to 2.5 A.cm^{-2} has a negative impact on R_{hf}, which increases despite the higher water production (figure 2.6(d)). This effect is observed across the entire tested range of relative humidity (20% to 70%) and has also been observed by Vandenberghe at al. [77, 78]. Instead of enhancing membrane and ionomer hydration-and thereby improving proton conductivity-there seems to be a net dehydration of the MEA at high current density. One possible explanation is the increased electro-osmotic drag of water from the anode to the cathode, which can deplete water from the anode compartment [83-85] and lead to significant membrane dehydration on that side [86, 87]. Another potential cause is membrane and/or electrode drying induced by the heat generated during the electrochemical half-reactions. This heat can produce substantial temperature gradients between the MEA and the bipolar plates, particularly under high current densities. Some

studies suggest that, under saturated vapor conditions, such temperature gradients lead to gradients in saturated water vapor pressure, driving water toward the cathode-side bipolar plate and further drying the membrane. This phenomenon is known as the heat pipe effect [88-92].

3.3 Origin of voltage drop at 95°C

Section 3.2 confirmed that water management, rather than mass transport, is the dominant factor behind the voltage drop and instabilities observed at high temperature*. However, although (figure 2.6(d)) shows an increase in R_{hf} with current density, it does not clarify whether the steep FC voltage drops or instabilities observed at 95°C are actually due to membrane dehydration (whether driven by electro-osmotic drag, thermal effects, or both) or to increased oxygen transport limitations, as is typically expected and accepted at lower temperatures [93, 94]. A deep understanding of these mechanisms required EIS measurements conducted near the inflection point of the polarization curves. Since this was not feasible in galvanostatic mode (section 2.2.1) due to the instability of the fuel cell voltage, we switched to potentiostatic mode for both the polarization curve and EIS measurements. Our focus was primarily on the high-frequency range, and we did not always record the full EIS spectra to enable rapid measurements and minimize changes in the MEA state.

Typical polarization curves measured with imposed voltage are presented at 70 and 95°C with 20, 30 an 50% gas inlet RH, at 3 bar and stoichiometry of 1.25/3 in hydrogen/air (figure 2.7).

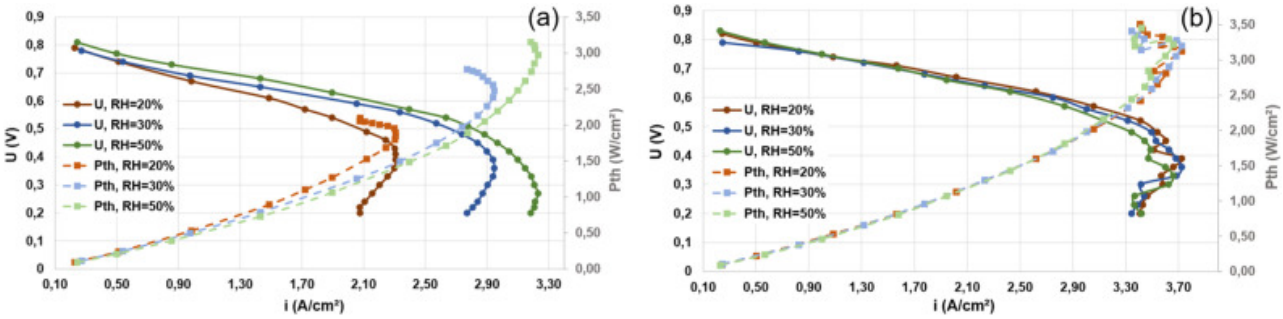

FIGURE 2.7 – Polarization curves and thermal power with 20, 30 and 50% gas RH at 95°C (a) and 70°C (b).

An unusual but normal behavior, compared to galvanostatic measurements, is the presence of a reversal point in the curves, corresponding to a maximum current density that cannot be exceeded. This reversal point is observed at both temperatures, but exhibits a much stronger dependence on the gas inlet RH at 95°C. At 95°C, the maximum current density increases significantly with RH, reaching 2.31, 2.95, and 3.23 A.cm^{-2} for 20, 30, and 50% RH, respectively. In contrast, at 70°C, the maximum current density shows almost no variation, ranging between 3.66 to 3.72 A.cm^{-2} (table 2.5).

Figure 2.7 and table 2.5 also present the evolution and the value at imax of the thermal power that results from the voltage losses, estimated as $P_{th} = (U_{rev} - U) \times j$, with Urev, the thermodynamic (reversible) FC voltage†. A striking result in figure 2.7 is the differing impact of RH at 95 and 70°C. At 95°C, increasing the gas inlet RH has a strong effect on the fuel cell voltage across the entire

*. This conclusion applies to the materials used here, *i.e.*, conventional Pt/C electrocatalysts. With Pt-free electrocatalysts, for instance, oxygen transport limitations would likely be more significant.

†. The reversible cell voltage U_{rev} was estimated using the following pseudo-Nernst equation, where p_i denotes the partial pressure of component i and P_0 the standard (reference) pressure (1 atm) ; T_0 stands for the standard temperature (298.15 K). The values of U_{rev} are given, for illustration, in the table below (with the cell temperature in °C for convenience).

$$U_{rev} = 1.184 - 2.3 \times 10^{-4}(T - T_0) + 4.3085 \times 10^{-5} T \left[\ln \left(\frac{p_{H_2} \times p_{O_2}^{1/2}}{p_{H_2O} \times p_0^{1/2}} \right) \right] \quad (2.2)$$

RH (%)	95°C			70°C		
	U (V)	i (A.cm^{-2})	P_{th} (W.cm^{-2})	U (V)	i (A.cm^{-2})	P_{th} (W.cm^{-2})
20	0.40	2.31	1.91	0.39	3.72	3.13
30	0.36	2.95	2.56	0.36	3.72	3.24
50	0.27	3.23	3.10	0.30	3.66	3.29

TABLE 2.5 – Voltage, current density, and thermal power at the current density limit.

current density range. Both the maximum current density and thermal power increase significantly. In contrast, at 70°C, neither the current density values nor the thermal power appear to be strongly dependent on the gas inlet RH. This suggests that the voltage drop observed at high current densities in figures 2.4, 2.5 and 2.7 may stem from different causes at 70 and 95°C. At the very least, it indicates that membrane and/or ionomer-related issues may play a significantly greater role in the voltage drop at 95 than at 70°C. To confirm this point, high-frequency resistance values were extracted from EIS measurements. The results show that at 95°C, increasing the gas inlet RH significantly affects R_{hf} across the entire polarization curve (figure 2.8(a)). Notably, R_{hf} is nearly halved between 20 and 50% RH at intermediate current densities, dropping from approximately 75 mΩ.cm^2 (20% RH) to 41 mΩ.cm^2 (50% RH) at 1.9 A.cm^{-2}. This reduction indicates that higher gas inlet RH improves the membrane-electrode assembly (MEA) hydration, thereby enhancing proton conductivity and overall fuel cell performance. Interestingly, this behavior is not observed at 70°C, as shown in the R_{hf} versus voltage plot in figure 2.8(b). In contrast to the results at 95°C, the R_{hf} curves at 70°C remain closely aligned regardless of the gas inlet RH, indicating a much weaker influence of humidity under these conditions.

Figure 2.8(a) also reveals a steep and sudden increase in R_{hf} near the maximum current density, reflecting most probably a rapid membrane dehydration. This may contribute to the increased instability of the operating point observed during polarization curve measurements in galvanostatic mode (figure 2.5) at 95°C. The increase in R_{hf} becomes less abrupt as the gas inlet RH rises, confirming that the phenomenon is related to water management issues. In contrast, at 70°C, no such increase is observed : the estimated R_{hf} values remain consistently close (around 35 mΩ·cm^2), regardless of the gas inlet RH. The slight R_{hf} increase of about 10 mΩ.cm^2 observed at low voltages (*i.e.*, high currents) at 70°C is minor compared to the behavior at 95°C, indicating that water management is not an issue at the lower temperature (table 2.6).

The gas composition within the cell is uniform and equal to that at gas inlets since the Nernst voltage is obtained at open circuit. The reversible voltage decreases slightly with the temperature : this is because the gas inlet RH stays identical at 70 and 95°C, resulting in a decrease in the reactant partial pressure. Nernst voltage depending on operating temperature, gas pressure and relative humidity.

RH (%)		5	10	20	30	40	50	60
T (°C)	P (bar)	U_{Nernst} (V)						
70	1	1.22	1.21	1.20	1.19	1.19	1.19	1.18
	3	1.25	1.24	1.23	1.22	1.22	1.21	1.21
95	1	1.20	1.19	1.18	1.17	1.16	1.16	1.15
	3	1.23	1.22	1.21	1.20	1.20	1.19	1.19

RH (%)	95°C		70°C	
	U (V)	R_{hf} (mΩ.cm^2)	U (V)	R_{hf} (mΩ.cm^2)
20	0.54	74	0.52	34
	0.20	159	0.20	44
30	0.52	54	0.52	33
	0.20	103	0.20	45
50	0.54	41	0.54	34
	0.22	69	0.22	40

TABLE 2.6 – R_{hf} values at 95 and 70°C and different voltages.

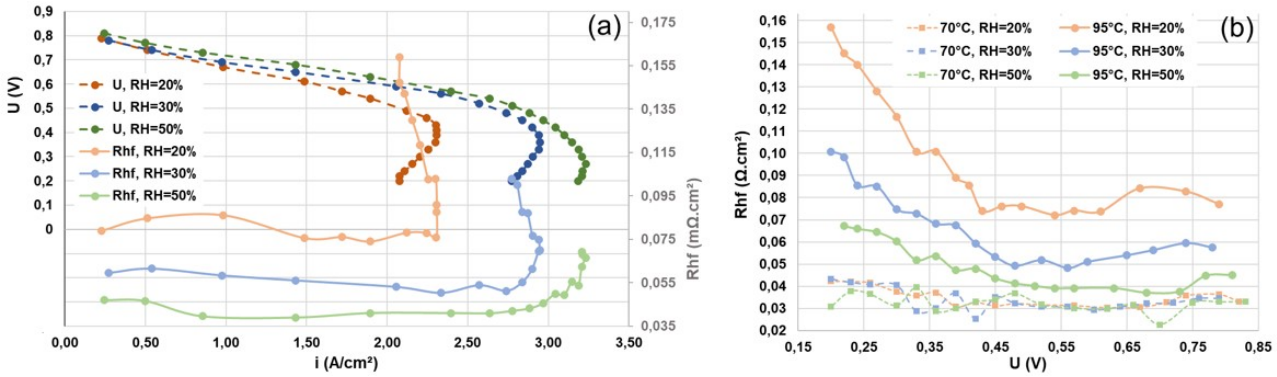

FIGURE 2.8 – R_{hf} and U evolution at 95°C (a) and R_{hf} evolution as a function of voltage at different RH and temperatures (b).

3.4 R_{hf} measurements during the AST

As highlighted in the preceding sections, the water management issues observed at high current densities and elevated temperatures may stem from two main causes : the so-called heat pipe effect [90-92], driven solely by thermal gradients within the MEA, and potentially localized drying on the anode side of the MEA due to electro-osmotic drag [34, 35, 83-85]. Electro-osmosis is driven solely by the current density and is independent on the fuel cell's electrochemical efficiency; in other words, it does not depend on the amount of heat generated by the MEA during operation. Naturally, both mechanisms may occur simultaneously, and their effects can be additive. To clarify this point, we performed an AST over eight days (section 2.3) measuring the current density and the high frequency resistance across a voltage range from approximately 0.8 to 0.2 V (figure 2.9(a)) every 48 hours. As shown in figure 2.9(a), the AST leads-as expected-to a decline in FC efficiency and voltage, thereby increasing the heat generated by the MEA at a given current density. Simultaneously, the maximum current density reached in potentiostatic mode tends to decrease and the associated rise in R_{hf} also tends to occur earlier. Interestingly, the R_{hf} values at low FC voltage remain of the same order of magnitude : approximately 100 mΩ.cm^2 at 0.2 V. This suggests that heat generation (and related membrane drying) is most likely the primary factor driving the increase in R_{hf} at high current density, and consequently, the voltage drop. Indeed, if electro-osmotic drag were the dominant mechanism, the increase in high-frequency resistance and the associated voltage drop would be expected to occur at the same current density, regardless of the amount of heat generated, *i.e.*, independently on the MEA material degradation over the course of the AST.

To confirm the minor role played by electro-osmotic drag in the observed increase of R_{hf}, we repeated the voltage and R_{hf} *vs.* current density measurements with an asymmetric gas inlet RH case, specifically

20% inlet RH on the hydrogen side and 50% on the air side, instead of 50% on both sides. Figure 2.9(b) clearly shows that this change has no significant effect on either the polarization curves or the estimated high frequency resistance values. If electro-osmosis was the cause of membrane dehydration, the reduction in anode humidification would have led to an increase in R_{hf} at a lower current density, as this effect dries out the membrane on the anode side. Consequently, membrane drying observed in the present conditions is primarily due to a thermal phenomenon that occurs at high current density.

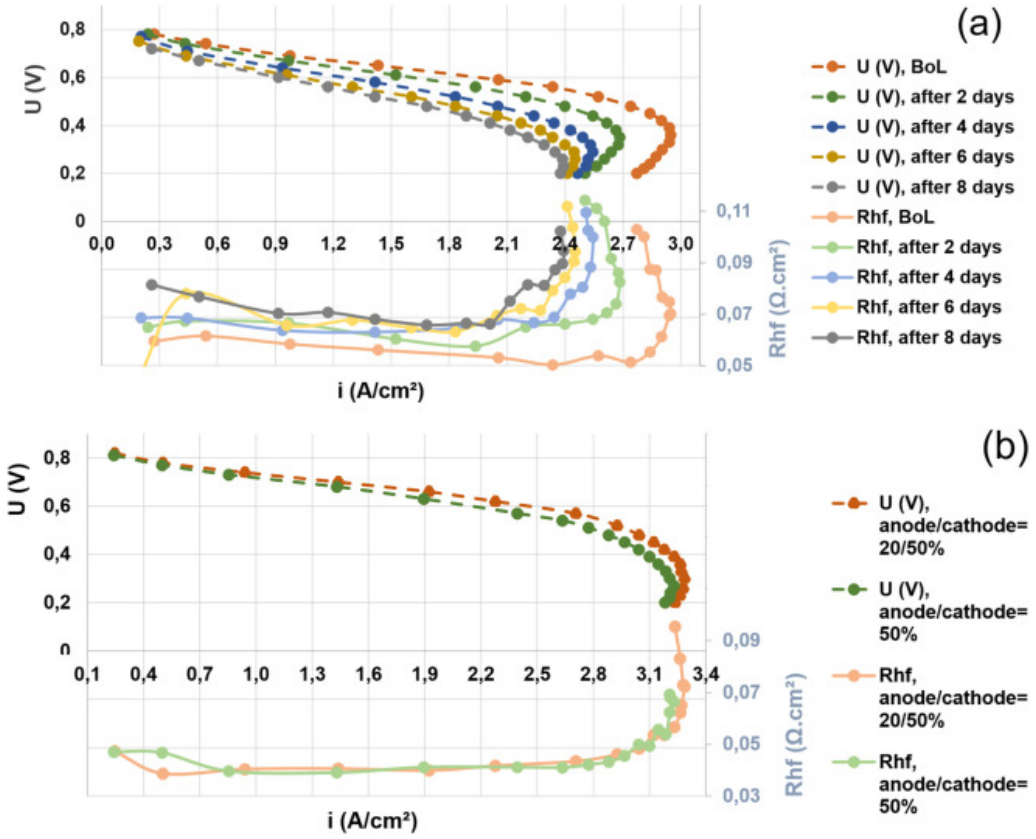

FIGURE 2.9 – R_{hf} and U evolution at 95°C (a) and R_{hf} evolution as a function of voltage at different RH and temperatures (b).

3.5 R_{hf} measurements at intermediate temperature

In real life, the operating temperature of PEMFC may vary depending on a variety of factors. For instance, Wang et al. [95] used a numerical model to assess the temperature field gradient within a stack with different cooling plate geometries. They found a significant temperature disparity between the membrane and the surface of the outermost cooling plate, depending on the current density (less than 3°C at low current density versus more than 18°C at high current density), as seen in other studies [96, 97]. We therefore measured R_{hf} in a temperature range between 70 and 95°C at 20 and 50% relative humidity. To save time, measurements were only made between 0.48 and 0.2 V to observe whether the increase in MEA dehydration begins at a specific temperature (only three voltage values are shown, table 2.7). Usual temperatures, such as 70-80°C, do not show a very significant increase in R_{hf}, which demonstrates that there are no major problems with MEA hydration at high current densities with the present MEA materials. However, a more significant increase in R_{hf} is observed at 85°C, with a value of 95 mΩ.cm^2 at 0.2 V and 20% relative humidity : the increase in MEA dehydration with current density is a gradual phenomenon, accentuated by the operating temperature. However, it can be counterbalanced with adequate gas RH, as the increase in R_{hf} is less significant at high RH.

R_{hf} ($\Omega.cm^2$)				
T (°C)	RH (%)	U (V)		
		0.48	0.3	0.2
70	20	0.034	0.039	0.044
	50	0.039	0.033	0.033
75	20	0.038	0.047	0.050
	50	0.032	0.039	0.038
80	20	0.042	0.052	0.066
	50	0.035	0.044	0.048
85	20	0.067	0.075	0.095
	50	0.040	0.054	0.054
90	20	0.056	0.084	0.108
	50	0.044	0.059	0.067
95	20	0.078	0.118	0.159
	50	0.043	0.062	0.069

TABLE 2.7 – R_{hf} measurements in potentiostatic mode at intermediate temperatures.

4 Discussion : on the main factors limiting the FC performance in the 90°C-100°C temperature range

Raising the cell operating temperature from standard (70 – 80°C) to higher levels under automotive conditions, *i.e.*, relatively dry conditions with low gas RH, alters the factors limiting fuel cell performance. While no increase in cell voltage is observed in the kinetics region, the voltage decreases in the ohmic region, and drops more significantly at high current densities (figure 2.4(a)), where voltage instabilities emerge, becoming more pronounced as the gas inlet RH is low (figure 2.5(a)). R_{hf} measurements across the entire polarization curve demonstrate that MEA hydration is responsible for that decline in performance at high current density. Similar trends have already been reported by Cho et al. at 120°C and 10% RH with SSC-PFSA ionomer [33]. Additional R_{hf} measurements taken during AST, as well as under reference conditions with asymmetric RH, support the conclusion that the heat flux generated by electrochemical reactions, rather than electro-osmotic drag, is the primary driver of MEA dehydration at 95°C and low gas RH. Complementary R_{hf} measurements, carried out to cover the full temperature range from 70 to 95°C in 5°C increments, demonstrated that this limiting factor is highly correlated with operating temperature and gas relative humidity (table 2.7) ; however, 85°C could be a critical operating point above which, MEA dehydration becomes a significant issue, at least in our operating conditions.

In addition, although, MEA dehydration can be counterbalanced by a higher gas RH, the increase in water content may create other issues that could become again the main limiting factor : actually, a threshold in gas inlet RH (app. 40%) was identified, above which no significant performance improvement was observed (figure 2.5(a)), suggesting that a trade-off exists between enhanced MEA hydration and the negative effects of oxygen dilution and/or increased mass transport resistance, as previously noted by Xu et al. [63]. Indeed, the iR-corrected polarization curves for 20, 30, and 50% inlet RH at fuel cell temperatures of 70 and 95°C (figure 2.10) confirm that the increase in R_{hf} at 95°C alone does not fully account for the lower performance compared to 70°C. A voltage difference of about 30 to 50 mV remains at low to moderate current densities (up to 1.8–2.0 $A.cm^{-2}$), and this difference increases at higher current densities. Impedance spectroscopy in galvanostatic mode has been carried out in the same conditions at 1 and 2 $A.cm^{-2}$ (only 30 and 50% RH are represented in figure 2.11). For both applied current density and relative humidity (RH), the mass transport loop

appears to be equivalent or smaller at 95 than 70°C, which suggests that larger mass transport limitations are unlikely at higher operating temperatures, at least within the low to mid-current density range. As mentioned above, the increase in water concentration with temperature (and constant RH) may be offset by a higher overall interdiffusion coefficient (table 2.3 and [62]). Therefore, the lower fuel cell voltage observed at 95°C is most likely due to the reduced oxygen partial pressure, resulting from the higher water vapor partial pressure. In addition, the results of the pseudo-Nernst equation (equation (1.2)) are in favor of that interpretation : for example, at 50% gas inlet RH and 3 bar, the oxygen inlet partial pressure diminishes from 0.6 to 0.54 bar when the temperature goes from 70°C to 95°C. This explains the app. 24 mV difference in Nernst voltage.

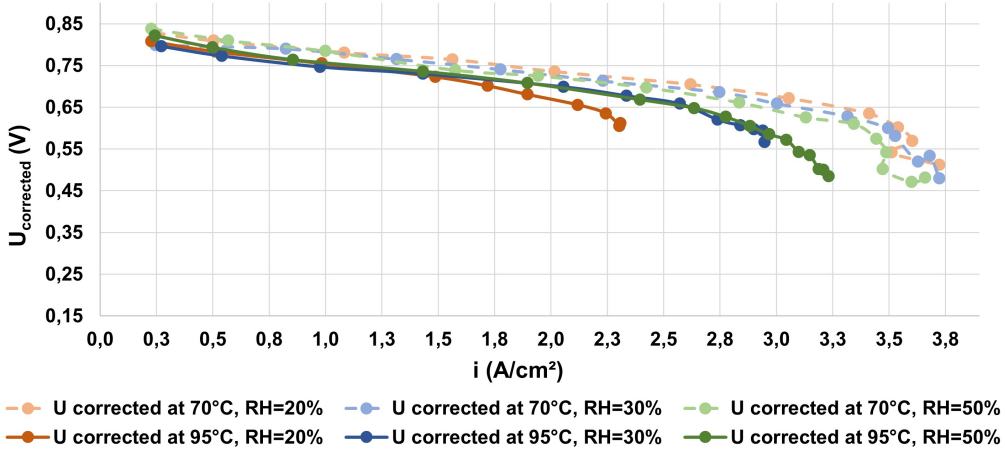

FIGURE 2.10 – 'U + i*R_{hf}' polarization curves for 20, 30 & 50% inlet RH gases and 70°C and 95°C FC temperature.

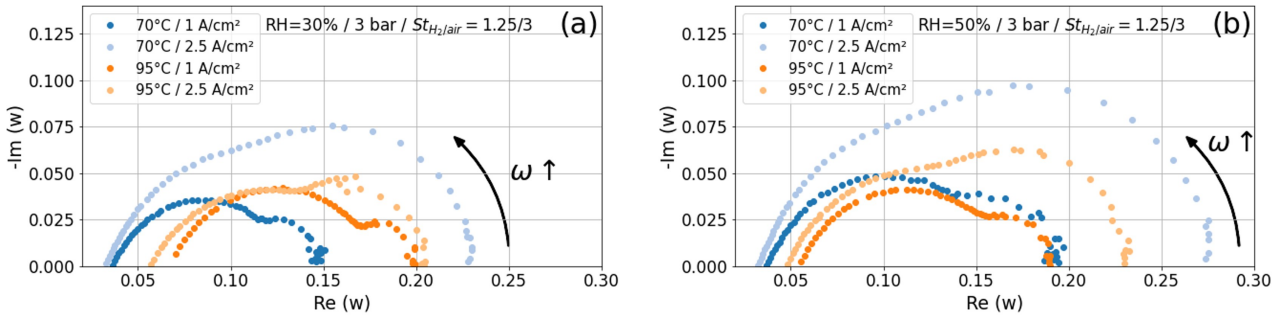

FIGURE 2.11 – EIS spectra at 70-95°C and 1-2.5 A.cm^{-2} for RH=30% (a) and 50% (b).

Butori et al. [98] reached similar conclusions after observing differences in iR-corrected polarization curves under varying temperature conditions at constant gas RH. In a subsequent experiment, they kept the gas RH and the oxygen partial pressure constant and found a good match between the iR-corrected polarization curves. This indicated that the increase in R_{hf} and the decrease in oxygen partial pressure jointly contribute to the voltage drop with increasing temperature. Saleh et al. [99] measured polarization curves at 70 and 90°C with various gas RH and concluded that FC operation at 70°C and high current densities is limited by oxygen transport, while MEA hydration becomes a major issue above 90°C as they observed that gas inlet RH is an essential parameter to control fuel cell performance ; their current density range (0-1.4 A.cm^{-2}) was smaller than ours. The hypothesis that oxygen dilution is the main factor responsible for the remaining discrepancies between iR_{hf}-corrected polarization curves could potentially be validated through impedance spectrum modeling and the de-

termination of the cathode charge transfer resistance ; however, this is out of the scope of this work. Considering only experimental results, and to summarize this discussion, four key observations lead to the conclusion that oxygen diffusion is not a performance-limiting factor at high temperature :

- Membrane drying at high temperature occurs at current densities that are usually much lower than those at which oxygen diffusion limitations appear at lower temperatures. For instance, with 20% RH inlet gases, the FC voltage drops to 0.4 V at a current density of 2.3 A.cm^{-2} at 95°C, *vs.* 3.7 A.cm^{-2} at 70°C (table 2.5). In addition, increasing the gas inlet RH at high temperature improves the current density limit, without any oxygen diffusion issue.
- Gas-phase interdiffusion coefficients improve with temperature : they are about 10 to 15% higher at 95 than at 70°C.
- All other conditions kept equal, EIS spectra do not show a larger diffusion loop at higher temperatures.
- Discrepancies between iR$_{hf}$-corrected polarization curves are observed over the entire current density range, including at very low current density. This suggests that the remaining phenomena (other than the increase in R$_{hf}$) explaining the drop in performance at high temperature are not governed by oxygen diffusion. They could possibly be driven by oxygen dilution.

Setting aside the sudden increase in R$_{hf}$ at high current density, it should be noted that there is already a significant difference in MEA hydration between different operating temperatures at low and medium current densities, affecting performance. In table 2.8, fuel cell voltage and current densities measurements, at respectively 1.5 A.cm^{-2} and 0.7 V, reveal slight voltage differences at 1.5 A.cm^{-2} from 70 to 90°C (a 40 mV drop with 20% RH inlet gases and a 50 mV drop with 50% inlet RH gases) while current densities at 0.7 V show more pronounced variations, mainly due to the increase in R$_{hf}$. This trend is confirmed above 90°C (table 2.8), although the FC voltage at 1.5 A.cm^{-2} is less sensitive to temperature with 50% gas inlet RH. On the other hand, increasing the temperature above 90°C under 20% inlet RH considerably accentuates the current density drop at 0.7 V, with only 0.624 A.cm^{-2} at 105°C, while R$_{hf}$ increases up to 0.108 Ω.cm^2.

Gas inlet RH : 20% RH				
T (°C)	U (V) @ i=1.5 A.cm^{-2}	R_{hf} (Ω.cm^2) @ i=1.5 A.cm^{-2}	i (A.cm^{-2}) @ U=0.7 V	R_{hf} @ U=0.7 V
70	0.71	0.033	1.708	0.032
75	0.70	0.033	1.616	0.033
80	0.71	0.035	1.568	0.035
85	0.70	0.044	1.476	0.043
90	0.67	0.058	1.124	0.063
95	0.62	0.079	0.748	0.087
100	0.59	0.096	0.748	0.097
105	-	-	0.624	0.108
Gas inlet RH : 50% RH				
T (°C)	U (V) @ i=1.5 A.cm^{-2}	R_{hf} (Ω.cm^2) @ i=1.5 A.cm^{-2}	i (A.cm^{-2}) @ U=0.7 V	R_{hf} @ U=0.7 V
70	0.73	0.030	1.844	0.029
75	0.72	0.030	1.800	0.029
80	0.72	0.030	1.772	0.029
85	0.70	0.032	1.552	0.033
90	0.68	0.036	1.528	0.035
95	0.71	0.040	1.492	0.040
100	0.70	0.044	1.400	0.043

TABLE 2.8 – Current density, fuel cell voltage, and R_{hf} measurements at usual operating points and different operating temperatures.

5 Local behavior assessment at 95°C

The previous section recapitulated performance limitations at 95°C, depending on gas RH. Excessive drying of the MEA was observed under low humidity conditions whereas mass transport limitations are susceptible to be detrimental under moderate conditions. Although R_{hf} trends are consistent, it represents an average value of MEA state, and there is therefore no indication about the local MEA state. That's why we conducted similar measurements on a restricted voltage range using a segmented single cell divided into 20 segments, enabling local current density and R_{hf} measurements, with the same channel geometry as previously (figure 2.12).

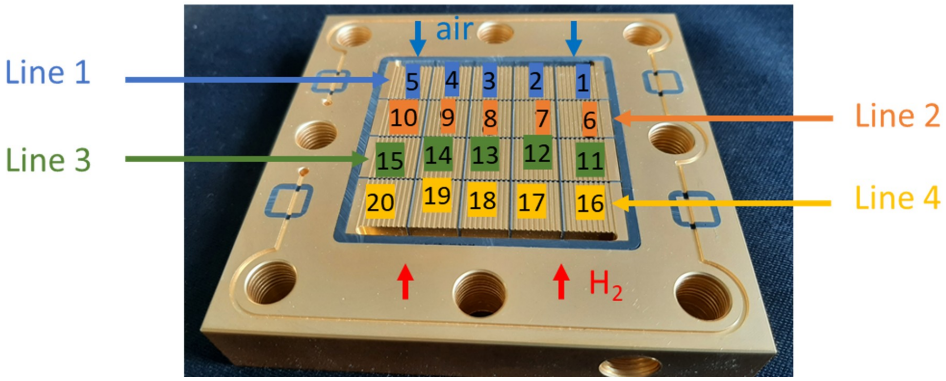

FIGURE 2.12 – Segmented monocell with straight parallel channels.

Local i and R_{hf} measurements were conducted at 95°C and under 20 or 50% gas inlet RH with

a restricted voltage range (0.30 to 0.45 V) under which significant drying was observed. As a complement, we also conducted the same measurements using Catalyst Coated Backing (CCB) MEA with thicker membrane to assess the effect of ionomer thickness on the phenomenon.

5.1 Local i and R_{hf} measurements with the state-of-the-art membrane

Although a sudden MEA drying appears at high current density, measurements in a non-segmented single cell cannot be affirmative about the globality of this phenomenon. One could think that localized areas experienced MEA drying, producing less current, while other ones could produce more current to compensate for the driest one, and possibly experience mass transport limitations due to the excessive water production. To investigate that, we measured the R_{hf} under conditions where we both observe, or did not observe, the MEA drying with the non-segmented cell. For an easier understanding, average values per line were represented (figure 2.12), enabling to assess MEA state along the channels. However, preliminary measurements showed an inhomogeneity in MEA state on each line with drier segment on the edge of each line, which could be due to an excessive reactant flowrate which could accentuate MEA drying. Nevertheless, the trends were consistent and we therefore chose to represent the average value of the 3 central columns, so that the error bars do not alter the conclusions.

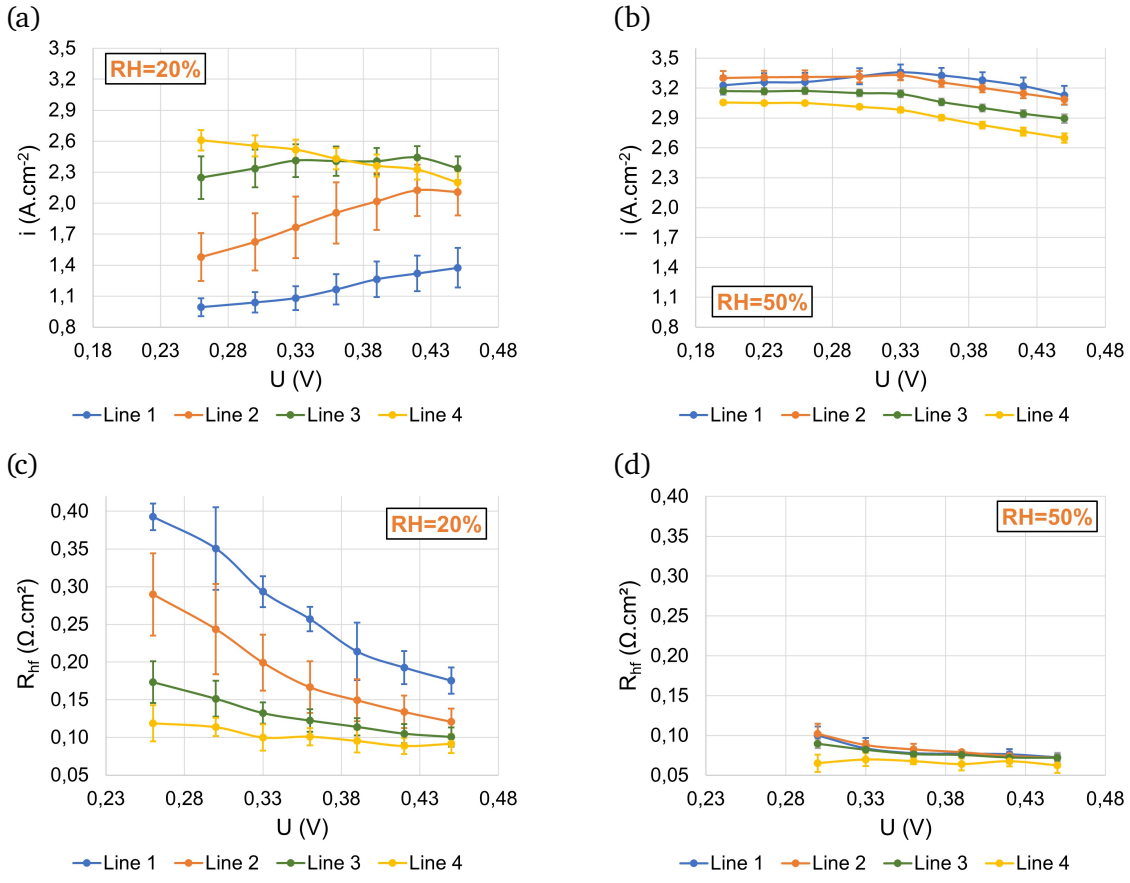

FIGURE 2.13 – Local current density and R_{hf} measurements in the 0.30-0.45 voltage range at 95°C under 20% (a)-(c) and 50% (b)-(d) gas inlet RH.

Significant differences in local current density were observed under low humidity conditions with a more pronounced local current drop near the air inlet (figure 2.13(a)). In addition, a more significant decrease is observed when reducing the fuel cell voltage, *i.e.*, increasing the average current density,

except at hydrogen inlet. In contrast, there was no such decrease under moderate humidity conditions (figure 2.13(b)) and local current productions are quite similar from one line to the other. Error bars are also very small under 50% gas RH, whereas they are particularly important under 20% gas RH, especially on line 2, close to air inlet.
These results are consistent with Rhf measurements under 20% gas RH, which showed that the highest values correspond to the lowest local current measurements. There is an increase of Rhf for all lines with decreasing fuel cell voltage which indicates that the MEA drying phenomenon is global, although it is less marked close to hydrogen inlet because of the self-humidification of the air flowrate. In addition, we observed that the highest local current values were on lines 3 and 4, which represent a compromise between MEA hydration and reactant concentration. In contrast, Rhf measurements under 50% gas RH indicated an overall stable MEA hydration state, corresponding to stable local current, with only a slight increase at low voltage.

These results confirm the trends observed in the non-segmented cell :

- Under low humidity conditions, there is a significant drying of the MEA, which is global, although more pronounced close to air inlet.
- Under moderate humidity conditions, MEA hydration state is relatively homogeneous, and the slight increase in R_{hf} at low voltage (0.28 to 0.20 V) indicates that MEA drying is significantly alleviated. Performance limitations at high current densities therefore result from a slight decrease in MEA hydration and oxygen dilution.

5.2 Effect of membrane thickness on MEA hydration

Performance limitations at high temperature and under low-humidity conditions were related to severe MEA drying due to the excessive thermal production at high current densities. R_{hf} measurements during an AST and under an asymmetrical gas RH case showed that the electroosmotic drag does not impact significantly this phenomenon. However, these conclusions were drawn with our materials, *i.e.*, a thin state-of-the-art membrane. Therefore, to go further, we performed complementary R_{hf} measurements using CCB MEA assembled by hot-pressing with thicker membranes : the 25 μm thick NR211 and the 50 μm thick NR212.

Although R_{hf} measurements were conducted under 50% gas RH, under which no significant drying was reported for the state-of-the-art membrane, significant differences in R_{hf} were observed between the lines at all voltages tested. These differences were more pronounced with the thicker membrane, indicating stronger differences in MEA hydration. In addition, the increase in R_{hf} at high current densities is more pronounced and appeared at higher voltage with increasing membrane thickness. Based on these observations, the following conclusions can be made :

- The increased differences observed along the gas flow, *i.e.*, between the lines, with thicker membranes indicate that the use of a thin state-of-the-art membrane enables a better redistribution and homogenization of water content within the MEA, limiting fuel cell voltage losses.
- The increased R_{hf} observed with NR211 and NR212 indicates a severe drying, although it was not the case with a thinner membrane. In these configurations, electroosmotic drag may be more detrimental for membrane humidification with possible water gradient within the membrane, limiting fuel cell performance.

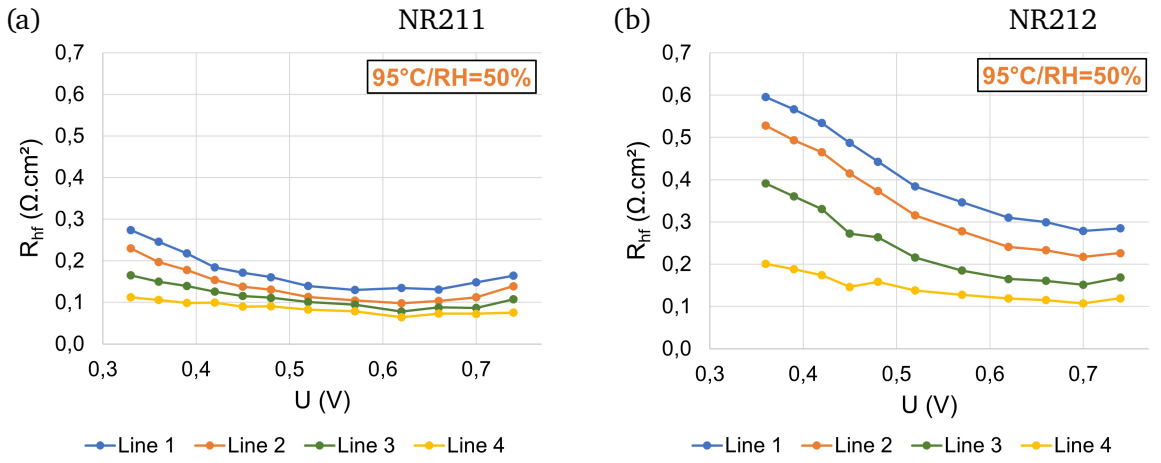

FIGURE 2.14 – R_{hf} measurements at 95°C under 50% gas RH from 0.77 to 0.33 V of CCB MEA made of NR211 (a) and NR212 (b).

6 Conclusion

We conducted extensive performance mapping using a commercial, state-of-the-art PEMFC MEA featuring a 12 µm thick LSC-PFSA membrane. The study was carried out over a temperature range of 70 to 105°C and under low to moderate gas inlet relative humidity (*i.e.*, 20 to 50% RH), representative of conditions encountered in automotive applications. Initial investigations examined the impact of external parameters, including gas relative humidity and pressure, cell temperature, and air stoichiometry. Within the tested range, results indicated that increasing gas pressure and relative humidity enhances the cell performance thanks to a higher MEA hydration, hence a smaller high frequency resistance. Additionally, an increase in air stoichiometry is beneficial, particularly at high current densities if the relative humidity of the gas is sufficient ; otherwise, a drop in performance is observed due to MEA dehydration. However, increasing the cell temperature was observed to negatively affect performance, especially under low or moderate RH, where a sudden voltage drop occurs at high current densities. Therefore, a second round of investigations was focused on the region of high current densities, where performance is typically limited by mass transport and reactant availability at standard temperatures. At 95°C, our results indicate that MEA dehydration becomes the dominant limiting factor, as low RH and elevated temperature significantly reduce membrane hydration and, consequently, proton conductivity. This was evidenced mostly through a sharp increase in the FC high frequency resistance. Additional measurements performed during an AST, *i.e.*, with a performance degradation over time, showed that membrane dehydration was most probably linked to the heat generated by the electrochemical reaction rather than by electro-osmotic drag ; indeed, this was supported by the absence of significant difference in the performance measured with symmetric gas inlet conditions (same inlet RH on the anode and cathode side : 50%) than with a lower inlet RH at the hydrogen inlet (20%) than at the air inlet (50%).

Although membrane dehydration is a major limiting factor at high temperatures, it only happens in dry conditions and non-usual operating points, *i.e.*, high current densities. Nevertheless, FC performance decreases across the entire current density range as temperature increases, mostly due to the rise in R_{hf}. However, iR-corrected polarization curves reveal that MEA hydration does not fully account for the lower performance of PEMFC when all other parameters (gas stoichiometry, pressure, and inlet RH) are held constant. We observed a residual 40 to 50 mV voltage difference up to 1.8–2.0 A.cm^{-2}, with the discrepancy increasing significantly at higher current densities. Impedance spectroscopy in

the low-to-moderate current density range showed no substantial differences in the mass transport loop between 70 and 95°C, suggesting that larger mass transport limitations at elevated temperatures are unlikely. This led us to the conclusion that oxygen dilution due to a higher water vapor concentration, was the most probable origin of the remaining voltage losses.
Finally, it should be emphasized that these findings are specific to the operating conditions, materials, and cell geometry used in this work. One cannot exclude that the optimization of both cell geometry and MEA materials could enable improved performance at high temperature in the future.

Future work will first focus on modeling the impedance spectra to accurately extract key parameters, particularly the cathode charge transfer resistance. This will enable a more precise assessment of the impact of oxygen dilution on fuel cell performance. In parallel, we plan to repeat this performance mapping using a segmented cell, to investigate the local effects of membrane and MEA dehydration on performance, impedance, and electrode potentials.

References

[1] D. A. Cullen et al., « New roads and challenges for fuel cells in heavy-duty transportation, » *Nature Energy*, t. 6, n° 5, p. 462-474, 2021, issn : 2058-7546. doi : 10.1038/s41560-021-00775-z

[2] Y. Zhao et al., « Reviews on the effects of contaminations and research methodologies for PEMFC, » *International Journal of Hydrogen Energy*, t. 45, n° 43, p. 23 174-23 200, 2020, issn : 03603199. doi : 10.1016/j.ijhydene.2020.06.145

[3] E. Gadducci et al., « Catalyst degradation under different test and poisoning conditions – Comparison parameters definition to map the effects on proton exchange membrane fuel cell voltage, » *Fuel Cells*, t. 22, n° 6, p. 241-253, 2022, issn : 1615-6854. doi : 10.1002/fuce.202200062

[4] Y. Devrim et al., « Experimental investigation of CO tolerance in high temperature PEM fuel cells, » *International Journal of Hydrogen Energy*, t. 43, n° 40, p. 18 672-18 681, 2018, issn : 03603199. doi : 10.1016/j.ijhydene.2018.05.085

[5] V. B. K.P et al., « Spatial analysis of CO poisoning in high temperature polymer electrolyte membrane fuel cells, » *International Journal of Hydrogen Energy*, t. 46, n° 11, p. 8179-8196, 2021, issn : 03603199. doi : 10.1016/j.ijhydene.2020.12.001

[6] R. K. Abdul Rasheed et al., « A review on modelling of high temperature proton exchange membrane fuel cells (HT-PEMFCs), » *International Journal of Hydrogen Energy*, t. 42, n° 5, p. 3142-3165, 2017, issn : 03603199. doi : 10.1016/j.ijhydene.2016.10.078

[7] Y. Nalbant et al., « Energy and exergy performance assessments of a high temperature-proton exchange membrane fuel cell based integrated cogeneration system, » *International Journal of Hydrogen Energy*, t. 45, n° 5, p. 3584-3594, 2020, issn : 03603199. doi : 10.1016/j.ijhydene.2019.01.252

[8] E. Jannelli et al., « Analyzing microcogeneration systems based on LT-PEMFC and HT-PEMFC by energy balances, » *Applied Energy*, t. 108, p. 82-91, 2013, issn : 03062619. doi : 10.1016/j.apenergy.2013.02.067

[9] A. Suzuki et al., « Evaluation for sintering of electrocatalysts and its effect on voltage drops in high-temperature proton exchange membrane fuel cells (HT-PEMFC), » *International Journal of Hydrogen Energy*, t. 37, n° 23, p. 18 272-18 289, 2012, issn : 03603199. doi : 10.1016/j.ijhydene.2012.09.016

[10] A. Chandan et al., « High Temperature (HT) Polymer Electrolyte Membrane Fuel Cells (PEMFC) – A Review, » *Journal of Power Sources*, t. 231, p. 264-278, 2013, issn : 0378-7753. doi : 10.1016/j.jpowsour.2012.11.126

[11] J. Zhang et al., « PEM fuel cells operated at 0% relative humidity in the temperature range of 23–120°C, » *Electrochimica Acta*, t. 52, n° 15, p. 5095-5101, 2007, issn : 00134686. doi : 10.1016/j.electacta.2007.02.002

[12] G. Alberti et al., « Polymeric proton conducting membranes for medium temperature fuel cells (110–160°C), » *Journal of Membrane Science*, t. 185, n° 1, p. 73-81, 2001, issn : 03767388. doi : 10.1016/S0376-7388(00)00635-9

[13] Y. Tang et al., « Temperature Dependent Performance and In Situ AC Impedance of High-Temperature PEM Fuel Cells Using the Nafion-112 Membrane, » *Journal of The Electrochemical Society*, t. 153, n° 11, A2036, 2006, issn : 1945-7111. doi : 10.1149/1.2337008

[14] Y.-T. Kim et al., « Nafion/ZrSPP composite membrane for high temperature operation of PEMFCs, » *Electrochimica Acta*, t. 50, n° 2-3, p. 645-648, 2004, ISSN : 00134686. DOI : 10.1016/j.electacta.2003.12.079

[15] P. Xiao et al., « Understanding of temperature-dependent performance of short-side-chain perfluorosulfonic acid electrolyte and reinforced composite membrane, » *International Journal of Hydrogen Energy*, t. 39, n° 28, p. 15 948-15 955, 2014, ISSN : 03603199. DOI : 10.1016/j.ijhydene.2014.01.204

[16] J. Li et al., « Understanding the Short-Side-Chain Perfluorinated Sulfonic Acid and Its Application for High Temperature Polymer Electrolyte Membrane Fuel Cells, » *RSC Advances*, t. 4, p. 3944-3965, 2014. DOI : 10.1039/c3ra43735c

[17] P. Xiao et al., « Physically stable and high performance Aquivion/ePTFE composite membrane for high temperature fuel cell application, » *Journal of Membrane Science*, t. 442, p. 65-71, 2013, ISSN : 0376-7388. DOI : 10.1016/j.memsci.2013.04.014

[18] Y. Jeon et al., « Temperature-dependent performance of the polymer electrolyte membrane fuel cell using short-side-chain perfluorosulfonic acid ionomer, » *International Journal of Hydrogen Energy*, t. 39, n° 22, p. 11 690-11 699, 2014, ISSN : 03603199. DOI : 10.1016/j.ijhydene.2014.05.105

[19] A. Stassi et al., « Performance comparison of long and short-side chain perfluorosulfonic membranes for high temperature polymer electrolyte membrane fuel cell operation, » *Journal of Power Sources*, t. 196, n° 21, p. 8925-8930, 2011, ISSN : 03787753. DOI : 10.1016/j.jpowsour.2010.12.084

[20] N. Zhao et al., « Superior Proton Exchange Membrane Fuel Cell (PEMFC) Performance Using Short-Side-Chain Perfluorosulfonic Acid (PFSA) Membrane and Ionomer, » *Materials*, t. 15, n° 1, p. 78, 2022, ISSN : 1996-1944. DOI : 10.3390/ma15010078

[21] L. Fan et al., « Effects of Side Chain Length on the Structure, Oxygen Transport and Thermal Conductivity for Perfluorosulfonic Acid Membrane : Molecular Dynamics Simulation, » *Journal of The Electrochemical Society*, t. 166, n° 8, F511, 2019, ISSN : 1945-7111. DOI : 10.1149/2.0791908jes

[22] T. Flottat et al., « Investigating percolation and clustering effects on aquivion and nafion membranes at the molecular scale, » *International Journal of Hydrogen Energy*, t. 48, n° 85, p. 33 283-33 296, 2023, ISSN : 03603199. DOI : 10.1016/j.ijhydene.2023.05.086

[23] S. Cui et al., « Comparison of the Hydration and Diffusion of Protons in Perfluorosulfonic Acid Membranes with Molecular Dynamics Simulations, » *The Journal of Physical Chemistry B*, t. 112, n° 42, p. 13 273-13 284, 2008, ISSN : 1520-6106, 1520-5207. DOI : 10.1021/jp8039803

[24] H. Nguyen et al., « Hydrocarbon-based Pemion™ proton exchange membrane fuel cells with state-of-the-art performance, » *Sustainable Energy & Fuels*, t. 5, n° 14, p. 3687-3699, 2021, ISSN : 2398-4902. DOI : 10.1039/D1SE00556A

[25] M. Kamal et al., « A Critical Review of the Advancement Approach and Strategy in SPEEK-Based Polymer Electrolyte Membrane for Hydrogen Fuel Cell Application, » *Energy & Fuels*, t. 38, n° 14, p. 12 337-12 386, 2024, ISSN : 0887-0624. DOI : 10.1021/acs.energyfuels.4c00462

[26] M. Daoudi et al., « Impact of sulfonated poly(ether ether ketone) membranes pretreatments on their physicochemical properties and fuel cell performances, » *Journal of Polymer Science*, t. 61, n° 9, p. 761-776, 2023, ISSN : 2642-4169. DOI : 10.1002/pol.20220649

[27] S. H. Mirfarsi et al., « High-temperature stability of hydrocarbon-based Pemion® proton exchange membranes : A thermo-mechanical stability study, » *International Journal of Hydrogen Energy*, t. 50, p. 1507-1522, 2024, issn : 03603199. doi : 10.1016/j.ijhydene.2023.07.236

[28] M. A. Hickner et al., « Understanding Liquid Water Distribution and Removal Phenomena in an Operating PEMFC via Neutron Radiography, » *Journal of The Electrochemical Society*, t. 155, n° 3, B294, 2008, issn : 1945-7111. doi : 10.1149/1.2825298

[29] Q. Liu et al., « Study on the influence of the hydrogen–oxygen stoichiometric ratio on the power performance improvement in a large-scale PEMFC stack, » *Journal of Power Sources*, t. 620, p. 235 279, 2024, issn : 03787753. doi : 10.1016/j.jpowsour.2024.235279

[30] H. Chen et al., « Optimal interval of air stoichiometry under different operating parameters and electrical load conditions of proton exchange membrane fuel cell, » *Energy Conversion and Management*, t. 205, p. 112 398, 2020, issn : 01968904. doi : 10.1016/j.enconman.2019.112398

[31] Z. Yang et al., « Effects of operating conditions on water and heat management by a transient multi-dimensional PEMFC system model, » *Energy*, t. 183, p. 462-476, 2019, issn : 03605442. doi : 10.1016/j.energy.2019.06.148

[32] B. Kim et al., « The effects of air stoichiometry and air excess ratio on the transient response of a PEMFC under load change conditions, » *Applied Energy*, t. 138, p. 143-149, 2015, issn : 03062619. doi : 10.1016/j.apenergy.2014.10.046

[33] M. K. Cho et al., « Effect of Catalyst Layer Ionomer Content on Performance of Intermediate Temperature Proton Exchange Membrane Fuel Cells (IT-PEMFCs) under Reduced Humidity Conditions, » *Electrochimica Acta*, t. 224, p. 228-234, 2017, issn : 0013-4686. doi : 10.1016/j.electacta.2016.12.009

[34] M. J. Cheah et al., « Effect of Interfacial Water Transport Resistance on Coupled Proton and Water Transport Across Nafion, » *The Journal of Physical Chemistry B*, t. 115, n° 34, p. 10 239-10 250, 2011, issn : 1520-6106. doi : 10.1021/jp204785t

[35] M. Ji et al., « A Review of Water Management in Polymer Electrolyte Membrane Fuel Cells, » *Energies*, t. 2, n° 4, p. 1057-1106, 2009, issn : 1996-1073. doi : 10.3390/en20401057

[36] T. Reshetenko et al., « Variation of PEM Fuel Cell Physical Parameters with Current : Impedance Spectroscopy Study, » *Journal of The Electrochemical Society*, t. 163, n° 9, F1100, 2016, issn : 1945-7111. doi : 10.1149/2.0981609jes

[37] W. Mérida et al., « Characterisation of proton exchange membrane fuel cell (PEMFC) failures via electrochemical impedance spectroscopy, » *Journal of Power Sources*, t. 161, n° 1, p. 264-274, 2006, issn : 03787753. doi : 10.1016/j.jpowsour.2006.03.067

[38] P. Moçotéguy et al., « Study of the impact of water management on the performance of PEMFC commercial stacks by impedance spectroscopy, » *International Journal of Hydrogen Energy*, t. 45, n° 33, p. 16 724-16 737, 2020, issn : 03603199. doi : 10.1016/j.ijhydene.2020.04.139

[39] D. Malevich et al., « Investigation of Charge-Transfer and Mass-Transport Resistances in PEMFCs with Microporous Layer Using Electrochemical Impedance Spectroscopy, » *Journal of The Electrochemical Society*, t. 156, n° 2, B216, 2008, issn : 1945-7111. doi : 10.1149/1.3033408

[40] N. Ge et al., « Membrane Dehydration with Increasing Current Density at High Inlet Gas Relative Humidity in Polymer Electrolyte Membrane Fuel Cells, » *Journal of Power Sources*, t. 422, p. 163-174, 2019, issn : 0378-7753. doi : 10.1016/j.jpowsour.2019.03.001

[41] M. Ciureanu, « Effects of Nafion® Dehydration in PEM Fuel Cells, » *Journal of Applied Electrochemistry*, t. 34, n° 7, p. 705-714, 2004, ISSN : 1572-8838. DOI : 10.1023/B:JACH.0000031102.32521.c6

[42] T. Miao, « Current density and temperature distribution measurement and homogeneity analysis for a large-area proton exchange membrane fuel cell, » *Energy*, t. 239, p. 121 922, 2022. DOI : 10.1016/j.energy.2021.121922

[43] B. Najafi et al., « Rapid Fault Diagnosis of PEM Fuel Cells through Optimal Electrochemical Impedance Spectroscopy Tests, » *Energies*, t. 13, n° 14, p. 3643, 2020, ISSN : 1996-1073. DOI : 10.3390/en13143643

[44] A. Schiefer et al., « Inductive Low-Frequency Processes in PEMFC-Impedance Spectra, » *Fuel Cells*, t. 20, n° 4, p. 499-506, 2020, ISSN : 1615-6854. DOI : 10.1002/fuce.201900212

[45] Z. Xia et al., « Effect of Channel-Rib Width Ratio and Relative Humidity on Performance of a Single Serpentine PEMFC Based on Electrochemical Impedance Spectroscopy, » *International Journal of Hydrogen Energy*, t. 47, n° 26, p. 13 076-13 086, 2022, ISSN : 0360-3199. DOI : 10.1016/j.ijhydene.2022.02.047

[46] J. Zhang et al., « PEM fuel cell relative humidity (RH) and its effect on performance at high temperatures, » *Electrochimica Acta*, t. 53, n° 16, p. 5315-5321, 2008, ISSN : 00134686. DOI : 10.1016/j.electacta.2008.02.074

[47] Y. Song et al., « High-Performance PEMFCs at Elevated Temperatures Using Nafion 112 Membranes, » *Journal of The Electrochemical Society*, t. 152, n° 3, A539, 2005, ISSN : 00134651. DOI : 10.1149/1.1855871

[48] S. Touhami et al., « Anode defects' propagation in polymer electrolyte membrane fuel cells, » *Journal of Power Sources*, t. 520, p. 230 880, 2022, ISSN : 03787753. DOI : 10.1016/j.jpowsour.2021.230880

[49] R. Sgarbi et al., « Impact of Transition Metals and Electrocatalyst Layer Thickness on the Pt-Based Cathodes of Proton Exchange Membrane Fuel Cells – Do Multimetallic Electrocatalysts Necessarily Yield an Improved Performance ? » *Advanced Energy Materials*, t. n/a, n° n/a, p. 2 403 212, ISSN : 1614-6840. DOI : 10.1002/aenm.202403212

[50] M. Daoudi et al., « Impact of Sulfonated Poly(Ether Ether Ketone) Pretreatments on Proton Exchange Membrane Fuel Cells Performances and Durability, » *ECS Meeting Abstracts*, t. MA2022-01, n° 35, p. 1406, 2022, ISSN : 2151-2043. DOI : 10.1149/MA2022-01351406mtgabs

[51] S. Touhami et al., « Anode aging in polymer electrolyte membrane fuel Cells I : Anode monitoring by ElectroChemical impedance spectroscopy, » *Journal of Power Sources*, t. 481, p. 228 908, 2021, ISSN : 03787753. DOI : 10.1016/j.jpowsour.2020.228908

[52] Y.-H. Lai et al., « Accelerated Stress Testing of Fuel Cell Membranes Subjected to Combined Mechanical/Chemical Stressors and Cerium Migration, » *Journal of The Electrochemical Society*, t. 165, n° 6, F3217, 2018, ISSN : 1945-7111. DOI : 10.1149/2.0241806jes

[53] Y.-H. Lai et al., « In-situ diagnostics and degradation mapping of a mixed-mode accelerated stress test for proton exchange membranes, » *Journal of Power Sources*, t. 274, p. 1162-1172, 2015, ISSN : 03787753. DOI : 10.1016/j.jpowsour.2014.10.116

[54] G. S. Harzer et al., « Cathode Loading Impact on Voltage Cycling Induced PEMFC Degradation : A Voltage Loss Analysis, » *Journal of The Electrochemical Society*, t. 165, n° 6, F3118, 2018, ISSN : 1945-7111. DOI : 10.1149/2.0161806jes

[55] D. Garcia-Sanchez et al., « Local impact of load cycling on degradation in polymer electrolyte fuel cells, » *Applied Energy*, t. 259, p. 114 210, 2020, ISSN : 03062619. DOI : 10.1016/j.apenergy.2019.114210

[56] S. Zhang et al., « Effects of open-circuit operation on membrane and catalyst layer degradation in proton exchange membrane fuel cells, » *Journal of Power Sources*, t. 195, n° 4, p. 1142-1148, 2010, ISSN : 03787753. DOI : 10.1016/j.jpowsour.2009.08.070

[57] S. Zhang et al., « Effect of open circuit voltage on degradation of a short proton exchange membrane fuel cell stack with bilayer membrane configurations, » *Journal of Power Sources*, t. 205, p. 290-300, 2012, ISSN : 03787753. DOI : 10.1016/j.jpowsour.2012.01.031

[58] G. Etienne et al., *On the main factors limiting the performance of state-of-art polymer electrolyte membrane fuel cells in the 90-100°C temperature range : data for replication*, 2025. DOI : 10.57745/6K5UR2

[59] J. B. Lu et al., « Pressure Effect on the PEMFC Performance, » *Fuel Cells*, t. 19, n° 3, p. 211-220, 2019, ISSN : 1615-6854. DOI : 10.1002/fuce.201800135

[60] D. Ko et al., « Investigation of the effect of operating pressure on the performance of proton exchange membrane fuel cell : In the aspect of water distribution, » *Renewable Energy*, t. 115, p. 896-907, 2018, ISSN : 09601481. DOI : 10.1016/j.renene.2017.08.063

[61] Q. Zhang et al., « Experimental study of variable operating parameters effects on overall PEMFC performance and spatial performance distribution, » *Energy*, t. 115, p. 550-560, 2016, ISSN : 03605442. DOI : 10.1016/j.energy.2016.08.086

[62] Bird Robert Byron, *Transport Phenomena*, Revised 2nd edition. New York [etc : John Wiley & Sons, Inc., 2007, ISBN : 978-0-470-11539-8.

[63] Y. Xu et al., « Investigation of Inlet Gas Relative Humidity on Performance Characteristics of PEMFC Operating at Elevated Temperature, » *World Electric Vehicle Journal*, t. 12, n° 3, p. 110, 2021, ISSN : 2032-6653. DOI : 10.3390/wevj12030110

[64] B. Wang et al., « Investigation of the effect of humidity at both electrode on the performance of PEMFC using orthogonal test method, » *International Journal of Hydrogen Energy*, t. 44, n° 26, p. 13 737-13 743, 2019, ISSN : 03603199. DOI : 10.1016/j.ijhydene.2019.03.139

[65] H. Cai et al., « Properties of composite membranes based on sulfonated poly(ether ether ketone)s (SPEEK)/phenoxy resin (PHR) for direct methanol fuel cells usages, » *Journal of Membrane Science*, t. 297, n° 1-2, p. 162-173, 2007, ISSN : 03767388. DOI : 10.1016/j.memsci.2007.03.040

[66] M. A. Barique et al., « Effect of Elevated Temperatures on the States of Water and Their Correlation with the Proton Conductivity of Nafion, » *ACS Omega*, t. 3, n° 1, p. 349-360, 2018. DOI : 10.1021/acsomega.7b01765

[67] A. B. Anderson et al., « Activation Energies for Oxygen Reduction on Platinum Alloys : Theory and Experiment, » *The Journal of Physical Chemistry B*, t. 109, n° 3, p. 1198-1203, 2005, ISSN : 1520-6106. DOI : 10.1021/jp047468z

[68] E. C. M. Tse et al., « Effect of Temperature and Pressure on the Kinetics of the Oxygen Reduction Reaction, » *The Journal of Physical Chemistry A*, t. 119, n° 8, p. 1246-1255, 2015, ISSN : 1089-5639. DOI : 10.1021/acs.jpca.5b00572

[69] M. Vinothkannan et al., « Toward improved mechanical strength, oxidative stability and proton conductivity of an aligned quadratic hybrid (SPEEK/FPAPB/Fe 3 O 4 -FGO) membrane for application in high temperature and low humidity fuel cells, » *RSC Advances*, t. 7, n° 62, p. 39 034-39 048, 2017. DOI : 10.1039/C7RA07063B

[70] R. Omrani et al., « PEMFC purging at low operating temperatures : An experimental approach, » *International Journal of Energy Research*, t. 43, n° 13, p. 7496-7507, 2019, ISSN : 1099-114X. DOI : 10.1002/er.4783

[71] M. Pérez-Page et al., « Effect of the Operation and Humidification Temperatures on the Performance of a PEM Fuel Cell Stack, » *ECS Transactions*, t. 25, n° 1, p. 733, 2009, ISSN : 1938-5862. DOI : 10.1149/1.3210625

[72] X. Liu et al., « Proton conductivity improvement of sulfonated poly(ether ether ketone) nanocomposite membranes with sulfonated halloysite nanotubes prepared via dopamine-initiated atom transfer radical polymerization, » *Journal of Membrane Science*, t. 504, p. 206-219, 2016, ISSN : 03767388. DOI : 10.1016/j.memsci.2016.01.023

[73] J. Peron et al., « Fuel cell catalyst layers containing short-side-chain perfluorosulfonic acid ionomers, » *Journal of Power Sources*, t. 196, n° 1, p. 179-181, 2011, ISSN : 03787753. DOI : 10.1016/j.jpowsour.2010.06.050

[74] H. Wu et al., « Novel sulfonated poly (ether ether ketone)/phosphonic acid-functionalized titania nanohybrid membrane by an in situ method for direct methanol fuel cells, » *Journal of Power Sources*, t. 273, p. 544-553, 2015, ISSN : 03787753. DOI : 10.1016/j.jpowsour.2014.09.134

[75] Z. Zhu et al., « Temperature Impacts on Oxygen Reduction Reaction Measured by the Rotating Disk Electrode Technique, » *The Journal of Physical Chemistry C*, t. 124, n° 5, p. 3069-3079, 2020, ISSN : 1932-7447. DOI : 10.1021/acs.jpcc.9b10173

[76] J. Mishler et al., « Probing the Water Content in Polymer Electrolyte Fuel Cells Using Neutron Radiography, » *Electrochimica Acta*, t. 75, p. 1-10, 2012, ISSN : 0013-4686. DOI : 10.1016/j.electacta.2012.04.040

[77] F. Vandenberghe et al., « Low-Loaded Catalyst Layers for Proton Exchange Membrane Fuel Cell Dynamic Operation Part 1 : Experimental Study, » *Electrochimica Acta*, t. 511, p. 145 364, 2025, ISSN : 0013-4686. DOI : 10.1016/j.electacta.2024.145364

[78] F. Vandenberghe et al., « Low-Loaded Catalyst Layers for Proton Exchange Membrane Fuel Cell Dynamic Operation Part 2 : Modeling Study, » *Electrochimica Acta*, t. 535, p. 146 542, 2025, ISSN : 0013-4686. DOI : 10.1016/j.electacta.2025.146542

[79] N. Takimoto et al., « Hydration behavior of perfluorinated and hydrocarbon-type proton exchange membranes : Relationship between morphology and proton conduction, » *Polymer*, t. 50, n° 2, p. 534-540, 2009, ISSN : 00323861. DOI : 10.1016/j.polymer.2008.11.029

[80] X. Yan et al., « Ion and water transport in functionalized PEEK membranes, » *Journal of Membrane Science*, t. 429, p. 13-22, 2013, ISSN : 03767388. DOI : 10.1016/j.memsci.2012.11.026

[81] C. Yin et al., « Positron annihilation characteristics, water uptake and proton conductivity of composite Nafion membranes, » *Physical Chemistry Chemical Physics*, t. 19, n° 24, p. 15 953-15 961, 2017, ISSN : 1463-9076, 1463-9084. DOI : 10.1039/C7CP03052E

[82] S. Nakamura et al., « The Diffusion Overpotential Increase and Appearance of Overlapping Arcs on the Nyquist Plots in the Low Humidity Temperature Test Conditions of Polymer Electrolyte Fuel Cell, » *Journal of Power Sources*, t. 186, n° 2, p. 278-285, 2009, ISSN : 0378-7753. DOI : 10.1016/j.jpowsour.2008.10.022

[83] X.-G. Yang et al., « Simultaneous Measurements of Species and Current Distributions in a PEFC under Low-Humidity Operation, » *Journal of The Electrochemical Society*, t. 152, n° 4, A759, 2005, ISSN : 00134651. DOI : 10.1149/1.1864492

[84] K. Jiao et al., « Water transport in polymer electrolyte membrane fuel cells, » *Progress in Energy and Combustion Science*, t. 37, n° 3, p. 221-291, 2011, ISSN : 03601285. DOI : 10.1016/j.pecs.2010.06.002

[85] Y. Park et al., « An experimental investigation of electro-osmotic drag coefficients in a polymer electrolyte membrane fuel cell, » *International Journal of Hydrogen Energy*, t. 33, n° 24, p. 7513-7520, 2008, ISSN : 03603199. DOI : 10.1016/j.ijhydene.2008.09.077

[86] D. G. Sanchez et al., « Oscillations of PEM Fuel Cells at Low Cathode Humidification, » *Journal of Electroanalytical Chemistry*, Special Issue Dedicated to Jacek Lipkowski, t. 649, n° 1, p. 219-231, 2010, ISSN : 1572-6657. DOI : 10.1016/j.jelechem.2010.04.005

[87] X. Li et al., « Dynamic behaviors of PEM fuel cells under load changes, » *International Journal of Hydrogen Energy*, t. 45, n° 39, p. 20 312-20 320, 2020, ISSN : 03603199. DOI : 10.1016/j.ijhydene.2019.12.034

[88] A. Thomas et al., « Thermal Effect on Water Transport in Proton Exchange Membrane Fuel Cell, » *Fuel Cells*, t. 12, n° 2, p. 212-224, 2012, ISSN : 1615-6846, 1615-6854. DOI : 10.1002/fuce.201100100

[89] A. Thomas et al., « Thermal and Water Transfer in PEMFCs : Investigating the Role of the Microporous Layer, » *International Journal of Hydrogen Energy*, t. 39, n° 6, p. 2649-2658, 2014, ISSN : 0360-3199. DOI : 10.1016/j.ijhydene.2013.11.105

[90] Y. Huang et al., « Thermal Management of Polymer Electrolyte Membrane Fuel Cells : A Critical Review of Heat Transfer Mechanisms, Cooling Approaches, and Advanced Cooling Techniques Analysis, » *Energy Conversion and Management*, t. 254, p. 115 221, 2022, ISSN : 0196-8904. DOI : 10.1016/j.enconman.2022.115221

[91] S. G. Kandlikar et al., « Thermal Management Issues in a PEMFC Stack – A Brief Review of Current Status, » *Applied Thermal Engineering*, Selected Papers from the 10th UK National Heat Transfer Conference, Edinburgh, Scotland, September 10-11, 2007, t. 29, n° 7, p. 1276-1280, 2009, ISSN : 1359-4311. DOI : 10.1016/j.applthermaleng.2008.05.009

[92] A. Thomas et al., « Measurements of Electrode Temperatures, Heat and Water Fluxes in PEMFCs : Conclusions about Transfer Mechanisms, » *Journal of The Electrochemical Society*, t. 160, n° 2, F191, 2012, ISSN : 1945-7111. DOI : 10.1149/2.006303jes

[93] F. Cai et al., « Proton Exchange Membrane Fuel Cell (PEMFC) Operation in High Current Density (HCD) : Problem, Progress and Perspective, » *Energy Conversion and Management*, t. 307, p. 118 348, 2024, ISSN : 0196-8904. DOI : 10.1016/j.enconman.2024.118348

[94] N. Ramaswamy et al., « Materials and Design Selection to Improve High Current Density in PEMFC, » *ECS Meeting Abstracts*, t. MA2018-01, n° 27, p. 1585, 2018, ISSN : 2151-2043. DOI : 10.1149/MA2018-01/27/1585

[95] Y. Wang et al., « Optimizing Temperature Distribution in a PEMFC Stack : A Computational Study on Cooling Plate and Coolant Dynamics, » *International Journal of Hydrogen Energy*, t. 97, p. 88-103, 2025, ISSN : 0360-3199. DOI : 10.1016/j.ijhydene.2024.11.339

[96] S. Cheng et al., « Model-Based Temperature Regulation of a PEM Fuel Cell System on a City Bus, » *International Journal of Hydrogen Energy*, t. 40, n° 39, p. 13 566-13 575, 2015, ISSN : 0360-3199. DOI : 10.1016/j.ijhydene.2015.08.042

[97] Y. Song et al., « Fixed Air Flow-Rate Selection by Considering the Self-Regulating Function of Low Power Air-Cooled PEMFC Stack, » *International Journal of Heat and Mass Transfer*, t. 158, p. 119 771, 2020, ISSN : 0017-9310. DOI : 10.1016/j.ijheatmasstransfer.2020.119771

[98] M. Butori et al., « The Effect of Oxygen Partial Pressure and Humidification in Proton Exchange Membrane Fuel Cells at Intermediate Temperature (80–120 °C), » *Journal of Power Sources*, t. 563, p. 232 803, 2023, issn : 0378-7753. doi : 10.1016/j.jpowsour.2023.232803

[99] M. M. Saleh et al., « Exploring the Effects of Symmetrical and Asymmetrical Relative Humidity on the Performance of H2/Air PEM Fuel Cell at Different Temperatures, » *Journal of Power Sources*, t. 164, n° 2, p. 503-509, 2007, issn : 0378-7753. doi : 10.1016/j.jpowsour.2006.11.065

Chapter 3

sPEEK Membranes : A Review of Structural and Physicochemical Properties

1 Introduction **98**
2 PEEK sulfonation **99**
3 Microstructure & Morphology **101**
4 Physicochemical properties **104**
4.1 Sorption, water uptake 105
4.2 Conductivity 107
4.3 Other transport properties 110
4.4 Mechanical properties 112
5 Ionomer durability **115**
5.1 sPEEK during *ex situ* degradation tests 115
5.2 sPEEK durability during fuel cell operation 117
6 Impact of manufacturing process **118**
6.1 Casting solvent 119
6.2 Pretreatment 121
6.2.1 Soaking treatments 121
6.2.2 Crosslinking 123
7 Conclusions/perspectives **124**
References **126**

Context

As explained previously, PFSA-based compounds are known to be costly and environmentally harmful due to their manufacturing process. For this reason, significant efforts have been devoted to the development of alternative materials capable of delivering comparable or improved performances while being less expensive and fluorine-free. Among these alternatives, hydrocarbon membranes-to which sPEEK membranes belong-are promising candidates.

The following chapters therefore aim to investigate sPEEK as an alternative membrane material. However, before presenting the experimental results, a dedicated literature review on sPEEK is provided in this chapter. An in-depth analysis of this ionomer was conducted, with particular emphasis on the relationship between its microstructure and functional properties. This review has been intentionally presented separately in order to ease the reading of the general state of the art (chapter 1), and because it is intended for submission to a scientific journal as a review article.

1 Introduction

Hydrogen technologies are considered a promising solution to limit greenhouse emissions from different sectors such as industries and transport. Different sectors such as fertilizer production and metallurgy use hydrogen, often produced from vapor reforming, which is a very polluting process. In these cases, electrolyzers supplied with energy from nuclear plant or renewable energy could significantly reduce their emissions. For transportation applications, several studies established potential scenarios where light and heavy-duty transportation such as train and trucks are equipped with a proton exchange membrane fuel cell, suitable thanks to its high-power density and rapid start-up/shut down process.

Numerous hydrogen technologies, such as proton exchange membrane (PEM) electrolyzers and fuel cells, are composed of bipolar plates, gas diffusion layers, catalyst layers, and an ionomer membrane. Nowadays, PerFluoroSulfonicAcid-based ionomers are considered the reference material both in the catalytic layer and as the membrane in low-temperature technologies because of their excellent proton conductivity and chemical stability. Although long-term operation has not revealed significant fluoride compound release, it is widely accepted that the pollution during manufacturing-due to fluorine chemistry-and the high cost are major drawbacks for the large-scale development of hydrogen technologies [1, 2]. Although comprehensive data are lacking, the cost of PerFluoroSulfonicAcid (PFSA) membranes is estimated to be around 300-500\$/m^2, depending on studies [3-5], which represents a significant part of the cost of the stack [6, 7]. Life cycle analysis enables comparison of the environmental impact of each material. Although conclusions depend strongly on methodological assumptions-for example, whether PFSA ionomer is recycled after operation-significant impacts of PFSA production on the ozone layer depletion, water ecotoxicity, and global warming have been consistently reported [6-9]. To reduce both economic and environmental costs, attention has focused on PFSA recycling via solvent-based separation processes. Robert et al. [10] significantly reduced the environmental impact, using isopropanol (IPA) solvent, and energy consumption in a fast and efficient electrode-membrane separation process. Nevertheless, Kutter et al. [11] observed differences in the properties of SSC-and LSC-PFSA membranes after reprocessing, notably in glass transition behavior, which resulted in different fuel cell performances between pristine and reprocessed membranes. This highlights that structural differences appear after PFSA recycling [12], which may require additional processing steps to recover its properties and enable effective re-employment in fuel cells. In comparison, hydrocarbon-based ionomers are considered as a serious alternative because of the less polluting manufacturing process and lower cost [13, 14]. Yuan et al. [4] compared alkaline-based flow battery

cost and performance made of sulfonated poly(ether ether ketone) (sPEEK) and Nafion 212. They reported a higher energy efficiency of sPEEK in a single-cell. In addition, given a 12.3\$/m^2 and 500\$/m^2 for sPEEK and Nafion 212, respectively, they reported that a 10 kW stack made of sPEEK cost 2652 \$ (sPEEK representing 3.5% of the price) whereas Nafion 212 represented 59.0% of the 6262\$ 10 kW stack.

In this context, sulfonated(poly ether ether ketone) (sPEEK) has long been considered as a promising candidate to replace PFSA-based component, thanks to superior thermal and mechanical properties. Its physicochemical properties strongly depends on its microstructure, which may enable its synthesis in accordance with the targeted operation. Despite this, its low chemical durability compared to PFSA ionomers and its high dependence on humidification have focused research on other hydrocarbon polymers. Nevertheless, more recent research reported increased fuel cell performance and durability through material modification strategies, including incorporation of functional additives.

Although the properties of sPEEK can be improved through chemical modification, composite formation (via incorporation of particulate additives) and hybridization, it is noteworthy that appropriate pretreatment can already yield significant improvements in sPEEK performance. However, optimizing these pretreatments requires a deep understanding of the influence of sPEEK microstructure on its properties. Nevertheless, the literature specifically dedicated to sPEEK alone, either in its pristine form or after pretreatment, remains limited. In most cases, the available information is embedded within studies focusing on hybrid materials, composite architectures, or chemical modification strategies, which makes it difficult to establish a clear understanding of the sPEEK behavior. Furthermore, in studies addressing pristine sPEEK, most investigations focus on property variations as a function of the degree of sulfonation (DS), without sufficiently addressing the role of microstructure or its impact on fuel cell performance. In this context, this review aims to focus on sPEEK as a standalone material by extracting and discussing the available information specifically related to its intrinsic behavior. Within this framework, the work further aims to bridge the existing knowledge gap by establishing a clear link between microstructure and physicochemical properties, and to examine how this relationship affects sPEEK stability and performance in fuel cells. Pretreatment strategies are also discussed to demonstrate the potential for performance improvement without the use of hybridization, chemical modification, or additive incorporation.

2 PEEK sulfonation

The sulfonation of polyether ether ketone (PEEK) is a necessary step to convert the polymer into an ionomer, enabling its use as a polyelectrolyte in PEM fuel cells or electrolyzers. This process involves introducing sulfonic acid groups onto the aromatic rings of the PEEK backbone. The extent of sulfonation is quantified by the degree of sulfonation (DS), which is defined as the number of sulfonic acid groups per mole of monomer :

$$DS = \frac{n_{PEEK-SO_3H}}{n_{PEEK-SO_3H} + n_{PEEK}} \tag{3.1}$$

The DS is directly related to the ion exchange capacity (IEC), which represents the number of sulfonic groups per gram of dry ionomer :

$$IEC = \frac{n_{SO_3H}}{m_{\text{sec}}} \times 1000 \tag{3.2}$$

Both parameters are related :

$$IEC = \frac{1000 \times DS}{M_{PEEK} + DS \times M_{SO_3H}} \tag{3.3}$$

with M_{PEEK}=288 g.mol^{-1} and M_{SO_3H}=80 g.mol^{-1}

Achieving an adequate DS, typically in the range of 50-65% according to Parnian et al. [15] and Portale et al. [16] is critical for ensuring the desired mechanical and physicochemical properties of the sPEEK [17]. To reach this optimal DS, various sulfonation methods have been described in the literature, generally classified into two categories [18-20] :

- Post-sulfonation techniques are the simplest and least time-consuming synthesis processes. They consist of an electrophilic substitution reaction, where a hydrogen atom on the aromatic ring is replaced by a sulfonic acid group. Several solutions can be used, such as sulfuric acid and chlorosulfonic acid. Among them, concentrated sulfuric acid (nearly 100%) is most commonly employed to limit side reactions and prevent polymer cross-linking [20], which could otherwise degrade the thermal and mechanical properties of the resulting ionomer [17].
- Pre-sulfonation techniques offer better control over both the degree of sulfonation [21] and the positioning of sulfonic acid groups on the aromatic ring of the PEEK monomer units. This method involves using pre-sulfonated monomers during polymer synthesis, allowing greater control over the ionomer structure. Indeed, it enables selective placement of the sulfonic groups, which can improve the chemical stability of the resulting polymer.

Except in rare cases [22, 23], studies in the literature use commercially available PEEK from various suppliers (Victrex, Gastone, Sigma Aldrich for example) as a starting point for sPEEK synthesis and follow a post-sulfonation approach. After sulfonation, a solution casting method is applied to form a membrane. Sulfonation is carried out by accurately mixing PEEK powder with an acid solution, whose composition varies across studies. Several studies [24-28] highlight that the DS of sPEEK is mainly influenced by three parameters : acid strength, reaction time, and temperature. Therefore, the most critical parameters are the temperature of the solution and the duration of the sulfonation step. The various protocols used–summarized in (table 3.1)-show that higher temperatures significantly increase the reaction rate, thus leading to much shorter durations than at room temperature to reach the same DS (generally a few hours at higher temperature and ranging from several tens to several hundreds of hours at ambient temperature). Once the reaction time, corresponding to the desired DS, is reached, the sPEEK is precipitated by addition of cold water. After filtration, the sPEEK precipitate is washed several times with water until a neutral pH is obtained. Finally, the sPEEK precipitate is dried mainly under air or vacuum for a few hours to several days at temperatures ranging from room temperature to over 100°C depending on the study. This drying step can be divided into several stages with different temperatures.

The second step consists of casting the sPEEK solution to form a membrane. To do this, the sPEEK powder is mixed with a solvent (DMAc, DMF, NMP, water/acetone, etc.) to obtain a concentrated solution with a weight fraction ranging from a few percent up to 15%. The solution is then cast onto an inert substrate and left to dry, following a series of controlled steps over several hours (table 3.1).

Step 1					Step 2		Ref.
Ratio $m_{PEEK}/V_{H_2SO_4}$	Temperature and time of stirring	Precipitation	Washing	Drying	Casting solvent and sPEEK/solvent ratio	Drying	
10 g / 100 mL	60°C / 4h	H_2O	H_2O until neutral pH	70°C vacuum oven	DMAc / 10% wt	T_{room}/12h + 70°C/24h	[29]
20 g / 500 mL	T_{room} / 24-140h	H_2O + stirring	H_2O until neutral pH	25-100°C 8-10h vacuum	DMAc, DMF 10-15% wt	Ambient / few days	[30]
5 g / 95 mL	T_{room}/1h + 47-63°C	H_2O + stirring	H_2O until neutral pH	100°C overnight	DMAc 2-4h 10% wt	100-110°C + 60°C/6h	[27]
5 g / 100 mL	50°C / 7h	H_2O + stirring	H_2O until neutral pH	60°C/12h + 110°C vacuum	DMAc 45°C 10% w/V	60°C/16h + 120°C vacuum	[31]
10 g / 50 mL MSA	30°C	H_2O neutral	H_2O until neutral pH	100°C / 5h	DMA, NMP 0.3g/9.7g	100°C/10h + 120°C/2h	[32]
40 g / 1.4 L	T_{room} or 55°C/10h	H_2O	H_2O until pH=6-7	T_{room}/48h + 80°C/24h	DMAc, DMF 15% wt	T_{room}/1d + 60°C/2d	[24]
20 g / 1 L	T_{room} / 24-112h	H_2O + stirring	H_2O until neutral pH	100°C 8-10h vacuum	DMAc / 5-10% wt	60°C/4-6h + 80-120°C	[33]
4-10% w/V	35-55°C / 3h	H_2O + stirring	H_2O until neutral pH	70°C / 12h	DMF + 3.3% sPEEK	No indication	[34]

Table 3.1 – Literature review of the two-step protocol for sPEEK membrane preparation.

At the end, an sPEEK membrane is formed, consisting of a hydrophobic poly(ether ether ketone) (PEEK) backbone with hydrophilic sulfonic acid groups directly attached to the aromatic ring (figure 3.1). The PEEK backbone ensures the mechanical strength of the ionomer while the sulfonic groups govern water uptake and proton conductivity.

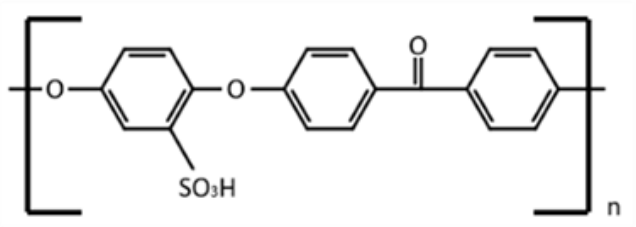

Figure 3.1 – sPEEK chemical structure.

3 Microstructure & Morphology

The complex microstructure and morphology of sPEEK are strongly influenced by its degree of sulfonation [35-37]. For this reason, several techniques were used to analyze these features, including X-ray diffraction (XRD) and small-angle X-ray scattering (SAXS). XRD was used to assess the degree of crystallinity, while SAXS provided information on the material morphology. In addition, the different relaxation processes of the sPEEK polymer chains were investigated using dynamic mechanical analysis (DMA).

XRD measurements show that a non-fluorinated PEEK membrane displays four diffraction peaks at 18.7°, 20.6°, 22.7°, and 28.7° (figure 3.2), characteristic of a crystalline orthorhombic structure [38]. After sulfonation, all four crystalline peaks disappear and only one broad peak remains, highlighting a shift from a crystalline to an amorphous state. As the DS increases, a decrease in intensity as well as a broadening is observed [35, 39] (figure 3.2(b)), indicating a loss of crystallinity. According to the authors, this loss of crystallinity is due to the sulfonic groups which act as a plasticizer, preventing

rearrangement and entanglement for the intercrystalline regions.

(a) (b)

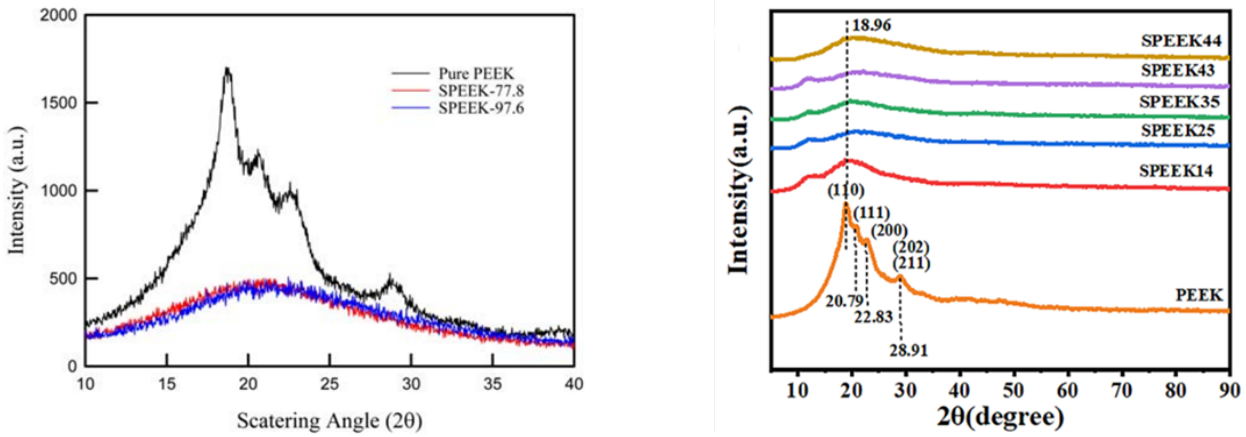

FIGURE 3.2 – XRD profiles of PEEK and sulfonated-PEEK (sPEEK) with different degrees of sulfonation : [36] (a) and [39] (b).

SAXS measurements make it possible to investigate the distance between hydrophilic and hydrophobic domains, phase separation, and the size of internal polymer structures [36, 40-42]. In particular, SAXS enables the observation of the ionomer peak, which is associated with the formation of hydrophilic domains. It should be noted that sPEEK membranes require the exchange of H^+ counter-ions to reveal the ionomer peak [40]. Indeed, SAXS profiles of dry sPEEK membranes in the H^+ form with various sulfonation levels show no ionomer peaks, in contrast to Nafion membrane, which exhibits a clear peak around 2 nm^{-1} (figure 3.3(a)). The sPEEK ionomer peak is too weak to be detected in the H^+ form because the electron density of the ionic clusters is too similar to that of the polymer backbone.

To enhance the scattering contrast, Yang et al. [40] introduced sodium and cesium counter-ions into sPEEK membranes and showed that cesium-neutralized membranes exhibit broad ionomer peaks (figure 3.3(b)). This peak reveals the presence of small ionic clusters separated by about 2.3 nm in sPEEK membranes. Moreover, SAXS measurements highlighted a shift of the ionomer peak toward higher q-values, *i.e.*, a decrease in distance between the ionic aggregates, with increasing DS [35, 36, 40], indicating an increase in the number of ionic aggregates.

(a) (b)

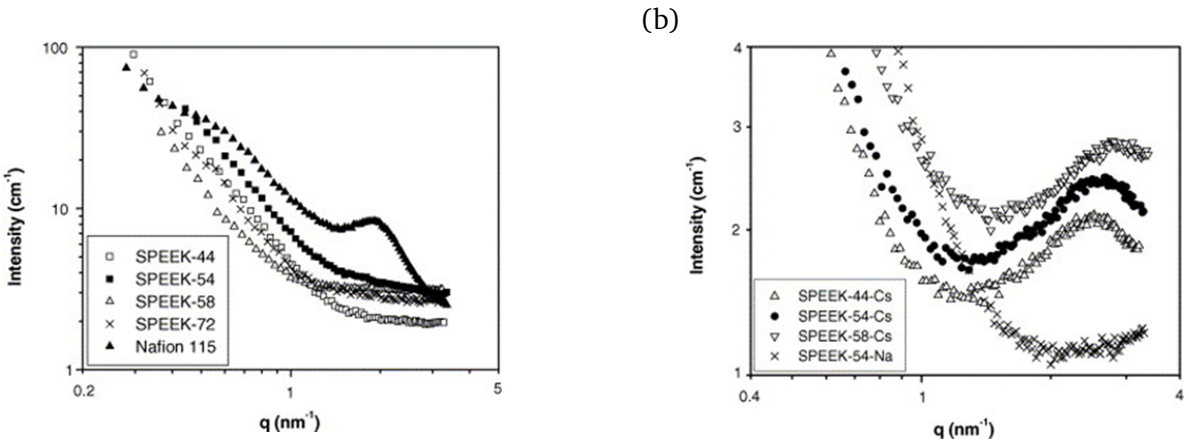

FIGURE 3.3 – SAXS profiles [40] : comparison between dry Nafion and sPEEK with different DS (a), and comparison of sPEEK neutralized with cesium or sodium (b).

(a) (b)

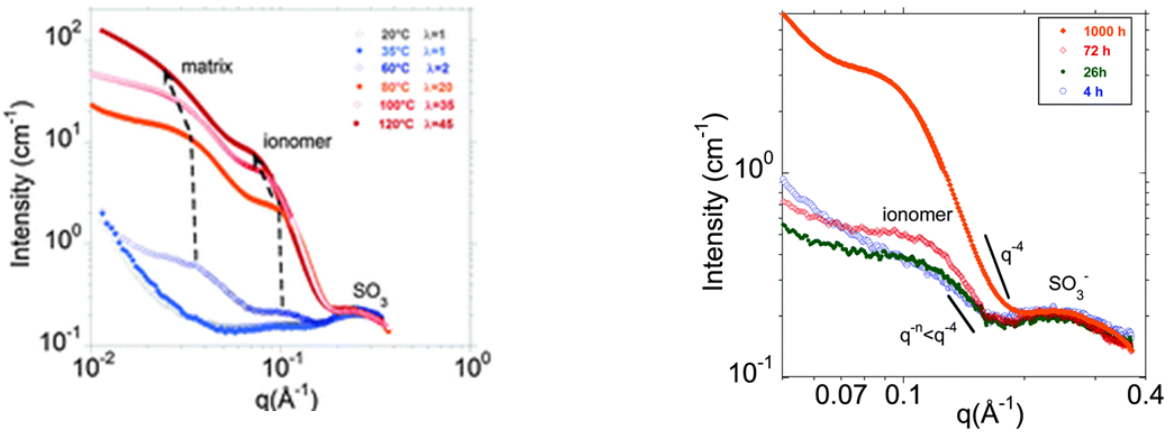

FIGURE 3.4 – SAXS profile of water swollen sPEEK membranes in the Cs^+ form at room temperature : after 96h of immersion in liquid water at different temperatures [41] (a) and after hydrothermal treatment at 80°C during various time [43] (b).

Mendil-Jakani et al. [41] investigated the nanostructure of commercial sPEEK membranes using Small-Angle X-Ray Scattering (SAXS) under different hydration states. They reported the appearance and evolution of up to three correlation peaks in the SAXS profiles upon membrane swelling and proposed a revised interpretation : two peaks associated with the polymer matrix and the ionomer domains, respectively, while the wide-angle peak reflects the average spacing between sulfonic acid groups. This reinterpretation, supported by temperature, contrast, and IEC-dependent studies, indicates that nano-phase separation in sPEEK is triggered by immersion in hot water. This work was carried out on sPEEK membranes with an Ion Exchange Capacity of 1.33 (IEC : number of millimoles of exchange sites per gram of exchanger), which were swollen in liquid water for 96 hours at 20, 35, 60, 80, 100 and 120°C. For immersion temperatures below 60°C (very low swelling, λ=2), the authors observed a low intensity, broad, wide-angle peak (large "q", labeled peak "3") at about 0.25 $Å^{-1}$ (d3 of 2π/q3 ~25 Å). At higher immersion temperatures, the membrane swelling increased dramatically ($\lambda \geq 20$) and two additional peaks emerged at smaller angles, labeled peaks "1" and "2". The evolution of the scattering profile with the swelling temperature followed a two-step process : in the first step, an abrupt increase in scattered intensity was observed between 60°C and 80°C, without significant peak shifting ; in the second step, for temperatures above 80°C, peaks "1" and "2" shifted toward smaller angles, accompanied by a further increase in their intensity. Above 80°C, peak "2" is followed by a "q^{-4}" behavior (Porod's law) in the wide-angle region, which is the typical signature of a sharp interface between two phases, certainly the hydrophobic and the hydrophilic ones. Peak "2" was therefore assigned to the so-called ionomer peak. From the observation of a macroscopic swelling, provided that the membrane is soaked in hot water, together with the appearance of an ionomer peak (fingerprint of the nano phase separation), the authors suggest that this immersion in water at elevated temperatures (from 60°C) allows sufficient molecular mobility to improve the self-assembly (hydrophilic-hydrophobic) which results in a better nanostructuration of the membrane and provides a well-defined interface between hydrophilic and hydrophobic phases. In other words, the ionic domains grow, up to making a continuous phase, and their separation with the rest of the membrane becomes sharper. It should be noted that this temperature-dependent nanostructuration contrasts drastically from what is known for Nafion® for which an ionomer peak, together with a "q^{-4}" behavior is observed from the very first step of hydration obtained at room temperature (low λ values, typically 2) : Nafion® is intrinsically nano-phase separated.

By investigating the effect of DS on the microstructure using DMA, SAXS, and other complementary techniques, Banerjee et al. [35] proposed a model describing the structural evolution of sPEEK as a

function of DS. At low DS, the distance between sulfonic acid groups becomes too large to enable the formation of ionic aggregates. This arises from the poor distribution of the sulfonic groups and the low mobility of the side chains, resulting from their direct attachment to the rigid PEEK backbone. As a result, only a small number of short and discontinuous conduction channels are formed, as illustrated in the left scheme figure 3.5. In contrast, a high DS reduces the distance between sulfonic acid groups and promotes the formation of hydrophilic clusters [35]. These domains are distinct from the hydrophobic backbone and form conduction channels and pathways for protons. Proton transport occurs either via the hopping mechanism or via the Grotthuss mechanism (section 4.2). When an adequate DS is reached, a homogeneous microstructure can be achieved characterized by long interconnected conduction channels, which can be assimilated to a well-developed network (figure 3.5, on the right).

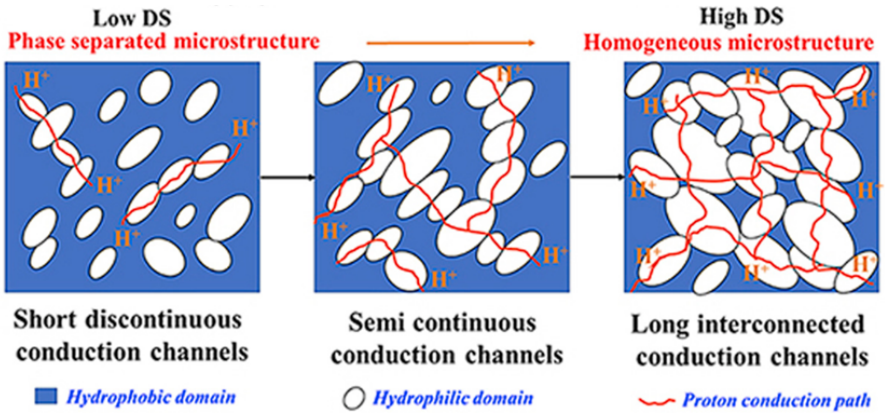

FIGURE 3.5 – Degree of sulfonation impact on the microstructure [35].

The difference in sPEEK physicochemical properties compared with other ionomers, such as PFSA-based ionomers, originates mainly from its different microstructure. Kreuer et al. [42] observed a less well-defined boundary between the hydrophilic and hydrophobic clusters in sPEEKK (chemically close to sPEEK) compared to Nafion 117, resulting in a narrower and less connected hydrophilic-cluster network with a higher fraction of dead ends. In contrast, simulations showed that Nafion exhibits an organization with well-defined hydrophilic and hydrophobic domains that are larger than those in sPEEK [44]. Although small ionic clusters remain in the sPEEK microstructure at high water content [45], limiting hydrophilic/hydrophobic phase separation, significant improvements occur at high water uptake. These improvements partially compensate for the less developed network and enable transport properties such as water diffusion and proton conductivity to reach values approaching those in PFSA ionomers [42, 46].

4 Physicochemical properties

As mentioned in the previous section, the microstructure of sPEEK is governed by the rigidity of its backbone and the short length of its side chains, leading to a poorly organized morphology that strongly depends on the DS. This significantly affects the physicochemical properties, including transport properties (gas permeability, water diffusion, proton conductivity) as well as sPEEK mechanical behavior.

4.1 Sorption, water uptake

Water uptake is a key property of an ionomer membrane since it governs proton conductivity, induces swelling, and impacts the mechanical properties (section 4.4). The results related to water uptake will be presented and discussed in two subsections, corresponding to immersion in liquid water and exposure to water vapor atmosphere.

Water uptake in liquid state

Numerous studies have reported an increase in water uptake with increasing degree of sulfonation [28, 35, 47-50]. A higher DS, *i.e.*, a higher density of sulfonic acid groups, improves the hydrophilicity of the ionomer [49, 51] and the formation of larger primary SO_3H-rich nanodomains, enabling greater water absorption [37].

Gebel et al. [52] investigated the microstructure of sPEEK at different DS values, water uptake, and temperatures using SANS and SAXS measurements. The sPEEK sample with a high IEC (1.9 mequiv.g^{-1}) dissolves in water above 60°C, whereas samples with lower IEC exhibit a progressive increase in water uptake followed by a sudden discontinuity at a temperature that depends on the IEC (figure 3.6). The authors hypothesized that this sharp increase in water uptake results from a structural reorganization of the ionic domains, driven by the volume expansion associated with water absorption.

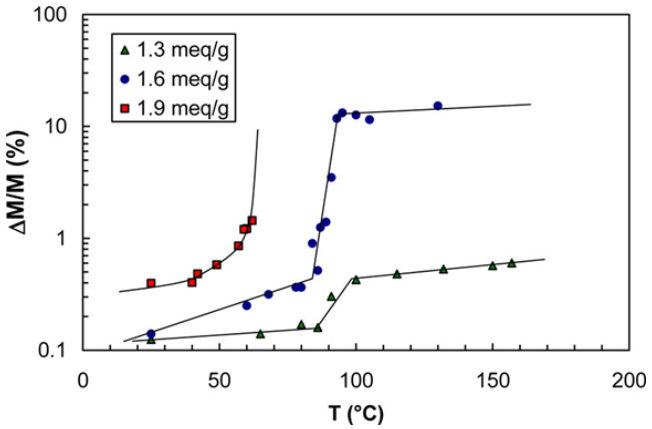

FIGURE 3.6 – Water uptake as a function of immersion temperature for sPEEK membranes with different IEC [52].

Note that a disparity in reported values can be found in the literature, making comparisons difficult. This variability may arise from differences in manufacturing processes, which can strongly influence sPEEK properties (section 6). For example, Tang et al. [47] reported water uptakes of approximately 28 and 37 wt% for sPEEK samples with DS close to 56 and 76%, respectively, whereas Yang et al. [53] reported significantly lower values of 5.1 and 25 wt% for similar DS levels.

Numerous studies have also reported an increase in water uptake with temperature [49, 50, 54-57] : for instance, Yang et al. [53] observed an increase from 5.1% to 140% (wt%) between 25°C and 80°C for sPEEK with 54% DS, and even reported dissolution at 80°C for samples with DS higher than 65%, demonstrating the detrimental effect of excessive sulfonation-and thus hydrophilicity-at elevated temperatures. Structural reorganizations in the ionomer occur at specific temperatures, depending on its chemical structure, leading to higher water uptake, with the effect being more pronounced at high DS [50]. Several studies have attributed this reorganization to increased mobility of sPEEK

chains and water molecules at elevated temperatures [58, 59]. This results in enhanced formation and interconnection of ionic clusters [40, 60] and, consequently, higher water uptake [39].

Water uptake in vapor state

In fuel cell environment, water can exist in both liquid and vapor states, which explains why several studies have focused on vapor sorption measurements. Jiang et al. [61] reported higher water-vapor uptake with increasing sPEEK DS and water activity. Vapor sorption experiments showed that increasing the DS from 41% to 78% has only a limited effect on the number of water molecules adsorbed per sulfonic acid site (λ) at low water activity. At a water activity of 0.34, λ ranged from 2.5 to 3.4, indicating that the large increase in liquid-water uptake observed at higher DS is not directly comparable to vapor sorption behavior. However, a much steeper increase in sorbed water was observed at high activity, with the number of water molecules per sulfonic site rising from 5.1 to 11.7 at an activity of 0.98, indicating greater membrane swelling at higher DS according to the authors. Nevertheless, it should be noted that Potreck et al. [62] reported greater water vapor sorption with an increase in water activity for DS from 59 to 75%, but that the number of water molecules per sulfonic site remained stable for DS values of 59 and 75%.

In comparison with Nafion, Jiang et al. [61] reported lower water-vapor sorption for sPEEK with 41% and 51% DS, and higher sorption for sPEEK with 60 and 78% DS, across almost all tested water activities. These differences arise from the large variations in microstructure and hydrophilicity, which can be compensated with a higher DS [47, 53]. Several models, such as BET type III, GAB, and others, have been developed to fit sorption isotherms and facilitate interpretation of the data. The New Dual Mode Sorption (NDMS) model [63-65] considers two types of sorption : one occurring in the matrix region of the glassy polymer and the other in the micro-voids. The model has the advantage of requiring only three parameters, which simplifies interpretation :

- **Cp** represents the mean sorption capacity of the polymer and depends on the ionomer's microstructure and state.
- **k'** indicates the difference in interactions among water molecules and between water molecules and the polymer matrix. A large k' corresponds to a strong increase in sorption at high activity, where newly sorbed molecules predominantly interact with each other. Hydrophobic polymers exhibit low k' values, whereas hydrophilic polymers exhibit higher ones.
- **A'** reflects the difference in interaction between the micro-voids and the first sorbed molecule, and between the micro-voids and water molecules in the subsequent layers. It represents the capacity of the ionomer to absorb additional water molecules beyond the first layer.

Li et al. [64] compared sorption isotherms of Nafion 117 and sPEEK using this model. Similar k' values indicated comparable levels of interaction between water molecules and the polymer matrix at high water activities. At low water activities, Nafion 117 showed a higher number of water molecules per site (higher Cp), which may be attributed to the greater acidity of its sulfonic group [66]. In contrast, significant differences appeared at intermediate water activities, where Nafion 117 displayed a larger multilayer sorption capacity (higher A').

Wu et al. [67] applied a hydration-shell model to describe water sorption in Nafion and sPEEK. They defined a first solvation layer associated with sulfonic groups, to which adsorbed water molecules are added, characterized by a lower adsorption energy. The first hydration shell was found to be more strongly bound with the sulfonic groups in Nafion, likely due to the greater acidity of these groups. In contrast, the energy association with the second hydration shell was found to be similar for both ionomers.

Membranes	C_p (mol.equiv^{-1})	k'	A'	R^2
Nafion 117	2.75 + 1[a]	0.75	9.2	0.999
sPEEK	2.60	0.77	2.77	0.999

[a] With '+1a' in the C_p value for Nafion 117 being a water molecule that remains bound to the sulfonic group.

TABLE 3.2 – Parameters C_p, k', and A' obtained for Nafion 117 and sPEEK membranes. From ref. [64]

Overall, significant differences in the water environment have been reported between sPEEK and Nafion [68]. Simulations by Mahajan et Ganesan [69] revealed that sPEEK forms smaller and more isolated water clusters at low water contents, as well as a less developed internal water network, compared with Nafion. These microstructural differences lead to different water percolation thresholds required to connect hydrophilic clusters. Because the hydrophilic/hydrophobic phase separation in PFSA membranes is well defined, a percolation threshold of about 0.1 was reported, much lower than the value of 0.3 estimated for sPEEK. Consequently, sPEEK ionomers require a higher water content to establish a connected network of hydrophilic pathways and, therefore, achieve proton conductivities comparable to PFSA-based membranes.

4.2 Conductivity

Proton transport occurs through two mechanisms : the Grotthuss mechanism (also called proton hopping) and the vehicle mechanism (figure 3.7).

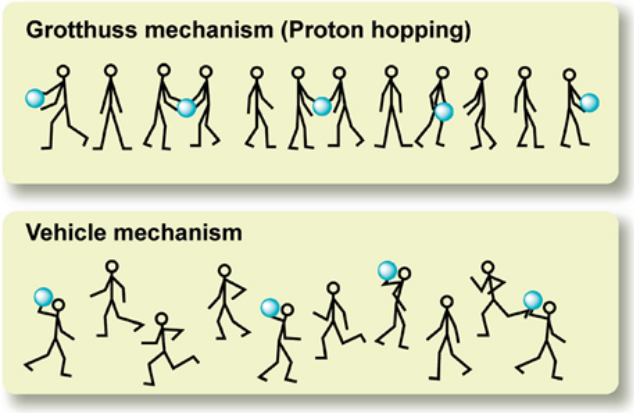

FIGURE 3.7 – Proton transport mechanisms [70].

The Grotthuss mechanism is based on proton transfer from one carrier to another without mass transport. It occurs through the formation and breaking of hydrogen bonds between water molecules and the proton, leading to charged complexes such as $H_5O_2^+$ or $H_9O_4^+$ [71]. Conversely, the vehicle mechanism involves mass transport : the proton is associated with several water molecules via hydrogen bonds and is transported across the membrane by diffusion. This mechanism is favored in bulk water, where the higher structural disorder weakens hydrogen bonds ; therefore, it becomes significant only above a minimum water content [72].

Proton conductivity depends on several factors [48] but is strongly influenced by the ionomer

structure. In the ionomer, sulfonate groups are located near the pore surfaces and strongly attract protons to form proton-sulfonate complexes. Even when these complexes lie within hydrated regions, the Coulombic barrier slows proton mobility, resulting in higher activation energies, as observed in membranes with narrow channels such as sPEEK [73] or under dry conditions in membranes with wider channels, like PFSA membranes for instance. In contrast, in well-hydrated membranes and/or membranes with wider channels, the increased distance between the sulfonic groups and the hydrated proton complex leads to an exponential decrease in the Coulombic barrier. Consequently, the activation energy decreases [48, 74], and the proton transport mechanism becomes closer to that observed in bulk solution [75].

The low mobility of sPEEK side chains, due to the direct attachment of sulfonic acid groups, [76], leads to a poor separation between hydrophilic and hydrophobic clusters, as evidenced by molecular simulation and SAXS. The resulting microstructure consists of narrower and less connected hydrophilic channels, which reduces the proton transport through sPEEK [77, 78]. Although this limitation is intrinsic to the polymer, a higher DS can partially counterbalance it by decreasing the distance between sulfonic groups, thereby promoting the formation of continuous hydrophilic pathways through ionic aggregation [79]. Numerous studies have assessed the impact of microstructure by varying the DS and water content of sPEEK samples. An increase in proton conductivity with increasing DS and water uptake has been consistently reported [22, 26, 28, 80-82], in agreement with the structural considerations mentioned above. Fan et al. [83] confirmed this trend, attributing the decrease in proton conductivity at lower RH to the disruption of the hydrogen-bonding network involved in the Grotthuss mechanism. The state of water also plays an important role, as higher proton conductivity has been observed when water is in the liquid phase [82], as is usually the case in ionomer membranes [84].

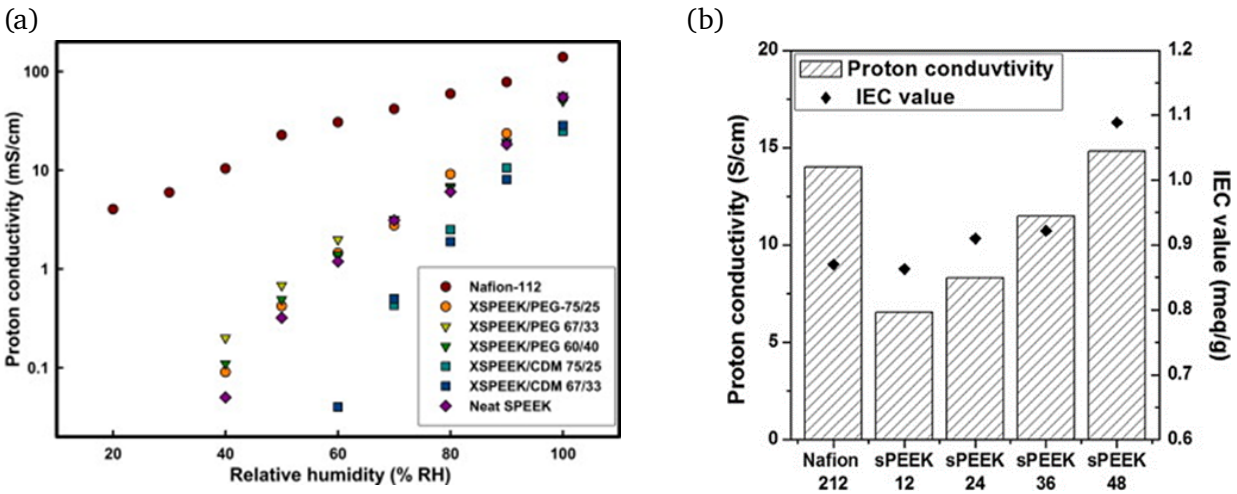

FIGURE 3.8 – Proton conductivity as a function of relative humidity at 100°C for different sPEEK samples compared to Nafion 112 [58] (a) and proton conductivity at room temperature under 100% relative humidity of sPEEK with different DS compared to Nafion 212 [56] (b).

Similarly to water uptake, operating temperature also has a significant and positive impact on proton conductivity [56, 58, 85]. Zaidi et al. [33] measured the conductivity of sPEEK with various DS values by clamping the samples in a cell after soaking them in water. Except for the sample with the lowest DS, all membranes exhibited the same behavior : an initial increase in proton conductivity with temperature, followed by a decrease at a specific temperature that depends on the DS. This increase in conductivity was expected since the proton transport is a thermally stimulated process, whereas the subsequent decrease resulted from the measurement procedure, which induced water evaporation during cell heating. However, it should be noted that membranes with higher DS exhibited a greater

ability to retain water, delaying dehydration to higher temperatures.

The increase in proton conductivity with temperature results from the higher mobility of sPEEK chains, enabling structural reorganization and improved water uptake, larger ionic cluster, and consequently a higher ionic cluster density [16, 73]. The enhanced development of a hydrophilic pathway network as expected leads to an increase in proton conductivity. In addition, the higher thermal energy facilitates proton transfer between sulfonic groups, thereby improving proton conductivity [15]. However, this effect is highly dependent on the membrane hydration state. If increasing temperature induces membrane dehydration, proton conductivity decreases due to the reduction in ionic clusters size and connectivity. Overall, proton conductivity is strongly governed by the coupling between temperature, water uptake, and the ionomer DS.

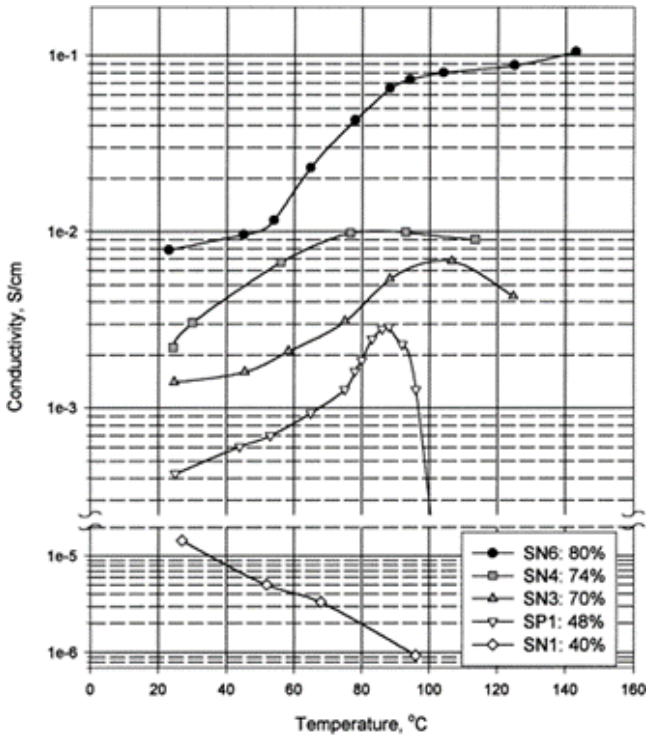

FIGURE 3.9 – Conductivity as a function of temperature for sPEEK with different DS [33].

Supplier	Solvent	T (°C)	State	DS (%)	Proton conductivity ($mS.cm^{-1}$)	Ref.
Victrex	DMAc	25	Fully hydrated	69 79 88 96	22 39 51 110	[30]
Sigma Aldrich	DMAc	25	Not precise	68 80	39 64	[29]
Victrex	DMF	25	Previous immersion in water (24h)	48 66 79	2 2.2 4.5	[24]
Victrex	DMAc	22	Previous immersion in water (24h)	59 65 73 78 93	4.1 4.7 5.2 6.7 9.3	[86]
Polysciences	DMAc	25 100	Soaked prior test	70 70	1.3 6.7	[33]
		25 100		74 74	2.1 9.5	
		25 100		80 80	8 76	
Aromatic nucl. substitution	DMSO	30 80	100% RH	58	41.1 122.8	[87]
Aromatic nucl. substitution	NMP	20 80	100% RH	71.4	57 190	[55]
Electrophilic substitution	DMF	20 120	20% RH 20% RH	52.8	2.18 7.68	[88]
		20 100	100% RH 100% RH		20.61 -	
Victrex	DMSO	100 140	< 25% RH	41.8	0.002 0.008	[89]
As received	-	30 60	Fully humidified	54	44 62	[90]
Victrex	DMAc	100	78% RH 90% RH 100% RH	35	0.57 17 67	[91]
		120	78% RH 90% RH 100% RH		0.93 38 93	
		100	78% RH 90% RH 100% RH	52	4 39 130	
		120	78% RH 90% RH 100% RH		3.4 57 100	

TABLE 3.3 – Review of proton conductivity of sPEEK membrane at different conditions of : solvent casting, temperature, relative humidity, degree of sulfonation.

4.3 Other transport properties

Permeability and diffusivity quantify the ability of a material to allow gas transport through the material under a pressure or a concentration gradient, respectively. These parameters strongly influence the mass-transfer dynamics of water and gases such as oxygen, hydrogen, carbon monoxide, etc, impacting fuel cell performance and durability :

- Gas crossover (H_2, O_2, N_2, CO, etc.) influences both fuel cell performance and durability. Oxygen and hydrogen crossover can lead to the formation of hydrogen peroxide H_2O_2, which can decompose into hydroxyl ($HO^\bullet$ and hydroperoxyl ($HOO^\bullet$) radicals. These species attack specific bonds of the ionomer [92], thereby reducing ionomer durability. Fuel cell performance can also be impaired by nitrogen crossover from cathode to anode, which dilutes hydrogen (reducing hydrogen partial pressure) and may eventually cause hydrogen starvation [93], although, to the best of our knowledge, this has mostly been observed under real-life operating conditions, with fuel cells operating with a dead-ended anode and excessively long delays between two successive purge events [94, 95]. Other gases, such as carbon monoxide and carbon dioxide, can contaminate the catalyst and block the active sites, reducing the electrochemical active surface area (ECSA) [96, 97].
- High water diffusivity in the membrane is essential to maintain homogeneous ionomer hydration, which is necessary for good proton conductivity and optimal fuel cell performances, as discussed previously.

Although the quantitative values of diffusivity and permeability depend on the gas-due to differences in molecular size-Arena et al. [98] reported a similar temperature-dependent trend for both oxygen and hydrogen diffusivity.

Hydrocarbon-based membranes (*e.g.*, sPEEK) generally exhibit low gas permeability and diffusivity compared with PFSA-based ionomers. Accordingly, these transport properties are reduced in sPEEK [99-101], which is beneficial during PEMFC operation because this limits gas crossover and thus mitigates chemical degradation. This behavior is linked to the microstructure : the reduced phase separation between hydrophilic and hydrophobic domains in sPEEK results in fewer free volumes and a less well-defined network of transport pathways [68, 76, 102]. However, external parameters also affect transport properties, as Mahajan et Ganesan [46] observed higher water diffusivity with the increase in water uptake and temperature.

Ionomer microstructure therefore strongly influences ionomer permeability and diffusivity properties [103]. Silva et al. [102] reported increased oxygen (0.17 to 0.35 Barrer) and carbon dioxide (0.12 to 0.26 Barrer) permeability coefficients with increasing ionomer DS from 52% to 71% at 20°C, whereas nitrogen permeability remained unchanged (0.10 Barrer). Increasing the DS generates a larger number of free volumes and leads to higher water uptake and swelling, which in turn increase both gas diffusivity and permeability [76, 102, 104]. As water uptake increases, the intermolecular distance between polymer chains expands due to swelling, thereby increasing the amount of free volume and creating or enlarging gas conduction pathways [104, 105]. Several studies reported an increased water vapor permeability with increasing water activity [65, 106].

Regarding the effect of temperature, the dependence of diffusivity and permeability must be distinguished : diffusivity generally increases with temperature because molecular motion is thermally activated (Brownian mechanism) [93, 105], whereas permeability also depends on gas solubility in the polymer. Azher et al. [104] compared water and CO_2 permeability of sPEEK with two different IEC values under various humidities. They observed an increase in permeability with temperature, up to about 50°C, followed by a decrease at higher temperatures. The authors attributed the initial increase to thermal expansion of the polymer between 30 and 50°C, which increases free volumes and thus gas permeability. Above 50°C, however, the higher water uptake reduces both the number and the size of free volumes, leading to lower gas permeability. Furthermore, the influence of temperature is strongly dependent on water activity. Indeed, the water permeability has been reported to decrease with temperature at water activity below 0.5, but increases between 30°C and 50°C when the water activity is above 0.5, before decreasing again at higher temperatures (figure 3.10(b)) [107].

(a) (b)

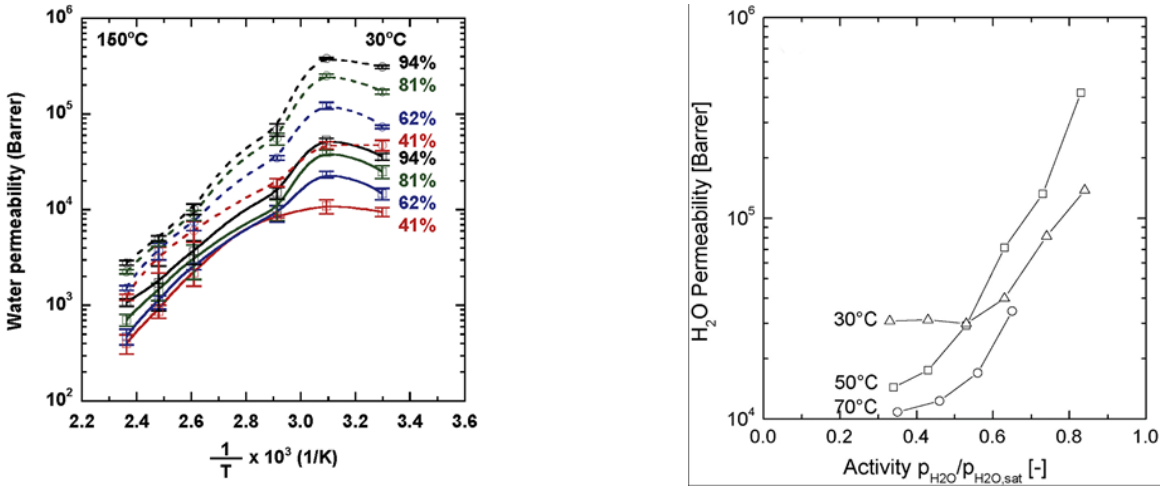

FIGURE 3.10 – Water permeability as a function of temperature and feed RH of sPEEK with IEC=1.6 (solid lines) and IEC=1.9 (dotted lines) [104] (a) and water permeability at 30°C, 50°C, and 70°C as a function of water activity of sPEEK (60% DS) [107] (b).

4.4 Mechanical properties

Mechanical properties are essential because the ionomer must be able to swell and shrink under high and low water contents while maintaining its mechanical integrity. For example, swelling/drying cycles generated by variations in gas inlet RH and/or by water produced during fuel cell operation induce mechanical stresses and may consequently lead to membrane damage [108, 109].

Mechanical properties are highly dependent on sPEEK microstructure, and thus on its DS. Xi et al. [110] reported a gradual decrease both in Young's modulus and breaking strength with increasing DS [51, 85]. Parnian et al. [15] reported the same trends at ambient RH and 25°C, and additionally reported a higher elongation at break at higher DS. Moreover, they observed a stress peak after the yield point, also reported by Park et al. [85], followed by a drop in stress to a stable level until failure, corresponding to a ductile behavior whose plastic deformation depends on the DS. Note that differences in elongation at break have been reported in the literature, which have been attributed to the presence of water acting as plasticizer [20, 111, 112], inducing higher elongation at break at higher DS [15].

sPEEK ionomer therefore exhibits a fragile behavior with a high Young's modulus at low DS, due to its high crystallinity. Increasing the DS modifies ionomer mechanical properties toward a more ductile behavior, associated with a more amorphous structure and a larger plastic deformation region. According to Reyna-Valencia et al. [113], the increased number of sulfonic groups generates significant encumbrance that prevents the formation of chain entanglements, thereby facilitating chain sliding. Sulfonic groups act therefore as plasticizers [35, 36] for the inter-crystalline regions by disrupting chain entanglement. Consequently, sPEEK transitions from an elastic and brittle behavior to a less elastic and more ductile one. Quantitative values must, however, be interpreted carefully, as they strongly depend on experimental conditions, particularly the presence of water, which acts as a plasticizer [114] ; therefore, sPEEK water content must be considered when evaluating mechanical properties : higher DS implies higher water uptake, which in turn influences the mechanical behavior of sPEEK. Hou et al. [111] compared the mechanical properties of sPEEK at ambient temperature under 0% and 43% RH. They reported a higher Young's modulus and yield strength, and a lower elongation at break, for the dry sPEEK sample at 0% RH. They explained that the presence of water increases the distance between polymer chains, reducing their interactions and thus decreasing mechanical properties. Similarly, the

state of water also plays an important role in mechanical response [115, 116]. Reyna-Valencia et al. [113] reported a significant decrease in Young modulus, yield stress, and stress at break, together with a substantial increase in elongation at break, when sPEEK sample was immersed in liquid water (table 3.4).

Sample	Conditions of the test	E (MPa)	Yield stress (MPa)	Elongation at break (%)	Stress at break (MPa)
sPEEK (DS=63%)	30% RH, 23°C	2404	62	50	51.5
	In water, 23°C	716	15.1	60	16.6
sPEEK (DS=69%)	30% RH, 23°C	2258	61.9	90	55.8
	In water, 23°C	781	14.4	120	23.6

TABLE 3.4 – Mechanical properties of sPEEK with DS=63 and 69% measured by Reyna-Valencia et al. [113]

As mentioned in the section 3, the temperature has a significant effect on sPEEK microstructure, and thus on its physicochemical properties, such as water uptake (subsection 4.1). sPEEK is characterized by several relaxations at specific temperatures inducing structural reorganization, and thus changes in mechanical properties. Sprugis et al. [117] reported a decrease in the sPEEK maximum strength with increasing temperature, highlighting the more pronounced amorphous behavior. Banerjee et al. [35] reported the evolution of the elastic modulus, showing two peaks of increase followed by a decrease. The second peak, observed between 75°C and 175°C, was attributed to a temperature-induced restructuring of the polymer in the glassy state. Concerning the first peak, the authors did not explain its origin, and the literature addressing the evolution of the mechanical properties of sPEEK as a function of temperature remains scarce. Sgreccia et al. [118] observed similar behavior for other hydrocarbon-based ionomers such as sulfonated poly-phenylsulfone (SPPSU), linking it to "*in situ*" crosslinking, although they did not report such behavior for sPEEK samples. A first increase is associated with the loss of plasticizing agents, such as water or residual casting solvent, followed by a decrease until the appearance of cross-linking which increases mechanical properties, among which the Young's modulus. The decrease that follows this phenomenon is explained by the approach of the glass transition temperature, at which the polymer will follow a more amorphous behavior. Banerjee et al. [35] reported a strong correlation between mechanical properties, such as the storage and loss modulus, and the transition in microstructure associated with increased temperature (figure 3.11).

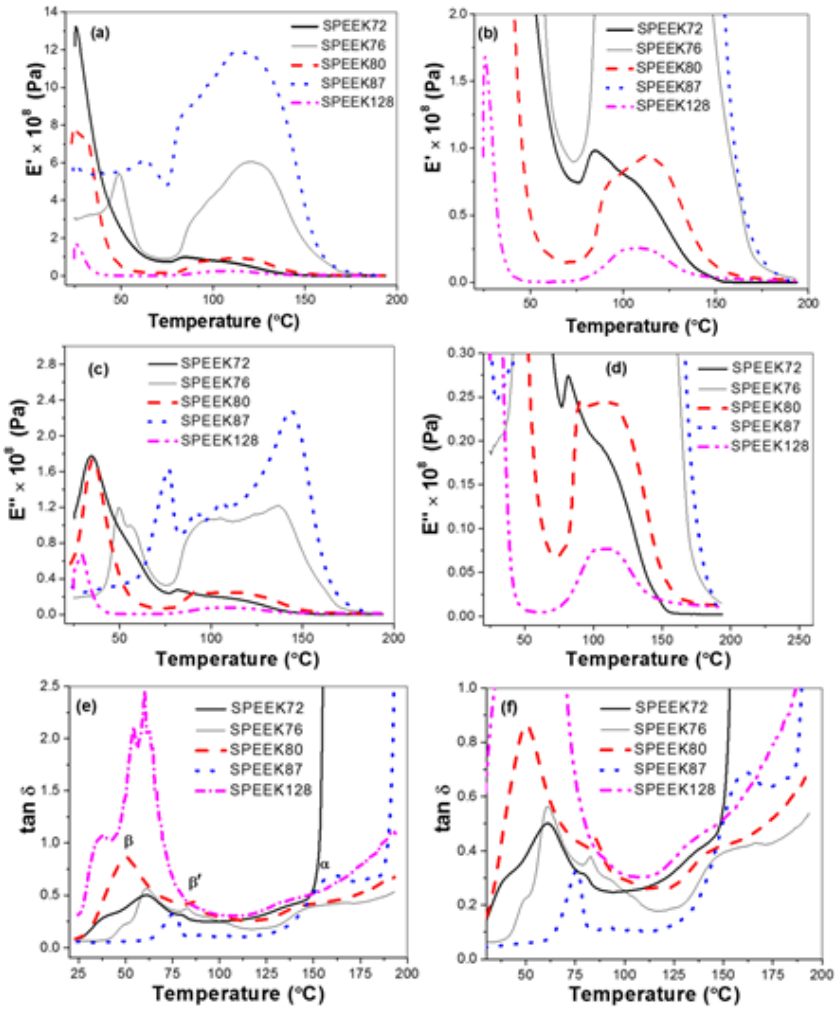

FIGURE 3.11 – sPEEK storage modulus (a-b), loss modulus (c-d), and tan(δ) (e-f) as a function of temperature in full scale (left column) and zoomed view (right column) [35].

Regarding the plastic deformation of the membrane, Reyna-Valencia et al. [113] reported a significant increase in elongation at break with increasing temperature for sPEEK samples with DS values of 63% and 83%. In water, an increase of approximately 50% and 43% in elongation at break was measured for sPEEK with DS of 63 and 83% sPEEK, respectively, when the temperature increased from 23 to 40°C. These results are consistent with mechanical tests carried out on PEEK, where a similar trend was observed [119]. This highlights the direct impact of temperature on the polymer's mechanical behavior, independent of DS or water uptake, since different DS levels correspond to different water uptake levels.

The mechanical properties of sPEEK are intrinsically linked to its microstructure and to the operating conditions. Increasing the DS induces a transition from a brittle behavior with a high Young's modulus to a ductile behavior characterized by a lower Young's modulus and a higher elongation at break. The introduction of sulfonic groups reduces chain entanglements, acting as plasticizers. In addition, a higher DS leads to an increased water uptake, which further acts as a plasticizer by increasing the distance between polymer chains and thereby impacting mechanical properties. Increasing temperature also alters mechanical properties through ionomer relaxations, inducing microstructure changes. In particular, ionomers exhibit reduced rigidity–reflected by a lower Young's modulus–when their temperature approaches or exceeds the glass transition temperature [120]. Although these ef-

fects have been presented independently, they are strongly coupled, as changes in DS influence both the relaxation temperatures and the water uptake.

5 Ionomer durability

5.1 sPEEK during *ex situ* degradation tests

Numerous studies have focused on the physicochemical properties of sPEEK (section 4) to assess how its properties depend on its structure, particularly its DS. However, far fewer studies have addressed the durability of this ionomer and, more specifically, the evolution of its properties over time. Although one ionomer may outperform another in terms of a given property, this advantage is not necessarily maintained under operating conditions. It is therefore essential to evaluate the durability of physicochemical properties.

During fuel cell operation, the degradation of each component can affect the durability of others. Touhami et al. [121] reported an increase in membrane permeation defects in the anode catalyst layer, while different catalyst types may induce different membrane degradation rates [122]. Dubau et al. [123] also reported increased carbon corrosion in cases of excessive membrane permeation. *Ex situ* accelerated stress tests have therefore been conducted to independently assess fuel cell component durability under various stress conditions.

Although mechanical and chemical degradation are coupled, several studies have analyzed degradation mechanisms independently in order to separately estimate chemical, mechanical, and thermal stability and to better understand the advantages of one ionomer over another. To evaluate chemical stability, it is necessary to expose the membrane to an environment containing hydroxyl $HO^{\bullet}$ hydroperoxyl $HOO^{\bullet}$ radicals. There are several ways to generate these species [124], two of which are the most commonly used :

- One method consists of heating a hydrogen peroxide solution. Perrot et al. [20] demonstrated that an optimal temperature of 80°C is sufficient to decompose hydrogen peroxide into free radicals.
- Another widely used test, known as the Fenton test, consists of immersing the membrane in a solution composed of H_2O_2 and Fe^{2+} ions, which catalyze radical formation [125, 126].

The limited chemical stability of sPEEK has been evidenced by accelerated chemical durability tests under such oxidative conditions. Indeed, Daoudi et al. [127] observed that sPEEK using a commercial process underwent partial fragmentation after soaking in a 0.1% H_2O_2 solution heated to 80°C for 24h, severe fragmentation in a 0.2% H_2O_2 solution, and a complete dissolution in a 1% H_2O_2 solution. Similar degradation trends were observed during Fenton tests, resulting in significant weight losses [116, 126, 128-130]. Chemical stability is strongly related to the sPEEK microstructure, particularly its DS [131]. A comparison of the time required for complete ionomer degradation during Fenton tests revealed a drastic decrease in lifetime with increasing DS, as reported by Parnian et al. [15] (200 and 2 min for DS values of 40.24% and 81.23%, respectively). Similarly, Song et al. [132] reported a degradation time approximately twice as short when the sPEEK DS increased from 51% to 62%.

A decrease in DS has been reported after H_2O_2 soaking or Fenton test by ATR-FTIR and H-Nuclear spectroscopy [127, 133]. Using ATR-FTIR, Karimi et al. [133] reported that the bond C—O in 1,2,4 substituted phenyl ring was much more affected by the chemical degradation than the asymmetric and symmetric S=O bonds, consistent with Salleh et al. observations [126]. Using half-cell design for degradation test, Zang et al. [134] reported a decreased absorption at 1010 cm^{-1} (p-substituted aryl ether), indicating the possible cleavage of ether bridges in the building block through FTIR

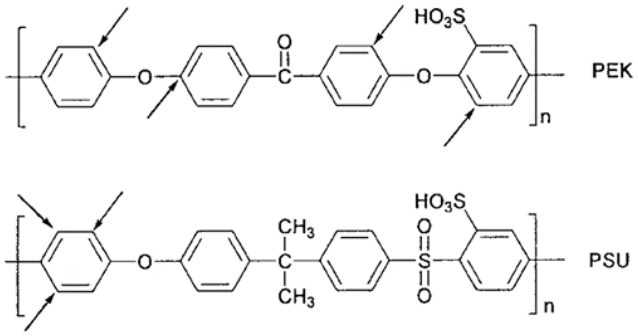

FIGURE 3.12 – Possible sites for HO• radical attack on PEK and PSU polymers [124].

measurements.

Finally, several studies using density functional theory (DFT) proposed hydrocarbon ionomer degradation mechanisms starting with the addition of an HO• radical to an aromatic ring [135, 136]. Hübner et al. [124] established with electron paramagnetic resonance measurement (EPR) that, in the presence of HO•, the dominant reaction implied its addition to aromatic rings (figure 3.12), although this radical can also lead to C-O-C bond breaking but only at pH > 5. Although fuel cell environment is often considered to be at low pH, Abdullah et al. [137] reported significant pH variations during fuel cell operation, exceeding 6, which does not exclude the latter degradation mechanism.

Chemical degradation induces microstructural changes, such as chain scission and loss of sulfonic groups, which severely affect the structural integrity of sPEEK. Increased sPEEK permeability as well as significant changes in mechanical properties have been observed, including reductions in Young's modulus, ultimate tensile stress, elongation at break, and toughness [126, 133], reflecting a marked loss of mechanical integrity. Karimi et al. [133] explained that the decrease in molecular weight and chain length, due to chain scission, reduces chain entanglements, thereby deteriorating mechanical properties, while the formation of microdefects enhances hydrogen permeability. Moreover, the loss of sulfonic groups also affects interchain interactions and entanglements, which can influence the glass transition temperature, although no consistent trend was reported [133].

As sPEEK DS decreases during chemical degradation, its physicochemical properties are inevitably affected. Higher water uptake and swelling ratios have been reported [133]. Several competitive effects can be identified. The decrease in ionomer DS reduces hydrophilicity and thus water uptake. However, the presence of defects and reduced chain entanglements can promote morphological changes, resulting in increased water uptake and swelling during chemical degradation. A decrease in proton conductivity as a consequence of chemical degradation has also been reported [134]. Parnian et al. [138] reported decreases in proton conductivity of more than 50% and 55% at room temperature and at 80°C, respectively, after a 100h Fenton test.

Because of its limited chemical stability, *ex situ* degradation studies have mainly focused on chemical aging, whereas relatively few have investigated the impact of mechanical degradation. Membrane creep occurs during swelling-shrinking cycles caused by variations in water uptake, leading to permanent deformation and chain rearrangement, which may significantly reduce fuel cell durability [85].

Mirfarsi et al. [139] conducted hygrothermal cycling tests (figure 3.13) by varying membrane temperature and gas relative humidity, and evaluated their effects on sPEEK properties. They reported the formation of small defects and an increase in crystalline ordering. Moreover, increased permanent

deformation and water uptake were observed with an increasing number of hygrothermal cycles, indicating microstructural rearrangements that are amplified at higher temperatures. These changes led to increased hydrogen permeability and altered mechanical properties. The authors reported increases in Young's modulus and ultimate tensile strength, along with a transition from ductile to brittle behavior, as evidenced by a large decrease in elongation at break. They suggested that elevated temperature during hygrothermal cycling, combined with available space generated by membrane creep, facilitate chains reorganization, resulting in modified mechanical behavior. Choi et al. [140] reported similar evolution by subjecting sPEEK samples to hygrothermal cycling consisting of immersion in water at 80°C for 2h, followed by drying under vacuum at 25°C, repeated 30 to 100 times (referred to as H-D cycle). The permanent deformation and brittle mechanical behavior were linked to nanostructural changes observed by SAXS, which revealed both permanent and reversible structural rearrangements, with increased nanophase separation under hydrated conditions that was partially reversible upon drying. Moreover, they reported improved performance after H-D cycling due to enhanced nanophase separation and higher proton conductivity, without any increase in hydrogen crossover.

(a) (b)

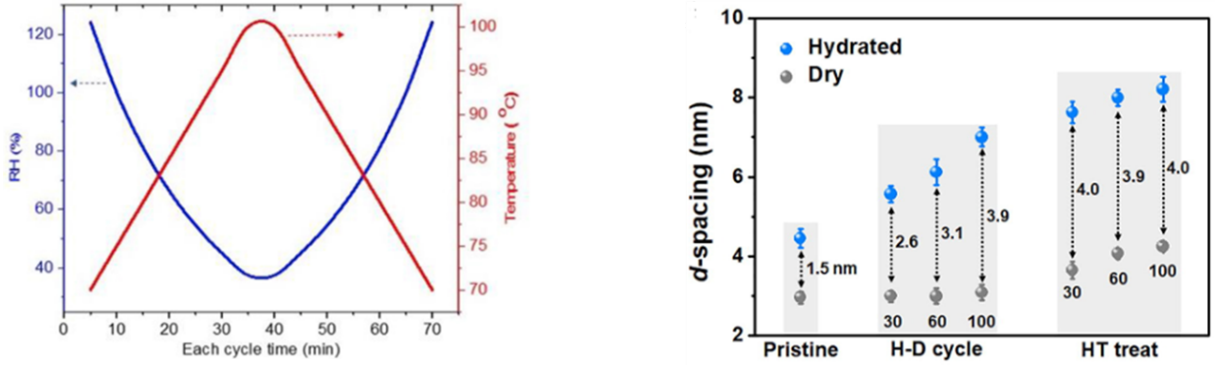

FIGURE 3.13 – Sinusoidal fluctuation of RH and temperature in each hygrothermal cycle employed [139] (a) and representation of d-spacing of sPEEK after hydration/dehydration cycling and hydrothermal treatment [140] (b).

Chemical and mechanical degradation lead to significant morphological changes, including chain scission, reversible and permanent deformation, and loss of sulfonic groups, which in turn induce changes in physicochemical properties such as proton conductivity, gas permeability, and mechanical properties. Ionomer durability therefore depends on both chemical and mechanical stability as degradation pathways are coupled [141, 142]. Despite the good intrinsic mechanical properties of sPEEK, further improvements must not neglect its long-term mechanical endurance to ensure durable operation.

5.2 sPEEK durability during fuel cell operation

The sPEEK ionomer has long been considered a credible alternative to PFSA-based membranes due to its superior mechanical and thermal properties; although, its chemical durability is significantly lower. Beyond optimization of its structure through an appropriate degree of sulfonation (DS), several studies have evaluated its durability under fuel cell operating conditions using accelerated stress tests (AST). A multitude of AST exists to induce accelerated membrane aging [143] :

- **Chemical degradation** is induced through the application of Open-Circuit Voltage (OCV), during which reactants cross the membrane and form hydrogen peroxide (H_2O_2), leading to chemical degradation of the ionomer.

- **Mechanical degradation** is induced via humidity cycling, either through variation of gas RH or through load cycling, during which water is produced at high current density. These processes induce microstructural changes, essentially characterized by an increased hydrogen permeation current [144-146].

Marrony et al. [147] conducted accelerated stress tests (AST) on sPEEK membranes consisting of load cycling at 70, 80, and 90°C under 100% inlet gas RH. Significant OCV degradation was observed at higher temperature, whereas a stable OCV was maintained at 70°C, indicating that humidity variations at higher temperatures are detrimental to sPEEK. Although sPEEK exhibits good mechanical properties, a lower OCV decrease was reported for Nafion under the same conditions, suggesting that mechanical properties at the beginning of life may not be an adequate indicator for assessing *in situ* durability. Monitoring mechanical properties during fatigue testing may therefore be more appropriate for evaluating relevant ionomer properties. For instance, sPEEK may exhibit a higher Young's modulus but less durable than PFSA membranes, or the larger elastic deformation range of PFSA ionomers may enable greater swelling without plastic deformation compared to sPEEK.

Regarding chemical durability, the OCV is widely considered a key indicator of membrane degradation [148]. While Nemeth et al. [149] reported a sudden decrease in OCV after approximately 81 h of an OCV accelerated stress test, Liu et al. [150] reported a 40% OCV loss after two days of an OCV test conducted at 90°C under 30% inlet gas RH, indicating poor chemical stability. In contrast, Parnian et al. [138] reported a much smaller OCV decay rate (0.52 $mV.h^{-1}$) under similar temperature and inlet gas relative humidity conditions for sPEEK membranes with a comparable DS, corresponding to an OCV loss of approximately 2.5% after 2 days of testing. This illustrates the significant variability reported in sPEEK durability, which is likely related to differences in membrane fabrication processes and resulting microstructure. Nevertheless, Song et al. [132] demonstrated higher durability for sPEEK with a lower DS (51% vs. 62%) during OCV tests conducted at 70°C under 100% inlet gas RH, highlighting the strong influence of membrane microstructure on chemical stability. Chemical degradation of sPEEK membranes resulted in a substantial increase in ohmic resistance and a marked decline in fuel cell performance [151], with the maximum power density decreasing from 745 to 499 $mW.cm^{-2}$ [138]. The degradation was characterized by severe membrane thinning with OCV-AST time, which was consistent with the observed decrease in high-frequency resistance values [152], and led to a significant increase in hydrogen permeation [138].

Overall, the durability of sPEEK is highly dependent on its microstructure, and particularly on its degree of sulfonation (DS). Higher DS increases water uptake and ionomer swelling, thereby enhancing mechanical stresses during humidity cycling and accelerating chemical degradation during OCV testing. Consequently, direct comparison of sPEEK durability results obtained through AST is challenging, as they strongly depend on the membrane manufacturing process (section 6).

6 Impact of manufacturing process

The literature reports significantly discrepant values for the physicochemical properties of sPEEK (section 4). These differences depend heavily on external conditions, but also on variations in manufacturing processes, which play a predominant role in determining the final microstructure of the ionomer. The effect of the casting solvent and the addition of a pretreatment have been shown to significantly influence the resulting properties, as detailed below.

6.1 Casting solvent

Different casting solvents such as dimethylsulfoxide (DMSO), N,N-dimethylacetamide (DMAc), dimethylformamide (DMF), N-methyl-2-pyrrolidone (NMP), or water/acetone mixture can be used to prepare sPEEK membranes. Their interaction with the ionomer directly affects the microstructure as well as its physicochemical properties such as proton conductivity, water uptake, and mechanical properties [118].

Luu et al. [32] compared the microstructure of sPEEK with various DS values (65%, 70%, and 75%) cast using DMA and NMP. Based on SAXS measurements, they reported changes in ionomer microstructure, with a larger ionic cluster size for the 65% DS sample cast with NMP (3.2 nm vs. 2.7 nm using DMAc). They also observed an increase in ionic cluster size with DS for films cast with NMP, whereas the changes were less significant for DMA. These microstructural differences resulted in a higher water uptake, thereby enhancing proton conductivity. For a similar DS, different water uptake values have been reported depending on the casting solvent [32, 115, 153, 154], generally with higher values for membranes cast from NMP, DMSO than from DMAc or DMF, although the exact order varies among studies. This may explain the dispersion observed in reported proton conductivity. H1 NMR measurements revealed that DMAc and DMF solvents are prone to establishing H-bonding with sulfonate groups, although hydrogen bonding with DMAc appeared only at higher temperature [30, 155]. Such interactions lead to sulfonic site deactivation, reducing the number of protons available for charge transport, decreasing the hydrophilicity and water content of the ionomer, and consequently lowering its proton conductivity.

Residual solvent in the membrane can also affect its properties. Jun et al. [154] studied the impact of DMSO, DMAc, NMP, and DMF casting solvents using two sample series : 'as-cast' samples, which were only dried after casting, and 'activated' samples, which underwent an additional H_2SO_4 soaking step to remove residual solvent not eliminated during drying. FTIR spectra confirmed the presence of residual solvent in the as-cast membranes. Compared with activated sPEEK samples, as-cast samples exhibited lower water uptake, suggesting that residual solvent hinders water absorption and thus reduces proton conductivity. It is also worth noting that acid activation led to a smaller dispersion in proton conductivity values, whereas the as-cast membranes showed variations of almost one order of magnitude (figure 3.14(b)). A similar trend was observed in fuel cell performances (figure 3.14(c)) : as-cast sPEEK performance depended strongly on the casting solvent, whereas activated samples exhibited much smaller differences, which may be due to structural modifications induced by the solvent during the manufacturing process.

The residual solvent (RS) content and its effect depend on the solvent's affinity with sPEEK. Liu et al. [156] reported that RS content increased with DS, and was higher for sPEEK casted with DMF and DMAc than with NMP and DMSO–consistent with their strong affinity. After removal of residual solvent, sPEEK casted with DMF or DMAc showed higher water uptake than samples casted with NMP or DMSO, which may be related to a larger volume initially occupied by casting solvent and later filled by water. For samples with fixed DS values of 43% and 75%, RS content was found to influence water uptake more strongly than the casting solvent nature itself. The authors further characterized sPEEK microstructure using SAXS and XRD. For sPEEK with 43% DS, the average size of hydrophilic domains was 1.79 nm for DMSO-cast film and 1.53 nm for films casted with DMF, DMAc, and NMP, which explained the higher proton conductivity of the DMSO-cast 43% sPEEK. Moreover, sPEEK casted with DMSO exhibited a semicrystalline structure, as also observed by Carbone et al. [157], whereas the other casting solvents induced a more amorphous structure. Together with SAXS results, this was attributed to a higher degree of nanophase separation in DMSO-cast sPEEK–at least for 43% DS, since no significant differences in SAXS or XRD were observed among the casting solvents for sPEEK with 75% DS.

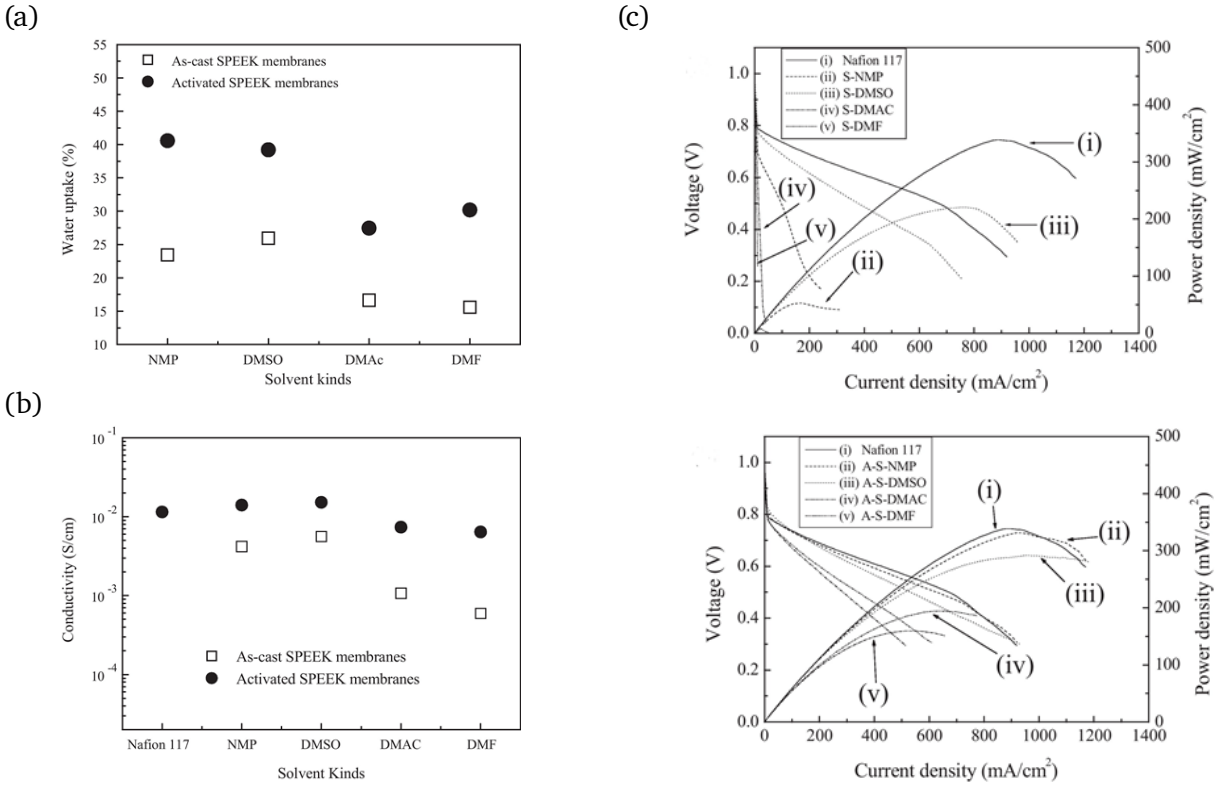

FIGURE 3.14 – Water uptake (a) and proton conductivity (c) of as-cast and pretreated sPEEK casted with different solvent. Fuel cell performance of as-cast sPEEK (top graph) and activated sPEEK (bottom graph) (c) [154].

Changes in sPEEK microstructure therefore depend on both the residual solvent content, even when an acidification step is used to remove it, and the solvent's affinity with the polymer, particularly at low DS. The initial residual solvent content affects the microstructure, with differences in hydrophilic domain size, affecting ionomer physicochemical properties [158]. Although minor differences were observed between sPEEK casted with NMP, DMAc, and DMF, notable structural variations occurred with DMSO. The stronger hydrophobic/hydrophilic separation phase induced higher proton conductivity, while the increased crystallinity was associated with variations in mechanical properties [156].

The manufacturing process is therefore an essential step, as the choice of casting solvent and the removal of residual solvent have been shown to impact strongly the physicochemical properties and thus, fuel cell performance [157]. Also it should be noted that comparisons between studies remain challenging, especially when manufacturing details are incomplete : for example, Do et al. [153] and Robertson et al. [155] used thermal drying in a vacuum oven between 25-140°C for a few days without further specification.

6.2 Pretreatment

A variety of processes are used to enhance ionomer properties prior to fuel cell operation. Numerous studies employ additives to improve physicochemical properties such as water uptake, proton conductivity, and mechanical behavior. Although this approach can lead to significant improvements, several processes are known to modify the microstructure without altering the chemical structure of sPEEK. While combining these pretreatments with additives may yield even greater improvements, we focus here solely on sPEEK pretreatments without additives to highlight the substantial benefits they offer.

6.2.1 Soaking treatments

One major characteristic of sPEEK microstructure is its relatively poor hydrophilic/hydrophobic phase separation compared to other ionomers, such as PFSA. As mentioned previously, this microstructure governs the physicochemical properties and, consequently, the fuel cell performance.

Mendil-Jakani et al. [43] studied the impact of hydrothermal treatments on sPEEK microstructure by soaking samples in water at temperatures ranging from 40 to 120°C for 10 to 1000 hours (figure 3.15). SAXS analysis revealed significant changes in the ionomer peak as a function of both time and temperature. At 80°C, longer treatment times led to an increase in the ionomer peak intensity and a transition from Porod's regime to a power law with n=-4, indicating a clearer separation between hydrophilic and hydrophobic clusters. The authors argued that temperatures above the β-relaxation threshold, combined with sufficient soaking time, allow segmental mobility that promotes pronounced hydrophilic/hydrophobic phase separation.

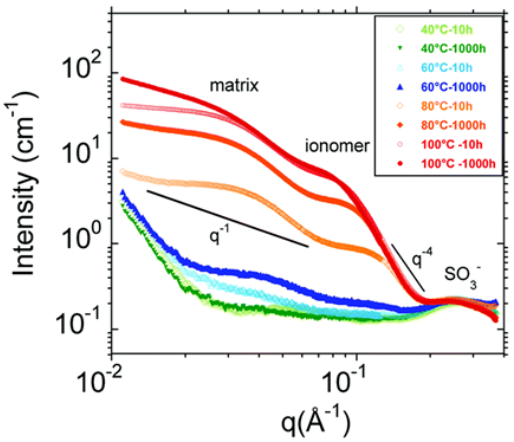

FIGURE 3.15 – SAXS measurements of sPEEK ionomer in Cs+ form for various soaking times in water at various temperatures [43].

Further experiments demonstrated the irreversibility of the process, showing that sPEEK exhibits a microstructural "memory", as also stated for ionomers by Van Der Linden et al. [159] and by Choi et Jin [140]. Measurements of water uptake and proton conductivity for samples soaked for 96 hours at various temperatures showed substantial increases with higher soaking temperatures : water uptake rose notably above 60°C, while proton conductivity increased sharply from 44°C at 70°C to 83 mS.cm^{-1} at 80°C (figure 3.16).

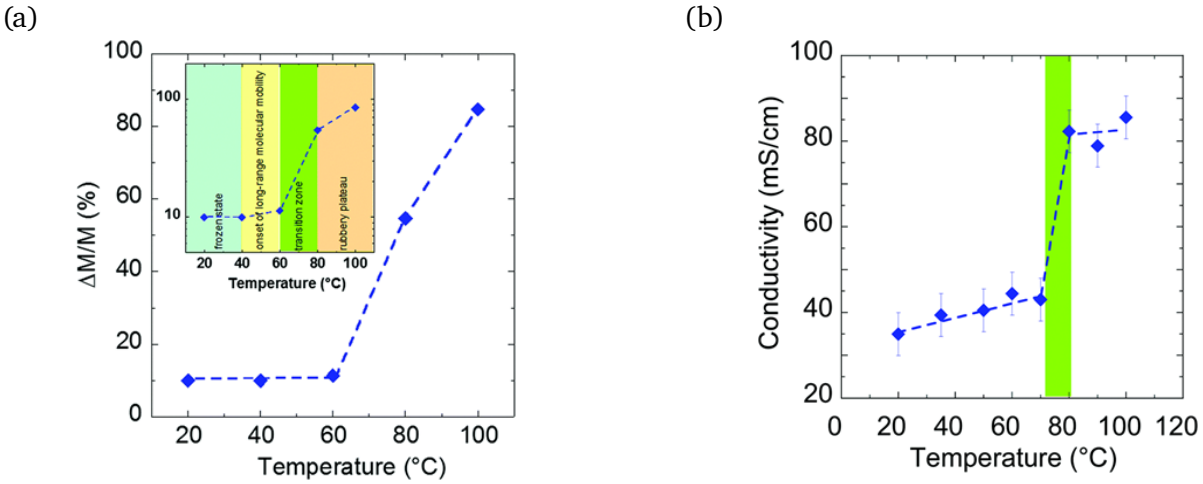

FIGURE 3.16 – Water uptake (a) and proton conductivity of sPEEK after soaking in water at various temperatures for 96h [43].

Daoudi et al. [127] investigated several pretreatments, including an acidification step (noted Acd), a hydrothermal step at 80°C (noted HT 1h and HT 72h for soaking durations of 1 and 72 hours in water, respectively), and a hydroalcoholic step (noted HA). The hydrothermal step increased the water self-diffusion coefficient above a given water uptake. The additional hydroalcoholic step induced further reorganization by enhancing chain mobility. Overall, combining the hydroalcoholic and hydrothermal steps resulted in lower high-frequency resistance and higher proton conductivity. As a consequence, a significant improvement in fuel cell performance was observed under H_2/O_2 operation (figure 3.17(a)), surpassing even that of a PFSA-based membrane (figure 3.17(b)).

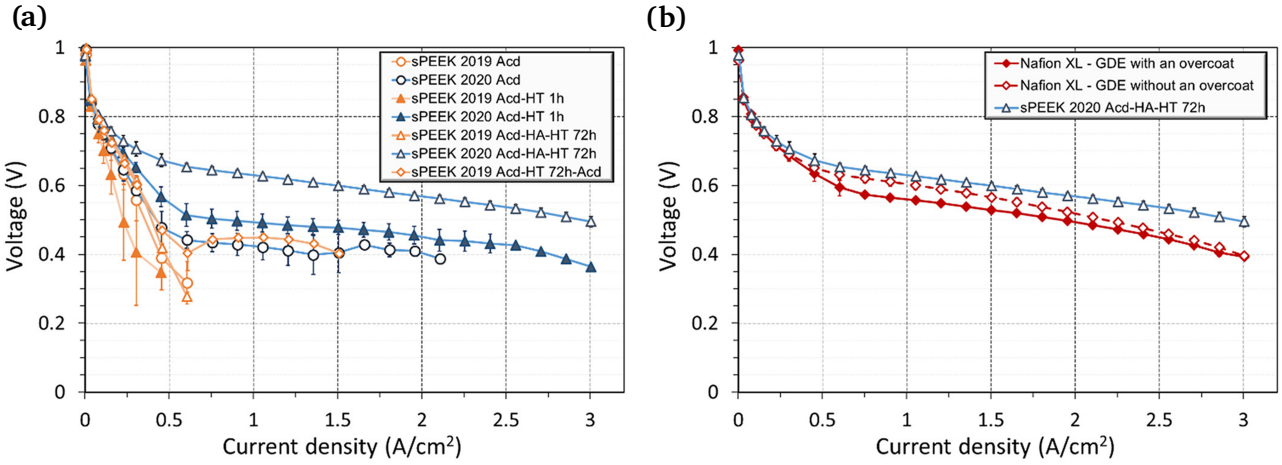

FIGURE 3.17 – Polarization curves of sPEEK under H_2/O_2 atmosphere at 70°C following various pretreatment protocols [160].

In addition to improving *in situ* performances, Daoudi et al. [127] also observed enhanced durability through *ex situ* accelerated stress tests. In the *ex situ* approach, FTIR measurements showed that sPEEK pretreated with the optimized protocol exhibited greater stability in a H_2O_2 solution heated to 80°C, highlighting the benefits of increased phase separation and improved chemical durability. However, a reduction in *in situ* durability was observed, which the authors attributed to the lower ionomer thickness resulting from the pretreatment.

6.2.2 Crosslinking

Crosslinking an ionomer is an effective way to improve its properties and can be applied on different chemical sites on the polymer. However, the location strongly affects ionomer properties. For example, crosslinking through the sulfonic acid groups reduces water uptake and therefore proton conductivity, whereas other crosslinking approaches target non-sulfonated positions to keep constant the ion exchange capacity.

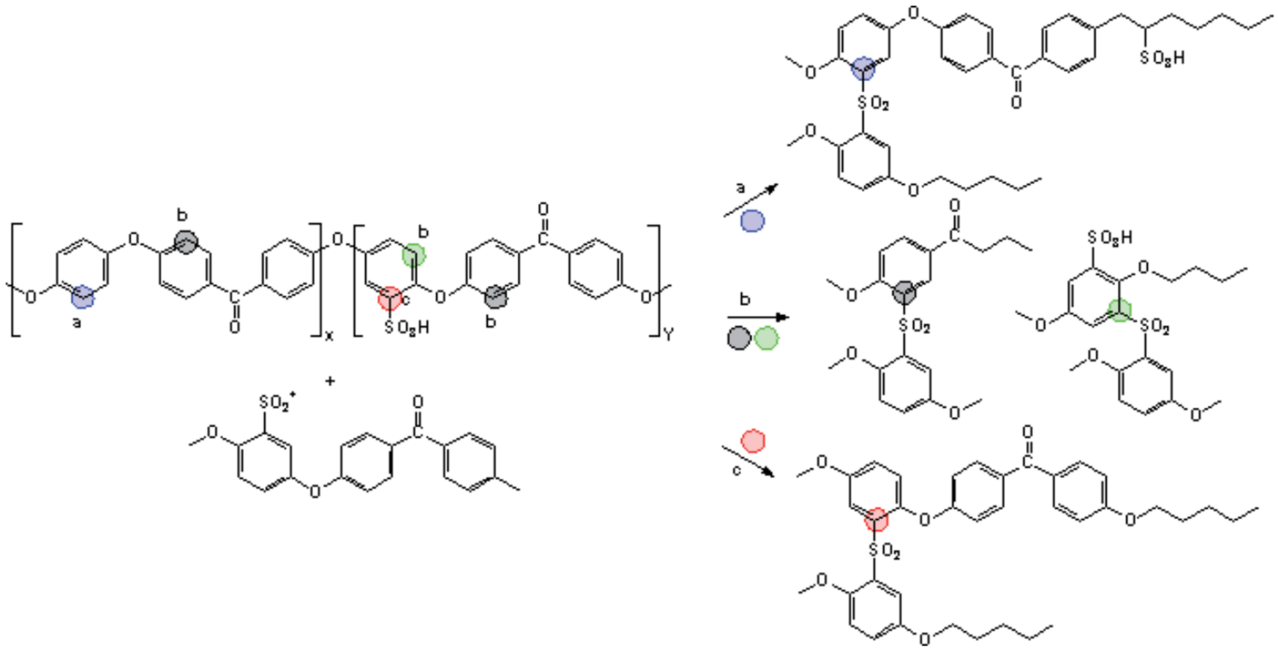

FIGURE 3.18 – Site position for sPEEK crosslinking [161].

Several processes can induce crosslinking between macromolecular chains, such as adding a chemical additive during the casting process, using irradiation [19, 162]. Thermal treatments are a common way with various temperatures and durations applied. However, Mikhailenko et al. [163] suggested that heating below about 120-150°C alone typically does not produce significant crosslinking and that a crosslinking reagent is therefore necessary. Residual casting solvent can facilitate crosslinking by acting as a crosslinking reagent, although this depends on its nature : DMAc and NMP have been reported not to induce crosslinking, contrary to DMSO [112, 161].

Di Vona et al. [112] applied different thermal treatments to sPEEK samples with various degrees of sulfonation and analyzed the process using XRD and NMR. While XRD consistently showed the same amorphous structure, NMR revealed that crosslinking became effective above 120°C for sPEEK cast with DMSO. Water uptake measurements showed significantly lower values for sample treated at 160°C, and even lower for samples treated sequentially at 120°C and at 160°C, compared to samples treated only at 120°C, as also reported by Narducci et al. [115]. Increasing crosslinking reduces ionomer deformation and thus membrane swelling, improving mechanical durability. A transition from ductile to more elastic behavior with increasing crosslinking degree has been reported, characterized by an increased Young's modulus and a decreased elongation at break ([164, 165] for SPPSU, [166]), although crystallinity was not affected [118].

Crosslinking can also be performed using chemical reagents in addition to thermal treatment. Hande et al. [164] performed Fenton's test on sPEEK that had been thermally crosslinked using

two aromatic compounds at various concentrations : BHMMP (2,6-bis(hydroxymethyl)-4-methyl phenol) and (1,4-bis(hydroxymethyl) benzene) BHMB as crosslinking reagents. After 1h of Fenton's test, uncrosslinked sPEEK was disintegrated, whereas crosslinked sPEEK exhibited less chemical degradation, as indicated by the lower weight loss and smaller changes in mechanical properties. They also reported increased durability with increasing crosslinking degree.

Overall, crosslinking is a simple way to improve dimensional stability and mechanical durability during fuel cell operation–such as under relative humidity cycling–by limiting water uptake and therefore swelling. However, increasing the degree of crosslinking reduces the ion-exchange capacity when sulfonic groups are used to form bonds between polymer chains [162, 164, 167], which in turn decreases proton conductivity [163, 166] and thus fuel cell performance. A trade-off must therefore be found between durability and performance. Barbieri et al., for example, reported better *in situ* performance with increasing crosslinking degree of sPEEK membranes [167]. In addition, the authors suggested that the proton conductivity of crosslinked membrane can be maintained, or even improved, despite the loss of sulfonic groups during the crosslinking reaction, by soaking the sPEEK membrane in boiling water and exploiting a "memory effect".

7 Conclusions/perspectives

The sPEEK synthesis process has a strong impact on its physico-chemical properties and therefore significantly affects its fuel cell performance. The casting solvent affects ionomer microstructure due to its affinity with it, whereas the increase in the degree of sulfonation enhances water uptake and proton conductivity while decreasing its mechanical properties to a more ductile behavior. Although sPEEK physicochemical properties can be equivalent to PFSA ones, notably for proton conductivity, lower fuel cell performance has systematically been reported. This behavior is mainly attributed to inherent microstructural differences, especially the lower degree of nanophase separation. Moreover, the lower chemical stability of sPEEK has led to its rejection for long-term operation. Nevertheless, adequate pretreatment involving annealing and hydrothermal or hydroalcoholic soaking resulted in substantial improvements both in terms of physicochemical properties, fuel cell performance and durability.

These encouraging results led us to explore the use of pretreated sPEEK. Our recent work, based on a pretreatment inspired by Daoudi et al. [127], showed similar performance to Nafion 211 under standard fuel cell conditions. These good performances were also measured at lower gas inlet RH, whereas most studies reported a crucial need for high gas RH for sPEEK operation. Accelerated stress tests also revealed close durability between the two ionomers, highlighting the potential of sPEEK ionomer when appropriate pretreatment is applied.

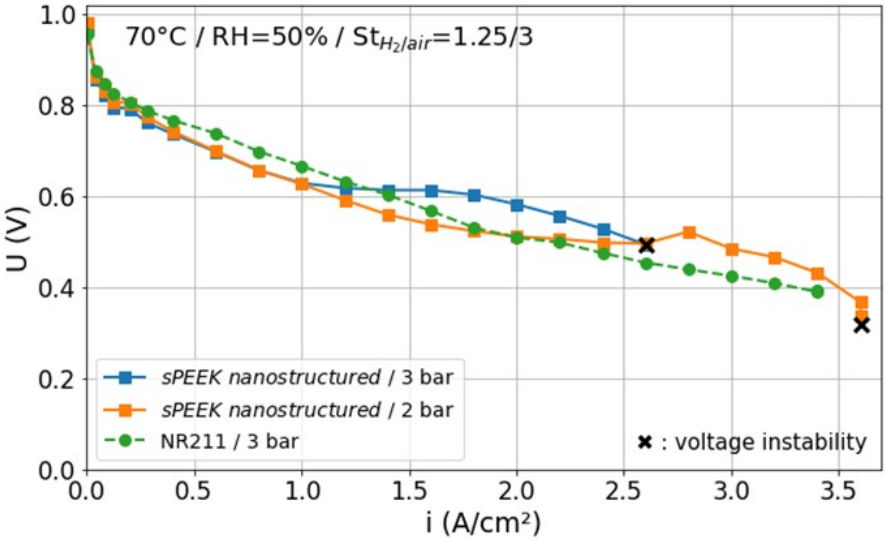

FIGURE 3.19 – sPEEK fuel cell performance compared to NR211 at 70°C under 50% gas inlet RH.

Thus, this review provides a new perspective on pristine sPEEK membranes, which exhibit significant potential without necessarily requiring hybridization or chemical modification. Future studies should focus on sPEEK synthesis, given the strong influence of the processing route, with a more systematic and rigorous investigation encompassing processing and membrane casting conditions, detailed microstructural characterization, and in-cell performance evaluation under relevant operating conditions. In particular, future work should also refocus on the pristine sPEEK membrane itself, with particular emphasis on optimizing pretreatment strategies, in order to further enhance performance and achieve durable membranes without hybridization, chemical modification, or additive incorporation.

References

[1] P. A. García-Salaberri, « Proton Exchange Membranes for Polymer Electrolyte Fuel Cells : An Analysis of Perfluorosulfonic Acid and Aromatic Hydrocarbon Ionomers, » *Sustainable Materials and Technologies*, t. 38, e00727, 2023, ISSN : 2214-9937. DOI : 10.1016/j.susmat.2023.e00727

[2] M. Adamski et al., « On the evolution of sulfonated polyphenylenes as proton exchange membranes for fuel cells, » *Materials Advances*, t. 2, n° 15, p. 4966-5005, 2021. DOI : 10.1039/D1MA00511A

[3] « Perfluorosulfonic Acid Proton Exchange Membranes - Global Industry Market Analysis Report 2020-2031, » Paco Research, rapp. tech., 2025.

[4] Z. Yuan et al., « Low-Cost Hydrocarbon Membrane Enables Commercial-Scale Flow Batteries for Long-Duration Energy Storage, » *Joule*, t. 6, n° 4, p. 884-905, 2022, ISSN : 2542-4351. DOI : 10.1016/j.joule.2022.02.016

[5] S. Ahmad et al., « An Overview of Proton Exchange Membranes for Fuel Cells : Materials and Manufacturing, » *International Journal of Hydrogen Energy*, t. 47, n° 44, p. 19 086-19 131, 2022, ISSN : 0360-3199. DOI : 10.1016/j.ijhydene.2022.04.099

[6] M. Miotti et al., « Integrated environmental and economic assessment of current and future fuel cell vehicles, » *The International Journal of Life Cycle Assessment*, t. 22, n° 1, p. 94-110, 2017, ISSN : 1614-7502. DOI : 10.1007/s11367-015-0986-4

[7] M. Mori et al., « Life Cycle Sustainability Assessment of a Proton Exchange Membrane Fuel Cell Technology for Ecodesign Purposes, » *International Journal of Hydrogen Energy*, Integrated Hydrogen Energy Systems, t. 48, n° 99, p. 39 673-39 689, 2023, ISSN : 0360-3199. DOI : 10.1016/j.ijhydene.2023.05.255

[8] O. M. Babatunde et al., « Environmental Impact Assessment of a 1 kW Proton-Exchange Membrane Fuel Cell : A Mid-Point and End-Point Analysis, » *Hydrogen*, t. 5, n° 2, p. 352-373, 2024, ISSN : 2673-4141. DOI : 10.3390/hydrogen5020020

[9] L. Duclos et al., « Environmental Assessment of Proton Exchange Membrane Fuel Cell Platinum Catalyst Recycling, » *Journal of Cleaner Production*, t. 142, p. 2618-2628, 2017, ISSN : 0959-6526. DOI : 10.1016/j.jclepro.2016.10.197

[10] M. Robert et al., « Investigation of Membrane–Electrode Separation Processes for the Recycling of Ionomer Membranes in End-of-Life PEM Fuel Cells, » *Energy & Fuels*, t. 39, n° 5, p. 2758-2771, 2025, ISSN : 0887-0624. DOI : 10.1021/acs.energyfuels.4c04930

[11] M. Kutter et al., « Recycling of Perfluorosulfonic Acid-Based Membranes and Their Reapplication in PEM Fuel Cells, » *Journal of Membrane Science*, t. 693, p. 122 370, 2024, ISSN : 0376-7388. DOI : 10.1016/j.memsci.2023.122370

[12] R. Sharma et al., « Recovery, Regeneration, and Reapplication of PFSA Polymer from End-of-Life PEMFC MEAs, » *ACS Applied Materials & Interfaces*, t. 15, n° 41, p. 48 705-48 715, 2023, ISSN : 1944-8244. DOI : 10.1021/acsami.3c11186

[13] H. Nguyen et al., « Fully Hydrocarbon Membrane Electrode Assemblies for Proton Exchange Membrane Fuel Cells and Electrolyzers : An Engineering Perspective, » *Advanced Energy Materials*, t. 12, n° 12, p. 2 103 559, 2022, ISSN : 1614-6840. DOI : 10.1002/aenm.202103559

[14] H. Nguyen et al., « Hydrocarbon-based Pemion™ proton exchange membrane fuel cells with state-of-the-art performance, » *Sustainable Energy & Fuels*, t. 5, n° 14, p. 3687-3699, 2021, ISSN : 2398-4902. DOI : 10.1039/D1SE00556A

[15] M. J. Parnian et al., « Comprehensive investigation of physicochemical and electrochemical properties of sulfonated poly (ether ether ketone) membranes with different degrees of sulfonation for proton exchange membrane fuel cell applications, » *Energy*, t. 125, p. 614-628, 2017, ISSN : 03605442. DOI : 10.1016/j.energy.2017.02.143

[16] G. Portale et al., « Microstructure, state of water and proton conductivity of sulfonated poly(ether ether ketone), » *Solid State Ionics*, t. 252, p. 62-67, 2013, ISSN : 01672738. DOI : 10.1016/j.ssi.2013.08.031

[17] A. Iulianelli et al., « Sulfonated PEEK-based polymers in PEMFC and DMFC applications : A review, » *International Journal of Hydrogen Energy*, The 2011 Asian Bio-Hydrogen and Biorefinery Symposium (2011ABBS), t. 37, n° 20, p. 15 241-15 255, 2012, ISSN : 0360-3199. DOI : 10.1016/j.ijhydene.2012.07.063

[18] C. Y. Wong et al., « Comparative Study On Water Uptake And Ionic Transport Properties Of Pre- And Post Sulfonated Chitosan/PVA polymer Exchange Membrane, » *IOP Conference Series : Materials Science and Engineering*, t. 458, n° 1, p. 012 017, 2018, ISSN : 1757-899X. DOI : 10.1088/1757-899X/458/1/012017

[19] P. Khomein et al., « Sulfonated aromatic polymer as a future proton exchange membrane : A review of sulfonation and crosslinking methods, » *Renewable and Sustainable Energy Reviews*, t. 137, p. 110 471, 2021, ISSN : 13640321. DOI : 10.1016/j.rser.2020.110471

[20] C. Perrot, « Degradation mechanisms of sulfonated polyaromatic membranes in fuel cell, » PhD Thesis, Université Joseph-Fourier - Grenoble I, 2006.

[21] X. Zhu et al., « Polymer Composites for High-Temperature Proton-Exchange Membrane Fuel Cells, » in *Polymer Membranes for Fuel Cells*, S. M. J. Zaidi et al., éd., Boston, MA : Springer US, 2009, p. 159-184, ISBN : 978-0-387-73532-0. DOI : 10.1007/978-0-387-73532-0_7

[22] M. Gil et al., « Direct synthesis of sulfonated aromatic poly(ether ether ketone) proton exchange membranes for fuel cell applications, » *Journal of Membrane Science*, t. 234, n° 1-2, p. 75-81, 2004, ISSN : 03767388. DOI : 10.1016/j.memsci.2003.12.021

[23] R. Araby et al., « Characterization and Sulfonation Degree of Sulfonated Poly Ether Ether Ketone Using Fourier Transform Infrared Spectroscopy, » *World Appl. Sci. J.*, t. 32, p. 2239-2244, 2014, ISSN : 1818-4952. DOI : 10.5829/idosi.wasj.2014.32.11.14561

[24] P. Xing et al., « Synthesis and characterization of sulfonated poly(ether ether ketone) for proton exchange membranes, » *Journal of Membrane Science*, t. 229, n° 1-2, p. 95-106, 2004, ISSN : 03767388. DOI : 10.1016/j.memsci.2003.09.019

[25] R. Ma et al., « Effects of different sulfonation times and post-treatment methods on the characterization and cytocompatibility of sulfonated PEEK, » *Journal of Biomaterials Applications*, t. 35, n° 3, p. 342-352, 2020, ISSN : 0885-3282. DOI : 10.1177/0885328220935008

[26] G. M. Shashidhara et al., « Proton Conductivity of SPEEK Membranes, » *Polymer-Plastics Technology and Engineering*, t. 49, n° 8, p. 796-806, 2010, ISSN : 0360-2559, 1525-6111. DOI : 10.1080/03602551003749601

[27] M. H. D. Othman et al., « Physico-Chemical Study of Sulfonated Poly(Ether Ether Ketone) Membranes for Direct Methanol Fuel Cell Application, » t. 2, n° 1, 2007.

[28] K. N. T. Do et al., « Comparison of homogeneously and heterogeneously sulfonated polyetheretherketone membranes in preparation, properties and cell performance, » *Journal of Power Sources*, t. 185, n° 1, p. 63-69, 2008, ISSN : 03787753. DOI : 10.1016/j.jpowsour.2008.06.087

[29] P. Salarizadeh et al., « Enhanced properties of SPEEK with incorporating of PFSA and barium strontium titanate nanoparticles for application in DMFCs, » *International Journal of Energy Research*, t. 43, n° 9, p. 4840-4853, 2019, ISSN : 1099-114X. DOI : 10.1002/er.4635

[30] S. Kaliaguine et al., « Properties of SPEEK Based PEMs for Fuel Cell Application, » *Catalysis Today*, t. 82, 2003. DOI : 10.1016/S0920-5861(03)00235-9

[31] F. Gashoul et al., « A new study on improving the physicochemical and electrochemical properties of SPEEK nanocomposite membranes for medium temperature proton exchange membrane fuel cells using different loading of zirconium oxide nanoparticles, » *International Journal of Hydrogen Energy*, t. 42, n° 1, p. 590-602, 2017, ISSN : 03603199. DOI : 10.1016/j.ijhydene.2016.11.132

[32] D. X. Luu et al., « SAXS and NMR Analysis for the Cast Solvent Effect on sPEEK Membrane Properties, » *The Journal of Physical Chemistry B*, t. 113, n° 30, p. 10 072-10 076, 2009, ISSN : 1520-6106, 1520-5207. DOI : 10.1021/jp904604u

[33] S. Zaidi et al., « Proton conducting composite membranes from polyether ether ketone and heteropolyacids for fuel cell applications, » *Journal of Membrane Science*, t. 173, n° 1, p. 17-34, 2000, ISSN : 03767388. DOI : 10.1016/S0376-7388(00)00345-8

[34] R. T. S. Muthu Lakshmi et al., « Sulphonated poly(ether ether ketone) : Synthesis and characterisation, » *Journal of Materials Science*, t. 40, n° 3, p. 629-636, 2005, ISSN : 1573-4803. DOI : 10.1007/s10853-005-6300-2

[35] S. Banerjee et al., « Impact of degree of sulfonation on microstructure, thermal, thermomechanical and physicochemical properties of sulfonated poly ether ether ketone, » *Polymer*, t. 109, p. 176-186, 2017, ISSN : 00323861. DOI : 10.1016/j.polymer.2016.12.030

[36] J.-M. Song et al., « Ionic aggregation characterization of sulfonated PEEK ionomers using by X-ray and DMA techniques, » *Macromolecular Research*, t. 20, n° 5, p. 477-483, 2012, ISSN : 2092-7673. DOI : 10.1007/s13233-012-0067-5

[37] C. A. Kawaguti et al., « Nanostructure and properties of proton-conducting sulfonated poly(ether ether ketone) (SPEEK) and zirconia–SPEEK hybrid membranes for direct alcohol fuel cells : effect of the nature of swelling solvent and incorporation of heteropolyacid, » *Polymer International*, t. 61, n° 1, p. 82-92, 2012, ISSN : 1097-0126. DOI : 10.1002/pi.3151

[38] O. Dupont et al., « Adaptation of the Rietveld Method for the Characterization of the Lamellar Microstructure of Polymers, » *Journal of Applied Crystallography*, t. 30, n° 6, p. 921-931, 1997, ISSN : 1600-5767. DOI : 10.1107/S0021889897003166

[39] Y. Zhang et al., « Investigation of sulfonation degree and temperature on structure, thermal and membrane's properties of sulfonated poly (ether ether ketone), » *International Journal of Hydrogen Energy*, t. 48, n° 37, p. 13 791-13 803, 2023, ISSN : 03603199. DOI : 10.1016/j.ijhydene.2022.12.332

[40] B. Yang et al., « Comparison of the small angle X-ray scattering study of sulfonated poly(etheretherketone) and Nafion membranes for direct methanol fuel cells, » *Journal of Power Sources*, t. 153, n° 1, p. 29-35, 2006, ISSN : 03787753. DOI : 10.1016/j.jpowsour.2005.03.185

[41] H. Mendil-Jakani et al., « A new interpretation of SAXS peaks in sulfonated poly(ether ether ketone) (sPEEK) membranes for fuel cells, » *Physical Chemistry Chemical Physics*, t. 16, n° 23, p. 11 243-11 250, 2014, ISSN : 1463-9084. DOI : 10.1039/C4CP00710G

[42] K. Kreuer, « On the development of proton conducting polymer membranes for hydrogen and methanol fuel cells, » *Journal of Membrane Science*, t. 185, n° 1, p. 29-39, 2001, issn : 03767388. doi : 10.1016/S0376-7388(00)00632-3

[43] H. Mendil-Jakani et al., « Optimization of Hydrophilic/Hydrophobic Phase Separation in sPEEK Membranes by Hydrothermal Treatments, » *Phys. Chem. Chem. Phys.*, t. 19, 2017. doi : 10.1039/C7CP00087A

[44] R. Wang et al., « Understanding of Nanophase Separation and Hydrophilic Morphology in Nafion and SPEEK Membranes : A Combined Experimental and Theoretical Studies, » *Nanomaterials*, t. 9, n° 6, p. 869, 2019, issn : 2079-4991. doi : 10.3390/nano9060869

[45] M. Tripathy et al., « Molecular Structuring and Percolation Transition in Hydrated Sulfonated Poly(Ether Ether Ketone) Membranes, » *The Journal of Physical Chemistry B*, t. 121, n° 18, p. 4873-4884, 2017, issn : 1520-6106. doi : 10.1021/acs.jpcb.7b01045

[46] C. V. Mahajan et al., « Atomistic Simulations of Structure of Solvated Sulfonated Poly(ether ether ketone) Membranes and Their Comparisons to Nafion : II. Structure and Transport Properties of Water, Hydronium Ions, and Methanol, » *The Journal of Physical Chemistry B*, t. 114, n° 25, p. 8367-8373, 2010. doi : 10.1021/jp1040794

[47] Y. Tang et al., « Ionic polymer–metal composite actuator based on sulfonated poly(ether ether ketone) with different degrees of sulfonation, » *Sensors and Actuators A : Physical*, t. 238, p. 167-176, 2016, issn : 09244247. doi : 10.1016/j.sna.2015.12.015

[48] L. Li, « Sulfonated poly(ether ether ketone) membranes for direct methanol fuel cell, » *Journal of Membrane Science*, t. 226, n° 1-2, p. 159-167, 2003, issn : 03767388. doi : 10.1016/j.memsci.2003.08.018

[49] S. Zhong et al., « Preparation and Evaluation of a Proton Exchange Membrane Based on Cross-linkable Sulfonated Poly(Ether Ether Ketone)s, » *Journal of Power Sources - J POWER SOURCES*, t. 162, p. 51-57, 2006. doi : 10.1016/j.jpowsour.2006.06.067

[50] D. Brush et al., « Phase Separation in Sulfonated Poly(ether ether ketone) (SPEEK) Ionomers by Spin Probe ESR : Effect of the Degree of Sulfonation and Water Content, » *Macromolecules*, t. 48, n° 3, p. 637-644, 2015, issn : 0024-9297, 1520-5835. doi : 10.1021/ma502359g

[51] Y. Zhang et al., « Sulfonated polysulfone proton exchange membrane influenced by a varied sulfonation degree for vanadium redox flow battery, » *Journal of Membrane Science*, t. 584, p. 173-180, 2019, issn : 03767388. doi : 10.1016/j.memsci.2019.04.073

[52] G. Gebel, « Structure of Membranes for Fuel Cells : SANS and SAXS Analyses of Sulfonated PEEK Membranes and Solutions, » *Macromolecules*, t. 46, n° 15, p. 6057-6066, 2013, issn : 0024-9297. doi : 10.1021/ma400314c

[53] B. Yang et al., « Sulfonated Poly(ether ether ketone) Membranes for Direct Methanol Fuel Cells, » *Electrochemical and Solid-State Letters*, t. 6, n° 11, A229, 2003, issn : 1944-8775. doi : 10.1149/1.1613073

[54] L. Du et al., « SPEEK proton exchange membranes modified with silica sulfuric acid nanoparticles, » *International Journal of Hydrogen Energy*, t. 37, n° 16, p. 11 853-11 861, 2012, issn : 03603199. doi : 10.1016/j.ijhydene.2012.05.024

[55] H. Li et al., « Composite membranes based on a novel benzimidazole grafted PEEK and SPEEK for fuel cells, » *International Journal of Hydrogen Energy*, t. 35, n° 20, p. 11 172-11 179, 2010, issn : 03603199. doi : 10.1016/j.ijhydene.2010.07.091

[56] D. J. Kim et al., « Characterization of the sulfonated PEEK/sulfonated nanoparticles composite membrane for the fuel cell application, » *International Journal of Hydrogen Energy*, t. 41, n° 13, p. 5793-5802, 2016, ISSN : 03603199. DOI : 10.1016/j.ijhydene.2016.02.056

[57] Z. Gaowen et al., « Organic/inorganic composite membranes for application in DMFC, » *Journal of Membrane Science*, t. 261, n° 1-2, p. 107-113, 2005, ISSN : 03767388. DOI : 10.1016/j.memsci.2005.03.036

[58] D. Gupta et al., « Studies on novel heat treated sulfonated poly(ether ether ketone) [SPEEK]/diol membranes for fuel cell applications, » *International Journal of Hydrogen Energy*, t. 36, n° 14, p. 8525-8535, 2011, ISSN : 03603199. DOI : 10.1016/j.ijhydene.2011.04.044

[59] H. Zhang et al., « Enhancement of proton conductivity of polymer electrolyte membrane enabled by sulfonated nanotubes, » *International Journal of Hydrogen Energy*, t. 39, n° 2, p. 974-986, 2014, ISSN : 03603199. DOI : 10.1016/j.ijhydene.2013.10.145

[60] A. Mayahi et al., « Effect of operating temperature on the behavior of promising SPEEK/cSMM electrolyte membrane for DMFCs, » *Separation and Purification Technology*, t. 106, p. 72-81, 2013, ISSN : 13835866. DOI : 10.1016/j.seppur.2012.12.027

[61] R. Jiang et al., « Investigation of membrane property and fuel cell behavior with sulfonated poly(ether ether ketone) electrolyte : Temperature and relative humidity effects, » *Journal of Power Sources*, t. 150, p. 120-128, 2005, ISSN : 03787753. DOI : 10.1016/j.jpowsour.2005.03.180

[62] J. Potreck et al., « Sorption induced relaxations during water diffusion in S-PEEK, » *Physical Chemistry Chemical Physics*, t. 11, n° 2, p. 298-308, 2009, ISSN : 1463-9084. DOI : 10.1039/B810638J

[63] H. Feng, « Modeling of vapor sorption in glassy polymers using a new dual mode sorption model based on multilayer sorption theory, » *Polymer*, t. 48, n° 10, p. 2988-3002, 2007, ISSN : 00323861. DOI : 10.1016/j.polymer.2006.10.050

[64] Y. Li et al., « Water Sorption Behavior in Different Aromatic Ionomer Composites Analyzed with a "New Dual-Mode Sorption" Model, » *Macromolecules*, t. 47, p. 6331-6342, 2014. DOI : 10.1021/ma501097k

[65] Y. Li et al., « Proton Exchange Membranes from Sulfonated Polyetheretherketone and Sulfonated Polyethersulfone-Cardo Blends : Conductivity, Water Sorption and Permeation Properties, » *Electrochimica Acta*, t. 111, p. 419-433, 2013, ISSN : 0013-4686. DOI : 10.1016/j.electacta.2013.07.158

[66] H.-L. Wu et al., « Swelling behavior and solubility parameter of sulfonated poly(ether ether ketone), » *Journal of Polymer Science Part B : Polymer Physics*, t. 44, n° 21, p. 3128-3134, 2006, ISSN : 1099-0488. DOI : 10.1002/polb.20964

[67] X. Wu et al., « Differences in water sorption and proton conductivity between Nafion and SPEEK, » *Journal of Polymer Science Part B : Polymer Physics*, t. 49, n° 20, p. 1437-1445, 2011, ISSN : 08876266. DOI : 10.1002/polb.22326

[68] J. M. Woudstra et al., « Investigating the Water in Hydrated sPEEK Membranes Using Multiple Quantum Filtered 2H NMR Spectroscopy, » *The Journal of Physical Chemistry B*, t. 116, n° 50, p. 14 724-14 730, 2012, ISSN : 1520-6106. DOI : 10.1021/jp309986x

[69] C. V. Mahajan et al., « Atomistic Simulations of Structure of Solvated Sulfonated Poly(Ether Ether Ketone) Membranes and Their Comparisons to Nafion : I. Nanophase Segregation and Hydrophilic Domains, » *The Journal of Physical Chemistry B*, t. 114, n° 25, p. 8357-8366, 2010, ISSN : 1520-6106. DOI : 10.1021/jp104078h

[70] T. Ueki et al., « Macromolecules in Ionic Liquids : Progress, Challenges, and Opportunities, » *Macromolecules*, t. 41, n° 11, p. 3739-3749, 2008, ISSN : 0024-9297, 1520-5835. DOI : 10.1021/ma800171k

[71] K.-D. Kreuer et al., « Transport in Proton Conductors for Fuel-Cell Applications : Simulations, Elementary Reactions, and Phenomenology, » *Chemical Reviews*, t. 104, n° 10, p. 4637-4678, 2004, ISSN : 0009-2665, 1520-6890. DOI : 10.1021/cr020715f

[72] M. Eikerling et al., « Electrophysical Properties of Polymer Electrolyte Membranes : A Random Network Model, » *The Journal of Physical Chemistry B*, t. 101, n° 50, p. 10 807-10 820, 1997, ISSN : 1520-6106, 1520-5207. DOI : 10.1021/jp972288t

[73] R. Wang et al., « Proton conductivity enhancement of SPEEK membrane through n-BuOH assisted self-organization, » *Journal of Membrane Science*, t. 479, p. 46-54, 2015, ISSN : 03767388. DOI : 10.1016/j.memsci.2014.12.054

[74] M. Cappadonia, « Conductance of Nafion 117 membranes as a function of temperature and water content, » *Solid State Ionics*, t. 77, p. 65-69, 1995, ISSN : 01672738. DOI : 10.1016/0167-2738(94)00289-5

[75] P. Commer et al., « The effect of water content on proton transport in polymer electrolyte membranes, » *Fuel Cells*, t. 2, n° 3-4, p. 127-136, 2002, ISSN : 1615-6854. DOI : 10.1002/fuce.200290011

[76] J. X. Leong et al., « Composite membrane containing graphene oxide in sulfonated polyether ether ketone in microbial fuel cell applications, » *International Journal of Hydrogen Energy*, t. 40, n° 35, p. 11 604-11 614, 2015, ISSN : 03603199. DOI : 10.1016/j.ijhydene.2015.04.082

[77] M. Eikerling et al., « Proton-Conducting Polymer Electrolyte Membranes : Water and Structure in Charge, » in *Fuel Cells I*, sér. Advances in Polymer Science, G. G. Scherer, éd., Berlin, Heidelberg : Springer, 2008, p. 15-54, ISBN : 978-3-540-69757-2. DOI : 10.1007/12_2008_132

[78] H. Wu et al., « Novel sulfonated poly (ether ether ketone)/phosphonic acid-functionalized titania nanohybrid membrane by an in situ method for direct methanol fuel cells, » *Journal of Power Sources*, t. 273, p. 544-553, 2015, ISSN : 03787753. DOI : 10.1016/j.jpowsour.2014.09.134

[79] H. Cai et al., « Properties of composite membranes based on sulfonated poly(ether ether ketone)s (SPEEK)/phenoxy resin (PHR) for direct methanol fuel cells usages, » *Journal of Membrane Science*, t. 297, n° 1-2, p. 162-173, 2007, ISSN : 03767388. DOI : 10.1016/j.memsci.2007.03.040

[80] X. Liu et al., « Proton conductivity improvement of sulfonated poly(ether ether ketone) nanocomposite membranes with sulfonated halloysite nanotubes prepared via dopamine-initiated atom transfer radical polymerization, » *Journal of Membrane Science*, t. 504, p. 206-219, 2016, ISSN : 03767388. DOI : 10.1016/j.memsci.2016.01.023

[81] R. Murmu et al., « Steady State Analysis of Water Transport through Sulfonated Polyether Ether Ketone (SPEEK) Membrane for Fuel Cell Application, » *JOURNAL OF POLYMER MATERIALS*, t. 35, 2018. DOI : 10.32381/JPM.2018.35.01.8

[82] X. Yan et al., « Ion and water transport in functionalized PEEK membranes, » *Journal of Membrane Science*, t. 429, p. 13-22, 2013, ISSN : 03767388. DOI : 10.1016/j.memsci.2012.11.026

[83] C. Fan et al., « Incorporating self-anchored phosphotungstic acid@triazole-functionalized covalent organic framework into sulfonated poly(ether ether ketone) for enhanced proton conductivity, » *Solid State Ionics*, t. 349, p. 115 316, 2020, ISSN : 01672738. DOI : 10.1016/j.ssi.2020.115316

[84] T. A. Zawodzinski et al., « Water Uptake by and Transport Through Nafion® 117 Membranes, » *Journal of The Electrochemical Society*, t. 140, n° 4, p. 1041-1047, 1993, ISSN : 0013-4651, 1945-7111. DOI : 10.1149/1.2056194

[85] G.-C. Park et al., « Porous PTFE reinforced SPEEK proton exchange membranes for enhanced mechanical, dimensional, and electrochemical stability, » *Polymer*, t. 218, p. 123 506, 2021, ISSN : 00323861. DOI : 10.1016/j.polymer.2021.123506

[86] S. Xue et al., « Methanol permeability in sulfonated poly(etheretherketone) membranes : A comparison with Nafion membranes, » *European Polymer Journal*, t. 42, n° 4, p. 776-785, 2006, ISSN : 00143057. DOI : 10.1016/j.eurpolymj.2005.10.008

[87] G. Li et al., « Intermolecular ionic cross-linked sulfonated poly(ether ether ketone) membranes with excellent mechanical properties and selectivity for direct methanol fuel cells, » *RSC Advances*, t. 6, n° 27, p. 23 025-23 032, 2016, ISSN : 2046-2069. DOI : 10.1039/C6RA02321E

[88] M. Vinothkannan et al., « Toward improved mechanical strength, oxidative stability and proton conductivity of an aligned quadratic hybrid (SPEEK/FPAPB/Fe 3 O 4 -FGO) membrane for application in high temperature and low humidity fuel cells, » *RSC Advances*, t. 7, n° 62, p. 39 034-39 048, 2017. DOI : 10.1039/C7RA07063B

[89] B. Campagne et al., « Novel Blend Membranes of Partially Fluorinated Copolymers Bearing Azole Functions with Sulfonated PEEK for PEMFC Operating at Low Relative Humidity : Influence of the Nature of the *N* -Heterocycle, » *Macromolecules*, t. 46, n° 8, p. 3046-3057, 2013, ISSN : 0024-9297, 1520-5835. DOI : 10.1021/ma400239f

[90] G. Rambabu et al., « Simultaneous tuning of methanol crossover and ionic conductivity of sPEEK membrane electrolyte by incorporation of PSSA functionalized MWCNTs : A comparative study in DMFCs, » *Chemical Engineering Journal*, t. 243, p. 517-525, 2014, ISSN : 13858947. DOI : 10.1016/j.cej.2014.01.030

[91] A. Carbone et al., « Composite S-PEEK membranes for medium temperature polymer electrolyte fuel cells, » *Journal of Power Sources*, t. 178, n° 2, p. 661-666, 2008, ISSN : 03787753. DOI : 10.1016/j.jpowsour.2007.10.023

[92] L. Gubler et al., « Perspective—Prospects for Durable Hydrocarbon-Based Fuel Cell Membranes, » *Journal of The Electrochemical Society*, t. 165, n° 6, F3100, 2018, ISSN : 1945-7111. DOI : 10.1149/2.0131806jes

[93] K. D. Baik et al., « Characterization of nitrogen gas crossover through the membrane in proton-exchange membrane fuel cells, » *International Journal of Hydrogen Energy*, t. 36, n° 1, p. 732-739, 2011, ISSN : 03603199. DOI : 10.1016/j.ijhydene.2010.09.046

[94] S. Abbou et al., « Local Potential Evolutions during Proton Exchange Membrane Fuel Cell Operation with Dead-Ended Anode – Part I : Impact of Water Diffusion and Nitrogen Crossover, » *Journal of Power Sources*, t. 340, p. 337-346, 2017, ISSN : 0378-7753. DOI : 10.1016/j.jpowsour.2016.11.079

[95] S. Abbou et al., « Local Potential Evolutions during Proton Exchange Membrane Fuel Cell Operation with Dead-Ended Anode – Part II : Aging Mitigation Strategies Based on Water Management and Nitrogen Crossover, » *Journal of Power Sources*, t. 340, p. 419-427, 2017, ISSN : 0378-7753. DOI : 10.1016/j.jpowsour.2016.10.045

[96] Z. Qi, « Effect of CO in the anode fuel on the performance of PEM fuel cell cathode, » *Journal of Power Sources*, t. 111, n° 2, p. 239-247, 2002, ISSN : 03787753. DOI : 10.1016/S0378-7753(02)00300-2

[97] R. Mohtadi et al., « Assessing durability of cathodes exposed to common air impurities, » *Journal of Power Sources*, t. 138, n° 1-2, p. 216-225, 2004, ISSN : 03787753. DOI : 10.1016/j.jpowsour.2004.06.036

[98] F. Arena et al., « Permeability and Diffusivity Measurements on Polymer Electrolyte Membranes, » *Fuel Cells*, t. 13, n° 1, p. 58-64, 2013, ISSN : 16156846. DOI : 10.1002/fuce.201200116

[99] A. Sivasankaran et al., « Influence of sulfonated SiO2 in sulfonated polyether ether ketone nanocomposite membrane in microbial fuel cell, » *Fuel*, t. 159, p. 689-696, 2015, ISSN : 00162361. DOI : 10.1016/j.fuel.2015.07.002

[100] S. Ayyaru et al., « Development of MFC using sulphonated polyether ether ketone (SPEEK) membrane for electricity generation from waste water, » *Bioresource Technology*, t. 102, n° 24, p. 11 167-11 171, 2011, ISSN : 09608524. DOI : 10.1016/j.biortech.2011.09.021

[101] D. M. Xing et al., « Characterization of Sulfonated Poly(Ether Ether Ketone)/Polytetrafluoroethylene Composite Membranes for Fuel Cell Applications, » *Fuel Cells*, t. 5, n° 3, p. 406-411, 2005, ISSN : 1615-6846, 1615-6854. DOI : 10.1002/fuce.200500089

[102] V. Silva et al., « Mass transport of direct methanol fuel cell species in sulfonated poly(ether ether ketone) membranes, » *Electrochimica Acta*, t. 51, n° 18, p. 3699-3706, 2006, ISSN : 00134686. DOI : 10.1016/j.electacta.2005.10.029

[103] S. Sambandam et al., « Estimation of electrode ionomer oxygen permeability and ionomer-phase oxygen transport resistance in polymer electrolyte fuel cells, » *Physical Chemistry Chemical Physics*, t. 15, n° 36, p. 14 994, 2013, ISSN : 1463-9076, 1463-9084. DOI : 10.1039/c3cp51450a

[104] H. Azher et al., « The effect of temperature on the permeation properties of Sulphonated Poly (Ether Ether) Ketone in wet flue gas streams, » *Journal of Membrane Science*, t. 519, p. 55-63, 2016, ISSN : 03767388. DOI : 10.1016/j.memsci.2016.07.015

[105] K. D. Baik et al., « Effects of operating parameters on hydrogen crossover rate through Nafion® membranes in polymer electrolyte membrane fuel cells, » *Renewable Energy*, t. 57, p. 234-239, 2013, ISSN : 09601481. DOI : 10.1016/j.renene.2013.01.046

[106] F. Hassan Akhtar et al., « Defining sulfonation limits of poly(ether-ether-ketone) for energy-efficient dehumidification, » *Journal of Materials Chemistry A*, t. 9, n° 33, p. 17 740-17 748, 2021. DOI : 10.1039/D1TA03690D

[107] H. Sijbesma et al., « Flue gas dehydration using polymer membranes, » *Journal of Membrane Science*, t. 313, n° 1-2, p. 263-276, 2008, ISSN : 03767388. DOI : 10.1016/j.memsci.2008.01.024

[108] S. Sarirchi et al., « An Overview of Organic/Inorganic Membranes Based on Sulfonated Poly Ether Ether Ketone for Application in Proton Exchange Membrane Fuel Cells, » *Journal of Renewable Energy and Environment*, t. 4, n° 1, p. 46-60, 2017, ISSN : 2423-5547. DOI : 10.30501/jree.2017.70106

[109] B. T. Huang et al., « Experimental Investigation of Air Relative Humidity (RH) Cycling Tests on MEA/Cell Aging in PEMFC Part II : Study of Low RH Cycling Test with Air RH at 62%/0%, » *Fuel Cells*, t. 12, n° 3, p. 347-355, 2012, ISSN : 1615-6846, 1615-6854. DOI : 10.1002/fuce.201100061

[110] J. Xi et al., « Effect of Degree of Sulfonation and Casting Solvent on Sulfonated Poly(Ether Ether Ketone) Membrane for Vanadium Redox Flow Battery, » *Journal of Power Sources*, t. 285, 2015. DOI : 10.1016/j.jpowsour.2015.03.104

[111] H. Hou et al., « Crosslinked SPEEK membranes : Mechanical, thermal, and hydrothermal properties, » *Journal of Materials Research*, t. 27, n° 15, p. 1950-1957, 2012, ISSN : 0884-2914, 2044-5326. DOI : 10.1557/jmr.2012.151

[112] M. L. Di Vona et al., « Analysis of Temperature-Promoted and Solvent-Assisted Cross-Linking in Sulfonated Poly(ether ether ketone) (SPEEK) Proton-Conducting Membranes, » *The Journal of Physical Chemistry B*, t. 113, n° 21, p. 7505-7512, 2009, ISSN : 1520-6106, 1520-5207. DOI : 10.1021/jp9006679

[113] A. Reyna-Valencia et al., « Tensile mechanical properties of sulfonated poly(ether ether ketone) (SPEEK) and BPO4/SPEEK membranes, » *Journal of Applied Polymer Science*, t. 98, n° 6, p. 2380-2393, 2005, ISSN : 1097-4628. DOI : 10.1002/app.22417

[114] L. Pasquini et al., « Stability of Proton Exchange Membranes in Phosphate Buffer for Enzymatic Fuel Cell Application : Hydration, Conductivity and Mechanical Properties, » *Polymers*, t. 13, n° 3, p. 475, 2021, ISSN : 2073-4360. DOI : 10.3390/polym13030475

[115] R. Narducci et al., « Cation-conducting ionomers made by ion exchange of sulfonated polyether-ether-ketone : Hydration, mechanical and thermal properties and ionic conductivity, » *Journal of Membrane Science*, t. 465, p. 185-192, 2014, ISSN : 03767388. DOI : 10.1016/j.memsci.2014.03.073

[116] P. Wei et al., « Sandwich-Structure PI/SPEEK/PI Proton Exchange Membrane Developed for Achieving the High Durability on Excellent Proton Conductivity and Stability, » *Journal of Membrane Science*, t. 644, p. 120 116, 2022, ISSN : 0376-7388. DOI : 10.1016/j.memsci.2021.120116

[117] E. Sprugis et al., « Mechanical Properties of Composite SPEEK Polymer Membranes Modified with Ionic Liquids, » *IOP Conference Series : Materials Science and Engineering*, t. 77, p. 012 043, 2015, ISSN : 1757-899X. DOI : 10.1088/1757-899X/77/1/012043

[118] E. Sgreccia et al., « Mechanical properties of proton-conducting sulfonated aromatic polymer membranes : Stress–strain tests and dynamical analysis, » *Journal of Power Sources*, t. 195, n° 23, p. 7770-7775, 2010, ISSN : 03787753. DOI : 10.1016/j.jpowsour.2009.09.061

[119] F. Chen et al., « Hot tensile fracture characteristics and constitutive modelling of polyether-ether-ketone (PEEK), » *Polymer Testing*, t. 63, p. 168-179, 2017, ISSN : 01429418. DOI : 10.1016/j.polymertesting.2017.07.032

[120] P. Knauth et al., *Solid State Proton Conductors : Properties and Applications in Fuel Cells*. John Wiley & Sons, 2012, ISBN : 978-0-470-66937-2.

[121] S. Touhami et al., « Anode defects' propagation in polymer electrolyte membrane fuel cells, » *Journal of Power Sources*, t. 520, p. 230 880, 2022, ISSN : 03787753. DOI : 10.1016/j.jpowsour.2021.230880

[122] V. O. Mittal et al., « Effect of Catalyst Properties on Membrane Degradation Rate and the Underlying Degradation Mechanism in PEMFCs, » *Journal of The Electrochemical Society*, t. 153, n° 9, A1755, 2006, ISSN : 1945-7111. DOI : 10.1149/1.2219708

[123] L. Dubau et al., « Carbon Corrosion Induced by Membrane Failure : The Weak Link of PEMFC Long-Term Performance, » *International Journal of Hydrogen Energy*, t. 39, n° 36, p. 21 902-21 914, 2014, ISSN : 0360-3199. DOI : 10.1016/j.ijhydene.2014.07.099

[124] G. Hübner et al., « EPR investigation of HO / radical initiated degradation reactions of sulfonated aromatics as model compounds for fuel cell proton conducting membranes, » *Journal of Materials Chemistry*, t. 9, n° 2, p. 409-418, 1999. DOI : 10.1039/A807129B

[125] J. Healy et al., « Aspects of the Chemical Degradation of PFSA Ionomers used in PEM Fuel Cells, » *Fuel Cells*, t. 5, n° 2, p. 302-308, 2005, ISSN : 1615-6846, 1615-6854. DOI : 10.1002/fuce.200400050

[126] M. T. Salleh et al., « Stability of SPEEK/Cloisite ® /TAP nanocomposite membrane under Fenton reagent condition for direct methanol fuel cell application, » *Polymer Degradation and Stability*, t. 137, p. 83-99, 2017, ISSN : 01413910. DOI : 10.1016/j.polymdegradstab.2016.12.011

[127] M. Daoudi, « Performances et Durabilité Des Membranes Alternatives Aux Membranes PFSA, » PhD Thesis, Université de Lorraine, 2023.

[128] S. Rowshanzamir et al., « Effect of Pt-Cs 2.5 H 0.5 PW 12 O 40 catalyst addition on durability of self-humidifying nanocomposite membranes based on sulfonated poly (ether ether ketone) for proton exchange membrane fuel cell applications, » *International Journal of Hydrogen Energy*, t. 40, n° 1, p. 549-560, 2015, ISSN : 03603199. DOI : 10.1016/j.ijhydene.2014.10.134

[129] M. J. Parnian et al., « Studies on the SPEEK membrane with low degree of sulfonation as a stable proton exchange membrane for fuel cell applications, » *Iranian Journal of Hydrogen & Fuel Cell*, t. 3, n° 3, 2016. DOI : 10.22104/ijhfc.2017.428

[130] C. Zhao et al., « Wet/Dry Cycling Durability and Fuel Cell Performance of the Thermal-Reinforced Pore-Filling ePTFE/SPEEK Membrane, » *Journal of Membrane Science*, t. 724, p. 123 980, 2025, ISSN : 0376-7388. DOI : 10.1016/j.memsci.2025.123980

[131] S. Sarirchi et al., « Simultaneous improvement of ionic conductivity and oxidative stability of sulfonated poly(ether ether ketone) nanocomposite proton exchange membrane for fuel cell application, » *International Journal of Energy Research*, t. 44, n° 4, p. 2783-2800, 2020, ISSN : 1099-114X. DOI : 10.1002/er.5094

[132] Y. Song et al., « Investigations of the Sulfonated Poly(ether ether ketone) Membranes with Various Degrees of Sulfonation by Considering Durability for the Proton Exchange Membrane Fuel Cell (PEMFC) Applications, » *Polymers*, t. 17, n° 16, p. 2181, 2025, ISSN : 2073-4360. DOI : 10.3390/polym17162181

[133] A. Karimi et al., « Vicious cycle during chemical degradation of sulfonated aromatic proton exchange membranes in the fuel cell application, » *International Journal of Energy Research*, t. 44, n° 11, p. 8877-8891, 2020, ISSN : 0363-907X, 1099-114X. DOI : 10.1002/er.5596

[134] L. Zhang et al., « Investigation of Durability Issues of Selected Nonfluorinated Proton Exchange Membranes for Fuel Cell Application, » *Journal of The Electrochemical Society*, t. 153, n° 6, A1062, 2006, ISSN : 00134651. DOI : 10.1149/1.2180715

[135] Y.-y. Zhao, « Theoretical studies on the degradation of hydrocarbon copolymer ionomers used in fuel cells, » *Journal of Membrane Science*, t. 487, p. 229-239, 2015, ISSN : 0376-7388. DOI : 10.1016/j.memsci.2015.04.005

[136] A. Panchenko, « DFT investigation of the polymer electrolyte membrane degradation caused by OH radicals in fuel cells, » *Journal of Membrane Science*, t. 278, n° 1-2, p. 269-278, 2006, ISSN : 0376-7388. DOI : 10.1016/j.memsci.2005.11.010

[137] A. Abdullah et al., « Effect of Relative Humidity on Temperature and Current Distributions within a Segmented H 2 /Air PEM Fuel Cell, » *ECS Transactions*, t. 35, p. 293-302, 2011. DOI : 10.1149/1.3654227

[138] M. J. Parnian et al., « Effect of ceria loading on performance and durability of sulfonated poly (ether ether ketone) nanocomposite membranes for proton exchange membrane fuel cell applications, » *Journal of Membrane Science*, t. 565, p. 342-357, 2018, issn : 03767388. doi : 10.1016/j.memsci.2018.08.029

[139] S. H. Mirfarsi et al., « Study of mechanical degradation of sulfonated poly (ether ether ketone) membrane using ex-situ hygrothermal cycles for polymer electrolyte fuel cell application, » *Journal of Power Sources*, t. 401, p. 73-84, 2018, issn : 03787753. doi : 10.1016/j.jpowsour.2018.08.067

[140] S.-Y. Choi et al., « Ex Situ Aging Effect on Sulfonated Poly(Ether Ether Ketone) Membrane : Hydration-dehydration Cycling and Hydrothermal Treatment, » *Journal of Energy Chemistry*, t. 70, p. 583-592, 2022, issn : 2095-4956. doi : 10.1016/j.jechem.2022.03.003

[141] M. Robert, « Impact of Degradation and Aging on Properties of PFSA Membranes for Fuel Cells, » PhD thesis, Université de Lorraine, 2021.

[142] S. velan Venkatesan et al., « Progression in the Morphology of Fuel Cell Membranes upon Conjoint Chemical and Mechanical Degradation, » *Journal of The Electrochemical Society*, t. 163, n° 7, F637, 2016, issn : 1945-7111. doi : 10.1149/2.0671607jes

[143] R. Mukundan et al., « Membrane Accelerated Stress Test Development for Polymer Electrolyte Fuel Cell Durability Validated Using Field and Drive Cycle Testing, » *Journal of The Electrochemical Society*, t. 165, n° 6, F3085, 2018, issn : 1945-7111. doi : 10.1149/2.0101806jes

[144] J. Kang et al., « Membrane electrode assembly degradation by dry/wet gas on a PEM fuel cell, » *International Journal of Hydrogen Energy*, t. 35, n° 23, p. 13 125-13 130, 2010, issn : 03603199. doi : 10.1016/j.ijhydene.2010.04.077

[145] Y. Jeon et al., « Accelerated life-time test protocols for polymer electrolyte membrane fuel cells operated at high temperature, » *International Journal of Hydrogen Energy*, t. 40, n° 7, p. 3057-3067, 2015, issn : 03603199. doi : 10.1016/j.ijhydene.2015.01.010

[146] Y. Jeon et al., « Accelerated Life-time Tests including Different Load Cycling Protocols for High Temperature Polymer Electrolyte Membrane Fuel Cells, » *Electrochimica Acta*, t. 148, p. 15-25, 2014, issn : 00134686. doi : 10.1016/j.electacta.2014.10.025

[147] M. Marrony et al., « Durability study and lifetime prediction of baseline proton exchange membrane fuel cell under severe operating conditions, » *Journal of Power Sources*, t. 182, n° 2, p. 469-475, 2008, issn : 03787753. doi : 10.1016/j.jpowsour.2008.02.096

[148] A. Sahin et al., « Improved performance and durability of sulfonated polyether ether ketone/cerium phosphate composite membrane for proton exchange membrane fuel cells, » *Ionics*, t. 25, n° 11, p. 5163-5175, 2019, issn : 0947-7047, 1862-0760. doi : 10.1007/s11581-019-03109-y

[149] T. Nemeth et al., *Chemical resilience of hydrocarbon-based PEMs in fuel cells : effect of aromatic electron density on molecular degradation and in-situ aging*, SSRN Scholarly Paper, Rochester, NY, 2026. doi : 10.2139/ssrn.6145030 Social Science Research Network : 6145030.

[150] X. Liu et al., « Durability enhancement of proton exchange membrane fuel cells by ferrocyanide or ferricyanide additives, » *Journal of Membrane Science*, t. 629, p. 119 282, 2021, issn : 03767388. doi : 10.1016/j.memsci.2021.119282

[151] M. J. Parnian et al., « High Durability Sulfonated Poly (Ether Ether Ketone)-Ceria Nanocomposite Membranes for Proton Exchange Membrane Fuel Cell Applications, » *Journal of Membrane Science*, t. 556, p. 12-22, 2018, issn : 0376-7388. doi : 10.1016/j.memsci.2018.03.083

[152] Z. Han et al., « Hydrocarbon Proton Exchange Membranes for Fuel Cells : An Antioxidant Study, » *ACS Applied Energy Materials*, 2026. doi : 10.1021/acsaem.5c03582

[153] K. N. T. Do et al., « Synthesis and characterization of homogeneously sulfonated poly(ether ether ketone) membranes : Effect of casting solvent, » *Journal of Applied Polymer Science*, t. 110, n° 3, p. 1763-1770, 2008, issn : 00218995, 10974628. doi : 10.1002/app.28150

[154] M.-S. Jun et al., « Solvent casting effects of sulfonated poly(ether ether ketone) for Polymer electrolyte membrane fuel cell, » *Journal of Membrane Science*, t. 396, p. 32-37, 2012, issn : 03767388. doi : 10.1016/j.memsci.2011.12.008

[155] G. P. Robertson et al., « Casting solvent interactions with sulfonated poly(ether ether ketone) during proton exchange membrane fabrication, » *Journal of Membrane Science*, t. 219, n° 1-2, p. 113-121, 2003, issn : 03767388. doi : 10.1016/S0376-7388(03)00193-5

[156] X. Liu et al., « The roles of solvent type and amount of residual solvent on determining the structure and performance of sulfonated poly(ether ether ketone) proton exchange membranes, » *Journal of Membrane Science*, t. 523, p. 163-172, 2017, issn : 03767388. doi : 10.1016/j.memsci.2016.10.007

[157] A. Carbone et al., « Sulphonated poly(ether ether ketone) membranes for fuel cell application : Thermal and structural characterisation, » *Journal of Power Sources*, t. 163, n° 1, p. 18-26, 2006, issn : 03787753. doi : 10.1016/j.jpowsour.2005.12.066

[158] X. Liu et al., « Effect of Residual Casting Solvent Content on the Structure and Properties of Sulfonated Poly(Ether Ether Ketone) Membranes, » *Journal of Membrane Science*, t. 492, p. 48-57, 2015, issn : 0376-7388. doi : 10.1016/j.memsci.2015.05.038

[159] F. van der Linden et al., « A Review on the Proton-Exchange Membrane Fuel Cell Break-in Physical Principles, Activation Procedures, and Characterization Methods, » *Journal of Power Sources*, t. 575, 233168 (17), 2023. doi : 10.1016/j.jpowsour.2023.233168

[160] M. Daoudi et al., « Impact of sulfonated poly(ether ether ketone) membranes pretreatments on their physicochemical properties and fuel cell performances, » *Journal of Polymer Science*, t. 61, n° 9, p. 761-776, 2023, issn : 2642-4169. doi : 10.1002/pol.20220649

[161] B. Maranesi et al., « Cross-Linking of Sulfonated Poly(ether ether ketone) by Thermal Treatment : How Does the Reaction Occur ? » *Fuel Cells*, t. 13, n° 2, p. 107-117, 2013, issn : 16156846. doi : 10.1002/fuce.201200010

[162] H. Hou et al., « Building bridges : Crosslinking of sulfonated aromatic polymers—A review, » *Journal of Membrane Science*, t. 423–424, p. 113-127, 2012, issn : 03767388. doi : 10.1016/j.memsci.2012.07.038

[163] S. D. Mikhailenko et al., « Proton conducting membranes based on cross-linked sulfonated poly(ether ether ketone) (SPEEK), » *Journal of Membrane Science*, t. 233, n° 1-2, p. 93-99, 2004, issn : 03767388. doi : 10.1016/j.memsci.2004.01.004

[164] V. R. Hande et al., « Crosslinking of sulphonated poly (ether ether ketone) using aromatic bis(hydroxymethyl) compound, » *Journal of Membrane Science*, t. 322, n° 1, p. 67-73, 2008, issn : 03767388. doi : 10.1016/j.memsci.2008.05.040

[165] M. Di Vona et al., « High ionic exchange capacity polyphenylsulfone (SPPSU) and polyethersulfone (SPES) cross-linked by annealing treatment : Thermal stability, hydration level and mechanical properties, » *Journal of Membrane Science*, t. 354, n° 1-2, p. 134-141, 2010, issn : 03767388. doi : 10.1016/j.memsci.2010.02.058

[166] S. Zhong et al., « Crosslinked sulfonated poly(ether ether ketone) proton exchange membranes for direct methanol fuel cell applications, » *Journal of Power Sources*, t. 164, n° 1, p. 65-72, 2007, issn : 03787753. doi : 10.1016/j.jpowsour.2006.10.077

[167] G. Barbieri et al., « LoLiPEM : Long life proton exchange membrane fuel cells, » *International Journal of Hydrogen Energy*, t. 41, n° 3, p. 1921-1934, 2016, issn : 03603199. doi : 10.1016/j.ijhydene.2015.10.096

Chapter 4

sPEEK-based MEA performances

1 Introduction 140
2 Materials & methods 143
2.1 sPEEK pretreatment 143
2.1.1 Drying step 144
2.2 Catalyst Coated Backing (CCB) based MEA 145
2.3 Catalyst Coated Membrane (CCM) based MEA 146
2.4 Test-bench, single cell, and performance mapping 147
2.5 Polarization curves and Electrochemical Impedance Spectroscopy (EIS) 148
3 Results 149
3.1 sPEEK-based MEA *vs.* Nafion 149
3.2 Impact of sPEEK pretreatment : *sPEEK nanostructured vs. sPEEK standard* 150
3.3 Impact of operating conditions 152
3.4 Comparison of electrodes deposition method effect 154
3.5 Effect of *Nafion overcoat* thickness on CCB MEA performance 157
4 Discussion 158
5 Conclusion 160
References 161

Context

This study aims to investigate the potential of sPEEK ionomer as a membrane for PEMFC and will be published soon. Owing to an appropriate pretreatment, the performance of sPEEK was compared with that of a reference material, namely Nafion 211. In addition, the effect of the electrode deposition process using a Catalyst Coating Membrane with the same membrane is investigated.

1 Introduction

The large-scale adoption of Proton Exchange Membrane Fuel Cells (PEMFC) relies on progress in sustainable material development : the manufacturing of key components such as gas diffusion layers, electrode ionomers, and membranes, remains energy-intensive and polluting. In particular, the synthesis of perfluorosulfonic acid (PFSA)-based ionomers which are widely used in electrodes and membranes and are considered the benchmark for performance and durability, is highly polluting due to the fluorine chemistry involved. This has motivated numerous studies on alternatives, including hydrocarbon-based ionomers, among which sulfonated poly(ether ether ketone) (sPEEK) has attracted significant attention.

The physicochemical properties of sPEEK make it a promising candidate for fuel cell operation. This ionomer is obtained by sulfonating the PEEK (polyether ether ketone) backbone, thereby introducing sulfonic acid groups. Its strong thermal and mechanical properties, inherited from the PEEK backbone, are among the main reasons for its interest. Sgreccia et al. [1] compared the mechanical properties of sPEEK and Nafion reported in the literature. For sPEEK, Young's modulus and tensile strength range from 680 to 2305 MPa and 25 to 75 MPa, respectively, depending on the casting solvent, Degree of Sulfonation (DS), and heat treatment. In contrast, Nafion 117 exhibits a tensile modulus of only 33 MPa [2]. This significant difference is due to the higher rigidity of the sPEEK backbone [3]. Regarding the physico-chemical properties of sPEEK, increasing the DS enhances water uptake and proton conductivity [4-6]. However, this improvement is often insufficient to reach the proton conductivity of PFSA ionomer [7]. Tang et al. [6] observed that sPEEK, with a higher Ion Exchange Capacity (IEC) than Nafion 117 (depending on the degree of sulfonation (DS) : 1.57 and 1.95 for sPEEK *vs.* 1.02 meq.g^{-1} for Nafion 117), exhibited significantly higher water uptake than Nafion 117 (28.1 and 36.9 *vs*. 16.6 wt%). However, its proton conductivity remained lower (0.023 and 0.064 S.cm^{-1} for sPEEK *vs*. 0.081 S.cm^{-1} for Nafion 117 in fully hydrated conditions), likely due to less efficient ionic pathway connectivity despite the higher IEC. Moreover, excessive sulfonation can lead to complete dissolution in water : according to Yang et al. [8], sPEEK dissolves when the DS exceeds 65%. The relatively low proton conductivity of sPEEK is partly attributed to the direct attachment of the sulfonic groups to the backbone : the limited mobility of the side chain prevents efficient aggregation of sulfonic groups, *i.e.*, a high degree of hydrophobic/hydrophilic phase separation, to form effective pathways for the proton conduction [9, 10]. Several studies also reported a low chemical stability of sPEEK, compared with that of PFSA membranes, when subjected to the Fenton test [11, 12].

In general, lower fuel cell performances are observed with sPEEK compared to PFSA membrane due to the above-mentioned properties [13, 14]. Similar conclusions are observed when using sPEEK ionomer in catalytic layers (CL). There is a delicate balance between an appropriate sPEEK content to promote sufficient proton conductivity, while avoiding electrode flooding and excessive mass transport resistance [15]. Several groups studied fuel cell performance with sPEEK-based catalytic layers [16, 17]. Due to the different properties of the ionomer, lower porosity was observed for the CL with sPEEK than with PFSA, with porosity decreasing as the sPEEK content increased. Although the increase in sPEEK content implied a higher connectivity of proton conductive channels, it can lead to mass trans-

port issues, particularly in conditions where flooding may occur. Furthermore, oxygen permeability through the ionomer film covering catalyst particles is lower for hydrocarbon-based ionomers than PFSA-based ionomer. Sambandam et al. [18] measured oxygen permeability to be an order of magnitude higher for Nafion than for sPEEK at 80°C and 75% RH (3.85 *vs.* 0.27 x 10^{-2}12 mol.cm^{-1}.s^{-1}), which explains the higher oxygen transport resistance through the sPEEK ionomer film.

To counterbalance the poor hydrophilic/hydrophobic phase separation in sPEEK, several groups suggest applying membrane pretreatment, with the objective of arranging the ionomer microstructure. The first step of such pretreatments is usually a classical acidification stage, allowing counterions to be completely substituted and remove residual solvent from the fabrication process : Jun et al. [13] reported an increase in proton conductivity and *in situ* performance after soaking sPEEK in a 80°C, 1M sulfuric acid solution for 12h. In addition, several studies observed that significant changes in the ionomer microstructure could be obtained by applying a hydrothermal step [9, 19-21]. For instance, Mendil-Jakani et al. [22] studied the impact of a hydrothermal pretreatment on the sPEEK microstructure by SAXS, varying both time and temperature : 40°C to 120°C for 10 h to 1000 h. They observed that hydrothermal treatments performed at a temperature near the β-relaxation temperature (related to backbone segmental motion [22, 23], *i.e.*, 75°C in dry state) induced a pronounced hydrophilic/hydrophobic phase separation. This was attributed to an increase in chain mobilities, enabling structural rearrangement, which was not observed in Nafion as its β-relaxation occurs at much lower temperature, *i.e.*, -20°C in dry state. Alternatively, a faster method to induce microstructural changes consists of using polar solvents at lower temperature [24].

Recently, in our group, Daoudi et al. [25] tested a pretreatment consisting of an acidification step followed by a hydro-alcoholic and hydrothermal step, aimed at enhancing nanophase separation in a commercial sPEEK membrane. They observed improved fuel cell performance and greater resistance to (*ex situ*) chemical aging compared with the sPEEK membrane pretreated according to the manufacturer's recommended procedure, which involves acidification followed by a 1 h hydrothermal treatment at 80°C only [26]. They also reported similar performance between the pretreated sPEEK membrane and the Nafion XL membrane under hydrogen/oxygen operation at atmospheric pressure, given that the sPEEK thickness is approximately 17 μm after pretreatment (*vs.* 27.5 μm for Nafion XL). They attributed this result to improved nanophase separation in the pretreated sPEEK membrane. However, despite significant improvements in the membrane's physical properties induced by the pretreatment, several challenges remain to achieve competitive performances in FC :

- **Membrane drying :** in the work of Daoudi et al. [25], a flattening step between plates at room temperature was applied before drying at 100°C in an oven. However, micro-folds, visible to the naked eye, systematically appeared at the end of this procedure. These micro-folds are likely to have a negative impact on the quality of the membrane-electrode interface formed during the hot-pressing process, and consequently on performance and durability. To address this issue, a new drying method has been developed in the present work, enabling the preparation of flatter membranes after pre-treatment, *i.e.*, without visible micro-folds.
- **MEA fabrication :** Daoudi et al. [25] prepared Membrane Electrode Assemblies (MEA) by hot-pressing commercial Gas Diffusion Electrodes (GDE, also referred to as Catalyst-Coated Backings, CCB) onto the membrane. However, they reported poor adhesion between the membrane and standard commercial GDE. Indeed, several studies have highlighted a lack of compatibility between hydrocarbon (HC) membranes and the PFSA ionomer commonly used in catalyst layers (CL) [27, 28]. For instance, Lee et al. [29] compared MEA made with an sPEEK membrane and CL containing either PFSA ionomer or sPEEK ionomer : at 70°C under H_2/O_2, they observed that sPEEK membranes combined with PFSA-based catalyst layers performed better at 100% RH, whereas the opposite trend was found at 30% RH. They suggested that under humid conditions, proton conductivity within CL was the main factor limiting performance, whereas at low RH, in-

terfacial resistance-rather than the ionomer's proton conductivity-became dominant. They also observed partial delamination between the PFSA-based CL and the sPEEK membrane after fuel cell characterizations, attributed to interfacial stresses arising under low humidity conditions. This indicates that the low quality of the interface between the sPEEK membrane and the PFSA-based catalytic layer can be detrimental to performance. Jeong et al. [30] observed that adding an interfacial bonding layer between a HC membrane and a PFSA CL increased durability, due to higher interfacial adhesion. Furthermore, it did not affect performance, which they attributed to a lower interfacial resistance. Similarly, Choo et al. [28] applied an interfacial layer consisting of a cross-linked sPEEK/PFSA blend to a sPEEK membrane hot-pressed to commercial Nafion-based Gas Diffusion Layers (GDE). Even though they observed slightly lower performance at low current density-attributed to the use of sulfonic groups for cross-linking, resulting in lower proton conductivity-a significantly higher adhesion was observed through wet/dry cycles, resulting in more stable overall performance. In a similar manner, Daoudi et al. [25] used GDE with a *Nafion overcoat* to overcome adhesion issues, which led to good FC performance. However, the impact-positive or negative-of the overcoat on MEA durability could not be clearly established.

- **Operation with air :** in most studies involving sPEEK membrane, poor performance was observed when the FC was fed with air at atmospheric pressure. Consequently, many authors chose to operate the cell with pure oxygen (table 4.1). Despite the variety of pretreatments applied to the membranes, the diversity of materials used, and the significant heterogeneity in MEA assembly processes, conditions enabling stable operation with air have, to the best of our knowledge, not yet been clearly identified. This diversity also results in significant variability in the reported performances, much of which actually concern sPEEK-based composite membranes, which aim to enhance material properties (proton conductivity, chemical durability, etc.). With pure sPEEK membranes, one of the primary challenges is therefore to identify operating conditions that allow efficient operation with air.

In this work, we re-evaluated the performance of the sPEEK membrane pretreated according to the protocol of Daoudi et al. [25]. However, to minimize microfold formation, the drying process was improved allowing to achieve flatter membrane leading to an improved membrane–electrode interfaces. The MEA were prepared by hot-pressing Gas Diffusion Electrodes with a *Nafion overcoat* (GDE) onto the membrane, and their performances were compared with that of a PFSA-based CCB. The effects of sPEEK pretreatment and operating parameters were analyzed using performance mapping under hydrogen/air operation across multiple conditions, including variations in gas inlet Relative Humidity (RH), air stoichiometry, cell temperature, and pressure. In addition, the impact of the electrode deposition method was evaluated using Catalyst-Coated Membranes (CCM) based on pretreated sPEEK, to assess the feasibility of directly sprayed PFSA-based electrodes onto the sPEEK membrane.

T (°C)	P	RH (%)	Atm	DS/IEC	i (A.cm^{-2}) @ 0.6 V	U (V) @ 1.5 A.cm^{-2}	@ maximum i		Ref
							i (A.cm^{-2})	U (V)	
				40	0.22	-	0.62	0.18	
80	Patm	100	H_2/air	48	0.44	-	1.04	0.13	[31]
				61	0.76	-	1.4	0.18	
70					0.60	-	0.94	0.43	
75	0.1 MPa	100	H_2/air	62	0.60	-	0.88	0.48	[7]
80					0.70	-	1.08	0.41	
30	1 bar	Dry H_2/saturated air	H_2/air	1.80	0.37	-	0.85	0.16	[32]
70	Patm	100	H_2/O_2	54	0.86	0.46	2.18	0.30	[33]
90	Patm	100	H_2/O_2	65	0.74	0.43	2.30	0.12	[34]
60	Patm	100	H_2/O_2	65	0.58	0.31	1.60	0.23	[35]
80					0.80	0.47	2.00	0.25	

sPEEK composite

Additives	T (°C)	P	RH (%)	Atm	DS/IEC	i (A.cm^{-2}) @ 0.6 V	U (V) @ 1.5 A.cm^{-2}	@ maximum i		Ref
								i (A.cm^{-2})	U (V)	
sPEEK/PVA (90/10) + 10% SiO_2					2.02	0.60	-	1.40	0.28	
sPEEK/PVA (70/30) + 10% SiO_2					1.86	0.17	-	1.40	0.17	
sPEEK/PVA (50/50) + 10% SiO_2	80	-	100	H_2/air	1.25	0.02	-	0.20	0.20	[36]
sPEEK/PVA (90/10)					1.39	0.05	-	0.40	0.20	
sPOP (2wt.%)-sPEEK	80	-	100	H_2/O_2	1.67	0.95	0.50	2.10	0.37	[33]
sPOP (4wt.%)-sPEEK					1.77	1.23	0.56	2.52	0.30	
sPEEK-BZY10	60	1 atm	-	H_2/O_2	69%	0.16	-	0.96	0.19	[37]
	80					0.19	-	1.10	0.19	
sPEEK-PS-T7.5	80	-	90%	H_2/O_2	68%	0.29	-	0.98	0.20	[38]
sPEEK-PA-T7.5						0.34	-	1.12	0.20	

Table 4.1 – Interpolated i/U performance of MEA made of sPEEK membrane at different operating conditions according to the literature.

2 Materials & methods

2.1 sPEEK pretreatment

The Fumapem E730 sPEEK membrane, purchased from Fumatech, has an IEC of 1.29 meq.g^{-1} and a thickness ranging from 29 to 33 μm. The two pretreatment protocols used here are identical to those reported by Daoudi et al.[25] :

- **Acidification-hydro alcoholic-hydrothermal 72 hours (Acd-HA-HT72h) :**
  - First, a re-acidification is performed by soaking the sample in 1M HCl at 30°C for 4h, followed by a triple rinsing step in distilled water. This ensures the protonation of all sulfonic groups and the removal of impurities and membrane processing additives.
  - The second step consists in soaking the sample in a hydroalcoholic solution (64/36 water/ethanol) at pH 4 and 60°C for 24h. This step is usually applied to swell the sPEEK membrane prior to sol-gel impregnation [39, 40] and is carried out here prior to the hydro-

thermal step in order to enhance its effect.
The sPEEK sample is then rinsed in distilled water for 4 hours to remove excess ethanol.

- Finally, the third step consists in a hydrothermal treatment : sPEEK samples are soaked in distilled water at 80°C for 72h. This step enhances phase separation known to improve the functional properties of the membrane [19, 22].

It should be noted that this protocol led to significant membrane thinning, with the thickness decreasing from 31.7 ± 0.9 μm to 16.7 ± 3.2 μm [26].

- **Acidification-hydrothermal 1 hour (Acd-HT1h) :**
  This pretreatment process follows the steps recommended by the supplier (Fumatech) :
  - The first step consists of an acidification in a 1M H_2SO_4 solution at 80°C for 16h, followed by a rinsing step.
  - A hydrothermal step is then conducted in distilled water at 80°C for 1h, followed by three successive rinsing steps in distilled water.

For simplicity, sPEEK pretreated with the *Acd-HA-HT72h* and *Acd-HT 1h* protocols will be referred to as *sPEEK nanostructured* and *sPEEK standard*, respectively.

2.1.1 Drying step

The drying process was based on the previous one developed in the lab. Indeed, after their pretreatment protocol, Daoudi et al.[25] applied a drying process in two steps :

1. The membranes were placed between two rigid PEEK plates, sandwiched between layers of 0.6 mm porous PE (polyethylene) and absorbent sheets (figure 4.1(a)), at ambient conditions during 24h, to remove as much water as possible while keeping the membrane flat.
2. The samples were removed from the plates and put in a drying oven at 100°C for 18 hours.

Although this process appears to be quite effective in producing a sufficiently flat membrane, the presence of micro-creases or folds was observed (figure 4.1(a)) which could affect the performance and possibly the durability in fuel cells. While the performance remained comparable to that of Nafion XL [26], it is likely that these microfolds absorb most of the stress during the hot-pressing process probably leading to an inhomogeneous membrane-electrodes interface.

Thus, in order to obtain an even flatter membrane-*i.e.*, free of micro-creases/folds-and to achieve improved performance, a *new process* was implemented. This process consists of the following steps :

1. The membranes were this time placed between two PEEK frames, without stretching, and small weights were used to keep the frames in position and maintain the sample in place (figure 4.1(a)). The assembly (sample/frame/weights) was placed in a drying oven at 60°C for 24 h.
2. The weights were removed to release the membrane, and the frame/membrane assembly was placed back in the drying oven at 100°C for 18 hours.

At the end of this *new process*, flatter samples without visible microfolds were obtained compared to those obtained with the previous one (figure 4.1(a)).

The effectiveness of this new drying process was assessed through fuel cell performance measurements in a 7.22 cm^2 single cell at 70°C/80% RH and ambient pressure under air or oxygen atmospheres. The pretreated membranes with the different drying processes (*Daoudi et al.* and the *new process*) were assembled in an MEA by hot-pressing GDE-with a *Nafion overcoat* onto the membrane (under the same condition as described in section 2.2). The polarization curves obtained (figure 4.1(b)) show

a clear improvement across the entire polarization curve for both conditions : under air and under oxygen.

(a)

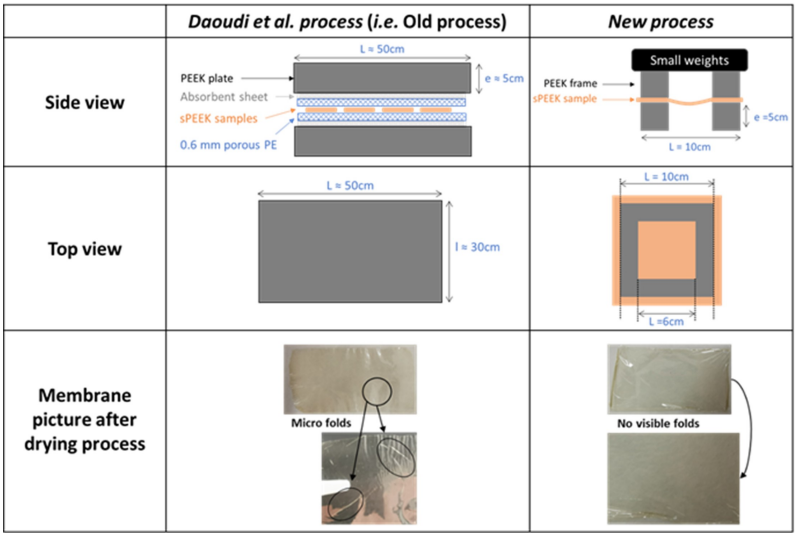

(b)

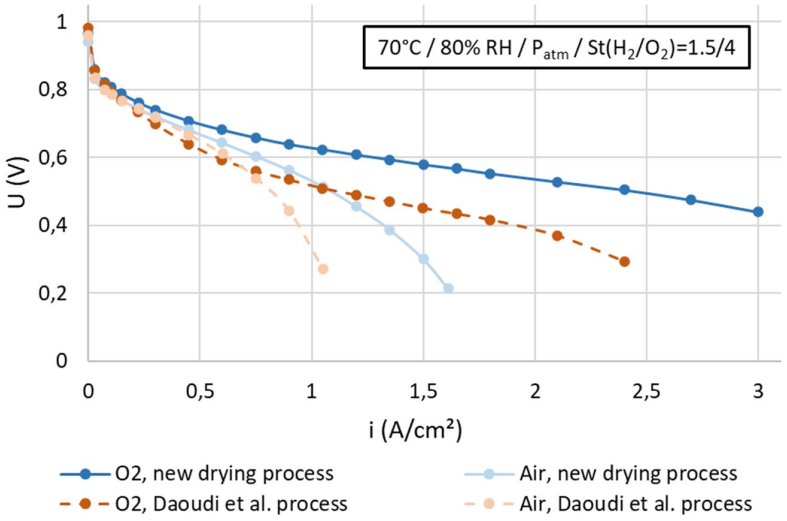

FIGURE 4.1 – Comparison of sPEEK macroscopic state after drying between the old and the new process with PEEK frames (a) and comparison of sPEEK performance at 70°C/80% RH/P_{atm}/$St_{H_2/O_2 \text{ or } air}$=1.5/4 on a 6.65 cm^2 single test cell after the old and new drying process (Daoudi et al. test bench [25]) (b).

2.2 Catalyst Coated Backing (CCB) based MEA

Gas diffusion electrodes (GDE), consisting of a Freudenberg H14CX653 gas diffusion layer (GDL) onto which electrodes with a Pt loading of 0.3 mg cm^{-2} are deposited, were purchased from HyPlat. In the case of GDE used for sPEEK membrane, the supplied GDE include, in addition, a *Nafion overcoat* (loading of 0.20 or 0.30 mg cm^{-2}) applied onto the electrode to improve adhesion between the electrode and the sPEEK membrane. Thus, for all sPEEK membranes, regardless of the pretreatment, GDE with *Nafion overcoat* were employed while basic GDE (*i.e.*, without *Nafion overcoat*) were applied for Nafion membrane.

The membrane electrode assembly was prepared using a CCB process. The MEA was prepared according to the following procedure (figure 4.2) :

- The membrane was sandwiched between two polyethylene naphthalate (PEN) sheets, each 25 µm thick and featuring an open window of 50 × 50 mm^2 that defines the active area.
- Two GDE (52 × 52 mm^2) were placed on both sides of the membrane, on top of the PEN layers, ensuring full coverage of the window of the PEN layers and thus a well-defined electrode-membrane contact over the 50 × 50 mm^2 active area.
- Two PTFE sheets with a 52.5 × 52.5 mm^2 window (PTFE n°1-2 in figure 4.2) were used to hold in place the GDE and prevent them from moving.
- This MEA was then placed between two aluminium plates covered by a PTFE layer (PTFE n°3-4 in figure 4.2) to prevent any direct contact between the aluminium plates and the GDE. Finally, the entire assembly was placed in a press and heated to 135°C, in order to carry out the hot-pressing step at a pressure of 4.5 MPa for 3 min 30 s.

It should be noted that the conditions used here differ from those employed by Daoudi et al. [25] (135°C / 6.9 MPa / 3 min 30 s) in terms of applied stress. Tests performed under these same conditions-with an applied stress of 6.9 MPa-on our sPEEK-based MEA showed large instabilities and significantly higher H_2 permeation, leading us to reduce the applied stress to that used for PFSA membranes [25]. One possible reason is that microfolds induced during the *Daoudi et al. drying process* absorbed part of the applied stress, which may explain why a higher stress was necessary to ensure a good electrode/membrane cohesion. In contrast, in the absence of microfolds, a pressure of 6.9 MPa appears excessive and detrimental to the membrane, resulting in increased H_2 permeation. Indeed, tests conducted at lower applied pressure confirmed improved performance and reduced H_2 permeation at 4.5 MPa.

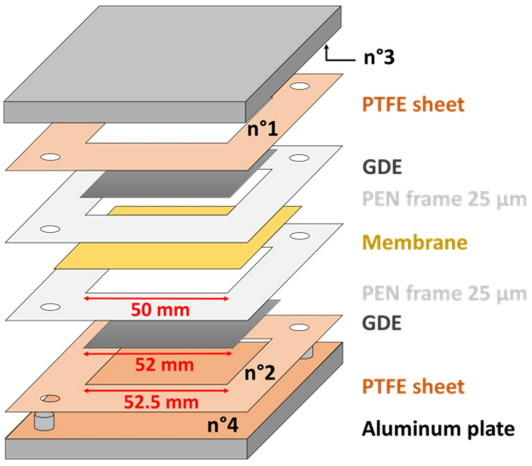

FIGURE 4.2 – Schematic representation of the MEA layers.

2.3 Catalyst Coated Membrane (CCM) based MEA

The catalyst inks used to form our CCM-based MEA were prepared according to a previous work [41]. The catalyst and ionomer components were incorporated in a water-alcohol solution (table 4.2) then magnetically stirred for 3h at 600 rpm with a 5-min sonification step every 1h. Ink parameters such as the solid content, the ionomer to carbon ratio, and ionomer concentration were fixed at 3.2 wt%, 0.72, and 10 $mg_{ionomer}/g_{solvent}$, respectively.

	Catalyst		Ionomer		Solvent
	Supplier	Composition	Supplier	Composition	Composition
Cathode	Tanaka (TEC10V50E)	40 wt% Pt/C	Ion Power	20 wt% Nafion D2021 (1100 EW)	20 wt% isopropanol - water
Anode	Tanaka (TEC10V30E)	30 wt% Pt/C			

TABLE 4.2 – Electrode inks composition : catalyst, ionomer, and solvent.

2.4 Test-bench, single cell, and performance mapping

The sPEEK MEA were characterized using the same test bench as in a previous study on MEA performance limitations at 95°C [42]. As a reminder, the characterizations were carried out using a single cell featuring 50 straight parallel channels made of gold-coated 316L stainless steel (figure 4.3). The channel depths on the anode and cathode sides were 0.15 mm and 0.25 mm, respectively. The cell temperature was controlled by an oil loop, and the gases were always fed in counter-flow.

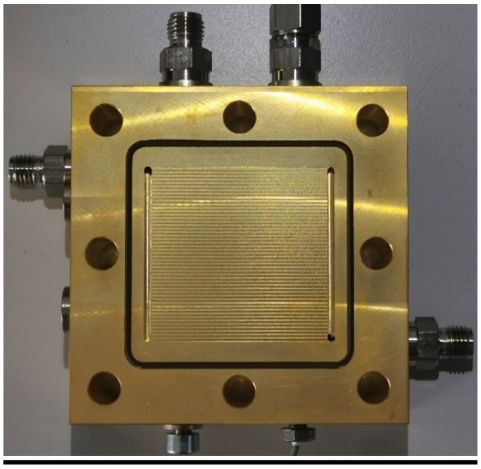

Number of channels	Depth	
	Anode	Cathode
50	0.15 mm	0.25 mm

FIGURE 4.3 – Straight parallel cell used for sPEEK MEA characterization.

The impact of the compression rate and break-in procedure was investigated through performance mapping. This involves polarization curve tests conducted at various gas relative humidities (30 and 50% RH), gas pressures (2 and 3 bar), and air stoichiometry (between 1.5 and 3), and two operating temperatures : 70 and 95°C. Three compression rates (12%, 25% and 31%) were considered to analyze whether changes in GDL porosity affect mass transport and water management. Two conditioning protocols, based on previous studies ([25, 43-45]), were tested. They consisted of potentiostatic holds at 0.3 V, 0.6 V, and open-circuit voltage (OCV) for approximately 2h15 at 50% gas inlet RH : one under medium humidity conditions (Stair=3 and P=1 bar) and another under humid conditions (St_{air}=1.5 to limit MEA drying and P=2 bar to enhance MEA hydration) as a high water content may favor ionomer rearrangement [46, 47]. Preliminary tests fixed the compression rate at 12%, due to the wider parameter window enabling proper fuel cell operation. The humid conditioning step was also adopted, as it led to significantly higher performance. Following this optimization, polarization curves

were recorded at 60°C and 80°C to determine the optimal operating temperature for the sPEEK-based MEA.

2.5 Polarization curves and Electrochemical Impedance Spectroscopy (EIS)

Polarization curves were measured in galvanostatic mode. The current density was first increased from OCV (Open-Circuit Voltage) in 200 s steps : initially in small increments (0.025 A cm^{-2}, 0.08 A cm^{-2}, and 0.12 A cm^{-2}) within the low current density region up to 0.2 A.cm^{-2}, followed by fixed increments of 0.2 A cm^{-2} at higher current densities, up to a cell voltage of 0.3 V. In our previous works, the current density was then decreased stepwise back to OCV [25, 43, 45] and the FC voltage was determined as the average of the values measured during the increasing and decreasing current density steps. However, under some operating conditions, a sudden voltage drop to approximately 50 mV was observed when increasing the current density (*i.e.*, decreasing the voltage ; figure 4.4) with recovery occurring only at a much lower current density.

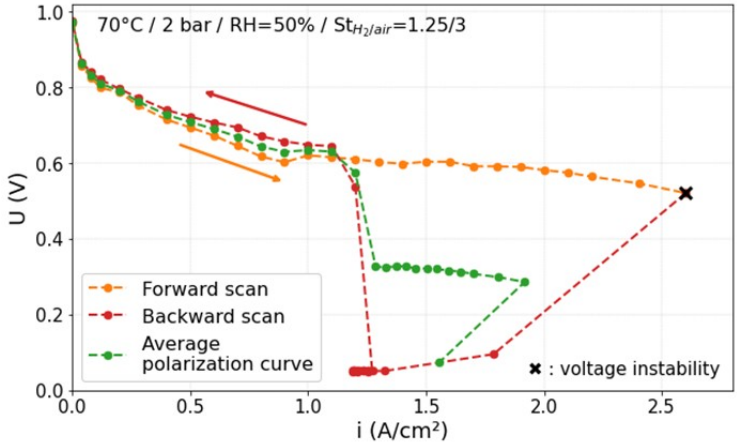

FIGURE 4.4 – Forward (orange) and backward (red) scan, and average polarization curve (green) at 70°C/2 bar/50% gas RH/St$_{H_2}$/air=1.25/3. The cross mark represents the point at which increasing current density resulted in a voltage drop to 50 mV.

Similar behavior had already been observed in a previous work for a PFSA-based membrane operated at 95°C under low inlet gas RH [42], and was attributed to significant drying of the MEA. Additional experiments performed in these conditions revealed that the thermal power generated at high current densities was responsible for a marked increase in R_{hf}. Considering that sPEEK requires significantly higher water uptake than PFSA to maintain adequate proton conductivity, at least at low to medium degrees of sulfonation ([48-50]), and given that exactly the same behavior is observed here, this sudden performance drop is most likely also due to sPEEK drying, despite the much lower temperature. In this work, as voltage instabilities were much more frequent than in previous studies with PFSA membranes, only the measurements recorded during the current increase (*i.e.*, forward scan) are shown in the polarization curves. When instabilities (*i.e.*, a sudden voltage drop) occur, they are indicated by a cross on the last data point of the curve.

Electrochemical impedance spectroscopy (EIS) was performed in galvanostatic mode by applying a ±10% sinusoidal perturbation around the current density setpoint and measuring the corresponding voltage response. A 30-min constant current density step, corresponding to the targeted setpoint, was applied before each measurement to ensure that the MEA reached a stable state. The spectra were recorded over a frequency range from 25 kHz to 0.05 Hz.

3 Results

3.1 sPEEK-based MEA *vs.* Nafion

Performance mapping tests were conducted on sPEEK pretreated with the Acd-HA-HT72h protocol, hereafter referred to as *sPEEK nanostructured* for simplicity, and compared with a Nafion membrane : NR211. Both membranes were assembled using the CCB process. As a reminder (section 2.2), GDE with an additional *Nafion overcoat* were used exclusively for sPEEK-based MEA.

A total of 32 polarization curves, repeated three times, were recorded while varying operating parameters, including gas pressure (2 and 3 bar), gas inlet RH (30 and 50%), and air stoichiometry (1.5 to 3). Similar performance was observed for *sPEEK nanostructured* and NR211 under equivalent operating conditions, although the polarization curves overlap exactly only at low current densities. In the example shown in figure 4.5, a slightly higher voltage was observed for NR211 from OCV up to 1.25 A.cm^{-2} at 2 bar and 1.8 A.cm^{-2} at 3 bar, beyond which *sPEEK nanostructured* exhibited superior performance. Notably, *sPEEK nanostructured* achieved higher performance at medium current densities when the pressure is lowered to 2 bar (see blue curve).

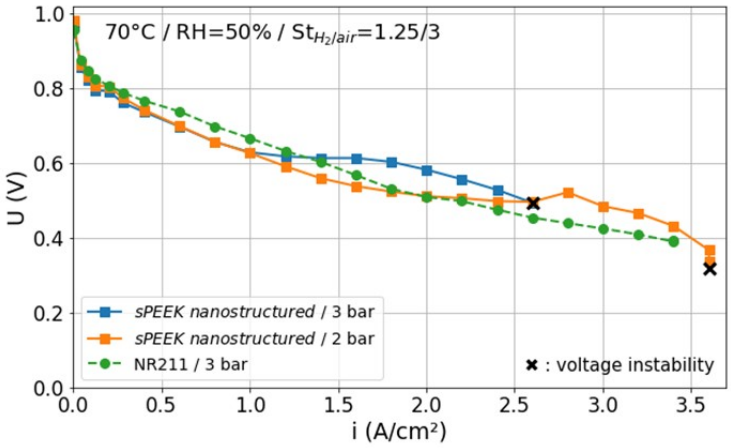

FIGURE 4.5 – Polarization curve of *sPEEK nanostructured* and NR211 at 70°C/50%gas RH/St$_{H_2}/air$=1.25/3. The cross mark represents the point at which increasing current density resulted in a voltage drop to 50 mV.

Note that similar performance mapping was conducted at 95°C with different MEA compression rates and conditioning steps (at 70°C under dry and humid conditions, and at 95°C) ; however, only the most humid conditions presented performance comparable to those of NR211, *i.e.*, 0.62 and 0.53 V at 1 and 2 A.cm^{-2} under 50% gas RH, 3 bar and 1.5 air stoichiometry. Although sPEEK is presented as a potential candidate at higher temperature for its mechanical and thermal properties, its high-water requirement to ensure sufficient proton conductivity is a major obstacle to its use above 80°C, at least with the commercial sPEEK and the pretreatment we used.
Nevertheless, the sPEEK membrane can therefore operate at usual temperature under an air atmosphere at moderate gas inlet RH with good performance, comparable to NR211, despite the common assumption that sPEEK cannot match PFSA performance. These results indicate that the application of an appropriate pretreatment can significantly enhance sPEEK properties, enabling *in situ* performance comparable to that of PFSA-based membranes.

Electrochemical impedance spectroscopy measurements were conducted at 1 and 1.5 A.cm^{-2} to assess the MEA state and to better understand the voltage differences observed at these operating points (figure 4.6). At 1 A.cm^{-2}, NR211 exhibited a higher voltage, which can be associated with smaller high-frequency and low-frequency loop. This suggests that the *Nafion overcoat* in the sPEEK-

based MEA may not be sufficiently hydrated to ensure optimal operation of the cathode catalyst layer (CL) or, more generally, that the interface created by the *Nafion overcoat* affects the operation of the cathode CL. The R_{hf} measurements showed that the values were similar for both MEA at 1 A·cm^{-2}, indicating no significant difference in overall ionic conductivity, while a slight difference was observed at 1.5 A·cm^{-2}. Moreover, NR211 exhibited a slightly larger low-frequency loop, indicating increased mass transport limitations.

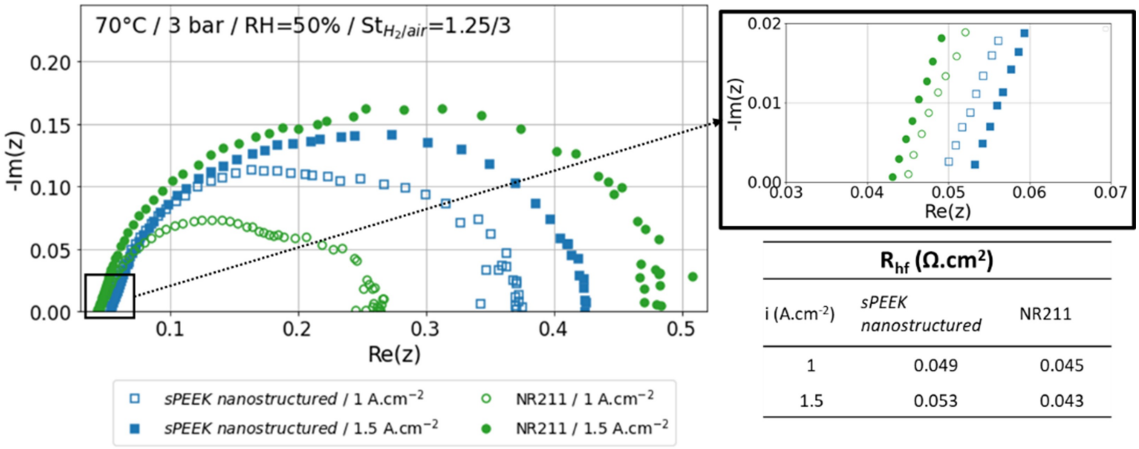

R_{hf} (Ω.cm²)		
i (A.cm^{-2})	*sPEEK nanostructured*	NR211
1	0.049	0.045
1.5	0.053	0.043

FIGURE 4.6 – EIS spectra of *sPEEK nanostructured* and NR211-based CCB MEA operating at 70°C/50% gas RH/St$_{H_2/air}$=1.25/3 and graphical R_{hf} measurements at 1 and 1.5 A.cm^{-2}

It should be noted that R_{hf} measurements are affected by membrane thickness. The sPEEK and NR211 membranes have thicknesses of 15-18 µm and 25.4 µm, respectively. Consequently, for equivalent R_{hf} values, the ionic conductivity of NR211 remains higher than that of sPEEK.

3.2 Impact of sPEEK pretreatment : *sPEEK nanostructured vs. sPEEK standard*

In order to investigate the impact of the pretreatment, the same performance mapping and conditioning protocol used in the previous section was also applied to MEA with *sPEEK standard* membrane.

sPEEK nanostructured showed significantly higher performance in almost all temperature/pressure/RH/air stoichiometry conditions. However, because of the large number of characterizations performed, only the best performances at 30% and 50% gas inlet RH are presented in figure 4.7.

Under 30% gas inlet RH, lower performances were observed for *sPEEK standard* across the entire polarization curve. In addition, a significantly higher maximum current density was measured for *sPEEK nanostructured*. Under moderate gas inlet RH (*i.e.*, 50% RH, figure 4.7(b)), the performance of the two pretreatments became closer : at 2 bar, similar voltage values were measured from OCV up to 1 A.cm^{-2}, above which *sPEEK nanostructured* exhibited higher voltages. Moreover, voltage instabilities associated with MEA dehydration were observed in both cases, but at higher current densities for *sPEEK nanostructured*, indicating more efficient water utilization than in *sPEEK standard*. At 3 bar, lower voltage values were measured between 1 and 2.2 A.cm^{-2} for *sPEEK nanostructured*, but a significantly higher maximum current density was achieved. Overall, an improved pretreatment enables higher performance and better water utilization, which is particularly notable given that sPEEK membrane is often considered to require high humidity levels to operate effectively [51-53]. It also expands the range of gas pressure, RH, and air stoichiometry conditions under which fuel cell operation is feasible.

Electrochemical impedance spectroscopy spectra of *sPEEK nanostructured* and *standard* measured

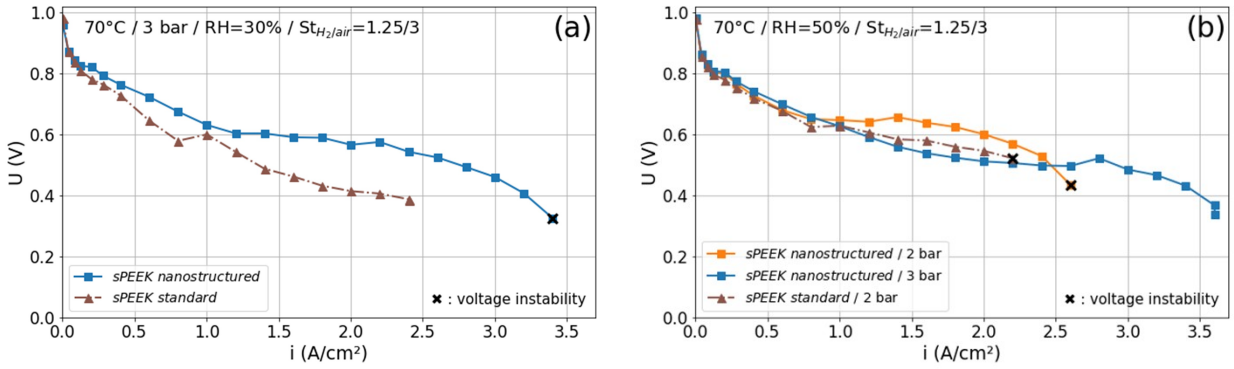

FIGURE 4.7 – *sPEEK standard vs. sPEEK nanostructured* : with a 1.25/3 hydrogen/air stoichiometries at 70°C/RH=30% (a) and 70°C/RH=50% (b). The cross mark represents the point at which increasing current density resulted in a voltage drop to 50 mV.

at 1 and 1.5 A.cm^{-2} (figure 4.8) revealed significantly different behaviors. *sPEEK standard* exhibited a larger low-frequency loop associated with cathode processes and/or mass transport limitations. This behavior suggests less effective operation of the cathode catalyst layer, which is consistent with water management issues and the lower performance compared to *sPEEK nanostructured* and the voltage instability observed at high current density under 2 bar and 50% gas inlet RH. These results further highlight the impact of membrane properties on cathode operation, which may appear counterintuitive but is consistent with the observations reported in the previous section when comparing sPEEK- and Nafion-based MEA.

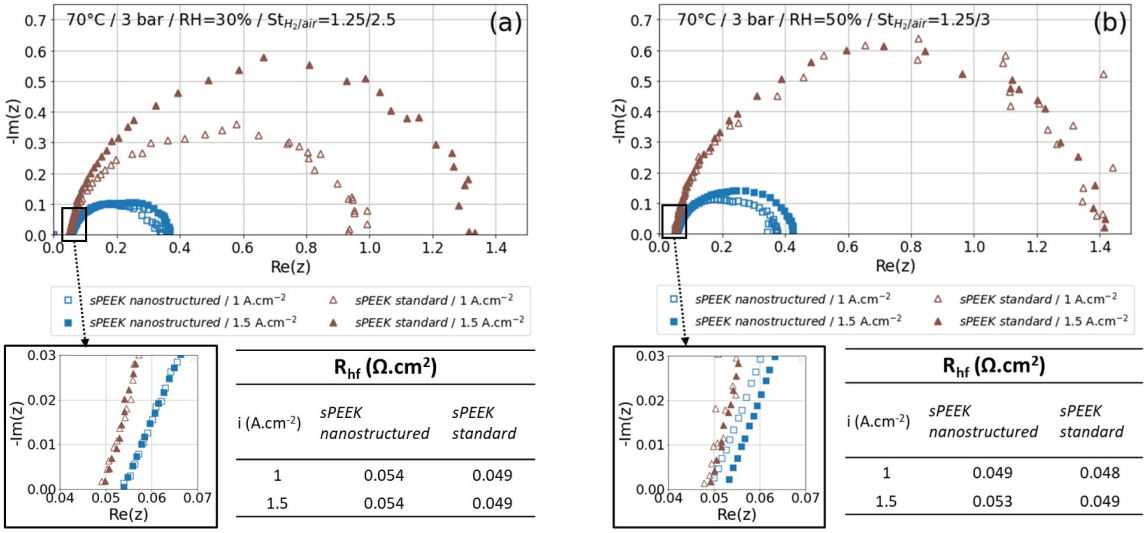

FIGURE 4.8 – EIS measurements on *sPEEK nanostructured* and *standard* at 70°C, 30% RH (a) and 50% RH (b) gas inlet RH under 1 and 1.5 A.cm^{-2}.

Overall, the estimated R_{hf} values were lower for *sPEEK standard* than for *sPEEK nanostructured*, except at high current density (≥ 1.5 A.cm^{-2} depending on the operating conditions), where *sPEEK standard* more frequently exhibited excessive drying. In contrast, *sPEEK nanostructured* showed excessive drying only at higher current densities. This is consistent with the trends observed in the polarization curves, further supporting improved water utilization with *sPEEK nanostructured*.
After reproducibility tests, good agreement of the EIS spectra was observed for both sPEEK membranes, although smaller low-frequency loops were observed for *sPEEK standard* at 30% RH and 1.5 A.cm^{-2},

as well as at 50% RH and 1.0-1.5 A.cm^{-2}. Moreover, minor variations in R_{hf} were measured for both sPEEK membranes while maintaining the same trend, as shown in figure 4.8.

Finally, it should be noted that *sPEEK nanostructured* membrane is approximately twice as thin as *sPEEK standard*, while the R_{hf} values are similar, around 50-55 mΩ·cm^2, with slight variations depending on the tested MEA and operating conditions. These results may be related to differences in sPEEK water sorption induced by the pretreatment : Daoudi et al. [25] previously reported lower water uptake for *sPEEK nanostructured* based on water sorption isotherms. The reduced water uptake of *sPEEK nanostructured* may therefore compensate for the greater thickness of *sPEEK standard*. Similarly, it is possible that the improved water management observed with *sPEEK nanostructured* membranes is largely due to their reduced thickness, which promotes water diffusion between the anode and cathode flow fields.

3.3 Impact of operating conditions

Performance mapping tests were conducted by varying gas RH (30-50%), operating pressure (2-3 bar), and air stoichiometry (1.5-2-2.5-3) at 60, 70 and 80°C, using polarization curves and electrochemical impedance spectroscopy measurements. Each *sPEEK nanostructured*-based MEA was conditioned under humid conditions (70°C, 50% gas RH, 2 bar, and H_2 and air stoichiometries equal to 1.5/1.5), with a compression rate of 12%. Performance mapping consisted of an initial characterization at 70°C to verify reproducibility, followed by a characterization at either 80°C or 60°C.

Impact of cell operating temperature

Low gas inlet humidities and/or pressure led to voltage instabilities at high current densities at 70 and 80°C, whereas stable voltage values were measured at 60°C, even up to 3 A.cm^{-2} under relatively dry conditions (2 bar and 30% gas inlet RH). This behavior illustrates the water requirement of the sPEEK membrane for adequate operation, although the effect is not strongly pronounced given the moderate gas inlet RH range investigated (30-50%), in contrast to most studies that employ high humidities (>50%). Overall, increasing the operating temperature from 60°C to 70-80°C resulted in higher performance, particularly at medium current densities. However, the increase from 70 to 80°C, under relatively dry conditions (low gas inlet RH and/or low pressure, *i.e.*, 30% gas RH and/or 2 bar) led to similar performance at medium current densities and poorer performance at high current densities. Although higher gas diffusion and proton conductivity are expected at higher temperature, hydration limitations restricted the maximum current densities, as evidenced by the observed voltage instabilities. Under more humid conditions (50% gas RH and 3 bar), higher performance was achieved at medium current densities, and voltage instability shifted at 80°C to higher current densities, confirming the dependence on membrane hydration. This phenomenon has already been reported for PFSA membranes, which exhibited increased performance between 65°C and 75°C and decreased performance above 80°C [54]. Although increasing temperature enhances mass transport and ionic conductivity [55], it induces lower membrane water content [56] and, consequently, higher membrane resistance [42]. As sPEEK requires a higher water content than PFSA for comparable proton conductivity, the decline in FC performance appeared at lower operating temperature.

Overall, 70°C proved to be the optimal cell operating temperature, delivering similar performance from low to medium current densities and a higher maximum current density than at 80°C, while outperforming operation at 60°C, except under the driest conditions.

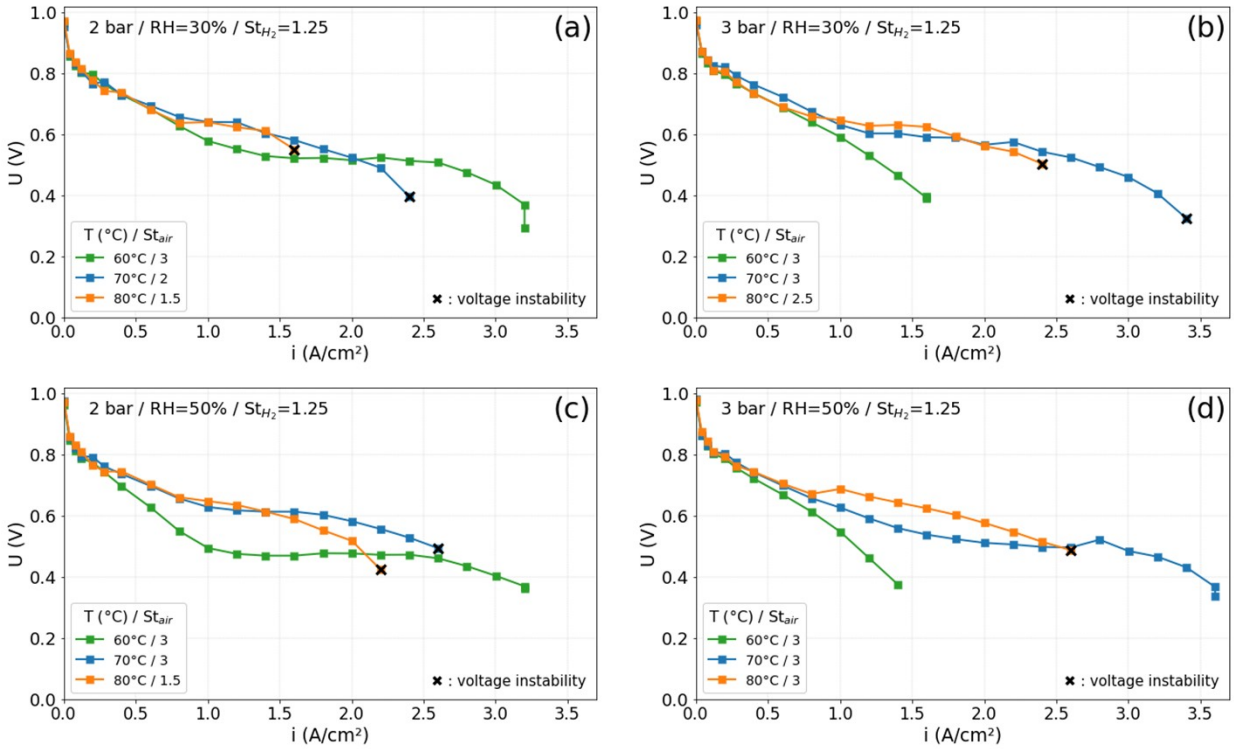

FIGURE 4.9 – Impact of temperature on polarization curves, for *sPEEK nanostructured*, at : 2 bar/30% RH (a), 3 bar/30% RH (b), 2 bar/50% RH (c) and 3 bar/50% RH (d). The cross mark represents the point at which increasing current density resulted in a voltage drop to 50 mV.

Impact of gas inlet RH

At a gas pressure of 2 bar, increasing the gas inlet relative humidity from 30% to 50% resulted in lower performance at 60°C and higher performances at 70-80°C. At low temperature, the membrane may already be sufficiently hydrated to ensure proton conduction, and an increase in RH mainly leads to enhanced oxygen dilution, whose negative effects are exacerbated by the poor, or at least non-optimal, operation of the cathode catalyst layer (section 3.1). In contrast, as membrane hydration becomes a more limiting factor at 70 and 80°C, increasing the gas inlet RH enhances proton conductivity and thus FC performance. At 3 bar and 60°C, increasing the gas inlet RH slightly decreased fuel cell performance, with the negative effect of oxygen dilution being compensated by the higher oxygen partial pressure. At 70 and 80°C, fuel cell performance was, in most cases, similar for both gas inlet RH tested. Although variations in air stoichiometry led to slight increases or decreases in performance, the overall trend was maintained. These observations highlight competing effects between enhanced membrane proton conductivity, increased oxygen partial pressure, and oxygen dilution combined with reduced gas diffusivity.

Overall, the influence of RH on fuel cell performance remains limited. Although the sPEEK membrane requires a significant water content, varying the gas inlet RH from 30 to 50% may not be sufficient to induce substantial changes. Nevertheless, low to moderate gas inlet RH values are sufficient to enable stable sPEEK operation with good performance when fed with air. The application of the Acd-HA-HT72h pretreatment (meaning *sPEEK nanostructured*) therefore reduces the dependence of sPEEK on its hydration state, although studies reported to date underline the need for high gas relative humidity [50-52].

Impact of cell operating pressure

Increasing gas pressure at 60°C decreased fuel cell performance at both gas inlet RH. In contrast, at 70°C, different effects were observed depending on operating conditions : under 30% gas inlet RH, fuel cell performance increased with increasing gas pressure, except at low air stoichiometry. Under 50% gas inlet RH, fuel cell performance was lower at medium current densities but higher maximal current densities were achieved at 3 bar. At 80°C, higher fuel cell performances were measured with increasing gas pressure for both gas inlet RH values, except at low air stoichiometry (1.5).

Overall, the effect of gas pressure strongly depends on the operating parameters. Increasing gas pressure raises the reactant partial pressures while simultaneously reducing gas interdiffusion [57] ; it is also expected to enhance membrane hydration. In the present case, the beneficial effect of increased gas pressure became more pronounced with increasing operating temperature. At 60°C, membrane hydration was likely sufficient, and performance losses were mainly attributed to reduced gas diffusion. At higher temperatures, membrane hydration became a dominant factor, and increased gas pressure enhanced membrane water content, leading to higher fuel cell performance. This explains why the effect of gas pressure at 70°C is contrasted and dependent on air stoichiometry : under 30% gas inlet RH, high air stoichiometry promotes membrane drying, which is compensated by increased gas pressure. At low air stoichiometry, membrane drying is less pronounced, and increasing gas pressure mainly reduces gas diffusivity, resulting in lower fuel cell performance. Once again, the negative impact of reduced gas interdiffusion at higher pressure is probably aggravated by the non-optimal operation of the cathode CL.

3.4 Comparison of electrodes deposition method effect

Fuel cell performance of CCM and CCB MEA

As previously shown, assembly using the CCB process required the use of GDE with a *Nafion overcoat* to ensure proper assembly, *i.e.*, good adhesion between the sPEEK membrane and the GDE. An electrode deposition process directly onto the membrane, followed by assembly with the GDLs, was therefore explored in order to eliminate the need for this *Nafion overcoat* and to investigate both CCB and CCM processes.
Performance mapping was therefore carried out using a Catalyst Coated Membrane (CCM) process, on *sPEEK nanostructured*, with a Pt loading of 0.3/0.3 mgPt.cm^{-2} on the anode and cathode, respectively. The experiments were conducted at 70°C and 80°C over the same range of operating parameters as those applied to the CCB MEA. For clarity, and since no significant improvement was observed with the CCM from 70°C to 80°C, only the results obtained at 70°C are shown (figure 4.10).

First, the successful fabrication of a CCM with sPEEK can be highlighted, as it exhibited overall good performance regardless of pressure and RH conditions. Compared to CCB MEA, the effect of gas pressure variation was comparable. At 70°C, increasing gas pressure improved performance under 30% RH (except at an air stoichiometry of 1.5) but led to reduced performance at 50% RH. This behavior reflects a trade-off between improved membrane hydration and reduced gas diffusion at higher pressure. At 80°C, membrane hydration became a dominant factor, and higher gas pressure enhanced fuel cell performance (except at an air stoichiometry of 1.5). Increasing gas inlet RH from 30% to 50% at 70°C generally improved performance at 2 bar due to enhanced hydration, but resulted in a slight overall decrease at 3 bar, where diffusion limitations may outweigh the benefits of improved membrane hydration. This is further supported by the increased performance observed at 80°C, where membrane hydration plays a more decisive role, when RH was increased from 30% to 50% at 3 bar. An exception was observed at an air stoichiometry of 1.5, where the lower O_2 concentration may

affect performance more than membrane hydration. As observed for CCB MEA, the trends were highly dependent on air stoichiometry, with higher values promoting MEA drying under dry conditions and generally enhancing performance under more humid conditions.

The direct comparison of the performance of CCM and CCB MEA was carried out in different gas inlet RH and pressure configurations, representing the best performances at 70°C (figure 4.10). For almost all pressure/RH configurations and at similar air stoichiometry, a distinct behavior was observed, with the CCM MEA showing higher performance up to medium current densities, beyond which CCB MEA performed better.

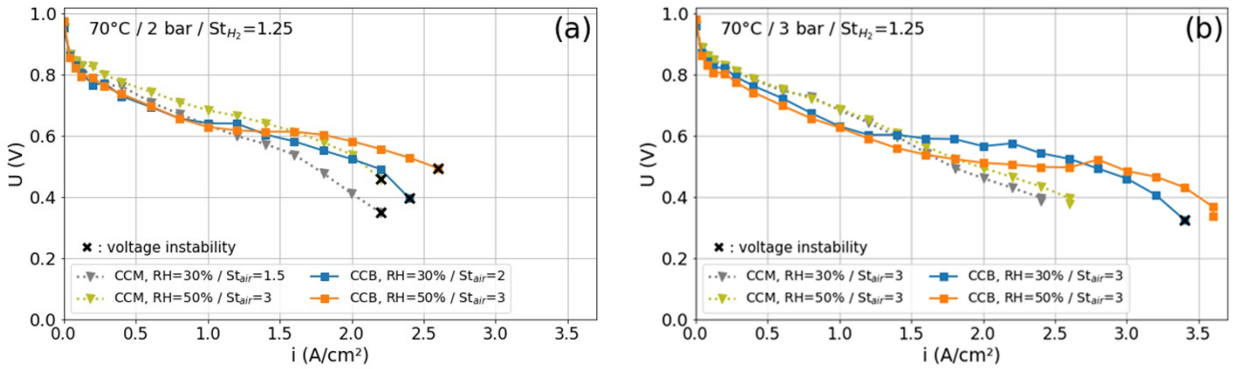

FIGURE 4.10 – Highest fuel cell performance of CCM and CCB MEA at 70°C/2 bar (a), 70°C/3 bar (b). The cross mark represents the point at which increasing current density resulted in a voltage drop to 50 mV.

At medium current densities, the lower voltage values exhibited by the CCB MEA may be attributed to the presence of the *Nafion overcoat*, which acts as an additional resistive layer. Conversely, the *Nafion overcoat* may provide benefits at high current densities, where significant MEA drying was observed, as indicated by the voltage drop (see cross marks in the previous figures). The presence of a *Nafion overcoat* may enhance interfacial contact, ensuring effective proton conduction pathways that would otherwise be diminished by MEA drying. This suggests that interfacial proton conduction becomes a significant limiting factor for the CCM MEA at high current densities. Note that differences in ink composition could also be responsible for different behavior, as the ratio I/C strongly affects electrodes hydration.

EIS measurements were performed at various current densities to assess the MEA state (figure 4.11). At 0.5 A.cm^{-2}, the CCB MEA exhibited a larger low-frequency loop, associated with cathode processes, whereas similar spectra were observed at 1 A.cm^{-2} for both CCM and CCB. At higher current densities (*i.e.*, 1.5 and 2 A.cm^{-2}), significantly larger low-frequency loops were observed for the CCM, consistent with its lower performance and suggesting less efficient operation of the cathode CL. This behavior is consistent with our hypothesis that MEA drying at high current densities may contribute to cathode limitations in CCM MEA, while the presence of a *Nafion overcoat* in CCB MEA may help maintain interfacial proton conduction under low-hydration conditions. The same measurements were conducted at 50% gas inlet RH which showed similar trends for both MEA.

R_{hf} measurements were conducted at identical operating points along the polarization curve, allowing us to assess interface resistance and membrane resistance, linked to MEA hydration state. Both CCM and CCB MEA exhibited an increase in R_{hf} with increasing current density, confirming progressive MEA drying due to increased heat generation, which leads to voltage instabilities (see cross marks on the previous graphs). The *Nafion overcoat* therefore did not affect MEA hydration behavior at high current densities, suggesting that the higher performance of the CCB MEA in this region is related to other phenomena, such as enhanced proton transfer between the electrode and the *Nafion overcoat*

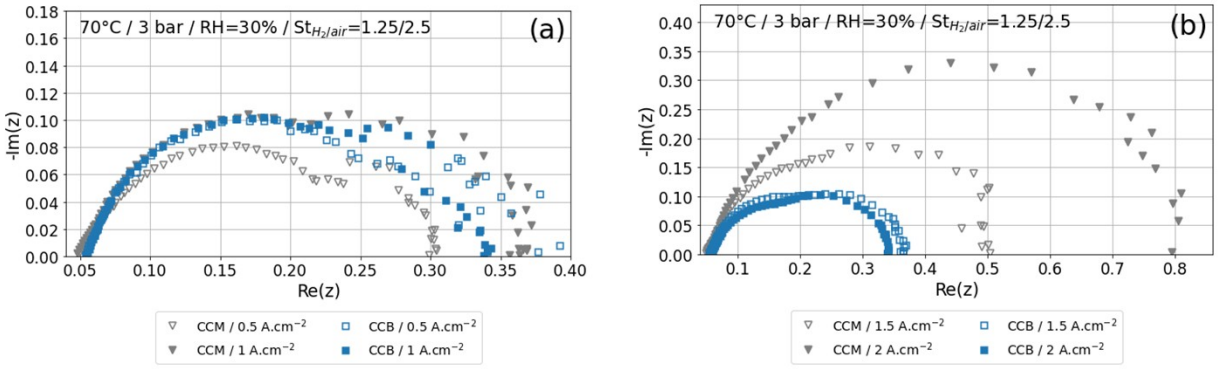

FIGURE 4.11 – EIS spectra of CCM and CCB MEA at 70°C and 3 bar under 30% gas inlet RH for various current densities setpoint : 0.5-1 A.cm^{-2} (a), and 1.5-2 A.cm^{-2} (b).

compared to the interface electrode/sPEEK membrane in the CCM MEA.

Overall, the respective effects of the *Nafion overcoat* and the electrode deposition method are not easy to disentangle. Nevertheless, significant differences were observed in both polarization curves and EIS spectra, highlighting the significant effect of a *Nafion overcoat*. These results suggest that the interface between the membrane and the electrode plays a decisive role in fuel cell performance.

Similar measurements were conducted with a CCM featuring a Pt loading of 0.1/0.3 mgPt.cm^{-2} on the anode and cathode, respectively (figure 4.12(a)). When comparing CCM MEA, significantly higher performance was observed for the lower Pt loading above 1 A.cm^{-2}. Nevertheless, comparison with the CCB MEA revealed trends similar to those observed for the 0.3/0.3 mgPt.cm^{-2} case : the lower performance at high current densities could be associated with a larger low-frequency loop, indicative of less efficient cathode operation. The performance gap could not be attributed to the R_{hf}, as the CCM with lower Pt loading exhibited higher performance until 2.6 A.cm^{-2} despite having higher R_{hf} values. This indicates that performance cannot be solely correlated with membrane resistance and membrane-electrode interface resistance.

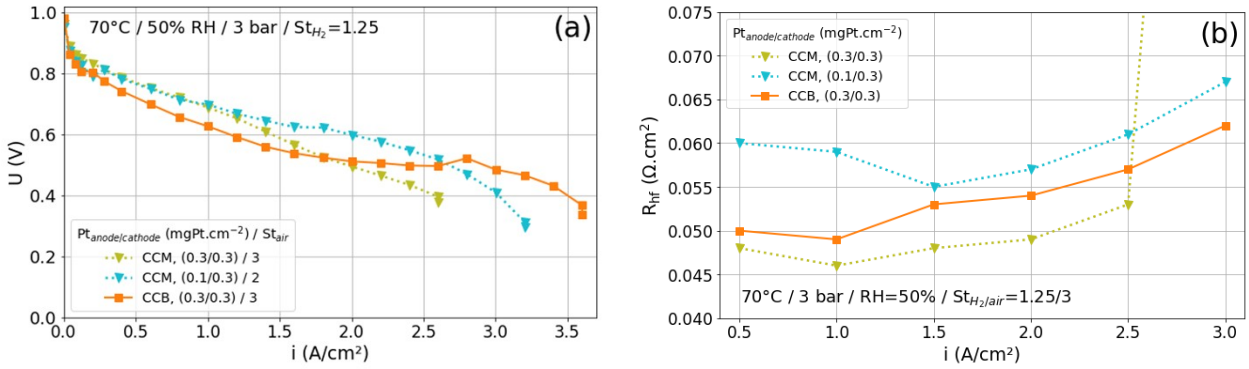

FIGURE 4.12 – Best polarizations curves at 70°C, 50% RH, and 3 bar (a) and R_{hf} measurements along the polarization curve at 70°C, 50% RH, 3 bar, and St(H_2/air)=1.25/3 (b) of CCB and CCM MEA with different Pt loadings. The sharp increase in Rhf to 0.19 Ω.cm^2 for the CCM MEA with (0.3/0.3 mgPt.cm^{-2}) above 2.5 A.cm^{-2} is related to excessive membrane drying.

These results show that further investigations, regarding ink composition/deposition, are required to elucidate the origin of this performance gap, as R_{hf} measurements suggest differences in the membrane-electrode interface between the two CCM.

3.5 Effect of *Nafion overcoat* thickness on CCB MEA performance

To clarify the impact of the *Nafion overcoat* on fuel cell performance, identical performance mappings were conducted on *sPEEK nanostructured*-based MEA using GDE with a 0.2 and 0.3 mg.cm^{-2} *Nafion overcoat*. Slight differences in voltage were observed at medium current densities between MEA with 0.2 and 0.3 mg.cm^{-2} *Nafion overcoats* (figure 4.13). Overall, performances were slightly higher with a lower overcoat thickness under all tested gas pressure, gas inlet RH, and air stoichiometry conditions, although voltage values remained generally similar.

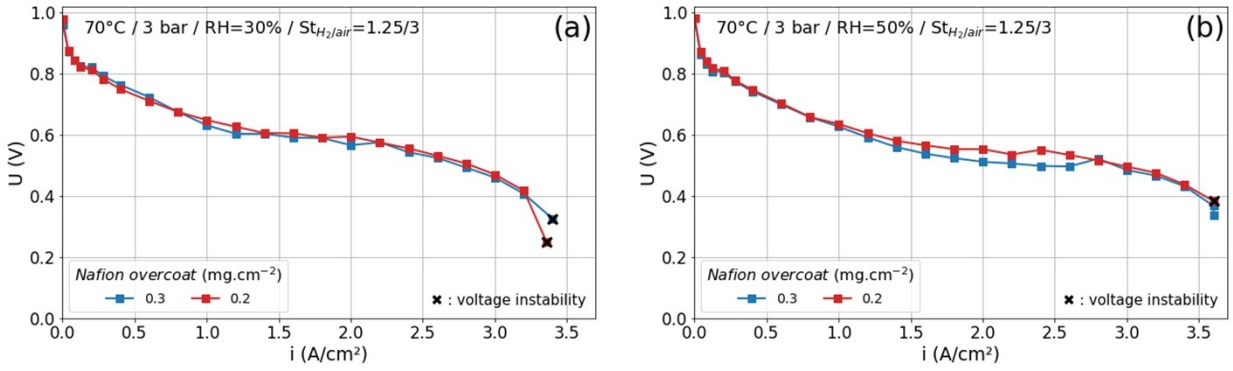

FIGURE 4.13 – Polarization curve of CCB MEA with different *Nafion overcoat* loadings at 70°C under 3 bar/30% gas RH (a), 3 bar/50% gas RH (b).

Similar R_{hf} values were obtained with *Nafion overcoat* loadings of 0.2 and 0.3 mg.cm^{-2}, with differences ranging from approximately 0.4 to 6.5 mΩ.cm^2 depending on gas inlet RH, pressure, and current density setpoints. The slight differences observed at high current densities suggest that the tested overcoat loading range does not significantly affect MEA operation. However, the *Nafion overcoat* may play a more decisive role under drier operating conditions, where the effect of the resistive layer would be more pronounced. For example, severe MEA drying occurred with a 0.3 mg.cm^{-2} overcoat at 3 bar/50% RH/3.5 A.cm^{-2}, resulting in a voltage drop to 50 mV and a current density below

RH (%)	St_{air}	i ($A.cm^{-2}$)	R_{hf} ($\Omega.cm^2$)	
			Overcoat 0.2 $mg.cm^{-2}$	Overcoat 0.3 $mg.cm^{-2}$
30	2.5	0.5	0.050	0.054
		1	0.049	0.054
		1.5	0.049	0.054
		2	0.053	0.057
50	3	0.5	0.048	0.050
		1	0.049	0.049
		1.5	0.047	0.053
		2	0.048	0.054
		2.5	0.050	0.057
		3	0.056	0.062
		3.5	0.063	0.226*

TABLE 4.3 – R_{hf} measurements of *sPEEK nanostructured* with 0.2 and 0.3 $mg.cm^{-2}$ *ionomer overcoat* on the GDE, operating at 70°C. Measurements were conducted in galvanostatic mode independently of the polarization curves measurements. *Corresponds to the R_{hf} measurement at a point where the current setpoint was not met due to the MEA drying out (voltage instability dropping to 50 mV and current below the setpoint, section 2.5).

the setpoint. In contrast, the MEA with a 0.2 $mg.cm^{-2}$ overcoat maintained a satisfactory hydration state (table 4.3).

Finally, polarization curves were also measured on an sPEEK-based MEA using a GDE without *Nafion overcoat* : low voltage values were observed across the entire polarization curve, along with a reduced maximum current density, confirming the necessity of a *Nafion overcoat* for the assembly of sPEEK membrane with PFSA-based electrodes by hot pressing.

4 Discussion

One of the main difficulties in making sPEEK-based MEA is achieving a high-quality membrane–electrode interface, especially when membrane pretreatments are applied : drying often creates micro-folds that degrade the interface. In this work, the application of a new drying process enabled membrane flattening without defects, resulting in significant performance under an air atmosphere, whereas numerous studies have investigated sPEEK under H_2/O_2 conditions [33-35, 58-61]. Furthermore, the use of an appropriate pretreatment led to higher performance compared to the *sPEEK standard* membrane, owing to enhanced nanostructuration and more efficient water utilization. This improvement was particularly evident under relatively low humidity conditions and at a usual operating temperature (30% and 70°C). These results indicate that the water requirement of sPEEK for effective proton conduction may not be as high as previously suggested when the material is nanostructured. Moreover, *sPEEK nanostructured*-based MEA achieved performance comparable to that of an NR211-based MEA, highlighting the benefits of ionomer nanostructuration. However, the lower thickness of the sPEEK membrane with *Nafion overcoat* compared to NR211 may partially contribute to performance : approximately 15 µm for the membrane and 1.52 µm of *Nafion overcoat* on each side, according to Daoudi et al. [25], resulting in a total thickness of 18 µm *vs.* 25 µm for NR211.

Although sPEEK has often been investigated for its superior mechanical and thermal properties, preliminary tests at 95°C showed that operation was not feasible, at least under our conditions (95°C, 3 bar, 20-60% gas inlet RH). Initial performance mapping indicated that sPEEK performance was highly dependent on operating parameters and system settings. For example, testing different MEA compression rates (12, 25, and 31%) revealed a trade-off between reduced porosity, decreasing gas diffusion,

and increased water retention with increasing compression. Overall, a 12% compression rate enabled operation under the largest number of feasible conditions. Moreover, performing the MEA conditioning stage under dry conditions at 70 and 95°C, and under humid conditions at 70°C, showed that humid conditions at 70°C led to a substantial increase in FC performance. This improvement is likely due, among other factors, to ionomer reorganization and enhanced ionic conductivity [46, 62]. Finally, performance measurements conducted at 60, 70, 80, and 95°C indicated that 70°C yielded the highest performance, likely representing a compromise between increased membrane conductivity at higher temperatures and reduced dehydration of sPEEK.

Similar characterizations were performed on a CCM MEA using *sPEEK nanostructured*, showing performances comparable to that of the CCB MEA. Nevertheless, slightly higher cell voltages were observed for the CCM MEA at low to intermediate current densities, whereas at high current densities the CCB MEA exhibited superior performance. Although the CCM MEA did not exhibit significant performance at high current densities, their better performance up to intermediate current densities compared to CCB MEA is noteworthy, as these conditions correspond to typical PEMFC operating points.

Additional electrochemical impedance spectroscopy (EIS) measurements indicated that the cathode in the CCM MEA operated more efficiently at low current densities but showed performance limitations at higher current densities. Based on these observations, the following assumptions can be proposed :

- **CCB MEA :** the *Nafion overcoat* may act as an additional resistive layer and affect MEA performance, depending on the current density setpoint. At low to intermediate current densities, it may reduce fuel cell voltage due to its added resistive contribution. In contrast, at higher current densities, it may help maintain efficient proton conduction pathways between the membrane and the cathode, despite reduced MEA water content caused by increased heat generation, as reflected by the increased R_{hf} for both CCM and CCB MEA.
- **CCM MEA :** improved performances were observed at low current densities, possibly due to the overall reduced MEA thickness. However, the lower performance at higher current densities may be associated with water management issues. Reduced water content due to increased MEA drying at higher current densities, together with potentially poorer interfacial compatibility between the sPEEK membrane and the catalyst layers, may decrease the number of proton conductive pathways.

Moreover, the significant differences in the tested CCM with different Pt loadings suggest that further performance improvements may be achieved through a better comprehension and optimization of the electrode deposition process.
In addition, it is noteworthy that the membrane-electrode interface may play an important role in cathode operation and thus, in fuel cell performance. Indeed, EIS measurements showed no significant differences in R_{hf}, whereas large differences in low-frequency loop size were observed, depending on membrane type, current density setpoint, and MEA configuration. This requires further investigations to elucidate the role of the membrane-electrode interface during fuel cell operation.

5 Conclusion

An exploratory study on the potential of sPEEK as a membrane for PEMFC applications was conducted. Although viable operating conditions enabling proper fuel cell operation at elevated operating temperature (95°C) could not be identified under the investigated conditions, significant performance was achieved at usual temperature of 70°C under air, comparable to that of the PFSA-based NR211 membrane. The application of an appropriate pretreatment, combined with a new drying process, resulted in significantly improved performance compared to the standard process. In addition, the feasibility of fabricating sPEEK-based CCM MEA was demonstrated, showing comparable or higher performance than that of the sPEEK CCB configuration at a representative current density relevant to PEMFC operation.

Several hypotheses have been proposed regarding the role of the *Nafion overcoat* in the sPEEK CCB configuration : however, complementary investigations are needed to elucidate its precise impact on fuel cell performance. Different ionomer loadings and an expanded range of gas inlet relative humidity could be investigated to determine whether the *Nafion overcoat* acts primarily as a resistive layer or whether interfacial resistances are predominant. Furthermore, the catalyst ink formulation used in the CCM MEA and the deposition method may not yet be fully optimized for the pretreated sPEEK membrane, and further investigations are required to assess the interaction between the ink and the membrane. Both sets of measurements could then help to better understand the impact of the membrane-electrode interface on cathode operation. This suggests additional potential for performance enhancement.

Overall, complementary investigations of sPEEK membrane performance in both CCB and CCM configurations are required to validate the proposed mechanisms and optimize fuel cell operation. Nevertheless, this study demonstrates the potential of sPEEK to compete with PFSA as a membrane in PEMFC applications, provided the operation temperature remains moderate.

References

[1] E. Sgreccia et al., « Mechanical properties of proton-conducting sulfonated aromatic polymer membranes : Stress–strain tests and dynamical analysis, » *Journal of Power Sources*, t. 195, n° 23, p. 7770-7775, 2010, issn : 03787753. doi : 10.1016/j.jpowsour.2009.09.061

[2] G. Alberti et al., « Effects of hydrothermal/thermal treatments on the water-uptake of Nafion membranes and relations with changes of conformation, counter-elastic force and tensile modulus of the matrix, » *Journal of Power Sources*, t. 178, n° 2, p. 575-583, 2008, issn : 03787753. doi : 10.1016/j.jpowsour.2007.09.034

[3] M. J. Parnian et al., « Comprehensive investigation of physicochemical and electrochemical properties of sulfonated poly (ether ether ketone) membranes with different degrees of sulfonation for proton exchange membrane fuel cell applications, » *Energy*, t. 125, p. 614-628, 2017, issn : 03605442. doi : 10.1016/j.energy.2017.02.143

[4] K. N. T. Do et al., « Comparison of homogeneously and heterogeneously sulfonated polyetheretherketone membranes in preparation, properties and cell performance, » *Journal of Power Sources*, t. 185, n° 1, p. 63-69, 2008, issn : 03787753. doi : 10.1016/j.jpowsour.2008.06.087

[5] S. Banerjee et al., « Impact of degree of sulfonation on microstructure, thermal, thermomechanical and physicochemical properties of sulfonated poly ether ether ketone, » *Polymer*, t. 109, p. 176-186, 2017, issn : 00323861. doi : 10.1016/j.polymer.2016.12.030

[6] Y. Tang et al., « Ionic polymer–metal composite actuator based on sulfonated poly(ether ether ketone) with different degrees of sulfonation, » *Sensors and Actuators A : Physical*, t. 238, p. 167-176, 2016, issn : 09244247. doi : 10.1016/j.sna.2015.12.015

[7] Y. Song et al., « Investigations of the Sulfonated Poly(ether ether ketone) Membranes with Various Degrees of Sulfonation by Considering Durability for the Proton Exchange Membrane Fuel Cell (PEMFC) Applications, » *Polymers*, t. 17, n° 16, p. 2181, 2025, issn : 2073-4360. doi : 10.3390/polym17162181

[8] B. Yang et al., « Sulfonated Poly(ether ether ketone) Membranes for Direct Methanol Fuel Cells, » *Electrochemical and Solid-State Letters*, t. 6, n° 11, A229, 2003, issn : 1944-8775. doi : 10.1149/1.1613073

[9] G. Portale et al., « Microstructure, state of water and proton conductivity of sulfonated poly(ether ether ketone), » *Solid State Ionics*, t. 252, p. 62-67, 2013, issn : 01672738. doi : 10.1016/j.ssi.2013.08.031

[10] R. Wang et al., « Understanding of Nanophase Separation and Hydrophilic Morphology in Nafion and SPEEK Membranes : A Combined Experimental and Theoretical Studies, » *Nanomaterials*, t. 9, n° 6, p. 869, 2019, issn : 2079-4991. doi : 10.3390/nano9060869

[11] M. T. Salleh et al., « Stability of SPEEK/Cloisite ® /TAP nanocomposite membrane under Fenton reagent condition for direct methanol fuel cell application, » *Polymer Degradation and Stability*, t. 137, p. 83-99, 2017, issn : 01413910. doi : 10.1016/j.polymdegradstab.2016.12.011

[12] L. Zhang et al., « Investigation of Durability Issues of Selected Nonfluorinated Proton Exchange Membranes for Fuel Cell Application, » *Journal of The Electrochemical Society*, t. 153, n° 6, A1062, 2006, issn : 00134651. doi : 10.1149/1.2180715

[13] M.-S. Jun et al., « Solvent casting effects of sulfonated poly(ether ether ketone) for Polymer electrolyte membrane fuel cell, » *Journal of Membrane Science*, t. 396, p. 32-37, 2012, issn : 03767388. doi : 10.1016/j.memsci.2011.12.008

[14] Erce Şengül et al., « Effects of sulfonated polyether-etherketone (SPEEK) and composite membranes on the proton exchange membrane fuel cell (PEMFC) performance, » *International Journal of Hydrogen Energy*, t. 34, n° 10, p. 4645-4652, 2009, ISSN : 03603199. DOI : 10.1016/j.ijhydene.2008.08.066

[15] T. Astill et al., « Factors Influencing Electrochemical Properties and Performance of Hydrocarbon-Based Electrolyte PEMFC Catalyst Layers, » *Journal of The Electrochemical Society*, t. 156, n° 4, B499, 2009, ISSN : 1945-7111. DOI : 10.1149/1.3082119

[16] J.-S. Park et al., « A Study on Fabrication of Sulfonated Poly(Ether Ether Ketone)-Based Membrane-Electrode Assemblies for Polymer Electrolyte Membrane Fuel Cells, » *Journal of Power Sources*, Selected Papers Presented at the 3rd INTERNATIONAL CONFERENCE ON POLYMER BATTERIES FUEL CELLS(PBFC 2007) on the Occasion of Professor Bruno Scrosati's70th Birthday, t. 178, n° 2, p. 642-650, 2008, ISSN : 0378-7753. DOI : 10.1016/j.jpowsour.2007.08.008

[17] J. Peron et al., « Microstructure–Performance Relationships of sPEEK-Based Catalyst Layers, » *Journal of The Electrochemical Society*, t. 157, n° 8, B1230, 2010, ISSN : 1945-7111. DOI : 10.1149/1.3454735

[18] S. Sambandam et al., « Estimation of electrode ionomer oxygen permeability and ionomer-phase oxygen transport resistance in polymer electrolyte fuel cells, » *Physical Chemistry Chemical Physics*, t. 15, n° 36, p. 14 994, 2013, ISSN : 1463-9076, 1463-9084. DOI : 10.1039/c3cp51450a

[19] H. Mendil-Jakani et al., « A new interpretation of SAXS peaks in sulfonated poly(ether ether ketone) (sPEEK) membranes for fuel cells, » *Physical Chemistry Chemical Physics*, t. 16, n° 23, p. 11 243-11 250, 2014, ISSN : 1463-9084. DOI : 10.1039/C4CP00710G

[20] G. Gebel, « Structure of Membranes for Fuel Cells : SANS and SAXS Analyses of Sulfonated PEEK Membranes and Solutions, » *Macromolecules*, t. 46, n° 15, p. 6057-6066, 2013, ISSN : 0024-9297. DOI : 10.1021/ma400314c

[21] K. Kreuer, « On the development of proton conducting polymer membranes for hydrogen and methanol fuel cells, » *Journal of Membrane Science*, t. 185, n° 1, p. 29-39, 2001, ISSN : 03767388. DOI : 10.1016/S0376-7388(00)00632-3

[22] H. Mendil-Jakani et al., « Optimization of Hydrophilic/Hydrophobic Phase Separation in sPEEK Membranes by Hydrothermal Treatments, » *Phys. Chem. Chem. Phys.*, t. 19, 2017. DOI : 10.1039/C7CP00087A

[23] J.-M. Song et al., « Ionic aggregation characterization of sulfonated PEEK ionomers using by X-ray and DMA techniques, » *Macromolecular Research*, t. 20, n° 5, p. 477-483, 2012, ISSN : 2092-7673. DOI : 10.1007/s13233-012-0067-5

[24] B. Yang et al., « Comparison of the small angle X-ray scattering study of sulfonated poly(etheretherketone) and Nafion membranes for direct methanol fuel cells, » *Journal of Power Sources*, t. 153, n° 1, p. 29-35, 2006, ISSN : 03787753. DOI : 10.1016/j.jpowsour.2005.03.185

[25] M. Daoudi et al., « Impact of sulfonated poly(ether ether ketone) membranes pretreatments on their physicochemical properties and fuel cell performances, » *Journal of Polymer Science*, t. 61, n° 9, p. 761-776, 2023, ISSN : 2642-4169. DOI : 10.1002/pol.20220649

[26] M. Daoudi, « Performances et Durabilité Des Membranes Alternatives Aux Membranes PFSA, » PhD Thesis, Université de Lorraine, 2023.

[27] X. Pu et al., « Understanding of Hydrocarbon Ionomers in Catalyst Layers for Enhancing the Performance and Durability of Proton Exchange Membrane Fuel Cells, » *Journal of Power Sources*, t. 493, p. 229 671, 2021, ISSN : 0378-7753. DOI : 10.1016/j.jpowsour.2021.229671

[28] M.-J. Choo et al., « New Cross-Linked Interfacial Layer on Hydrocarbon Membrane to Improve Long-Term Stability of Polymer Electrolyte Fuel Cells, » *Electrochimica Acta*, t. 92, p. 285-290, 2013, ISSN : 0013-4686. DOI : 10.1016/j.electacta.2013.01.038

[29] J. Lee et al., « Binder Effect on Fuel Cell Performance and Interfacial Stability of Membrane Electrode Assembly Fabricated with Sulfonated Poly(ether ether ketone) Membrane, » *Macromolecular Research*, t. 27, n° 2, p. 175-181, 2019, ISSN : 2092-7673. DOI : 10.1007/s13233-019-7063-y

[30] H. Y. Jeong et al., « Novel Interfacial Bonding Layers with Controlled Gradient Composition Profile for Hydrocarbon-Based Membrane Electrode Assemblies, » *Journal of Power Sources*, t. 398, p. 1-8, 2018, ISSN : 0378-7753. DOI : 10.1016/j.jpowsour.2018.07.045

[31] S. D. Mikhailenko et al., « Properties of SPEEK based membranes modified with a free radical scavenger, » *Journal of Membrane Science*, t. 345, n° 1-2, p. 315-322, 2009, ISSN : 03767388. DOI : 10.1016/j.memsci.2009.09.017

[32] A. Carbone et al., « Porphyrin/sPEEK Membranes with Improved Conductivity and Durability for PEFC Technology, » *ACS Applied Energy Materials*, t. 1, n° 4, p. 1664-1673, 2018, ISSN : 2574-0962, 2574-0962. DOI : 10.1021/acsaem.8b00126

[33] R. Gutru et al., « Synthesis of sulfonated poly(bis(phenoxy)phosphazene) based blend membranes and its effect as electrolyte in fuel cells, » *Solid State Ionics*, t. 296, p. 127-136, 2016, ISSN : 01672738. DOI : 10.1016/j.ssi.2016.09.011

[34] M. J. Parnian et al., « High Durability Sulfonated Poly (Ether Ether Ketone)-Ceria Nanocomposite Membranes for Proton Exchange Membrane Fuel Cell Applications, » *Journal of Membrane Science*, t. 556, p. 12-22, 2018, ISSN : 0376-7388. DOI : 10.1016/j.memsci.2018.03.083

[35] M. J. Parnian et al., « Effect of ceria loading on performance and durability of sulfonated poly (ether ether ketone) nanocomposite membranes for proton exchange membrane fuel cell applications, » *Journal of Membrane Science*, t. 565, p. 342-357, 2018, ISSN : 03767388. DOI : 10.1016/j.memsci.2018.08.029

[36] A. Sahin, « The Development of Speek/Pva/Teos Blend Membrane for Proton Exchange Membrane Fuel Cells, » *Electrochimica Acta*, t. 271, p. 127-136, 2018, ISSN : 0013-4686. DOI : 10.1016/j.electacta.2018.03.145

[37] P. Hosseinabadi et al., « Synthesis and optimization of nanocomposite membranes based on SPEEK and perovskite nanoparticles for polymer electrolyte membrane fuel cells, » *New Journal of Chemistry*, t. 43, n° 41, p. 16 232-16 245, 2019, ISSN : 1369-9261. DOI : 10.1039/C9NJ03980E

[38] P. Salarizadeh et al., « Novel Proton Exchange Membranes Based on Proton Conductive Sulfonated PAMPS/PSSA-TiO2 Hybrid Nanoparticles and Sulfonated Poly (Ether Ether Ketone) for PEMFC, » *International Journal of Hydrogen Energy*, t. 44, n° 5, p. 3099-3114, 2019, ISSN : 0360-3199. DOI : 10.1016/j.ijhydene.2018.11.235

[39] C. Tougne et al., « Total Oxidation Stress Protection of Thiourea-Based Hybrid Fuel Cell Membranes, » *Electrochimica Acta*, t. 541, p. 147 338, 2025, ISSN : 0013-4686. DOI : 10.1016/j.electacta.2025.147338

[40] E. Ferri et al., « Thiourea-Based Hybrid sPEEK Membranes Using a Sol-Gel Approach : Elaboration of Stabilized Hybrid sPEEK Membranes, » *Reactive and Functional Polymers*, t. 219, p. 106 588, 2026, ISSN : 1381-5148. DOI : 10.1016/j.reactfunctpolym.2025.106588

[41] M. S. Ripa et al., « Catalyst Ink Solvent Composition and its Impact on Polarization of Proton Exchange Membrane Fuel Cells Under Hydrogen/Air Operation, » *Journal of The Electrochemical Society*, t. 172, n° 5, p. 054 513, 2025, ISSN : 1945-7111. DOI : 10.1149/1945-7111/add9d6

[42] G. Etienne et al., « On the Main Factors Limiting the Performance of State-of-the-Art Polymer Electrolyte Membrane Fuel Cells in the 90–100 °C Temperature Range, » *Electrochimica Acta*, t. 541, p. 147 320, 2025, ISSN : 0013-4686. DOI : 10.1016/j.electacta.2025.147320

[43] R. Sgarbi et al., « Impact of Transition Metals and Electrocatalyst Layer Thickness on the Pt-Based Cathodes of Proton Exchange Membrane Fuel Cells – Do Multimetallic Electrocatalysts Necessarily Yield an Improved Performance ? » *Advanced Energy Materials*, t. n/a, n° n/a, p. 2 403 212, ISSN : 1614-6840. DOI : 10.1002/aenm.202403212

[44] W. Aït-Idir et al., « Oxygen Diffusion Impedance in Proton Exchange Membrane Fuel Cells – Insights into Electrochemical Impedance Spectra and Equivalent Electrical Circuit Modeling, » *Electrochimica Acta*, t. 472, p. 143 430, 2023, ISSN : 0013-4686. DOI : 10.1016/j.electacta.2023.143430

[45] S. Touhami et al., « Anode aging in polymer electrolyte membrane fuel Cells I : Anode monitoring by ElectroChemical impedance spectroscopy, » *Journal of Power Sources*, t. 481, p. 228 908, 2021, ISSN : 03787753. DOI : 10.1016/j.jpowsour.2020.228908

[46] M. Kostelec et al., « Fundamental and Practical Aspects of Break-In/Conditioning of Proton Exchange Membrane Fuel Cells, » *The Chemical Record*, t. 24, n° 10, e202400114, 2024, ISSN : 1528-0691. DOI : 10.1002/tcr.202400114

[47] T. A. M. Suter et al., « Engineering Catalyst Layers for Next-Generation Polymer Electrolyte Fuel Cells : A Review of Design, Materials, and Methods, » *Advanced Energy Materials*, t. 11, n° 37, p. 2 101 025, 2021, ISSN : 1614-6832, 1614-6840. DOI : 10.1002/aenm.202101025

[48] X. Wu et al., « Differences in water sorption and proton conductivity between Nafion and SPEEK, » *Journal of Polymer Science Part B : Polymer Physics*, t. 49, n° 20, p. 1437-1445, 2011, ISSN : 08876266. DOI : 10.1002/polb.22326

[49] K. Kreuer, « On the development of proton conducting materials for technological applications, » *Solid State Ionics*, t. 97, n° 1-4, p. 1-15, 1997, ISSN : 01672738. DOI : 10.1016/S0167-2738(97)00082-9

[50] N. Takimoto et al., « Hydration behavior of perfluorinated and hydrocarbon-type proton exchange membranes : Relationship between morphology and proton conduction, » *Polymer*, t. 50, n° 2, p. 534-540, 2009, ISSN : 00323861. DOI : 10.1016/j.polymer.2008.11.029

[51] A. Karimi et al., « Investigation, Modeling, and Optimization of Parameters Affecting Sulfonated Polyether Ether Ketone Membrane-Electrode Assembly, » *International Journal of Hydrogen Energy*, t. 44, n° 2, p. 1096-1109, 2019, ISSN : 0360-3199. DOI : 10.1016/j.ijhydene.2018.10.225

[52] Y. Jiang et al., « A novel porous sulfonated poly(ether ether ketone)-based multi-layer composite membrane for proton exchange membrane fuel cell application, » *Sustainable Energy & Fuels*, t. 1, n° 6, p. 1405-1413, 2017. DOI : 10.1039/C7SE00240H

[53] R. Jiang et al., « Investigation of membrane property and fuel cell behavior with sulfonated poly(ether ether ketone) electrolyte : Temperature and relative humidity effects, » *Journal of Power Sources*, t. 150, p. 120-128, 2005, ISSN : 03787753. DOI : 10.1016/j.jpowsour.2005.03.180

[54] Q. Yan et al., « Steady State and Dynamic Performance of Proton Exchange Membrane Fuel Cells (PEMFCs) under Various Operating Conditions and Load Changes, » *Journal of Power Sources*, t. 161, n° 1, p. 492-502, 2006, ISSN : 0378-7753. DOI : 10.1016/j.jpowsour.2006.03.077

[55] D. N. Ozen et al., « Effects of Operation Temperature and Reactant Gas Humidity Levels on Performance of PEM Fuel Cells, » *Renewable and Sustainable Energy Reviews*, t. 59, p. 1298-1306, 2016, ISSN : 1364-0321. DOI : 10.1016/j.rser.2016.01.040

[56] J. Zhang et al., « Experimental and Numerical Simulation Study of Oxygen Transport in Proton Exchange Membrane Fuel Cells at Intermediate Temperatures (80 °C–120 °C), » *Membranes*, t. 14, n° 4, p. 72, 2024, ISSN : 2077-0375. DOI : 10.3390/membranes14040072

[57] Bird Robert Byron, *Transport Phenomena*, Revised 2nd edition. New York [etc : John Wiley & Sons, Inc., 2007, ISBN : 978-0-470-11539-8.

[58] A. M. Martos et al., « Synthesis and Characterization of Sulfonated PEEK-WC-PES Copolymers for Fuel Cell Proton Exchange Membrane Application, » *European Polymer Journal*, t. 93, p. 390-402, 2017, ISSN : 0014-3057. DOI : 10.1016/j.eurpolymj.2017.06.013

[59] M. Vinothkannan et al., « Facile enhancement in proton conductivity of sulfonated poly (ether ether ketone) using functionalized graphene oxide—synthesis, characterization, and application towards proton exchange membrane fuel cells, » *Colloid and Polymer Science*, t. 294, n° 7, p. 1197-1207, 2016, ISSN : 1435-1536. DOI : 10.1007/s00396-016-3877-8

[60] P. Martina et al., « Nanosulfonated Silica Incorporated SPEEK/SPVdF-HFP Polymer Blend Membrane for PEM Fuel Cell Application, » *Ionics*, t. 26, 2020. DOI : 10.1007/s11581-020-03478-9

[61] R. Patel et al., « Integrated Proton Transport Architecture in Fiber-Reinforced Sulfonated Membrane for High-Performance Proton Exchange Membrane Fuel Cell, » *Journal of Power Sources*, t. 653, p. 237 763, 2025, ISSN : 0378-7753. DOI : 10.1016/j.jpowsour.2025.237763

[62] F. van der Linden et al., « A Review on the Proton-Exchange Membrane Fuel Cell Break-in Physical Principles, Activation Procedures, and Characterization Methods, » *Journal of Power Sources*, t. 575, 233168 (17), 2023. DOI : 10.1016/j.jpowsour.2023.233168

Chapter 5

PFSA-based durability at higher operating temperature and comparison with alternative membrane

1 Introduction 168
2 Materials, methods & protocol 169
2.1 Materials & methods 169
2.2 Protocol 170
3 Durability evaluation of state-of-the-art materials 172
3.1 Impact of operating parameters on MEA performance evolution 172
3.2 Post-mortem analysis 182
3.3 Summary and discussion 188
4 Comparison with alternative membrane ionomers 191
4.1 sPEEK durability : effect of pretreatment and comparison with PFSA membranes durability 191
4.2 Effect of *Nafion overcoat* and electrodes deposit method (CCM) on sPEEK durability 194
4.3 Summary and discussion 197
5 Conclusions 198
References 201

1 Introduction

Although only a few studies have investigated the effect of temperature on fuel cell membrane durability, they consistently report a significant increase in the membrane degradation rate. Several of these studies reported lower chemical durability, as evidenced by a greater decrease in OCV [1, 2], along with structural degradation of the membrane : increased pinhole formation and higher degradation product formation rates [1]. According to the same studies, this effect is all the greater when the gas inlet RH is low [3], due to increased production of H_2O_2 radicals [4, 5]. Regarding mechanical degradation, drive cycle tests induced reduced mechanical properties of the membrane and structural defects such as cracks, especially at higher operating temperature [6, 7]. Near the glass transition temperature, membrane properties are changed and automotive conditions, *i.e.*, relatively dry conditions and load cycling, induce high constraints with notably drastic dehydration and significant heat release, which could potentially lead to significant alterations in the ionomer. When coupled chemical/mechanical degradation tests were applied, the also results showed an accelerated degradation of the membrane with earlier crossover onset and significant structural changes highlighted by enhanced thinning and/or pinhole formation [8].

In this chapter, we evaluated, first, the durability of the IRD MEA through accelerated stress test (AST) with various operating parameters to assess the impact of cell operating temperature and gas RH. An overview of the global performance decrease is made, as well as a diagnostic of the electrodes and membrane state thanks to ECSA and permeation tests. Then, post-mortem analysis has been performed by partners to assess the microstructural changes, with the evaluation of material thickness.

Although Gore membrane is operating well in various conditions, there is still a need to investigate the potential of alternative fluorine-free ionomers. As observed in the previous chapter, sPEEK ionomer used as membrane with an adequate pretreatment (*sPEEK nanostructured*) demonstrated interesting in-operando performances, close to that of Nafion 211 one. Despite higher water requirements to ensure proton conduction, the nanostructuration of the ionomer enables a more efficient water utilization and thus, fuel cell operation under an air atmosphere. There is therefore a requirement to evaluate sPEEK durability under these conditions, although *ex situ* aging tests showed a significantly poorer chemical stability compared to PFSA ionomer.

Accelerated stress test (AST) at 70°C/50% RH, regardless of the membrane type, were therefore conducted and their performance and membrane state were evaluated through polarization curve, permeation current, and high-frequency resistance measurements. Further investigations were carried out to assess the effect of the pretreatment on sPEEK membranes by analyzing samples treated according to the protocol recommended by the supplier (*sPEEK standard*). In addition, the influence of the amount of Nafion deposited on the GDE (*i.e.*, *Nafion overcoat* loading) was evaluated. The effect of eliminating this overcoat was also investigated through the fabrication of home-made CCM-type MEA prepared by our partner ZSW, in which the electrodes were deposited directly onto the membrane. Finally, to enable a more relevant comparison with sPEEK, NR211 membranes-which, like sPEEK and unlike Gore membranes, do not contain mechanical reinforcement or radical scavengers-were also included in the study.

2 Materials, methods & protocol

2.1 Materials & methods

PFSA-based materials

The same commercial MEA employed during the performance evaluation at higher operating temperatures (chapter 2) was also used in the durability study to assess the impact of temperature on the 12 μm state-of-the-art membrane. A reminder of the composition is given below :

- Anode : Pt/HSAC 50 wt% (Tanaka TKK TEC10E50E) - 0.1 $mg.cm^{-2}$
- Cathode : Pt/HSAC 50 wt% (Tanaka TKK TEC10E50E) - 0.3 $mg.cm^{-2}$
- Nafion D2020CS as the electrode ionomer for both anode and cathode side with an ionomer/carbon ratio equal to 0.8
- Gore788.12 membrane
- Freudenberg H14CX653 GDL

sPEEK-based materials

In parallel with the study of temperature effects on the state-of-the-art membrane, MEA based on pretreated sPEEK (*sPEEK nanostructured*) were tested at usual temperature. Details of the composition, the pretreatment, and the hot-pressing process are provided below (for more information, refer to chapter 4) :

Composition	Membrane	Pretreated sPEEK
	GDL	H14CX653
	Electrodes	0.3 $mg.cm^{-2}$ Pt loading
Membrane pretreatment (*sPEEK nanostructured*)	Acidification	4 h in HCl 1M at 30°C
	Rinsing	Distilled water
	Hydro-alcoholic	24 h in water/ethanol at pH = 4 and 30°C
	Rinsing	Distilled water
	Hydro-thermal	72 h in distilled water at 80°C
	Drying	24 h at 60°C on PEEK frame 18 h at 100°C
Hot-pressing process	Constrain	4.5 MPa
	Temperature	135°C
	Time	210 s

Table 5.1 – Summary of sPEEK MEA composition, sPEEK Acd-HA-HT72h pretreatment (*i.e.*, *sPEEK nanostructured*) and parameters employed during the hot-pressing process.

In addition to the *sPEEK nanostructured* membrane, the pretreatment recommended by the supplier was also tested on sPEEK (referred to as *sPEEK standard*), assembled in MEA under the same conditions and with the same GDE/overcoated as the *sPEEK nanostructured*. The *sPEEK standard* protocol consists of an acidification step (H_2SO_4 at 80°C for 16 h) followed by a hydrothermal step (water at 80°C for 1 h).

Each MEA has been tested in the same straight parallel channel design as for the performance mapping and limitation study in the chapter 2 (figure 2.1). Although it could be interesting to assess the impact of cell channel geometry by testing the serpentine design, the duration of each test being approximately between 10 and 20 days (*i.e.*, AST duration in addition to characterizations every 24h)

did not allow us to compare it. Nevertheless, we estimate that changing cell geometry design should not change the measured trends and therefore, testing one cell channel design may be enough to assess the impact of operating parameters.

The conditioning step before each AST is identical to that used for the performance mapping, *i.e.*, constant voltage step at OCV, 0.6 and 0.3 V during approximately 2h for IRD MEA and less than 3h for sPEEK MEA (see corresponding chapters for operating conditions). Also, to simplify the number of tests, we fixed gas pressure and gas stoichiometries to the reference conditions established during the performance mapping, *i.e.*, 3 bar and 1.25/3. The operating temperature and gas inlet RH at 95°C were varied to evaluate their impact on IRD MEA durability. However, for sPEEK-based MEA, AST were conducted only at 70°C and 50% RH as no stable operating conditions could be established at 95°C. All the operating conditions tested for the different types of MEA are summarized in table 5.2.

MEA type			P (bar)	St(H_2/air)	T (°C)	RH (%)
CCM		IRD (Gore 788.12)	3	1.25/3	70	20
						50
					95	20
						30
						50
		sPEEK nanostructured	3	1.25/3	70	50
CCB	Overcoat 0.3 mg.cm^{-2}	*sPEEK nanostructured*	3	1.25/3	70	50
	Overcoat 0.2 mg.cm^{-2}	*sPEEK nanostructured*				
	Overcoat 0.3 mg.cm^{-2}	*sPEEK standard*				
	No overcoat	NR211				

TABLE 5.2 – Summary of operating conditions and membrane-based MEA tested during the AST for each type of MEA : CCM or CCB with GDE with or without *Nafion overcoat*.

2.2 Protocol

The choice of AST is not evident because of the multitude of possibilities. Beyond variations in operating parameters, there is a wide variety of AST based on chemical, mechanical or combined chemical and mechanical degradation. For simplicity, an AST based on previous works was chosen [9-11], which also provided a basis for comparison. It was observed that this AST resulted in significant aging of the membrane and electrodes, with a notable reduction in the active surface area of the electrodes due to Ostwald ripening [11]. The AST consists of a 60 s repeated cycle divided in load cycling and Open Circuit Voltage (OCV) :

- The load cycling stage lasts 43 s and consists in cycling in galvanostatic mode between 0 A for 2 s, *i.e.*, OCV, and a current density setpoint corresponding to approximately 0.5-0.55 V for 3s.
- The second stage consists in holding OCV, *i.e.*, zero current density, during 17 s.

Gas flowrates are set to a fixed value corresponding to the current density at low voltage. The repetition of both stages induces a coupled chemical and mechanical aging of the materials :

- Electrodes' aging is induced by the load, and thus potential, cycling period [12, 13].

- Chemical aging is induced during the 17s OCV period, in addition to OCV periods occurring during load cycling. At this operating point, no electrochemical consumption of reactants takes place ; hydrogen and oxygen permeate through the membrane and recombine with the opposite reactant, leading to the formation of H_2O_2 and subsequently radical species. As discussed previously (chapter 1, section 1.5.2), these radicals chemically attack specific bonds within both the membrane and the ionomer in the electrodes, resulting in chain scission, desulfonation, and ultimately ionomer deformation, which may lead to the formation of pinholes.
- Mechanical aging thanks to the period of load cycling and OCV. During the load cycling, there is a significant production of water, which hydrates both the membrane and the ionomer in the electrodes, resulting in ionomer swelling. On the contrary, the OCV period contributes to dehydrate the ionomer, as the gas flowrates remove the water from the cell, and then shrink the ionomer. It results in a swelling/shrinking cycle every 60 s, inducing repeated mechanical constraints.

Finally, it should be kept in mind that the decrease in the cathode ECSA observed during the AST is mainly due to catalyst oxidation/reduction cycles. This particular AST does not involve any potential excursions, such as those occurring during start/stop cycles, that would lead to significant carbon corrosion.

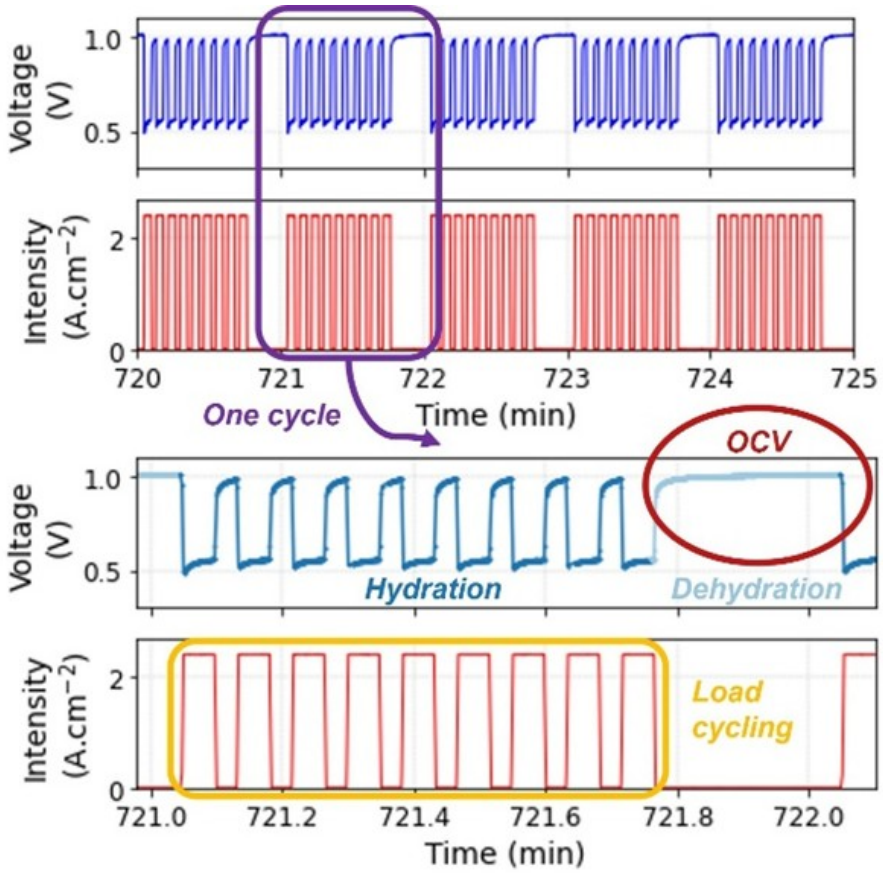

FIGURE 5.1 – Description of the applied AST, voltage (blue line) and current density (red line) cycling [14].

Each AST lasted 14 days, unless the membrane failed earlier, during which characterizations were performed every 24h to assess the evolution of each material. Permeation and ECSA tests are carried out to assess the state of the membrane and the electrodes while polarization curves and impedance spectroscopy at 1 and 1.5 A.cm^{-2} in galvanostatic mode are performed to assess global MEA performance. Permeation and voltammetry measurements were performed based on previous studies [9, 15, 16]. The Electrochemical Impedance Spectroscopy (EIS) and polarization curve measurement protocols are identical to those described in the previous chapters. As a reminder, all operating parameters are given in table 5.3.

Test	Gas flowrate (10 slph)		U (V)	i (A.cm^{-2})	Comment
	Anode	Cathode			
Permeation	H_2	N_2	120 s at 0 V, then 120 s at 0.6 V	Measured	Gas reversible
Voltammetry	H_2	N_2	0.1–0.7 V at 50 mV.s^{-1}	Measured	Gas reversible
Spectroscopy	St H_2	St air	Measured	1–1.5 A.cm^{-2}	[0.05Hz–25kHz]
Polarization curve	St H_2	St air	Measured	Imposed	OCV to 0.3 V
IRD : average value from forward/backward scan with 100 s current density step sPEEK : forward scan with 200 s current density step					

TABLE 5.3 – Summary of operating conditions during characterization stage of the AST.

3 Durability evaluation of state-of-the-art materials

This section is dedicated to evaluating the durability of the IRD MEA, with particular focus on the state-of-the-art membrane under various operating conditions. AST were conducted to assess the impact of cell operating temperature and gas relative humidity on IRD MEA performance over time, and to determine whether performance degradation originates from the membrane or the electrodes. In particular, this study aims to determine whether automotive operating conditions, with maintaining a moderate temperature, are compatible with usual materials. For clarity, the evolution of MEA performance is presented every two days, whereas the state of the electrodes and membrane state is monitored daily throughout the AST.

3.1 Impact of operating parameters on MEA performance evolution

Impact of cell operating temperature

The effect of cell operating temperature was assessed through AST conducted at 70 and 95°C, under two different gas RH levels. Polarization curves recorded over time showed a progressive decrease in fuel cell performance, but it remained difficult to determine which operating conditions were harsher for MEA durability. One noteworthy observation occurred at 95°C/20% RH, where a significant increase in performance was measured between the Beginning of Life (BoL) and after one day of AST, but could not be explained.

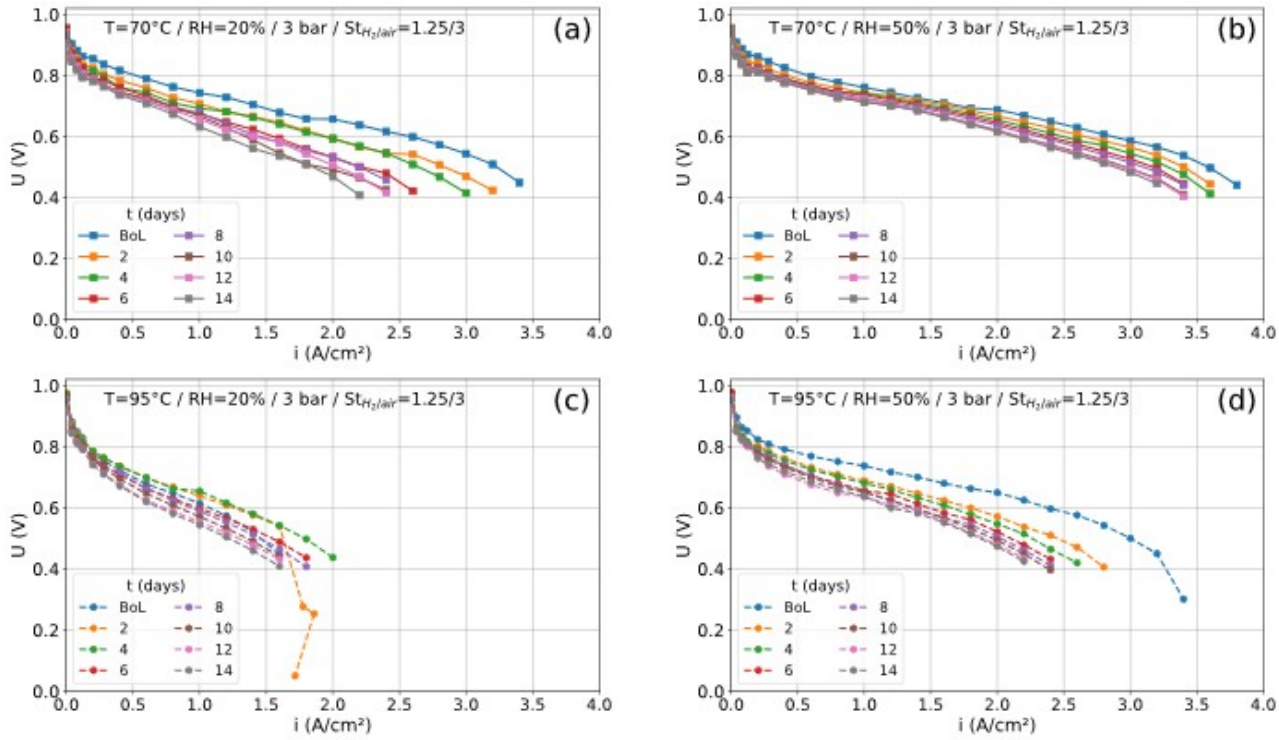

FIGURE 5.2 – IRD-MEA performance evolution over time under AST at : 70°C/20% RH (a), 70°C/50% RH (b), 95°C/20% RH (c), and 95°C/50% RH (d).

Performance decrease was evaluated at different fuel cell operating points, including voltages (0.5 and 0.7 V) and current densities (0.5, 1, and 1.5 A.cm^{-2}), to assess the impact of operating conditions on fuel cell performance (figure 5.3 and table 5.4). Higher relative performance losses were observed with increasing operating temperature at 50% RH, with the MEA aged at 70°C/50% RH exhibiting the lowest overall relative losses. In contrast, performance losses at 70°C/20% RH were significantly higher than those at 70°C/50% RH and were comparable to those at 95°C/50% RH. The MEA aged at 95°C/20% RH exhibited slightly higher relative losses than that aged at 70°C/50% RH, but significantly lower losses than those observed at 70°C/20% and 95°C/50% RH. Although performance losses remained lower, comparisons across operating conditions are complicated by the performance increase observed after the first day of AST.

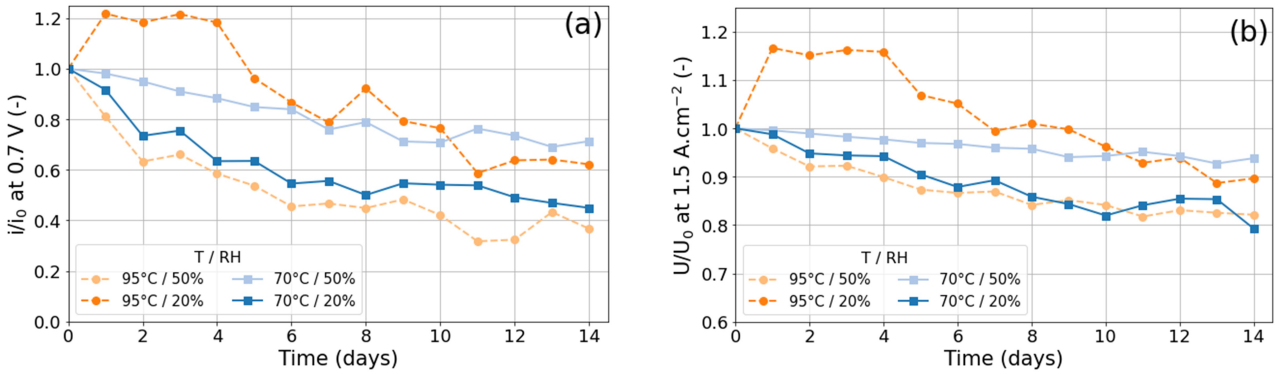

FIGURE 5.3 – Relative i and U states of the IRD MEA at usual operating points with AST time at : 0.7 V (a), 1.5 A.cm^{-2} (b).

AST conditions	Relative losses (%)				
	i @ 0.7 V	i @ 0.5 V	U @ 0.5 A.cm^{-2}	U @ 1 A.cm^{-2}	U @ 1.5 A.cm^{-2}
70°C / 50% RH	29%	20%	6%	6%	6%
95°C / 50% RH	63%	38%	10%	14%	18%
70°C / 20% RH	55%	43%	10%	15%	21%
95°C / 20% RH	38%	16%	8%	11%	10%

TABLE 5.4 – Relative voltage and current densities losses at different operating points after 14 days of AST.

The performance monitoring is therefore difficult to interpret. Nevertheless, the results indicate that humidity may have a mixed effect on performance durability, depending on temperature, with increased losses at 70°C and decreased losses at 95°C under low-humidity conditions.

The evolution of the electrodes and membrane was monitored using ECSA, permeation, and high-frequency resistance measurements performed during each AST day. Regarding the active surface area (figure 5.4), different trends were observed at the cathode and anode :

- On the **cathode side** (figure 5.4(a)), a similar decrease exceeding 60% was observed under all operating conditions, except at 95°C/20% RH, where the decrease did not exceed 40%. Moreover, a stable ECSA value was observed during the first day of AST. This trend may be related to the enhanced performance observed after the first day, although no clear explanation can be provided at this stage.
  Regarding the other conditions, the absence of significant differences suggests that cathode ECSA degradation is not sensitive to temperature under moderate gas RH and our AST protocol.

- On the **anode side** (figure 5.4(b)), a small decrease appeared at 70°C/20% RH on the first day, followed by a relatively stable value, whereas no losses were observed at 70°C/50% RH, indicating that no significant changes in active surface area were detected at 70°C. In contrast, higher temperature appears to affect the anode side, with substantial declines observed at 95°C under both gas RH conditions : approximately 40% and 34% losses at 20 and 50% RH, respectively.

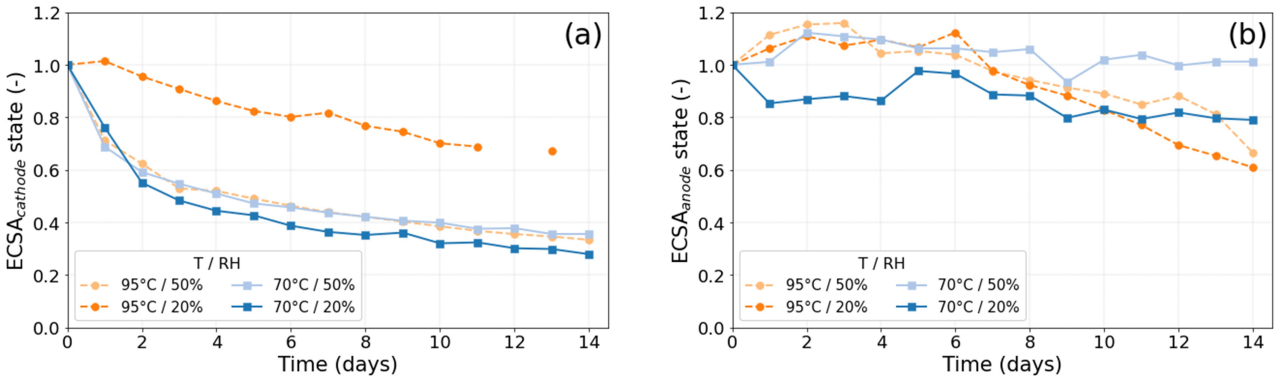

FIGURE 5.4 – ECSA state evolution over time of the IRD MEA at 70-95°C and 20-50% gas inlet RH on cathode (a) and anode side (b).

In all cases, no increase in permeation current was observed (figure 5.5(a)), a result that was confirmed with the same measurement performed on the anode side. Interestingly, drier conditions at 95°C led to higher permeation currents ; however, the values remained stable throughout the entire AST. Moreover, higher values were observed on day 12 and 14 for the MEA aged at 95°C/20% RH, although no clear explanation could be identified. Nevertheless, the overall stability of the permeation does not indicate significant membrane rupture, and the higher values may therefore originate from measurement artifacts. This suggests that the membrane did not undergo significant deterioration such as cracks or pinholes. However, it should be noted that this result is valid only for the IRD MEA, and that using other MEA based on the same Gore membrane, supplied within the framework of the PEMFC95 project (CEA, Hynology) or other projects in our group, might lead to different conclusions.
R_{hf} measurements showed a slight increase at 20% RH for both temperatures, whereas no increase was observed at 50% RH. Although no sign of membrane degradation was detected through the permeation test, this may indicate a slow but progressive degradation of the membrane or of the membrane/electrode interface through coupled chemical and mechanical degradation. However, no clear trend can be identified, as 95°C/20% gas RH represents dry conditions, whereas 70°C/20% RH represents more humid conditions than 95°C/50% RH.

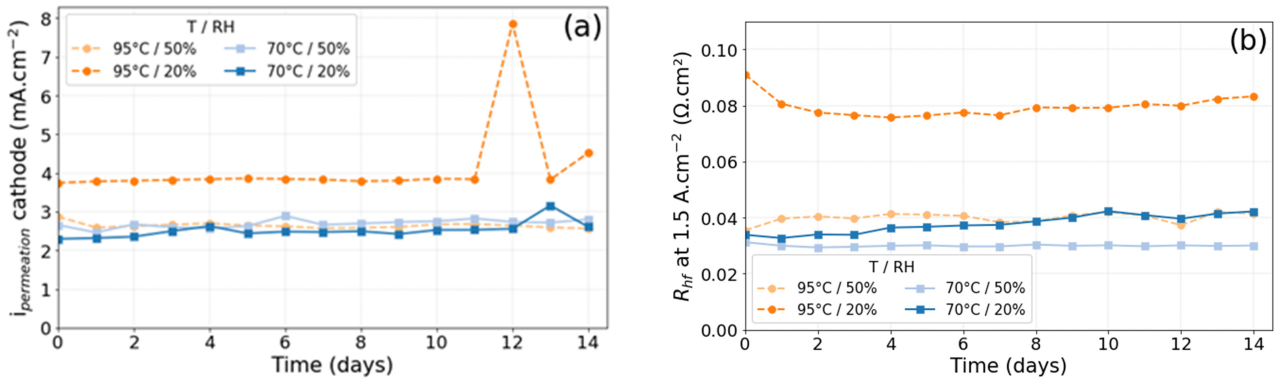

FIGURE 5.5 – Permeation of the IRD MEA on the cathode side (a) and R_{hf} evolution at 1.5 A.cm^{-2} over time (b)

At this stage, it is difficult to evaluate the effect of operating temperature at constant gas RH with the current AST protocol. No significant trend was observed through performance degradation measurements, and permeation and R_{hf} measurements indicated a relatively stable, non-degraded membrane, despite the slight increase in R_{hf} that was observed at 20% gas RH for both temperatures discussed in the section “Temperature effect“ of the summary and discussion section.

Impact of gas inlet RH

The impact of gas inlet RH was evaluated through accelerated stress tests conducted at 95°C. Tests at 20%, 30%, and 50% RH were performed to assess the effect of water content on MEA performance, as well as the membrane and electrodes state, using the characterizations tests described in the previous section.

The evolution of current density and voltage during the AST at characteristic operating points revealed contrasting trends with respect to gas RH (figure 5.6). Lower relative current density losses were observed at 0.7 and 0.5 V with decreasing gas inlet RH. In contrast, relative voltage losses at 0.5, 1 and 1.5 A.cm^{-2} remained similar for the MEA aged under 30% and 50% gas inlet RH. However, MEA aged at 95°C/20% RH exhibited results that depended on the performance increase observed on the first day. In the first test, losses similar to those obtained at higher gas inlet RH were observed at 0.5 and 1 A.cm^{-2}, whereas lower losses were measured at 1.5 A.cm^{-2}. In the second test, increased relative voltage losses were observed at 0.5, 1, and 1.5 A.cm^{-2}. Overall, decreasing gas RH at 95°C may help limit relative performance losses at low current densities, although values remained close at certain operating points and the trends cannot be confirmed with certainty.

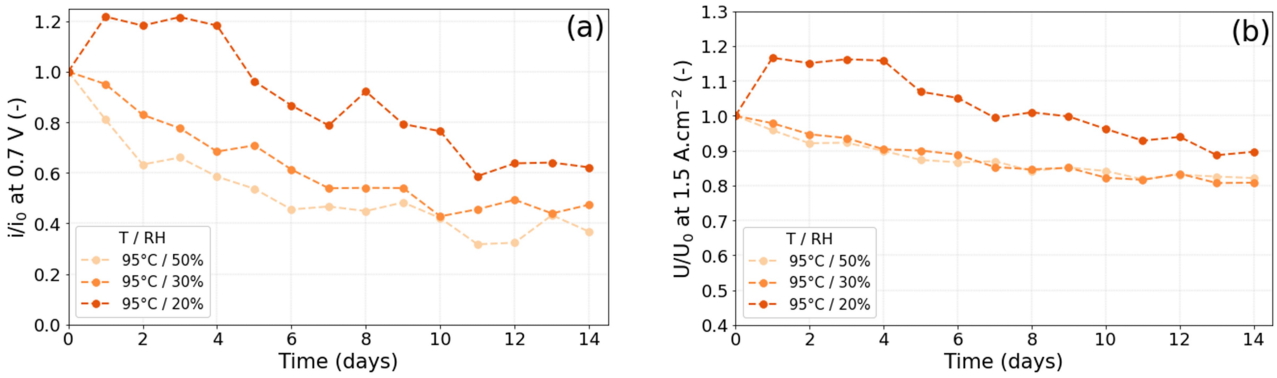

FIGURE 5.6 – Relative i and U states of the IRD MEA at usual operating points over time at : 0.7 V (a), 1.5 A.cm^{-2} (b).

Regarding the active surface area on the cathode side (figure 5.7(a)), a clear trend was observed : ECSA degradation increased with increasing gas RH, with losses ranging from more than 60% after 14 days at 50% RH to less than 40% at 20% RH. On the anode side, a systematic degradation of the active surface area was observed, which was more pronounced at low gas RH. This suggests that ECSA degradation at the anode side increases as gas humidity decreases, although higher degradation was also observed at 30% RH. However, higher permeation was measured for the MEA aged at 95°C/30% RH (figure 5.8(a)), likely related to the sample itself. Therefore, ECSA degradation at the anode may possibly be associated with the higher permeation under drier conditions. In other words, a higher crossover rate may lead to increased H_2O_2 formation, which could enhance Pt degradation through ionomer binder or carbon support degradation. Touhami et al. [9] and Tavassoli et al. [17] suggested that membrane thinning near anode electrode defects and delamination could result from a higher production of H_2O_2 consecutive from gas crossover. Nevertheless, further analyses would be required to confirm this hypothesis in the present study.
As with the hydrogen permeation current measurements, ECSA could not be determined on the cathode side for the MEA aged at 95°C/20% RH on days 12 and 14, due to test bench malfunctions (figure 5.7(g)).

The evolution of performance is therefore difficult to correlate with those of the ECSA : although no significant difference in relative performance degradation was observed, the gas inlet RH impacted

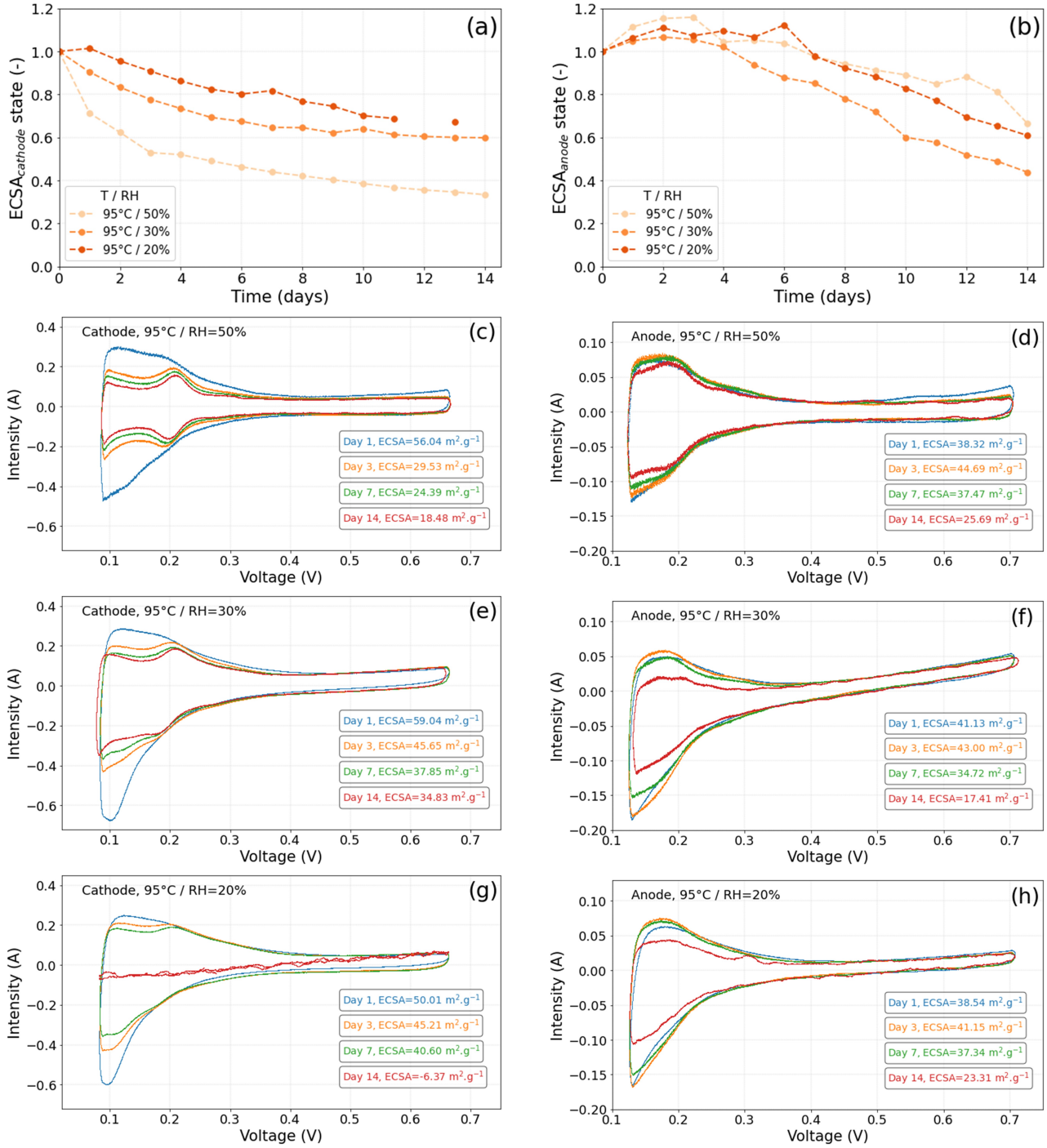

FIGURE 5.7 – Relative ECSA state evolution over time of the IRD MEA at 95°C and different gas inlet RH on the cathode side (a) and on the anode side (b). Voltammograms on cathode (c-d-e) and anode (d-f-h) side at different aging time during AST at 95°C and 50% RH (c-d), 30% RH (e-f), and 20% RH (g-h).

significantly the ECSA degradation, particularly on the cathode side. This may suggest that structural changes have occurred within the catalytic layers, significantly affecting the ECSA while having a limited impact on overall MEA performance.

Regarding the membrane state, permeation and R_{hf} measurements (figure 5.8) did not show any trends indicative of significant membrane degradation. Permeation values remained stable, despite differences in initial values likely attributable to variations in hydration state. Higher permeation values were observed for the MEA aged at 95°C/30% RH, likely due to intrinsic sample-to-sample variability. At 95°C/20% RH, the MEA exhibited a significant decrease in R_{hf} between day 0 and the first few days of testing. Ionomer reorganization in dry conditions, driven by hydration cycling may explain the improved performance observed. Moreover, the progressive increase from day-7 to the end of the test, as previously noted, was not observed at higher gas RH (although technical issues precluded measurements at 95°C/30% RH). This could indicate a negative impact of low humidity conditions on the state of the membrane and/or the membrane/electrode interface, whereas the stable R_{hf} and permeation values at higher gas RH may suggest that no significant changes in membrane thickness or at the membrane-electrode interface occurred.

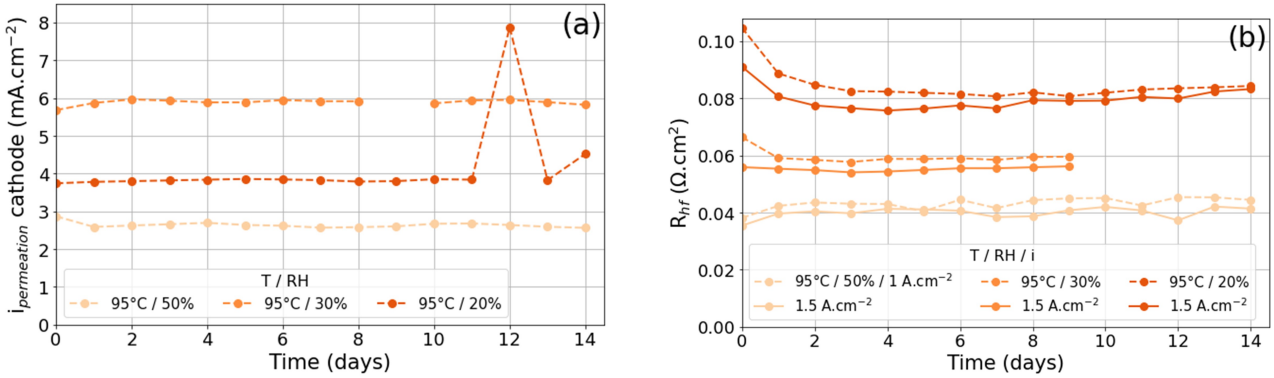

FIGURE 5.8 – Evolution of permeation of the IRD MEA on the cathode side (a) and R_{hf} at 1 and 1.5 A.cm^{-2} (b) over time

Performance improvement at 95°C and 20% gas inlet RH during early AST days

As previously mentioned, a noticeable improvement in performance was observed for the MEA aged at 95°C/20% RH after the first day of AST. In parallel, a significant decrease in R_{hf} was measured after one day of AST, suggesting an enhanced hydration state. A likely explanation involves the rehydration and reorganization of the membrane and ionomer binder, driven by hydration/dehydration cycling during the AST. To validate this hypothesis, an AST at 95°C/20% RH was conducted, including a constant current step at 1 A.cm^{-2} for over 9 hours prior to the first AST day, to assess whether any voltage improvement could be attributable to ionomer rehydration.

Fuel cell voltage remained stable at approximately 0.69 V throughout the constant current step, suggesting no significant changes in hydration state occurred (figure 5.9). The observed voltage drops are due to water drainage at the fuel cell outlet. This is because the reactant flowrates are cooled after leaving the fuel cell outlet and before reaching the pressure regulators, and the condensed water is collected in a small tank. When this reservoir is full, the water is drained, creating a temporary void that causes a transient drop in reactant concentration and gas pressure within the fuel cell, leading to a decrease in cell voltage.

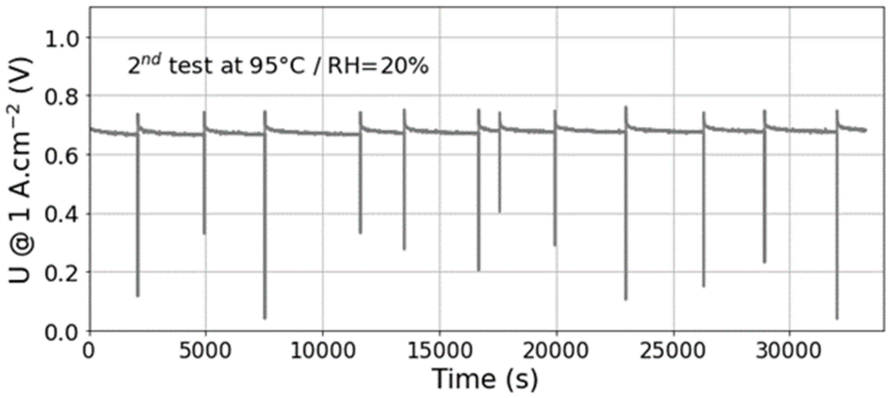

FIGURE 5.9 – Fuel cell voltage of the IRD MEA during a constant current step recorded after characterization at day 0 and before the first AST day.

When comparing the performance of the second test at day 0 and day 1, no improvement was observed on the polarization curve (figure 5.10(a)). Moreover, performance at day 1 remained almost identical, showing no significant effect of the constant current step conducted prior to the AST. A significant performance gap therefore existed between the two tests. This discrepancy may be explained by differences in R_{hf} behavior : the first MEA showed a more pronounced decrease after the first day, enhancing fuel cell performance. These results suggest differences in MEA hydration state at BoL, which diminish over the course of the AST. This may be associated with ionomer reorganization, driven by hydration/dehydration cycling. On the other hand, a 5-10 $m\Omega.cm^2$ gap still exists despite very close performance at day 1, showing that fuel cell performance is not governed solely by R_{hf}.

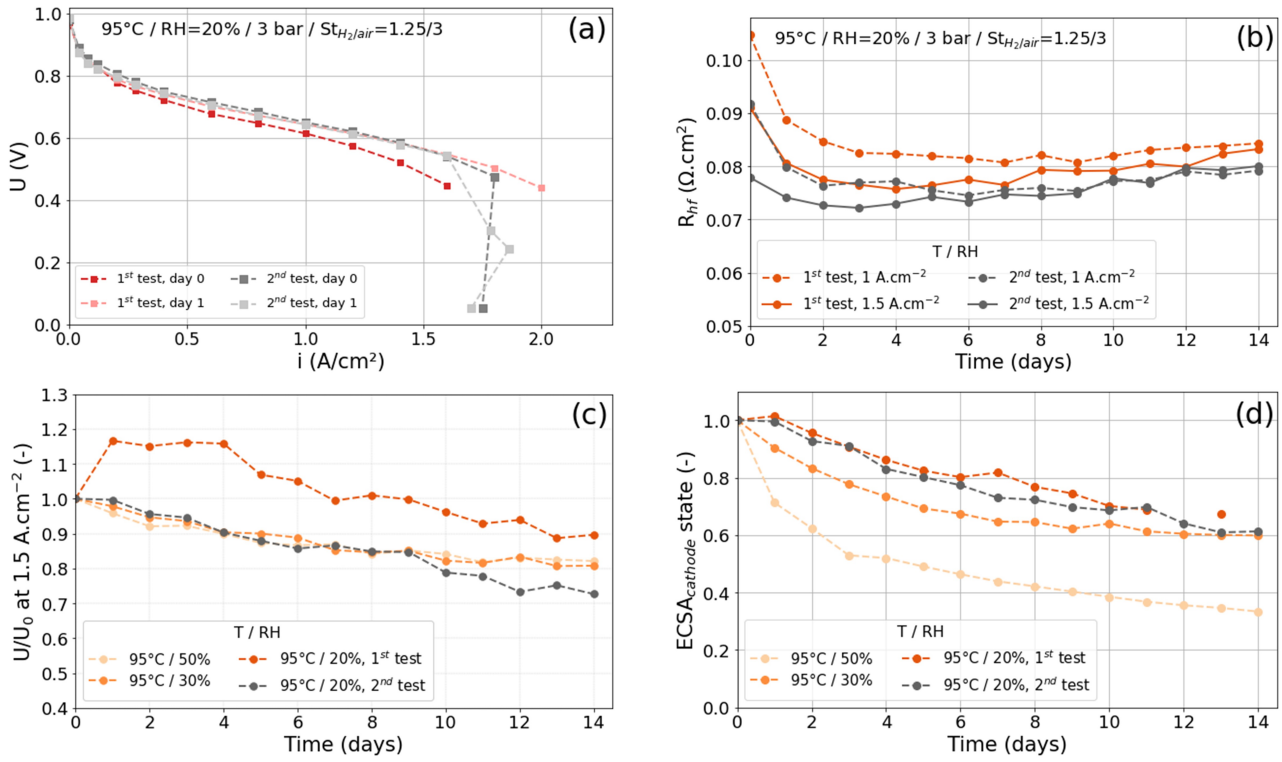

FIGURE 5.10 – Comparison of AST conducted on the IRD MEA at 95°C and 20% RH : polarization at day 0 and 1 (a), R_{hf} at 1 and 1.5 $A.cm^{-2}$ (b), relative voltage at 1.5 $A.cm^{-2}$ (c), and cathode ECSA state (d).

These differences in performance at BoL lead to differing performance trends, making it difficult to identify clearly the effect of gas inlet RH at 95°C. Despite significant differences in performances and R_{hf}, very similar ECSA state trends were observed for both the anode and cathode catalytic layers.

Repeatability of *in situ* characterizations during AST

The previous sections showed that trends concerning relative performance under various operating conditions remained unclear. However, it is noteworthy that performance evolutions are represented in relative terms, and a few percent difference in fuel cell voltage does not represent a significant voltage gap. Nevertheless, reproducibility remains to be determined, as only the test at 95°C/20% RH was repeated.

A similar AST protocol has already been used during previous works in our team [18, 19]. In particular, Aït-Idir conducted reproducibility tests applying a similar AST to four different commercial MEA based on a similar membrane (Gore 775.15) but with different Pt loadings (two MEA with 0.1/0.3 mg.cm^{-2} and two with 0.05/0.1 mg.cm^{-2} anode/cathode Pt loading) [20]. At equivalent loading, high reproducibility was observed in terms of performance at BoL and EoL. Moreover, similar cathode ECSA evolution was observed regardless of Pt loading, whereas anode ECSA evolution remained similar at equivalent Pt loading. These results underlined the high reproducibility of the AST protocol employed at usual operating temperature of 80°C.

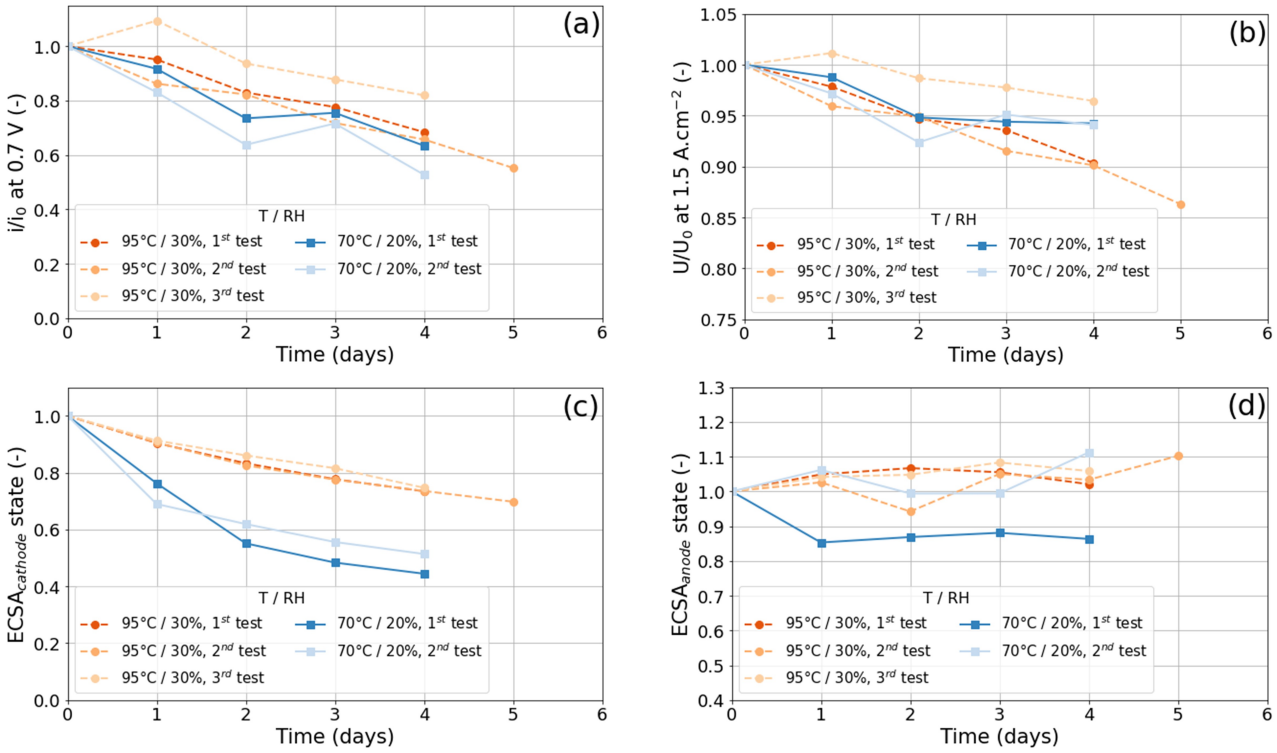

FIGURE 5.11 – Comparison of the evolution of the IRD MEA performance and ECSA during the first five days of AST at 95°C/30% RH and 70°C/20% RH : relative current at 0.7 V (a), relative voltage at 1.5 A.cm^{-2} (b), relative cathode ECSA (c), and relative anode ECSA (d).

Preliminary trials at 70°C/20% RH and 95°C/30% RH were conducted and then stopped due to technical issues before 14 days. Nevertheless, comparison on the first few days can be made to assess AST reproducibility. Regarding performance, relatively similar evolutions were observed at 0.7 V and 1.5 A.cm^{-2} under identical conditions. For the MEA aged at 95°C/30% gas RH, the performance at day 0

determined the relative performance evolution, as similar trends were observed when no performance increase occurred after the first day of AST. Regarding electrode state, the relative evolution is almost identical under fixed conditions, demonstrating good reproducibility of the measurements.

These results demonstrate overall that the *in situ* characterizations and performance monitoring are reproducible and that the AST protocol enables controlled aging of the MEA over the period investigated (additional long-duration tests are required to confirm its robustness over the full 14-day timescale). Moreover, this confirmed that no significant trends in relative performance across different operating conditions can be assessed, but that ECSA measurements are valid and partly confirm the trends mentioned above.

3.2 Post-mortem analysis

To extend the analysis, post-mortem characterization of the IRD MEA was performed in order to provide a more detailed understanding of the trends observed during *in situ* AST, as well as to identify potential degradation phenomena not accessible through *in situ* characterization techniques. In relation to the performance evolution reported in figure 5.3, the 95°C/50% RH and 70°C/20% RH conditions were selected for optical microscopy, scanning electron microscopy (SEM), and energy-dispersive X-ray spectroscopy (EDS) analyses for which the analyses were carried out by our partners at LEPMI. In addition, the MEA aged at 95°C/20% was characterized by transmission electron microscopy (TEM) by our partners at CEA, in view of the significant decrease in anode ECSA observed exclusively at high temperature and slightly more pronounced at 20% than at 50% relative humidity (figure 5.4(b)). TEM was specifically employed for this MEA to further investigate potential changes in platinum particle size, as well as other possible structural evolutions. All measurements were carried out by the project partners (LEPMI and CEA).

Optical microscopy and SEM characterizations were performed in two distinct regions corresponding to the air inlet and outlet, referred to as Seg#3 and Seg#18*, respectively (figure 5.12), for all analyzed MEA. The same regions were also investigated for the pristine reference MEA.

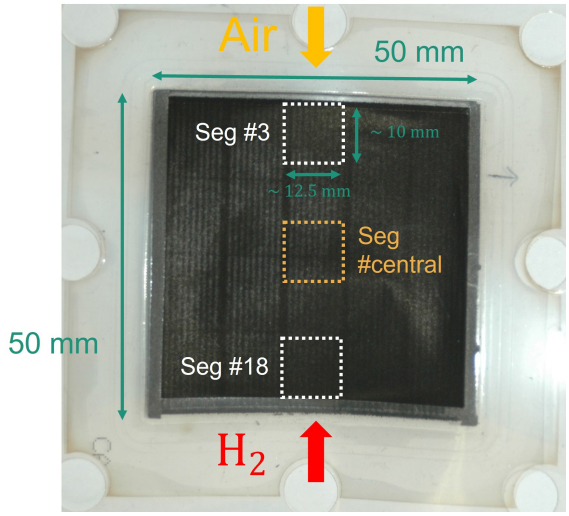

FIGURE 5.12 – Illustration of an MEA showing the regions of interest selected for optical microscopy and SEM analyses (seg #3 and #18) & TEM measurements (seg #central), together with the gas flow direction during fuel cell operation.

The cross-sectional observation of the MEA revealed significant variations in electrode thicknesses shown by the optical image (figure 5.13(a)). Layer thicknesses were determined through image post-processing based on grayscale level detection, enabling thickness mapping of the different layers. The resulting thickness distributions are presented as violin plots in figure 5.13(b), highlighting significant variations in electrode thicknesses and confirming the optical observations, which reveal a pronounced heterogeneity in ink deposition during MEA fabrication. Due to this high heterogeneity in the pristine state, any membrane thickness variation of less than or equal to 30% after AST cannot be considered reliable and therefore may not be regarded as significant.

*. The segments refer to the position within the segmented cell used in chapter 2, section 5

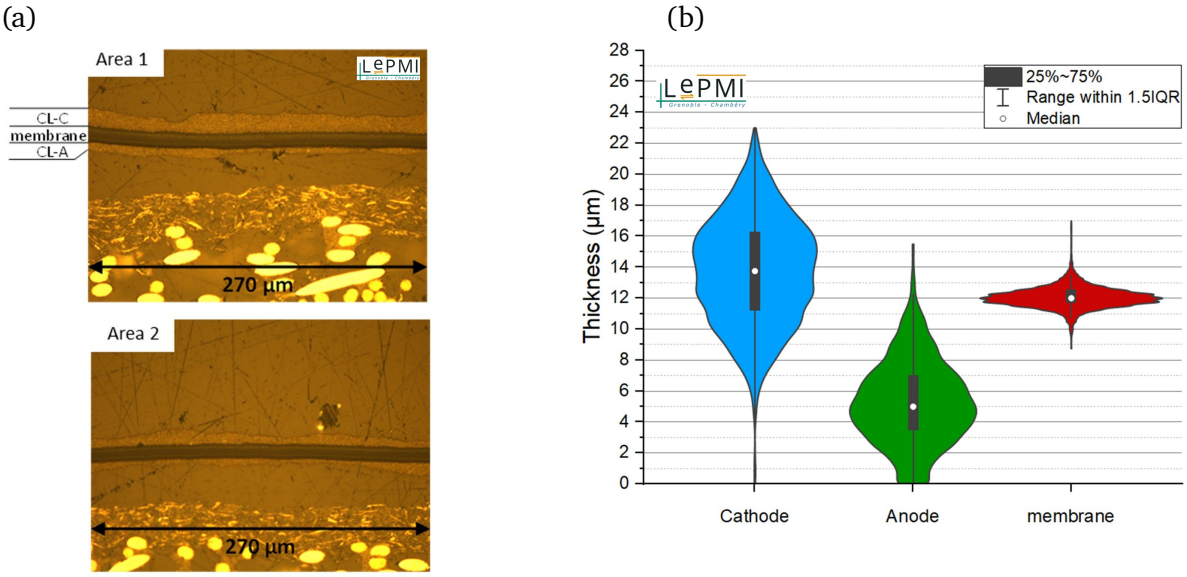

FIGURE 5.13 – Optical image of a pristine MEA in two different areas of the same segment (a) and thickness distributions of the cathode, anode, and membrane layers of the pristine MEA (b).

Using the same analysis approach, membrane and electrode thicknesses of the MEA after AST performed under 95°C/50% RH and 70°C/20% RH conditions were measured in the same regions (Seg#3 and Seg#18). The variations relative to the pristine MEA are summarized in table 5.5. The following observations can be highlighted :

- No significant variation in membrane thickness was observed for the MEA aged at 95°C/50% RH, in agreement with the stable permeation and R_{hf} values recorded throughout the 14 days of AST (figure 5.5). In contrast, the MEA aged at 70°C/20% RH exhibited an average membrane thickness increase of approximately 1 µm, with localized regions in Seg#18 showing increases of up to 3 µm. These observations suggest that the slight increase in R_{hf} measured at the end of the AST may be significant. To further support this hypothesis, additional analyses of the membrane chemical structure and morphology are required and will therefore be considered in future work.

- Regarding the electrodes, the measured mean thickness variations remained smaller than the thickness heterogeneity observed in the pristine MEA, making the interpretation of potential electrode thinning not clearly interpretable. Thus, as a precaution, these cases will be classified as *'difficult to conclude'* in table 5.5. Consequently, it is difficult to correlate the decreases in cathode and anode ECSA measured during fuel cell operation with possible variations in electrode thickness. An exception was, however, identified for seg #3 of the MEA aged under 70°C/20% RH conditions, which exhibited a severe decrease in cathode thickness (greater than 80% relative to the average pristine value). As this pronounced decrease was not observed in seg #18, these results may indicate heterogeneous degradation within the MEA, possibly associated with the gas flow direction. These observations highlight the need for further investigations over a larger number of regions, which may additionally improve correlation with the *in situ* measurements. Future work should also include experiments in a segmented cell configuration, in order to improve the correlation between post-mortem segment analysis and local electrochemical characterization.

	Thickness change		
	Anode	Cathode	Membrane
95°C/50% RH Seg #3	*difficult to conclude*	*difficult to conclude*	None
95°C/50% RH Seg #18	*difficult to conclude*	*difficult to conclude*	None
70°C/20% RH Seg #3	*difficult to conclude*	Decrease (-80%)	Slight overall swelling (+1 μm)
70°C/20% RH Seg #18	*difficult to conclude*	*difficult to conclude*	Slight overall swelling (+1 μm) *with some localized swelling (+3 μm)*

TABLE 5.5 – Membrane, anode and cathode thickness changes, compared to pristine MEA, of the aged MEA under 95°C/50% RH or 70°C/20% RH of seg #3 and seg #18.

In addition to optical microscopy, scanning electron microscopy (SEM) and energy-dispersive X-ray spectroscopy (EDS) analyses were performed to investigate the morphological evolution of the MEA and to assess potential platinum migration within the membrane. Figure 5.14 unambiguously shows migration of platinum into the membrane with the presence of a platinum band in the aged MEA (figure 5.14(c-d)), as observed by SEM and confirmed by EDS elemental mapping of Pt. The platinum band was not observed in the pristine MEA (figure 5.14(a-b)) confirming that platinum migration occurred during the AST.

A closer examination of the MEA cross-section after AST at 95°C/50% RH reveals the presence of a dark region within the cathode at the membrane interface, which appears to be a Pt-depleted area. Upon closer inspection of this region, as shown in figure 5.15, a detailed zoom with an analysis of the grayscale levels of the cross-section confirm that this region is indeed depleted in Pt (named as Pt depletion zone). Using this grayscale-based analysis approach, it was possible to investigate the presence or absence of Pt bands and Pt depletion zones across all aged samples with the corresponding results reported in table 5.6. The presence of a platinum band within the membrane was detected for both AST conditions and in both segments (seg #3 et #18). However, a greater platinum band thickness is observed after aging at 95°C/50% RH. For this aging condition, a Pt depletion zone is also identified within the cathode at the cathode–membrane interface, which is not observed for the 70°C/20% RH condition. This may suggest that, at 95°C/50% RH, the system undergoes a more advanced and severe degradation state, leading to significant platinum migration and resulting in Pt depletion within the electrode. Nevertheless, regardless of the underlying mechanism, the strong differences observed between the samples aged at 95°C /50% RH and 70°C/20% RH do not appear to explain the cathode ECSA loss, which is similar for both MEA (figure 5.4(a)).

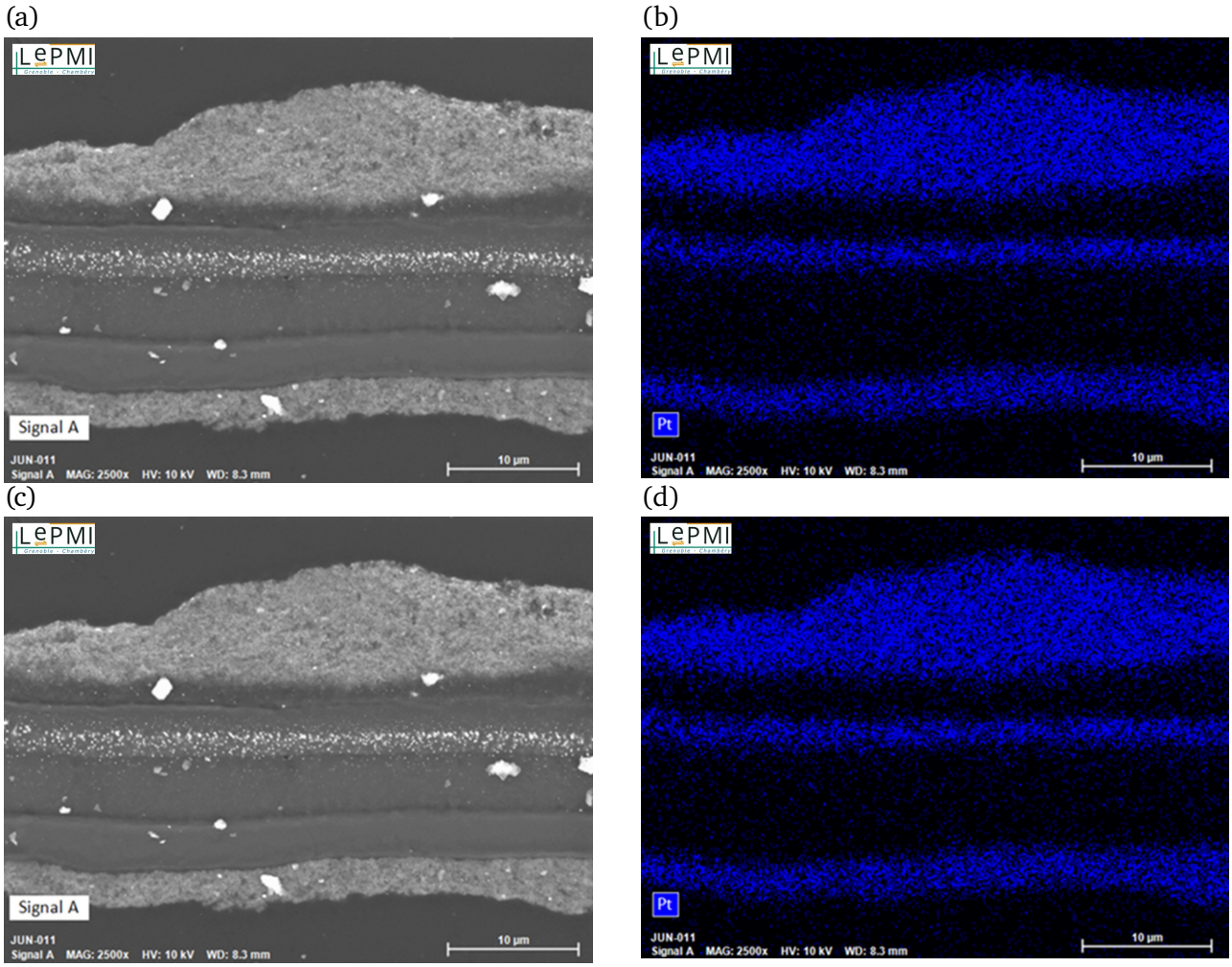

FIGURE 5.14 – Cross-section SEM images and corresponding EDS elemental map of Pt with cathode on top of : pristine MEA (a), (b) and MEA after AST under 95°C/50% RH condition (c), (d).

	Evidence of platinum migration	
	Pt band (in the membrane) thickness	Pt depletion zone (in the cathode thickness)
95°C – 50% RH Seg #3	2.2	1.4
95°C – 50% RH Seg #18	3.5	1.3
70°C – 20% RH Seg #3	1.2	None
70°C – 20% RH Seg #18	1.1	None

TABLE 5.6 – Evidence of platinum migration, through measurement of : Pt band thickness in the membrane and Pt depletion zone in the cathode, of MEA after AST under 95°C/50% RH or 70°C/20% RH of Seg #3 and Seg #18.

To establish more robust conclusions and better understand this depletion phenomenon, further analyses are required. In this context, a second TEM study was performed on the MEA aged at 95°C/20% RH. This was done, first, to confirm the presence of the depletion zone at 95°C under different humidity conditions, and second, to investigate platinum particle size evolution, as this sample

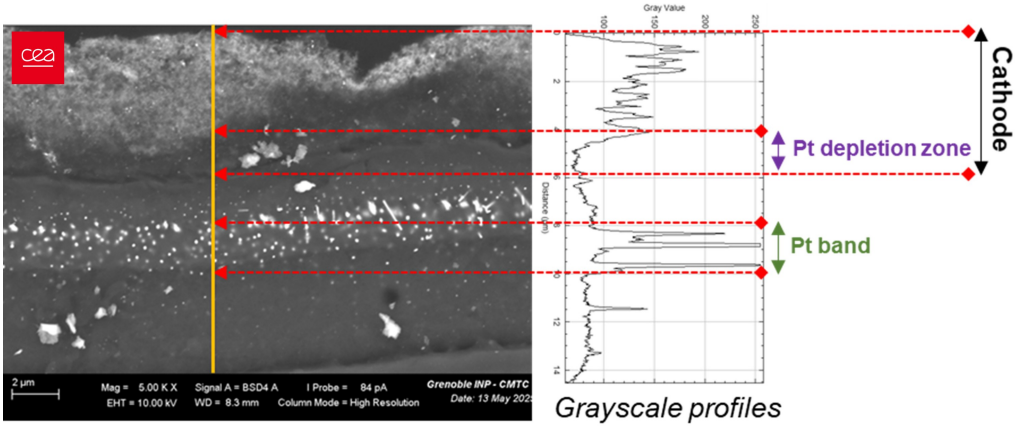

FIGURE 5.15 – Zoomed SEM image of the MEA after AST under 95°C/50% RH conditions with grayscale profiles of the cross-section (yellow line) highlighting the Pt band and Pt depletion zone.

exhibits the most pronounced anode ECSA loss. The TEM cross-section of the MEA first reveals the presence of a platinum band within the membrane (figure 5.16(a)), as well as the confirmation of a Pt depletion zone in the cathode (figure 5.16(b)). The TEM analysis confirmed, in agreement with the SEM observations, that no depletion zone is present in the anode (figure not shown here).

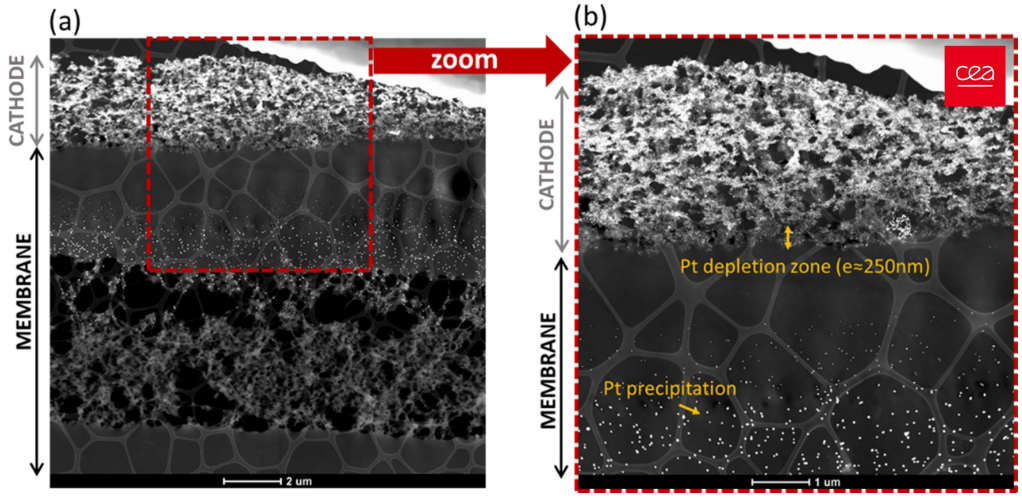

FIGURE 5.16 – TEM image of cross-section of MEA after AST under 95°C/20% RH (a) and zoomed TEM image to underline Pt depletion zone & Pt precipitation in the membrane (*i.e.*, Pt band) (b).

A closer view of the cathode near the membrane interface (figure 5.17(b)) reveals a region depleted in Pt particles-absent in the pristine MEA (figure 5.17(a))-confirming the ~250 nm depletion zone observed in figure 5.16(b). This depletion is exclusively located at the cathode/membrane interface, as the TEM image of the cathode at the MPL side (figure 5.17(c)) does not show any evidence of Pt depletion. A comparison of the Pt depletion zone thickness in the cathode measured by SEM for 95°C/50% RH and by TEM for 95°C/20% RH, with values of approximately 1.3–1.4 µm and 250 nm respectively, suggests that relative humidity influences the extent of this depletion zone. Indeed, higher humidity appears to be associated with a larger depletion zone thickness. This observation requires further confirmation through analysis of MEA aged under 95°C/30% RH conditions as well as through AST repeatability tests.

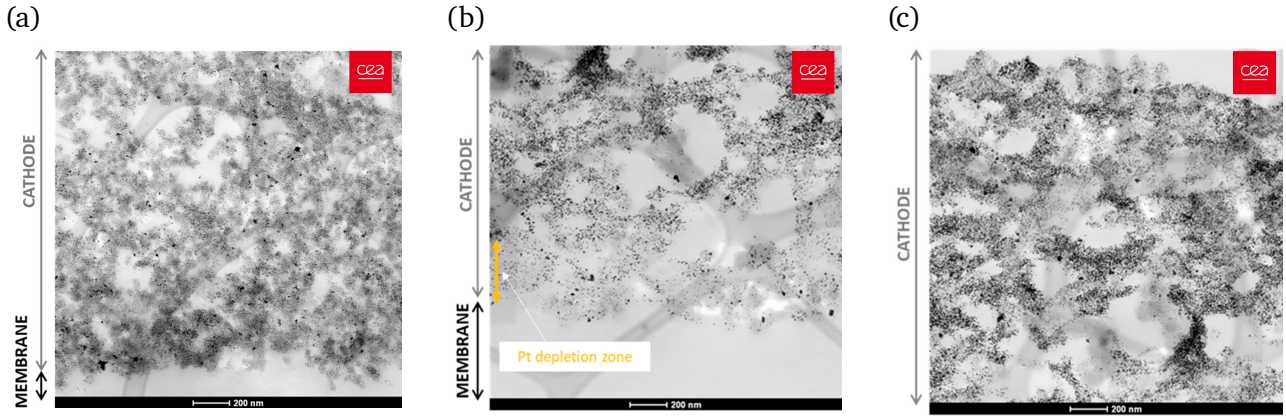

FIGURE 5.17 – TEM image of pristine MEA (a) & of MEA after AST under 95°C/20% RH at the interface cathode/membrane (b) and at the interface cathode/microporous layer (MPL) (c).

In addition to the Pt depletion zone observed in the cathode, a significant growth of Pt nanoparticles (NPs) is observed after aging at 95°C/20% RH, as evidenced by the TEM images in figure 5.18(b-c). This increase in particle size is found both in the cathode at the membrane side-*i.e.*, within the depletion zone-figure 5.18(b) and in the cathode at MPL side (figure 5.18(c)), indicating that Pt particle growth occurs throughout the entire cathode thickness and is not specific to the depletion zone. A quantitative analysis of particle size distribution should be performed to more precisely evaluate the extent of Pt nanoparticle growth, and extended to other aging conditions. This would help determine whether this phenomenon could account for the ECSA loss observed during fuel cell operation. Even though an additional indication could suggest that the loss of ECSA cannot be directly correlated with an increase in particle size and/or Pt depletion, it may also point toward the existence of multiple degradation mechanisms leading to ECSA loss, with or without Pt nanoparticle growth. Indeed, for this aged MEA under 95°C/20% RH which showed a significant decrease in anode ECSA (figure 5.4(b)), no increase in Pt particle size is observed (figure 5.19).

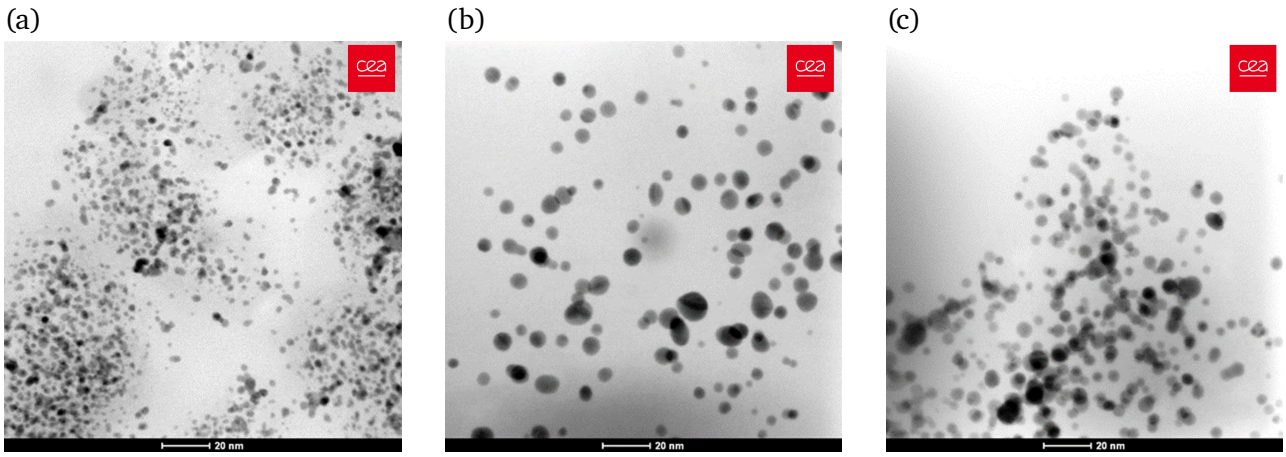

FIGURE 5.18 – TEM image of pristine cathode (a) & of cathode after AST under 95°C/20% RH at membrane side (b) and at microporous layer (MPL) side (c).

(a) (b)

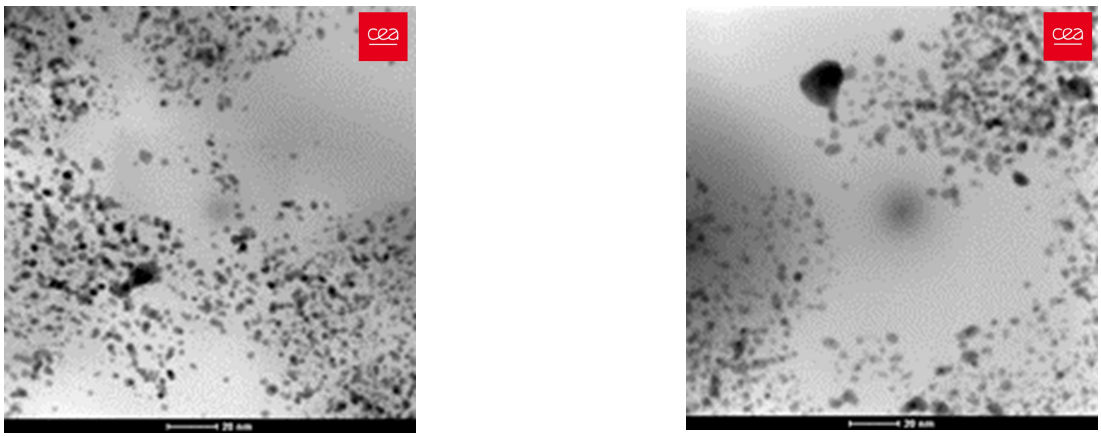

FIGURE 5.19 – TEM image measured in the middle of the MEA of pristine anode (a) & after an AST conducted at 95°C/20% RH (b).

In conclusion, post-mortem characterization does not account for all *in situ* observations related to electrode evolution and the effects of temperature and/or humidity. This is partly due to the difficulty in accurately assessing thickness variations after AST, as a result of the inherent heterogeneity already present in the pristine MEA (linked to the electrode coating process), and partly due to the complexity of degradation phenomena in fuel cells. A given *in situ* performance loss, such as ECSA reduction, may indeed result from different underlying material degradation mechanisms.

Nevertheless, these analyses represent a complementary tool, both to propose hypotheses and to identify trends correlated with *in situ* observations. For instance, the decrease in cathode ECSA at 95°C is more pronounced when increasing relative humidity from 20 to 50% (figure 5.4(a)). In this context, post-mortem analysis reveals the presence of a Pt depletion zone in the cathode with a greater thickness observed for the MEA aged at 50% relative humidity.

Furthermore, post-mortem characterization provides an additional and essential perspective beyond the correlation between *in situ* observations and material evolution in the MEA. It enables the identification of degradation phenomena that are either not detected, or not readily detectable, under *in situ* AST conditions, or that exhibit variations too small to be considered significant. For example, in the case of the AST at 70°C/20% RH, the increase in membrane thickness (table 5.5), suggesting possible membrane degradation, provides new insight into the slight change in R_{hf} observed (figure 5.5(b)).

3.3 Summary and discussion

The operating conditions applied during the AST aimed to evaluate the effect of temperature at constant gas humidity, as well as the effect of gas humidity at higher operating temperature. Significant decreases in performance were observed in all cases, and the states of the membrane and electrodes were analyzed through *in situ* and post-mortem measurements. Based on the previous results, the following conclusions can be made :

Temperature effect

No significant temperature effect on fuel cell performance loss trends was observed under the applied AST conditions. Increasing the temperature at 50% RH led to higher relative performance losses, although these remained close to those observed at 70°C/20% RH. Moreover, the comparison

with the MEA aged at 95°C/20% RH proved challenging due to the improvement in performance observed after the first day of AST. The additional test, during which no improvement in performance was observed after one day of AST, revealed higher relative performance losses, further complicating the comparison.

Regarding component states, the effect of temperature affected cathode ECSA only at 20% RH, where a smaller decrease was observed at 95°C. In contrast, a systematic decrease in anode ECSA was observed at higher temperature. Thickness measurements do not allow definitive conclusions to be drawn, as large deviations were already observed for the pristine sample. Nevertheless, significant thinning of the cathode electrode was observed for the MEA aged at 70°C/20% RH. Regarding thickness variations on the anode side, no conclusions could be drawn, despite the systematic decrease in anode ECSA. These results were not surprising, since the AST to which the MEA was subjected did not include high-potential excursions that may lead to excessive carbon corrosion and thus cathode catalyst layer collapse. Nevertheless, this first part of the chapter highlighted the difficulty of correlating performance losses with ECSA degradation. Additional measurements to assess electrode composition could provide insight into structural changes within the electrodes, particularly on the anode side, where the mechanism responsible for the decrease in ECSA could not be identified.

Regarding the membrane, permeation values and R_{hf} values remained stable, in agreement with the unchanged membrane thickness. Only the MEA aged at both temperatures and 20% RH exhibited slight membrane swelling, more pronounced at the air outlet at 70°C, consistent with a progressive increase in Rhf. Moreover, greater degradation was observed at 70°C/20% RH compared to AST conditions at higher operating temperature. This highlights the limitations of the applied AST conditions, in which mechanical aging is highly dependent on operating parameters. The aging profile presented in figure 5.20 shows that the MEA underwent severe hydration cycling at 70°C/20% RH (see the voltage undershoot after the OCV period) due to high reactant flowrate, whereas no such mechanical stress was observed at 70-95°C and 50% RH. In contrast, aging under 95°C/20% RH induced mechanical stress due to rapid hydration/dehydration cycling during the short (2-3 s) high current/OCV periods. Conditions promoting drying corresponded to MEA that exhibited a progressive increase in Rhf, suggesting a possible coupled chemical/mechanical degradation.

Gas relative humidity effect at higher operating temperature

Relative current density and voltage measurements during the AST did not show a consistent trend, with very similar relative losses after 14 AST days. However, a larger decrease in cathode ECSA was observed at higher RH, whereas stronger anode ECSA losses occurred at low RH. This behavior is consistent with several studies reporting greater cathode ECSA loss under higher water content [21, 22], due to higher water-activity, which may lead to an increased Pt dissolution and oxide formation. This was confirmed by post-mortem characterization, which revealed a thicker Pt depletion zone with increasing gas RH. Note that a different mechanism likely explains the opposite trend observed on the anode side. As mentioned previously, one possible explanation is a higher H_2O_2 formation rate at low gas RH, which could enhance Pt degradation, via ionomer binder degradation. Several studies have reported increased membrane thinning, and thus greater chemical degradation, near anode electrodes defects and delamination, potentially associated with higher H_2O_2 formation on the anode side [9, 17]. However, no analyses could be conducted to test this hypothesis. Similarly, to the effect of temperature, the membrane state remained stable after 14 days, as indicated by stable permeation value, although a slight increase in R_{hf} was observed at lower gas humidity. This could indicate lower membrane stability under drier conditions, even though it was previously noted that mechanical cycling induced by this AST was more pronounced at low humidity. Post-mortem analyses revealed slight membrane swelling, which may be attributed to the more pronounced hydration/dehydration cycling observed through the

aging profile (figure 5.20).

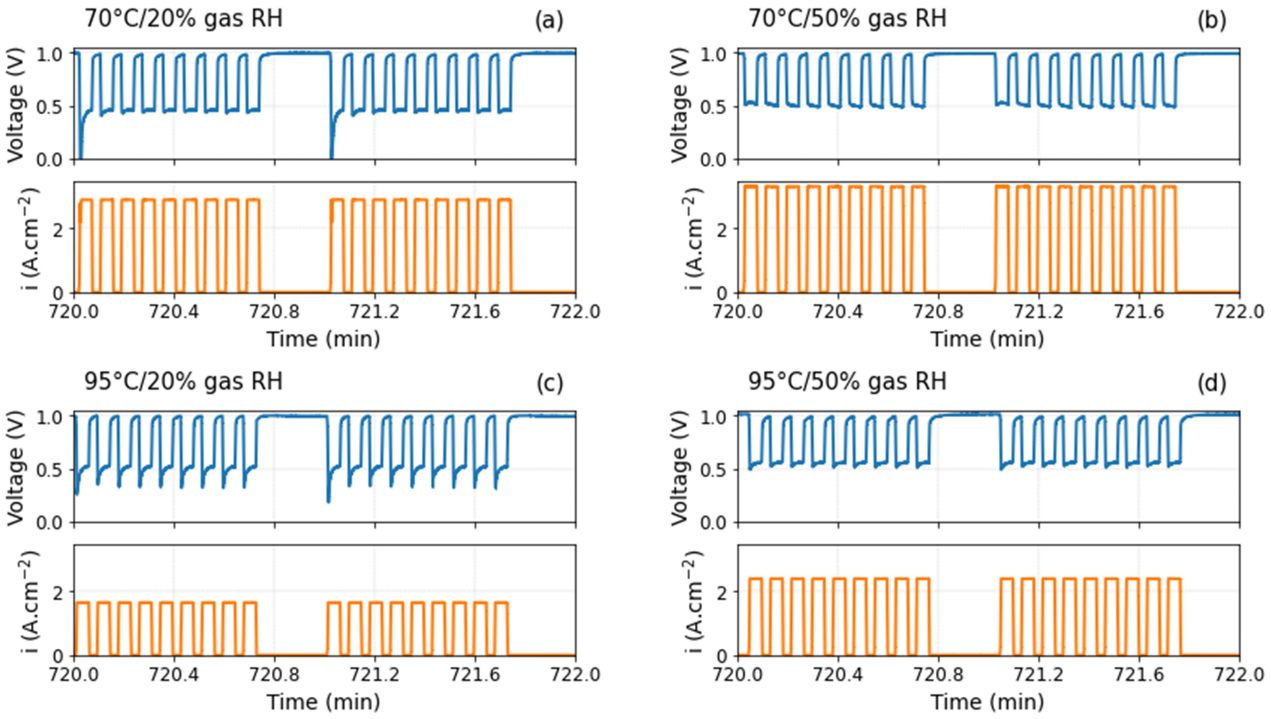

FIGURE 5.20 – Aging profile during the AST on MEA aged at 70°C/20% RH (a), 70°C/50% RH (b), 95°C/20% RH (c), and 95°C/50% RH (d).

Conclusions

The AST applied in different temperature/RH conditions revealed no significant effect of temperature on MEA performance durability. Although no effect was observed on cathode ECSA, the systematic degradation of anode ECSA suggests that different degradation mechanisms may occur at higher temperatures. We also observed that the correlation between *in situ* measurements and post-mortem analysis via SEM measurements is complex and therefore requires complementary measurements. Regarding the effect of gas humidity, a decrease in cathode degradation was observed with decreasing gas humidity, whereas similar anode degradation was reported across conditions.

In all cases, the membrane remained overall stable, as indicated by the low variations in membrane permeation and R_{hf}. Nevertheless, these observations are valid for this commercial MEA under the applied aging conditions. Indeed, the application of alternative AST protocols could result in more significant MEA degradation, whether originating from chemical, mechanical, or coupled chemical/mechanical stressors.

4 Comparison with alternative membrane ionomers

Comparison with sPEEK and NR211 membranes was carried out using IRD MEA durability as a reference. As mentioned in the previous chapter, the sPEEK ionomer cannot operate with satisfactory performance at 95°C, at least without additives [23] enhancing water content and proton conductivity. Durability measurements were therefore conducted at 70°C and 50% RH. This study is divided into several parts :

- **The first section** focuses on evaluating the effect of sPEEK pretreatment with the commercial and the nanostructured one, and compares the durability to that of PFSA ionomer, *i.e.*, NR211 and the state-of-the-art membrane from IRD MEA.
- **The second section** examines the impact of overcoat layers on the GDE as well as the influence of electrode deposition methods on MEA durability.
- **The third section** discusses the results from the two previous sections to provide a global overview of the findings.

4.1 sPEEK durability : effect of pretreatment and comparison with PFSA membranes durability

Durability tests were performed twice for *sPEEK nanostructured* with GDE/*Nafion overcoat* (0.3 $mg.cm^{-2}$) and compared to *sPEEK standard*. Additional comparisons were made with NR211-based CCB MEA using GDE without an overcoat, as well as with IRD MEA. The forward scans of polarization curve were compared (figure 5.21) as severe MEA drying can occur at high current densities (see chapter 4, section 2.5).

The results (not shown here) revealed poor reproducibility : *sPEEK nanostructured* aging tests lasted 8 and 12 days, respectively, before excessive membrane permeation occurred. Although the measured H_2 permeation currents showed only minor differences (0.29 and 0.16 $mA.cm^{-2}$ on the cathode side for the 8 and 12-day AST), a 10-mV difference in OCV was observed at the BoL, suggesting potential defects in the sPEEK membrane. Identifying the origin of this discrepancy is challenging, as several steps precede *in situ* operation. Variability may arise from the pretreatment, the hot-pressing step, or simply from inconsistencies in the materials themselves. Nevertheless, only the MEA exhibiting the longer durability was considered in the subsequent analysis.

Polarization curves show a significant performance decrease for all MEA over time (figure 5.21). However, only the AST on the IRD MEA was stopped at 14 days, as no sign of membrane degradation was detected. PFSA-based membranes exhibited a gradual decline in fuel cell performance throughout the AST, except for the NR211-based MEA, whose performance increased between BoL and day 1. Similarly, sPEEK-based MEA showed an initial performance increase up to a few days, after which their performance began to decline. This behavior suggests that additional adjustments may be required to optimally condition the sPEEK ionomer or MEA, as similar voltage variations were previously observed during the polarization curves measurements in the design-of-experiment optimization (chapter 4). Nevertheless, one major difference compared with PFSA-based ionomers is the presence of stronger voltage fluctuations and a larger voltage drop at EoL in the sPEEK-based MEA.

For easier comparison, current densities and voltage losses at 0.7 V and 1.5 $A.cm^{-2}$ were evaluated to classify performance degradation (figure 5.22). At 0.7 V, the IRD MEA experienced significant current density loss and strong fluctuations as a small variation in voltage induce large variations in current densities. In contrast, sPEEK and NR211-based MEA showed relatively small decreases until excessive membrane permeation few days before the EoL. At medium current densities (1.5 $A.cm^{-2}$), the measured voltages remained relatively stable, indicating stable fuel cell performance over the AST duration.

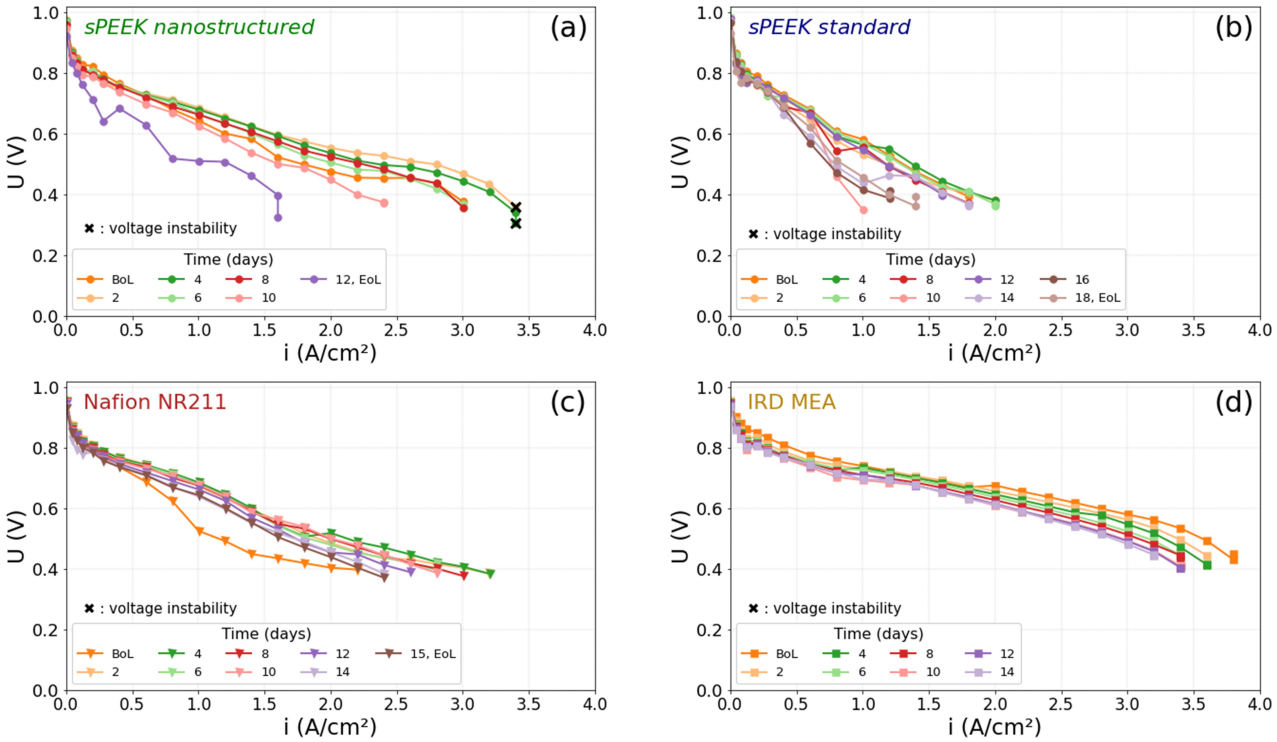

FIGURE 5.21 – Performance evolution during AST at 70°C/50% RH/3 bar and St(H_2/air)=1.25/3 of : *sPEEK nanostructured* MEA (a), *sPEEK standard* MEA (a), NR211 MEA (c), and IRD MEA (d).

A more pronounced decrease was observed for *sPEEK nanostructured* MEA near EoL. In particular, the *sPEEK nanostructured*-based MEA exhibited an abrupt performance drop, most likely associated with membrane failure.

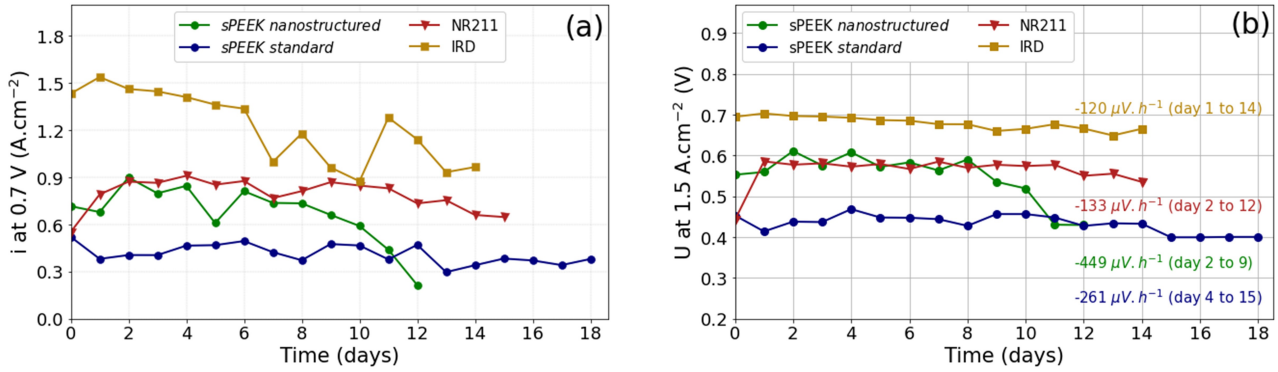

FIGURE 5.22 – Current density and voltage evolution during AST for *sPEEK nanostructured* (green), *sPEEK standard* (blue), Nafion NR211 (red), and IRD MEA (yellow) at 0.7 V (a) and 1.5 A.cm^{-2} (b)

To identify the origin of the fuel cell performance losses, R_{hf}, ECSA, and H_2 permeation current measurements were performed and compared (figure 5.23). Note that ECSA values at the end of the test are not shown when the high H_2 permeation did not allow their measurement. The initial cathode ECSA value of the IRD MEA was significantly higher–approximately 78.2 m^2.g^{-1} compared to 50-55 m^2.g^{-1} for the sPEEK and NR211 MEA, which partly explains its superior performance. For the sPEEK and NR211 MEA, the values were reproducible, with similar initial ECSA levels.

A significant decrease in relative cathode ECSA was observed for all MEA, with a remarkably simi-

lar degradation trend, although the IRD MEA showed a slightly lower decline (figure 5.23(a)). On the anode side, no decrease in anode ECSA was observed for any MEA, indicating the absence of meaningful degradation in the anode catalytic layer (figure 5.23(b)). Overall, the ECSA degradation trends were similar across all MEA. Interestingly, the substantial decrease in cathode ECSA did not correspond to a similar decrease in fuel cell voltage. In fact, an increase in performance was observed over the first few days of AST for both the NR211-and sPEEK-based MEA, despite this period corresponding to the highest ECSA degradation rate. This suggests that additional mechanisms contribute to fuel cell performance degradation until end of life, as the ECSA degradation rate is strongly reduced after a few days of AST. This may be linked to material conditioning or to the MEA hot pressing process. It would be of interest to perform physico-chemical analyses at different aging stages, rather than relying only on post-mortem analyses, in order to achieve a better understanding of the mechanisms occurring during these early stages

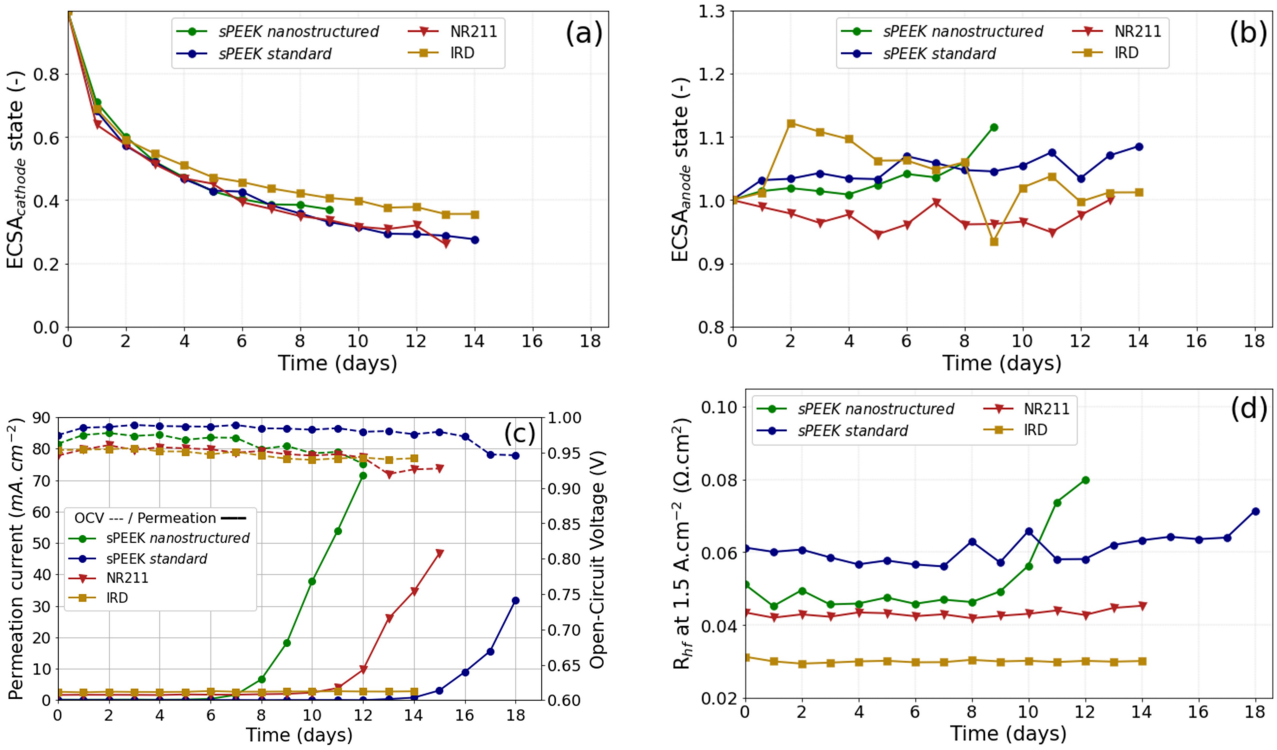

FIGURE 5.23 – Relative ECSA losses on the cathode side (a) and on the anode side (b). Evolution of H_2 permeation current and Open-Circuit voltage (c), and evolution of R_{hf} at 1.5 A.cm^{-2}.

Regarding the membrane state (figure 5.23(c)), higher OCV values and lower H_2 permeation currents were measured for the sPEEK-based MEA at BoL, which is consistent with the intrinsically lower gas permeability of hydrocarbon ionomers. It should be noted that the *sPEEK nanostructured* sample exhibited higher permeation than the *sPEEK standard* one, which may be attributed to its lower thickness and to a more pronounced hydrophilic/hydrophobic phase separation [24]. In contrast, PFSA-based membranes exhibited higher H_2 permeation currents, in agreement with the lower OCV, due to higher gas permeability compared to hydrocarbon ionomers, typically reported in the literature [1, 25, 26]. The IRD membrane exhibited higher permeation than NR211, which can be explained by its lower thickness : 12 µm against 25 µm.
The membrane from the IRD MEA exhibited the highest durability, reflecting its state-of-the-art material design. This is unsurprising given the combined mechanical and chemical reinforcement with the presence of radical scavengers ; and this is of course consistent with the results presented in the first

part of this chapter. The *sPEEK nanostructured* membrane showed the lowest durability, with permeation increasing after 7 days, followed by NR211 (10 days), *sPEEK standard* (16 days), and finally the membrane from IRD MEA, which showed no damage after the 14-day AST.

Although the *sPEEK nanostructured* membrane showed a lower lifetime, it is worth noting that the gap with NR211 durability is not as large as *ex situ* studies might suggest [18], especially considering its reduced thickness (15-18 μm compared with 25 μm for NR211). Interestingly, the *sPEEK standard* membrane exhibited the highest durability among the CCB MEA, which can be attributed to its lower H_2 permeation at BoL. In addition, the AST was conducted under galvanostatic load cycling between OCV and 0.5-0.55 V, determined from the BoL fuel cell performance. However, the substantially lower performance of the *sPEEK standard* MEA resulted in a lower current density range (table 5.5). While voltage cycling resulted in similar ECSA degradation–since the voltage limits were identical–the hydration/dehydration cycles necessarily differ, as water production is lower at reduced current densities. The improved durability of *sPEEK standard* may therefore be linked to reduced mechanical stress, as sPEEK can be significantly affected by RH cycling. Overall, these results remain encouraging for the use of sPEEK in PEMFC applications.

MEA type	*sPEEK nanostructured*	*sPEEK standard*	Nafion NR211	IRD MEA
Load cycling range ($A.cm^{-2}$)	0–1.9	0–1.2	0–2.5	0–3.32

TABLE 5.7 – Load cycling range for all tested MEA

R_{hf} measurements at 1.5 $A.cm^{-2}$ (figure 5.23(d)) partly explain the superior performance of the IRD MEA, which combines a very thin membrane with a well-assembled membrane-electrode interface. The sPEEK-based MEA exhibited higher R_{hf} values, likely due to reduced compatibility between the PFSA overcoat and the sPEEK. However, a notable gap remained between the *sPEEK standard* and *nanostructured* samples, which may be attributed to differences in membrane thickness.

Regarding R_{hf} evolution, the IRD MEA exhibited stable values throughout the AST. A slight increase was observed for both NR211-and sPEEK-based MEA during the final days of the AST, particularly for *sPEEK nanostructured*, corresponding to the period of increased H_2 permeation and thus enhanced degradation. A similar trend was observed for the *sPEEK standard* with relatively stable values until day-12, indicating a stable membrane/electrode interface and a non-degraded membrane. From day-14 to day-18, the strong rise in permeation likely explains the sharper increase in R_{hf}.

Overall, there is no clear evidence of degradation of the membrane/electrode interface, whereas MEA failure can be attributed to membrane degradation, as indicated by the sharp increase in H_2 permeation current prior to the end of the tests. Nevertheless, the state of the interface cannot be conclusively determined, as the stable R_{hf} values may result from two competitive effects : membrane thinning, which decreases the R_{hf}, and interface degradation, which increases it. Therefore, definitive conclusions require post-mortem analyses to visualize the interface and measure membrane thickness.

4.2 Effect of *Nafion overcoat* and electrodes deposit method (CCM) on sPEEK durability

The effects of the electrode deposition method (CCM) and of the *Nafion overcoat* loading on durability were evaluated using the same AST protocol at 70°C/50% RH, in conditions identical to the previous section. All MEA were based on *sPEEK nanostructured*, onto which electrodes were either deposited by coating or applied by hot-pressing GDE with *Nafion overcoat* (0.2 or 0.3 $mg.cm^{-2}$) to improve membrane/electrode adhesion. Two sPEEK-based CCM were tested, showing lower performances than those observed previously (chapter 4), as well as lower lifetimes of 7.75 and 9 days before excessive H_2 permeation occurred. Since these correspond to two CCM batches produced at different times, this

may indicate heterogeneity in the CCM fabrication process, highlighting the potential need to optimize the assembly parameters, which could differ significantly from those used in standard Nafion-based CCM. Nevertheless, despite this heterogeneity, it should be noted that the fabrication of sPEEK-based CCM, thereby eliminating the need for the overcoat required in the CCB process, was a clear success, yielding good performance. To the best of our knowledge, this represents a first report in the literature. Furthermore, two MEA with a 0.2 mg.cm^{-2} overcoat were also tested, showing 10.55-and 12.9-days lifetime before failure.

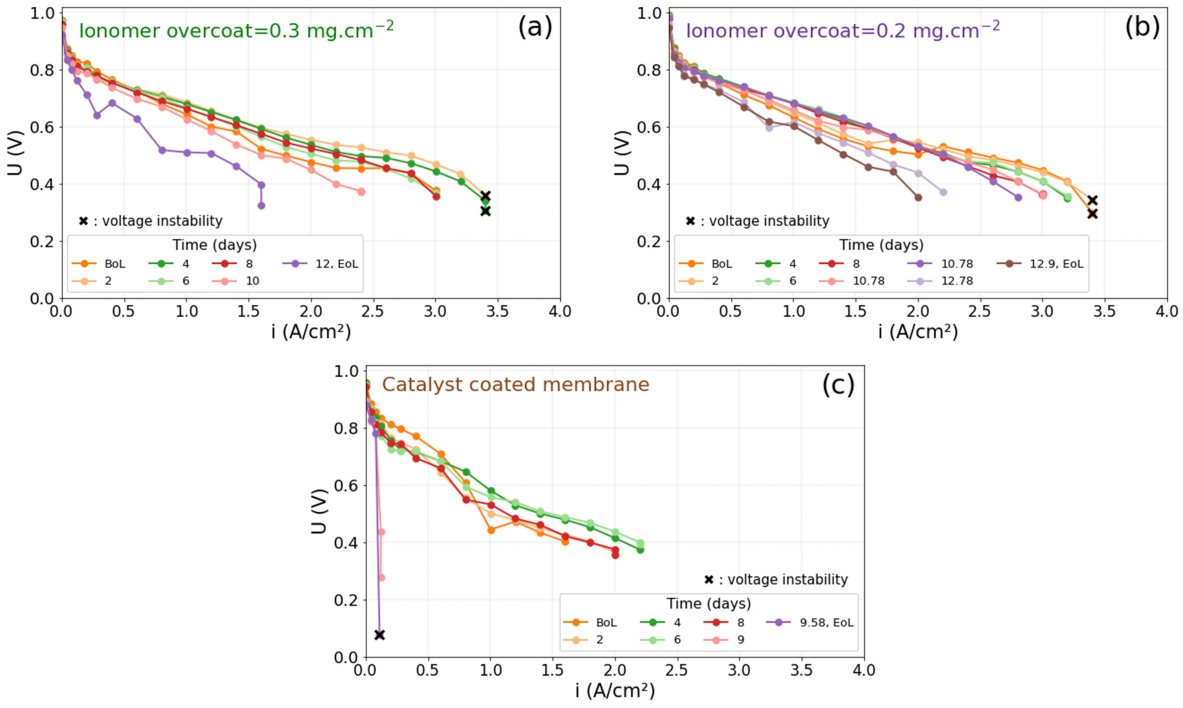

FIGURE 5.24 – Performance evolution during AST at 70°C/50% RH/3 bar of *sPEEK nanostructured* MEA : CCB with 0.3 mg.cm^{-2} ionomer overcoat (a), CCB with 0.2 mg.cm^{-2} ionomer overcoat (b), and CCM from partners (c).

The performance evolution showed improved durability for the MEA with the 0.2 mg.cm^{-2} overcoat (12.9 days), followed by the MEA with the 0.3 mg.cm^{-2} overcoat, and finally the CCM (figure 5.24). Regarding the CCM performance evolution, decreased performance was observed at low current densities, whereas increased performance was measured at medium current densities (1 and 1.5 A.cm^{-2}) during the first 4-6 days, after which a significant decline occurred. Moreover, although performance remained relatively stable over each 24-hour interval, the CCM MEA exhibited a sudden failure at day-9, with almost no current production, whereas the CCB MEA did not reach zero performance by the end of the test. Thus, sPEEK-based CCM exhibited two major drawbacks compared with the CCB configuration incorporating GDE with *Nafion overcoat* : reduced durability and a reliability issue that remains not fully understood, as performance dropped to zero within a single day.

Current density at 0.7 V and voltage at 1.5 A.cm^{-2} showed significant fluctuations at different stages of the AST, the origin of which remained unclear. The CCM MEA exhibited the lowest performances, with a gradual decrease in current density at 0.7 V, whereas the fuel cell voltage remained relatively stable at 1.5 A.cm^{-2}. Overall, fuel cell performance remained stable during most of the AST, until a sharp decrease in both voltage and current density occurred, preceding MEA failure.

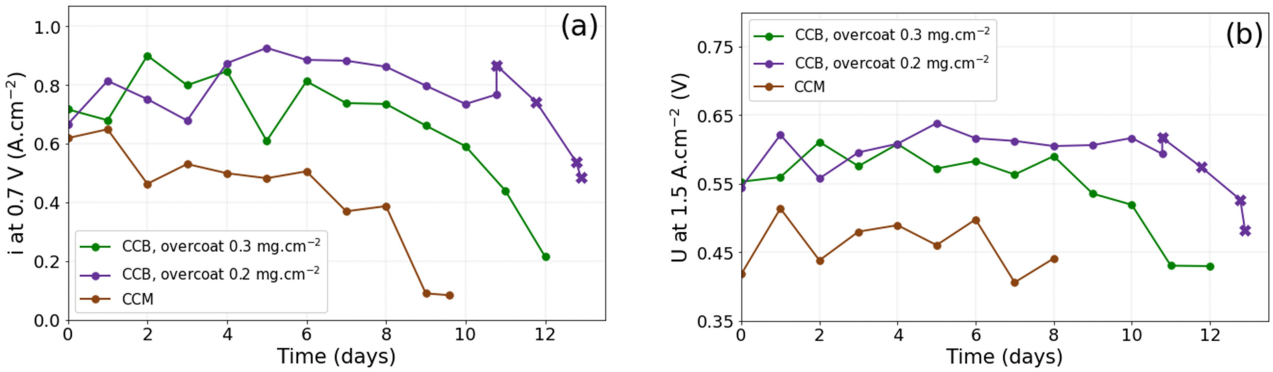

FIGURE 5.25 – i and U evolution over time at : 0.7 V (a) and 1.5 A.cm^{-2}. Cross markers represent the evaluation conducted after the experiment was resumed due to laboratory's closure.

The analysis of performance losses was established using ECSA measurements and H_2 permeation current tests to assess the state of both the electrodes and the membrane (figure 5.26). The objective was to determine the origin of the sudden failure observed in the CCM MEA and to evaluate the effect of the ionomer overcoat.

Regarding the cathode and anode active surface areas, similar behaviors were observed : an exponential decrease in cathode ECSA and stable anode ECSA values. This trend mirrors that of PFSA-based MEA (NR211 CCB and IRD CCM), indicating that the membrane ionomer type, the presence of an overcoat with different loadings, and the electrode deposition method did not significantly affect the relative ECSA losses behavior. It should be noted that the cathode ECSA values for both CCM and CCB MEA were inconsistent at some point due to excessive membrane permeation.

The increase in H_2 permeation with time showed a reduced durability of the CCM MEA compared to CCB MEA, indicated by an earlier onset of increased H_2 permeation after only a few days of AST. In contrast, the CCB with the 0.2 mg.cm^{-2} overcoat displayed significantly higher durability, with H_2 permeation rising only after 10-11 days. In addition, an increased H_2 permeation from 0.32 to 1.66 mA.cm^{-2} was observed after AST resumed, which may have negatively affected MEA durability and may suggest higher durability without interruption. This suggests that the ionomer overcoat may be detrimental for membrane durability, as underlined by Daoudi et al. [18]. In contrast, the CCM fabrication process may require further optimization to improve MEA durability, as the CCM MEA exhibited significantly lower durability, despite being based on the same membrane. Several studies have investigated the introduction of an interfacial bonding layer, such as a gradient composition one [27] or a crosslinked one [28]. These approaches were reported to enhance durability under humidity cycling conditions. OCV parameter is also used to characterize membrane state, although H_2 permeation measurements enable earlier detection of membrane degradation. In all cases, the OCV remained relatively stable, even when the H_2 permeation current had already started to increase. The OCV only began to decrease when the permeation current reached approximately 5-10 mA.cm^{-2}. In practice, OCV variations on the order of 10 mV already correspond to a substantial increase in H_2 permeation–high enough to prevent proper fuel cell operation.

R_{hf} measurements at 1.5 A.cm^{-2} indicated first a globally stable membrane/electrode interface, followed by a significant increase before the EoL, which may be influenced by rising H_2 permeation. At BoL, the R_{hf} measured for the CCM MEA was significantly higher than that of the CCB MEA (results reproduced twice), which may illustrate poor compatibility between the sPEEK membrane and the electrodes, similar to that observed between hydrocarbon ionomers and PFSA [29, 30]. However, lower R_{hf} values were measured under the same conditions during performance mapping, indicating that

further improvements are required to ensure reproducibility in MEA manufacturing. Nevertheless, the CCM MEA exhibited significantly lower durability, suggesting that the use of GDE with *Nafion overcoat* may have a beneficial effect on MEA durability. Indeed, several studies reported that enhancing the cohesion between a PFSA-based electrode and a hydrocarbon-based through an interfacial bonding layer improves MEA durability [27, 28]. However, the Nafion loading must be carefully optimized, as higher durability was observed with a lower loading. Overall, no substantial increase or decrease in R_{hf} was observed during the test, except when H_2 permeation began to rise, suggesting that the limited compatibility between the membrane and the electrodes may not be the primary factor affecting MEA durability. This also indicates that neither sPEEK nor state-of-the-art membranes exhibited conductivity losses, and thus no significant changes in Ion Exchange Capacity (IEC).

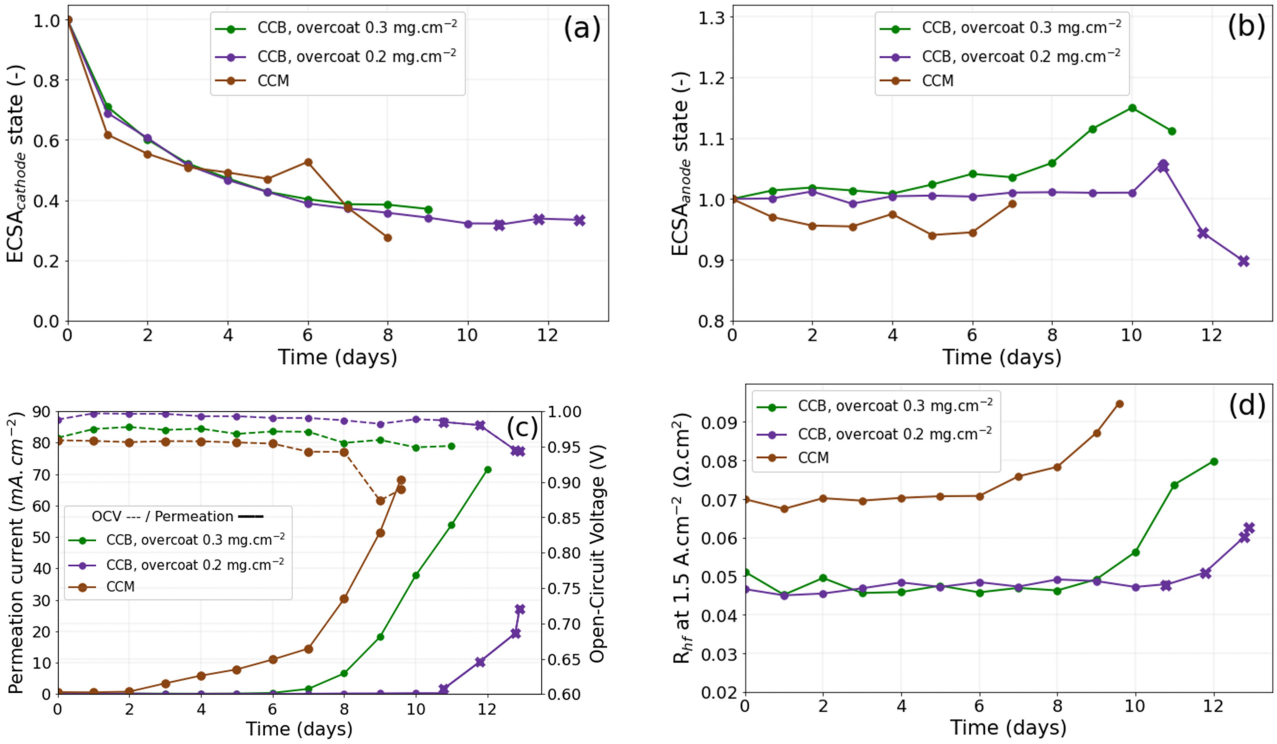

FIGURE 5.26 – Relative ECSA losses over time on the cathode side (a) and on the anode side (b). Evolution of H_2 permeation current and Open-Circuit voltage (c), and evolution of R_{hf} at 1.5 A.cm^{-2}. Cross markers represent the evaluation conducted after the experiment being resumed due to laboratory's closure.

4.3 Summary and discussion

The comparison of state-of-the-art materials with NR211 and pretreated sPEEK highlights the significant progress achieved in their development, resulting in substantially higher and stable performance and durability. The state-of-the-art membrane exhibited a stable hydrogen permeation value, indicating superior integrity after a 14-days AST. In comparison, the NR211-based MEA showed lower durability, with hydrogen permeation starting to increase after 11 days. *sPEEK nanostructured* exhibited lower durability, characterized by an increase in hydrogen permeation starting after 7 days and failure occurring after 12 days. In contrast, *sPEEK standard* exhibited unexpectedly high durability and stable performance, with hydrogen permeation increasing only after 14 days. These results raise several questions as the *ex situ* durability study conducted by Daoudi et al. [18] reported significantly higher chemical durability for NR211 than for sPEEK, particularly for *sPEEK standard*, which exhi-

bited poor stability during chemical degradation tests. Indeed, the differences in durability between *sPEEK nanostructured* and NR211 observed in this study are smaller than those reported by *ex situ* tests, and the higher durability observed for *sPEEK standard* suggests that MEA durability during fuel cell operation is not determined solely by chemical degradation. Several hypotheses may account for the discrepancies between these *in situ* durability results and the *ex situ* degradation data reported by Daoudi et al. [18] :

- **Impact of hydrogen permeation :** hydrogen membrane permeation at beginning of life may be a determining factor for MEA lifetime. *sPEEK standard* exhibited a very low permeation value (0.05 $mA.cm^{-2}$ *vs.* 0.16 $mA.cm^{-2}$ for *sPEEK nanostructured*), which may delay the onset of hydrogen permeation increase and, consequently, chemical degradation. In contrast, hydrogen permeation is much higher for the NR211 membrane (1.64 $mA.cm^{-2}$ at EoL), but this may be mitigated by the higher chemical durability of PFSA, explaining why the onset of permeation increase lies between *sPEEK nanostructured* and *standard*.
- **Non-homogeneous AST conditions :** load cycling conditions are determined by the BoL performance, which defines the current setpoints for cycling between 0.5-0.55V and OCV. As a result, mechanical constraints during wet and dry phases of the AST differ significantly. For NR211, the higher current setpoint (60 A vs. 30 A and 47.5 A for *sPEEK standard* and *nanostructured*, respectively) induces greater water production and thus increased swelling. In addition, it implies higher reactant flowrates, leading to more pronounced drying of the MEA during the OCV phase. Consequently, mechanical aging may be more severe at higher current setpoints, which could explain the higher durability observed for *sPEEK standard*.

Regarding the effect of the *Nafion overcoat*, the results suggest a trend toward higher durability at lower ionomer loading ; however, additional reproducibility tests are required to confirm this observation. This observation is consistent with the work of Daoudi et al. [18], who reported lower durability for NR211-based MEA composed of GDE with *Nafion overcoat* compared to NR211-based MEA with GDE without *Nafion overcoat*. Although no definitive conclusions can be drawn, *Nafion overcoat* loading did not significantly impact electrode aging or the membrane-electrode interface. Nevertheless, differences in OCV may have affected these results, as lower values were generally observed with a 0.3 $mg.cm^{-2}$ *Nafion overcoat*, compared to values above 0.98 V for a 0.2 $mg.cm^{-2}$ *Nafion overcoat*. These differences may arise from variations in the pristine samples, during the pretreatment process, or the ionomer overcoat loading itself. Finally, AST conducted on *sPEEK nanostructured*-based CCM MEA showed poorer durability, with H_2 permeation increasing after only a few days. At this stage, further investigations are required to better understand these results and to extend this work by optimizing the electrode deposition parameters in order to achieve CCM with even higher performance.

5 Conclusions

The durability of state-of-the-art materials was evaluated through AST testing. The IRD MEA, which incorporates a 12 μm reinforced membrane, exhibited a significant performance decline after 14 days of aging, regardless of the temperature and gas inlet RH at which the tests were conducted. Nevertheless, during AST at 70 and 95°C under 20 and 50% RH, performance measurements at different operating points revealed no clear influence of operating temperature. In parallel, *in situ* measurements indicated a substantial decrease in cathode ECSA, with no significant difference between the two temperatures, while the membrane showed no structural degradation, as confirmed by *in situ* characterizations and post-mortem analysis. Overall, increasing the operating temperature from 70 to 95°C did not appear to affect the membrane state under the AST conditions applied in this

study. Indeed, the aging profile is highly dependent on operating conditions and high load setpoint, as mechanical aging is dependent on the reactant flowrate for the drying phases. In contrast, a systematic decrease in ECSA on the anode side was observed at 95°C, whereas stable values were obtained for MEA aged at 70°C.
The effect of gas RH at 95°C was also evaluated through AST conducted at 20%, 30%, and 50% RH. Although no significant impact was observed on overall fuel cell performance evolution or on membrane condition, higher ECSA losses were measured on the cathode side with increasing gas RH, while the opposite trend was observed at the anode. The presence of water therefore appears detrimental to cathode ECSA, possibly due to enhanced platinum oxide formation. In contrast, the higher decrease in anode ECSA at lower gas RH may be related to a lack of water, as such behavior was not observed at 70°C. Under these conditions, the increased gas permeation may promote H_2O_2 production, which is known to be detrimental to electrodes durability.

Globally, increasing cell operating temperature from 70 to 95°C under low to moderate gas RH does not impact membrane state, as observed through R_{hf}, H_2 permeation tests, and post-mortem analyses. Although no impact has been observed on the cathode ECSA, a systematic decrease in anode ECSA was observed. From these observations, three main conclusions can be drawn :

- The AST protocol used does not reveal any significant effect of cell operating temperature, at least within the 70°C-95°C range.
- The applied AST does not allow adequate mechanical or combined mechanical/chemical aging of the MEA. More severe operating conditions or alternative protocols are required to more solicit the membrane.
- The impact of increasing cell operating temperature is not detectable through *in situ* characterizations, except for the anode ECSA, at least over the duration of the applied AST. Post-mortem analyses are therefore necessary to identify potential structural defects in the materials that are not reflected in fuel cell performance over the timescale of the AST.

To confirm these findings, longer AST duration and/or harsher conditions (*e.g.*, lower gas RH) would be necessary.

The replacement of PFSA-based membranes was assessed through accelerated aging using a hydrocarbon-based membrane. sPEEK has long been considered as a promising ionomer due to its mechanical and thermal properties, particularly at higher temperatures. However, performance mapping conducted at 95°C over a wide gas inlet RH range showed that operation was challenging due to poor proton conductivity.

Nonetheless, and since the performances was promising in these conditions (chapter 4), AST were conducted at usual operating temperature on sPEEK membranes pretreated with the Acd-HA-HT72h and Acd-HT1h processes and compared to a reference material and NR211-based MEA. The *sPEEK nanostructured* exhibited relatively stable performance until a sudden failure associated with excessive membrane permeation. Performance evolution indicated that the state-of-the-art membrane is at a significantly more advanced development stage due to mechanical reinforcement and the presence of radical scavengers, showing no sign of deterioration, whereas NR211 exhibited an increase in permeation starting at day 11. In contrast, sPEEK membranes exhibited variable durability depending on pretreatment, likely due to differences in thickness and initial hydrogen permeation values, which may delay the chemical degradation onset.

The effect of *Nafion overcoat* loading on the GDE in terms of durability, as well as the use of sPEEK-based CCM, was also investigated. In this context, CCM fabrication was explored as a means to eliminate the *Nafion overcoat* typically required in the CCB configuration, and was found to be successful. Significantly higher durability was observed with lower ionomer overcoat loading, whereas the lowest durability was obtained for the sPEEK-based CCM MEA. These findings highlight :

- The ionomer overcoat may have a detrimental effect on fuel cell performance, as previously observed by Daoudi et al. [18] on NR211-based MEA. Further measurements are required to understand its potential negative impact on mechanical or chemical MEA integrity.
- The manufacturing process of sPEEK-based CCM may not be sufficiently optimized, and interactions between ink solvents and the membrane may affect sPEEK durability. Indeed, the two tests conducted showed an early increase in hydrogen permeation, particularly sudden in one case. Additional measurements are therefore required to clarify the aging mechanisms and then to optimize the manufacturing process.

Further tests are therefore required to assess the repeatability of the AST results, particularly regarding MEA lifetime. In addition, further AST specifically targeting chemical or mechanical degradation pathways could help determine whether the different configurations are more susceptible to one degradation mechanism over another.

References

[1] V. A. Sethuraman et al., « Durability of Perfluorosulfonic Acid and Hydrocarbon Membranes : Effect of Humidity and Temperature, » *Journal of The Electrochemical Society*, t. 155, n° 2, B119, 2007, ISSN : 1945-7111. DOI : 10.1149/1.2806798

[2] N. Zhao et al., « Effects of Fuel Cell Operating Conditions on Proton Exchange Membrane Durability at Open-Circuit Voltage, » *Fuel Cells*, t. 20, n° 2, p. 176-184, 2020, ISSN : 1615-6854. DOI : 10.1002/fuce.201900173

[3] C. Chen et al., « The Effect of Humidity on the Degradation of Nafion® Membrane, » *Polymer Degradation and Stability*, t. 94, n° 9, p. 1436-1447, 2009, ISSN : 0141-3910. DOI : 10.1016/j.polymdegradstab.2009.05.016

[4] V. A. Sethuraman et al., « Hydrogen Peroxide Formation Rates in a PEMFC Anode and Cathode : Effect of Humidity and Temperature, » *Journal of The Electrochemical Society*, t. 155, n° 1, B50, 2007, ISSN : 1945-7111. DOI : 10.1149/1.2801980

[5] C. Chen et al., « H2O2 Formation under Fuel-Cell Conditions, » *ECS Transactions*, t. 11, n° 1, p. 1127-1137, 2007, ISSN : 1938-5862, 1938-6737. DOI : 10.1149/1.2781025

[6] Y. Lu et al., « Degradation Mechanism Analysis of a Fuel Cell Stack Based on Perfluoro Sulfonic Acid Membrane in Near-Water Boiling Temperature Environment, » *Renewable Energy*, t. 234, p. 121 166, 2024, ISSN : 0960-1481. DOI : 10.1016/j.renene.2024.121166

[7] M. Marrony et al., « Durability study and lifetime prediction of baseline proton exchange membrane fuel cell under severe operating conditions, » *Journal of Power Sources*, t. 182, n° 2, p. 469-475, 2008, ISSN : 03787753. DOI : 10.1016/j.jpowsour.2008.02.096

[8] Y.-H. Lai et al., « Accelerated Stress Testing of Fuel Cell Membranes Subjected to Combined Mechanical/Chemical Stressors and Cerium Migration, » *Journal of The Electrochemical Society*, t. 165, n° 6, F3217, 2018, ISSN : 1945-7111. DOI : 10.1149/2.0241806jes

[9] S. Touhami et al., « Anode defects' propagation in polymer electrolyte membrane fuel cells, » *Journal of Power Sources*, t. 520, p. 230 880, 2022, ISSN : 03787753. DOI : 10.1016/j.jpowsour.2021.230880

[10] M. Daoudi et al., « Impact of Sulfonated Poly(Ether Ether Ketone) Pretreatments on Proton Exchange Membrane Fuel Cells Performances and Durability, » *ECS Meeting Abstracts*, t. MA2022-01, n° 35, p. 1406, 2022, ISSN : 2151-2043. DOI : 10.1149/MA2022-01351406mtgabs

[11] R. Sgarbi et al., « Impact of Transition Metals and Electrocatalyst Layer Thickness on the Pt-Based Cathodes of Proton Exchange Membrane Fuel Cells – Do Multimetallic Electrocatalysts Necessarily Yield an Improved Performance ? » *Advanced Energy Materials*, t. n/a, n° n/a, p. 2 403 212, ISSN : 1614-6840. DOI : 10.1002/aenm.202403212

[12] D. Garcia-Sanchez et al., « Local impact of load cycling on degradation in polymer electrolyte fuel cells, » *Applied Energy*, t. 259, p. 114 210, 2020, ISSN : 03062619. DOI : 10.1016/j.apenergy.2019.114210

[13] G. S. Harzer et al., « Cathode Loading Impact on Voltage Cycling Induced PEMFC Degradation : A Voltage Loss Analysis, » *Journal of The Electrochemical Society*, t. 165, n° 6, F3118, 2018, ISSN : 1945-7111. DOI : 10.1149/2.0161806jes

[14] G. Etienne et al., « On the Main Factors Limiting the Performance of State-of-the-Art Polymer Electrolyte Membrane Fuel Cells in the 90–100 °C Temperature Range, » *Electrochimica Acta*, t. 541, p. 147 320, 2025, ISSN : 0013-4686. DOI : 10.1016/j.electacta.2025.147320

[15] M. Daoudi et al., « Impact of sulfonated poly(ether ether ketone) membranes pretreatments on their physicochemical properties and fuel cell performances, » *Journal of Polymer Science*, t. 61, n° 9, p. 761-776, 2023, ISSN : 2642-4169. DOI : 10.1002/pol.20220649

[16] Z. Zhang et al., « Deciphering Degradation in Porous Transport Layer-Based Hydrogen-oxygen PEMFCs : Insights from 6600-Cycle Operando Durability Tests, » *Applied Energy*, t. 415, p. 127 863, 2026, ISSN : 0306-2619. DOI : 10.1016/j.apenergy.2026.127863

[17] A. Tavassoli et al., « Effect of Catalyst Layer Defects on Local Membrane Degradation in Polymer Electrolyte Fuel Cells, » *Journal of Power Sources*, t. 322, p. 17-25, 2016, ISSN : 0378-7753. DOI : 10.1016/j.jpowsour.2016.05.016

[18] M. Daoudi, « Performances et Durabilité Des Membranes Alternatives Aux Membranes PFSA, » PhD Thesis, Université de Lorraine, 2023.

[19] S. Touhami, « Apparition, détection et propagation des défauts à l'anode des piles à combustible à membrane échangeuse de protons, » PhD Thesis, Université de Lorraine, 2022.

[20] W. Aït-Idir, « Performance et durabilité des piles à combustible basse température à faible chargement en platine, » PhD Thesis, Université de Lorraine, 2024.

[21] N. Ramaswamy et al., « Mitigation of PtCo/C Cathode Catalyst Degradation via Control of Relative Humidity, » *Journal of The Electrochemical Society*, t. 168, n° 12, p. 124 512, 2021, ISSN : 1945-7111. DOI : 10.1149/1945-7111/ac4374

[22] P. Schneider et al., « The Effect of Ionomer to Carbon Ratio and Relative Humidity on Cathode Catalyst Degradation in PEM Fuel Cells, » *Journal of The Electrochemical Society*, t. 170, n° 10, p. 104 505, 2023, ISSN : 1945-7111. DOI : 10.1149/1945-7111/acff1f

[23] M. Vinothkannan et al., « Toward extended durability and power output of high temperature proton exchange membrane fuel cells with Gd2Zr2O7-C3N4 composite membrane, » *Ionics*, t. 32, n° 1, p. 57-68, 2026, ISSN : 1862-0760. DOI : 10.1007/s11581-025-06120-8

[24] H. Mendil-Jakani et al., « Optimization of Hydrophilic/Hydrophobic Phase Separation in sPEEK Membranes by Hydrothermal Treatments, » *Phys. Chem. Chem. Phys.*, t. 19, 2017. DOI : 10.1039/C7CP00087A

[25] M. Han et al., « Accelerated Testing of Polymer Electrolyte Membranes under Open-Circuit Voltage Conditions for Durable Proton Exchange Membrane Fuel Cells, » *International Journal of Hydrogen Energy*, t. 42, n° 52, p. 30 787-30 791, 2017, ISSN : 0360-3199. DOI : 10.1016/j.ijhydene.2017.10.160

[26] D. M. Xing et al., « Characterization of Sulfonated Poly(Ether Ether Ketone)/Polytetrafluoroethylene Composite Membranes for Fuel Cell Applications, » *Fuel Cells*, t. 5, n° 3, p. 406-411, 2005, ISSN : 1615-6846, 1615-6854. DOI : 10.1002/fuce.200500089

[27] H. Y. Jeong et al., « Novel Interfacial Bonding Layers with Controlled Gradient Composition Profile for Hydrocarbon-Based Membrane Electrode Assemblies, » *Journal of Power Sources*, t. 398, p. 1-8, 2018, ISSN : 0378-7753. DOI : 10.1016/j.jpowsour.2018.07.045

[28] M.-J. Choo et al., « New Cross-Linked Interfacial Layer on Hydrocarbon Membrane to Improve Long-Term Stability of Polymer Electrolyte Fuel Cells, » *Electrochimica Acta*, t. 92, p. 285-290, 2013, ISSN : 0013-4686. DOI : 10.1016/j.electacta.2013.01.038

[29] D. M. Yu et al., « Thin Bonding Layer Using Sulfonated Poly(Arylene Ether Sulfone)/PVdF Blends for Hydrocarbon-Based Membrane Electrode Assemblies, » *Electrochimica Acta*, t. 173, p. 268-275, 2015, ISSN : 0013-4686. DOI : 10.1016/j.electacta.2015.05.031

[30] S.-W. Nam et al., « Synthesis and Properties of Bonding Layer Containing Flexible and Fluorinated Moieties for Hydrocarbon-Based Membrane Electrode Assemblies, » *International Journal of Hydrogen Energy*, t. 41, n° 25, p. 10 884-10 895, 2016, ISSN : 0360-3199. DOI : 10.1016/j.ijhydene.2016.04.174

Chapter 6

Ex situ durability measurements in vapor phase

1 Introduction 206
2 Materials & methods 208
2.1 Materials 208
2.2 Methods 209
3 Preliminary tests : sPEEK vs NR211 and parameters adjustment 210
4 Impact of chemical and coupled chemical-mechanical stresses on sPEEK membrane . . . 214
4.1 sPEEK chemical structure 214
4.2 Crystallinity evolution through FTIR measurements 218
4.3 Impact on fuel cell performance 220
4.4 Discussion 222
5 Conclusions 225
References 227
6 Appendix 231

1 Introduction

While *in situ* (*i.e.*, using MEA in single cells or stacks) performance mapping and characterization tests provide valuable insights into MEA behavior, they do not always allow for an accurate assessment of changes in individual material or component properties. They also do not always enable characterization of potential structural changes (morphology, chemistry) that may explain the observed changes in fuel cell performance. These limitations arise from the interdependent degradation pathways of MEA components, which obscure the isolation of membrane specific degradation. Several studies illustrate these coupled failure modes ; different membrane degradation rates have been reported depending on the catalyst type [1], while several studies have shown that defects in the anode catalyst layer can lead to accelerated performance degradation and membrane durability issues [2, 3], as evidenced by a greater reduction in membrane thickness near electrode defects. Similarly, Tavassoli et al. [4] reported increased membrane thinning near local delaminated anode areas, while Taylor et al. [5] suggested that cracks in the Gas Diffusion Electrode (GDE) may contribute to the formation of cracks in the membrane, thereby reducing MEA lifetime. Conversely, Dubau et al. [6] reported that excessive membrane permeation leads to increased H_2 crossover, which in turn promotes significant carbon corrosion.

The chemical, mechanical, thermal, or hydrothermal causes and thus degradation mechanisms of individual components are difficult to assess during *in situ* operation. This has motivated the development of *ex situ* accelerated degradation tests that target specific elements of the MEA and apply controlled/defined stressor(s). A large number of studies have been conducted using these approaches, including chemical aging tests such as the Fenton test [7, 8], hygrothermal test [9, 10], and mechanical tests [11, 12], to better understand membrane degradation mechanisms. In particular, these studies have helped identify the mechanisms responsible for chemical degradation, which originates from the decomposition of H_2O_2 into radical species [13-15] (section 1.5.2 in chapter 1) that attack the chemical structure of the membrane. These findings have helped guide mitigation strategies, for example, the development of PFSA membranes with end-groups free of carboxylic acid functionalities that are prone to chemical degradation, as well as the incorporation of radical scavengers. These *ex situ* approaches also enable direct comparison between different membranes–differing in chemical structure, IEC/DS, pretreatment, or hybridization–under controlled conditions and allow assessment of their durability without interference from other components. For example, Feng et al. [16] reported that PFSA-based membranes-Nafion HP, Nafion 212, and Gore M788.12-underwent significant weight loss and structural changes during Fenton testing, resulting in pronounced performance degradation and increased hydrogen permeation current. Shi et al. [17] observed increased crack propagation with increasing degrees of chemical degradation during mechanical cycling for Nafion 212 and Nafion XL following Fenton tests. Several studies have investigated the effect of pretreatment and additives on the chemical durability of sPEEK by immersing samples in a thermally activated H_2O_2 solution [13, 14]. Enhanced chemical durability was reported with the incorporation of various radical scavengers, as evidenced by lower weight loss and reduced concentrations of degradation products in the resulting solutions [18, 19].

The study of stressors applied exclusively to the membrane has therefore been, and remains, essential. However, to better replicate fuel cell operation, it has become necessary to investigate the effects of combined stressors. *Ex situ* degradation tests have thus been developed by coupling chemical and mechanical stresses to more closely reproduce the conditions encountered in an operating fuel cell, where degradation pathways are inherently coupled. Robert et al. [20] investigated the durability of Nafion XL and Nafion 211 using Fenton tests combined with various mechanical stresses. They observed reduced membrane stability when mechanical stresses were applied, as indicated by an increased fluoride emission rate (FER). Kusoglu et al. [21] reported similar findings, with accelerated degradation under additional mechanical stresses. Although such coupled tests provide a more realistic assessment of

membrane durability, the fuel cell environment remains multiphasic, involving both liquid and vapor states. This strongly affects membrane stability due to changes in physicochemical properties, particularly mechanical properties [22, 23]. It is therefore also important to evaluate ionomer durability under vapor-phase conditions. Several studies have performed *ex situ* accelerated stress tests in the vapor phase and under mechanical stresses [24-26]. While Lai et al. [25] did not observe a significant effect of mechanical stresses in the vapor phase, Yoon et al. [26] reported a higher degradation rate of PFSA membranes, as evidenced by increased FER and changes detected via FTIR measurements when mechanical stresses were added.

The effect of coupled chemical and mechanical degradation, whether on PFSA or sPEEK membranes, is therefore not yet fully understood. Further studies are therefore required, particularly in vapor environments, where comparatively few investigations have been conducted. To address this gap, *ex situ* chemical degradation tests in vapor phase were carried out using a home-made chemical/mechanical degradation test bench designed to generate a controlled vapor environment. H_2O_2 vapor was generated under controlled operating conditions to evaluate the durability of sPEEK ionomer under various chemical and coupled chemical/mechanical stress conditions. Although the chemical durability of sPEEK is lower than that of PFSA [13, 27, 28], its degradation mechanisms in the vapor phase – under either purely chemical or coupled chemical/mechanical stresses – have not yet been thoroughly investigated. Following preliminary tests at high H_2O_2 concentrations in the vapor phase on both PFSA and sPEEK samples, the study focuses specifically on degradation tests of sPEEK membrane. Its durability was investigated under both purely chemical and coupled chemical/mechanical stressors. Post-degradation characterizations were then carried out to assess the impact of degradation on the ionomer's chemical structure, as well as on properties relevant to fuel cell performance.

2 Materials & methods

2.1 Materials

Membranes

The tests were conducted on sPEEK (Fumapem E730) and PFSA (Nafion NR211) membranes. Prior to the experiments, pretreatments were applied (for details, see chapter 4) :

- Regarding the sPEEK membrane, protocols were :
  - (i) an acidification step (HCl at 30°C for 4h) followed by a hydroalcoholic (water/ethanol at 30°C for 24h) and hydrothermal step (water at 80°C for 72h), referred to as *sPEEK nanostructured*.
  - (ii) acidification (H_2SO_4 at 80°C for 16h) and hydrothermal step (water at 80°C for 1h) referred to as *sPEEK standard*.
- For Nafion NR211, the pretreatment consisted of boiling the sample in 3% H_2O_2, soaking in HNO_3, boiling in H_2SO_4, boiling in distilled water (1 hour for each step) before drying at 60°C for 24 hours.

Experimental setup

H_2O_2 generation in vapor phase was controlled thanks to the HPP272 sensor from Vaisala operating from 0 to 2000 ppm with two relative humidity sensors. The first measures the RH induced by water vapor, while the second catalyzes H_2O_2 decomposition into H_2O through a membrane and then measures the resulting RH. The H_2O_2 concentration is subsequently determined from the difference between the two measurements. The H_2O_2 sensor operates over a temperature range of 5-50°C, which prevents placement immediately upstream of the cell, whose temperature can reach values higher than 50°C. Therefore, a specific home-made device was designed to allow us to generate a controlled H_2O_2 vapor sent to a cell which can be installed in a compression testing machine. The device is composed of three main parts : the H_2O_2 vapor flow generator, the mechanically constrained cell where the sample is placed, and the condensation section where the steam flow is condensed (figure 6.1) :

- **H_2O_2 vapor generation :** a small flow of liquid H_2O_2 is injected into this pipe using a syringe pump in drip-injection mode. The entire injected H_2O_2 flow is evaporated within the heating pipe and then conveyed by a controlled dry air flow (flow n°1). Two additional air flows are introduced : one (n°3) is water-saturated via a bubbler at controlled temperature, and the other (n°2) is added directly to the water-saturated flow. Finally, the three flows are mixed before entering the cell. The RH of the total flow is controlled by adjusting flows n°2 and n°3.
- **Mechanically constrained cell :** a 5x5 cm^2 stainless-steel cell with 50 straight parallel channels was used (figure 6.2). Its dimensions were chosen to match those used in the performance and durability studies in the previous chapters to avoid discrepancies arising from differences in cell design. The cell temperature is controlled, and mechanical stress is applied using a compression engine. All mechanical parameters are controlled, including static or cyclic stress, as well as the number and frequency of cycles.
- **Condensation part :** the H_2O_2/water air flow is condensed after the cell using a Peltier condenser. The gas is condensed to allow analysis of the solution, either to verify the H_2O_2 concentration and/or the presence of degradation products.

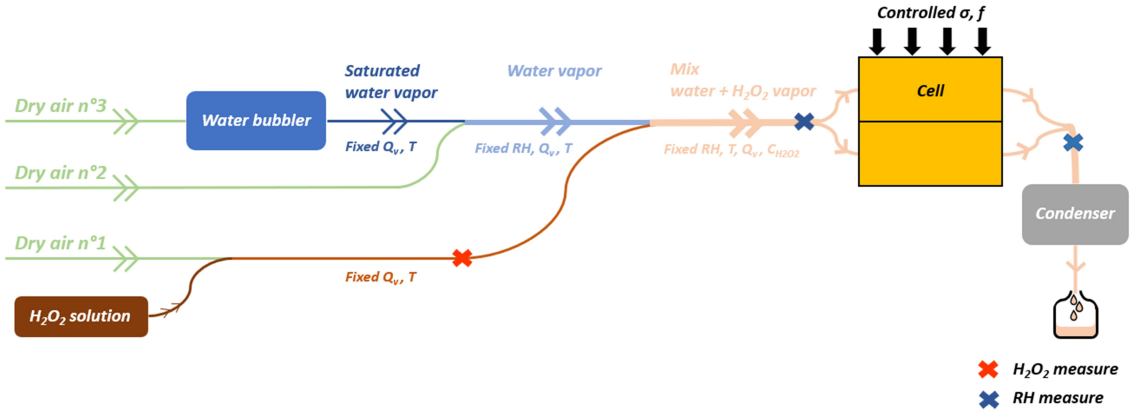

FIGURE 6.1 – Schematic representation of the home-made bench for H_2O_2 generation in vapor phase.

First tests of the bench– without membrane samples-showed fluctuations in the concentration of generated vapor-phase H_2O_2 (noted $[H_2O_2]_{vap}$) over time (example in Appendix 2.1.). The observed fluctuations in the measured H_2O_2 vapor concentration can be attributed to the non-ideal evaporation behavior of aqueous H_2O_2 solutions. The higher volatility of water compared to H_2O_2 leads to preferential evaporation of water, and thus to fluctuations in the composition of the generated vapor over time. The temperature of the pipe where liquid H_2O_2 is injected, the air flowrate used as a carrier gas for the evaporated solution (flowrate n°1), as well as the flowrate of the liquid H_2O_2 solution affect significantly the measured concentration. Some examples of these impacts are provided in the Appendix 2.2. It is therefore important to carry out preliminary tests and adjust the parameters prior to the main study, this constituting the objective of the first part of this work.

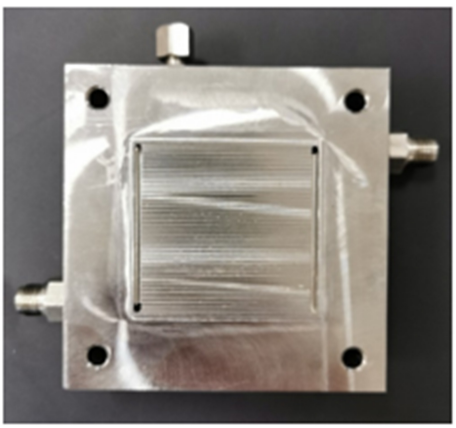

Straight parallel channels	Number of channels	50
	Channels depth	0.5 mm
	Channels width	0.6 mm
	Rib width	0.4 mm

FIGURE 6.2 – Straight parallel channels cell used and its dimensions.

2.2 Methods

Ex and *in situ* characterizations were conducted to assess membrane state and the effect on its structure and performance :

- **1. Attenuated Total Reflectance-Fourier Transform Infrared spectroscopy (ATR-FTIR) :** ATR-FTIR spectroscopy in reflectance mode was used to investigate changes in the ionomer chemical structure. This technique was chosen for its rapid, non-destructive measurement capability, while providing a fast assessment of changes in the degree of sulfonation (DS) of sPEEK membranes, which is a key parameter affecting the membrane's functional properties.

Measurements were carried out using a Bruker ITRF Vertex 80v spectrometer. Each sample was subjected to a dry N_2 flow (1 NL.min^{-1}) for 13 min prior to measurement, to ensure the same drying state for all the samples and enable reliable comparative analysis ; a duration shorter than 13 min did not lead to satisfying results. ATR-FTIR spectra were then recorded from 450 to 6000 cm^{-1} at several points on each sample to ensure reproducibility and evaluate degradation homogeneity. A spectral resolution of 1-2 cm^{-1} and 200 scans were systematically applied for precise measurements.
Deconvolution of FTIR spectra using Gaussian curves was performed to extract area and intensity of individual peaks, allowing us to compare the 1280/1305 ratio, linked to ionomer crystallinity (see section 4.2).

- **2. Ultraviolet-visible (UV-Vis) spectroscopy :** UV-Vis spectroscopy was used to detect and quantify degradation products in the condensed solution. This technique enables the quantification of sPEEK degradation products at 295 nm corresponding to aromatic ring absorption [29] highlighted as a degradation product of sPEEK chemical degradation. UV-Vis spectroscopy was performed on approximately ten condensed solutions of tests for which significant chemical degradation of the membrane was detected by ATR-FTIR spectroscopy.
- **3. *In situ* electrochemical characterizations :** the impact of membrane degradation was evaluated using the same single cell employed for the performance and durability characterizations (chapters 2, 4, and 5). The dimensions and channel geometry were identical to those of the *ex situ* cell. Aged membranes that could be handled were hot-pressed onto Gas Diffusion Electrodes (Freudenberg H14CX653) under 4.5 MPa at 135°C for 210 s. *In situ* characterizations were conducted to assess MEA performance (polarization curve) and membrane state (permeation current test), using fixed test parameters (see previous chapters).

3 Preliminary tests : sPEEK vs NR211 and parameters adjustment

Preliminary tests were performed to evaluate the reproducibility of the H_2O_2 generation setup and to define the concentration range (starting under high-concentration conditions), while also allowing a comparison of the degradation behavior of *sPEEK nanostructured* with that of Nafion. The membranes were exposed to a 45% H_2O_2 solution at a flowrate of 15 µL.min^{-1} in a heated pipe at 160°C with an air flowrate of 60 NL.h^{-1} for 2 hours at 95°C, corresponding to a measured H_2O_2 concentration of 970 ± 278 ppm. The H_2O_2 concentration corresponds to the mean value and fluctuations over the 2 hours tests. As explained previously, a fluctuation on H_2O_2 concentration is systematically observed due to the higher volatility of water compared to H_2O_2. No macroscopic changes were observed for the NR211 membrane, whereas the sPEEK membrane showed significant alteration and a very brittle structure (figure 6.3).

(a) **sPEEK** (b) **NR211**

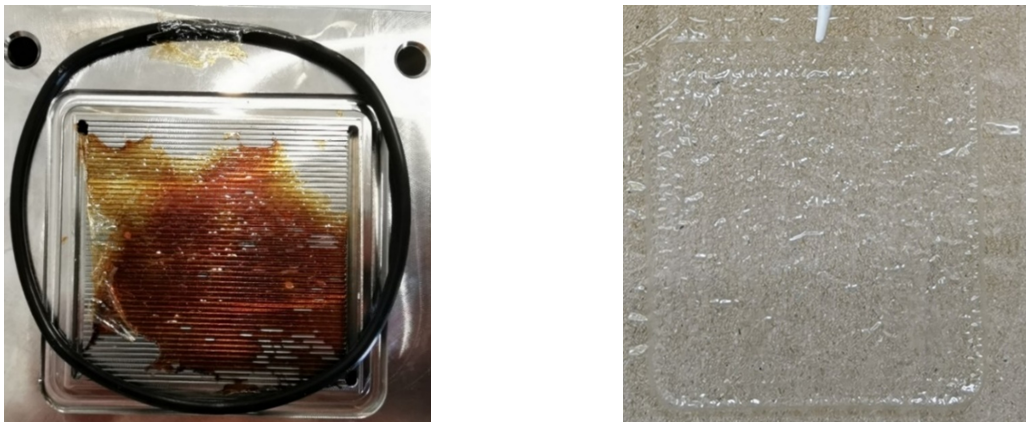

FIGURE 6.3 – *sPEEK nanostructured* (a) and NR211 (b) after degradation under [970 ± 278 ppm] $[H_2O_2\}_{vap}$

Nevertheless, FTIR spectroscopy measurements were conducted on an NR211 sample to assess potential chemical structural changes not visible at the macroscopic scale. Measurements were performed at different locations on the sample, and the spectra were normalized to the characteristic peak at 1145 cm^{-1} corresponding to the CF_2 bond [30-33]. This analysis (figure 6.4) revealed no significant evolution except a slight shift of the peak at 1057 cm^{-1} corresponding to SO_3^- stretching (symmetric) of the sulfonic group.

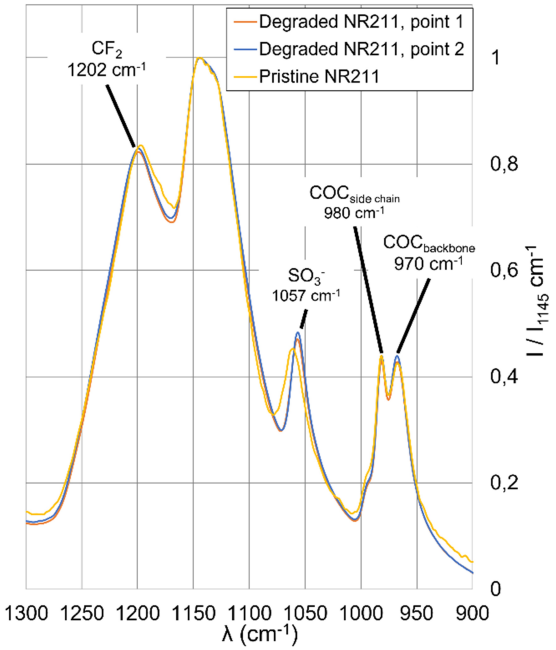

FIGURE 6.4 – NR211 FTIR spectra-with peaks identification based on [30-33] after a 2h degradation under a 970 ± 278 ppm $[H_2O_2]_{vap}$

These preliminary results showed the very good chemical stability of PFSA compounds exposed to high H_2O_2 concentrations, as illustrated by the absence of macroscopic defects and by the lack of significant changes in chemical structure as probed by FTIR analysis. Inducing chemical degradation of the PFSA structure may require harsher conditions, such as longer exposure times and/or the

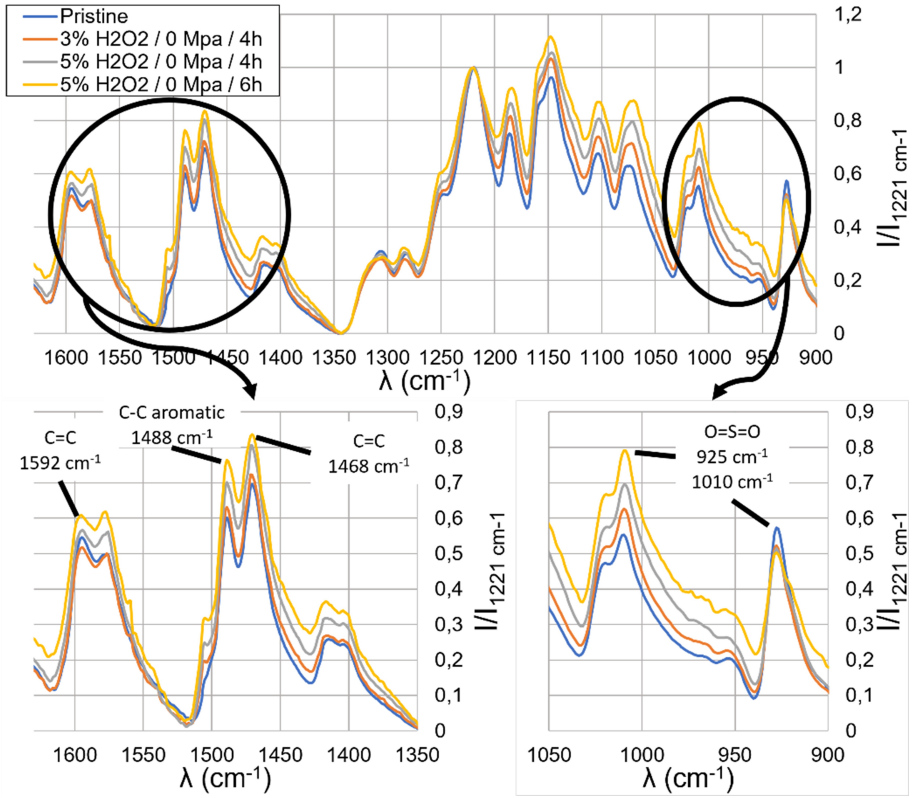

FIGURE 6.5 – : IR spectra of *sPEEK nanostructured* before (pristine) and after exposure to 33 ± 28 ppm $[H_2O_2]_{vap}$ (3% $[H_2O_2]_{liq}$), 116 ± 48 ppm $[H_2O_2]_{vap}$ (5% $[H_2O_2]_{liq}$) during 4h or 6h.

presence of ferrous ions (Fe^{2+}) to catalyze radical formation. In contrast, the significant degradation observed for sPEEK membrane demonstrated the effectiveness of the test bench and also highlighted the lower chemical stability of sPEEK compared to Nafion under vapor phase H_2O_2 exposure, revealing a similar trend to that previously reported in the liquid phase by Daoudi et al. [13]. Based on these observations, subsequent tests therefore focused on the sPEEK ionomer. In addition, the concentration range was reduced, as the initial high concentration (i) led to excessively severe degradation, making post-analyses difficult, and (ii) was intentionally chosen to assess the effectiveness of the test bench.

After further optimization of the operating parameters, *sPEEK nanostructured* membranes were exposed to 33 ± 28 ppm and 116 ± 48 ppm $[H_2O_2]_{vap}$ (corresponding to initial liquid H_2O_2 solutions of 3% and 5%, respectively) at 95°C for a short time at first (4 or 6 hours), with $T_{pipe\ injection}$=150°C / $Q_{air\ carrier}$=60 nL.h^{-1} / $Q_{H_2O_2,liq}$=20 µL.min^{-1}. Under these conditions, the resulting structural changes were investigated by FTIR spectroscopy. The spectra were represented in the region of interest (900 and 1650 cm^{-1}) between which most of the characteristic peaks are present based on literature [34-36]. Significant variations of peak intensity were observed in both the polymer backbone at 1468, 1488, and 1592 cm^{-1} and the sulfonic acid groups at 1010 cm^{-1} highlighting structural changes (figure 6.5).

Although variations in several peaks were observed, the analysis was deliberately focused on those enabling the assessment of changes in the degree of sulfonation (DS), as it plays a key role in the functional properties of the membrane, particularly proton conductivity. Given its direct impact on these properties, DS was used here as the main descriptor to evaluate the effect of degradation. A more detailed interpretation of all peak variations and understanding degradation mechanisms was intentionally beyond the scope of this work. In this aim, the evaluation of the DS was based on Al

Lafi et al. work [34], who investigated the sulfonation of PEEK using FTIR spectroscopy, among other techniques. They demonstrated a strong correlation between the normalized intensity of the 1490 cm^{-1} peak and the DS, measured by NMR, expressed by the following equation :

$$DS = \frac{(1.84 \pm 0.04) - A_{1490}}{(0.0180 \pm 0.0006)} \text{ with } A_{1490} = \frac{I_{1490}}{I_{1600}} \tag{6.1}$$

Based on this equation 6.1, the DS for *sPEEK nanostructured* before and after *ex situ* chemical degradation was evaluated (table 6.1) and highlight significant decreases in all conditions. Significant degradation of sPEEK DS was observed under both H_2O_2 concentrations. Interestingly, for the same exposure time the increase in H_2O_2 concentration-between 3 and 5%-showed not significantly impact on the DS. Similarly, increasing the exposure time to 6 hours only slightly decreased the DS, from 34 to 32%.

Time (h)	$[H_2O_2]_{vap}$ (ppm)	DS (%)
Pristine		40
4	33 ± 28	35
	116 ± 48	34
6	116 ± 48	32

TABLE 6.1 – Estimation of sPEEK DS by FTIR spectroscopy after chemical degradation tests under various H_2O_2 concentrations and times.

Considering these results, which confirmed the feasibility of post-test measurements and highlighted an impact on the chemical structure through variations in the degree of sulfonation (DS), a second phase of operating parameter adjustment was undertaken. This phase aimed to adopt a concentration range consistent with that used by Daoudi et al. [13] in their study of liquid-phase degradation : 0.5 to 3%. In addition, longer exposure times of 8 hours were implemented, with a duration selected to match that employed in the study of coupled degradation of Nafion membranes conducted by Robert et al. [20], in order to enable potential correlations between these studies.

All preliminary tests highlighted that the H_2O_2 concentration measured in the vapor phase strongly depends on the operating parameters ($T_{\text{pipe injection}}$, $Q_{\text{air carrier}}$) and did not match the expected concentration regarding the H_2O_2 solution one injected. Thermal decomposition of H_2O_2 seems to occur during evaporation (prior to H_2O_2 measurement probe) and possibly upon contact with the warmed stainless-steel surfaces. Therefore, to ensure a rigorous comparative study, the operating parameters were re-evaluated and fixed at values considered relevant and optimized (details are not provided here for the sake of simplicity) for the remainder of the study. The selected values were :

- $\mathbf{T_{pipe\ injection}}$**=100°C** to increase $[H_2O_2]_{vap}$ value while potentially limiting thermal decomposition compared to higher initial values (≈150°C)
- $\mathbf{Q_{air\ carrier}}$**=90 NL.h**$^{-1}$, the maximum flowrate value, to enhance vaporization and $H_2O_{2,\ vap}$ concentration.
- $\mathbf{T_{cell}}$**=60°C** to reduce H_2O_2 thermal decomposition while still allowing radical formation.
- $\mathbf{Q_{H_2O_2,\ liq}}$**=40 µL.min**$^{-1}$ to provide sufficient volume for post-characterization despite the relatively short experiment time.
- **Relative humidity of the total flow maintained at ≈15%** (oscillating between 10 and 20%) to ensure consistent water vaporization from the H_2O_2 solution.

- **$[H_2O_2]_{liq}$ concentration** was varied between **0 and 3%**.

In this context, it was also decided to express and discuss the results as a function of the injected liquid-phase H_2O_2 concentration ($[H_2O_2]_{liq}$), after confirming that the corresponding vapor-phase concentrations exhibited a sufficiently coherent and reproducible trend (figure 6.6).

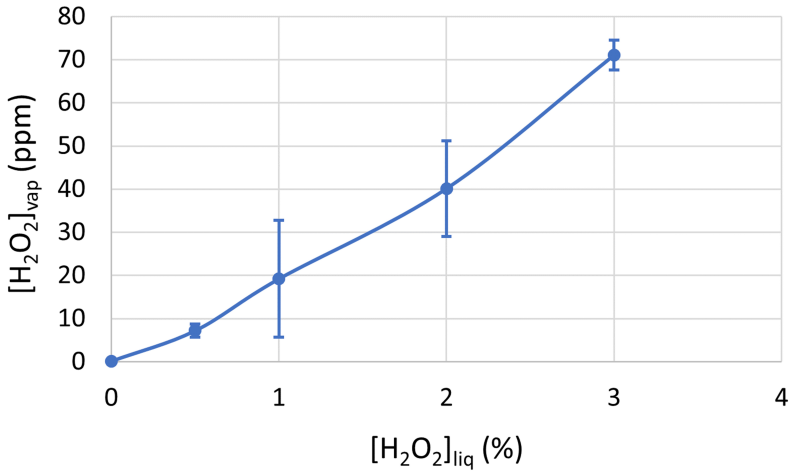

FIGURE 6.6 – H_2O_2 concentration in vapor phase as a function of the concentration of the H_2O_2 liquid solution. Each measurement has been repeated at least three times for repeatability (except for the test under water vapor).

4 Impact of chemical and coupled chemical-mechanical stresses on sPEEK membrane

4.1 sPEEK chemical structure

Impact of $[H_2O_2]_{liq}$ concentration

The impact of H_2O_2 concentration on the chemical stability of *sPEEK nanostructured* in a vapor environment was evaluated through degradation tests using injected H_2O_2 solutions with concentrations ranging from 0.5 to 3%. Each sample was analyzed using FTIR spectroscopy to assess its chemical structure. The spectra illustrated in figure 6.7(a) correspond to the average of two to three measurements per sample as well as repeatability tests. Measurements showed very good reproducibility and homogeneity within a single sample, as shown in Appendix 3.

Figure 6.7(a) shows significant evolution of peak intensities compared to the reference, with increasingly pronounced changes as the H_2O_2 concentration increases. Using again the equation proposed by Al Lafi et al. [34], the degree of sulfonation was evaluated for each spectrum and plotted as a function of $[H_2O_2]_{liq}$ (figure 6.7(b)). The DS decreases significantly with increasing H_2O_2 concentration, reaching nearly half of its initial value for 3% $[H_2O_2]_{liq}$. It is also observed that even at a low concentration of 0.5% $[H_2O_2]_{liq}$, the DS decreases from 41% to 35%, highlighting the high sensitivity of the *sPEEK nanostructured* to radical attack generated by H_2O_2 decomposition and, consequently, its low chemical stability.

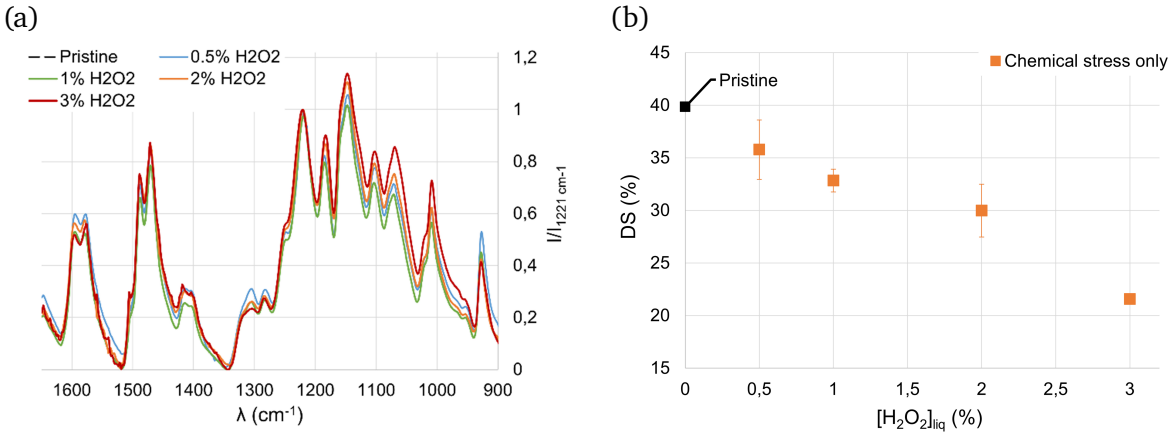

FIGURE 6.7 – Average FTIR spectra (a) and corresponding calculated degree of sulfonation (b) of degraded sPEEK with different H_2O_2 concentrations.

Impact of sPEEK pretreatment

Chemical degradation tests were conducted at 1% and 2% $[H_2O_2]_{liq}$ on *sPEEK standard* in order to assess the effect of the pretreatment and to verify whether the behavior reported during liquid-phase degradation [13] is also observed.

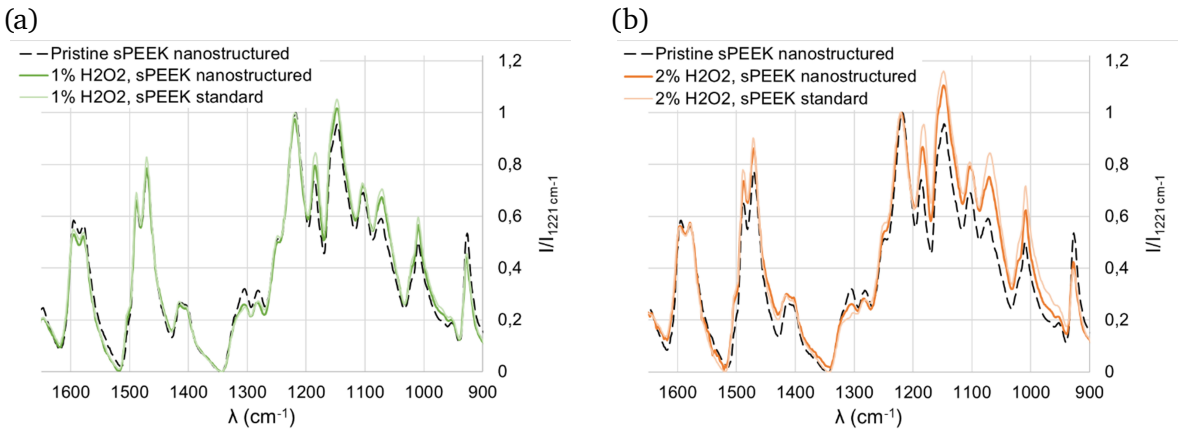

FIGURE 6.8 – FTIR spectra of sPEEK pretreated with the optimized (*nanostructured*) and the process advised by the manufactured (*standard*) degraded under 1% H_2O_2 (a) and 2% H_2O_2 (b).

Regardless of the H_2O_2 concentration, both types of sPEEK exhibit variations in peak intensities (figure 6.8) indicative of chemical structure evolution. A marked difference between *sPEEK standard* and *sPEEK nanostructured* is observed only at 2% $[H_2O_2]_{liq}$. This is confirmed by DS (table 6.2) showing that the DS of *sPEEK standard* decreases to the same extent as that of *sPEEK nanostructured*, relative to the pristine material, at 1% $[H_2O_2]_{liq}$. It is only at 2% H_2O_2 that a significant difference between the two materials emerges, highlighting the higher stability of *sPEEK nanostructured*. This observation is consistent with the study of Daoudi et al. [13] work in liquid-phase H_2O_2 degradation, who demonstrated that the applied pretreatment leading to *sPEEK nanostructured* improves the chemical stability of sPEEK membrane.

As *sPEEK nanostructured* exhibits higher fuel cell performance (see chapter 4), the following experiments are conducted on *sPEEK nanostructured*.

$[H_2O_2]_{liq}$ (%)	DS (%)	
	sPEEK nanostructured	*sPEEK standard*
1	32.8	32.3
2	30.0	24.5

TABLE 6.2 – DS values of *sPEEK nanostructured* and *standard* after chemical degradation in vapor phase.

Impact of added mechanical stress

To evaluate the impact of added mechanical stresses on the chemical stress, static (5 MPa) and cyclic (3 to 7 MPa at 0.1 Hz sinusoidal frequency) mechanical pressures were applied under similar $[H_2O_2]_{liq}$ concentrations to assess the effects of coupled chemical and mechanical stress compared to chemical stress alone. Static compression at 5 MPa was targeted to achieve stress levels comparable to those in previous studies investigating coupled chemical/mechanical degradation [20, 21, 25, 26]. To mimic severe swelling/shrinking cycling-induced by wet/dry cycling-a cyclic constraint between 2 and 7 MPa (corresponding to +/- 2 MPa around the 5 MPa used in static test) was applied.

Surprisingly, FTIR measurements showed no changes in peak intensities up to 1% $[H_2O_2]_{liq}$ with the addition of either static or cyclic constraints compared to chemical stress only, indicating similar degradation of the *sPEEK nanostructured* chemical structure. Indeed, as shown by the DS evolution in figure 6.9, the addition of mechanical constraint-static or cyclic-does not lead to any significant differences, at least within the measurement uncertainty, up to 2% $[H_2O_2]_{liq}$. It is only at the highest tested concentration (3% $[H_2O_2]_{liq}$) that a difference from purely chemical degradation begins to emerge. Interestingly, the addition of mechanical constraint, regardless of its nature, results in a less pronounced decrease in DS compared to chemical stress alone.

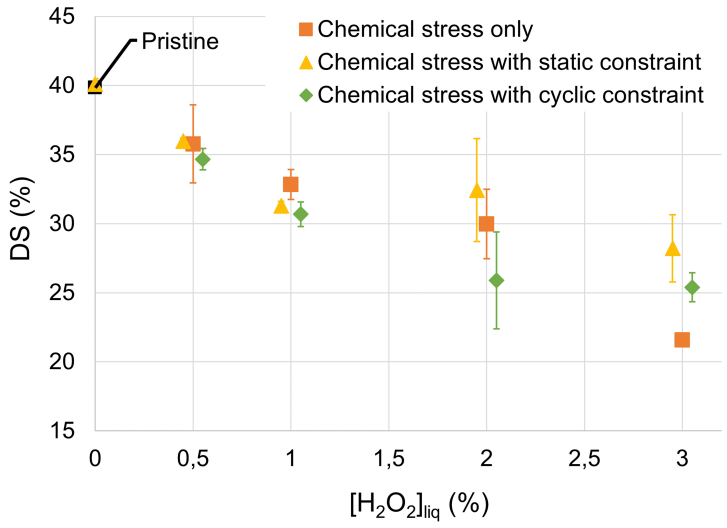

FIGURE 6.9 – Degree of sulfonation calculated from the average FTIR spectra of degraded sPEEK under various chemical and mechanical conditions.

The addition of mechanical constraints under our experimental conditions does not appear to exacerbate chemical degradation regarding the DS (figure 6.9). This could be because the low humidity conditions (approximately 15%) used here may not be sufficient to induce significant ionomer swelling and, consequently, significant local mechanical stress. Moreover, it is tempting

to further support this hypothesis by the observation that, despite the *nanostructured* deviations, a slightly greater decrease in DS at high $[H_2O_2]_{liq}$ is observed at higher stress levels under cyclic loading compared to static loading. In addition, it is important to note that the analysis of degradation solutions can be a useful complement to FTIR measurements for detecting degradation products as indicators of chemical degradation, thereby highlighting degradation mechanisms that do not alter the repeat unit. Indeed, in the case of Nafion, Robert et al. [37] observed no significant alteration in the chemical structure of Nafion via ATR-FTIR measurements, despite detecting an increased fluoride emission rate (FER) in degradation solution when mechanical stress was applied.

It is noted that, in this study, the analysis of the degradation solution was not conclusive. Indeed, UV-Vis spectroscopy analysis of the condensed vapors after the degradation tests did not detect any degradation products, suggesting that these products may have been trapped within the sample. An attempt to elute potential degradation products was made, but samples were too brittle and completely fragmented upon contact with water.

Impact of temperature

The effect of temperature on *sPEEK nanostructured* degradation was evaluated through degradation tests conducted at 70°C under : (i) 0.5, 2 and 3% $[H_2O_2]_{liq}$ without constraint and (ii) at 2% $[H_2O_2]_{liq}$ under static or cyclic mechanical stress. This temperature was specifically selected because the highest performance of the sPEEK-based MEA in fuel cells was obtained at 70°C during the performance mapping study (chapter 4). Moreover, the fuel cell ASTs were also carried out at 70°C (see chapter 5). Therefore, to enable a meaningful comparison between *ex situ* observations and in-cell aging, it is important to verify whether the behavior observed at 60°C is confirmed at 70°C. It is also necessary to determine whether the impact of applied stresses (chemical alone or coupled chemo-mechanical) is sensitive to temperature.

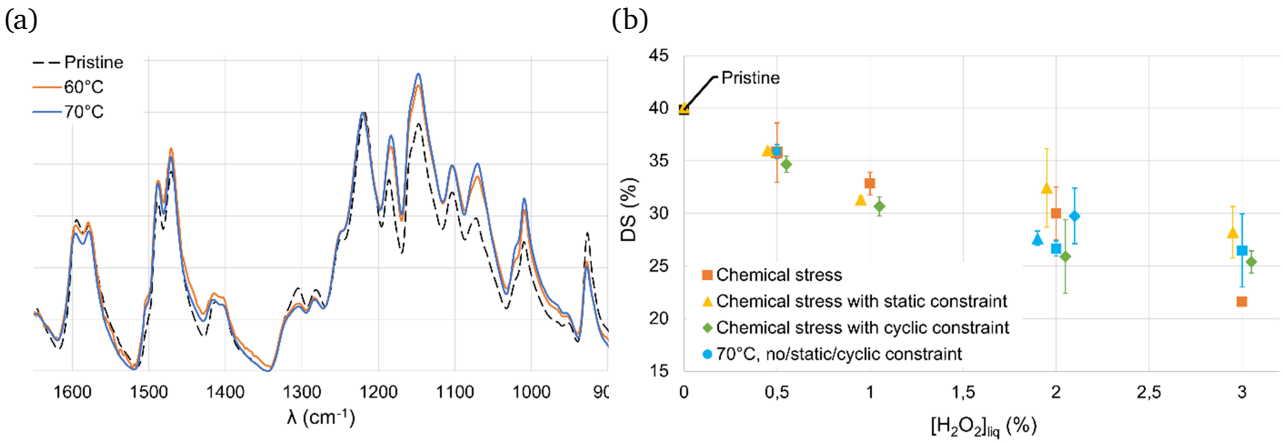

FIGURE 6.10 – Effect of temperature on chemical degradation under 2% $[H_2O_2]_{liq}$ without constraint (a) and DS evolution under various chemical and mechanical degradant conditions (b).

Without constraint, and at 70°C, the FTIR spectrum (figure 6.10(a)) of *sPEEK nanostructured* after degradation test under 2% $[H_2O_2]_{liq}$ highlight, similarly to the observations at 60°C, significant changes in peak intensities. At 70°C and 2% $[H_2O_2]_{liq}$, a significant decrease in DS (figure 6.10(b)) is observed for both chemical and coupled chemical/mechanical degradation. However, the addition of a cyclic constraint appears to slightly affect the DS, with lower degradation (*i.e.*, lower DS decrease

compared to pristine sPEEK). The evolution of DS as a function of $[H_2O_2]_{liq}$ concentration (figure 6.10(b)) shows a trend similar to that observed at 60°C. A more detailed comparison of DS values at 70°C compared to 60°C shows :

(i) Identical DS values at the lowest concentration (0.5% $[H_2O_2]_{liq}$).
(ii) Slightly lower DS values are observed at 1%.
(iii) Higher DS values at 2%.

Overall, it remains difficult to draw clear conclusions regarding the effect of temperature for each varying parameter. However, since the DS remains of the same order of magnitude as those obtained at 60°C, this suggests that increasing the temperature from 60 to 70°C under the tested conditions does not significantly affect the DS.

4.2 Crystallinity evolution through FTIR measurements

It has been previously shown that FTIR spectra can be used to determine the degree of sulfonation of sPEEK. In addition, FTIR can also provide insights into its crystallinity. Indeed, several studies [35, 38, 39] have reported correlations between the evolution of specific FTIR band ratios, crystallinity, and DS, as determined by complementary characterization techniques. In particular, a linear relationship has been observed between FTIR peak ratios and crystallinity, which is itself related to the DS of sPEEK.

More specifically, Chalmers et al. [38] investigated the crystallinity of poly(aryl-ether-ether-ketone) using FTIR and WAXS measurements, reporting increased crystallinity associated with higher band ratios of 1305/1280 cm^{-1} and 970/952 cm^{-1}. Conversely, Regis et al. [39] examined the crystallinity of thermally annealed PEEK by comparing DSC results to the 1280/1305 cm^{-1} ratio. Although their analysis used the inverse ratio compared with Chalmers et al. [38], they also observed a linear increase in the 1280/1305 cm^{-1} ratio with the increase in crystallinity measured by DSC. Despite the opposite trend which may be due to different polymers and crystallinity measurement methods, a clear linear correlation was found in both studies. More closely to our case, Rangasamy et al. [35] correlated the crystallinity of sulfonated PEEK membranes measured by DSC with the 1280/1305 cm^{-1} band ratio. They observed a linear relationship between this band ratio and crystallinity, which they also linked to the sPEEK DS. An increase in DS led to a decrease in both the band ratio and the crystallinity by DSC. It is not surprising that this band ratio is related to DS, as Al Lafi et al. [34] reported that the peaks at 1280 and 1305 cm^{-1}, associated respectively with the asymmetric stretching of the diphenyl ether group and the carbonyl linkage within the PEEK repeat unit, vary with sulfonation time. Several studies have also reported a decrease in sPEEK crystallinity with the DS, which has been attributed to the hindering effect of the-SO_3H groups on the formation of an ordered polymer structure [22, 40, 41].

This method was therefore employed to attempt to extract information on the evolution of the crystallinity degree from the measured FTIR spectra. The 1280/1305 cm^{-1} band ratios were calculated after the deconvolution of FTIR spectra using Gaussian curves (figure 6.11) and were then compared with the DS evolution (figure 6.12).

Although an increased trend in the 1280/1305 cm^{-1} ratio is observed with chemical degradation without mechanical constraint (orange squares in figure 6.12), the large deviations at each point prevent conclusions about changes in sPEEK crystallinity. Similarly, samples aged under combined chemical/mechanical stresses showed no clear trend : ratios remained nearly constant despite various DS, with persistent large deviation. It should be noted that spectral deconvolution is a mathematical approach that does not necessarily yield a unique solution, which may obscure underlying trends. Moreover, in the present case, the variation in DS does not arise from synthesis conditions but from

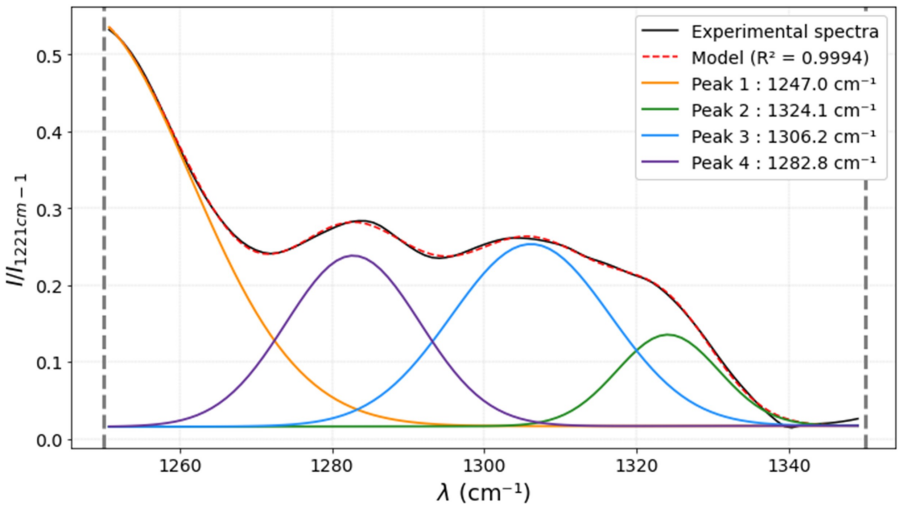

FIGURE 6.11 – FTIR spectra from a *sPEEK nanostructured* sample degraded under 2% $[H_2O_2]_{liq}$ and its deconvolution into four gaussian curves.

chemical degradation, with degradation products potentially retained within the membrane. Indeed, as a reminder UV–Vis spectroscopy analysis of the condensed solutions after degradation tests did not detect any degradation products. Consequently, the morphological organization within the membrane may be fundamentally different from that driven solely by variations in DS, and it is therefore not possible to correlate this ratio with the degree of crystallinity in a direct and straightforward manner. In any case, this highlights that, in the context of ionomer degradation studies, crystallinity is more reliably assessed using techniques specifically dedicated to its direct characterization, such as WAXS.

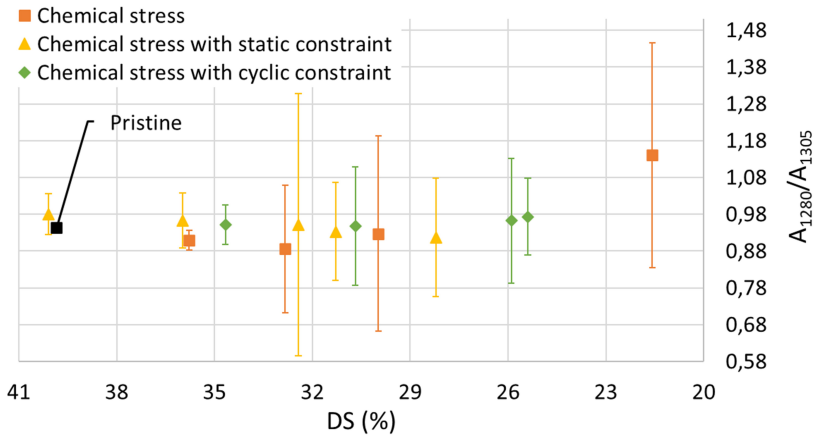

FIGURE 6.12 – Band ratio A1280/A1305 evolution as a function of the DS after degradation test in vapor phase.

4.3 Impact on fuel cell performance

sPEEK samples were often too damaged (*i.e.*, brittle) to be handled and successfully assembled by hot-pressing with GDEs, making it impossible to investigate all *ex situ* degradation conditions in fuel cell test. Nevertheless, measurements could be carried out under the least severe *ex situ* degradation conditions, namely :

(i) Comparison between *sPEEK nanostructured* and *sPEEK standard* after *ex situ* aging at 0.5% $[H_2O_2]_{liq}$ without mechanical constraint.

(ii) Assessment of the mechanical impact (static and cyclic) at 0% $[H_2O_2]_{liq}$ for *sPEEK nanostructured*. A comparison between *sPEEK nanostructured* and *standard* samples was successfully tested after *ex situ* aging conducted at 0.5% $[H_2O_2]_{liq}$ without constraint.

Polarization curves and permeation current were measured, using the test bench described in the previous chapters, at 70°C, 30-50% RH, 3 bar, with H_2 and air stoichiometries of 1.25 and 3, namely our reference conditions, described in chapter 2).

During the conditioning step (figure 6.13(a)), *sPEEK nanostructured* membranes after 8h under 0.5% $[H_2O_2]_{liq}$ without mechanical constraint exhibited current densities consistent with those obtained with the pristine membrane (observed for two aged membranes), values around 2.2 A.cm^{-2} at 0.3 V (compared to average values of 2.2-2.3 A.cm^{-2} observed during performance measurements in the chapter 4). However, a lower initial OCV value was observed (0.91-0.92 V *vs.* 0.98 V for the fresh membrane) along with a significant decrease during the conditioning step, dropping to 0.83-0.89 V by the end, while the current density at 0.3 V remained at appropriate levels (around 2.2 A.cm^{-2}). This indicates a functional MEA but with a severely degraded membrane, leading to a low initial OCV that further deteriorates during potentiostatic cycling. Similar observations were made for *sPEEK standard* (figure 6.13(b)), which exhibited a stable but significantly lower OCV than the pristine samples (0.915 *vs.* 0.97-0.98 V), along with a progressive decrease in the current density at 0.3 V.

The first aged *sPEEK nanostructured* could not be fully characterized, as the hydrogen permeation current reached a high value (123.3 mA.cm^{-2}), leading to premature test termination. Similarly, the second sample exhibited high permeation after a single polarization curve, reaching approximately 120 mA.cm^{-2}. Regarding *sPEEK standard*, the permeation current reached 7 mA.cm^{-2} after the first polarization curve and subsequently increased to 116 mA.cm^{-2} after the second measurement. These results suggest a very low stability of the sPEEK ionomer after chemical degradation even though it was at a low 0.5% $[H_2O_2]_{liq}$ concentration with a small decrease of DS (figure 6.10(b)). It is noteworthy that Electrochemical Impedance Spectroscopy (EIS) measurements showed a consistent high-frequency resistance (R_{hf}) for the second *sPEEK nanostructured* sample (around 53 mΩ.cm^2), whereas *sPEEK standard* exhibited a lower value (approximately 43 mΩ.cm^2), which suggests significant membrane thinning.

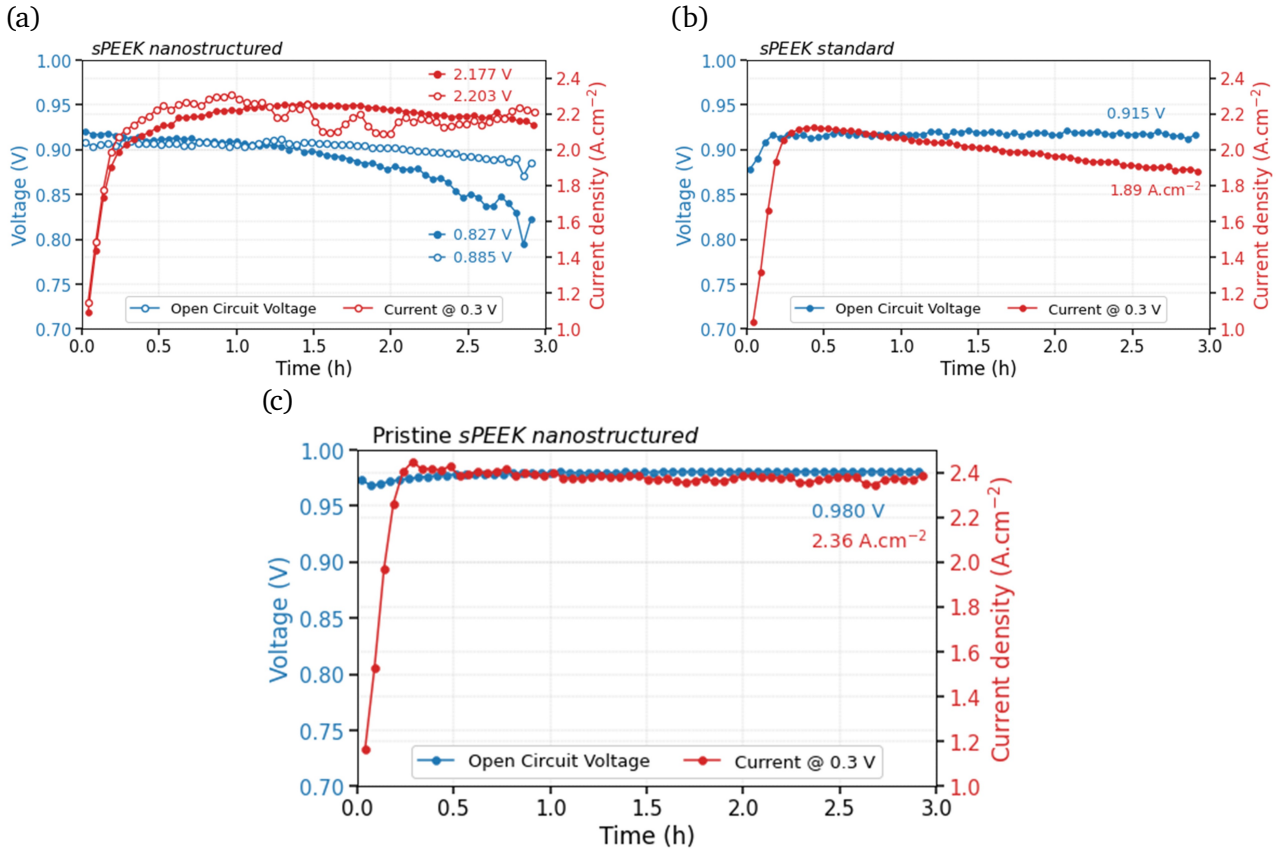

FIGURE 6.13 – Open circuit voltage and current density at 0.3 V evolution during the conditioning step for : *sPEEK nanostructured* (a) and *sPEEK standard* (b) after 8h under 0.5% H_2O_2 without mechanical constraint, and pristine *sPEEK nanostructured* (c).

These results indicate that the consequences of an *ex situ* aging test under conditions presumed to be mildly degrading, evidenced by the slight decrease in DS (approximately 36% compared to 40% for the pristine membrane), are indeed prohibitive for fuel cell operation, the membrane becoming unusable due to high hydrogen permeation.

In addition, we were interested to observe if degradations under mechanical constraint-static or cyclic-and water vapor (*i.e*, 0% $[H_2O_2]_{liq}$) could impact fuel cell performance, while no degradation of the DS was observed (figure 6.10(b)). These aged *sPEEK nanostructured* membranes were compared to the pristine *sPEEK nanostructured*, using the forward scan of the polarization curve at 30 and 50% RH. The polarization curve for the pristine sample was derived from the average value of three tests for both RH. Aged sPEEK exhibited lower performance under both RH, characterized by voltage instabilities and significant performance degradation from low to medium current densities regions (figure 6.14). This effect was particularly pronounced for membranes aged under cyclic constraints, which exhibited a voltage drop at substantially lower current densities. However, and interestingly, the static constraint had also a negative impact, also less pronounced. Although the addition of mechanical stress did not strongly affect the chemical structure, for instance, the DS remained nearly unchanged (40.1% for sPEEK aged at 0% $[H_2O_2]_{liq}$ under cyclic constraint *vs.* 39.8% for the pristine membrane), mechanical degradation nonetheless had a significant impact on fuel cell performance. However, a vapor-phase degradation test performed without chemical or mechanical stress should be conducted to confirm these results.

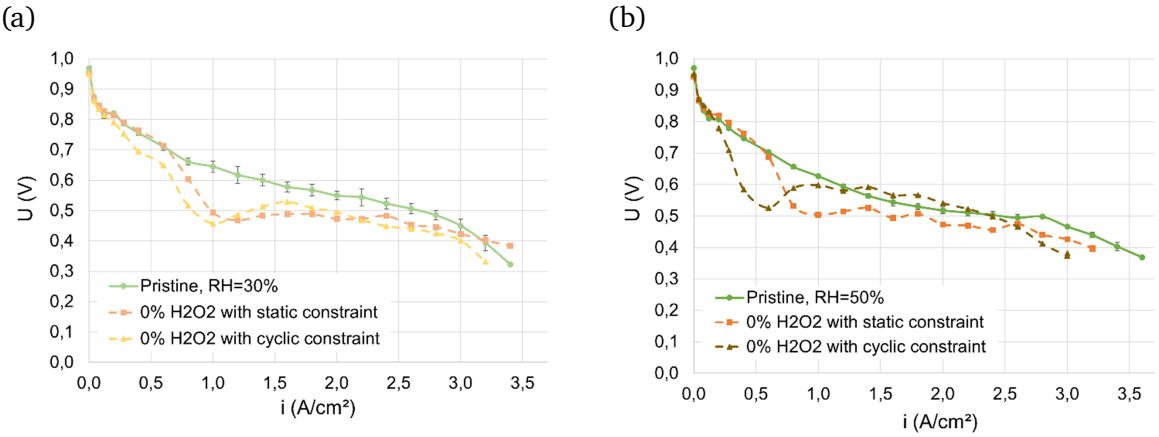

FIGURE 6.14 – Forward scan of polarization curves of pristine (solid lines) and (dashed lines) *sPEEK nanostructured* after 8h at 0% $[H_2O_2]_{liq}$ under mechanical constraint (static or cyclic) : at 30% (a) and 50% (b) gas inlet RH.

However, the effect of mechanical degradation on sPEEK must be distinguished from potential degradations arising from the hot-pressing process. To this end, R_{hf} measurements were used to evaluate the electrodes/membrane interface, while permeation current tests were conducted to assess the membrane integrity. Note that permeation current and R_{hf} values for the pristine sPEEK correspond to the average values obtained directly after the conditioning step.

An increase of Rhf is observed at 1 A.cm^{-2} for sPEEK subjected to static mechanical stress (figure 6.15(a)), which may indicate a slightly lower quality of the membrane electrodes interface, or a possibly modified membrane microstructure. However, this could not be correlated with the performance loss observed as the sample aged under cyclic constraint exhibited the same performance loss with a R_{hf} comparable to the pristine sample. Overall, the difference in R_{hf} between the static and the other cases may not be significant. Regarding the membrane state, the application of a static constraint led to a significant increase in permeation current, exceeding 0.7 mA.cm^{-2}, while adding a cyclic constraint caused only a moderate increase on the cathode and the anode sides, respectively, with values remaining within the error bars of the pristine membrane. These results align with the OCV values, which showed an approximate decay of 10 to 20 mV. The application of a mechanical constraint could therefore deteriorate membrane permeability properties, although the slight variations may come from the samples themselves and/or their pretreatments.

There is therefore a strong impact of static mechanical constraint on the properties of sPEEK, which is not detectable through its chemical structure. It is likely that the membrane state is affected by stress differences between the ribs and the channels, although the effect on the R_{hf} is mitigated. Nevertheless, a slight increase in H_2 permeation current was observed with the addition of a mechanical constraint, indicating that the effect of mechanical degradation may be more related to ionomer microstructure instead of its chemical structure.

4.4 Discussion

Chemical degradation has a severe effect on the sPEEK membrane at high H_2O_2 concentrations where sample fragmentation occurred. Nevertheless, lower H_2O_2 concentrations were sufficient to induce significant chemical structure changes, observed by the decrease in DS. However, the addition of a mechanical stress does not appear to significantly affect the degradation of the chemical structure of sPEEK, since no significant variation in DS was observed. These results could highlight two points :

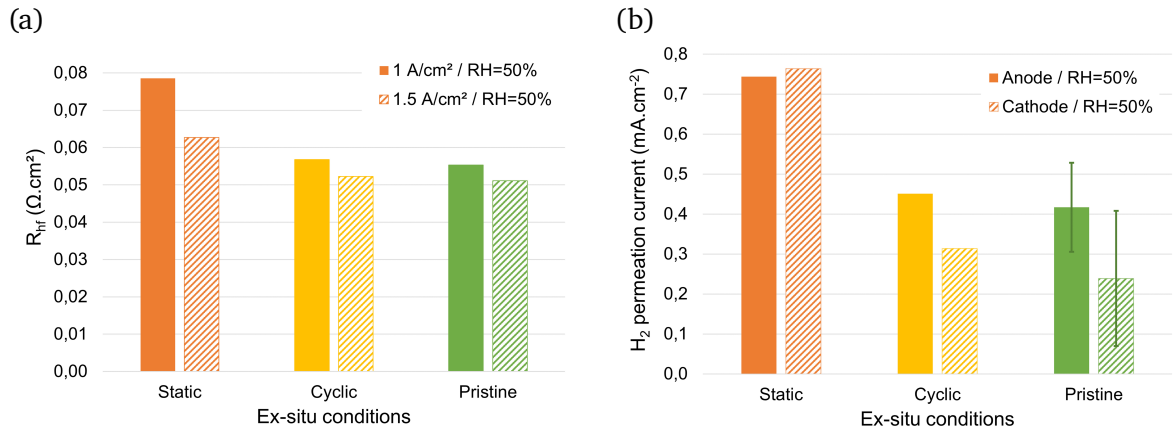

FIGURE 6.15 – R_{hf} at 1 and 1.5 A.cm^{-2} (a), and permeation current (b) of pristine sPEEK (green bars), sPEEK after *ex situ* degradation under static constraint (orange bars) or under cyclic constraint (yellow bars)

- It is likely that the relative humidity is too low in the present study (≈15%) to significantly reveal the impact of the applied mechanical constraint, and that a higher level of mechanically induced stress would be required. Further investigations involving RH variation, as well as RH cycling without H_2O_2, could provide better insight.
- Complementary analysis of the membrane morphology must be done. Indeed, mechanical constraints may alter the ionomer microstructure without significantly affecting specific chemical bonds, in contrast to chemical degradation.

This second point is partly supported by the *in situ* (*i.e.*, in single cell) characterizations, which show a significant effect of both static and cyclic constraints on fuel cell performance while no decrease in DS was measured. In addition, slightly higher permeation values were measured, suggesting that microstructural modifications or damages may have been induced during the *ex situ* degradation tests.

Chemical degradation appears to be more detrimental than mechanical degradation, as indicated by the low OCV value at the beginning of the conditioning step and the sharp increase in permeation measured at the end of this stage. This leads to an important conclusion : the degradation induced during *ex situ* testing is significantly more severe than that occurring during *in situ* operation, despite relatively minor changes in DS. This suggests that chemical degradation primarily affects the ionomer microstructure, inducing structural damage that can ultimately lead to membrane failure. In contrast, changes in ionomer DS, and thus proton conductivity, may have a smaller impact during fuel cell operation, as membrane failure is likely to occur first.

Moreover, *ex situ* aging tests are of interest when compared with *in situ* AST, but care must be taken when establishing correlations between the two approaches, and *ex situ* experiments should be regarded solely as an accelerated representation of chemical degradation. Indeed, H_2O_2 concentrations in fuel cells are generally lower. An even more important point is that, under fuel cell operation, H_2O_2 is generated during ASTs and depends-according to mechanisms proposed in the literature-on hydrogen permeation through the membrane. Thus, any comparative analysis between *in situ* ASTs and *ex situ* experiments must be interpreted in light of this key factor, which is explicitly accounted for in the present work.
This may explain why the significant difference in chemical stability between PFSA and sPEEK ionomers is not clearly reflected during the *in situ* accelerated stress tests (figure 6.16). *sPEEK standard* exhibited higher durability than *sPEEK nanostructured*, owing to its higher thickness (approximately 25 *vs.* 15-18 µm), while NR211 exhibited an intermediate lifetime due to a compromise between moderate thickness (25 µm) and higher initial permeation value.

In contrast, in the analysis of chemical degradation resistance presented above, it was clearly shown that Nafion exhibits higher chemical stability than sPEEK, and that the pretreatment leading to nanostructured sPEEK improved its resistance to radical attack. In other words, the resistance to chemical degradation followed the order : Nafion NR211 > *sPEEK nanostructured* > *sPEEK standard*. In the case of *in situ* accelerated stress tests (AST), as shown in figure 6.16, this order is not confirmed. Indeed, *sPEEK standard* exhibits the highest durability, followed by Nafion NR211, whereas *sPEEK nanostructured* is the least durable, showing a noticeable increase in permeation and a decrease in OCV after 7 days. The explanation for these differences lies in hydrogen permeation, which governs H_2O_2 formation and therefore occurs at later stages in initially less permeable membranes. PFSA-based membranes exhibited higher H_2 permeation currents, in agreement with the lower OCV, due to higher gas permeability compared to hydrocarbon ionomers, typically reported in the literature [42-44]. A lower gas permeability of *sPEEK standard*-conferred by its chemical structure-compared to Nafion is therefore measured, which accounts for the higher durability of *sPEEK standard* relative to Nafion. Although expected to be less prone to chemical degradation than *sPEEK standard*, the *sPEEK nanostructured* exhibits an earlier increase in permeation during the AST (figure 6.16) and thus earlier membrane degradation. This can be explained by its higher initial permeation, attributed to membrane thinning during the pretreatment step, with the thickness decreasing from approximately 25 to 15-18 µm.

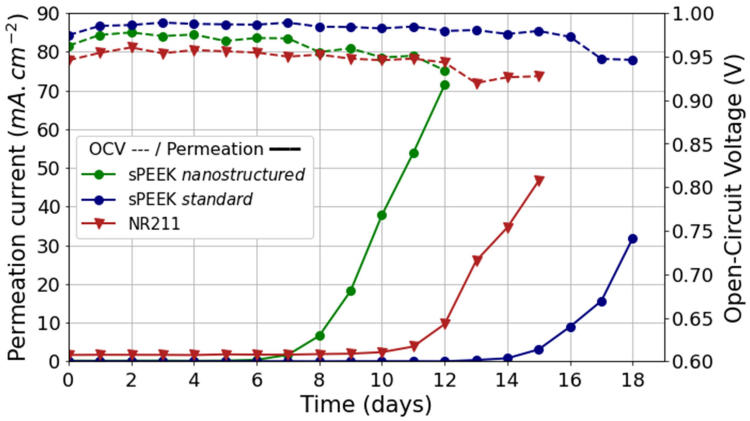

FIGURE 6.16 – Hydrogen permeation current and OCV values for sPEEK and PFSA-based MEA during an *in situ* accelerated stress test.

In light of these observations, one might be tempted to conclude that the *ex situ* approach, which does not reproduce the trends observed in *in situ* ASTs, provides limited relevant information. On the other hand, this comparative conclusion between *ex situ* and *in situ* approaches highlights :

- Firstly, that the initial membrane permeation is a key parameter in fuel cell operation to improve membrane durability.
- Secondly, the *ex situ* approach enables the assessment of the intrinsic resistance of membranes to chemical degradation under controlled and comparable conditions, which represents a major asset for their optimization.

In the present case, it can thus be concluded that one possible route for improvement consists of developing an optimized *sPEEK nanostructured* membrane, to combine the advantages of the chemical nature of sPEEK and nanostructuring, while mitigating the detrimental effects associated with high initial hydrogen permeation. Optimizing the drying process and pretreatment to minimize refining are areas for improvement to render this material competitive with both Nafion and *sPEEK standard*.

5 Conclusions

sPEEK membrane durability was assessed through *ex situ* tests. Although H_2O_2 generation in the vapor phase is a challenging process, a homemade bench was designed to induce coupled chemical and mechanical degradation of sPEEK under controlled relative humidity and temperature. Preliminary tests indicated that improvements could be made to achieve a more efficient H_2O_2 vaporization process. Nevertheless, initial degradation tests conducted under high H_2O_2 concentration revealed severe degradation of the sPEEK chemical structure, whereas no significant changes were observed for NR211. This behavior can be explained by the significantly higher chemical stability of PFSA membranes, which would require long degradation test durations in vapor phase ; therefore, this study focused on sPEEK membrane.

At 60°C and under reduced H_2O_2 concentration, significant changes in FTIR peak intensities were observed. These changes increased with the H_2O_2 concentration, indicating a strong impact of degradation on the sPEEK chemical structure. Under the most aggressive conditions, the sPEEK samples exhibited brittle behavior after testing, demonstrating that these conditions were excessively degradant for sPEEK. To further investigate degradation mechanisms, crystallinity evolution (via band ratio analysis) and the degree of sulfonation, determined from peak intensity ratio were evaluated.

For crystallinity, overall results did not reveal any consistent trend, except maybe under chemical degradation alone ; however, the error bars remained too large to draw firm conclusions. In contrast, a pronounced decrease in DS was observed with increasing H_2O_2 concentration, highlighting the detrimental effect of chemical degradation on sPEEK physicochemical properties. Surprisingly, the addition of static or cyclic mechanical constraints did not significantly enhance DS degradation. Similarly, the addition of mechanical stress did not impact much the chemical structure with similar FTIR spectra. On the contrary, it seems that the degradation was reduced in some cases with the addition of mechanical constraint. Similarly, increasing the temperature to 70°C did not significantly affect the DS, but minor changes in peak intensities were observed, indicating potentially increased chemical degradation.

Although no significant effect of mechanical constraint could be reported, this kind of stress may be more impactful for ionomer microstructure than the chemical structure. Therefore, *in situ* characterizations were conducted following the degradation tests to evaluate the effect of chemical degradation on fuel cell performance and to determine whether mechanical stress had an impact. While chemically degraded samples were often too brittle to be handled in fuel cell, sPEEK degraded under 0.5% H_2O_2 exhibited excessive hydrogen permeation, indicating that even minor changes in chemical structure can be sufficient to cause fuel cell failure. The application of mechanical constraints alone affected both fuel cell performance and hydrogen permeation in the case of static constraint. Although it is difficult to distinguish the effects of degradation from those induced by the hot-pressing process, these results demonstrated that mechanical constraints can have a significant impact on membrane performance and durability without substantially altering its chemical structure. *Ex situ* and *in situ* approaches appear complementary but not directly correlated, with observed discrepancies mainly driven by operating conditions, in particular initial permeation and H_2O_2 formation under fuel cell operation. The *ex situ* approach nevertheless enables the evaluation of the intrinsic chemical stability of membranes under controlled and comparable conditions, making it a relevant tool for material optimization. In this context, developing a thicker nanostructured sPEEK membrane appears as a promising strategy to combine the benefits of sPEEK chemistry and nanostructuring while mitigating the detrimental effects associated with high initial permeation.

As perspectives, additional experiments should be carried out to gain a better understanding of the hydrogen peroxide evaporation process. Repeatability tests should also be conducted to ensure the reliability of the observed trends. In addition, post *ex situ*-aging morphological analyses of the mem-

branes should be further developed to better elucidate the structural changes induced by degradation. In addition, studies of relative humidity effects-both in the presence and absence of H_2O_2-are required to better understand and highlight the role of coupled mechanical–chemical stress on the chemical degradation. Finally, the development of a nanostructured membrane process that avoids undesired thinning should be pursued.

References

[1] V. O. Mittal et al., « Effect of Catalyst Properties on Membrane Degradation Rate and the Underlying Degradation Mechanism in PEMFCs, » *Journal of The Electrochemical Society*, t. 153, n° 9, A1755, 2006, ISSN : 1945-7111. DOI : 10.1149/1.2219708

[2] S. Touhami et al., « Anode defects' propagation in polymer electrolyte membrane fuel cells, » *Journal of Power Sources*, t. 520, p. 230 880, 2022, ISSN : 03787753. DOI : 10.1016/j.jpowsour.2021.230880

[3] Y. Bultel et al., « Anode Defects' Propagation in Polymer Electrolyte Membrane Fuel Cells Stack, » *International Journal of Hydrogen Energy*, t. 82, p. 257-264, 2024, ISSN : 0360-3199. DOI : 10.1016/j.ijhydene.2024.07.403

[4] A. Tavassoli et al., « Effect of Catalyst Layer Defects on Local Membrane Degradation in Polymer Electrolyte Fuel Cells, » *Journal of Power Sources*, t. 322, p. 17-25, 2016, ISSN : 0378-7753. DOI : 10.1016/j.jpowsour.2016.05.016

[5] A. K. Taylor et al., « The Influence of Electrode Crack Dimensions on the Durability of Polymer Electrolyte Membrane Fuel Cells, » *Journal of Power Sources*, t. 628, p. 235 884, 2025, ISSN : 0378-7753. DOI : 10.1016/j.jpowsour.2024.235884

[6] L. Dubau et al., « Carbon Corrosion Induced by Membrane Failure : The Weak Link of PEMFC Long-Term Performance, » *International Journal of Hydrogen Energy*, t. 39, n° 36, p. 21 902-21 914, 2014, ISSN : 0360-3199. DOI : 10.1016/j.ijhydene.2014.07.099

[7] C. Chen et al., « XPS Investigation of Nafion® Membrane Degradation, » *Journal of Power Sources*, t. 169, n° 2, p. 288-295, 2007, ISSN : 0378-7753. DOI : 10.1016/j.jpowsour.2007.03.037

[8] L. Ghassemzadeh et al., « Evaluating chemical degradation of proton conducting perfluorosulfonic acid ionomers in a Fenton test by solid-state 19F NMR spectroscopy, » *Journal of Power Sources*, t. 196, n° 5, p. 2490-2497, 2011, ISSN : 03787753. DOI : 10.1016/j.jpowsour.2010.11.053

[9] F. M. Collette et al., « Hygrothermal aging of Nafion®, » *Journal of Membrane Science*, t. 330, n° 1-2, p. 21-29, 2009, ISSN : 03767388. DOI : 10.1016/j.memsci.2008.11.048

[10] F. M. Collette et al., « Structure and Transport Properties of Solution-Cast Nafion® Membranes Subjected to Hygrothermal Aging, » *Journal of Membrane Science*, t. 435, p. 242-252, 2013, ISSN : 0376-7388. DOI : 10.1016/j.memsci.2013.02.002

[11] A. Sadeghi Alavijeh et al., « Ex-Situ Tensile Fatigue-Creep Testing : A Powerful Tool to Simulate in-Situ Mechanical Degradation in Fuel Cells, » *Journal of Power Sources*, t. 312, p. 123-127, 2016, ISSN : 0378-7753. DOI : 10.1016/j.jpowsour.2016.02.053

[12] S. H. Mirfarsi et al., « Study of mechanical degradation of sulfonated poly (ether ether ketone) membrane using ex-situ hygrothermal cycles for polymer electrolyte fuel cell application, » *Journal of Power Sources*, t. 401, p. 73-84, 2018, ISSN : 03787753. DOI : 10.1016/j.jpowsour.2018.08.067

[13] M. Daoudi, « Performances et Durabilité Des Membranes Alternatives Aux Membranes PFSA, » PhD Thesis, Université de Lorraine, 2023.

[14] M. Zatoń et al., « Current understanding of chemical degradation mechanisms of perfluorosulfonic acid membranes and their mitigation strategies : a review, » *Sustainable Energy & Fuels*, t. 1, n° 3, p. 409-438, 2017. DOI : 10.1039/C7SE00038C

[15] A. B. LaConti et al., « Mechanisms of membrane degradation, » in *Handbook of Fuel Cells*, John Wiley & Sons, Ltd, 2010, ISBN : 978-0-470-97400-1.

[16] Y. Feng et al., « Degradation Study and Diagnostic Technology for Nafion Membrane, » *Journal of Power Sources*, t. 613, p. 234 880, 2024, ISSN : 0378-7753. DOI : 10.1016/j.jpowsour.2024.234880

[17] S. Shi et al., « Fatigue Crack Propagation Behavior of Fuel Cell Membranes after Chemical Degradation, » *International Journal of Hydrogen Energy*, t. 45, n° 51, p. 27 653-27 664, 2020, ISSN : 0360-3199. DOI : 10.1016/j.ijhydene.2020.07.113

[18] C. Tougne et al., « Total Oxidation Stress Protection of Thiourea-Based Hybrid Fuel Cell Membranes, » *Electrochimica Acta*, t. 541, p. 147 338, 2025, ISSN : 0013-4686. DOI : 10.1016/j.electacta.2025.147338

[19] E. Ferri et al., « Thiourea-Based Hybrid sPEEK Membranes Using a Sol-Gel Approach : Elaboration of Stabilized Hybrid sPEEK Membranes, » *Reactive and Functional Polymers*, t. 219, p. 106 588, 2026, ISSN : 1381-5148. DOI : 10.1016/j.reactfunctpolym.2025.106588

[20] M. Robert et al., « The Impact of Chemical-Mechanical Ex Situ Aging on PFSA Membranes for Fuel Cells, » *Membranes*, t. 11, n° 5, p. 366, 2021, ISSN : 2077-0375. DOI : 10.3390/membranes11050366

[21] A. Kusoglu et al., « Effect of Mechanical Compression on Chemical Degradation of Nafion Membranes, » *ECS Electrochemistry Letters*, t. 3, n° 5, F33-F36, 2014, ISSN : 2162-8726, 2162-8734. DOI : 10.1149/2.008405eel

[22] A. Reyna-Valencia et al., « Tensile mechanical properties of sulfonated poly(ether ether ketone) (SPEEK) and BPO4/SPEEK membranes, » *Journal of Applied Polymer Science*, t. 98, n° 6, p. 2380-2393, 2005, ISSN : 1097-4628. DOI : 10.1002/app.22417

[23] Y. Tang et al., « An experimental investigation of humidity and temperature effects on the mechanical properties of perfluorosulfonic acid membrane, » *Materials Science and Engineering : A*, t. 425, n° 1-2, p. 297-304, 2006, ISSN : 09215093. DOI : 10.1016/j.msea.2006.03.055

[24] Y.-H. Lai et al., « Chemical Degradation of Fuel Cell Membranes Subjected to Mechanical Stresses in a Hydrogen Peroxide Vapor Test, » *ECS Meeting Abstracts*, t. MA2021-02, n° 38, p. 1128, 2021, ISSN : 2151-2043. DOI : 10.1149/MA2021-02381128mtgabs

[25] Y.-H. Lai et al., « The Effect of Differential Pressure Driven Tensile Stress on Chemical Degradation of Perfluorosulfonic Acid Membranes Using a Hydrogen Peroxide Vapor Flow Cell Test, » *Journal of The Electrochemical Society*, t. 172, n° 2, p. 024 504, 2025, ISSN : 1945-7111. DOI : 10.1149/1945-7111/adb188

[26] W. Yoon et al., « Acceleration of Chemical Degradation of Perfluorosulfonic Acid Ionomer Membrane by Mechanical Stress : Experimental Evidence, » *ECS Meeting Abstracts*, t. MA2010-02, n° 10, p. 776, 2010, ISSN : 2151-2043. DOI : 10.1149/MA2010-02/10/776

[27] S. Rowshanzamir et al., « Effect of Pt-Cs 2.5 H 0.5 PW 12 O 40 catalyst addition on durability of self-humidifying nanocomposite membranes based on sulfonated poly (ether ether ketone) for proton exchange membrane fuel cell applications, » *International Journal of Hydrogen Energy*, t. 40, n° 1, p. 549-560, 2015, ISSN : 03603199. DOI : 10.1016/j.ijhydene.2014.10.134

[28] M. T. Salleh et al., « Stability of SPEEK/Cloisite ® /TAP nanocomposite membrane under Fenton reagent condition for direct methanol fuel cell application, » *Polymer Degradation and Stability*, t. 137, p. 83-99, 2017, ISSN : 01413910. DOI : 10.1016/j.polymdegradstab.2016.12.011

[29] C. Perrot, « Mécanismes de dégradation des membranes polyaromatiques sulfonées en pile à combustible, » PhD Thesis, Université Joseph-Fourier - Grenoble I, 2006.

[30] A. Gruger et al., « Nanostructure of Nafion® Membranes at Different States of Hydration, » *Vibrational Spectroscopy*, t. 26, n° 2, p. 215-225, 2001, issn : 0924-2031. doi : 10.1016/S0924-2031(01)00116-3

[31] K. A. Mauritz et al., « State of Understanding of Nafion, » *Chemical Reviews*, t. 104, n° 10, p. 4535-4586, 2004, issn : 0009-2665. doi : 10.1021/cr0207123

[32] Z. Liang et al., « FT-IR Study of the Microstructure of Nafion® Membrane, » *Journal of Membrane Science*, t. 233, n° 1, p. 39-44, 2004, issn : 0376-7388. doi : 10.1016/j.memsci.2003.12.008

[33] C. Korzeniewski et al., « Transmission Infrared Spectroscopy as a Probe of Nafion Film Structure : Analysis of Spectral Regions Fundamental to Understanding Hydration Effects, » *Applied Spectroscopy*, t. 60, n° 6, p. 599-604, 2006, issn : 0003-7028. doi : 10.1366/000370206777670620

[34] A. G. Al Lafi, « The sulfonation of poly(ether ether ketone) as investigated by two-dimensional FTIR correlation spectroscopy, » *Journal of Applied Polymer Science*, t. 132, n° 2, 2015, issn : 00218995. doi : 10.1002/app.41242

[35] V. S. Rangasamy et al., « Vibrational spectroscopic study of pure and silica-doped sulfonated poly(ether ether ketone) membranes, » *Spectrochimica Acta Part A : Molecular and Biomolecular Spectroscopy*, t. 138, p. 693-699, 2015, issn : 13861425. doi : 10.1016/j.saa.2014.12.004

[36] S. D. Mikhailenko et al., « Properties of SPEEK based membranes modified with a free radical scavenger, » *Journal of Membrane Science*, t. 345, n° 1-2, p. 315-322, 2009, issn : 03767388. doi : 10.1016/j.memsci.2009.09.017

[37] M. Robert, « Impact of Degradation and Aging on Properties of PFSA Membranes for Fuel Cells, » PhD thesis, Université de Lorraine, 2021.

[38] J. M. Chalmers et al., « Crystallinity in poly(aryl-ether-ketone) plaques studied by multiple internal reflection spectroscopy, » *Polymer Bulletin*, t. 11, n° 5, p. 433-435, 1984, issn : 1436-2449. doi : 10.1007/BF00265483

[39] M. Regis et al., « Characterization of thermally annealed PEEK and CFR-PEEK composites : Structure-properties relationships, » *Polymer Degradation and Stability*, t. 136, p. 121-130, 2017, issn : 01413910. doi : 10.1016/j.polymdegradstab.2016.12.005

[40] S. Banerjee et al., « Impact of degree of sulfonation on microstructure, thermal, thermomechanical and physicochemical properties of sulfonated poly ether ether ketone, » *Polymer*, t. 109, p. 176-186, 2017, issn : 00323861. doi : 10.1016/j.polymer.2016.12.030

[41] Y. Zhang et al., « Investigation of sulfonation degree and temperature on structure, thermal and membrane's properties of sulfonated poly (ether ether ketone), » *International Journal of Hydrogen Energy*, t. 48, n° 37, p. 13 791-13 803, 2023, issn : 03603199. doi : 10.1016/j.ijhydene.2022.12.332

[42] V. A. Sethuraman et al., « Durability of Perfluorosulfonic Acid and Hydrocarbon Membranes : Effect of Humidity and Temperature, » *Journal of The Electrochemical Society*, t. 155, n° 2, B119, 2007, issn : 1945-7111. doi : 10.1149/1.2806798

[43] M. Han et al., « Accelerated Testing of Polymer Electrolyte Membranes under Open-Circuit Voltage Conditions for Durable Proton Exchange Membrane Fuel Cells, » *International Journal of Hydrogen Energy*, t. 42, n° 52, p. 30 787-30 791, 2017, issn : 0360-3199. doi : 10.1016/j.ijhydene.2017.10.160

[44] D. M. Xing et al., « Characterization of Sulfonated Poly(Ether Ether Ketone)/Polytetrafluoroethylene Composite Membranes for Fuel Cell Applications, » *Fuel Cells*, t. 5, n° 3, p. 406-411, 2005, ISSN : 1615-6846, 1615-6854. DOI : 10.1002/fuce.200500089

6 Appendix

Appendix 1 - Technical scheme of the home-made bench

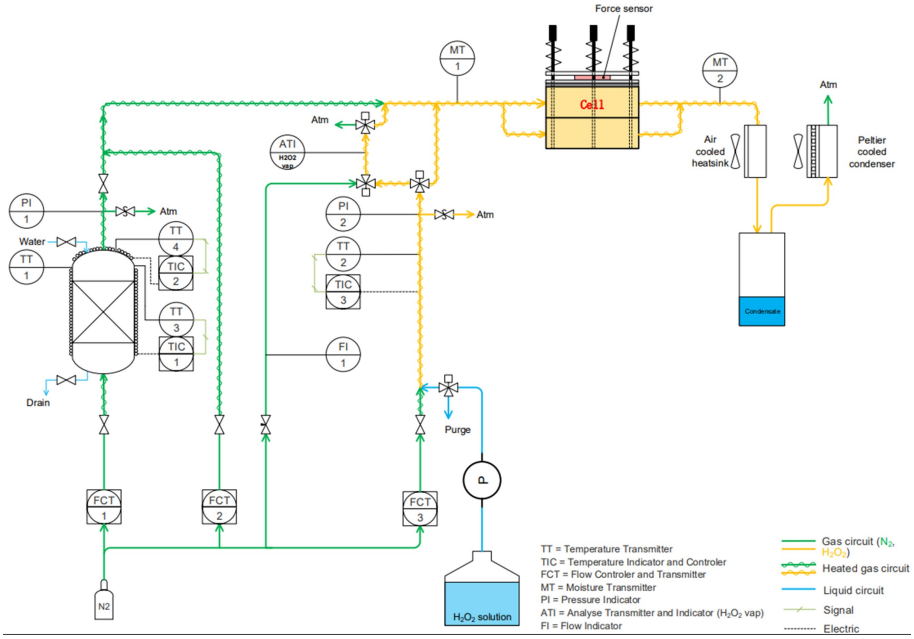

FIGURE 6.17 – Technical scheme of the degradation in vapor phase bench.

Appendix 2 – Impact of bench parameters on H_2O_2 vapor concentration

1. H_2O_2 concentration measured in the vapor phase with various H_2O_2 liquid flowrate

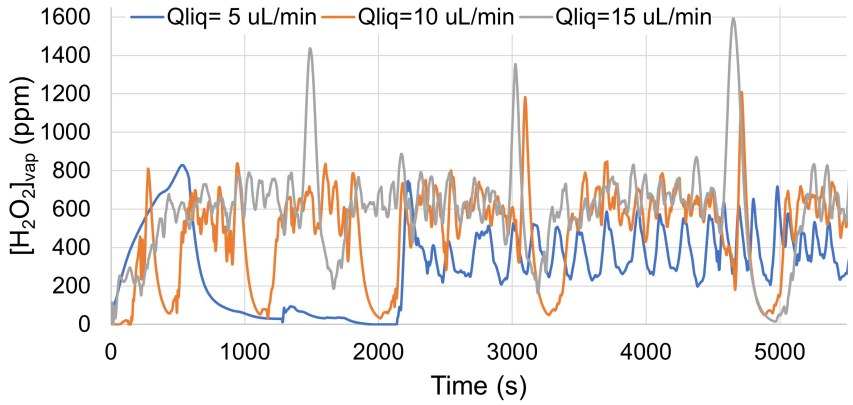

FIGURE 6.18 – H_2O_2 concentration in the vapor phase over time for different liquid flow rates.

2. H_2O_2 concentration measured in vapor phase with various H_2O_2 liquid concentration and flowrate

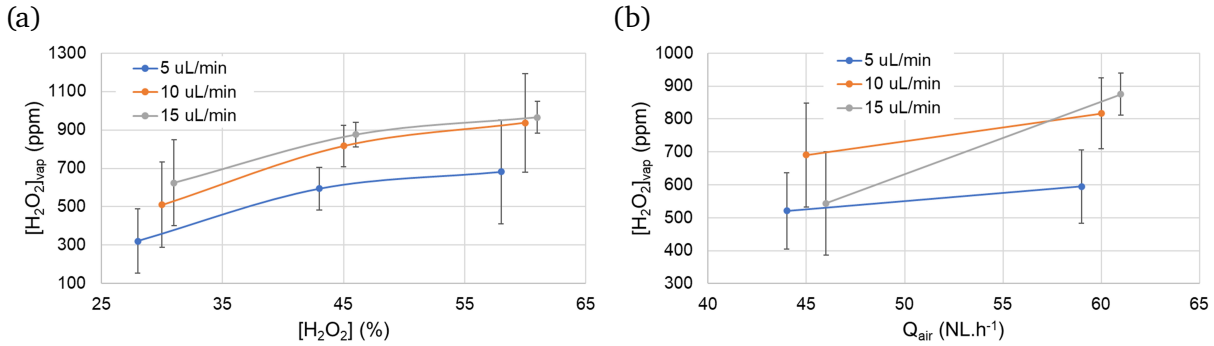

FIGURE 6.19 – Preliminary tests of H_2O_2 generation in vapor phase with heated pipe at 150°C for all experiments except for $[H_2O_2]_{liq}$ =60% (heated pipe at 170°C) : impact of H_2O_2 concentration in liquid state with an air flowrate of 60 NL.h^{-1} (a) and impact of the air flowrate with 45% H_2O_2 concentration in liquid state.

High H_2O_2 concentration (30, 45 and 60%) were used to validate the experimental setup. High average amounts of H_2O_2 in vapor phase were generated, large error bars corresponding to the concentration fluctuations observed. Increasing the $Q_{H_2O_2,\,liq}$ from 5 to 10 µL.min^{-1} increases the measured $H_2O_{2,\,vap}$ concentration, whereas almost no difference is observed between 10 and 15 µL.min^{-1}, indicating the existence of an optimal liquid flowrate under these conditions. Furthermore, good proportionality of the vapor concentration is observed between 30 and 45% liquid concentrations, with the vapor concentration being approximately 1.5 times higher. However, this trend does not hold at 60% liquid concentration, where the vapor concentration is less than twice that measured for 30% liquid concentration. In this latter case, it should be noted that the higher injection pipe temperature (170°C instead of 150°C) may have led to greater thermal decomposition. In all cases, the vapor-phase concentration remains lower than that of the liquid solution. Several hypotheses can be proposed to explain this difference :

- When H_2O_2 solution is injected into the heated pipe, part of H_2O_2 is decomposed by thermal degradation. Due to a difference in boiling points between H_2O and H_2O_2, a two-step evaporation process occurs : first, water vaporized because of its lower boiling point ; subsequently, the remaining liquid–mainly H_2O_2–is vaporized. The longer residence time of H_2O_2 molecules in contact with the heated pipe before vaporization could enhance thermal decomposition, explaining why the vapor concentration is lower than that of the liquid solution.
- As in the Fenton test, metal cations can catalyze the decomposition of H_2O_2 into water and oxygen. Although all pipes are made of stainless-steel due to its high stability, to best of our knowledge, no data are available regarding the interaction between heated stainless-steel and H_2O_2 solutions.

3. Effect of different heated materials on H_2O_2 decomposition

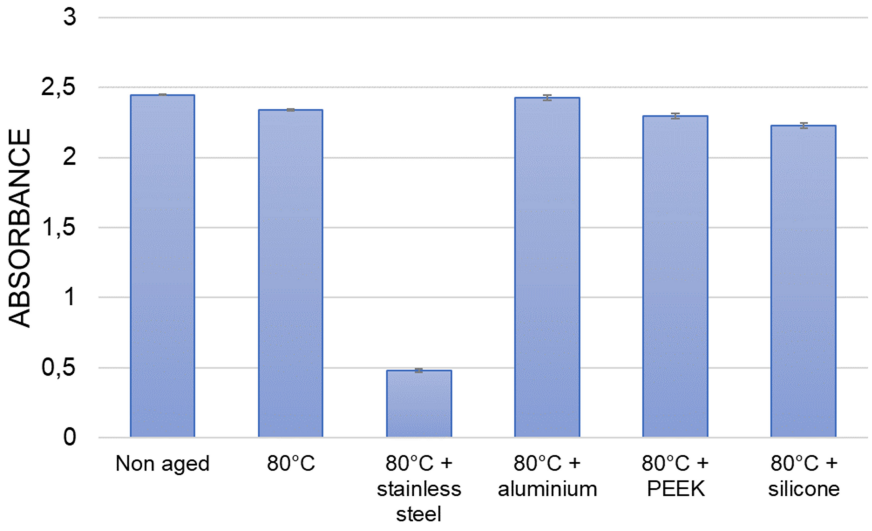

FIGURE 6.20 – UV measurements of H_2O_2 solution after exchange with a 2M KI solution.

A simple experiment was conducted by immersing pieces of stainless-steel, aluminium, silicone and PEEK in a 30% H_2O_2 liquid solution at 80°C for approximately 7h to study H_2O_2 decomposition. Macroscopically, significant gas release was observed in contact with stainless-steel, indicating significant decomposition of H_2O_2 into O_2. To obtain a more quantitative assessment, the H_2O_2 concentration was measured by colorimetry. After the experiment, 10 µL of the H_2O_2 solution was added to 50 mL of a 2M KI solution, and the absorption peak at 350 nm was measured three times using UV-Vis spectroscopy.

A lower H_2O_2 concentration in the liquid phase after contact with stainless-steel was confirmed by UV-Vis spectroscopy, supporting the macroscopic observations of significant H_2O_2 decomposition. Although these results cannot be directly correlated with those obtained using the test bench (due to different temperatures and the fact that materials were not immersed during test bench operation), they provide a strong indication that could explain the difference in concentration between the liquid and vapor phases. It should also be noted that, in the case of liquid H_2O_2 in contact with aluminium, the decomposition rate did not appear to increase ; however, the aluminium surface showed visible alterations, suggesting that some elements may have been released into the solution. Due to time constraints, we were unable to replace the stainless-steel pipe to confirm these results. Nevertheless, this option remains under consideration for future improvements to the test bench.

Appendix 3 - ATR-FTIR spectra of *sPEEK nanostructured* after contact with H_2O_2 in vapor phase from a 1% and 2% H_2O_2 liquid solution measured in several points

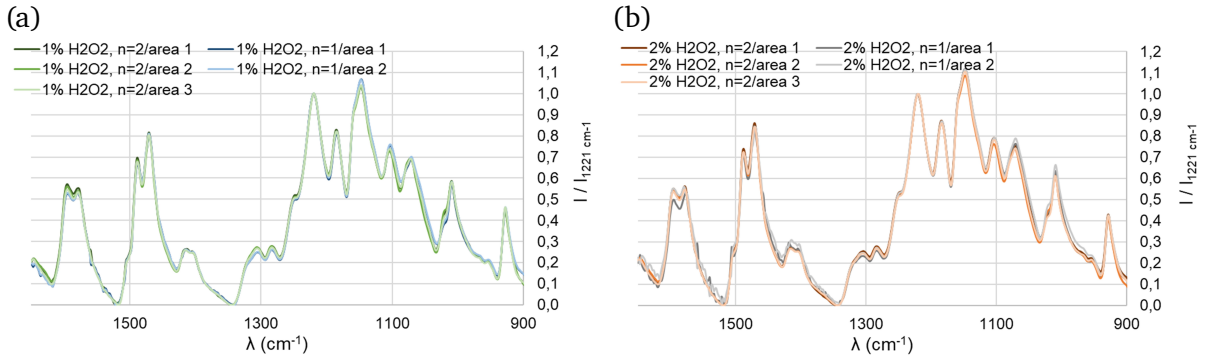

FIGURE 6.21 – FTIR spectra of *sPEEK nanostructured* degraded with 1% $[H_2O_2]_{liq}$ (green lines) and 2% $[H_2O_2]_{liq}$ (orange lines).

Conclusions & perspectives

This work was focused on the effect of PEMFC operating temperature on performance and durability, as well as on the utilization of alternative materials to replace PFSA-based membranes. A comprehensive review of the literature revealed a significant lack of data regarding the performance and the durability of state-of-the-art materials operating at near-boiling temperatures. Nevertheless, several studies have shown that increased operating temperatures negatively affect conventional membranes (PFSA-LSC), leading to higher degradation rates, notably through the formation of pinholes and cracks. At the PEMFC system level, advanced materials for various components (bipolar plates, GDL, CL, and the membrane) have also exhibited significantly higher degradation rates under accelerated stress tests, especially under load cycling conditions. As we have seen, our results do not fully confirm these conclusions.

In parallel, this work investigated the use of sulfonated poly(ether ether ketone) (sPEEK) as an ionomer membrane for PEMFC applications. The literature indicates that no direct alternatives fully match the performance of PFSA-based materials due to their inherent properties. However, growing concerns regarding cost and the environmental impact of fluorinated materials are driving research into alternative materials. This study therefore evaluated the performance and durability of sPEEK membranes in PEMFC, after they were subjected to a pretreatment to improve their functional properties.

This work was divided into four parts, the conclusions and perspectives of which are summarized below.

Chapter 2 : effect of operating temperature on fuel cell performance

Fuel cell performance was investigated at usual and near-boiling temperatures (70 *vs.* 95°C) using a commercial MEA based on a state-of-the-art membrane. Polarization curves showed that increasing temperature has a negative effect on fuel cell performance, partly attributed to membrane dehydration and oxygen dilution under equivalent gas inlet relative humidity (RH). Performance mapping at 95°C revealed several trade-offs : increasing gas pressure enhances MEA hydration and gas partial pressure but reduces gas diffusivity, while increasing air stoichiometry improves oxygen availability but can reduce fuel cell voltage under dry conditions. Fuel cell performance was particularly enhanced with increasing gas inlet RH due to improved membrane hydration, up to approximately 40-50% RH, above which mass transport issues may arise. Under the driest conditions tested (*i.e.*, 95°C and below 30% gas humidity), voltage instabilities-*i.e.*, a voltage sudden drop-appeared at high current densities, which was not observed under moderate gas inlet RH. High-frequency resistance (R_{hf}) measurements conducted at 70 and 95°C in potentiostatic mode showed a sharp increase at low voltage-*i.e.*, high current density-associated with significant MEA drying, whereas a more stable and better-hydrated state was observed at usual temperature. Further investigations indicated that the thermal production from electrochemical reactions was responsible for this sudden MEA drying, rather than the electro-osmotic drag. This phenomenon appeared to be global, starting above 80°C, although more pronounced at the

air inlet. Of course, it could be counterbalanced with an adequate gas inlet RH, possibly at the expense of FC performances above 40-50%.

These results underline the critical importance of a well-hydrated MEA to ensure proper operation at higher operating temperature. Moreover, they indicate that performance limitations at higher operating temperatures and under low humidity conditions are primarily related to MEA drying, whereas they are mainly associated with mass transport limitations at usual operating temperature.

Further investigations could focus on similar studies involving other components. For example, characterizations conducted at 95°C and 50% gas inlet RH on thicker membranes (*e.g.*, Nafion 211 and Nafion 212) showed significant differences compared to the reference case : variations in local hydration state and the onset of drying at higher fuel cell voltages were observed with increasing membrane thickness, suggesting that electroosmosis effects may be more detrimental under these conditions.

Chapter 4 : sPEEK-based MEA performance

sPEEK as an ionomer membrane has been investigated as a potential substitute for PFSA-based membranes in PEMFC. Although lower proton conductivity, particularly under dry conditions, and reduced chemical stability have been reported compared to PFSA ionomers, previous studies have also shown that the application of a specific pretreatment can induce enhanced nanophase separation, leading to improved fuel cell performance. In addition, the implementation of a new drying process, resulting in a much flatter membrane, led to significantly improved performance under both air and oxygen conditions. Pretreated sPEEK membranes were assembled using a hot-pressing process with Gas Diffusion Electrodes (GDE) and an ionomer overcoat to allow adhesion between the membrane and the electrodes. Optimization of MEA compression rate and conditioning procedure showed that a low compression rate (12%, compared to 25 or 31%) provided the widest range of operating conditions, while a humid conditioning step improved fuel cell performance.

Following these optimizations, a comparison was performed between CCB MEA using sPEEK membranes prepared *via* the optimized and standard processes (referred to as *sPEEK nanostructured* and *sPEEK standard*, respectively). Performance mapping at various temperatures, gas humidities, pressures, and air stoichiometries showed a significant improvement with *sPEEK nanostructured*, attributed to more efficient water utilization. Moreover, performance comparable to that of NR211-based MEA was achieved at 70°C/50% gas RH. These results demonstrate that sPEEK membranes can deliver competitive performance relative to PFSA-based membranes when their microstructure is optimized. However, performance mapping at different temperatures also revealed that sPEEK membranes cannot operate effectively at 95°C, even over a wide RH range (20-70%), due to increased resistance. In contrast, tests conducted at 60, 70, and 80°C highlighted a trade-off between improved membrane conductivity and reduced hydration with increasing temperature, with 70°C providing the best performance across a broad range of operating conditions.

The effect of *ionomer overcoat* used to improve the membrane-electrode interface was investigated using GDE with different loadings (0.2 and 0.3 mg.cm^{-2}). No significant impact on performance was observed, although small differences in R_{hf} suggest a possible resistive contribution of the overcoat. However, additional R_{hf} measurements are required to investigate the effect of loading on MEA hydration at higher current density, where increased MEA drying was observed. A comparison with Catalyst Coated Membrane (CCM) MEA was then carried out to assess the feasibility of removing the *ionomer overcoat*. Similar overall performances were obtained, with CCM MEA exhibiting higher voltages at low to intermediate current densities, while CCB MEA performed better at higher current densities. These differences may be attributed to the *ionomer overcoat*, which may introduce addi-

tional resistance at low current densities but help maintain proton conduction pathways under drier conditions at high current densities. Further tests with CCM MEA featuring lower Pt loading showed significantly improved performance despite a higher R_{hf}, indicating that this parameter alone does not govern performance. This highlights the need for further investigation and optimization of the membrane-electrode interface, particularly during the electrode deposition process.

Overall, this study demonstrates the feasibility of using sPEEK membranes in PEMFC applications under air and at low to moderate humidity conditions (30-50% gas RH), provided that appropriate pretreatment and operating temperature are applied. In addition, satisfactory performance was achieved with sPEEK-based CCM, particularly in the typical operating range of PEMFC applications (low current densities). However, the variability observed for CCB MEA and the more pronounced differences for CCM MEA, likely related to pretreatment, drying process, and electrodes deposition process, indicate that further characterizations are required to fully understand and optimize these systems. In particular, the effect of *ionomer overcoat* could be further investigated through similar characterizations using different loadings. In addition, exploring alternative ink compositions and/or electrode deposition processes could help improve overall CCM MEA performance.

Chapter 5 : durability of the state-of-the-art membrane and comparison with sPEEK ionomer

In addition to the performance characterization of both state-of-the-art and pretreated sPEEK membranes, durability studies were conducted to evaluate the effect of higher operating temperatures and alternative membranes on MEA durability. An accelerated stress test, based on previous studies, was employed to induce both electrode and ionomer/membrane aging through combined chemical and mechanical stresses.

The first part focused on AST conducted at 70 and 95°C under various humidity conditions on the state-of-the-art membrane, over 14 days. Performance monitored at specific current density and voltage points revealed no significant effect of temperature on MEA performance losses, whereas decreasing gas RH at 95°C may slightly reduce performance losses at low current densities. Moreover, temperature did not affect the evolution of ECSA on the cathode side, whereas reduced losses were observed at low RH. In contrast, a systematic decrease in anode ECSA was observed at 95°C, while it remained stable at 70°C. Temperature may therefore affect the anode catalyst layer, possibly due to an enhanced H_2O_2 production under drier conditions. However, thickness measurements from SEM images could not confirm this, as no significant changes were observed on the anode side regardless of the AST conditions. Moreover, no consistent trends were observed for the cathode side. These results were not surprising, since the AST to which the MEA was subjected did not include high-potential excursions that may lead to excessive carbon corrosion and thus cathode catalyst layer collapse. Nevertheless, this first part of the chapter highlighted the difficulty of correlating performance losses with ECSA degradation. Regarding the membrane, no signs of increased permeation were observed in all cases, indicating a stable state. However, a slight increase in R_{hf} was observed under 70-95°C/20% gas RH conditions. In addition, post-mortem measurements of the membrane thickness revealed a slight increase for this MEA, the origin of which remains to be clarified : chemical degradation and/or changes in structure and morphology. The aging profiles revealed that the mechanical stresses induced during the AST are highly dependent on operating conditions, with higher mechanical stress at low gas RH at both temperatures. Conclusions are therefore highly dependent on the AST protocol and the materials tested. Further tests could therefore focus on mechanical and chemical degradation pa-

thways to independently assess the effect of temperature on membrane stability. In addition, further tests could explore higher temperatures (*i.e.*, above 100°C) to investigate a wider operating range. Intermediate-duration AST could also be carried out to better understand the relationship between ECSA evolution and component degradation through physico-chemical analyses.

Regarding the stability of sPEEK-based MEA, ASTs could not be conducted at 95°C due to the absence of viable operating conditions. A comparison at 70C° was therefore performed between *sPEEK standard* and nanostructured CCB, sPEEK-based CCM, and NR211-based MEA. Low durability of the sPEEK-based CCM MEA, compared to other MEA, was observed. Nevertheless, considering the strong dependence of MEA performance on CCM fabrication conditions (composition, processing method, etc.), this finding motivates further development of optimized CCM for sPEEK-based systems, with the potential to improve durability. The *sPEEK nanostructured* in CCB configuration showed interesting durability, although approximately 30% lower than that of the NR211-based MEA. Moreover, a test conducted with a thinner ionomer overcoat exhibited significantly higher durability, similar to that of NR211-based MEA, showing that substantial improvements are possible. *sPEEK standard* showed higher durability than NR211, likely due to its very low initial permeation value. Compared to *sPEEK nanostructured*, the higher durability was justified by the slightly lower permeation in addition to a higher thickness. Furthermore, these results highlight that conclusions from *ex situ* chemical degradation tests, showing higher degradation of sPEEK than Nafion, should be considered in direct comparison with the fact that they are performed under identical hydrogen peroxide (and thus radical) concentration conditions. Indeed, the lower permeability of sPEEK, which results in lower H_2O_2 formation, can lead to higher durability under fuel cell AST compared to Nafion.

Compared with referenced materials, a significant gap was observed, reflecting the higher level of development of the state-of-the-art PFSA membrane. Indeed, this membrane is both mechanically and chemically reinforced, making direct comparison difficult. Nevertheless, these results provide a foundation for future work on the durability of alternative ionomers, as they demonstrated promising performance. Further tests could therefore focus on the durability of *sPEEK nanostructured* CCB using GDEs with different ionomer overcoat loadings to assess its effect. Additional measurements could also be conducted on *sPEEK nanostructured* CCM with different ink compositions, in particular using hydrocarbon-based catalyst layers, to evaluate whether higher cohesion can enhance MEA durability.

Chapter 6 : ionomer durability during *ex situ* aging test in vapor phase

The increase in fuel cell operating temperature requires characterizations of the effect of H_2O_2 on membrane durability. Although numerous studies have investigated membrane degradation in liquid phase using H_2O_2 solutions or the Fenton test, only a few works have characterized degradation in the vapor phase, with or without mechanical stress.

Ex situ degradation tests were therefore conducted using a home-made bench, enabling the generation of H_2O_2 in the vapor phase while mechanically constraining the membrane in a cell with the same channel design as in the previous chapters. Post-degradation characterizations were performed using ATR-FTIR spectroscopy to evaluate changes in the ionomer chemical structure. ATR-FTIR spectroscopy was chosen for its rapid, non-destructive measurement capability, while providing a fast assessment of changes in the degree of sulfonation (DS) of sPEEK membranes, which is a key parameter affecting the membrane's functional properties.

Initial tests conducted at very high H_2O_2 concentrations showed that, even under these extreme conditions, the NR211 membrane exhibits no change in its chemical structure, unlike sPEEK. These results are consistent with literature reports indicating the lower chemical stability of sPEEK membranes. Further investigations on the sPEEK membranes revealed a strong decrease in DS with increasing H_2O_2

concentration, while no significant effect of static or cyclic mechanical constraints or temperature (between 60 and 70°C) was observed. These results highlight the high sensitivity of sPEEK ionomer to radical attack under the studied conditions. *In situ* characterizations were then performed following *ex situ* degradation to evaluate their impact on performance. Permeation tests showed that low H_2O_2 concentrations were sufficient to induce dramatic structural changes, as indicated by the excessive H2 permeation currents exceeding 100 mA.cm^{-2}. In contrast, mechanical constraint affected performance, although no significant differences were observed in R_{hf} or permeation measurements.

These results provide further insight into the differences between *ex situ* and *in situ* degradation. FTIR spectroscopy measurements showed that small changes in chemical structure can significantly affect membrane integrity, as indicated by excessive hydrogen permeation. Moreover, chemical structure characterization may not be the most appropriate indicator for quantifying mechanical degradation. Additional characterizations are therefore required to achieve a deeper understanding of ionomer chemical and microstructural degradation, for example : Wide-Angle & Small-Angle X-ray Scattering (WAXS & SAXS), Scanning Electron Microscopy (SEM). Further studies on mechanical constraints could also be conducted using RH cycling instead of compression cycling, as this may be more representative of fuel cell operating conditions.

Perspectives

The work carried out in this thesis opens several perspectives, presented below according to short-, medium-, and long-term research directions :

- **Extended post-mortem analysis**
  Post-mortem analyses should be further extended, first to assess platinum particle size and determine whether it can account for the observed ECSA evolution, as well as to analyze additional MEA. The identification-for the first time, to the best of our knowledge-of a platinum depletion zone during tests at 95°C, whose thickness may depend on relative humidity, is a key finding requiring further investigation. It would be of interest to examine whether this depletion zone exhibits a distinct electrode structure in terms of ionomer distribution and carbon support. Finally, additional experiments should be carried out to confirm whether this phenomenon is exclusively observed at high temperature (95°C) and whether its thickness is indeed governed by the RH during AST.

- ***ex situ* degradation set-up**
  Further investigations could be conducted to gain a better understanding of the H_2O_2 evaporation process, enabling optimization of the operating parameters for a more effective vaporization process. Additional *ex situ* degradation tests could also be conducted to improve understanding of sPEEK degradation using complementary characterization techniques. It would also be of interest to investigate the impact of relative humidity variations in the absence of H_2O_2, using humidification/dehumidification cycles, to better reproduce the mechanical stresses experienced in fuel cells. Finally, experiments involving MEA could be considered (i) to enable distinction between membrane degradation and degradation potentially induced during the hot-pressing process when the membrane is assembled prior to fuel cell test and (ii) to assess the effects of coupled chemical/mechanical degradation on the membrane in the presence of the electrodes, MPL and GDL.

- **sPEEK-based CCM**
  It has been successfully demonstrated that CCM-type MEA can be obtained, allowing the elimination of the Nafion overcoat on the GDE, which is required to ensure MEA adhesion, and exhibiting promising performance. However, it is well established that both the deposition and the composition of the catalyst ink in CCM have a strong impact on electrode structure and/or electrode/membrane interface, and consequently on performance. Thus, in light of the promising results obtained here, it would be particularly interesting to pursue this work through a dedicated study aimed at optimizing CCM fabrication for sPEEK membranes. This study should not be limited to *sPEEK nanostructured*, even though it shows higher performance, but should also be extended to *sPEEK standard*, which exhibits better durability.

- ***sPEEK nanostructured* improvement**
  The fuel cell performance and durability of sPEEK membranes in fuel cells showed that *sPEEK nanostructured* exhibits higher performance but lower durability compared to *sPEEK standard*. However, *ex situ* tests (in vapor and liquid phase) conversely evidenced that *sPEEK nanostructured* displays better resistance to chemical degradation. The lower durability observed in fuel cell operation is explained by its higher permeation, resulting from membrane thinning after the pre-treatment steps. Thus, using a thicker membrane while preserving the same nanostructured architecture should make it possible to achieve improved durability surpassing that of *sPEEK standard*. It would therefore be of interest to further investigate this approach by developing a nanostructured but thicker membrane.

- **Temperatures above 100°C for state-of-the-art PFSA-LSC-based membrane**
  This work demonstrates the feasibility of using the state-of-the-art PFSA-LSC-based membrane in the 95-100°C range under adequate operating conditions. Future works could therefore complement these results by investigating temperatures above 100°C using the same materials, in order to identify limiting operating conditions.

- **PFSA-SSC membrane and ionomer binder**
  Since severe MEA drying was observed at high current densities and elevated temperatures in PFSA-LSC-based MEA under the operating conditions explored in this work, a dedicated investigation of PFSA-SSC materials in both the membrane and electrode layers at 95°C could be of particular interest. Indeed, several studies have reported improved water retention and promising transport properties for PFSA-SSC materials at temperatures above 100°C. In addition, SSC-PFSA ionomers have been shown to exhibit enhanced thermo-mechanical stability arising from higher crystallinity and reduced swelling compared to conventional LSC materials. These characteristics make SSC-PFSA promising candidates not only as membrane materials but also as electrode ionomers for PEMFC operation in the 80–120°C temperature range.

Résumé élargi

Contexte

"We also highlight, once again, two critical areas where the world is clearly falling short : universal energy access and climate change.", tels sont les mots de Dr Fatih Birol en introduction du rapport "World Energy Outlook 2025". La demande mondiale en énergie atteint des sommets et est, dans l'ensemble, satisfaite majoritairement par le recours aux énergies fossiles, principales contributrices au réchauffement climatique. Dans le même temps, cette demande croissante met en évidence l'interdépendance énergétique des états, illustrée par les nombreuses tensions observées dans les conflits récents. Dans ce contexte, le développement des énergies renouvelables et du nucléaire pour la production d'électricité bas carbone constitue la principale réponse face à ces défis. Néanmoins, l'intermittence de l'éolien et du solaire, ainsi que le stockage de l'électricité, constituent des défis majeurs pour la transition énergétique. C'est pourquoi plusieurs pays ont engagé des politiques de développement des filières de l'hydrogène, susceptibles de se substituer, dans certains usages, à l'électricité. Plus facilement stockable que cette dernière, l'hydrogène peut être produit grâce à des technologies telles que les électrolyseurs, alimentés par les surplus d'électricité issus des énergies renouvelables, et ainsi contribuer à la stabilisation du réseau. Au-delà du stockage, l'hydrogène peut être mobilisé dans de nombreuses filières, telles que l'industrie et le transport, soit par combustion directe, soit par l'utilisation de piles à combustible.

Différents types de piles à combustible existent. Ils se distinguent notamment par la nature de l'électrolyte utilisé et trouvent des applications variées selon leurs caractéristiques propres. Les piles à combustible à membrane échangeuse de protons (Proton Exchange Membrane Fuel Cell, PEMFC, figure 6.22) présentent un intérêt particulier pour les applications de transport, ou plus largement, pour celles nécessitant un démarrage rapide. En effet, elles se caractérisent notamment par une densité de puissance élevée ainsi qu'une grande rapidité lors des phases de démarrage et d'arrêt. Elles sont donc particulièrement adaptées aux applications de transport, pour lesquelles l'utilisation de batteries impliquerait des masses embarquées trop importantes, notamment dans le cas des camions ou des navires.

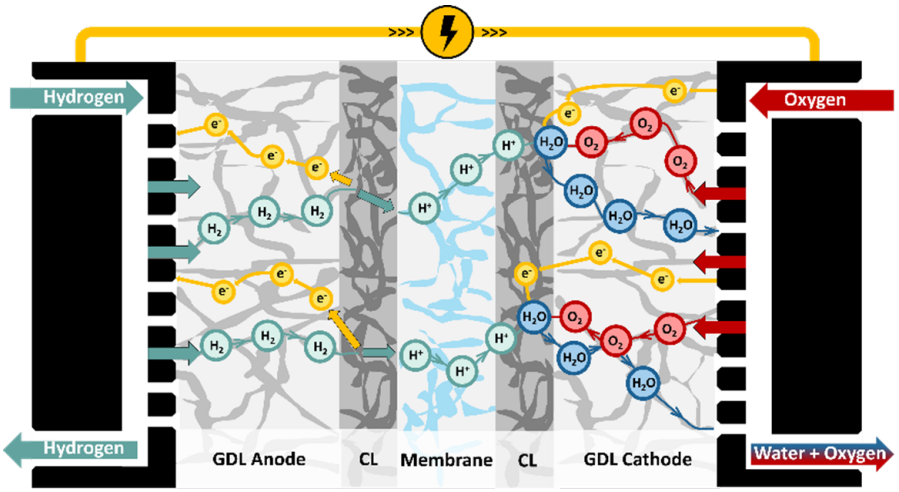

FIGURE 6.22 – Schéma de principe d'une PEMFC opérant sous oxygène.

L'architecture de cette pile est classique : elle comprend des plaques bipolaires ainsi que des couches de diffusion des gaz (Gas Diffusion Layer), assurant l'alimentation en réactifs et leur acheminement jusqu'aux couches catalytiques, nommées anode et cathode. L'oxydation de l'hydrogène à l'anode et la réduction de l'oxygène à la cathode sont rendues possibles par la présence d'une membrane conductrice de protons et isolante vis-à-vis des électrons, ce qui permet la production simultanée d'électricité et d'eau. Les performances et la durabilité de chacun des composants dépendent fortement des conditions opératoires.

L'intérêt des PEMFC pour les applications de transport est d'autant plus marqué que les seuls produits de la réaction sont l'électricité, la chaleur et l'eau. Malgré ces avantages, plusieurs verrous subsistent et freinent encore le déploiement de cette technologie à grande échelle. Des métaux précieux et coûteux, tels que le platine, sont généralement utilisés dans les couches catalytiques. L'ionomère de référence constituant la membrane et jouant le rôle de liant dans les électrodes est quant à lui à base d'acide perfluorosulfonique (PFSA), également coûteux et présentant des enjeux environnementaux, tant lors de sa synthèse que de son utilisation. De plus, les électrodes sont particulièrement sensibles à l'empoisonnement par certaines impuretés, ce qui peut entraîner des pertes de performances plus ou moins irréversibles.
Afin de pallier ces inconvénients, une augmentation de la température de fonctionnement peut être envisagée. Celle-ci permet d'accroître la cinétique des réactions électrochimiques, améliorant la tolérance aux impuretés, et de réduire la taille des systèmes de refroidissement, rendant ainsi le système plus compact et plus efficace. Cependant, une élévation de la température est également susceptible d'affecter les performances et la durabilité de la pile. Par exemple, le transport des protons à travers la membrane nécessite une teneur en eau minimale, or cette quantité d'eau peut diminuer lorsque la température augmente. De même, les propriétés mécaniques et physicochimiques des matériaux peuvent évoluer, entraînant des mécanismes de dégradation différents et/ou plus marqués lors d'un fonctionnement prolongé.

Le projet PEMFC95 vise ainsi à étudier les performances et la durabilité d'une PEMFC basée sur une membrane à l'état de l'art, à température élevée (95°C *vs.* 70°C), à l'échelle de la monocellule et du stack (ensemble de monocellules reliées en série ou parallèle). Ce projet regroupe différents laboratoires se répartissant les différentes tâches telles que la synthèse de nouveaux matériaux et leur caractérisation, l'étude des performances et de la durabilité en monocellule ou en stack, ou encore l'analyse de cycle de vie des composants. Dans ce cadre, le laboratoire LEMTA se focalise sur l'effet d'une température de fonctionnement plus élevée sur les performances et la durabilité des assemblages

membrane-électrodes (AME) en monocellule. Deux thèses s'inscrivent dans ce projet : celle d'Aouatef OUHAMMI, qui se concentre sur l'étude des électrodes, et la présente, plutôt focalisée sur la membrane.

Résultats

Ce travail s'articule autour de plusieurs tâches visant à comprendre l'effet de la température sur une membrane commerciale de référence, ainsi qu'à évaluer une membrane alternative sans PFSA, le sPEEK (sulfonated poly(ether ether ketone)). Les deux premières parties portent respectivement sur l'effet de la température sur les performances d'une AME IRD, référence du projet, puis sur celles d'AME constituées d'une membrane sPEEK prétraitée, avec une attention particulière portée aux différentes configurations d'assemblage : *Catalyst Coating Backing* (CCB) et *Catalyst Coated Membrane* (CCM). Dans un second temps, la durabilité en pile des AME IRD est étudiée dans différentes conditions de température et d'humidité, tandis que celle des AME sPEEK est évaluée dans des conditions fixes, en comparant plusieurs configurations (CCB, CCM et différents prétraitements). Enfin, une dernière partie s'intéresse à l'impact de la dégradation chimique et couplée chimique/mécanique des membranes sPEEK sous H_2O_2 en phase vapeur, dans le cadre d'une approche *ex situ*. Cette configuration a été choisie car, en fonctionnement en pile, le composé H_2O_2 généré est principalement sous forme vapeur. Les dégradations *ex situ* en phase liquide sont quant à elles plus représentatives des cas où un noyage local de l'AME peut se produire.

Performances des PEMFC à température élevée

La première partie aborde les performances d'une AME commerciale composée d'une membrane à l'état de l'art de 12 µm et évalue l'effet de la température sur le fonctionnement de la pile et de la membrane. Plusieurs cartographies de performance ont été réalisées, permettant d'évaluer l'influence de la température, de la pression, de l'humidité des gaz et de la stœchiométrie d'air.

Bien que les résultats aient montré qu'il était possible d'opérer à plus haute température, les performances de la pile ont été affectées négativement par l'augmentation de la température, principalement en raison d'un état d'hydratation plus faible de la membrane et d'une diminution de la concentration en oxygène. De plus, une chute de tension a été observée à haute densité de courant dans les conditions les plus sèches, c'est-à-dire à faible humidité de gaz. Des mesures complémentaires ont permis de montrer qu'un assèchement sévère et global de l'AME, dû à la chaleur produite par les réactions, apparaît dans ces conditions. Il en résulte une augmentation drastique de la résistance de la membrane au transport protonique, ce qui réduit significativement les performances. Bien que ce phénomène soit compensé avec l'augmentation de l'humidité des gaz, ces résultats mettent en évidence des limitations de performance différentes à haute densité de courant selon la température de fonctionnement : à température usuelle, les limitations sont principalement liées à des phénomènes de dilution et de diffusion des gaz, tandis qu'à une température supérieure à 85°C et à faible humidité des gaz, elles sont dominées par un assèchement sévère de l'AME. Néanmoins, ces conclusions restent valables dans le cadre des conditions de tests et des matériaux étudiés ici. Des mesures complémentaires ont également montré que l'utilisation de membranes plus épaisses conduisait à un état d'hydratation moins homogène que dans le cas d'une membrane plus fine, ce qui pourrait traduire un effet plus marqué de l'électro-osmose.

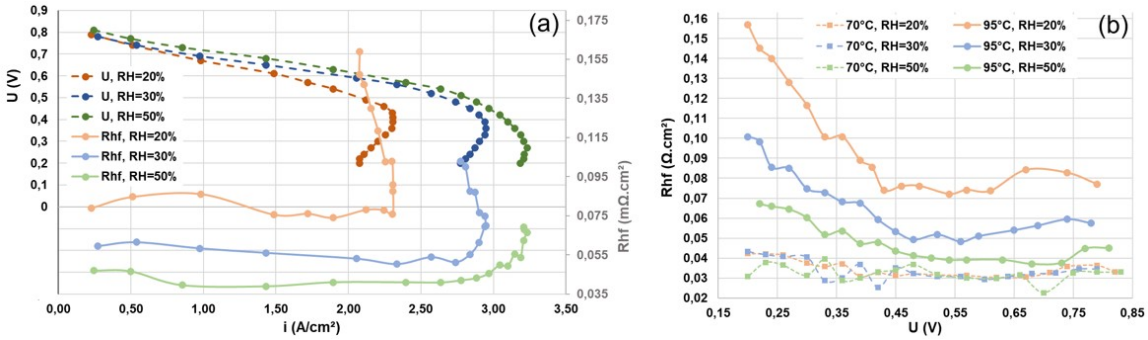

FIGURE 6.23 – Evolution de la R_{hf} et de la tension à 95°C (a) et évolution de la R_{hf} en fonction de la tension à différentes humidités (HR) et températures (b).

Bien que dépendantes des matériaux employés, ces conclusions soulignent l'aspect essentiel de l'hydratation de l'AME dans la limitation de l'impact négatif de la température sur les performances de la pile.

Performances d'AME basées sur du sPEEK prétraité

La deuxième partie aborde les performances d'AME basées sur du sPEEK prétraité selon deux procédés distincts : un procédé commercial, désigné comme *sPEEK standard*, et un procédé optimisé, nommé sPEEK *nanostructuré*. Bien que les performances du *sPEEK nanostructuré* restent nettement inférieures à celles de la membrane de référence, en raison d'un niveau de développement technologique moins avancé, des performances comparables à celles du Nafion 211 (PFSA) ont été obtenues sous air à 70°C et 50% d'humidité des gaz. Malgré les propriétés intrinsèques nettement supérieures du PFSA, l'application d'un prétraitement nanostructurant permet d'obtenir des performances significatives sous air et à humidité faible ou modérée (30-50%), en dépit des hypothèses généralement admises concernant le sPEEK. En effet, la comparaison avec le prétraitement commercial a montré que la nanostructuration améliorait significativement les performances, grâce à une meilleure gestion de l'eau. En revanche, aucunes conditions opératoires n'ont pu être trouvées à 95°C pour un fonctionnement viable à cause d'un assèchement important induisant une faible conductivité protonique.

La comparaison entre les configurations CCM et CCB à base de *sPEEK nanostructuré* a montré que le dépôt des électrodes par spray était possible, avec des performances similaires entre les deux configurations. Cependant, cette comparaison a également mis en évidence l'impact de la surcouche de PFSA présente sur les Gas Diffusion Electrode (GDE) dans le cas des CCB, utilisée afin d'améliorer l'adhésion entre les électrodes et la membrane sPEEK. Les essais de performances ont révélé une tension plus faible à basse densité de courant, mais de meilleures performances à haute densité de courant. Ces résultats suggèrent un effet résistif de la surcouche de PFSA, pénalisant les performances à faible densité de courant en raison de sa faible hydratation, tout en contribuant au maintien des performances à forte densité de courant grâce au maintien de la conduction protonique entre les électrodes et la membrane.

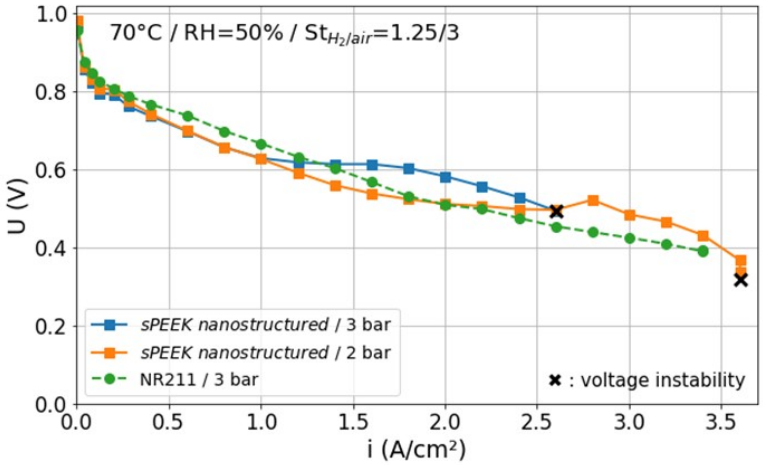

FIGURE 6.24 – Courbes de polarisation du *sPEEK nanostructuré* et du Nafion 211 à 70°C/50%gas RH/St$_{H_2/air}$=1.25/3. La croix représente le point de fonctionnement à partir duquel l'augmentation de la densité de courant induit une chute de tension à 50 mV.

Bien que de nombreux essais restent encore nécessaires afin d'optimiser les procédés de fabrication et de mieux comprendre les mécanismes à l'origine des performances, ces résultats soulignent les performances significatives pouvant être obtenues avec le sPEEK dans des conditions considérées défavorables à ce type d'ionomère, à savoir un fonctionnement sous air et à faible humidité.

Durabilité des membranes à l'état de l'art et des membranes sPEEK prétraitées

Les tests de durabilité menés sur l'AME de référence n'ont pas mis en évidence d'effet significatif des conditions opératoires, telles que la température et l'humidité des gaz, sur l'évolution des performances. En effet, des pertes relatives importantes de tension et de densité de courant ont été observées, associées à une diminution de la surface active du catalyseur, sans qu'un lien clair avec les conditions opératoires puisse être établi. En revanche, les tests complémentaires réalisés sur les électrodes ont montré qu'une dégradation systématique de l'ECSA côté anode apparaissait à 95°C. Par ailleurs, si la température ne semblait pas affecter l'ECSA côté cathode à une humidité de 50%, les pertes relatives semblaient plus limitées lorsque l'humidité des gaz diminuait à 95°C, ce qui pourrait suggérer un effet de l'eau sous forme liquide. Les caractérisations *in situ* et post-mortem n'ont révélé aucune dégradation structurelle de la membrane, avec une perméation stable et une épaisseur conservée. Cela montre que la membrane de référence présente une résistance mécanique et chimique suffisante pour supporter ces conditions supposées plus dégradantes, du moins sous les conditions opératoires étudiées.

La comparaison avec les AME à base de sPEEK prétraité a montré que les membranes de référence étaient à un niveau de développement nettement plus avancé. En effet, les membranes prétraitées sPEEK et NR211 ont toutes présenté une augmentation significative de la perméation à l'hydrogène à 70°C et 50% d'humidité à l'issue du même test de vieillissement accéléré. En revanche, les résultats ont mis en évidence une durabilité intéressante du sPEEK, inférieure à celle du NR211 pour le *sPEEK nanostructuré*, mais supérieure pour le *sPEEK standard*. Ces résultats indiquent que, bien que le PFSA présente une résistance chimique intrinsèque nettement supérieure à celle du sPEEK, la durabilité en pile dépend fortement de la perméation initiale de l'ionomère ainsi que de son épaisseur. De plus, des optimisations des procédés de prétraitement et dépôt des électrodes restent nécessaires, puisqu'une durabilité limitée a été observée pour les sPEEK en configuration CCM, alors qu'une durabilité comparable à celle du NR211 a été observée pour le *sPEEK nanostructuré* en réduisant l'épaisseur de la surcouche de PFSA sur les GDE.

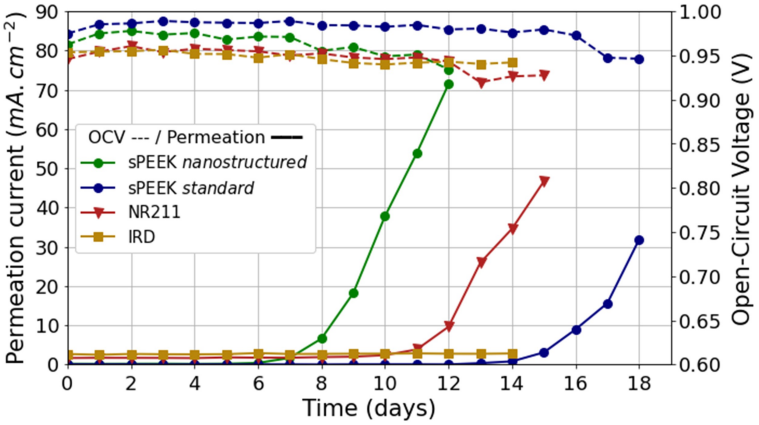

FIGURE 6.25 – Evolution du courant de perméation à l'hydrogène et de la tension à vide (Open-Circuit voltage) durant le vieillissement accéléré d'AMEs faites de différentes membranes.

Essais de durabilité *ex situ* en phase vapeur

Les tests de dégradation *ex situ* sous une phase vapeur d'H_2O_2 ont été conduits grâce à un banc développé au laboratoire LEMTA. Ce procédé vise à reproduire, mais de manière plus sévère (test accéléré), l'environnement radicalaire présent lors du fonctionnement en pile, issu de la décomposition du H_2O_2 en radicaux, lesquels attaquent la structure chimique de la membrane. L'expérience se déroule avec des paramètres opératoires contrôlés, à savoir la température, humidité du flux et concentration d'H_2O_2 sous forme vapeur imposée par la concentration de la solution d'H_2O_2 injectée dans le dispositif. Après une phase d'optimisation de ces paramètres, des tests de dégradation ont été appliqués aux *sPEEK nanostructuré* et *standard*, étant donné que les tests préliminaires n'ont pas révélé de dégradation du NR211 (PFSA), même à forte concentration d'H_2O_2. Les résultats ont montré une importante dégradation de la structure de l'ionomère, visible macroscopiquement et par spectroscopie infrarouge à transformée de Fourier (IRTF). Le suivi du degré de sulfonation (DS) a été réalisé, selon l'étude d'Al Lafi et al. * qui établit une corrélation entre ce paramètre et le ratio des pics situés à 1490 et 1600 cm^{-1}. Ce paramètre a été choisi en raison de son impact prépondérant sur les propriétés fonctionnelles de la membrane, notamment la conductivité protonique.

Une diminution importante du DS avec l'augmentation de la concentration en H_2O_2 a été observée, indiquant une faible stabilité chimique du sPEEK face à une phase vapeur d'H_2O_2. L'ajout d'une contrainte mécanique statique et cyclique semble avoir impacté la structure chimique de l'ionomère avec des variations notables de l'intensité des pics des spectres IRTF. Néanmoins, aucun impact de la contrainte mécanique sur le DS n'a pu être observé. Finalement, plusieurs caractérisations *in situ* ont été réalisées après les tests de dégradation *ex situ*. Seuls les échantillons de *sPEEK nanostructuré* dégradés chimiquement à faible concentration de H_2O_2 ont pu être caractérisés en pile à cause de la fragilité importante à plus forte concentration. Une forte perméation de la membrane a été mesurée, indiquant qu'une faible dégradation chimique *ex situ* n'est pas comparable aux dégradations mesurées en pile lors de vieillissement accéléré.

*. *The sulfonation of poly(ether ether ketone) as investigated by two-dimensional FTIR correlation spectroscopy*, DOI.10.1002/app.41242

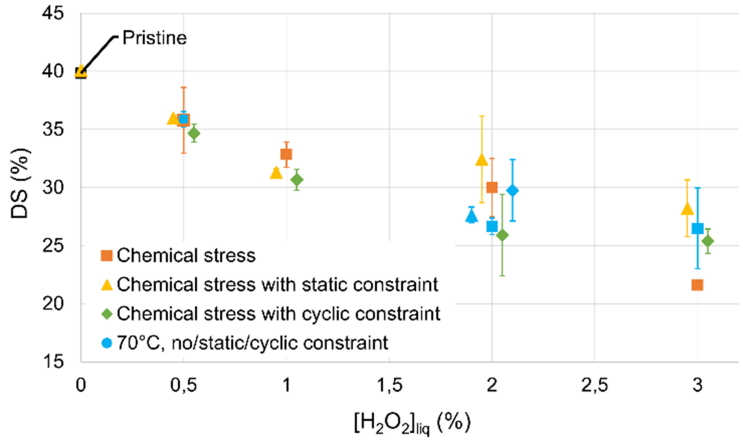

FIGURE 6.26 – Evolution du DS du sPEEK prétraité après dégradation sous différentes contraintes chimiques et mécaniques.

Conclusions & perspectives

L'ensemble des mesures présentées permet une compréhension approfondie du fonctionnement des PEMFC sous différentes configurations. L'effet de la température sur les performances et la durabilité est détaillé pour des AME commerciales composées de matériaux à l'état de l'art. Parallèlement, une comparaison avec des membranes hydrocarbonées prétraitées a révélé un potentiel intéressant en termes de performance et de durabilité, bien qu'un retard significatif persiste en matière de développement.

Bien que détaillées, ces résultats ouvrent des perspectives de recherche importantes. Des tests de durabilité à des températures supérieures et dans des conditions plus sèches semblent pertinents pour induire un vieillissement accéléré et mieux comprendre l'effet de ces conditions opératoires. Concernant le sPEEK, plusieurs tests d'optimisation pourraient être menés pour approfondir la compréhension des performances et de l'effet de la surcouche d'ionomère sur les GDE. Par exemple, l'optimisation du pressage à chaud, du conditionnement, du chargement de la surcouche d'ionomère pour les CCB, ainsi que l'ajustement de la composition de l'encre pour les CCM, représentent des pistes majeures d'amélioration.

Performance et durabilité des membranes ionomères pour pile à combustible entre 70°C et 100°C Approches *ex situ* et *in situ*

Le déploiement à grande échelle des piles à combustible à membrane échangeuse de protons constitue une solution prometteuse pour la décarbonation des applications de transport lourd, telles que les camions, les bateaux, voire à terme l'aviation. Toutefois, plusieurs verrous doivent encore être levés afin d'améliorer leurs performances et leur durabilité. Parmi ceux-ci, l'augmentation de la température de fonctionnement présente plusieurs avantages, notamment une meilleure tolérance des électrodes aux impuretés et une réduction de la taille des systèmes de refroidissement. En revanche, elle peut également accélérer la dégradation des performances et des composants, bien que cet effet reste encore très peu documenté.

Ce travail étudie l'impact de l'augmentation de la température de fonctionnement sur les performances et la durabilité de matériaux commerciaux de référence, notamment d'une membrane à l'état de l'art de 12 µm d'épaisseur. Une cartographie des performances a été réalisée afin d'évaluer l'effet de la pression, de l'humidité des gaz et de la stœchiométrie en air à 70°C et 95°C, voire au-delà. Les résultats ont été comparés à ceux d'un ionomère alternatif, le sPEEK, réputé peu polluant et peu coûteux. En suivant un protocole similaire, une étude intégrant différents taux de compression en cellule et étapes de conditionnement a été menée, permettant d'aboutir à un fonctionnement sous air et sous humidité faible à modérée. Une comparaison a également été réalisée avec des AME basés sur des membranes Nafion 211, du sPEEK prétraité selon un procédé commercial, ainsi qu'avec des AME de type CCM à base de sPEEK nanostructuré.
La question de la durabilité a ensuite été abordée via deux approches : *in situ* et *ex situ*. La première repose sur un protocole établi dans des travaux antérieurs. L'effet de la température sur les matériaux de référence a été étudié, ainsi que la comparaison avec les mêmes membranes alternatives sPEEK. La seconde approche s'appuie sur la conception d'un banc expérimental développé au laboratoire, permettant la génération d'une phase vapeur chimiquement dégradante. Après une phase d'optimisation, une série d'essais a permis de mesurer la dégradation du sPEEK prétraité sous différents degrés de contraintes chimiques et mécaniques.

Mots-clés – IT-PEMFC, Performance, Durabilité, Membrane, Electrodes, sPEEK, PFSA

Performance and Durability of Ionomer Membranes for Fuel Cells between 70°C and 100°C *Ex Situ* and *In Situ* Approaches

The large-scale deployment of proton exchange membrane fuel cells (PEMFC) represents a promising solution for the decarbonization of heavy-duty transport applications, such as trucks, ships and possibly aircraft. However, several challenges still need to be addressed in order to improve their performance and durability. Among the possible strategies, increasing the operating temperature offers several advantages, including improved electrode tolerance to impurities and a reduction in cooling system size. On the other hand, it may also accelerate the degradation of both performance and cell components, although this effect remains poorly documented.

This work investigates the impact of increasing operating temperature on the performance and durability of commercial reference materials, with a particular focus on a 12 µm-thick state-of-the-art membrane. A performance mapping study was carried out to evaluate the effects of pressure, gas humidity, and air stoichiometry at 70 and 95°C. The results were compared with those obtained using an alternative ionomer, sPEEK, known for its reduced cost and potentially lower environmental impact. Following a similar protocol, a complementary study was conducted on different cell compression levels and conditioning procedures, leading to operation under air and under low to moderate humidity conditions. Finally, a comparison was performed using membrane electrode assemblies (MEAs) based on Nafion 211 membranes, commercially pretreated sPEEK, and nanostructured sPEEK in a CCM configuration.
Durability was then investigated through two complementary approaches : *in situ* and *ex situ*. The first approach relied on a protocol established in previous studies and was used to evaluate the effect of temperature on the reference materials, as well as to compare their behavior with that of the alternative sPEEK membranes. The second approach was based on the development of a dedicated in-house experimental setup designed to generate a chemically degrading vapor phase. Following an optimization stage, a series of tests was carried out to quantify the degradation of pretreated sPEEK under different levels of chemical and mechanical stress.

Keywords – IT-PEMFC, Performance, Durability, Membrane, Electrodes, sPEEK, PFSA